THE DESIGN OF COUPLED FRAME-WALL STRUCTURES FOR SEISMIC ACTIONS

A thesis
submitted in partial fulfilment
of the requirements for the Degree
of
Doctor of Philosophy in Civil Engineering
at the
University of Canterbury
by

WILLIAM JOHN GOODSIR

University of Canterbury,
Christchurch, New Zealand

1985

THE DESIGN OF COUPLED FRAME-WALL STRUCTURES
FOR SEISMIC ACTIONS

Errata

p.7	12 lines up	"intertia" → "inertia
p.22	8 lines up	"V = M/αH"
p.29	5 lines down	"right" → "rigid"
p.30	14 lines down	- remove the words "post elastic"
p.53	Table 3.13	"A_v" → "Δ_v"
p.78	8 lines up	"restrict the maximum allowable"
p.86	3 lines down	"subjects" → "subjected"
p.107	10 lines up	"modes" → "models"
p.112	11 lines down	"demanda" → "demands"
p.158	10 lines down	"walls which can"
p.161	6 lines up	"$0.15\ell_w$ from the extreme compression fibre."
p.165	4 lines down	"6.2.4" → "6.2.5"
p.177	Bottom line of text - replace full stop with comma	
p.178	19 lines down	"6.10" → "6.8"
p.188	2 lines down	"playwood" → "plywood"
p.189	7 lines up insert "These potentiometers were located 150 mm from the east end of the wall."	
p.217	The last two sentences should read as follows: Flexural deformations are approximately equal to shear deformations for negative loading and twice the shear deformations for positive loading at $\mu_\Delta = 4$. Sliding shear at the base construction joint level constituted at most 11% of shear deformations and less than 5% of total first floor displacement.	
p.218	3 lines down	"2.23" → "7.23"
p.220	7 lines down	"negative" → "positive"
p.258	Points marked	$\mu_\Delta = \pm 6$ should be $\mu_\Delta = \pm 5$
p.272	Point marked	$\mu_\Delta = -6$ should be $\mu_\Delta = -5$
p.280	Table 7.1, item 4, lower case c	
p.285	7 lines down	"pracice" → "practice"
p.286	Table 7.2	"$\mu_\Delta = 4$"
p.288	10 lines down	"negative loading stiffness"
p.296	4 lines up	"0.66" → "0.81"
p.D.11	5 lines up	"s = 80 mm" → "s = 100 mm"

For A.M.P.

ABSTRACT

A methodology for the design of reinforced concrete frame-wall structures for seismic resistance is presented. By using capacity design principles, plasticity is restricted to well detailed beam and wall base hinge zones where energy is expected to be dissipated primarily via the flexural yielding. Numerous inelastic time history analyses, simulating earthquake attacks, were performed for simplified 6 and 12 storey buildings. Major variables examined included relative frame:wall stiffness, wall base fixity and wall: frame height. Response to the NS El Centro 1940 accelerogram indicated the likelihood of very satisfactory seismic response for prototype structures. Member actions were able to be estimated with good accuracy although the dynamic magnification of wall base shear forces is viewed with concern.

Complementary to the analytical study, four approximately 1/3 scale model cantilever structural wall units were tested under a regime of cyclic lateral loading. The units exhibited very good hysteretic behaviour prior to failure via out of plane buckling or material compression failure accelerated by the former mode of response. Features of behaviour of wall sections with large concrete compression strains and lateral instability were the major targets of study in these experiments. Recommendations are made regarding confining hoop reinforcement and dimensional limitations for the plastic hinge zones of structural walls.

ACKNOWLEDGEMENTS

The research described in this thesis was carried out in the Department of Civil Engineering, University of Canterbury, under the overall guidance of its Head, Professor R. Park.

I wish to acknowledge the great debt of gratitude I owe to Professor T. Paulay for his tireless assistance and encouragement during this project.

The guidance of Dr. A.J. Carr regarding computational aspects of the project is also gratefully acknowledged.

My thanks are extended to the Technical Staff of the Department, especially Messrs. P.G. Mitchell and G.W. Sim (specimen construction) and Messrs. G.E. Hill and G.H. Clarke (specimen testing). I also wish to thank Mrs V.J. Grey for assistance with the draughting work, Mr. L.H. Gardner for photographic work, and Mrs A. Watt for typing the manuscript.

The financial assistance provided by the Ministry of Works and Development and the University Grants Committee is gratefully acknowledged.

TABLE OF CONTENTS

Page

NOTATION

A_b = Area of reinforcing bar

A_c = Area of concrete or Area of confined concrete core measured to the outside of confining hoops

A_g = Gross area of section

A_s = Area of tension reinforcement

A_{sh} = Total effective area of hoop bars and supplementary cross ties in direction under consideration within spacing s_h

A_{st} = Total area of vertical flexural reinforcement in a section

A_{sv} = Area of shear reinforcement within a spacing s

A_{te} = Area of one leg of a stirrup tie

A_v = Area of cross section effective in resisting shear stresses

A_{vf} = Area of shear friction reinforcement

A^*_c = Area of concrete core extending over the outer half of the neutral axis depth which is subject to compression, measured to the outside of peripheral hoops

A^*_g = Gross area of concrete section extending over outer half of the neutral axis depth which is subject to compression

b = Width of wall section, subscripted R for rectangular section or I for I section wall

b_f = Flange width for a tee section wall

b_w = Width of web sustaining shear stress

b' = Width of flange in a flanged wall

c = Distance from extreme compression fibre to neutral axis

c_{av} = Average value of c calculated from experimental readings on opposite sides of a test unit

c_c = Critical value of c

c_i = Value of c at ideal moment capacity

C = Basic seismic coefficient for the derivation of C_d

C_d = Lateral force coefficient for equivalent static analysis = CRSM

d = Distance from extreme compression fibre to centroid of tension reinforcement

d_b = Diameter of bar

d_h = Diameter of hoop leg

d' = Distance from extreme compression fibre to centroid of compression reinforcement

D = Dead load or Prefix for reinforcing bar size denoting deformed mild steel bar

e = Eccentricity of axial load from elastic centroid of section

E = Earthquake load or Modulus of elasticity

E_c = Modulus of elasticity for concrete

E_s = Modulus of elasticity for steel

E_t = Tangent modulus for steel

$E_{t,crit}$ = Value of E_t at the onset of section instability

$E_{t,x}$ = Value of E_t at a general point x

f_s = Reinforcement stress

$f_{s,crit}$ = Value of f_s at the onset of section instability

$f_{s,x}$ = Value of f_s at a general point x

f_{ult} = Ultimate strength of reinforcement

f_y = Specified minimum yield strength of reinforcement

f_{yh} = Specified minimum yield strength of hoop reinforcement

f'_c = Specified minimum 28 day concrete cylinder strength or Cylinder strength for experimental units at the time of testing. MPa or psi units are implied for non homogeneous equations involving the term $\sqrt{f'_c}$

g = Acceleration of gravity = 9.81 m/s^2 or Subscript denoting gross section property

G = Shear modulus

h = Storey height

h_b = Overall depth of beam

h_i = Height of action of force $V_{code,i}$

h_w = Height of a structural wall element

h'' = Dimension of concrete core of section measured perpendicular to the direction of the hoop leg, to the outside of the peripheral hoop

H = Total height of a building

HD = Prefix for bar diameter denoting high strength (nominal f_y = 380 MPa) deformed bar

I = Second moment of area of a section, may be subscripted w for a wall

jd = Lever arm between centre of compression block and centroid of the tension steel of a reinforced concrete section

k = UBC [26] lateral force coefficient

K = UBC [26] horizontal force factor

K_o = Initial loading stiffness

K_1 = Post yield (bilinear) stiffness

ℓ = Member length or Height between end rollers in prism units tested

ℓ_c = Clear span of column

ℓ_e = Effective length for buckling

ℓ_f = Flange length for a tee section wall

ℓ_n = Length of clear span of a member

ℓ_p = Plastic hinge length

ℓ_v = Shear span, defined as the ratio of the effective height of application of the shear force acting on a wall to the wall dimension ℓ_w

ℓ_w = Major dimension of a structural wall section, may be subscripted I or R for an I or rectangular section

ℓ_{FI} = Length of flange for an I section wall

ℓ' = Distance between interior and exterior columns used in overturning moment calculations

L = Live load

L_R = Reduced live load

max,min = Subscripts denoting maximum or minimum values of a variable

M = Bending moment or Structural material factor used in the derivation of C_d

M_b = Balanced failure moment from column interaction diagram

M_{code} = Bending moment derived from code specified lateral seismic loading only (taken at the beam centreline for column members)

$M_{code,top}$ = Value of M_{code} at the top of a bottom floor column

M_{col} = Column centreline design moment

$M_{col,red}$ = Column design moment at the face of the beam-column joint

$M_{col_{base}}$ = Base level column moment occurring during a dynamic analysis

M_d = Dependable moment capacity

M_i = Ideal moment capacity

M_{max} = Maximum moment recorded during dynamic analyses or Maximum flexural strength of a wall test unit

M_o = Overturning moment at the base of a building

M_u = Factored moment at a section acting with shear force V_u

M_{wall} = Wall design moment

$M_{wall_{base}}$ = Base level wall moment occurring during a dynamic analysis

M_y = Yield moment

M_B, M_T = Flexural strengths of bottom and top sections of a column

$M_{1,2,3,4}$ = Moment associated with axial loads of 0, $\frac{1}{3}P_*$, $\frac{2}{3}P_*$ and P_* on the simplified column interaction diagram

M_y^{min} = Minimum wall base moment used by the PCA [37]

M^o = Overstrength moment capacity, may be subscripted col for a column

n = Number of storeys in a building or Number of primary flexural bars restrained from buckling by a hoop leg

p = Moment - rotation bilinear factor

P = Axial load, may be subscripted D for dead load or LR for reduced live load

P_b = Balanced axial compression load

$P_{e,max}$, $P_{e,min}$ = Maximum and minimum design axial forces acting on a column during an earthquake

P_{eq} = Earthquake induced column force resulting from beam overstrength shear force inputs = $R_v \Sigma V_{oe}$

P_u = Design axial compression force normal to cross section occurring simultaneously with V_u

P_{yc}, P_{yt} = Ultimate column compression and tension strengths on the simplified column interaction diagram

P^* = Compressive axial force for simplified interaction diagram = $0.6f'_c A_g$

r = User supplied bilinear factor for the program RUAUMOKO

r_v = Shear force reduction factor used by PCA [37,38]

R = Risk factor used in the derivation of C_d or Prefix for bar diameter denoting mild steel (nominal f_y = 275 MPa) plain round bar

R_m = Moment reduction factor dependent on axial load level and ω

R_v = Reduction factor accounting for the likelihood of beam overstrength occurring at all levels of a frame

s = Spacing of shear stirrup sets

s_h = Spacing of transverse hoop sets

s_v = Pseudo 5% damped velocity or Horizontal spacing of vertical reinforcement in a wall

S = Structural type factor used in the derivation of C_d

T_i = ith mode period of vibration, i = 1,2...

UB = Universal beam section

v = Shear stress

v_c = Concrete shear strength capacity

v_i = Total shear strength index

$v_{i,max}$ = Maximum allowable value of v_i

v_{max} = Maximum allowable design shear stress or Maximum shear stress sustained by wall test units

v_s = Steel shear stress = $v_i - v_c$

V = Shear force, may be subscripted i or base floor level i of base level

V_{code} = Shear force in a member due to code specified lateral loading, may be subscripted i for member i

$V_{code,total,base}$ = Total code base shear force for a frame-wall building

$V_{code,wall,base}$ = Value of V_{code} at the base of a wall in a wall-frame building

V_{col} = Column design shear force

V_{max} = Maximum shear force recorded during dynamic analysis, may be subscripted base or i for base level or level i or Maximum shear force sustained by experimental wall units

V_{oe} = Maximum earthquake induced shear force at the development of beam flexural overstrengths

V_u = Factored shear force at a section acting with moment M_u

V_{wall} = Wall design shear force

V_T = Code wall base shear force used by PCA [37]

V_T^{dyn} = Dynamic wall base shear force used by PCA [37]

w = Mass per unit length of a member

W , W_t = Total seismic weight of a building

W_i = Reactive seismic weight acting at height h_i

x = Cracking factor, i.e. the proportion of gross section properly assumed to be effective after the effects of cracking

z = Distance between layers of wall end zone reinforcement measured in the out of wall plane direction

α = Height of application of dynamic wall shear force normalised with respect to wall height or Unloading stiffness factor in the Takeda Hysteresis Relationship [28], or Fraction of compression block requiring confinement

β = Height of application of code wall shear force normalised with respect to wall height or Constant used in Newmark [45] integration scheme or Reloading stiffness factor in Takeda Hysteresis Relationship [28]

γ = Internal bilinear factor used in the program RUAUMOKO [15]

δ = Interstorey drift (displacement)

Δ = General displacement or Building top horizontal deflection

Δ_f = Flexural displacement

Δ_{fe} = Fixed end displacement

Δ_v = Shear displacement

Δtop, +ve, Δtop, -ve = Positive or negative wall top displacement normalised with respect to wall height

Δsv = Change in pseudo 5% damped velocity

Δt = Time step used for numerical integration in time history analysis

ΔT_1 = Change in first mode period

ε_c = Concrete compression strain

ε_s = Reinforcement strain

$\varepsilon_{s,crit}$ = Value of ε_s at the onset of section instability

$\varepsilon_{s,max}$ = Maximum tensile strain in reinforcement prior to section instability

$\varepsilon_{s,x}$ = Value of ε_s at a general point x

ε_y = Yield strain of reinforcement

θ = General rotation

θ_p = Plastic rotation

θ_y = Yield rotation

λ = Fraction of critical damping, may be subscripted i for the ith mode

μ = Coefficient of friction

μ^a = Section rotational ductility capacity used by PCA [37

μ_Δ = Displacement ductility factor

μ_θ = Rotational ductility factor

μ_ϕ = Curvature ductility factor

ρ = Flexural steel reinforcement ratio = $A_s/(b_w d)$

ρ_d = $A_s/(0.8\ell_w b_w)$

ρ_f = Ratio of main flexural reinforcement area to end zone area

ρ_h = Ratio of distributed flexural reinforcement area to gross concrete area of a vertical section of wall

ρ_ℓ = Area ratio of primary vertical tension reinforcement in wall spaced at s_v

ρ_s = Volumetric ratio of hoop reinforcement to confined core (measured to the outside of hoops)

ρ_t = Ratio of total vertical reinforcement area to gross section area

ρ_v = Ratio of shear reinforcement area to gross concrete area of a vertical section of wall

Σ = Symbol denoting the summation of a variable

ϕ = Strength reduction factor (Section 4.3.1.2, Ref. 34)
or Curvature

ϕ_o = Flexural overstrength factor, defined as the ratio M^o/M_{code}

ϕ_u = Ultimate curvature

ϕ_y = Yield curvature

ω = Dynamic magnification factor or Natural circular frequency

ω_c = Column shear dynamic magnification factor

ω_v = Dynamic shear magnification factor for a cantilever structural wall

ω_v^* = Dynamic magnification factor for a wall in a frame-wall building

$\rightarrow$ or $\leftarrow$ placed over a variable signifies the direction of earthquake attack.

DEFINITION OF MEMBER FLEXURAL STRENGTHS

The various levels of member flexural strength used in the following chapters are defined here as follows:

1. Ideal strength (M_i) theoretical strength calculated using specified (nominal) steel and concrete strengths.

2. Dependable strength - ideal strength multiplied by strength reduction factors (ϕ) to give an extreme lower bound for member strength.

3. Probable strength - theoretical strength calculated using expected mean material strengths. In this report, column probable flexural strength was taken to be $1.13\,M_i$.

4. Overstrength (M^o) expected maximum strength allowing for probable mean yield strength and strain hardening of reinforcement. In this report, typical beam and wall flexural overstrengths of $1.39\,M_i$ and $1.45\,M_i$ respectively were used.

REFERENCES

1. PARK, R. and PAULAY, T., "Reinforced Concrete Structures", John Wiley and Sons, New York, 1975, 769pp.
2. GOODSIR, W.J., "The Response of Coupled Shear Walls and Frames", Master of Engineering Report, University of Canterbury, New Zealand, 1982, 156pp.
3. ASCE, "Monograph on Planning and Design of Tall Buildings: Volume CB, Structural Design of Tall Concrete and Masonry Buildings", ASCE, 1978, 938pp.
4. COULL, A. and STAFFORD-SMITH, B., "Analysis of Shear Wall Structures (A Review of Previous Research)", Tall Buildings, Proceedings of a Symposium held at the University of Southampton, Pergamon Press, April 1966, pp.139-156.
5. DERECHO, A.T., "Design of Frame-Wall Structures", Workshop on Earthquake-Resistant Reinforced Concrete Building Construction (ERCBC), University of California, Berkeley, July 11-15, 1977, pp.1281-1310.
6. KONG, F.K., EVANS, R.H., COHEN, E. and ROLL, F., "Handbook of Structural Concrete", Pitman, 1983, 1968pp.
7. SINGH, G. and SCHWAIGHOFER, J., "A Bibliography on Shear Walls", University of Toronto, Department of Civil Engineering Report 76-02, May 1976.
8. UMEMURA, H. and TAKIZAWA, H., "Dynamic Response of Reinforced Concrete Buildings", Structural Engineering Document 2, International Symposium for Bridge and Structural Engineering, Zurich,1982, pp.1-64.
9. NZS 4203:1976, "Code of Practice for General Structural Design and Design Loadings for Buildings", Standards Association of New Zealand, Wellington, 80pp.
10. ROSMAN, R., "Laterally Loaded Systems Consisting of Walls and Frames", Tall Buildings, University of Southampton, 1966, pp.273-289.
11. WYNHOVEN, J.H. and ADAMS, P.F., "Analysis of Three-Dimensional Structures", Journal of the Structural Division, ASCE, Vol. 98, ST1, Jan. 1972, pp.233-248.
12. MACGREGOR, J.G. et al, "Approximate Inelastic Analysis of Shear Wall-Frame Structures", Journal of the Structural Division, ASCE, Vol. 98, ST11, November 1972, pp.2351-2362.
13. KHAN, F.R. and SBAROUNIS, J.A., "Interaction of Shear Walls with Frames in Concrete Structures under Lateral Loads", Journal of the Structural Division, ASCE, Vol. 90, No. ST3, June 1964, pp.285-335.

14. KAANAN, A.E. and POWELL, G.H., "DRAIN-2D, A General Purpose Computer Program for Dynamic Analysis of Planar Structures", Report UCB/EERC-73/6, Earthquake Engineering Research Center, University of California, Berkeley, 1973, 101pp. plus appendices.

15. CARR, A.J., "RUAUMOKO", Computer Program Library, Department of Civil Engineering, University of Canterbury, New Zealand, 1984, 34pp.

16. YUZUGULLU, O., and SCHNOBRICH, W.C., "Finite Element Approach for the Prediction of Inelastic Behaviour of Shear Wall Frame Systems", University of Illinois at Urbana-Champaign, Civil Engineering Studies, Structural Research Series No. 386, May 1972, 125pp.

17. SPURR, D.D., "Post Elastic Behaviour of Reinforced Concrete Frame-Wall Components and Assemblages Subjected to Simulated Seismic Loading", Ph.D. Thesis, Department of Civil Engineering, University of Canterbury, New Zealand, 1984, 498pp.

18. ZIENKIEWICZ, O.C., "The Finite Element Method in Engineering Science", McGraw-Hill, 1971, 521pp.

19. OTANI, S., "Nonlinear Dynamic Analysis of 2-D Reinforced Concrete Building Structures", IASS Symposium - Nonlinear Behaviour of R.C. Spatial Structures, Darmstadt, July 1978.

20. EMORI, K. and SCHNOBRICH, W.C., "Computed Behaviour of a Ten Storey Reinforced Concrete Frame-Wall Structure for Static Lateral Loads", 7th WCEE, Istanbul, Turkey, Sept. 1980, Vol. 5, pp.529-536.

21. ABRAMS, D.P. and SOZEN, M.A., "Experimental Study of Frame-Wall Interaction in Reinforced Concrete Structures Subjected to Strong Earthquake Motions", University of Illinois at Urbana-Champaign, Civil Engineering Studies Structural Research Series No. 460, May 1979, 386pp.

22. BERTERO, V.V., "State of the Art and Practice in Seismic Resistant Design of R/C Frame-Wall Structural Systems", Proceedings 8th WCEE, San Francisco, 1984, Vol. V, pp.613-620.

23. AKTAN, A.E. and BERTERO, V.V., "States of the Art and Practice in the Optimum Seismic Design and Analytical Response Prediction of R/C Frame-Wall Structures", Report No. UCB/EERC - 82/06, Earthquake Engineering Research Center, University of California, Berkeley, 61pp.

24. CHARNEY, F.A. and BERTERO, V.V., "An Evaluation of the Design and Analytical Seismic Response of a Seven Storey Reinforced Concrete Frame-Wall Structure", Report UCB/EERC - 82/08, Earthquake Engineering Research Center, University of California, Berkeley, 1982, 176pp.

25. PENZIEN, J., "Recommendations for a U.S.-Japan Cooperative Research Program Utilizing Large Scale Testing Facilities", U.S.-Japan Planning Group Report No. UCB/EERC - 79/26, Sept. 1979.

26. INTERNATIONAL CONFERENCE OF BUILDING OFFICIALS, "Uniform Building Code (UBC 79)", 1979, 734pp.

27. ACI COMMITTEE 318, "Building Code Requirements for Reinforced Concrete (ACI 318-83)", American Concrete Institute, Detroit, 1983, 111pp.

28. TAKEDA, T., SOZEN, M.A. and NIELSEN, N.N., "Reinforced Concrete Reponse to Simulated Earthquakes", Journal of the Structural Division ASCE, Vol. 96, No. ST12, 1970, pp.2557-2573.

29. FINTEL, M. and GHOSH, S.K., "Inelastic Response History Analysis of Earthquake Resistant Building Structures with Yielding Walls and Elastic Frames", 7th WCEE, Istanbul, Turkey, Sept. 1980, Vol. 5, pp.435-438.

30. FINTEL, M. and GHOSH, S.K., "Seismic Resistance of a 31-Storey Shear Wall-Frame Building using Dynamic Inelastic Response History", 7th WCEE, Istanbul, Turkey, Sept. 1980, Vol. 4, pp.379-386.

31. SAATCIOGLU, M., TAKAYANGI, T. and DERECHO, A.T., "Dynamic Response of Reinforced Concrete Wall Systems", 7th WCEE, Istanbul, Turkey, Sept. 1980, Vol. 5, pp.49-56.

32. MOEHLE, J.P. and SOZEN, M.A., "Experiments to Study Earthquake Response of R/C Structures with Stiffness Interruptions", University of Illinois at Urbana-Champaign, Civil Engineering Studies Structural Research Series No. 482, August 1980, 421pp.

33. NIKHED, R.P., MACGREGOR, J.G. and ADAMS, P.F., "Studies of Reinforced Concrete Shear Wall-Frame Structures", Structural Engineering Report No. 25, Department of Civil Engineering, University of Alberta, June 1970, 241pp plus appendices.

34. NZS 3101:1982, Parts 1 and 2, "Code of Practice for the Design of Concrete Structures", Standards Association of New Zealand, Wellington, 283 pp.

35. SHIBATA, A. and SOZEN, M.A., "The Substitute Structure Method for Earthquake-Resistant Design of Reinforced Concrete Frames", University of Illinois at Urbana-Champaign, Civil Engineering Studies, Structural Research Series No. 412, October 1974.

36. BLAKELEY, R.W.G., COONEY, R.C. and MEGGET, L.M., "Seismic Shear Loading at Flexural Capacity in Cantilever Walls", Bulletin N.Z. National Society for Earthquake Engineering, Vol. 8, No. 4, Dec. 1975, pp.278-290.

37. FINTEL, M., et al, "Structural Walls in Earthquake Resistant Structures, Analytical Investigation Dynamic Analysis of Isolated Structural Walls - Parts A and B", Portland Cement Association, Skokie, 1976, 279pp.

38. FINTEL, M, et al., "Structural Walls in Earthquake Resistant Structures, Analytical Investigation Dynamic Analysis of Isolated Structural Walls - Part C, Interim Report", Portland Cement Association, Skokie, 1976, 266pp.

39. PAULAY, T., "The Design of Reinforced Concrete Ductile Shear Walls for Earthquake Resistance", Research Report 81-1, Department of Civil Engineering, University of Canterbury, Christchurch, New Zealand, Feb. 1981, 133pp.

40. ARCHER, J.S., "Consistent Mass Matrix for Distributed Mass Systems", Journal of the Structural Division, ASCE, Vol. 89, No. ST4, August 1963, pp.161-178.

41. SHARPE, R.D., "The Seismic Response of Inelastic Structures", Ph.D. Thesis, University of Canterbury, New Zealand, 1974, 188pp.

42. GIBERSON, M.F., "The Response of Nonlinear Multi-Storey Structures Subjected to Earthquake Excitation", Earthquake Engineering Research Laboratory, California Institute of Technology, Pasadena, 1967.

43. KESHAVARZIAN, M. and SCHNOBRICH, W.C., "Computed Nonlinear Seismic Response of R/C Wall-Frame Structures", Civil Engineering Studies Structural Research Series No. 515, University of Illinois at Urbana-Champaign, May 1984, 219pp.

44. EMORI, K. and SCHNOBRICH, W.C., "Analysis of Reinforced Concrete Frame-Wall Structures for Strong Motion Earthquakes", University of Illinois at Urbana-Champaign, Civil Engineering Studies Structural Research Series No. 457, December 1978, 209pp.

45. NEWMARK, N.M., "A Method of Computation for Structural Dynamics", Journal of the Engineering Mechanics Division, ASCE, Vol. 85, No. EM3, July 1959, pp.67-94.

46. HANSEN, S.D., "A Study of Interacting Structural Walls and Foundations in Seismic Design", Master of Engineering Report, University of Canterbury, New Zealand, 1984, 113pp plus appendices.

47. DERECHO, A.T. and IQBAL, M., "Inertial Forces Over Height of Reinforced Concrete Structural Walls During Earthquakes", Reinforced Concrete Structures Subjected to Wind and Earthquake Forces, ACI Publication SP-63, 1980., pp.173-196.

48. SAATCIOGLU, M., DERECHO, A.T. and CORLEY, W.G., "Modelling Hysteretic Behaviour of Coupled Walls for Dynamic Analysis", Earthquake Engineering and Structural Dynamics, Vol. 11, 1983, pp.711-726.

49. CARTER, B.H.P., "The Seismic Behaviour of Reinforced Concrete Frame-Shear Wall Structures", Master of Engineering Report, University of Canterbury, New Zealand, 1980, 118pp.

50. NEW ZEALAND PORTLAND CEMENT ASSOCIATION, "New Zealand Reinforced Concrete Handbook",NZPCA, 1979.

51. TOMPKINS, D.M., "The Seismic Response of Reinforced Concrete Multistorey Frames", Research Report 80-5, Department of Civil Engineering, University of Canterbury, New Zealand, Feb. 1980, 141pp.

52. NAKASHIMA, M. et al, "Seismic Resistance Characteristics of Reinforced Concrete Beam-Supported Floor Slabs in Building Structures", Report No. 422-9, Lehigh University, April 1981, 349pp.

53. OESTERLE, R.G., et al, "Earthquake Resistant Structural Walls - Tests of Isolated Walls Appendix B - Test Results", Portland Cement Association, Skokie, 1976, 233pp.

54. OESTERLE, R.G., et al, "Earthquake Resistant Structural Walls - Tests of Isolated Walls, Phase II", Portland Cement Association, Skokie, 1979, 84pp plus appendices.

55. WANG, T.Y., BERTERO, V.V. and POPOV, E.P., "Hysteretic Behaviour of Reinforced Concrete Framed Walls", Report UBC/EERC 75/23, Earthquake Engineering Research Center, University of California, Berkeley, 1975, 367pp.

56. VALLENAS, J.M., BERTERO, V.V. and POPOV, E.P., "Hysteretic Behaviour of Reinforced Concrete Structural Walls", Report UBC/EERC 79/20, Earthquake Engineering Research Center, University of California, Berkeley, 1979, 234pp.

57. MANDER, J.B., "Seismic Design of Bridge Piers", Research Report 84-2, Department of Civil Engineering, University of Canterbury, New Zealand, 1984, 442pp.

58. SCARPAS, A., "The Inelastic Behaviour of Earthquake Resistant Reinforced Concrete Exterior Beam-Column Joints", Master of Engineering Report, University of Canterbury, New Zealand, 1981, 114pp.

59. PARK, R., PRIESTLEY, M.J.N. and GILL, W.D., "Ductility of Square Confined Concrete Columns", Proceedings ASCE, Vol. 108, ST4, April 1982, pp.929-950.

60. LESLIE, P.D., "Ductility of Reinforced Concrete Bridge Piers", Master of Engineering Report, University of Canterbury, New Zealand, 1974, 147pp.

Chapter One INTRODUCTION

The frame-wall structural form, comprising interconnected moment resisting space frames and cantilevered structural walls, is an efficient configuration for medium-rise reinforced concrete buildings at risk from seismic activity. The form combines the advantages of its constituent elements. Structural walls are capable of providing the deformation control necessary to prevent damage to a building and its contents during minor earthquakes, and the strength and inelastic deformation capacity needed to ensure that major earthquakes are resisted without collapse. Moment resisting frames, which become less efficient at resisting lateral forces at upper storeys, are well suited to transfer gravity load to the foundations. Both components are capable of dissipating considerable seismic energy via flexural yielding in zones to be detailed for this purpose. Although the research effort devoted to frame-wall behaviour has increased in recent years, the current state of knowledge regarding such structures is less advanced than that of isolated frames or walls.

This report presents a design methodology for frame-wall buildings, utilising the capacity design philosophy [1]. Numerous computer based nonlinear dynamic analyses, modelling seismic attack on simplified prototype structures, were carried out in order to develop and to assess the design process.

In view of the significant structural ductility demands which may be imposed during a major seismic event, critical regions of the structural walls must be able to sustain high local deformations. Thus, complementary to the theoretical study, an experimental investigation of the behaviour of relatively slender cantilever structural walls was undertaken. Special attention was given to hoop reinforcement requirements and the tendency for out of plane instability of the compression zone of the walls in the potential plastic hinge region.

The topics are presented in the following order: Chapter 2 summarises previous literature regarding analytical and experimental studies, and design philosophy for frame wall buildings. Chapter 3 describes an investigation via computer modelling of parameters which

significantly affect plain cantilever structural wall behaviour. These include wall geometry, stiffness, fixity, damping properties, base excitation and the analytical modelling used. Chapter 4 examines the force and deformation response of simplified 6 and 12 storey frame-wall buildings to the NS El Centro 1940 and S15°W Pacoima Dam 1971 accelerograms, the structures being designed according to a previously postulated method [2]. Chapter 5 extends this analytical investigation to examine the influence of wall foundation flexibility and wall height on overall structural performance. Chapter 6 forms an introduction to an experimental investigation of cantilever structural wall behaviour, describing the current New Zealand design methodology, and reviewing previous experimental studies. Chapter 7 contains detailed results of the 4 wall tests performed and a discussion of the behaviour observed. Chapter 8 briefly describes a series of axial load tests made on wall subassemblage units. Finally, Chapter 9 summarises the work undertaken and restates the main conclusions and recommendations made regarding the design methodology and the detailing of structural wall units.

Chapter Two A SUMMARY OF LITERATURE REGARDING THE ANALYSIS , DESIGN AND EXPERIMENTAL STUDY OF FRAME-WALL BUILDINGS

2.1 INTRODUCTION

Although a considerable body of literature devoted to the study of isolated beam-column frames and cantilever structural walls exists, there has been comparatively little work on coupled frame-wall buildings. However, as well as specific papers and reports on the subject, some general references containing bibliographies do exist [3,4, 5, 6, 7, 8]. This chapter surveys previous literature on the analysis, design and experimental study of frame-wall buildings. Some work is presented in more detail in order to give an illustration of existing approaches to the subject.

2.1.1 Basic Interaction

The existence of the phenomenon of force interaction between beam-column frame elements and cantilever structural walls constrained to act together is well known. These interactive or internal forces arise from the essentially different modes of response of frame and walls to a given distribution of lateral load. Isolated frames adopt displacement profiles similar to those of cantilever beams dominated by shear deformations, while free standing structural walls are dominated by flexural deformations.

It is unfortunate that this fact is often obscured by the widespread use of the term "shear" walls: in fact shear deformations need not be significant in the response of structural walls to any form of loading.

Because frame and wall elements in the one building are constrained by the floor diaphragms to adopt a similar displacement profile for a particular external lateral load, the deformation patterns that would be adopted on both elements, were they to be de-coupled, are modified (Fig. 2.1). This modification is responsible for the existence of interactive forces between frames and walls, forces which must be taken into account in the analysis of this type of structure. If the frame component is sufficiently stiff, it may effectively restrain the (more flexible) upper regions of the

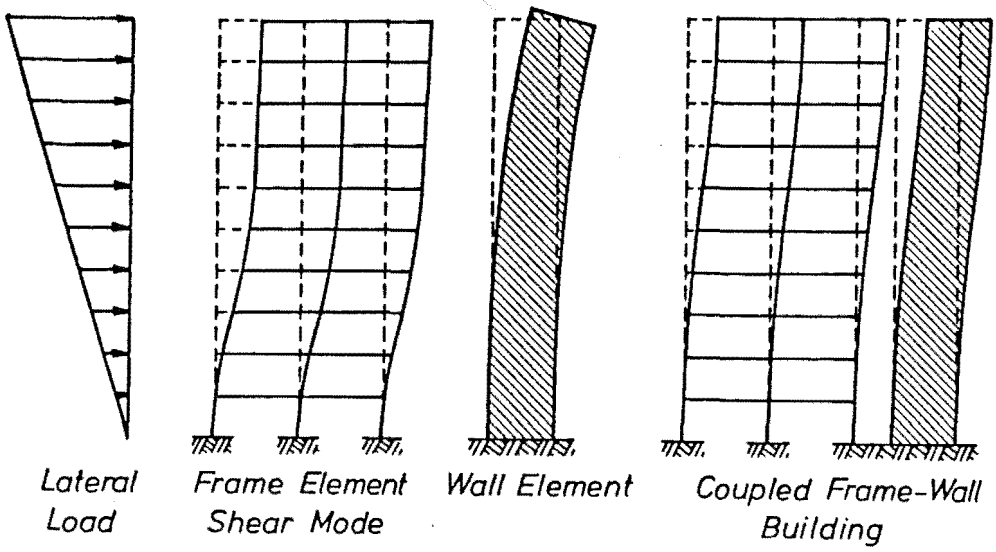

Fig. 2.1 Deformation Patterns of Frame, Wall, and Coupled Frame-Wall Elements.

walls. This causes both the existence of a point of contraflexure in the walls, and a reversal in the sense of the shear force carried by the wall above the point. This latter phenomenon has the effect of requiring the upper part of the frame to sustain a load greater than the applied external force in this upper region.

It is reiterated that the recognition of and appropriate allowance for this basic aspect of frame-wall behaviour is central to the analysis of this class of structure.

2.2 ANALYSIS

2.2.1 Static Elastic Analysis Techniques

The majority of existing analytic techniques, and almost all those of the pre 1970 era, are limited to describing the elastic response of frame wall structures. Despite the fact that satisfactory seismic response of these buildings usually requires a level of inelastic response, elastic analyses are an invaluable tool in the initial design of a structure, and are in fact often a mandatory stage in strength design [9]. The design method described in this thesis is intended to ensure good seismic response by apportioning strength on the basis of suitably

factored elastic load patterns. Three successively more sophisticated methods of static elastic analyses have emerged, and are briefly described below. Modelling techniques commonly used in these approaches are also briefly noted.

1. Continuous connection approach: The frame component of the structure is replaced by an equivalent shear cantilever, a single member with stiffness properties modelling those of the frame. This member is connected to a flexural cantilever element (representing the predominantly flexurally deforming wall elements in the structure) in a continuous manner, similar to that used in the laminar analysis of coupled shear walls. Such approaches commonly assume uniform geometrical properties with height and can usually cope with only simple forms at static lateral loading [10].

2. Simplified frame approach: In this method multi-bay frames are simplified to one [11] or two [12] bay frames. This substitute frame is coupled to a lumped structural wall via rigid pin-ended links. The two systems are generally considered separately and a compatible deformation pattern is derived using an iterative procedure to determine the distribution of forces between the structural components. Influence curves based on such procedures have been prepared [13].

Methods 1 and 2 suffer from two major difficulties. Firstly, in determining stiffness properties for the simple lumped members which allow accurate representation of the more complex elements being modelled, e.g. finding stiffnesses for a single bay frame used to represent a multi-bay frame. Secondly, it can be difficult to extract member actions relevant to the real structural elements from the force distributions determined for the simplified, lumped model, e.g. deriving actions for the beams and columns of a multi-bay frame modelled simply as a single bay frame.

3. Discrete frame approach: There is a direct one-to-one correspondence between the members of the prototype and analytical model structures in this method. Elements of similar dimensional details may be lumped together in this approach, and the force distribution determined via the computer based solution of a finite element formulation of the problem [14,15,16,17]. Such approaches are becoming more widespread because of the increasing availability to designers of static analysis

package programs. This approach enables the distribution of member forces throughout the structure to be determined for arbitrary patterns of external forces, such as gravity or code specified lateral loading. The finite element formulation is also usually used in analysis of frame-wall structures which take account of inelastic structural response. These more sophisticated approaches are discussed in Section 2.2.2.

2.2.1.1 Common modelling assumptions: There are a number of assumptions commonly used in the modelling of frame-wall structures. These are listed subsequently, although in no particular order of importance. These assumptions are typically made for both elastic and inelastic analyses of frame-wall buildings.

1. Analyses are generally restricted to plane (2 dimensional) structures. This means that torsional or skew loading effects can usually be taken account of in only an approximate manner.

2. Identical frame or wall elements may be readily lumped together to form a fictitious sub assemblage of similar form with stiffness properties found simply by multiplying the single element properties by the number of like elements.

3. Multi-bay frames are commonly represented by simpler elements such as single bay frames. Such techniques must be treated with caution when member actions derived for such simpler elements are used to determine prototype member actions: these cannot be simply determined from considerations of relative member stiffnesses, but must be based on compatibility of deflected shapes.

4. Computational expense is often reduced by simplifying the number of unknown degrees of displacement and rotational freedom to 3 per storey (2 translations and one rotation).

5. Members are usually idealised as line elements, although allowance can often be made for the finite size of member joints (which are usually assumed to be rigid, i.e. deformation free).

6. Structures are commonly assumed to have floor slabs of infinite inplane rigidity so that all parts of a structure at a particular level undergo identical horizontal translations. To ensure that walls and frames are constrained to act in this manner, one of two methods of connection of these lateral load resisting elements is commonly used. Either adjacent floor levels are joined by

fictitious pin-ended, axially rigid members or adjacent horizontal degrees of freedom are "slaved" (i.e. constrained to be equal).

7. Axial deformations of members are sometimes neglected, as are shear deformations.

8. Analyses are usually "first order" in the sense that calculations are based on the initial (undeformed) structural geometry. The presence of relatively stiff structural walls is likely to control lateral deformations sufficiently to make second order ($P-\Delta$) moments of minor importance.

9. Full foundation fixity for column and wall members is commonly assumed in analysis, although foundation compliance can be simulated by the provision of a rotational spring at ground level. The problem then becomes one of selecting an appropriate spring constant to simulate soil stiffness.

2.2.2 Inelastic Analysis Techniques

Computer based finite element techniques have become increasingly prominent in recent years, coupled to the desire for more accurate modelling of structural components and the development of more powerful computers. Since the likelihood of inelastic structural response during a significant seismic event has become widely accepted, analytical techniques able to model this behaviour have been developed. Such analyses make allowance for various modes of nonlinear response and may be used to predict the response of subassemblages or entire structures to external loading. Situations which can be modelled include monotonic external loading into the nonlinear response range, patterns of variable loading such as those used in experimental studies and simulated seismic loading, using accelerogram records to generate inertia loading histories. SEE ERRATA Although summaries of the finite element method [18], and available modelling techniques exist [19], several selected methods of inelastic analysis specifically relevant to frame-wall buildings are subsequently presented.

2.2.2.1 General purpose dynamic analysis programs: Several general purpose programs (e.g. DRAIN-2D [14], RUAUMOKO [15]) exist which permit the piece-wise time-history response of nonlinear structures to ground acceleration records to be modelled. These programs, which are not discussed in detail here, allow the geometry, stiffness and strength properties of each element in the structure to be modelled. Member types specifically suited to beams, columns and walls are commonly available.

Beam-column frames and structural wall elements are modelled separately but constrained to undergo equal horizontal displacements. Programs of this type are used most commonly in the analytical modelling of frame-wall buildings.

2.2.2.2 Other inelastic analysis methods: Emori and Schnobrich [20] developed an analysis program incorporating member models of increasing sophistication. These were (a) a concentrated spring model wherein inelastic deformations occur only at hypothetical point rotational springs, (b) a multiple spring model which allows for the more even distribution of member plasticity, and (c) a layered model for which inelasticity occurs in a finite sized plastic hinge and changes in flexural rigidity due to varying axial load and moment are recognised. The program was used to simulate the experimental work of Abrams and Sozen [21] (Section 2.4.4.1) with only fair success. It was concluded that even relatively sophisticated analytical procedures can simulate response in only an approximate manner.

Other finite element formulations and models also exist. Yuzugullu and Schnobrich [16] describe a program wherein line elements are used for frame members and walls are modelled with quadrilateral elements. The behaviour of experimentally tested deep beams and shear panels was simulated with good accuracy. Spurr [17] developed a sophisticated member model comprising of a number of layered segments. Deformations due to flexure (including the effects of diagonal shear cracking), bar anchorage pull out, sliding shear and imperfect crack closure were modelled. Although the model was able to simulate the experimental behaviour of subassemblage and frame wall units (Section 2.4.3), this was computationally expensive despite the consideration attention given to coding efficiency.

2.3 DESIGN METHODOLOGIES AND EXAMPLES

2.3.1 Introduction

The techniques described previously, encompassing both the elastic and inelastic modelling of structural response, have been oriented towards analysis rather than design. Very few detailed formulations of design practices suitable for frame-wall buildings have been published. This is in spite of the fact that good seismic response results from the advantageous distribution of strength and deformation capacity, rather than a knowledge of the distribution of member forces and moments under

some arbitrary loading regime. Clearly analytical techniques are important but the limitations resulting from the numerous assumptions on which analytical techniques are based should be recognised. In addition, due to the random nature of seismic events, the equivalent static forces used in building design are at best crude approximations. It is unfortunate that the formulation of design philosophies has been accorded an importance secondary to the refinement of analytical techniques.

In the subsequent section, work representing current American frame-wall design is described in some detail. (See also Refs. 22,23). The design of several other specific frame-wall structures is also briefly outlined. Previous research [2] on the development of the design philosophy presented in this thesis is described in Chapter 4.

2.3.2 Charney and Bertero [24]

The authors describe procedures used to assess the design of a prototype 7 storey frame-wall structure, studied as part of a joint US-Japan research programme [25] into this class of structure. The behaviour of the building (shown in Fig. 2.2) was modelled analytically using linear and nonlinear computer programs.

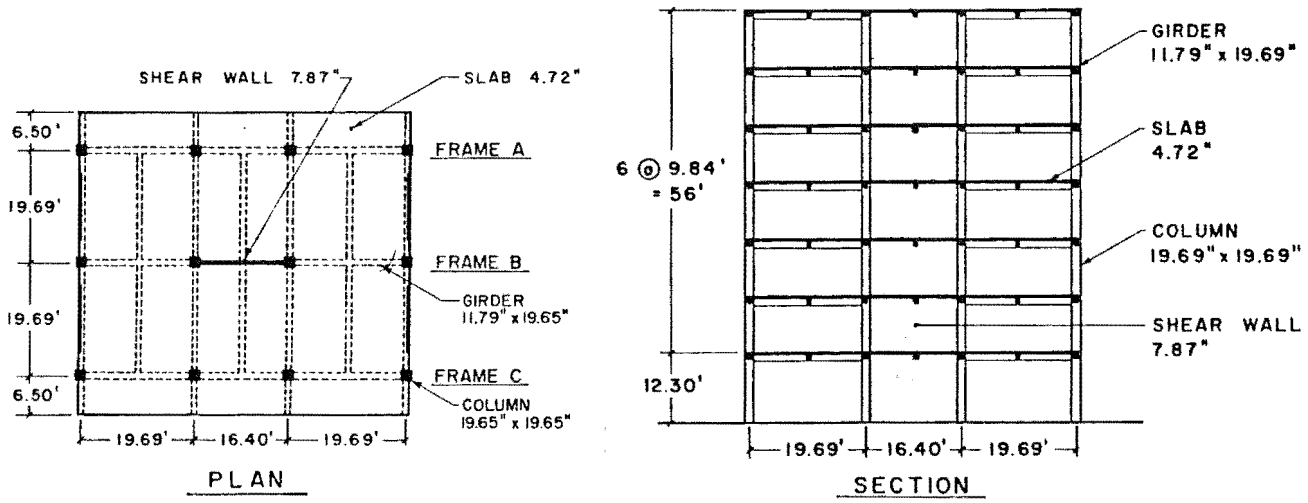

Fig. 2.2 Prototype Structure Analysed by Charney and Bertero [24].

2.3.2.1 Description of the prototype structure: It is not clear to precisely which specifications the prototype structure was originally designed, although the reinforcement layout appears to be a compromise between American and Japanese viewpoints. The beam shear reinforcement supplied was adequate to allow development of full beam flexural over-strength. Column shear strength was sufficient to sustain the force $V = 1.25 \times (M_T + M_B)/\ell_c$, where M_T and M_B are the flexural strengths of the top and bottom sections of a column of clear span ℓ_c. Prototype column confinement details were shown to provide curvature ductility capacities of between only 2 and 4. Charney and Bertero recommend a tie spacing of 3 times the flexural bar diameter in critical column zones from considerations of confinement and the prevention of local inelastic bar buckling. Recommendations for closer joint hoop spacing and supplementary cross ties in beam hinge zones were also made.

The structural wall elements had relatively well confined boundary elements. Wall shear strength was estimated at 574 kips (2560 kN), composed of approximately equal proportions of steel and concrete resisting mechanisms, the latter based on a stress of $3.3\sqrt{f'_c}$ psi ($0.27\sqrt{f'_c}$ MPa).

2.3.2.2 UBC [26] Static lateral loading: A static lateral load analysis was performed for the structure, using seismic coefficient of 0.0967 and a load factor of 1.4. The structural wall element dominated response, taking 92% of total base shear force. Factored gravity load moments were combined with the earthquake actions to give design, "code" actions. These strength demands were compared with prototype strengths calculated according to ACI [27] specifications and including a flexural streng reduction factor of 0.9. Prototype beam strength was shown to be adequate only if 20% vertical moment redistribution was allowed. Prototype column design was very conservative while the calculated wall flexural and shear strengths were 60% in excess of the design actions.

If the frame-wall structure was to qualify as "ductile" under the provisions of the UBC (i.e. have a UBC "K" factor of 0.8), and permit a 20% reduction in design force level stated above, certain conditions (given in Table 2.1) had to be met. These requirements could not be satisfied. They are considered by Charney and Bertero to be unduly harsh because the actual frame strength is not recognised and wall flexural strength is markedly in excess of the code requirements.

TABLE 2.1 : HORIZONTAL FORCE FACTOR K FOR BUILDINGS AND OTHER STRUCTURES

(From Table 23-I of UBC [26])

For buildings with a dual bracing system consisting of a ductile moment resisting space frame and a shear wall using the following criteria K shall be taken as 0.80.
(a) The frames and shear walls shall resist the total lateral forces in accordance with their relative rigidities considering the interaction of shear walls and frames.
(b) The shear walls acting independently of the ductile moment resisting space frame shall resist the total required lateral forces.
(c) The ductile moment resisting space frame shall have the capacity to resist not less than 25 percent of the required lateral forces.

2.3.2.3 Strength under monotonically increasing lateral load: A computer program was used to trace the response of the structure loaded incrementally until a collapse mechanism had formed. Members were given simplified yield surface envelopes with bilinear hystersis rules. For various lateral load patterns, load-displacement curves indicated approximately linear response up to the point of wall hinge formation, which occurred relatively early in the load history. After wall yield, stiffness was reduced to 60% of the initial value as load was absorbed by the frames. Beam hinge collapse mechanisms eventually formed, with base level column hinges last to form. P-Δ effects were insignificant due to the control on deflections exerted by the wall.

2.3.2.4 Response to earthquake loading: The computer program DRAIN-2D [14] was used to model the response of the prototype structure to (a) the Miyagi-Oki record (normalized to a peak acceleration of 0.36 g), and (b) the Pacoima Dam record (normalized to 0.4 g) . Simplified interaction diagrams were used for column members with bilinear hysteresis, while degrading Takeda [28] hysteresis was used for beam and wall sections. A Rayleigh damping scheme giving an average of 6% of damping to the first 3 modes of vibration was used. The integration time step used was 0.01 sec.

Displacement response was controlled by the wall, with peak normalized top level displacements of -0.0083 and 0.0132 recorded. Wall base shear force history had a greater higher mode component than wall base moment, although both were predominantly governed by first mode response. High base moments and shear forces generally occurred simultaneously. UBC [26] design wall base moments and shears were exceeded by up to 86% and 109% respectively. Maximum beam hinge plastic rotation of 0.016 radians was recorded. Significant lateral load was resisted by the frames only after wall hinging occurred.

2.3.2.5 Sources of inaccuracy in computed response: Several sources of error were cited:

1. Global modelling errors - coupling between exterior and interior frames via transverse beams, large displacement ($P-\Delta$) and foundation flexibility effects were citedas being potentially significant.

2. Local modelling errors - the use of simple elastic stiffnesses which are independent of the level of axial load in the member was viewed with concern. Because of the high wall shear forces indicated in analyses, the modelling of inelastic shear deformations may be warranted.

3. Miscellaneous - the use of the tributary area approach for gravity load distributionwas questioned, as was the use of the tangential stiffness matrix in the Rayleigh damping model. The need for a small integration time step to ensure numerical stability was stressed.

2.3.2.6 Conclusions: Charney and Bertero drew the following conclusions from the analytical work which has been described herein.

1. The prototype structure could have been classified as a dual bracing system ($K = 0.8$), had adequate column and beam tie reinforcement been present and if the requirement regarding the carrying of all lateral load by the wall was to be neglected.

2. The structure embodies the strong column-weak beam design philosophy and has good energy dissipation capabilities.

3. The analytical response to both static and dynamic loading was controlled by the structural wall. Although not allowed for in analysis, large inelastic shear deformations may occur in the

wall base region.

4. After wall flexural hinging, the beam column frames to which the wall was coupled were capable of resisting significant additional lateral load.

5. The results of the dynamic analyses should be viewed with some caution, given the possible sources of inaccuracies listed previously.

2.3.3 Other Design Approaches

Fintel and Ghosh [29] present a methodology whereby frame response is kept elastic and yielding is restricted to structural wall elements. Such an approach is dependent on wall sections possessing sufficient ductility capacity and in addition, it is unclear whether wall base yielding alone can dissipate sufficient seismic energy to give good seismic performance.

In an alternative approach [30], the same authors illustrate an iterative procedure using inelastic analyses to refine the preliminary design of a 31 storey frame-coupled wall building. Plasticity was restricted to main and coupling beams. Although such approaches are likely to become more popular, current practice would generally be to use dynamic analyses as a design checking aid rather than as a direct design tool. The problem of finding a reasonable preliminary design remains.

Saatcioglu et al [31] discusses the performance of a 20 storey frame-coupled wall structure, paying special attention to axial force-moment interaction and inelastic shear deformation effects. The former was found to be markedly more important than the latter.

2.4 EXPERIMENTAL INVESTIGATION OF FRAME-WALL INTERACTION

2.4.1 Introduction

To date very few experimental studies of frame-shear wall interaction have been made, although significant contributions to knowledge in this field may soon be made as a result of the US-Japan cooperative research program [25]. The expense of making scale models of frame-wall structures and difficulties in testing these models are responsible for this absence of a large body of research. Four experimental investigations are described in this section, with the

first two outlining the behaviour of what could more properly be described as well-outrigger frame specimens. Subsequently, small scale shake table tests carried out at the University of Illinois [21,32] are described.

2.4.2 Wall-Outrigger Frame Tests

Nikhed et al. [33] describe a 1/3 scale model 4 storey structure comprising a structural wall connected rigidly via beams to a full height column. With gravity load on wall and column, lateral load was increased monotonically until failure. The primary conclusion was that the importance of wall-frame interaction should be recognised in design. An analytical procedure also described by the authors was found to model the observed response reasonably well. The authors refer to pre 1970 experimental testing of frame-wall structures, although this is not discussed herein because of the lack of applicability of those structural forms studied to the modern conception of frame-wall buildings.

Two ½ scale 7 storey outrigger frame-wall units were tested by Spurr [17]. Although the units were wall dominated, the frame component resisted 25% of total base flexural strength. The units were tested pseudo-statically at increasing structural displacement ductilities, with equal lateral loads at the 3rd, 5th and 7th floors. An identical reinforcement layout was used for each unit except for beam flexural reinforcement which was conventionally horizontal in one and diagonally inclined in the other. The units were designed using capacity design principles [1] and the detailing requirements of NZS 3101 [34].

Due to the control on deformations exerted by the wall, and specifically, the control on beam yielding, beam flexural strength was selected arbitrarily. Columns and beam-column joints were designed to remain elastic under peak beam input forces. Axial load was applied to the wall and column stack to give base section compressions of 0.04 and $0.11 f'_c A_g$.

Shear reinforcement was supplied to beams and the wall to sustain the forces associated with flexural overstrength in those members. The maximum unsupported length of wall end region flexural reinforcement was limited to six times the diameter of the bar so restrained.

The following conclusions were drawn from the observed response of the units:

1. Beam behaviour was good for both horizontally and diagonally reinforced members, although the latter exhibited better resistance to sliding shear deformations. Beam ductility demands were high compared with overall structural ductilities, with plastic rotations of approximately 0.040 radians recorded (equivalent to a rotational ductility factor of approximately 10). Anchorage pullout in beams constituted between 25 and 35% of total deformations, independent of the level of applied load.

2. Column response remained essentially elastic except at the base section which must hinge to enable the development of a full structure mechanism. The limited yielding of the column base section was controlled by the much stronger wall element.

3. Column, joint and beam tie reinforcement apportioned according to capacity design principles proved adequate to ensure a beam hinge mechanism.

4. Wall plastic hinge zone behaviour was good, with plastic rotations of up to 0.025 radians sustained. Large sliding shear deformations did not develop due to the presence of net axial compression on the section.

5. Although the tie spacing limitation of $6d_b$ proved sufficient to prevent individual flexural bar buckling, the need to tie the wall end zone bar bundle to the web adequately was established.

6. Out of plane instability of the wall compression zone can limit load carrying capacity. Reversed cyclic loading to appreciable displacement ductilities leads to an accumulation of wide tensile cracks and a loss in the integrity of the concrete. The application of compression forces to such sections may result in uneven crack closure and sudden out of plane movement of the compression zone.

7. Although the units tested were strongly dominated by the wall, the applicability of the capacity design approach to frame-wall systems was demonstrated.

2.4.3 University of Illinois Tests

Two valuable series of experimental studies of frame-shear wall interaction have been carried out at the University of Illinois [21,32].

2.4.3.1 Abrams and Sozen [21]: Four small scale (approximately 1/12 full size) 10 storey frame wall structures were constructed and tested on a shake table. The model structures comprised two three-bay frames and one structural wall constrained to act in parallel (see Fig. 2.3). Inertia loads on the structures were due to the equal lumped storey masses used. The experimental program was undertaken in order to examine nonlinear wall-frame interaction and to test the adequacy of the design process used.

The structures were designed according to the Substitute Structure Method [35], whereby, on the basis of arbitrarily selected damage ratios, elements of a building are assigned substitute stiffnesses and effective damping factors to take account of the intended inelastic behaviour. This was to make the primary demands for inelastic behaviour on the beams, a reduced inelastic demand on the wall and prohibit the yielding of column members. While the geometrical details of all 4 structures were identical, two buildings had relatively heavily reinforced walls, while two were lightly reinforced. Conservative shear strength and anchorage details were provided.

The structures were subject to three earthquake simulations of progressively increasing severity, corresponding to peak accelerations of 0.4 g (design level excitation) 0.8 g and 1.2 g. The N21°E Taft 1952 and NS El Centro 1940 components were used. The following behaviour was observed:

1. A decrease in natural frequencies occurred with increased inelastic behaviour, coupled to an increase in energy dissipation.
2. Nonlinear behaviour occurred primarily in the beams, walls and base level columns.
3. Overall structural load resistance remained high even at large lateral displacements.
4. Permanent, locked in displacements developed and were associated with residual forces resisted by the walls.
5. Wall elements failed (at very high deformation) by rupture of tension reinforcement.

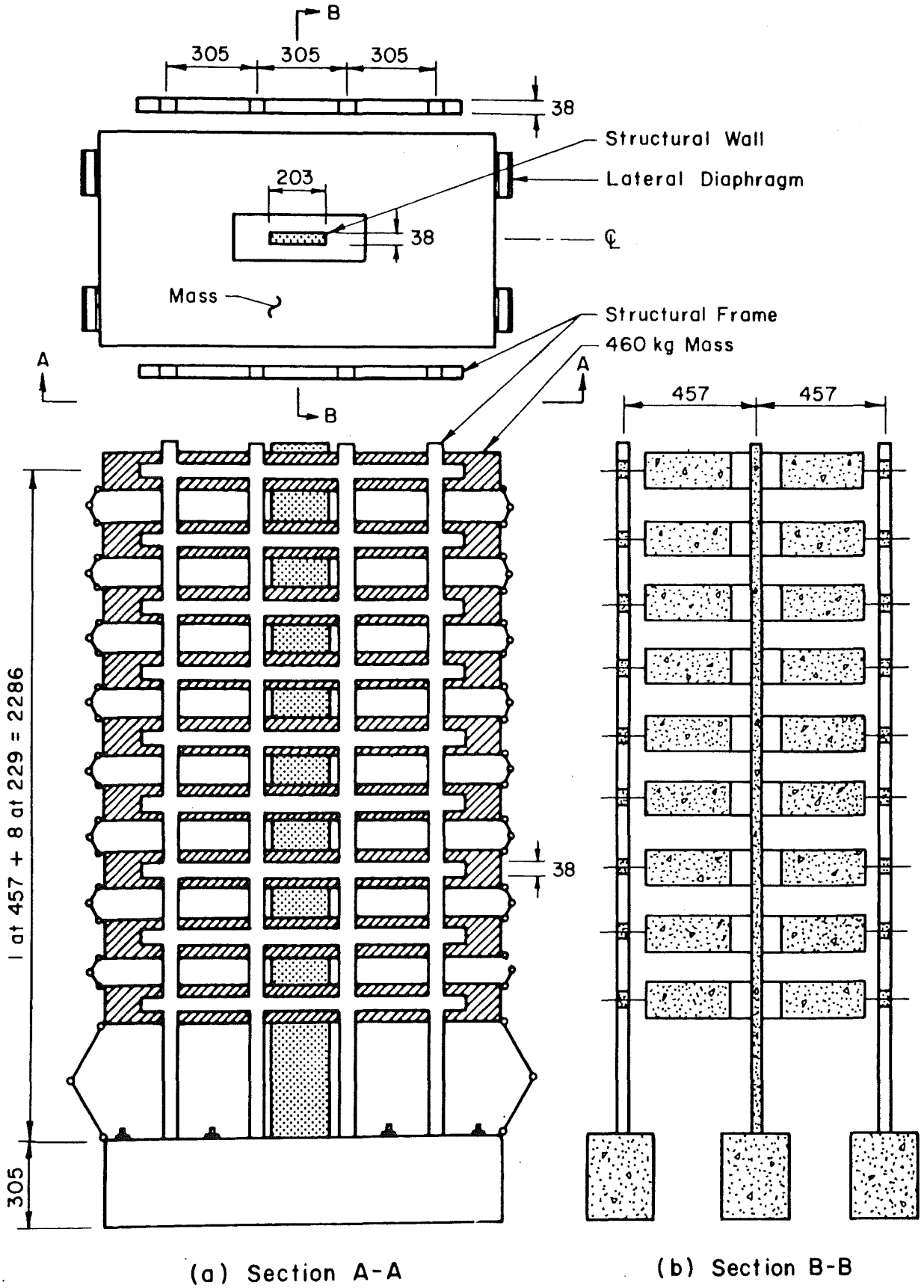

Fig. 2.3 Model Frame-Wall Structure Tested by Abrams and Sozen [21].

6. High values of wall shear force and moment generally occurred simultaneously.

7. Wall and frame shear forces were often in opposite senses even at the base level.

8. Time histories of wall base shear and moment were dominated by first mode response, although the shear history indicated significant higher mode participation.

It was concluded that the design method led to acceptable structural response and that,while the deformation response would be reasonably well predicted by a single degree of freedom model, the force response of individual frames or wall members could not.

2.4.3.2 Moehle and Sozen [32]: In an extension of the previously described research, Moehle and Sozen conducted a study of frame-wall structures with walls of less than full height. Four model structures were constructed to the same general specifications as described previously, but with variations in wall height and geometry as follows: the first storey height was double that used previously, giving a 9 rather than a 10 storey building. Three structures had wall heights of 9, 4 and 1 storeys, respectively, while the fourth structure was comprised of two frames only acting in parallel. In addition to investigating the seismic performance of these buildings, the suitability of simple linear and nonlinear numerical models for the description of various aspects of structural response was studied. A similar test procedure to that described previously was used.

The major aspects of observed structural response are summarised as follows:

1. Top level displacements of all structures was similar (approximately 1% of height during the design intensity excitation). Maximum interstorey drift indices recorded were 0.020, 0.019, 0.014 and 0.014 for the frames only, the 1, 4 and 9 storey walled structures respectively.

2. The three walled structures had similar total base moment strengths, with a lesser strength for the frames-only structure. The total base shear force resisted by the buildings increased with increasing wall height, although the forces resisted by the structural walls only did not necessarily increase with wall height.

(3) The hysteretic relationship between top displacement and total base moment was approximately bilinear with post-yield stiffness 15% of the pre-yield value. The structural response characteristics (period, damping) depended on the maximum previously attained displacement and the response amplitide at which the measurements were made.

(4) The wall component of the 4 and 9 storey walled structures consistently took approximately 60% of the total base shear force, the proportion rising to 95% for the 1 storey wall.

(5) Primary inelastic behaviour occurred in the beam members. High wall shear forces and moments were observed to occur simultaneously in general.

The authors show that for design purposes, equivalent static lateral load procedures compare well with more elaborate modal spectral analysis. Maximum experimental base level actions could not be well estimated from static load patterns however.

2.5 CONCLUSIONS

Of the three aspects briefly addressed in this literature review, namely analysis, design and experimental investigation of frame-wall buildings, the first-mentioned has been accorded the most extensive study. The hand and graphical techniques developed in order to determine simple static force distributions between interacting frame and structural wall components are now commonly used in only preliminary calculations. Reliable computer based techniques are routinely used, these formulations often incorporating numerous comparatively sophisticated modelling features. These techniques enable the study of the load and deflection response of structures to static, monotonically increasing and simulated seismic loading, and take account of inelastic member behaviour. It is stressed, however, that such techniques are based heavily on many simplifying assumptions. This fact should be borne in mind when interpreting the results of these analyses.

The state of development of design philosophies specifically for frame-wall buildings is less advanced. Although design techniques obviously hinge on a knowledge of generated member forces and moments (i.e. analysis), relatively little consideration has been given to the

formulation of design philosophies which recognise the inter-relationship of indivdual member detailing and the response of the entire structure to seismic events.

Similarly, the body of experimentally derived knowledge of the behaviour of frame-wall structures is not extensive. Considerations of scale have to date prohibited all but small scale modelling of realistic complete structural configurations, although considerable work has been done regarding the performance of isolated subassemblages or components. The logistical difficulties and high expense of conducting large scale tests are likely to continue to influence the acquisition of more reliable experimentally derived knowledge in spite of increasing interest in the subject.

Continued progress in the fields of analysis, design and experimental study of frame-wall buildings is desirable, with particular value attached to the closer integration and co-development of research in these areas.

Chapter Three DYNAMIC MAGNIFICATION OF SHEAR FORCE IN STRUCTURAL WALLS

3.1 INTRODUCTION

As stated previously, the primary thrust of the theoretical studies reported herein was directed towards the aseismic design of frame-wall structures, in an extension of a previously postulated approach [2]. Relatively early in the investigation it became clear that the most critical aspect of the design method hinged on the shear design of the wall component of these hybrid structures. This is based on a magnification of code specified shear forces used for uncoupled plain cantilevered structural walls [34]. Because of the importance of the prohibition of a shear failure in a structural wall, the work described in this chapter was undertaken: a re-examination of some aspects of the recommended shear design practice for the more fundamental lateral load resisting elements of isolated structural walls.

While few structural walls have failed in shear during seismic attack, this is largely because of earlier failure via some other mechanism such as bond failure, foundation failure, etc. Thus what are believed to be generally poor shear design practices world wide have not been revealed as such during previous seismic events. Although the trend towards better detailing is likely to circumvent many previously observed failure modes, the avoidance of the less commonly manifested shear failure is regarded as being of great importance.

In this chapter the phenomenon of dynamic magnification is described, together with some previous research into the subject.

A series of simplified structural walls were designed in an approximate manner with respect to flexural strength. The seismic response of these structures to several historical accelerograms was investigated using dynamic analysis time history programs. An initial series of analyses were made encompassing a wide but credible range of structural parameters. Selected results for these analyses are presented first, and discussed. Two separate computer programs, RUAUMOKO [15] and DRAIN 2D [14], were used for the analyses made in this section. The causes of discrepancies between results obtained from these programs for identical input data are discussed separately (Section 3.7.1). Subsequently, individual parameters, not considered in the first series of analyses,

were studied. This was usually done with reference to one particular structure and accelerogram, i.e. in a less comprehensive manner than the first series.

Of primary interest in the study was the magnification of the code load wall base shear force observed during dynamic response, and how this crucial design parameter is affected by various input parameters.

3.2 A DEFINITION - DYNAMIC MAGNIFICATION

Most code approaches to the design of buildings for earthquake resistance specify a distribution of static lateral loads which the structure must be able to resist safely. These static forces purport to give a force distribution equivalent to that induced in a structure by seismic base excitation but of reduced magnitude, if it is accepted that inelastic deformations and associated hysteretic damping will occur. The form of such code lateral load distributions typically has load increasing linearly with height and is an approximation of the loading pattern associated with the first mode of vibration of the structure. The force patterns throughout a structure due to such codified lateral static loading are subscripted "code" hereafter (e.g. V_{code}) and are generally synonymous with first mode behaviour. While this first mode response often dominates the deflection response of a structure, the participation of 2nd and higher modes is often of significance in force patterns in individual members.

The effect of higher mode participation (revealed in a quantitative manner by dynamic time history analyses) is to vary the height of the centroid of action of the inertia forces acting on that wall.

Typically the centroid of a code static load distribution is about 0.72H above wall base (Fig. 3.1(a)), where H is the total wall height. A very different loading pattern may exist during a dynamic response with the inertia load centroid situated lower down the wall (Fig. 3.1(b)). The base shear in this situation is $V = M/\alpha H$. In SEE ERRATA order to obtain an estimate of the upper bound on V, maximum and minimum values of M and α respectively must be assessed. It is assumed that a flexural failure is desired in preference to a shear failure, which necessitates the calculation of an upper bound on V.

The value of wall base moment M realised during an earthquake is likely to be larger than M_{code} due to (i) probable material strength in excess of minimum dependable design strength, (ii) additional member

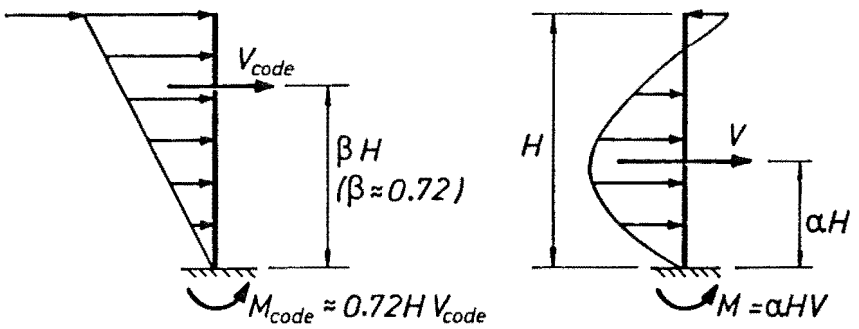

Fig. 3.1 Static and Dynamic Lateral Load Distributions.

strength developed by the strain hardening of reinforcement in a member subject to significant inelastic deformations, (iii) concrete strength being in excess of the specified 28 day strength, and (iv) flexural reinforcement having been provided in excess of that derived in the design calculations. Thus the value of M is taken to be $M^o = \phi_o M_{code}$, where the factor ϕ_o is the flexural overstrength factor and is generally about 1.45 for a wall.* Hence the design shear V can be expressed as $V = \phi_o M_{code}/\alpha H$. Since $M_{code} = \beta H V_{code}$, where $\beta \doteq 0.72$ typically, and $V = \phi_o \left(\frac{\beta H}{\alpha H}\right) V_{code} = \phi_o \omega_v V_{code}$, where ω_v is

---

* A typical value of the flexural overstrength factor ϕ_o may be evaluated as follows: for an ideal design moment of M_i, flexural reinforcement is required [34] to give a dependable strength of $M_i/\phi = M_d$, where $\phi = 0.9$. Assuming that mild steel (Grade 275) reinforcement is used, the enhancement of section strength above the dependable value (due to factors (ii) and (iii) listed previously) may be of the order of 25%. Thus the section overcapacity strength $M^o > (M_i/0.9) \times 1.25 \cong 1.45 M_i$, and the flexural overstrength factor, ϕ_o, which is by definition the ratio of M^o to $M_{code} = M_i$, is 1.45.

defined as a wall dynamic shear magnification factor. ω_v may be thought of as a measure of the drop in centroid of the distributed inertia forces associated with the dynamic response of the wall, as compared to the code static first mode force distribution.

In the analyses reported herein, dynamic shear magnification factors were obtained by determining the maximum wall base shear from time history analyses (for structures designed for "code" loading) and calculating the ratio $\omega_v = V_{max}/(\phi_o V_{code})$.

3.3 PREVIOUS RESEARCH INTO SHEAR MAGNIFICATION

Although the notion of ω_v factors is primarily a concept used in New Zealand, the investigation of dynamic magnification of shear forces has not been restricted to this country. Two previous studies of this topic are outlined in this section, firstly that of Blakeley et al [36] and secondly work performed by the Portland Cement Association (PCA) [37,38].

3.3.1 Blakeley, Cooney and Megget [36]

This work is of more direct application to the problem, being the study on which the New Zealand code [34] approach to structural wall shear design is based. Three cantilever structural walls (of 6, 15 and 20 storeys) were subjected to 5 different ground motions, and their response investigated using DRAIN 2D[14]. The structures were modelled by dividing the wall into beam elements, using up to 6 elements to represent the lst storey and a reducing number per storey up the height of the wall. The assumed stiffness variation was based on a linear decrease in the extent of wall cracking from the base upwards, while basic wall thickness decreased with height. Flexural strength was reduced with height up the walls. A Rayleigh damping model of 5% of critical damping on the first and second modes of vibration was apparently used. Hysteretic response of inelastic members was bilinear, with a post yield stiffness of nominally 2% of the pre-yield value.

It was found that the ratio of maximum wall base shear observed during seismic attack to code specified base shear increased with wall height. A series of storey dependent dynamic shear magnification factors were suggested, and have since been recommended by NZS 3101 [34]. With the exception of the range of accelerograms used, little consideration was given in this study to establishing the sensitivity of the analyses to variation in input parameters.

The design approach recommended by Blakeley et al. involved the factoring up of code shear forces by the product of the flexural overstrength factor (ϕ_o) and a dynamic magnification factor (ω_v). Shear reinforcement was to be apportioned neglecting the contribution of the concrete to shear resistance in the potential plastic hinge zone at the base of the wall. For a typical structural wall with light axial load and medium strength concrete, codified [34] allowable concrete shear stress (v_c) in a plastic hinge zone is of the order 0.8MPa, a significant fraction of the likely total design shear stress. Thus it is apparent that wall shear design according to NZS3101 [34], where v_c need not be neglected, is significantly less conservative than the practice suggested by Blakeley et al.

3.3.2 Portland Cement Association [37,38]

The PCA has carried out an extensive paremeter study regarding factors believed to influence structural wall response to seismic excitation. Variations in both excitation and structural parameters were considered. Those most significant were found to be (a) (accelerogram related) intensity, frequency, character and duration, and (b) (structure related) base yield moment and fundamental period of vibration (i.e. stiffness). Many more parameters were considered, however, including strength and stiffness variation, wall height, number of elements in the model, hysteresis rules, base fixity and viscous damping.

The basic reference structure on which the bulk of the analyses were performed was a 12 element model of a 20 storey structure of fundamental period (T_1) = 1.4 sec. and base yield moment of 500 000 in.kip (56.5 MNm). Stiffness was assumed constant with height, while strength decreased linearly to 250 000 in.kip (28.25 MNm) at wall top. Full base fixity was assumed, and a Rayleigh damping model (based on the initial stiffness and mass matrices) assigning 5% of critical damping to modes 1 and 2 was used.

The findings of this series of analyses, together with observations made during a series of experimental investigations undertaken by the PCA, were combined to formulate a method for the design of cantilever structural walls.

The primary steps in the PCA design procedure for the base of a structural wall of a given section and fundamental period T_1 are as follows:

(1) On the basis of experimental tests and estimated design shear stress, a section rotational ductility capacity is assummed - μ^a.

(2) Using T_1 and μ^a, a minimum base yield moment M_y^{min} is found from a chart prepared using the results of the PCA parameter study. This value of yield moment is such that assumption of a lesser value may result in the imposition of ductility demands greater than the assumed capacity μ^a.

(3) The UBC-76 [26] distribution of base shear is used together with M_y^{min} to determine the lateral force coefficient k and thus code base shear force $V_T = kW$ may be found. (This process may be achieved via the use of a second design chart).

(4) A further design chart based on PCA studies is used to obtain a dynamic base shear V_T^{dyn}, a function of T_1 and M_y^{min}. The ratio V_T^{dyn} / V_T can then be calculated.

(5) The wall base section may now be designed for a moment of M_y^{min} and a shear force of $r_v V_T^{dyn}$, where r_v is an arbitrary reduction factor (0.7) intended to relate critical dynamic shears to the "design shears corresponding to the laboratory test results" [38].

(6) The assumed design shear stress is checked against that value assumed in step (1) and the design is modified if necessary.

Although, as has been noted, the PCA design method does incorporate a shear magnification factor, the structuring of the method is such as to make a direct comparison between this and the current New Zealand code approach impossible. Appendix A however shows how the New Zealand approach compares with a sample calculation given by the PCA [38]. The salient features of the comparison are (1) the considerably higher flexural strength required by the PCA method, and (2) the relatively lower design shear force associated with this base moment (as measured by the moment/shear ratio).

3.4 DESCRIPTION OF STRUCTURES STUDIED

3.4.1 General

Six simple structural walls were chosen as the basis for this study. They comprised 3 pairs of walls of height 6, 12 and 18 storeys with a constant storey height of 3.5 m. Of the 2 walls of each particular height, one was rectangular in section, the other was I shaped.

The thicknesses of the walls tapered with height, as indicated in Fig. 3.2. The dimensions of the pairs of walls were chosen so as to ensure that the 2 walls had nearly identical stiffnesses (or equivalently, first mode period) (see Table 3.1). A linear distribution of the wall flexural rigidity was assumed as an allowance for cracking present in the walls (refer to Fig. 3.3) and used to reduce gross section properties in a decreasing manner with height up the walls. Consideration of typical loading and tributary area assumptions enabled estimates of lumped floor weights to be made (see Table 3.1), considered constant for each floor.

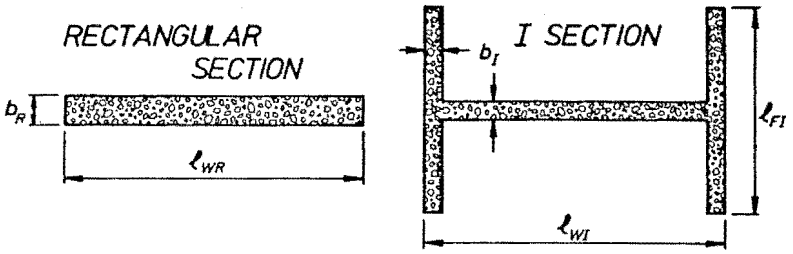

Wall height (number of storeys)	Floors	Rectangular Section		I Section		
		ℓ_{WR} (m)	b_R (m)	ℓ_{WI} (m)	ℓ_{FI} (m)	b_I (m)
3	1 - 3	2.65	0.350	2.00	1.00	0.35
6	1 - 2	5.50	0.450	4.00	2.00	0.40
	3 - 4	"	0.400	"	"	0.35
	5 - 6	"	0.350	"	"	0.30
12	1 - 3	9.00	0.400	6.00	3.00	0.40
	4 - 6	"	0.350	"	"	0.35
	7 - 9	"	0.350	"	"	0.30
	10 - 12	"	0.250	"	"	0.25
18	1 - 6	18.00	0.600	12.00	5.00	0.70
	7 - 10	"	0.525	"	"	0.60
	11 - 14	"	0.450	"	"	0.50
	15 - 18	"	0.400	"	"	0.40

Fig. 3.2 Rectangular and I Section Wall Geometry.

TABLE 3.1 : PERIODS OF VIBRATION AND DESIGN DETAILS FOR THE PROTOTYPE WALLS

Structure	(1) T_1 (s)	(2) T_2 (s)	(3) T_3 (s)	(4) T_4 (s)	(5) T_5 (s)	(6) W (kN)	(7) V_{code} (kN)
3 Storey						800	288
Rectangular	0.440	0.0714	0.0598	0.0316	0.0197		
I Section	0.441	0.0749	0.0551	0.0340	0.0181		
6 Storey						2000	1180
Rectangular	0.712	0.126	0.108	0.0527	0.0357		
I Section	0.725	0.135	0.101	0.596	0.0386		
12 Storey						3000	2160
Rectangular	1.661	0.292	0.222	0.119	0.0734		
I Section	1.692	0.306	0.193	0.129	0.0786		
18 Storey						6500	7020
Rectangular	1.549	0.290	0.268	0.124	0.0902		
I Section	1.560	0.303	0.238	0.134	0.0840		

(1) - (5) Periods of the first 5 modes of structural vibration.

(6) Assumed constant lumped storey weight.

(7) Code [9] specified base shear, calculated as the product of the seismic design coefficient C_d, the lumped floor mass (6) and the number of storeys, n.

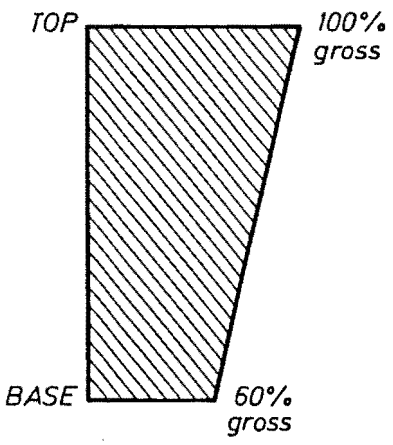

Fig. 3.3 Assumed Distribution of Wall Section Stiffness, $E_c I_w$.

3.4.2 Design

Simplified flexural design of the walls was carried out as follows: for an assumed first mode period (subsequently verified by modal analysis) the basic seismic coefficient C [9] was determined assuming the wall to be founded on ~~rigid~~ rigid subsoils in Seismic Zone A and that the wall was one of several similar elements in a structure. Thus the seismic design coefficient C_d was obtained (SM = 0.8) and code lateral static load calculated as the product of C_d and the total reduced gravity load W_t. This shear force was distributed in accordance with clause 3.4.6(a) of NZS 4203 [9] as shown in Fig. 3.4. M_{code} at wall base was calculated and a brief check made as to the practicality of flexural reinforcement required.

SEE ERRATA

To determine an approximate base yield moment, the code moment was factored by

(i) $\frac{1}{0.9}$ to account for dependable rather than ideal strength.

(ii) 1.13 to account for probable over dependable strength.

(iii) 1.05 higher strength due to increased axial compression load likely to be present during an earthquake as compared to design axial load (D + L/3 compared to 0.9D).

Curtailment of flexural strength was in accordance with the linear envelope recommended for cantilever shear walls [39] as shown in Fig. 3.5. The

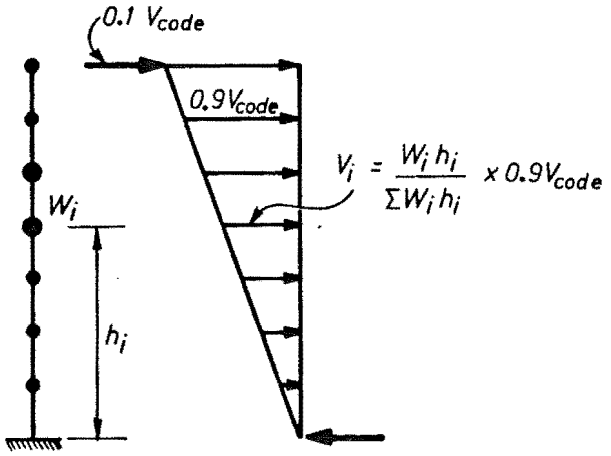

Fig. 3.4 Code Wall Shear Force Distribution.

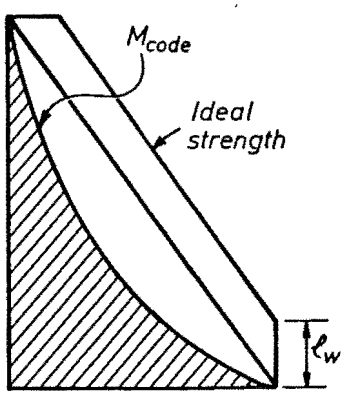

Fig. 3.5 Design Wall Moment Envelope.

intention of this procedure is to restrict significant inelastic deformations to the base of the wall, which is specifically detailed for this purpose. A brief check was also made as to the practicality of shear resistance at wall base level.

3.4.3 Computer Modelling

For the majority of analyses made, the following modelling assumptions were used:

- one beam element was used per floor, so that the number of members equalled the number of storeys.
- mass was lumped at floor levels, with a rotational inertia of the same order as the term in a consistent mass matrix used in association with the rotational degree of freedom at each node [40].
- Young's and shear moduli of 25 and 11 GPa respectively were used.
- a bilinear hysteresis model was used to describe the ~~post-elastic~~ SEE ERRATA response of the members, with a bilinear factor of 0.02.
- for time history analyses, an integration time step of 1/100 sec. was used.

3.5 RESULTS OF THE GENERAL STUDY

In the course of a time history analysis, a great deal of information is generated, and it is obviously possible to present only a restricted summary of this data. The maximum values of member actions and deformations are of critical interest. Because the base (ground level) region of a structural wall generally experiences the largest member actions, peak shear and moment at this zone are recorded. Dynamic shear magnification factors calculated using $\phi_o = 1.45$ are shown, as are the ratios M_{max}/M_y.

Deformations output include maximum normalised top floor deflection, ground floor and maximum interstorey drift indices, and maximum plastic rotation recorded at the point of the plastic hinge which formed adjacent to the base of the bottom wall element. The results are presented sequently in tabular form.

TABLE 3.2 : 6 STOREY WALL RESULTS - RAYLEIGH DAMPING; $\lambda_1 = \lambda_5 = 5\%$

	El Centro		Bucharest		Parkfield	
PROGRAM	RUAUMOKO	DRAIN 2D	RUAUMOKO (10)	DRAIN 2D	RUAUMOKO	DRAIN 2D
Rectangular Wall						
$V_{max,base}$ (1) kN	3194	3220	2784	2706	3324	3365
ω_v (2)	1.87	1.88	1.60	1.58	1.94	1.97
Δ_{top} +ve (3)	0.0014	0.0014	0.0075	0.0072	0.0106	0.0100
Δ_{top} -ve (4)	-0.0039	-0.0059	-0.0072	-0.0084	-0.0040	-0.0042
Base drift (5)	0.0029	0.0043	0.0055	0.0074	0.0069	0.0077
Max. drift (6)	0.0048	-	0.0083	-	0.0119	-
θ_p (7) rad.	0.0023	0.0037	0.0049	0.0067	0.0062	0.0071
M_{max} (8) kN.m	27154	25228	31983	27219	34257	27472
M_{max}/M_y (9)	1.19	1.11	1.40	1.19	1.50	1.20
I Section Wall						
$V_{max,base}$ kN	3005	3742	3419	2462	3239	3102
ω_v	1.76	2.18	2.00	1.44	1.89	1.81
Δ_{top} +ve	0.0014	0.0013	0.0072	0.0072	0.0098	0.0099
Δ_{top} -ve	-0.0040	-0.0051	-0.0072	-0.0085	-0.0040	-0.0042
Base Drift	0.0031	0.0049	0.0056	0.0071	0.0066	0.0083
Max Drift	0.0047	-	0.0079	-	0.0110	-
θ_p rad.	0.0025	0.0039	0.0049	0.0067	0.0059	0.0074
M_{max} kN.m	27412	25260	32009	27004	33957	27428
M_{max}/M_y	1.20	1.11	1.40	1.18	1.49	1.20

Notes

(1) Maximum base level wall shear force.

(2) Dynamic shear magnification factor = $V_{max,base}/(1.45V_{code})$

(3),(4) Maximum positive and negative wall type deflection normalised with respect to wall height.

(5),(6) Maximum base level and overall interstorey drift index.

(7) Maximum plastic rotation at base level hinge.

(8),(9) Maximum and maximum normalised base moment.

(10) This analysis made using $\Delta t = 1/200$ sec. (numerically unstable at $\Delta t = 1/100$ sec, the value used for the other analyses).

TABLE 3.3 : 6 STOREY WALL RESULTS - RAYLEIGH DAMPING $\lambda_1 = \lambda_2 = 5\%$

		El Centro		Bucharest		Parkfield	
PROGRAM		RUAUMOKO	DRAIN 2D	RUAUMOKO	DRAIN 2D	RUAUMOKO	DRAIN 2D
Rectangular Wall							
$V_{max,base}$	kN	2566	2898	2592	2420	3089	2896
ω_v		1.52	1.72	1.54	1.44	1.84	1.72
Δ_{top} +ve		0.0014	0.0014	0.0072	0.0072	0.0100	0.0099
Δ_{top} -ve		-0.0038	-0.0050	-0.0070	-0.0083	-0.0040	-0.0042
Base Drift		0.0028	0.0043	0.0055	0.0071	0.0066	0.0077
Max Drift		0.0047	-	0.0079	-	0.0112	-
θ_p	rad.	0.0022	0.0037	0.0049	0.0066	0.0059	0.0072
M_{max}	kN.m	27027	25326	31878	27144	33816	25781
M_{max}/M_y		1.19	1.11	1.40	1.19	1.48	1.21
I Section Wall							
$V_{max,base}$	kN	2694	3400	2595	2342	3138	3035
ω_v		1.60	2.02	1.54	1.39	1.86	1.80
Δ_{top} +ve		0.0014	0.0014	0.0073	0.0071	0.0098	0.0098
Δ_{top} -ve		-0.0038	-0.0050	-0.0071	-0.0084	-0.0085	-0.0042
Base Drift		0.0031	0.0044	0.0056	0.0074	0.0068	0.0080
Max Drift		0.0046	-	0.0082	-	0.0110	-
θ_p	rad.	0.0024	0.0037	0.0048	0.0066	0.0059	0.0074
M_{max}	kN.m	27233	25122	31934	26933	33955	27391
M_{max}/M_y		1.19	1.10	1.40	1.18	1.49	1.20

TABLE 3.4 : 6 STOREY WALL RESULTS - LINEAR DAMPING; $\lambda_1 = 5\%$, $\lambda_{18} = 100\%$

		El Centro	Bucharest	Parkfield
PROGRAM		RUAUMOKO	RUAUMOKO	RUAUMOKO
Rectangular Wall				
$V_{max,base}$	kN	2459	2580	2928
ω_v		1.44	1.51	1.71
Δ_{top} +ve		0.0015	0.0073	0.0102
Δ_{top} -ve		-0.0038	-0.0070	-0.0040
Base Drift		0.0028	0.0055	0.0068
Max Drift		0.0047	0.0081	0.0115
θ_p	rad.	0.0022	0.0048	0.0061
M_{max}	kN.m	26972	31610	34135
M_{max}/M_y		1.18	1.39	1.50
I Section Wall				
$V_{max,base}$	kN	2799	2770	3467
ω_v		1.64	1.63	2.03
Δ_{top} +ve		0.0016	0.0065	0.0101
Δ_{top} -ve		-0.0040	-0.0056	-0.0054
Base Drift		0.0023	0.0030	0.0042
Max. Drift		0.0047	0.0075	0.0121
θ_p	rad.	0.0016	0.0023	0.0038
M_{max}	kN.m	31566	36025	41678
M_{max}/M_y		1.38	1.58	1.83

TABLE 3.5 : 12 STOREY WALL RESULTS - RAYLEIGH DAMPING; $\lambda_1 = \lambda_5 = 5\%$

		El Centro		Bucharest		Parkfield	
PROGRAM		RUAUMOKO	DRAIN 2D	RUAUMOKO	DRAIN 2D	RUAUMOKO	DRAIN 2D
Rectangular Wall							
$V_{max,base}$	kN	6542	8860	7366	5795	8183	10401
ω_v		2.09	2.83	2.35	1.85	2.61	3.32
Δ_{top} +ve		0.0028	0.0030	0.0171	0.0038	0.0113	0.0124
Δ_{top} -ve		-0.0035	-0.0054	-0.0117	-0.0122	-0.0078	-0.0038
Base Drift		0.0011	0.0031	0.0084	0.0080	0.0074	0.0043
Max Drift		0.0047	-	0.0207	-	0.0141	-
θ_p	rad.	0.0007	0.0024	0.0092	0.0072	0.0097	0.0038
M_{max}	kN.m	88735	89103	150270	100440	155300	92330
M_{max}/M_y		1.06	1.06	1.80	1.20	1.86	1.10
I Section Wall							
$V_{max,base}$	kN	8311	8957	6965	5360	9789	10146
ω_v		2.65	2.86	2.21	1.71	3.13	3.24
Δ_{top} +ve		0.0029	0.0031	0.0053	0.0038	0.0115	0.0122
Δ_{top} -ve		-0.0041	-0.0060	-0.0118	-0.0123	-0.0039	-0.0038
Base Drift		0.0019	0.0037	0.0051	0.0077	0.0043	0.0046
Max Drift		0.0055	-	0.0140	-	0.0140	-
θ_p	rad.	0.0009	0.0027	0.0042	0.0070	0.0035	0.0041
M_{max}	kN.m	90165	89560	113470	98641	108410	92974
M_{max}/M_y		1.08	1.07	1.36	1.18	1.30	1.11

TABLE 3.6 : 12 STOREY WALL RESULTS - RAYLEIGH DAMPING; $\lambda_1 = \lambda_2 = 5\%$

		El Centro		Bucharest		Parkfield	
PROGRAM		RUAUMOKO	DRAIN 2D	RUAUMOKO	DRAIN 2D	RUAUMOKO	DRAIN 2D
Rectangular Wall							
$V_{max,base}$	kN	6596	7952	6431	5357	9063	9323
θ_v		2.11	2.54	2.05	1.71	2.89	2.98
Δ_{top} +ve		0.0029	0.0030	0.0053	0.0039	0.0113	0.0120
Δ_{top} -ve		-0.0035	-0.0046	-0.0116	-0.0120	-0.0038	-0.0038
Base Drift		0.0011	0.0023	0.0046	0.0071	0.0037	0.0051
Max Drift		0.0047	-	0.0138	-	0.0138	-
θ_p		0.0007	0.0015	0.0039	0.0066	0.0031	0.0046
M_{max}	kN.m	88625	87183	112150	98743	106290	94219
M_{max}/M_y		1.06	1.04	1.34	1.18	1.27	1.13
I Section Wall							
$V_{max,base}$	kN	7088	8298	6452	5097	9414	10142
ω_v		2.26	2.65	2.06	1.63	3.00	3.24
Δ_{top} +ve		0.0033	0.0031	0.0054	0.0040	0.0118	0.0128
Δ_{top} -ve		-0.0038	-0.0051	-0.0117	-0.0121	-0.0039	-0.0038
Base Drift		0.0013	0.0029	0.0048	0.0074	0.0038	0.0051
Max Drift		0.0051	-	0.0139	-	0.0138	-
ω_p	rad	0.0006	0.0020	0.0039	0.0067	0.0032	0.0043
M_{max}	kN.m	87711	87889	111510	98028	106060	92946
M_{max}/M_y		1.05	1.05	1.33	1.17	1.27	1.11

TABLE 3.7 : 12 STOREY WALL RESULTS - LINEAR DAMPING; $\lambda_1 = 5\%$, $\lambda_{36} = 100\%$

		El Centro	Bucharest	Parkfield
PROGRAM		RUAUMOKO	RUAUMOKO	RUAUMOKO
Rectangular Wall				
$V_{max,base}$	kN	6767	6482	9710
ω_v		2.16	2.07	3.10
Δ_{top} +ve		0.0032	0.0060	0.0115
Δ_{top} -ve		-0.0037	-0.0116	-0.0038
Base Drift		0.0011	0.0047	0.0037
Max Drift		0.0056	0.0143	0.0140
θ_p	rad.	0.0006	0.0043	0.0030
M_{max}	kN.m	87871	119240	105920
M_{max}/M_y		1.05	1.43	1.27
I Section Wall				
$V_{max,base}$	kN	7378	6355 (1)	9837
ω_v		2.36	2.03	3.14
Δ_{top} +ve		0.0033	0.0056	0.0116
Δ_{top} -ve		-0.0039	-0.0118	-0.0038
Base Drift		0.0014	0.0049	0.0041
Max Drift		0.0052	0.0141	0.0140
θ_p	rad.	0.0006	0.0040	0.0033
M_{max}	kN.m	87831	112250	107140
M_{max}/M_y		1.07	1.35	1.28

Note: (1) This analysis made using $\Delta t = 1/400$ sec; all others made using $\Delta t = 1/200$ sec. Numerical instability resulted at $\Delta t = 1/100$ sec.

TABLE 3.8 : 18 STOREY WALL RESULTS - RAYLEIGH DAMPING; $\lambda_1 = \lambda_5 = 5\%$

		El Centro		Bucharest		Parkfield	
PROGRAM		RUAUMOKO	DRAIN 2D	RUAUMOKO	DRAIN 2D	RUAUMOKO	DRAIN 2D
Rectangular Wall							
$V_{max,base}$	kN	22290	33442	23764 (2)	21070	35554 (1)	37024
ω_v		2.19	3.28	2.33	2.07	3.50	3.64
Δ_{top} +ve		0.0018	0.0018	0.0037	0.0027	0.0073	0.0080
Δ_{top} -ve		-0.0024	-0.0030	-0.0077	-0.0081	-0.0023	-0.0023
Base Drift		0.0009	0.0017	0.0022	0.0040	0.0021	0.0029
Max. Drift		0.0031	-	0.0091	-	0.0089	-
θ_p	rad.	0.0042	0.0011	0.0018	0.0035	0.0017	0.0022
M_{max}	kN.m	467180	457960	584060	518878	576260	486490
M_{max}/M_y		1.09	1.07	1.36	1.21	1.34	1.13
I Section Wall							
$V_{max,base}$	kN	26626 (1)	33813	24136	19099	35921 (2)	39545
ω_v		2.61	3.32	2.37	1.88	3.53	3.88
Δ_{top} +ve		0.0020	0.0019	0.0038	0.0030	0.0073	0.0084
Δ_{top} -ve		-0.0025	-0.0031	-0.0077	-0.0080	-0.0023	-0.0023
Base Drift		0.0008	0.0020	0.0024	0.0043	0.0022	0.0034
Top Drift		0.0033	-	0.0092	-	0.0090	-
θ_p	rad.	0.0004	0.0012	0.0018	0.0034	0.0017	0.0021
M_{max}	kN.m	465460	459639	586600	516846	580650	483156
M_{max}/M_y		1.08	1.07	1.38	1.20	1.35	1.12

Notes:

(1) $\Delta t = 1/200$ sec. $\Delta t = 1/100$ sec. used elsewhere except

(2) $\Delta t = 1/400$ sec.

TABLE 3.9 : 18 STOREY WALL RESULTS - RAYLEIGH DAMPING; $\lambda_1 = \lambda_2 = 5\%$

		El Centro		Bucharest		Parkfield	
PROGRAM		RUAUMOKO	DRAIN 2D	RUAUMOKO	DRAIN 2D	RUAUMOKO	DRAIN 2D
Rectangular Wall							
$V_{max,base}$	kN	21396	29807	22676	19422	33244	34719
ω_v		2.10	2.93	2.23	1.91	3.27	3.41
Δ_{top} +ve		0.0018	0.0018	0.0038	0.0029	0.0072	0.0077
Δ_{top} -ve		-0.0024	-0.0027	-0.0076	-0.0079	-0.0023	-0.0023
Base Drift		0.0006	0.0013	0.0021	0.0042	0.0020	0.0032
Max. Drift		0.0030	-	0.0090	-	0.0087	-
θ_p	rad.	0.0004	0.0008	0.0017	0.0033	0.0016	0.0024
M_{max}	kN.m	466730	449533	575610	514397	566430	490564
M_{max}/M_y		1.09	1.05	1.34	1.20	1.32	1.14
I Section Wall							
$V_{max,base}$	kN	20890	31083	22583	18199	34293	36439
ω_v		2.05	3.05	2.22	1.79	3.38	3.58
Δ_{top} +ve		0.0018	0.0019	0.0039	0.0031	0.0072	0.0081
Δ_{top} -ve		-0.0026	-0.0028	-0.0077	-0.0079	-0.0023	-0.0023
Base Drift		0.0012	0.0012	0.0023	0.0042	0.0021	0.0035
Max. Drift		0.0033	-	0.0090	-	0.0087	-
θ_p	rad.	0.0004	0.0008	0.0017	0.0033	0.0015	0.0022
M_{max}	kN.m	465290	450226	576040	513383	566240	485810
M_{max}/M_y		1.08	1.05	1.34	1.19	1.32	1.13

TABLE 3.10 : 18 STOREY WALL RESULTS - LINEAR DAMPING $\lambda_1 = 5\%$, $\lambda_{54} = 100\%$

		El Centro	Bucharest	Parkfield
PROGRAM		RUAUMOKO	RUAUMOKO	RUAUMOKO
Rectangular Wall				
$V_{max,base}$	kN	21960 (1)	(2)	(2)
ω_v		2.16		
Δ_{top} +ve		0.0017		
Δ_{top} -ve		-0.0025		
Base Drift		0.0007		
Max. Drift		0.0031		
θ_p	rad.	0.0004		
M_{max}	kN.m	469139		
M_{max}/M_y		1.09		
I Section Wall				
$V_{max,base}$	kN	26042 (1)	(2)	(2)
ω_v		2.56		
Δ_{top} +ve		0.0018		
Δ_{top} -ve		-0.0025		
Base Drift		0.0017		
Max. Drift		0.0033		
θ_p	rad.	0.0004		
M_{max}	kN.m	466840		
M_{max}/M_y		1.09		

Note:

(1) $\Delta t = 1/200$ sec.

(2) These analyses were unstable at $\Delta t = 1/800$ sec.

3.6 DISCUSSION OF RESULTS

The effect on response of each aspect of the structure's modelling is addressed in turn, although some overlap of aspects does occur. The discussion is made with an emphasis on the influence of the input parameters on wall base shear force.

3.6.1 DRAIN 2D vs RUAUMOKO Comparison

Moment and plastic rotation at base. The same nominal strain hardening factor of 0.02 was used in the time history programs. It is evident, however, that for a given degree of plasticity, RUAUMOKO indicates a greater strength gain for the wall due to movement along the 2nd branch of the assumed bilinear hysteresis. The ratio $\frac{\text{moment increase}}{\text{plastic rotation}}$ for analyses done using the program RUAUMOKO is about 3 times that for the DRAIN 2D analyses. This is due to differing methods of application of the factor accounting for plastic strength gain.

This means that for most analyses, base moments calculated by RUAUMOKO are larger than those found by DRAIN 2D, although the DRAIN 2D analyses indicate generally larger plastic rotation demands. This tends to equalise the energy dissipation implied by the 2 programs as measured by the area under the M-θ curve.

The increases in flexural strength suggested by both programs are not considered likely to be available in reality for most walls - increases of up to 86% on nominal M_y are predicted. These very large values are indicative of numerical instability, e.g. Table 3.5, M_{max}/M_y ratios for the rectangular section wall under the Bucharest and Parkfield excitations are much larger than for the I section wall. The M_{max}/M_y ratio is generally not greatly affected by section type, (rectangular or I shaped), whereas base shear for example is.

Deflections and deformations.

1. Top deflections. Generally good agreement exists between DRAIN 2D and RUAUMOKO results. The damping model chosen does not affect maximum deformations nearly as much as it affected other parameters (shear force, etc.), primarily because deflection is largely dominated by first mode response which for the analyses reported herein was consistently given 5% of critical damping.
2. Base drift

   It would generally be thought that 1st storey drift should correlate with shear force in some manner. However, although DRAIN 2D gave

consistently larger first storey drifts for all accelerograms, wall height and damping models, this was not correlated with consistently larger base shears. This suggests that high mode influence on observed shear force is considerable. Cases of smaller base drift and larger base shear occurring in RUAUMOKO are not unusual.

3. Maximum drift

The version of DRAIN 2D used had no facility for assessment of this parameter. Maximum drift generally occurred in the top two or three storeys of walls and was not often more than twice the maximum base level drift. Values were usually less than 0.01, a level of deformation commonly deemed to be a reasonable upper bound ensuring protection for non-structural components.

Maximum base shear force

Analyses made using the program DRAIN 2D indicate a larger scatter of base shear force than do those made using RUAUMOKO, ignoring some of the clearly unstable analyses made with this latter program.

The values of maximum base shear are not consistently different between the two programs, but vary according to wall cross sectional shape, accelerogram, wall height, etc. ω_v values calculated from the analyses using both programs are consistently larger than those values suggested by Blakeley et al.[36] (who used DRAIN 2D).

The values of dynamic magnification factor derived from PCA [37,38] analyses cannot be directly compared with the values reported herein because of the structure of the design method proposed by that organisation. PCA shear magnification factors depend on an assumed rotational ductility capacity. In addition, reinforcement was provided to develop a section yield moment well in excess of the "code" moment demand. The differences between the shear force magnification factors implied by the PCA design approach and those implied by the reported analyses can thus not be presented in a general fashion. A comparison for a particular structural wall is presented in Appendix A.

Time histories of base shear force confirm previous observations (PCA) that this quantity is subject to more rapid fluctuations during seismic attack than say base moment or top floor deflections.

The differences in maximum base shear force typically recorded using the two dynamic analysis package programs (for identical input parameters) is viewed with concern. These differences are both erratic, and large

on occasions and given the importance of adequate shear resistance in a structural wall, indicate the imperfect knowledge of structural response that even these relatively advanced techniques can provide.

3.6.2 Phenomenon of Numerical Instability

Some analyses performed using RUAUMOKO exhibited a form of instability whereby the number of plastic hinges in the wall would gradually increase and eventually spread over the whole wall. An incompatible combination of clockwise and anti-clockwise rotations was usually indicated. It was not possible to establish the cause of this phenomenon, which clearly resulted from some computational instability rather than being an indication of likely structural performance. Internal member forces, damping and inertia forces all increased while maintaining equilibrium during the development of this phenomenon. Structural deflections did not increase significantly above values indicated by stable analyses, although plastic rotations were several times larger, associated with large flexural strength gains due to strain hardening. The actual sizes of forces generated are of an order of 10 greater than expected. It was noted (see Sections 3.6.3 and 3.7.2) that variation in the damping model or integration time step, keeping all other parameters unchanged, could cause instability to occur.

It is also believed that some analyses made with DRAIN 2D were also close to instability, although this was not manifested in the dramatic manner described above. This is suggested by the magnitude of some of the ω_v values indicated by DRAIN 2D - the highest value of 3.88 is difficult to accept. It should be noted that both RUAUMOKO and DRAIN 2D use numerical integrations schemes which are not unconditionally stable in the inelastic regime.

3.6.3 Influence of Damping Model

3 damping models were considered in the reported analyses:

(i) Rayleigh model 5% of critical on 1st and 2nd mode.

(ii) " " " " 1st and 5th mode.

(iii) Linear model, 5% mode 1 rising to 100% for the highest mode.

The Rayleigh model fits a hyperbolic distribution of damping through 2 specified points. The models are shown in Fig. 3.6 which illustrates both the overall scheme and details of damping at lower modes. It is important to note that these schemes are simply mathematically convenient ways of assigning damping to the modes of vibrations of the

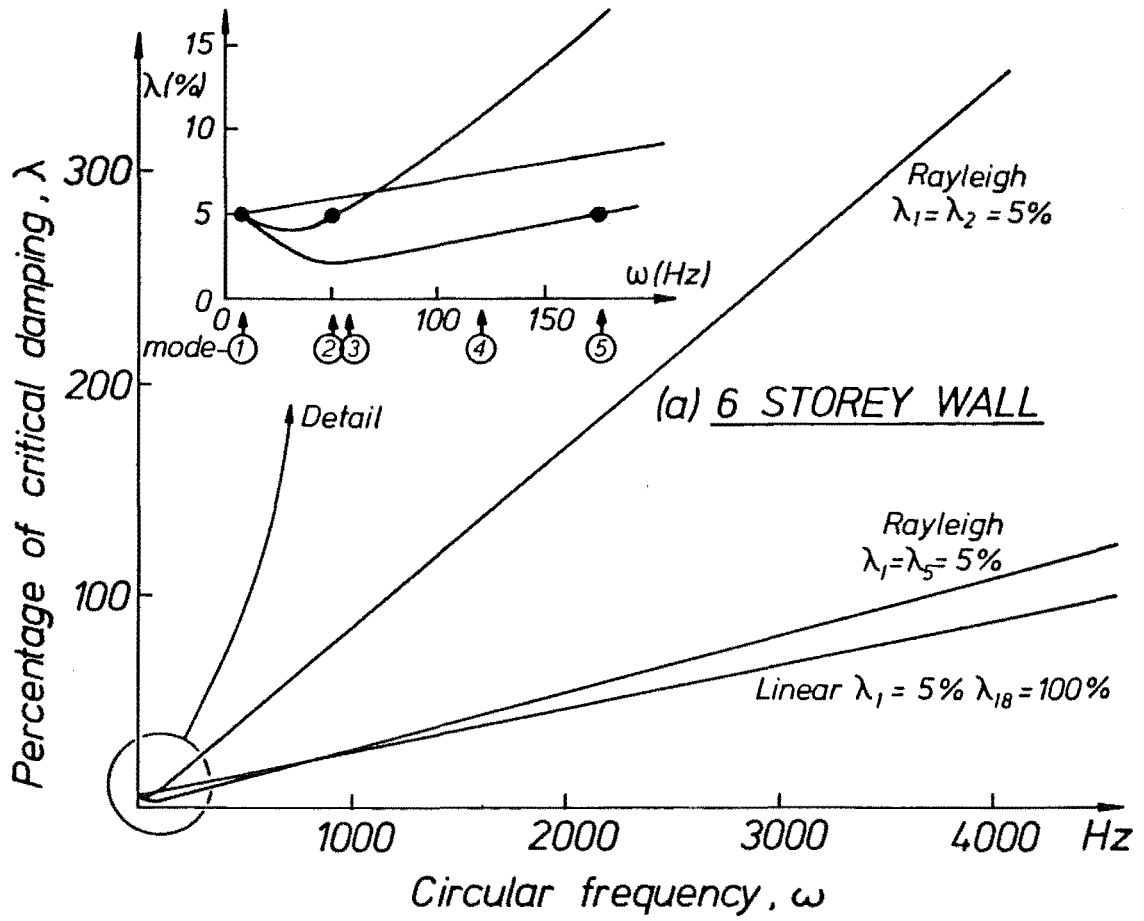

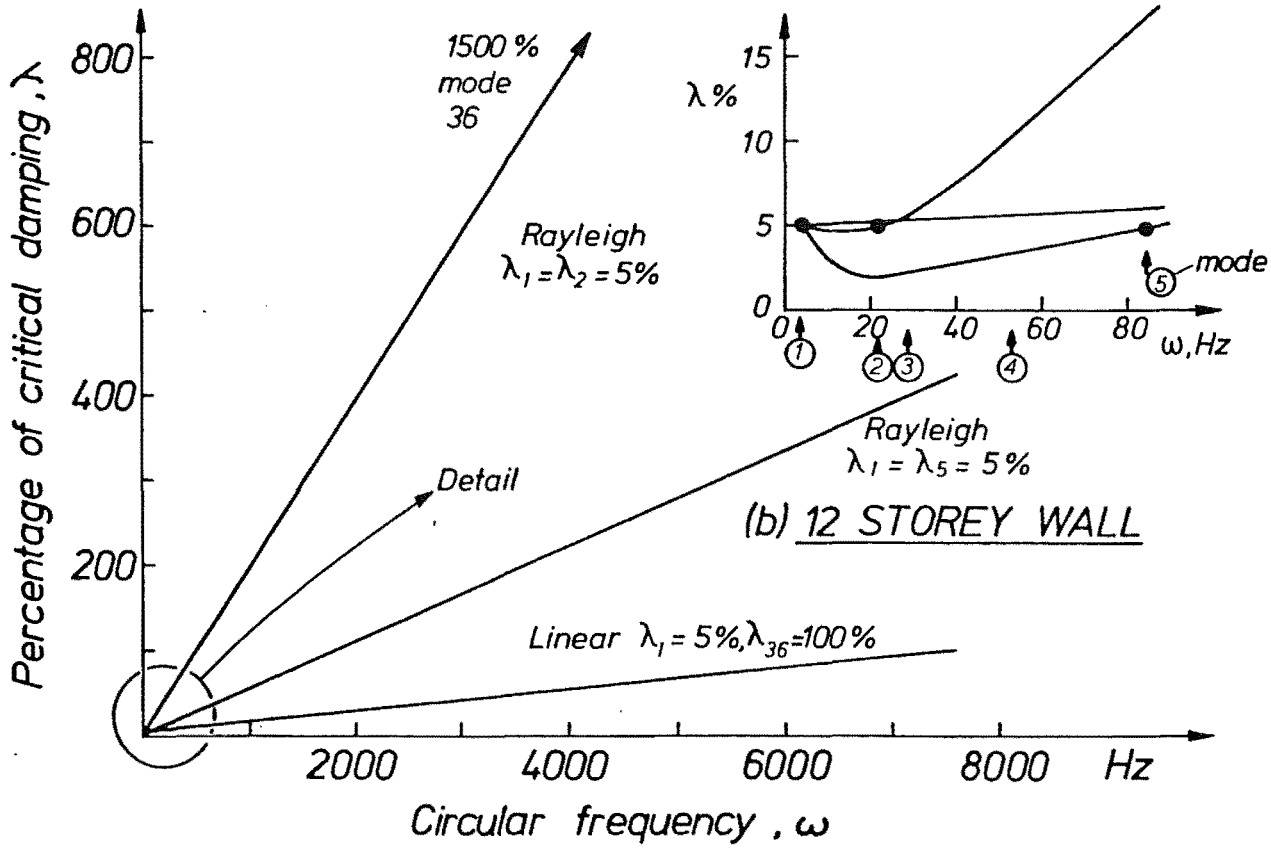

Fig. 3.6 Damping Schemes for 6, 12 and 18 Storey Walls.

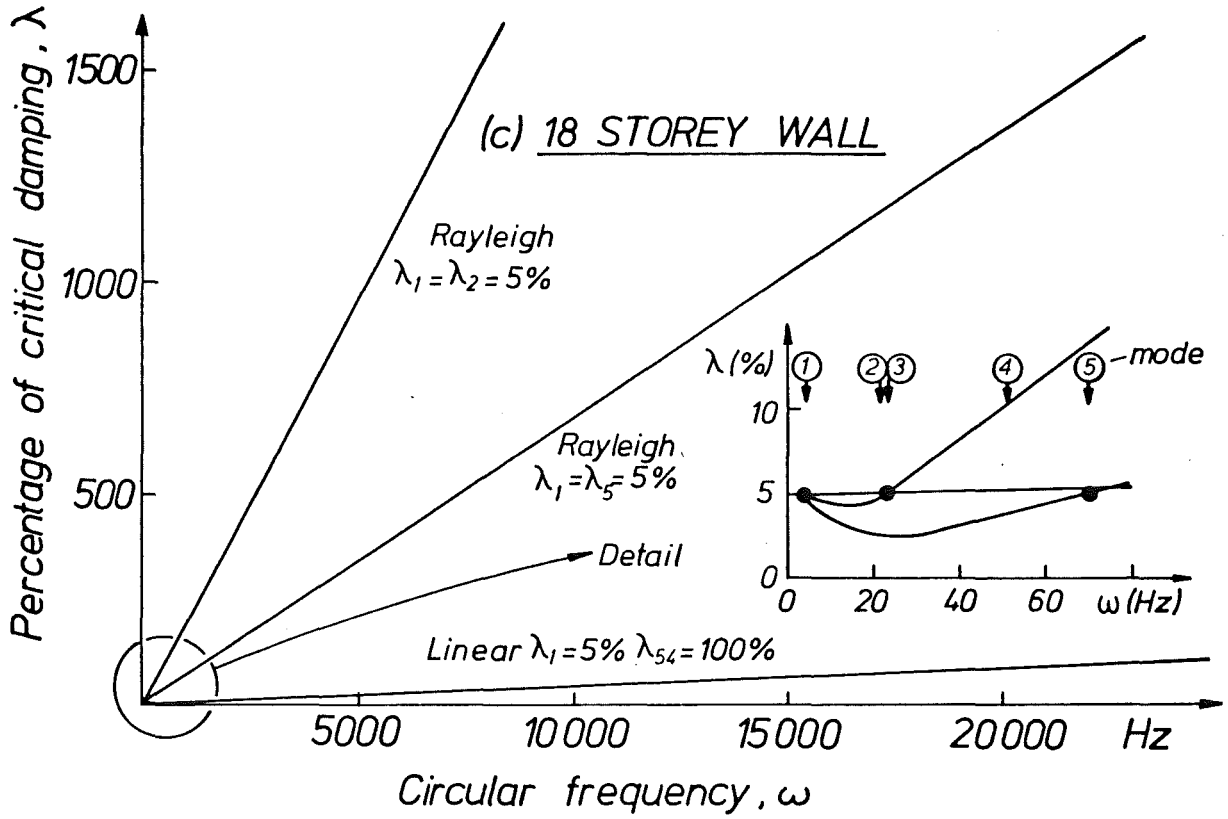

Fig. 3.6 (Continued)

structure. The full equations of motion require a damping coefficient for each mode of vibration. The values assigned are based on the notion of viscous damping, which is not the primary source of damping in inelastic structures (see Ref. 19). It is unfortunate that damping, which is so poorly defined, can exert so significant an influence on structural response in the inelastic domain. The damping schemes and values commonly used have been influenced by several views:

(1) It seems reasonable that high modes of vibration should not affect response unduly and should thus be more highly damped than lower modes.

(2) Although assigning equivalent viscous damping to a mode of vibration does not make much physical sense, it would seem to be unreasonable to assign either very low or very high percentages of critical damping (λ) to any mode. i.e. it would seem reasonable to have $1\% < \lambda < 100\%$. Critical damping is the least amount of damping which leads to no oscillation in the case of free response.

(3) The damping scheme used should be computationally as simple as possible. (A Rayleigh damping scheme is based on mass and stiffness matrices which are calculated routinely for a time history analysis, and thus is not an expensive process).

A value of 5% of critical damping on mode 1 was used throughout the analyses. This value is commonly accepted as being reasonable for reinforced concrete. With reference to the damping models in Fig. 3.6, it may be noted that a Rayleigh scheme tends to put low (< 5%) damping on some low modes and high (> 100% i.e. critical) damping on high modes. The linear damping model (available only in RUAUMOKO) can allow this under- and over-damping to be avoided. It must be conceded, however, that the analyses performed using the linear damping option did not exhibit noticeably superior stability characteristics. In the analyses performed with RUAUMOKO it was found that when using equivalent viscous damping less than about 2% for low modes (2,3,4) or greater than several hundred percent for the highest modes, instability would usually result as reported previously. A mode with damping in excess of the critical amount is non oscillatory. It has been demonstrated [41] that instability can occur in analyses in which the time step of integration is comparable to the highest subcritically damped mode of vibration. This condition could apply in the case of Rayleigh damping based on specified fractions of critical damping on modes 1 and 2.

As may be seen from Fig. 3.6, the use of a Rayleigh scheme can make the avoidance of such damping values impossible, especially in systems with many degrees of freedom.

With regard to the "blow up" of analyses discussed earlier, it is considered that very high damping, even if associated with low velocities, can cause abnormally large damping forces which are compensated for by larger member forces. In the meantime load may have reversed, leaving a large out of balance force at the node, etc. leading to a snowballing effect and, ultimately, formation of plastic hinges throughout the system as all member strengths are exceeded. Also, very low damping at low modes (2,3,4) which are likely to contribute significantly to response of the structure may cause an imbalance in force distribution because of an inability to absorb damping forces which are passed elsewhere.

The phenomenon of an equilibrium imbalance associated with the damping modelling in DRAIN 2D has been reported [14]. This imbalance was observed to exist for several time steps after member yield had occurred and the damping degrees of freedom are believed to absorb any force excess. This is done more rapidly for more strongly damped systems. The problem is likely to be minimized if the node where yield occurs has elastic members framing into it, which help to stabilize the node [14]. It is apparent that the problem is potentially more serious at the base of a structural wall model, where there is only one yielding member. This observation should be borne in mind when the results of analyses performed using DRAIN 2D are being considered.

It was noted that in some cases the chosen damping model makes little difference to wall base shear for both DRAIN 2D and RUAUMOKO, e.g. 6 storey wall, rectangular section, Bucharest earthquake where ω_v varies from 1.44 - 1.60. In other cases, even where the analyses remained stable, a much greater scatter was obtained, e.g. 6 storey wall, I section Bucharest record.

3.6.4 Influence of Wall Cross-Sectional Shape (Rectangular vs I Section)

Wall geometry was chosen so as to give very nearly the same first mode period of vibration for the rectangular and I section walls, i.e. similar moments of inertia. The differing shear stiffness of the sections was, however, expected to produce different inelastic responses. Both DRAIN 2D and RUAUMOKO assume elastic shear deformations,

with inelastic deformations occurring in the flexural mode only. A similarity of first mode period to within 1% was generally achieved. However, it must be noted that from consideration of typical response spectra, a very small period shift can have a large associated change in response (spectral velocity) due to the highly irregular nature of some spectra.

There is no evidence of a consistent trend in the differences between results for rectangular and I section walls which exists independently of other variables such as wall height, accelerogram, etc. A choice of rectangular or I section can make a significant difference to wall shear, however, presumably attributable to both the differing degree of shear deformation and the slightly unequal frequency characteristics between the rectangular and I section walls.

It may be concluded that categorisation of walls according to stiffness (or first mode period) only, can be misleading in the assessment of seismic response.

3.6.5 Effect of Number of Storeys

Larger ω_v factors were observed with increasing number of storeys ("n"), confirming the trend of observations made by Blakeley et al. [36]. Although some ω_v values for the 6 storey wall were larger than those for 18 storey structures, the general trend of proportionally greater dynamic magnification of wall shear with increasing n is not in serious doubt. However, it may equally well be claimed that a similar correlation can be made using 1st mode period (T_1) rather than number of storeys. The former would seem to be a more fundamental parameter than n. The 12 and 18 storey walls chosen had stiffnesses (first mode periods) more similar than their numbers of storeys and also similar ω_v factors. Thus on the basis of this evidence it cannot be claimed with certainty that ω_v should be considered related to n rather than T_1.

PCA investigations [37]indicate the converse. Two series of analyses were made as follows: (i) for constant period and base yield moment, maximum base shears were found via time history analyses for 10, 20, 30 and 40 storey walls. (ii) shears were found for three 20 storey walls of the same strength as those in (i) and of periods 0.8, 1.4 and 2.0 secs. The larger variation in shear was observed in case (i). Some doubts may be entertained as to the reasonableness of the case (i) structures, however. This cast doubt on the conclusions which are drawn.

In a subsequent section, the behaviour of a stiff 12 storey wall is described in a further attempt to determine whether ω_v is better considered height or period dependent (Section 3.7.6).

3.6.6 Effect of Input Accelerogram

Considerable work was done by the PCA [37] investigating the effect of accelerogram characteristics on response. Variables considered were intensity (defined in this case as the area under the 5% damped velocity spectrum between periods of 0.1 and 3.0 seconds), duration and frequency content of the earthquake records. The primary conclusions were:

1. Higher member actions were generally encountered in records of greater intensity.
2. Although peak forces and deformations generally occur within the first 10 secs. of strong shaking, cumulative plastic rotation demands and the like may not be maximised at the end of this time, due to continued strong shaking.
3. The frequency charcteristics of the accelerogram are probably the most important in relation to how a structure of a given stiffness (period) will respond to the record. This is conventionally assessed in an approximate way by considering where the first mode period lies on the pseudo velocity spectrum curve. If a high pseudo velocity is indicated, than a considerable structural excitation may be anticipated. Unfortunately no simple way exists of estimating higher mode participation in response despite the potential importance of this phenomenon.

The accelerograms chosen in a study obviously greatly affect the response and hence the deduced performance of a structure. It is unfortunate that no consistent approach is taken world wide in this problem. This is analogous to the absence of a standard loading program for experimental investigations. The desire to subject structures to a wide variety of accelerograms must be tempered by the dual constraints of time and expense. As mentioned previously, the 3 accelerograms used were: (i) NS El Centro 1940

(ii) NS Bucharest 1977

(iii) N50E Parkfield 1966.

These were used in an unmodified state.

The El Centro 1940 record was the first strong motion accelerogram to be recorded and has over the years become inseparably linked with

both parametric studies of structural response and design methods for structures. It should be observed, however, that this record is not a "typical" accelerogram and analyses performed with this particular record are not of inherently greater value than others. The El Centro event was associated with a multiple slippage failure at contintental plate boundaries, and could be described as having a peaking response spectrum.

The Bucharest event was recorded some 160 km from the epicentre, the seismic waves having propagated through extensive alluvial deposits. This record has an unusual broad band ascending velocity spectrum which is such that higher period structures are likely to undergo unusually large excitations. In addition, softening of the structure (due to poor foundation fixity for example) may not lead to reduced response, as normally occurs for most accelerograms.

The Parkfield accelerogram is associated with a single isolated seismic event, and corresponds with essentially one large pulse with relatively minor aftershocks.

The general trend of the analyses was to predict the largest ω_v values for response to the Parkfield accelerogram and smallest values for the Bucharest event. For the 18 storey walls,(Δt = 1/100 s), instability occurred with all analyses made using RUAUMOKO and the Parkfield and Bucharest accelerograms. Analyses made with DRAIN 2D often gave unreasonably high shear magnification for the Parkfield excitation. Analyses made with the El Centro excitation were generally the most stable. Table 3.11 shows the spectrum intensities and classification types of the 3 records. It is evident that the conclusion made by the PCA,that larger reponse actions are generally associated with higher spectrum intensity, is not supported by the analyses reported herein.

TABLE 3.11 : ACCELÉROGRAM SPECTRUM CHARACTERISTICS

	PCA Spectrum Intensity(1)	Spectrum Type
El Centro	1.78 m	Peaking descending
Bucharest	0.90 m	Broad band ascending
Parkfield	0.20 m	Broad band constant

Note:

(1) Defined as the area under the 5% damped velocity spectrum between periods of 0.1 and 3.0 seconds.

3.6.7 Effect of Member Modelling

In the analyses performed using both the RUAUMOKO and DRAIN 2D programs, the structural walls were modelled with the beam elements incorporated in each program. It was not considered necessary to use column elements (which can take account of the influence of varying axial load on yield strength) because of the small changes in axial load experienced by a cantilever structural wall during seismic excitation. The two programs use different basic beam elements which are briefly described subsequently.

3.6.7.1 RUAUMOKO - Giberson [42] one component non-linear beam: This model is a one dimensional prismatic member with independent point rotational springs at each end. (Fig. 3.7a). Plasticity is modelled when the yield moment of the rotational spring is exceeded, and the stiffness of this spring is reduced according to the specified bilinear factor. The remainder of the member remains elastic. In RUAUMOKO the

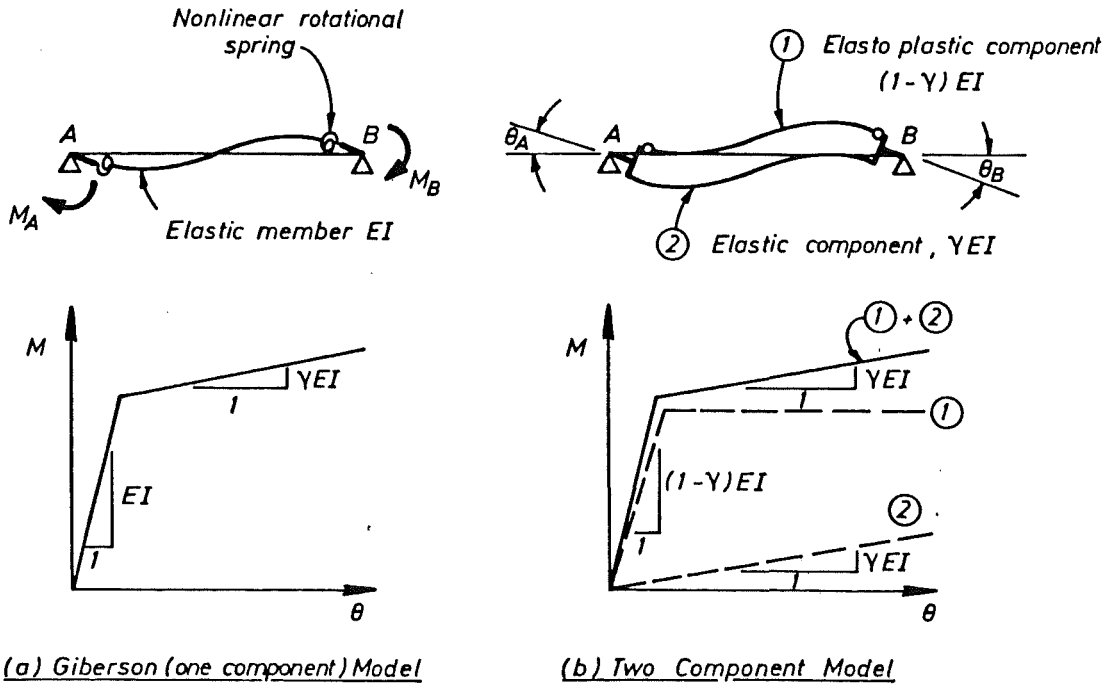

(a) Giberson (one component) Model

(b) Two Component Model

Fig. 3.7 One and Two Component Member Models.

specified bilinear factor, r, is related to the internal factor, γ, (Fig. 3.7 (a)) via the expression

$$\gamma = \frac{\ell}{4\ell_p}\left(\frac{r}{1-r}\right)$$

where ℓ is the member length and ℓ_p is the plastic hinge length assumed to be 1.0 m by default in the program.

For the bulk of the analyses reported in this section, with member length equal to the storey height of 3.5 m,

$\gamma = \frac{3.5}{4 \times 1.0} \times \frac{0.02}{0.98} = 0.0179$ which does not significantly differ from the external or program-user supplied factor of $r = 0.02$ which was used for the analyses reported. This element was developed as a representation of relatively slender beam members, in which significant plastic deformations would extend over a relatively short length, and the point rotational hinge approximation is reasonable. Modifications have been made to the basic Giberson model which allow for:

(1) the presence of deformation-free rigid end blocks
(2) shear deformations of the member, which are considered to remain elastic and assume greater importance for squat members, and
(3) fixed end moments, which represent for example gravity load present on a beam.

The fact that inelastic deformations at either end of the member are assumed to be independent is computationally advantageous. It is also a major weakness of the model. This is because the rotation at one end should depend on the curvature distribution along the member, and hence the moment at the other end.

3.6.7.2 DRAIN 2D - Two component model: The two component model incorporates two parallel elements, an elastic member and an elasto-plastic member, this latter modelling the behaviour of a concentrated point hinge at the member ends (Fig. 3.7 (b)). The hinges in the elasto-plastic component yield at a particular moment, while the moment in the elastic component may increase, thus providing for the effects of strain hardening. If moment is relatively constant along the member, the moment-curvature and moment-rotation relationships are proportional and the element performs best. Shear deformations are modelled via modification of flexural stiffness. Initial and fixed end forces can also be taken into account.

Both the Giberson and 2 component models are considered inadequate to model the inelastic behaviour of a prototype structural wall. The plastic hinge zone at the base of a wall, where significant inelastic deformation is expected during seismic attack, generally extends over a height approximately equal to the wall length (i.e. $\ell_p \simeq \ell_w$). This zone may extend over a height of 2 or 3 storeys for a large wall. This is vastly different to the concept of point rotational hinges embodied in the models discussed previously. The analyses described in this chapter generally used one beam element per storey, and plasticity was observed to be confined to the ends of the bottom three members at most. Instead of a "smeared" plasticity over the bottom 2 or 3 storeys, it is concentrated at several distinct points with the intermediate regions of the members deforming only elastically.

It is felt that by the summation of plastic rotations at the lower hinge locations, a reasonable estimate of total plastic rotation demand can be made. (For simultaneous hinging at several levels, base plastic rotation is usually considerably larger than rotations at the other levels). However, the use of yield rotation and maximum plastic rotation at the base hinge to calculate a rotational ductility demand, and hence section curvature ductility demand, is viewed with considerable suspicion. The critical dependence of ductility calculations on yield level deformations is well known, and it is not considered that rotation at a point hinge is sufficiently meaningful to form a basis for theoretical rotational and curvature ductility demand predictions for a structural wall.

3.6.8 High Shear Force and Moment at Wall Base Sections

In view of the high values of wall base shear frequently recorded (compared with code level forces) and the design ramifications of these observations, the following aspects of response were investigated:

(1) the frequency of occurrence of high base shear forces,
(2) the duration of these high forces, and
(3) the coincidence of high levels of both base shear and bending moment.

Although a rigorous statistical analysis of this data was not undertaken, it is believed that the results obtained are of value if viewed with the aid of engineering judgement.

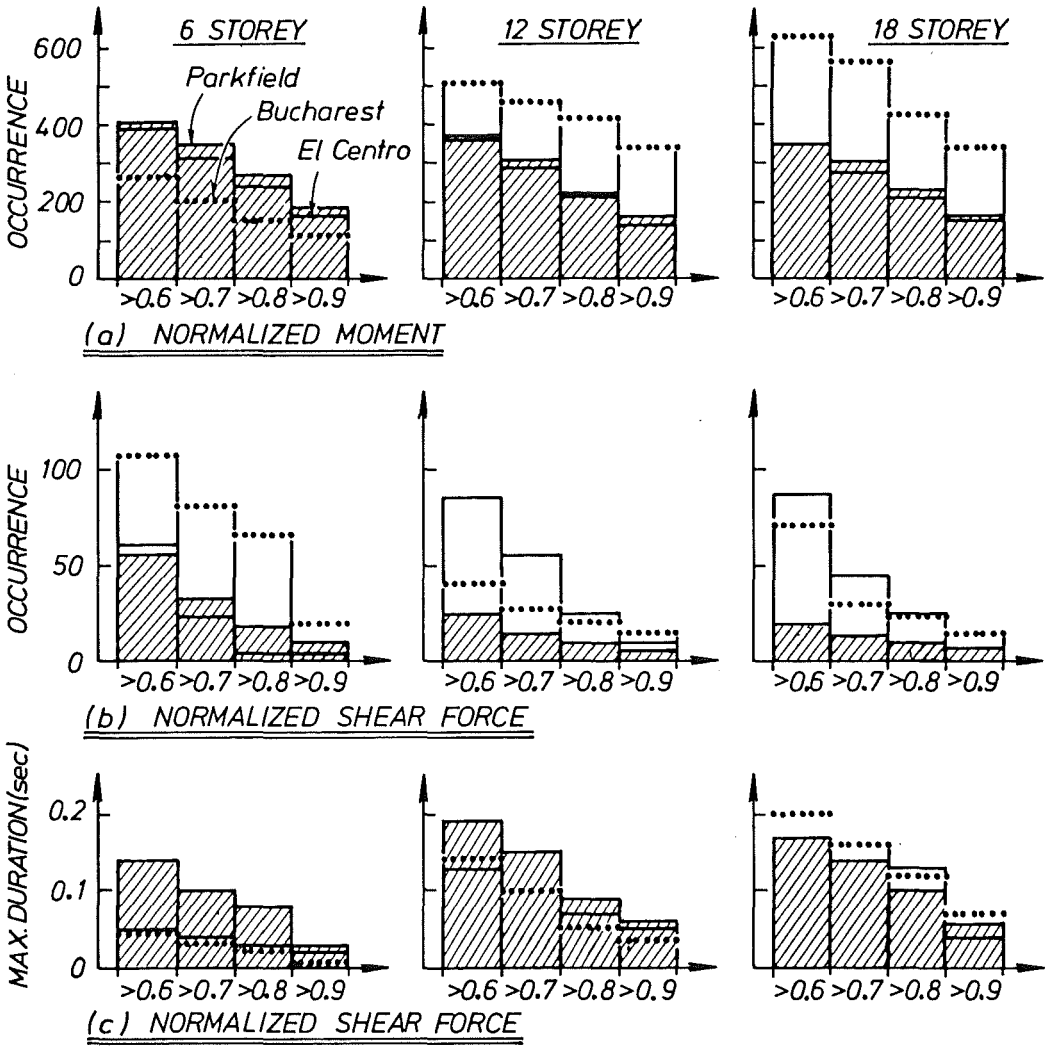

Fig. 3.8 Incidence and Duration of Wall Base Moments and Shear Forces.

Nine cases were selected for study, comprising the 6, 12 and 18 storey rectangular section walls, with Rayleigh damping of $\lambda_1 = \lambda_5 = 5\%$, subjected to the El Centro, Parkfield and Bucharest excitations. Histories of base section moment and shear force were obtained at 1/100 sec. intervals for the first 10 seconds of the accelerogram records. Shear forces were split into four intervals: $0.6 - 0.7\ V_{max}$, $0.7 - 0.8\ V_{max}$, $0.8 - 0.9\ V_{max}$ and $0.9 - 1.0\ V_{max}$, where V_{max} for a particular wall denotes the peak base shear force recorded during the analysis. Moments were split into similar intervals, based on the yield moment, M_y for the wall under consideration. Force and moment levels less than 60% of V_{max} and M_y were considered to be too low to be of concern. The number of times that base shear or moment fell into these intervals was recorded and used to derive Fig. 3.8. These diagrams show the number of times out of 1000 (the number of 1/100 sec. intervals in the 10 sec. of earthquake record considered) that shear force and moment exceeded 60%, 70%, etc. of V_{max} and M_y respectively.

The peak duration times of occurrence of the various levels of shear force are shown in Fig. 3.8(c). These times represent the maximum time for which a particular level of shear force was sustained during any of the response pulses undergone by the structure.

The following observations are made with reference to Fig. 3.8:

(1) High levels of base shear force occur markedly less frequently than base moment. For example, shear forces in excess of 90% of V_{max} occur for less than 2% of the 10 seconds of accelerograms considered. Moments in excess of 90% of M_y occurred as frequently as 35% of the time.

(2) The peak duration times of the various levels of wall base shear force decrease from 0.20 sec. (for $V \geq 0.6V_{max}$) to 0.07 sec. (for $V \geq 0.9V_{max}$).

(3) High levels of base shear force were invariably accompanied by high levels of base moment.

The magnitudes of plastic rotations indicated by both time history programs are generally small but consistently different, with maximum rotations of the order 0.004 and 0.008 radians for RUAUMOKO and DRAIN 2D respectively. The rotational ductilities associated with these plastic rotations may be approximated as follows:

approximate yield curvature $\phi_y \simeq \frac{\varepsilon_y}{0.9\ell_w}$

where ε_y = flexural reinforcement yield strain.

Assuming constant curvature over a plastic hinge zone of $\ell_p = \ell_w$, yield rotation can be estimated as $\theta_y \simeq \varepsilon_y/0.9$. For reinforcement of nominal yield strengths 275 and 380 MPa, with probable strength 13% in excess of these values, wall yield rotations of 0.0018 to 0.0023 might be expected. Using an average value of 0.002 radians, it may be seen that the extreme plastic rotations of 0.004 and 0.008 radians (RUAUMOKO and DRAIN 2D respectively) indicate approximate rotational ductility demands of 2 or 4 respectively. Such demands can be readily met by well detailed structural wall sections.

In a subsequent section (3.7.3) the effect on wall behaviour of a finer subdivision of the critical base region of the wall is considered. It is shown that the modelling of inelastic deformations is not significantly improved.

Given the critical effect that deformations in the bottom region of structural walls has on overall response, it appears reasonable to use more sophisticated member modelling [43,17,44] in that region than is available from the simple one or two component representation. Such refinement of analyses was not carried out in this study.

It is believed that these observations have important implications for the design of cantilever structural walls. The recommended practice for wall shear design in New Zealand [39] is based on dynamic shear magnification factors calculated on the basis of the maximum wall shear force levels observed in a series of dynamic analyses [36]. It has been demonstrated, however, that extreme shear forces occur infrequently, and then for short durations. For example, it would seem to be unlikely that a structure would be fatally damaged by a shear force acting for less than 1/10 sec, in which case a design force level based on $0.9V_{max}$ might be deemed appropriate. Such considerations should be borne in mind, together with others (e.g. the need for more sophisticated modelling of wall base regions and the uncertainties associated with assumptions made in dynamic analyses) when the results of time history analyses are interpreted.

3.7 STUDY OF INDIVIDUAL PARAMETERS

In this section further aspects of the analyses and modelling, believed to be of importance, are discussed. The investigation of these features generally involved time history analyses additional to those discussed previously.

3.7.1 Choice of Analysis Program - DRAIN 2D [14] vs RUAUMOKO [15]

In Section 3.6.1 the two time history programs used in this study were taken purely as variables or parameters in the analyses. In this section an attempt is made to determine the source of the discrepancies noted between the results the two programs indicate for identical input data.

DRAIN 2D was developed in 1973 by G.H. Powell at the EERC, Berkeley since which time it has been used in many time history analyses to make it the most widely accepted package of its type in current usage. RUAUMOKO is the current form of a program, written at the University of Canterbury by Sharpe in 1973, since which time it has been considerably modified and extended by Carr to its present form. Both programs were written to model the force-deformation response of plane structural systems to simulated seismic attack. Both use a direct stiffness formulation of the full equations of motion which are solved for nodal displacements with a time-wise step by step numerical integration. The programs were compared with reference to their prediction of response to the NS Bucharest 1977 earthquake for the 6 storey I section wall, used previously.

Four separate pairs of analyses were made in an attempt to isolate the causes of the differences illustrated in the previous section (3.6.1). These analyses were with all input parameters as given in Section 3.4 except:

Run	Input data variation
1	shear deformations suppressed, bilinear factor = 0
2	" " permitted, " " = 0
3	" " suppressed, " " = 2%
4	" " permitted, " " = 2%

Run 4 corresponds to the usual modelling situation.

Table 3.12 illustrates the difference made to the periods of vibration of the structure by the suppression of the shear deformation mode. The incorporation of shear deformations renders the structure more flexible, and alters the frequency characteristics of the structure considerably. Major results for the 4 analyses are given in Table 3.13.

The most important features to note are:

(1) in no cases were the results identical,

(2) greater discrepancies were apparently caused by differences in application of the bilinear factor, rather than differences from shear deformation calculations,

(3) for a stated plastic rotation, the associated strength increase is larger in RUAUMOKO than DRAIN 2D (1887 MN.m rad^{-1} compared to 706 MN.m rad^{-1}). This indicates a greater effective strain hardening in the case of RUAUMOKO despite a nominally equal post-yield stiffness factor of 0.02.

TABLE 3.12 : COMPARISON OF PERIODS OF VIBRATION OF MODES 1 - 5 FOR THE SIX STOREY WALL

	Shear Deformations Suppressed	Shear Deformations Allowed
T_1 sec.	0.69754	0.72491
T_2 sec.	0.10570	0.13507
T_3 sec.	0.10080	0.10080
T_4 sec.	0.03716	0.05961
T_5 sec.	0.03360	0.03859

TABLE 3.13 : COMPARISON OF ANALYSES MADE USING RUAUMOKO AND DRAIN 2D

SEE ERRATA

	RUN 1 $A_v = 0$ $r = 0$		RUN 2 $A_v \neq 0$ $r = 0$		RUN 3 $A_v = 0$ $r \neq 0$		RUN 4 $A_v \neq 0$ $r \neq 0$	
PROGRAM	RUAUMOKO	DRAIN 2D	RUAUMOKO	DRAIN 2D	RUAUMOKO	DRAIN 2D	RUAUMOKO	DRAIN 2D
$V_{max,base}$ kN	2296	2307	2764	2650	2818	2561	3419	2462
ω_v	1.34	1.35	1.62	1.55	1.65	1.50	2.00	1.44
Δ_{top} +ve	0.0029	0.0029	0.0041	0.0046	0.0068	0.0058	0.0072	0.0073
Δ_{top} -ve	-0.0090	-0.0090	-0.0095	-0.0094	-0.0069	-0.0070	-0.0072	-0.0085
Base Drift	0.0080	0.0080	0.0084	0.0083	0.0052	0.0046	0.0056	0.0071
θ_p rad	0.0009	0.0015	0.0009	0.0077	0.0048	0.0040	0.0049	0.0067
M_{max} kN.m	22800	22800	22800	22800	31773	29839	32009	27004

Note: Definition of the tabulated variables is as given in the footnote for Table 3.2.

3.7.2 Time Step of Numerical Integration

The time step (Δt) used for the numerical integration procedures in a time history program is an important parameter. RUAUMOKO has an implicit numerical integration based on the Newmark $\beta = \frac{1}{4}$ scheme [45] which is unconditionally stable for any Δt. It should be noted, however, that unconditional stability has not been proven for a nonlinear, damped multi-degree-of-freedom system. Therefore instabilities in analysis can arise if Δt is not sufficiently small due to response phase shift, the implicit equivalent damping of the integration technique, and amplitude modification [41], The two primary factors in the choice of Δt are (i) the economic feasibility of the value, and (ii) the need for a value sufficiently small to ensure numerical stability. It is generally considered that a time step will be adequate if it is smaller than the lowest period of vibration of the structural system being studied. This is clearly impractical for the walls considered (see Fig. 3.6). Traditionally, Δt = 1/100 sec. has been found adequate for frame structures. This value was used for the majority of the wall analyses reported in this chapter. It was found that a significant number of these analyses, especially the 18 storey walls, exhibited numerical instability. The re-running of these analyses with time steps of 1/200 or 1/400 gave greater apparent stability, although the results indicated by some of these analyses are rather extreme. ω_v values in excess of 3 are not uncommon in such circumstances. The use of a yet finer time step was not observed to significantly alter the results. This suggests a general conclusion, that if an analysis appears stable at some particular Δt, the differences arising from the use of a smaller value will be insignificant. This is illustrated in Table 3.14 for the case of the rectangular section 18 storey wall subjected to the Parkfield accelerogram, with Rayleigh damping of $\lambda_1 = \lambda_5 = 5\%$. This analysis "blew up" with Δt = 1/100 sec. It shows, however, similar stable results for time steps of 1/200 and 1/400 secs. Also shown are analyses run for the 12 storey I section wall using DRAIN 2D. Despite the high ω_v values indicated, it is clear that these analyses are stable and a time step of 1/100 sec. seems adequate.

3.7.3 Number of Elements Used in Wall Modelling

It might be thought intuitively that the finer subdivision of a wall into separate beam-column elements, the more accurate the modelling of that wall would be. However,the nature of the elements themselves should be considered. Dividing a wall into more (vertically aligned) elements makes these members more squat, so that shear deformations are

TABLE 3.14 : EFFECT OF VARIATION OF TIME STEP USED IN NUMERICAL INTEGRATION

		12 Storey Rectangular Section, Rayleigh Damping $\lambda_1 = \lambda_2 = 5\%$, Parkfield, DRAIN 2D			18 Storey Rectangular Section, Rayleigh Damping $\lambda_1 = \lambda_5 = 5\%$, Parkfield RUAUMOKO		
Time Step	sec.	1/100	1/200	1/400	1/100	1/200	1/400
$V_{max,base}$	kN	10142	10179	10181	Unstable(2)	35554	35466
ω_v		3.24	3.25	3.25		3.50	3.49
Δ_{top} +ve		0.0128	0.0128	0.0128		0.0073	0.0073
Δ_{top} -ve		-0.0038	-0.0038	-0.0038		-0.0023	-0.0023
Base Drift		0.0074	0.0049	0.0049		0.0021	0.0021
Max. Drift		-	-	-		0.0089	0.0089
θ_p	rad.	0.0043	0.0043	0.0043		0.0017	0.0017
M_{max}	kN.m	92946	92945	92945		576260	575470
M_{max}/M_y		1.11	1.11	1.11		1.34	1.34

Notes:

(1) Definition of the tabulated variables is as given in the footnote for Table 3.2.

(2) Numerical instability gave unreasonable results.

TABLE 3.15 : EFFECT OF NUMBER OF ELEMENTS USED TO MODEL A 12 STOREY WALL

Number of Elements		12 Elements		16 Elements		28 Elements	
Program		RUAUMOKO	DRAIN 2D	RUAUMOKO	DRAIN 2D	RUAUMOKO	DRAIN 2D
$V_{max,base}$	kN	6542	8860	6571	8854	6500	8979
ω_v		2.09	2.83	2.10	2.83	2.08	2.87
Δ_{top} +ve		0.0028	0.0030	0.0028	0.0030	0.0028	0.0030
Δ_{top} -ve		-0.0035	-0.0054	-0.0035	-0.0052	-0.0035	-0.0050
Base Drift		0.0013	0.0031	0.0014	0.0029	0.0014	0.0026
Max Drift		0.0047	-	0.0046	-	0.0046	-
θ_p	rad.	0.0007	0.0024	0.0007	0.0020	0.0007	0.0020
M_{max}	kN.m	88735	89104	88378	92122	87374	93384
M_{max}/M_y		1.06	1.06	1.06	1.10	1.04	1.12

Note: Definition of the tabulated variables is as given in the footnote for Table 3.2.

likely to be of increasing importance. This may not be advantageous, given the generally unsophisticated nature of shear displacement calculations in many package programs, especially in the inelastic range. In addition, the number of structure degrees of freedom are increased and have lower inertias and thus higher associated frequencies of vibration. This can cause stability problems with regard to the selection of a suitable damping model. It might be hoped that fine division of the wall, especially at base level, would better model the plasticity in this area than would the one element per storey representation used for the bulk of the reported analyses.

The 12 storey rectangular section wall was used as the basis for a brief investigation of the effect of an increased number of wall elements.

12, 16 and 28 element representations of the wall were used, with a closer nodal spacing in the wall base region. A Rayleigh damping scheme of 5% on modes 1 and 5 was used for each wall model. A comparison was also made between the trends exhibited by the two programs RUAUMOKO and DRAIN 2D. The results of the analyses, summarised in Table 3.15, show good consistency between the 3 models although large differences between the 2 programs are evident. It would seem that the use of 1 element per storey is sufficient to model a structural wall adequately, provided that the wall is reasonably slender. One element modelling of a very squat wall is unlikely to be satisfactory, for example. Despite the relatively close nodal spacing in the wall base region used in the 28 element model, plastic deformations were restricted to the 2 lowermost nodes, i.e. to a maximum height of only 1.75 m ($\simeq 0.2\ell_w$) above the base level. Thus it would appear that apparently more accurate modelling does nothing to reproduce better the base level plasticity of a structural wall.

3.7.4 Effect of Assumed Section Stiffness Properties

Present dynamic analysis programs require the specification of stiffness properties (axial and shear areas, moment of inertia, Young's and shear moduli) which are considered constant throughout the time history analysis. No adjustment is made to member stiffness (below flexural yield conditions) which might represent the effects of cracking, previous inelastic deformations and changing axial load in vertical members. A common practice is to assume some degree of member cracking reflected in the use of areas and moment of inertias

less than those based on the gross section. Guidelines have been given [39] although work by Hansen [46] suggests that for walls stiffness is often considerably overestimated. The rationale for this practice is that by the onset of strong shaking, the structure will have cracked to the assumed degree, and the influence of the first seconds of loading, when the structure is actually stiffer, is small.

The effect of the assumed degree of cracking on performance was investigated for the 12 storey rectangular walled structure subject to the El Centro accelerogram.

The range of distributions of second moment of wall area assumed as allowance for cracking is shown in Fig. 3.9. Because wall geometry assumes a decreasing web thickness with height (Fig. 3.2) properties based on gross area decrease up the structure. A summary of the results of these analyses is given in Table 3.16. For a constant degree of cracking with height, it is of interest to look at the correlation between first mode period and second moment of area. Classical theory for a single degree of freedom oscillator relates period^2 to stiffness, quantities which are shown in Table 3.17. Despite the fact that the walls are modelled as multi-degree-of-freedom systems and have variable section properties with height, a nearly classical correlation exists

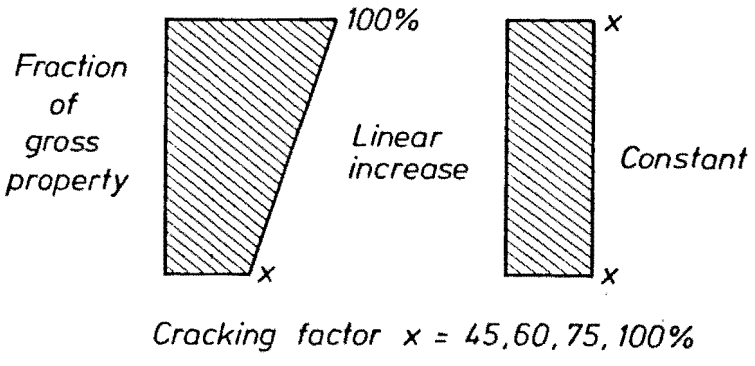

Fig. 3.9 Assumed Variation of Wall Stiffness Properties.

TABLE 3.16 : EFFECT OF ASSUMED EXTENT OF WALL CRACKING - 12 STOREY WALL - EL CENTRO

Cracking factor[2]		x = 100%		x = 75%		x = 60%		x = 45%	
Cracking Distribution[2]		Constant	Linear	Constant	Linear	Constant	Linear	Constant	Linear
$V_{max,base}$	kN	8551	8851	6453	6198	9280	6542	8129	8782
ω_v		2.73	2.73	2.06	1.98	2.96	2.09	2.60	2.80
Δ_{top} +ve		0.0018	0.0018	0.0026	0.0023	0.0032	0.0028	0.0039	0.0033
Δ_{top} -ve		-0.0034	-0.0034	-0.0035	-0.0032	-0.0051	-0.0035	-0.0070	-0.0053
Base Drift		0.0020	0.0020	0.0012	0.0013	0.0026	0.0011	0.0031	0.0029
Max. Drift		0.0043	0.0043	0.0046	0.0041	0.0069	0.0047	0.0092	0.0069
θ_p	rad.	0.0013	0.0013	0.0008	0.0009	0.0019	0.0007	0.0023	0.0018
M_{max}	kN.m	99331	99331	90961	92086	97185	88735	96021	93658
M_{max}/M_y		1.19	1.19	1.09	1.10	1.16	1.06	1.15	1.12
T_1[3]	sec.	1.36	1.36	1.57	1.53	1.76	1.66	2.03	1.85
s_v[4]	m/s	0.51	0.51	0.49	0.47	0.51	0.51	0.58	0.53

Notes: (1) Definition of the tabulated variables is as given in the footnote for Table 3.2
(2) See Fig. 3.9.
(3) First mode period.
(4) Pseudo 5% damped velocity (NS El Centro 1940 accelerogram)

between first mode period^2 and cracking factor, in the case of constant cracking. For variable cracking the correlation is less good due to the stiffening effect of the upper part of the wall.

TABLE 3.17 : CORRELATION BETWEEN CRACKING FACTOR AND FIRST MODE PERIOD

	Constant Cracking			Linear Cracking		
Cracking Factor	0.45	0.60	0.75	0.45	0.60	0.75
$T_1/T_{1,gross}$	0.67	0.77	0.87	0.74	0.82	0.89
$(T_1/T_{1,gross})^2$	0.44	0.59	0.76	0.55	0.67	0.79

Consideration of Table 3.16 shows that large variations in response can be achieved by altering the parameter allowing for the degree of cracking. It is interesting to correlate these results with the associated spectral velocities for the El Centro accelerogram, as a function of first mode period. This is also shown in Table 3.16. As may be seen there is reasonable correlation between the observed response (moment, shear and drift) and the excitation, as measured by first mode spectral velocity. The primary way in which the assumed stiffness distribution affects response is via the associated change to the frequency characteristics of the structure. As has been documented in the past, such a period shift may increase or decrease the structural response depending on the accelerogram used, and the degree of participation of higher modes.

3.7.5 The Effect of Foundation Compliance

The structure chosen for a brief investigation of the effect of foundation compliance was the 6 storey I section wall, with Rayleigh damping of $\lambda_1 = \lambda_5 = 5\%$, subjected to the El Centro excitation. A simple model of foundation complience was used (Fig. 3.10) whereby the stiffness and span of an imaginary foundation beam can be chosen to give any desired rotational stiffness. Soil hysteresis is notoriously difficult to model accurately and this has not been attemped in this study. The foundation beam stiffness was chosen to give base rotations

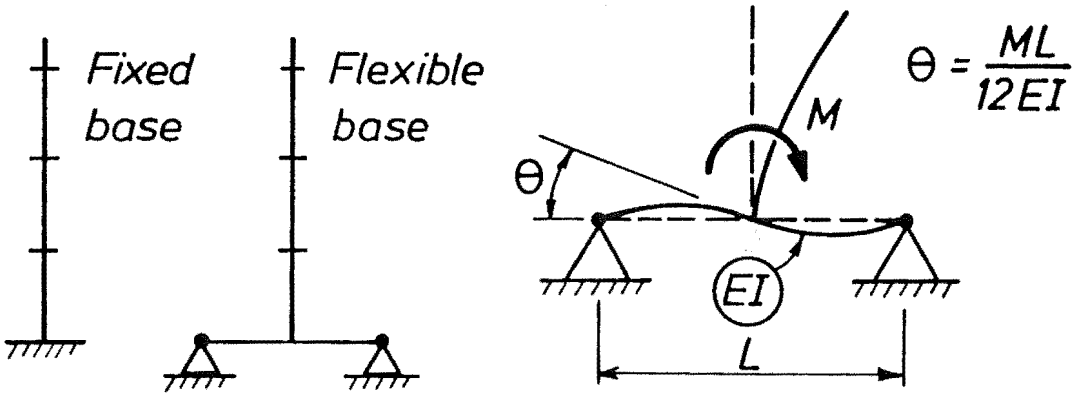

Fig. 3.10 Simple Foundation Compliance Model.

at wall yield moment of 0.0001, 0.001 and 0.01 radians. Summarised results of the analyses performed using the program RUAUMOKO are given in Table 3.18.

The following observations may be made from a consideration of the data provided in this table:

(1) There is no consistent effect on base shear with increasing foundation flexibility.

(2) A potentially large first mode period shift may result, depending on the assumed degree of compliance.

(3) High foundation flexibility leads to increased deformations and drifts, coupled to a lesser degree of inelastic behaviour.

(4) It may be concluded that the main effect of foundation compliance is to increase the first mode period of the structure, and the effect that this has is dependent on the characteristics of the accelerogram chosen. This is a similar conclusion to that drawn for the effect of assumed wall stiffness variation (Section 3.7.4).

TABLE 3.18 : EFFECT OF FOUNDATION COMPLIANCE ON WALL RESPONSE
6 STOREY WALL - EL CENTRO

$\theta^{(2)}$ radians	0.01	0.001	0.0001	0 (fixed base)
$T_1^{(3)}$ seconds	2.11	0.96	0.75	0.73
$V_{max,base}$ kN	3136	3558	2557	3005
ω_v	1.86	2.12	1.52	1.78
Δ_{top} +ve	0.0128	0.0039	0.0014	0.0014
Δ_{top} -ve	-0.0127	-0.0064	-0.0044	-0.0040
Base Drift	0.0121	0.0053	0.0035	0.0031
Max. Drift	0.0137	0.0072	0.0049	0.0047
θ_p rad.	0.0076	0.0033	0.0027	0.0025
M_{max} kN.m	24240	29051	27914	27412
M_{max}/M_y	1.06	1.27	1.22	1.20

Notes: (1) Definition of the tabulated variables is as given in the footnote for Table 3.2.
(2) Rotation of wall base at yield moment, see Fig. 3.10.
(3) First mode period.

3.7.6 Dependence of Dynamic Shear Magnification on Period

In order to investigate the dependence of ω_v on stiffness (period), a 12 storey rectangular section wall, relatively stiffer than those discussed previously, was designed and studied. The first mode period was 0.97 sec, considerably less than the value of 1.66 secs. obtained for the previous 12 storey walls. Assumed damping was a Rayleigh model with 5% of critical damping on modes 1 and 5. Wall geometry and details are summarised as follows:

ℓ_w = 12.0 m, b_w = 0.50, 0.45, 0.40 and 0.35 m over floors 1-3, 4-6, 7-9 and 10-12, respectively, V_{code} = 2820 kN and M_y = 109.3 MN.m.

As may be seen from the results summarised in Table 3.19, the ω_v values obtained are quite similar to those indicated in Table 3.5, the maximum difference for a given accelerogram being 15%. This suggests that ω_v values are not strongly dependent on first mode period of vibration.

TABLE 3.19 : EFFECT OF PERIOD CHANGE ON WALL RESPONSE

	12 Storey Wall, T_1 = 0.97 sec.			12 Storey Wall, T_1 = 0.71 sec.		
Accelerogram	El Centro	Bucharest	Parkfield	El Centro	Bucharest	Parkfield
$V_{max,base}$ kN	9380	6930	10925	6210	4244	5407
ω_V	2.29	1.69	2.67	2.25	1.54	1.96
Δ_{top} +ve	0.0009	0.0058	0.0061	0.0007	0.0032	0.0051
Δ_{top} -ve	-0.0038	-0.0061	-0.0025	-0.0020	-0.0036	-0.0021
Base Drift	0.0029	0.0043	0.0043	0.0017	0.0026	0.0034
θ_p rad.	0.0024	0.0037	0.0039	0.0013	0.0023	0.0031
M_{max} kN.m	124915	130964	134467	81954	88922	93720
M_{max}/M_y	1.14	1.20	1.23	1.10	1.20	1.27

The behaviour of the stiff 12 storey wall was further studied by reducing the nodal weights associated with the structure and thus reducing the first mode period to 0.709 s which is approximately the same as the 6 storey wall periods. This change in stiffness is reflected in changed values of V_{code} and M_y (1906 kN and 73.9 kN.m respectively). The summary of associated results in Table 3.19 shows similar results to the previous stiff wall except for the Parkfield accelerogram. The similarity of the ω_v values in this tables compared with the range of values obtained for the 6 storey walls (Tables 3.2 - 3.5) does nothing to clarify the question of period or height dependence of dynamic magnification.

3.7.7 Hysteresis Model

The analyses reported previously were all made using a bilinear hysteresis model with a post yield branch of nominal stiffness 2% of the pre-yield branch. In order to assess the sensitivity of structural wall response to the hysteresis model used, a series of analyses were conducted using a Modified Takeda Degrading Stiffness model [28]. The structure used was the 6 storey rectangular wall, with Rayleigh damping of 5% on modes 1 and 5 subjected to the 1940 El Centro N-S accelerogram.

The Takeda model is shown in Fig. 3.11. The model is more sophisticated than the simple bilinear model and is generally believed to follow quite closely the hysteresis loops obtained from Japanese laboratory tests of model structural walls. It should be noted, however, that many laboratory test units indicate a level of performance considerably inferior to that which may be obtained from well detailed walls subjected to moderate ductility demands. The shape of the Takeda model loops is controlled by the parameters α and β, as shown in Fig. 3.11. α is a factor representing the degree to which an unloading branch is less stiff than the initial loading branch, while β determines how closely to the point of previous maximum deformation a subsequent ascending load branch is directed. It was assumed that low values of both α and β were most representative of the likely behaviour of walls constructed according to New Zealand practices. The summarised results of a series of analyses covering the range $\alpha = 0 \rightarrow 0.4$, $\beta = 0$, 0.2 and both DRAIN and EMORI unloading [15] are given in Table 3.20. As may be seen, some of these analyses indicate unreasonably high base shear forces, while most other aspects of behaviour remain credible. Discounting

TABLE 3.20 : EFFECT OF TAKEDA HYSTERESIS MODEL ON WALL RESPONSE
6 STOREY WALL - EL CENTRO

$\beta = 0$		$\alpha = 0.0$		$\alpha = 0.2$		$\alpha = 0.4$		Bilinear Model
Unloading Option		EMORI	DRAIN	EMORI	DRAIN	EMORI	DRAIN	
$V_{max,base}$	kN	2761	2761	2978	4969	4368	10293	3194
ω_v		1.61	1.61	1.74	2.90	2.55	6.02	1.87
Δ_{top} +ve		0.0021	0.0021	0.0022	0.0026	0.0027	0.0044	0.0014
Δ_{top} -ve		-0.0045	-0.0045	-0.0046	-0.0046	-0.0047	-0.0048	-0.0039
Base Drift		0.0035	0.0035	0.0035	0.0035	0.0035	0.0039	0.0029
Max. Drift		0.0051	0.0051	0.0053	0.0052	0.0043	0.0061	0.0048
θ_p	rad.	0.0030	0.0030	0.0029	0.0028	0.0029	0.0033	0.0023
M_{max}	kN.m	28140	28140	28218	28273	28187	28416	27154
M_{max}/M_y		1.23	1.23	1.24	1.24	1.24	1.25	1.19
$\beta = 0.2$								
$V_{max,base}$	kN	2697	2564	2815	2758	4470	2854	3194
ω_v		1.58	1.50	1.65	1.61	2.61	1.67	1.87
Δ_{top} +ve		0.0020	0.0020	0.0021	0.0025	0.0028	0.0026	0.0014
Δ_{top} -ve		-0.0042	-0.0042	-0.0043	-0.0044	-0.0044	-0.0045	-0.0045
Base Drift		0.0032	0.0032	0.0033	0.0033	0.0033	0.0034	0.0029
Max. Drift		0.0049	0.0049	0.0050	0.0050	0.0050	0.0052	0.0048
θ_p	rad.	0.0028	0.0026	0.0027	0.0025	0.0027	0.0028	0.0023
M_{max}	kN.m	27595	27540	27769	27849	27761	28041	27154
M_{max}/M_y		1.21	1.21	1.22	1.22	1.22	1.23	1.19

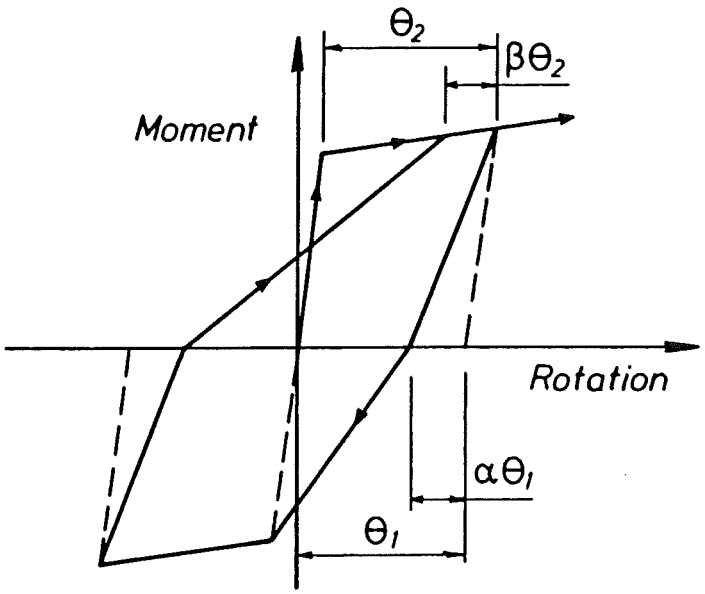

Fig. 3.11 Takeda Degrading Stiffness Model [28].

these it may be observed that lower values of ω_v factors were calculated, as compared with the bilinear model calculation. However, both drifts and base plastic rotation demands are larger for the Takeda model analyses, the increases being greatest for the case of $\beta = 0$. This may be explained from a consideration of energy dissipation: if it accepted that approximately equal energy is dissipated by a bilinear and a Takeda model (i.e. equal areas are enclosed by the hysteretic response curves) it is clear that larger rotations must occur for the Takeda model. If, however, first mode structural period is such that the equal energy concept is not considered valid, such an explanation becomes less reasonable. The DRAIN and EMORI options (which give slightly different unloading stiffnesses) made little difference to the analyses. It is considered that although some differences exist between results of analyses made using bilinear and Takeda models, this is not the most disturbing source of variations in structural wall response.

3.7.8 Shear Force Envelope

From the analyses made using RUAUMOKO and the two cases of Rayleigh damping[+], values of $V_{max,i}/V_{max,base}$ (where $V_{max,i}$ is the shear force at level i) were calculated. The distributions of maximum values of this parameter are shown in Fig. 3.12, together with an envelope of Code [9] design shear force normalised in a similar way. In a few cases, values of the former ratio in excess of unity above the base level were obtained. These were discarded, however, because they were associated with analyses of doubtful numerical stability. It may be observed that the code shear distribution conservatively estimates maximum shear force over the bottom 75% of the walls, above which this trend is reversed. The discrepancy is worst at the wall top. On the basis of these observations, a proposal is made to enable a modified shear design envelope to be obtained from the code distribution (Fig. 3.12(d)). Although the 50% increase at wall top may seem high, it should be noted that in the upper levels of most structural walls, shear design is seldom critical and an increase in design force of this size is likely to be readily accommodated. Although the increase is based on a continuous rather than a stepwise code force distribution, common sense should be used to adapt the procedure to a finite number of floors. The increases in upper floor design force are similar to those of the scheme proposed by Derecho [47]. This uses a period dependent magnification of UBC-76[26] shear force over the top 25% of structural walls.

3.8 SOURCES OF INACCURACY IN TIME HISTORY ANALYSES

It is considered that dynamic time history analyses should not be accorded undue credence because of the inaccuracies inherent in the selection of input data and the relatively unsophisticated nature of the modelling on which most such analyses are based. It is unfortunate that because of the expense and very large volume of output generally associated with these analyses, the calculated results are often regarded as being of unquestionable validity and accuracy. Some sources of inaccuracies are listed subsequently. Typical effects on structural response of variation in the parameters cited are also presented.

3.8.1 Input Data

1. Stiffnesses of lateral load resisting elements which accurately reflect the degree of cracking or degradation of the elements.

+ i.e. 12 analyses were used to construct the figure for each wall height.

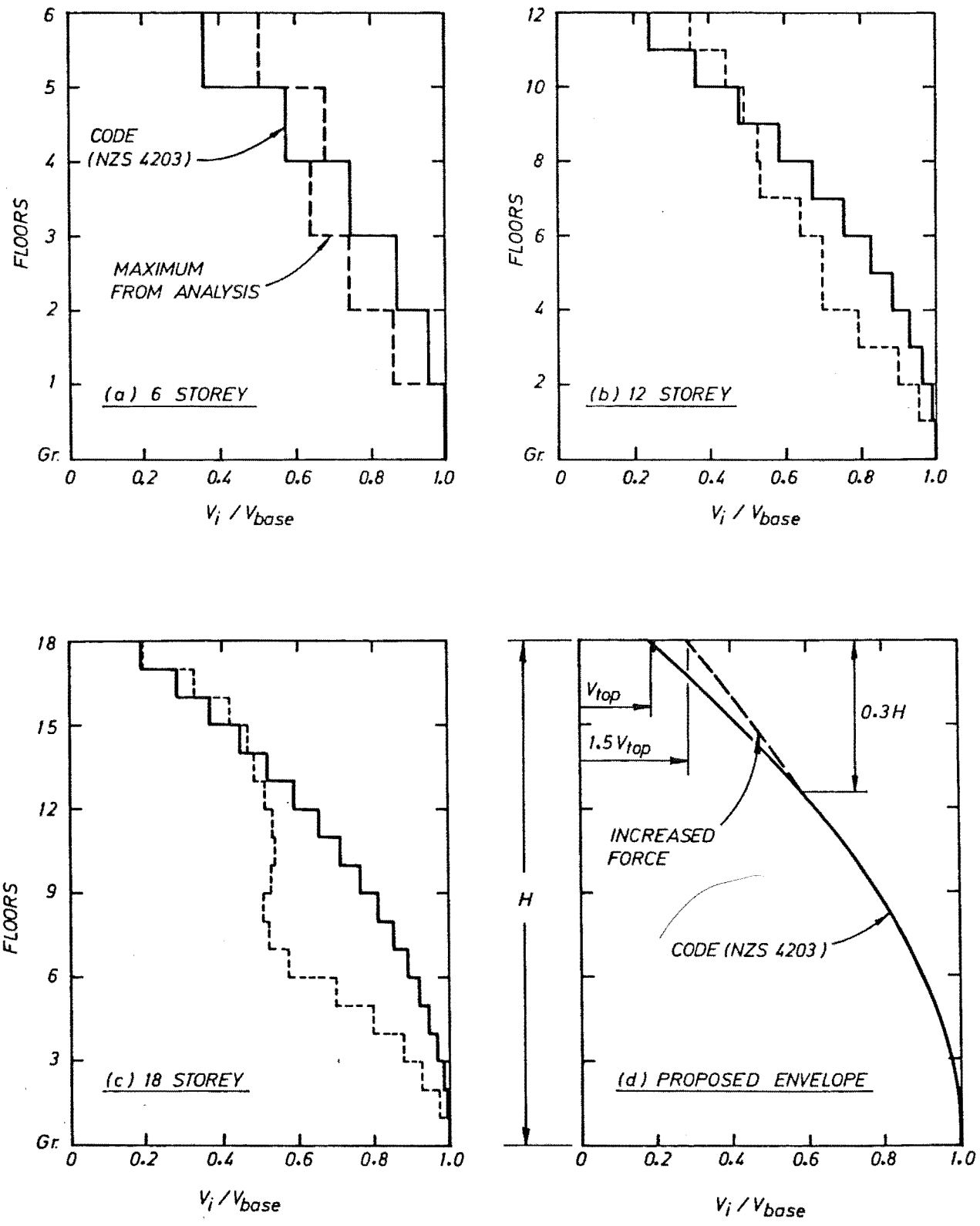

Fig. 3.12 Wall Shear Force Distributions.

Stiffness affects structural frequency characteristics which, depending on the accelerogram used, may lead to different strength or deformation capacity demands.

2. True strengths of members, which may not be accurately estimated for the purposes of time history analyses. The onset of member yielding during the earthquake may be affected and thus the overall response influenced.
3. Assumptions regarding base fixity and floor slab rigidity. As has been shown, loss of wall base fixity may substantially affect both force and deformation levels.
4. Approximate representation of the true lateral load resisting system. Elements not considered to contribute to load resistance may in fact do so, thus modifying response, or they may be subjected to displacements which cause damage.
5. The use of historical earthquake records which will never re-occur. In addition, many accelerograms are strongly influenced by local conditions at the recorder site.

3.8.2 Modelling

1. The assumed deformation patterns on which finite element models are based may not be well suited to some prototype member types. This is especially true of squat elements such as structural wall segments whose behaviour may control total structural response.
2. The basic stiffness of members is generally held constant throughout an analysis, despite the influence of varying axial load. This may be of importance in the case of coupled wall systems [48].
3. Point plastic hinges are usually assumed, which is reasonable only for relatively slender members. Little credence may be placed on calculated hinge rotations for members in which hinge lengths are a significant proportion of the total member length.
4. Arbitrary viscous damping models are often used which do not accurately reflect the true nature of the phenomenon. It has been demonstrated (Section 3.6.3) that the choice of damping model used can influence response markedly.
5. The modelling of 3 dimensional effects and torsion is generally not possible except at considerable expense, although structural behaviour obviously depends upon these influences.

6. The influence of nominally non-structural items is seldom taken into account.
7. The modifying effects of site conditions on base excitation are seldom modelled.

3.9 SUMMARY OF MAJOR FINDINGS

1. The basic approach to structural wall shear design advocated by the New Zealand Code [34] is a reasonable engineering solution to a complex problem. However, the evaluation of a more credible set of shear force dynamic magnification factors (ω_v) remains to be made. This could be achieved on the basis of a large number of dynamic analyses in which a realistic finite element model of the critical (base) region of the walls is used. The effect of parameters such as wall geometry, damping model, base fixity and excitation accelerograms must be taken into account.
2. The analyses performed suggest that the dynamic shear magnification factors advocated by Blakeley, Cooney and Megget [36] are approximately 30% too small. However, consideration of the probability of occurrence and duration of large magnitude shear forces suggests that the use of higher ω_v factors may not be appropriate. In addition, the analyses on which the assessment of shear magnification is based are, like any dynamic analyses, founded on assumptions which make the unreserved acceptance of analysis results a dubious proposition. Engineering judgement should be used in this issue, given the already high levels of design forces recommended in New Zealand [34].
3. It has been shown that structural wall response can be greatly affected by such parameters as the assumed damping model, stiffness, base fixity and wall geometry.
4. The modelling of the inelastic behaviour of the plastic hinge zones of structural walls, using either the Giberson or 2 component models (Section 3.6.7) is rather questionable. Both representations assume members to be slender and with inelastic deformations concentrated in "point hinges": both assumptions are incompatible with realistic wall geometries and behaviour patterns.
5. It is not clear whether dynamic magnification should be considered solely a function of either the number of storeys (as is assumed in the code approach [34])or first mode period, as the phenomenon is dependent on both these parameters.

Chapter Four THE SEISMIC RESPONSE OF SIX AND TWELVE STOREY FRAME-WALL BUILDINGS

4.1 INTRODUCTION

This chapter describes a series of analyses performed in order to further investigate and extend a previously postulated [2] method of design for seismic resistance of frame-wall buildings. The general approach to this problem involved three steps: firstly a series of simplified buildings were designed according to an established procedure (summarized below). Secondly, the structures were subject to simulated seismic attack via computer based analysis using an inelastic time history analysis program [15]. Finally, on the basis of the analytically predicted structural performance, the design method was modified as appropriate. The behaviour of buildings of height 6, 12 and 18 storeys was investigated in this manner.

4.1.1 Existing approach to the design of frame-wall buildings

Set out in this introductory section is a step by step exposition of an existing approach [2] suggested for the design of coupled frame-wall buildings. The general design procedure is an extension of a capacity design philosophy previously postulated for ductile frames [34]. The principal feature of this approach is the "a priori" selection and hence appropriate detailing of primary energy dissipating elements (so called plastic hinges). Other structural elements are provided with sufficient reserve strength to ensure that significant inelastic deformations occur only at regions specially detailed for that purpose. This design philosophy is deterministic. In multi-storey buildings with an appreciable frame content, the desirable heirarchy in plastic hinge formation involves beams rather than columns. Column hinge mechanisms (referred to as soft storeys) are avoided by providing columns with strength in excess of the maximum load input from adjacent beams.

The structural wall components of the coupled frame-wall building are also apportioned strength in accordance with capacity design principles, using procedures established for cantilever structural walls [39]. Because of the desirability of energy dissipation in walls via flexural yielding, the most appropriate design procedure is to restrict this inelastic behaviour to zones (usually at the wall base) specially detailed for this purpose. The wall must also be provided with sufficient shear strength to prohibit a shear failure.

The summarized design method is presented subsequently. Some aspects of the process are described in greater detail in Section 4.2.2. The method is based largely on a recommended method for the evaluation of column actions in ductile multistorey frames [34]. The procedure covers the flexural design of beams, columns and walls, and the evaluation of design shear forces for columns and walls.

Step 1: Derive the bending moments and shear forces for all members of the frame-wall system for the specified lateral static earthquake load only, using an appropriate elastic analysis. These actions are subscripted "code".

Step 2: Superimpose the beam bending moments so obtained upon the appropriately factored gravity load moments. Subsequently carry out a horizontal and vertical moment redistribution allowing a reduction of up to 30% of beam moments.

Step 3: Design all critical beam sections so as to provide the required dependable flexural strengths and hence determine and detail the reinforcement for all beams of the frame.

Step 4: For both directions of applied lateral load, compute the flexural overstrength of each potential plastic beam hinge, and determine the corresponding moment induced shear forces, V_{oe}, in each beam span.

Step 5: Determine the beam overstrength factor, ϕ_o, at the centreline of each column for both directions of loading, using fixed values of $\phi_o = 1.4$ and 1.1 for ground and roof levels respectively.

Step 6: Derive the column design shear forces at each level,

$$V_{col} = \omega_c \phi_o V_{code} \tag{4.1}$$

where the column dynamic shear magnification factor w_c is 2.5, 1.3 and 2.0 for the bottom, intermediate and top storey, respectively. For the bottom storey, a design shear force of

$$V_{col} = (M^o_{col} + 1.3\phi_o M_{code,top})/(\ell_n + 0.5h_b) \tag{4.2}$$

may be used if it exceeds $2.5\phi_o V_{code}$, where M^o_{col} is the flexural overstrength of the column base section, and $M_{code,top}$ is the value of M_{code} at the first floor level of the column.

Step 7: Estimate in each storey the maximum likely earthquake induced column axial load

$$P_{eq} = R_v \Sigma V_{oe} \tag{4.3}$$

where

$$R_v = (1 - n/67) \geq 0.7 \tag{4.4}$$

is a reduction factor that takes the number of storeys n into account [34].

Step 8: Determine the total design axial load on columns

$$P_{e,max} = P_D + P_{LR} + P_{eq} \quad (4.5)$$

and

$$P_{e,min} = 0.9P_D - P_{eq} \quad (4.6)$$

where P_D and P_{LR} are forces due to dead and reduced live gravity loads respectively.

Step 9: The design moments for columns are

$$M_{col,red} = R_m(\omega\phi_o M_{code} - 0.3h_b V_{col}) \quad (4.7)$$

where R_m is an axial load dependent reduction factor applicable to columns subjected to tension or compression stresses not exceedings 10% of the compression strength of the concrete [34] and V_{col} is found in Step 6. The value of ω is given in Fig. 4.1.

Step 10: Determine the design axial forces due to appropriately factored gravity and earthquake loads on the walls.

Step 11: From the maximum earthquake load induced bending moment at the wall base and the above axial loads, determine the necessary vertical wall reinforcement. When curtailing bars with height, follow the linear moment envelope of Fig. 4.2.

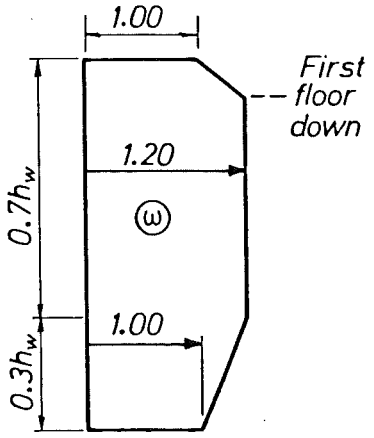

Fig. 4.1 Column Dynamic Moment Magnification Factor for Frame-Wall Structures.

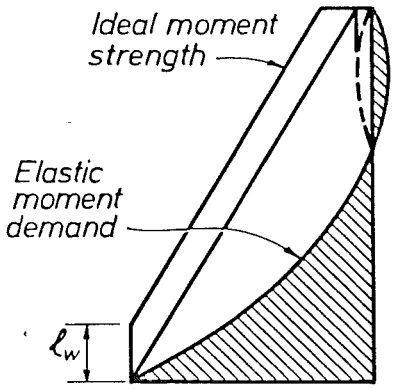

Fig. 4.2 Design Wall Moment Envelope for Frame-Wall Structures.

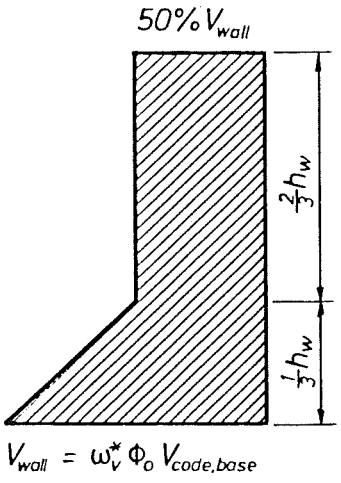

Fig. 4.3 Design Wall Shear Force Envelope for Frame-Wall Structures.

Step 12: Having completed the detailing of the wall flexural reinforcement, determine the flexural overstrength factor ϕ_o with respect to the base moment, i.e. $\phi_o = (M^o/M_{code})_{base}$

Step 13: From the elastic analysis determine the "shear ratio" as

$$\text{shear ratio} = (V_{code,wall}/V_{code,total})_{base} \qquad (4.8)$$

Step 14: Determine the value of dynamic shear magnification (ω_v) appropriate for an uncoupled free standing cantilever wall of the same number of storeys as the wall being designed from the following equations

$$\omega_v = 0.9 + n/10 \quad \text{when } n \leq 6 \qquad (4.9)$$

$$\omega_v = 1.3 + n/30 \leq 1.8 \quad \text{when } n > 6 \qquad (4.10)$$

where n is the number of storeys.
Finally, the dynamic shear magnification factor appropriate for a wall in a frame-wall structure, ω_v^*, is calculated as

$$\omega_v^* = 1 + (\omega_v - 1) \times (\text{shear ratio}) \qquad (4.11)$$

Step 15: With wall shear force at the base, obtained from the elastic analysis, determine the maximum wall design shear force

$$V_{wall} = \omega_v^* \phi_o V_{code,base} \qquad (4.12)$$

and from Fig. 4.3 construct the shear design envelope.

Step 16: Determine the necessary horizontal wall shear reinforcement in accordance with appropriate code requirements.

4.1.2 Choice of accelerogram for dynamic analysis

The choice of historical seismic excitation to which a building is exposed (via computer based modelling) is clearly of critical importance if the response of the structure is to be used as the means of evaluating the design method used. Ideally, a structure should be exposed to many excitations in order to determine envelopes of response that are likely to encompass the response of a prototype building to a future seismic event. The practical constraints of available time and the expense of computer analyses serve to greatly reduce the scope of most such investigations, and the work reported on herein is no exception.

Traditionally, the NS El Centro 1940 component has commonly been used as a benchmark for comparisons of structural performance. This is despite the relatively unusual nature of this record, which is not at all of a "typical" seismic event. However, this accelerogram has been used as the basis for the design lateral load coefficients used in New Zealand Code of Practice for Design Loadings [9] (amongst other documents). Thus it was considered appropriate to use the response of the frame-wall buildings to this accelerogram as the primary means of assessing the adequacy of the postulated design method.

In addition, the buildings studied were also exposed to the S15 W Pacoima Dam 1970 component. Although some controversy exists as to the levels of horizontal accelerations recorded during this event, it is considered that this accelerogram represents an upper bound to a possible seismic event, in the context of New Zealand seismicity. It is further suggested that although the survival of a structure exposed to this excitation indicates an acceptable design, the non-survival of a structure would not necessary condemn the design.

4.1.3 Choice of dynamic analysis program

The 2-dimensional inelastic time history program "RUAUMOKO" [15] developed in original form by Sharpe [41] and substantially modified by Carr [15] was used to investigate the response of the structures discussed in this chapter to simulated seismic attack. In this program, a step by step numerical integration process (based on the constant acceleration or Newmark's $\beta = \frac{1}{4}$ method) is used to solve the equations of motion governing the response of a structure to a given input base excitation. Detailed discussion of the essential features of this program, which may also be used to perform elastic and modal analyses, may be found in reference 15. Section 4.2.3 outlines the input data required by the program, and these requirements are discussed at greater length in reference 2 .

Output data from the program consisted of three main parts: displacement and force states of selected nodes and members at specified time intervals throughout the analysis, diagrammatic representation of the structure at times of plasticity alteration, and envelopes of maxima/ minima of nodal and member data recorded during the analysis. Constraints of time and space permit the presentation of only a fractional amount of the information generated in each analysis. The University of

Canterbury's B6900 Burroughs computer was used for all the analyses reported herein.

4.2 SIX STOREY BUILDINGS

Two six-storey frame-wall buildings were selected for study. The subsequent sections describe the configurations of these structures, the application of the previously postulated design method to establish appropriate member strengths and the behaviour of the buildings under simulated seismic attack.

4.2.1 Structural layout and description of buildings

The six-storey frame-wall structures studied were based on the twelve storey buildings originally studied by Carter [49]. As shown in Fig. 4.4 the basic dimensions are 8 bays x 2 bays, each bay spanning

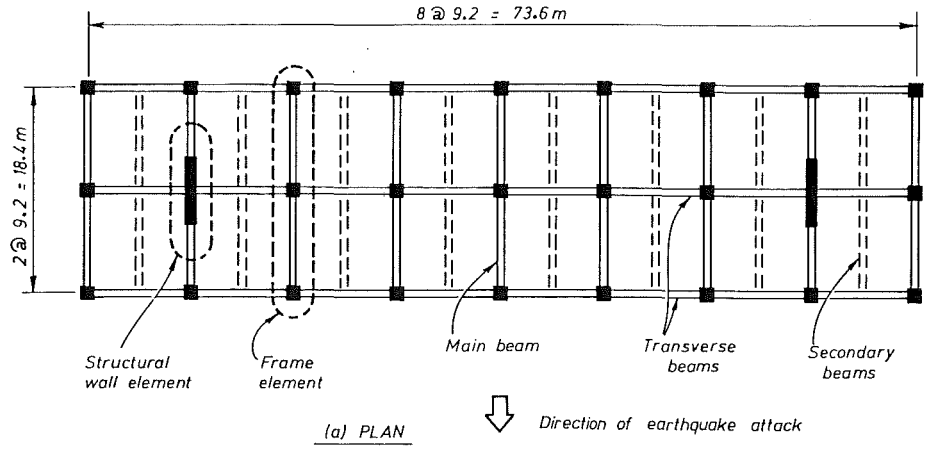

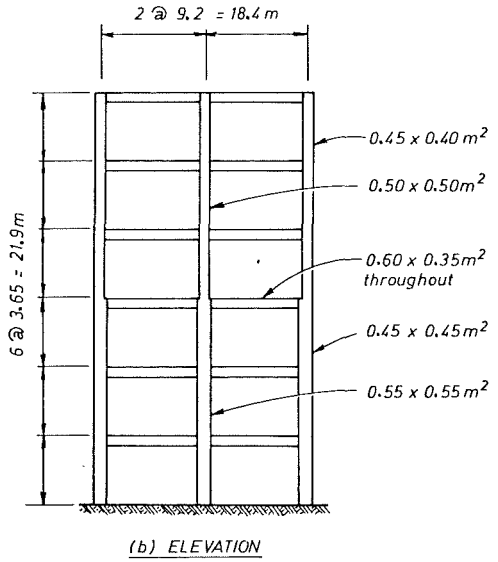

Fig. 4.4 Plan and Elevation of 6 Storey Building.

9.2 m, with a constant floor height of 3.65m. All beams (main, secondary and transverse) have dimensions 350 x 600 mm, and a slab thickness of 160 mm was used throughout the buildings. The two buildings studied

have a constant frame component, with variation in stiffness distribution between frame and wall elements provided by varying the structural wall dimensions as indicated in Table 4.1. Simplified loading, as detailed in the subsequent section, was assumed for the buildings which themselves should be viewed as representative of a class of structures rather than prototype buildings. The buildings are identified subsequently by reference to the size (ℓ_w) of their structural wall component. e.g. 2 m walled buildings.

TABLE 4.1 : DIMENSIONAL VARIATION OF STRUCTURAL WALLS USED IN THE SIX STOREY BUILDINGS

		2 m Walled Structure	4 m Walled Structure
Floors 1 - 3	ℓ_w (m)	2.00	4.00
	b_w (m)	0.50	0.40
Floors 3 - 6	ℓ_w (m)	2.00	4.00
	b_w (m)	0.40	0.30

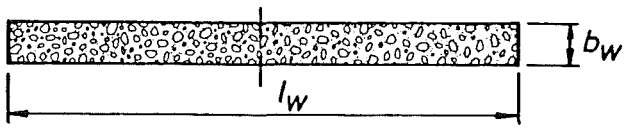

4.2.2 Design of buildings

The 6 storey buildings were designed according to the recommendations [2] formulated in the precursor to this study, differing only in the use of a Material Factor (M) for reinforced concrete of 0.8 instead of 1.0. Details of dead loading on the buildings are summarised as follows: a unit weight of 23 kN/m^3 was assumed for concrete, a distributed dead load of 0.5 kPa and unreduced live load of 2.5 kPa (as for a general office building - Table 2, NZS 4203 [9]) were assumed, and the seismic live load was taken to be 0.3 x 2.5 = 0.75 kPa$^+$.

The buildings were designed to resist a seismic base shear $V = C_d W_t$, where W_t is the total dead and seismic live loads, and C_d, the seismic design coefficient is the product of four factors - C_d = CRSM, as specified in NZS 4203 [9]. The factors are itemized as follows:

+ Seismic live load is a fraction of the specified live load assumed to be present in the event of seismic attack and is thus included in the equivalent mass.

C = Basic seismic coefficient (dependent on first mode period). The buildings were assumed to be founded on rigid to intermediate subsoils in seismic Zone A. Modal analyses were performed to establish the frequency characteristics of the buildings, and enable the basic seismic coefficients to be calculated. First mode period of vibration and seismic coefficients for the 6 storey buildings were 1.37 sec (0.075) and 1.08 sec (0.087) for the 2 and 4 m walled buildings, respectively.

S = Structural type factor = 1.0 for a hybrid wall-frame structure.

M = Material type factor = 0.8 for reinforced concrete.

R = Risk factor = 1.0 for a structure exposed to no unusual risk.

As required by NZS 4203 [9] elastic analyses for the static lateral loads specified by that Code of Practice were carried out, with member stiffnesses as shown in Table 4.2. The structural model used, and the

TABLE 4.2 : ASSUMED STIFFNESSES OF STRUCTURAL ELEMENTS IN THE SIX STOREY BUILDINGS

Property	Beams	Columns	Walls
Area	$0.5A_g$	$0.8A_g$	$0.6A_g$
Shear Area	$0.5A_v$	$0.8A_v$	$0.6A_v$
2nd Moment of Area	$0.5I_g$	$0.8I_g$	$0.6I_g$

Note: Subscript 'g' refers to gross section property.

code lateral design loads, are shown in Fig. 4.5. Standard engineering practice was used to derive this model: the two exterior and five interior frame elements were lumped into 1 frame which was coupled to the lumped wall in such a manner as to constrain the two types of lateral load resisting elements to have equal horizontal displacements at each floor level. This assumed the floor slab to be of infinite rigidity. Full base fixity of wall and column elements was also assumed. The beam-column outrigger frames in the plane of the structural walls were ignored in this lateral load analysis. The values of the shear ratio as defined in equation 4.8 were 0.47 and 0.74 for the 2 and 4 m walled buildings respectively.

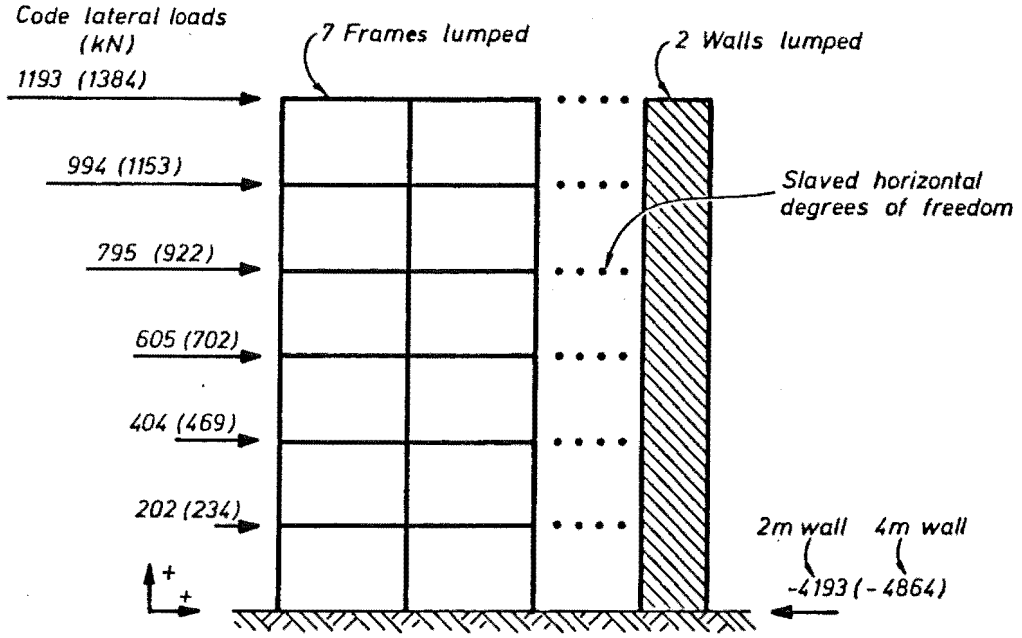

Fig. 4.5 Structural Model of 6 Storey Buildings.

Detailed flexural design only was carried out, with brief checks made as to the feasibility of providing shear and hoop reinforcement. This is in line with the capacity design philosphy used for frame-wall buildings whereby failure by any but a flexural mode is proscribed. A description of the flexural design of the frame elements and walls is presented subsequently.

4.2.2.1 Beam Design

Separate elastic analyses for gravity and static lateral (earthquake) loading were carried out. The appropriately factored [9] beam moments were superimposed in the standard manner to determine design actions. The load combination $D + 1.3L_R + E$ was generally critical, although at the first and sixth floor levels, gravity load ($1.4D + 1.7L_R$) sometimes dominated. Horizontal redistribution of beam moments (at column centrelines) was carried out, within the codified limits [34], which generally restrict the maximum allowable reduction of any moment to 70% of its original value. A vertical moment redistribution of up to 20% was then made, as indicated in Fig. 4.6 which permits the adoption of only one or two beam reinforcement configurations over the height of the building. The beams were apportioned flexural reinforcement, with dependable strength calculated as $M_d = \phi A_s f_y jd$, $jd = d - d'$; the strength reduction factor ϕ taking a value of 0.9. For all beams, f_y = 275 MPa was used.

SEE ERRATA

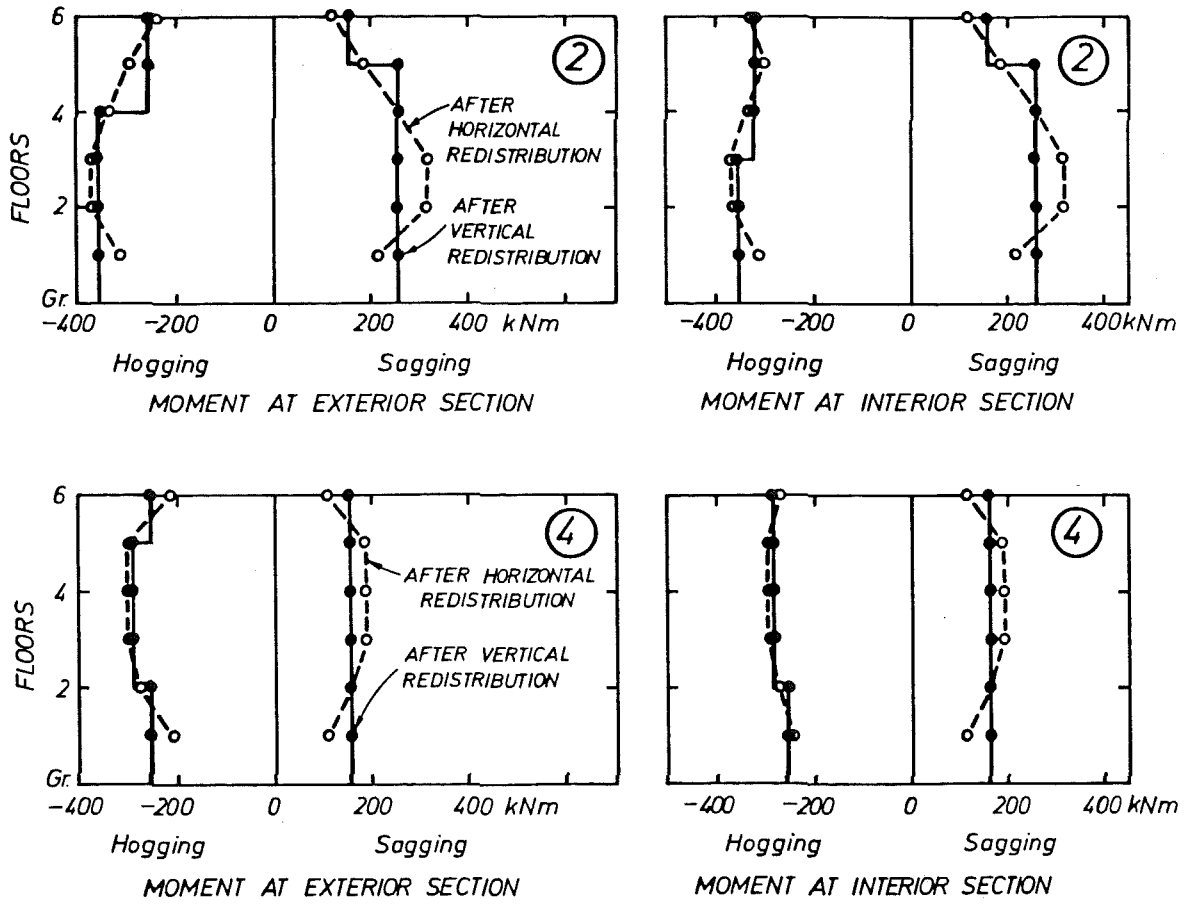

Fig. 4.6 Vertical Redistribution of Beam Moments - 6 Storey Buildings (circled numbers, used throughout, refer to wall size).

Consideration was given to practical arrangement of available bar sizes in the values of A_s used. The range in reinforcement contents used in the beams is $\rho = 0.67 \rightarrow 1.70\%$. Flexural overstrength factors (as defined in the Notation) were calculated for both directions of loading.

4.2.2.2 Column Design

The design of columns for the frame-wall structures was based on the procedure suggested for the columns of moment resisting frames given in the commentary to NZS 3101 [34]. In this approach, the code earthquake moment, M_{code}, is magnified to take account of both beam overstrength moment input and dynamic magnification. Because of the control exerted on high mode participation (and the associated dynamic magnification of member actions) by the structural walls present in these hybrid buildings, a lower value of dynamic magnification factor (ω) than that used for pure frame structures is appropriate [34]. A basic value of $\omega = 1.2$ was used in the design of these columns.

The basic equation used to evaluate the critical design column moment $M_{col,red}$ was given previously (Eq. 4.7).

Initially the factors ω and ϕ_o (as calculated in the previous section) are used to magnify the column moment determined in the static lateral analysis (M_{code}). This moment, $\omega\phi_o M_{code}$ is evaluated at the column centreline and consequently reduced (by an amount $0.3h_b V_{col}$) to give a moment occurring at the critical column section, level with the beam soffit. The value used for V_{col} is generally taken to be $1.3\phi_o V_{code}$ where V_{code} is the column shear force associated with M_{code} (see Eq. 4.1). A further reduction factor (R_m) is permitted when column axial load is low [34].

Design axial forces were also calculated in the manner suggested for beam-column frames [34]. Tributary area considerations were used to evaluate dead and live loads, while beam shear input associated with earthquake induced loading is estimated as the summation of those shear forces associated with the development of beam flexural overstrength capacity. Thus $P_{eq} = R_v \Sigma V_{oe}$, where R_v is a reduction factor which recognises the reducing probability of every beam developing overstrength shear, with distance from the top of the building. Design axial loads were $P_{e,min} = 0.9P_D - P_{eq}$ and $P_{e,max} = P_D + P_{LR} + P_{eq}$, the former generally being critical, as column axial loads were generally less than that associated with balanced failure. Critical combinations of column moment and axial load were determined, and assuming material properties of f'_c = 25MPa and f_y = 380 MPa, using interaction charts [50] to determine the required reinforcement contents. These values were rounded to the nearest 0.1%, with no detailed consideration given to the combination of actual bar sizes necessary to provide the required reinforcement content, which ranged from the code minimum [34] of 0.8% to 2.2%. Appendix B contains tables illustrating the steps in the design process used for the 6 storey building columns.

4.2.2.3 Wall Design

Flexural design of the structural wall elements was based on the linear moment envelope shown in Fig.4.2. Critical axial load on the lightly loaded base section was $P_{e,min} = 0.9P_D$, the shear input from the beams in the plane of the walls being neglected. Standard engineering principles were used to determine the required flexural reinforcement content: strength reduction factor ϕ = 0.9, extreme fibre

compression strain ε_c = 0.003, linear strain profile, inclusion of vertical web reinforcement [of area ratio approximately 0.3%] in strength calculations, etc. Only the base section was designed in detail, to check that reinforcement contents were reasonable. It was then assumed that upper levels could be supplied with flexural strength equal to the strength demand at those levels. The main (vertical) flexural reinforcement contents, expressed as $\rho = A_s/(b_w d)$ at wall base sections were 0.0123 and 0.0077 for the 2 and 4 m walls respectively. f_y = 380 MPa was used for wall design.

4.2.3 Input for Dynamic Analyses

The 2-dimensional inelastic analysis program RUAUMOKO [15] discussed earlier was used to investigate the response of the frame-wall buildings to simulated seismic attack. This program requires the following information as input data, discussed in more detail in reference 2.

1. Nodal Geometry - the geometrical position of the nodes necessary to define the structure must be provided, together with information regarding possible nodal fixity or inter-nodal coupling.

2. Member positions - the various members making up the structure are specified by reference to the nodes which bound these members.

3. Stiffness properties - for each member values of cross-sectional area shear and second moment of area are required, together with Young's and shear moduli. Values of 25 and 11 GPa were used respectively for the latter, while those properties used for the elastic analyses (Table 4.2) were assumed also for the dynamic analyses.

TABLE 4.3 : APPARENT FIRST MODE PERIODS - SIX STOREY BUILDINGS

First Mode Period T_1 - sec.	2 m Walled Structure	4 m Walled Structure
Modal Analysis	1.37	1.08
Apparent-El Centro	1.3 - 1.4	1.1 - 1.2
Apparent-Pacoima Dam	1.4 - 1.5	1.2 - 1.3

4. Strength properties - flexural strengths were supplied for all members. For beams and walls (modelled as beams with constant axial load), these are simply positive and negative moments based on the required dependable strength values as determined

in design and factored as follows:

(i) x 1.13 to estimate the probable strength of the sections

(ii) x 0.95 to compensate for the phenomenon of moment-overshoot [41].

The strength of column members was supplied in the form of a simplified moment-axial interaction diagram (Fig. 4.7). Moments on the column interaction diagram are subject to the same multipliers as were the beam strengths. Beam and column elements were given bilinear hysteretic behaviour rules, as shown in Fig. 4.8. The factor controlling post yield stiffness was taken to be 0.02 for beams and columns, and 0.03 for walls.

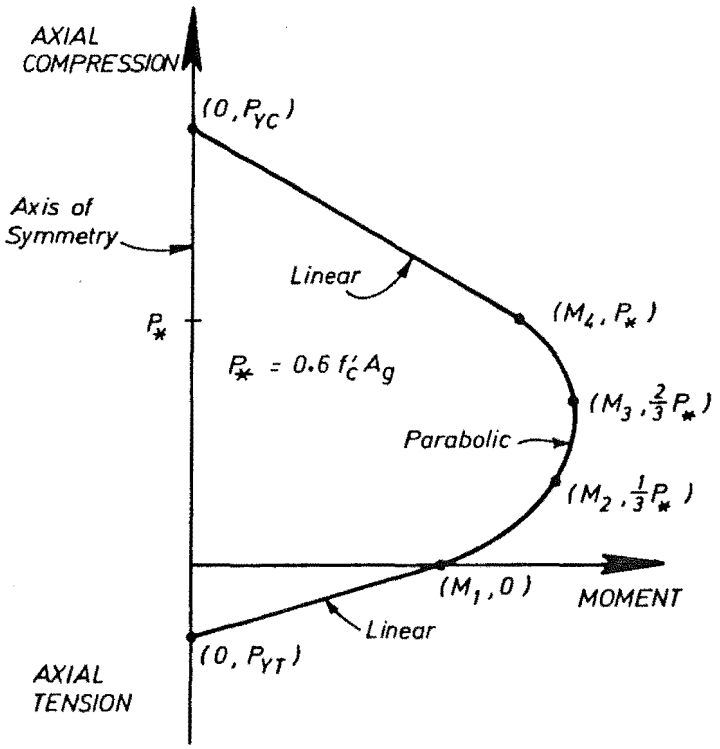

Fig. 4.7 Simplified Column Interaction Relationship.

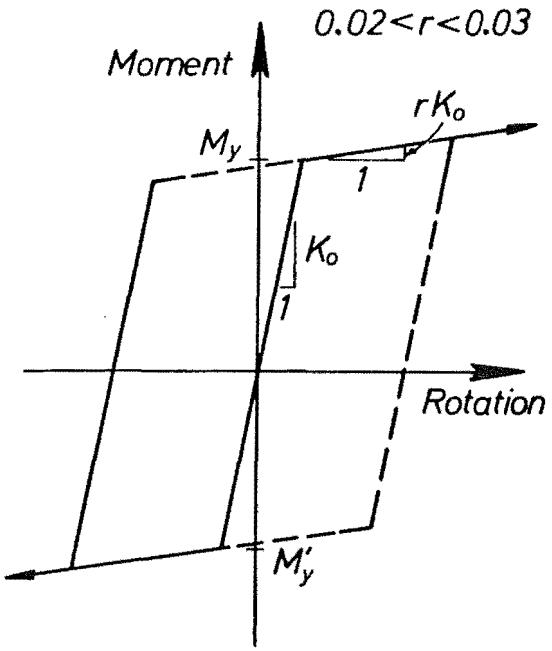

Fig. 4.8 Bilinear Hysteresis Loop.

5. Nodal masses - lumped nodal masses (and inertias for rotational degrees of freedom) are required to calculate inertia forces and moments. A tributary area approach was used to assess masses for horizontal and vertical degrees of freedom, while rotational inertias were approximated as the off diagonal term in the constistent mass matrix [40]. i.e.

$\Sigma \frac{4w\ell^3}{420}$, where w is the mass per unit length of a member of length ℓ framing into the node and the summation is made over all members meeting at the node.

6. Earthquake record - a digitized representation (in Berg format [15]) of historical earthquake records was supplied, with structures generally subjected to the first 10 seconds of strong shaking only. As discussed earlier, the two excitations primarily used in this study of frame-wall buildings were the NS El Centro 1940 and S15°W Pacoima Dam 1970 components. The former constitutes what is believed to be a credible seismic event in New Zealand, while the latter constitutes an upper bound to likely excitation in this context.
7. Miscellaneous data - these include such information as the time step (Δt) used in the numerical solution of the full equations of motion governing structural response, and a damping scheme. In the analyses of frame-wall buildings described herein, a value of $\Delta t = {}^{1}/_{100}$ sec. was generally used. A Rayleigh damping model, based on the initial stiffness and mass matrices was used to give 5% of critical damping to the first and tenth modes of vibration. The Rayleigh model interpolates values of damping for other modes of vibration on the basis of a hyperbolic curve through the two specified points. Also provided for beam members were the fixed end moments and shear forces associated with the seismic gravity load (assumed to be D + L/3) actions which are combined as appropriate with seismically induced moments and shears.

4.2.4 Response of the six storey buildings

The response of the buildings to simulated seismic attack is described by means of diagrams showing envelopes of extreme structural deformation and member actions. It should be noted that these maxima did not occur concurrently. (The results presented are relevant to a single member, not the artificial "lumped" members used in analysis). Where appropriate, comparisons are made with design level actions or code limitations [9] in the case of deformations. Comments are made as to the apparent adequacy of the design method in the light of these comparisons. It is stressed that response to the El Centro excitation is considered more relevant to the assessment of the design method, rather than response to the extreme Pacoima Dam accelerogram.

Also shown on some diagrams are envelopes relevant to frame-wall structures with pin-base walls which are discussed in Chapter 5.

4.2.4.1 Displacement response

Figure 4.10 shows time histories of the horizontal deflections undergone by the 2 and 4 m walled structures subjected to the El Centro and Pacoima Dam excitations. Maximum deflections, normalized with respect to the total building height, were 0.0071, 0.0047 (El Centro) and 0.0225, 0.0178 (Pacoima Dam) for the 2 and 4 m walled buildings respectively. The response curves to the El Centro record indicate a predominantly first mode response, the curves being approximately sinusoidal in nature. No "locked in" displacement occurred for the 4 m walled structure, while only slight permanent plastic displacements developed for the 2 m walled structure after 10 seconds of strong shaking. As would be expected, deformations due to the Pacoima Dam excitation were much larger. A greater degree of high mode participation is evident, and large permanent drifts are indicated. Apparent periods of vibration, estimated from the figures, are shown in Table 4.3 and are slightly in excess of the values calculated via modal analyses.

Envelopes of interstorey drifts, expressed as fractions of the storey height, are shown in Fig. 4. 9. Peak drifts are approximately constant above the second storey, and below the value of 0.01 for the El Centro excitation. There is no specific codified limit on permissible levels of interstorey drift for frame-wall buildings. The value of 0.01 is used as a reference value, this being the maximum value allowed [9] in buildings where nonstructural elements are separated from the lateral load resisting system. The Pacoima Dam record produced drift indices approximately two times this limit for both structures.

Although the magnitudes of structural deflections depend heavily on the assumptions made regarding member stiffnesses, it is considered that these structures demonstrated acceptable levels of deformations

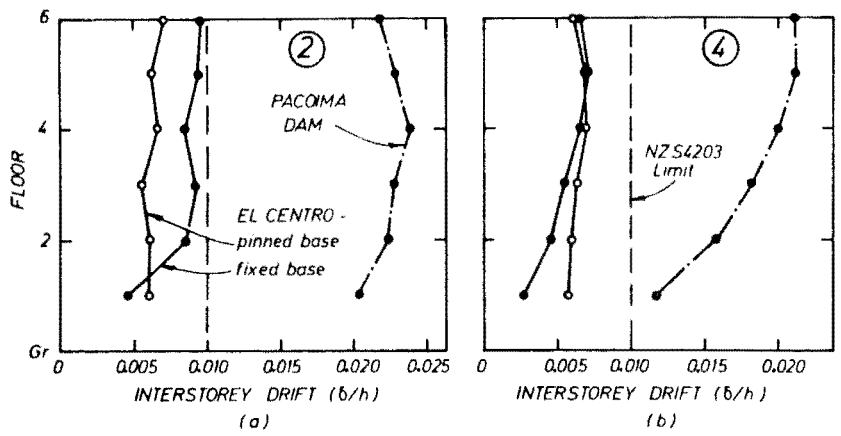

Fig. 4.9 Interstorey Drift Envelopes - 6 Storey Buildings.

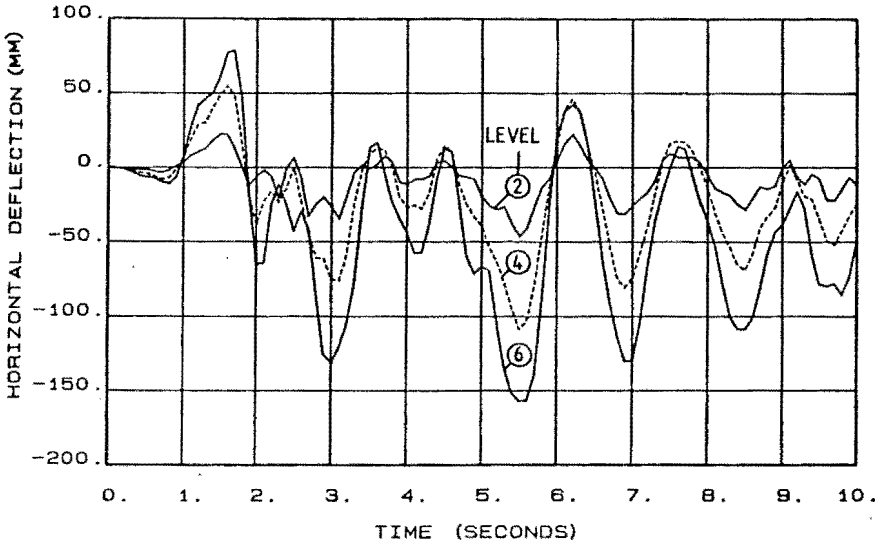

(a) 6 STOREY BUILDING 2M WALL FIXED BASE ELCENTRO

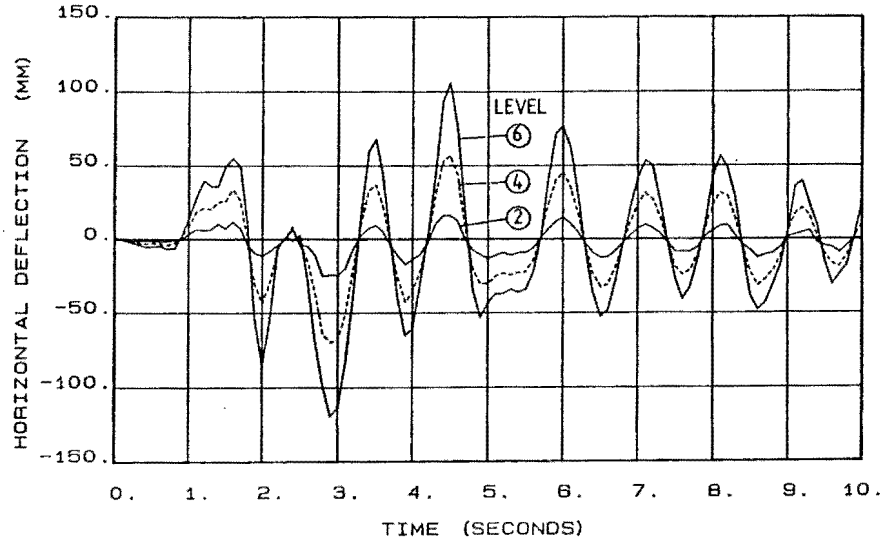

(b) 6 STOREY BUILDING 4M WALL FIXED BASE EL CENTRO

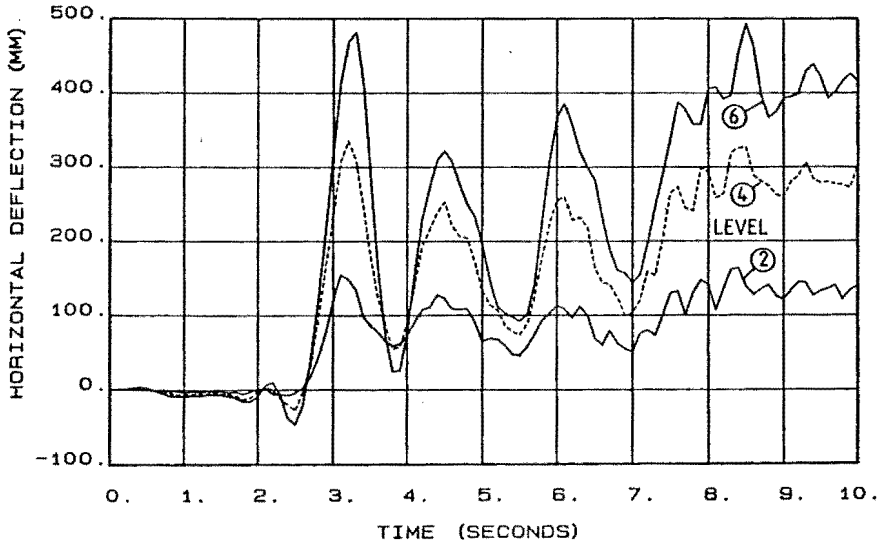

(c) 6 STOREY BUILDING 2M WALL FIXED BASE PACOIMADAM

Fig. 4.10 Horizontal Displacement Histories - 6 Storey Buildings.

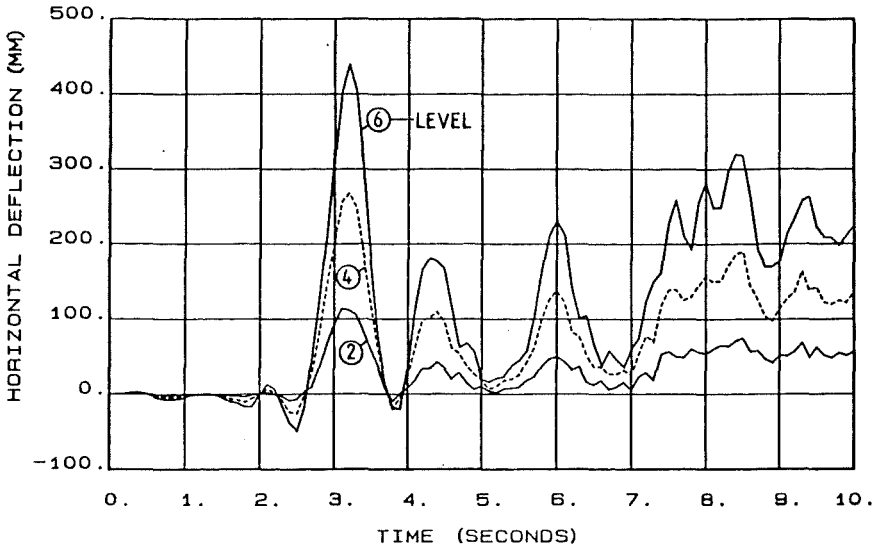

(d) 6 STOREY BUILDING 4M WALL FIXED BASE PACOIMADAM

Fig. 4.10 (Continued)

4.2.4.2 Wall bending moment

Envelopes of peak (positive or negative) moments are shown in Fig. 4.11. Yielding occurred at the base level only for both walls subjected ~~subjects~~ to the El Centro excitation. Under the Pacoima Dam excitation however, inelastic activity is indicated at most levels, although the plastic rotations involved are generally very small (see Section 4.2.4.7). These analyses indicate that the linear design envelope for wall bending moment appears to be satisfactory.

SEE ERRATA

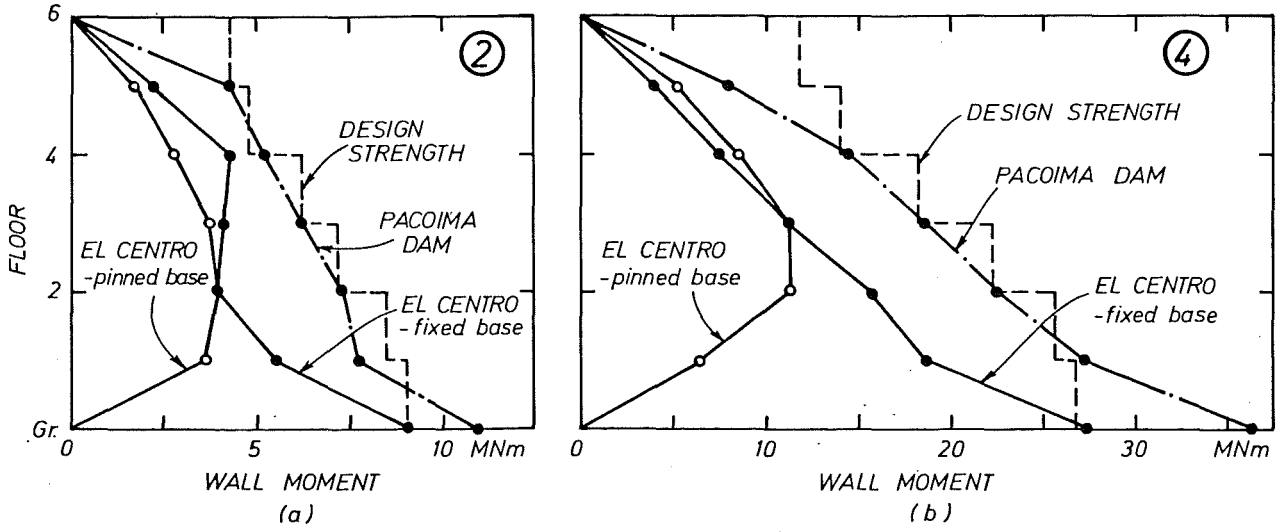

Fig. 4.11 Wall Moment Envelopes - 6 Storey Buildings.

4.2.4.3 Wall shear force

Figure 4.12 indicates that for the El Centro excitation, wall shear force levels are generally well estimated by the design method except at the most critical (base) level. For both the 2 and 4 m walled structures, the maximum recorded shear forces exceeds the design value by close to 20% for the El Centro excitation. The basic shape of the design force envelope matches the force demand well. The sign of the forces is as indicated in Fig. 4.5. Shear force levels encountered during the Pacoima Dam event are up to two times the design values. However, it should be borne in mind that the design force levels are calibrated more to an excitation of the severity of the El Centro event [2].

4.2.4.4 Column axial force

Figure 4.13 indicates the peak axial load distributions for the exterior columns only, as the interior column was subject to only small variations from the dead plus seismic live load values. The force levels recorded under the Pacoima Dam excitation are generally slightly more extreme than those for El Centro. Minimum design force levels estimated the recorded minimum forces accurately, while maximum forces were conservatively over-estimated by the design scheme.

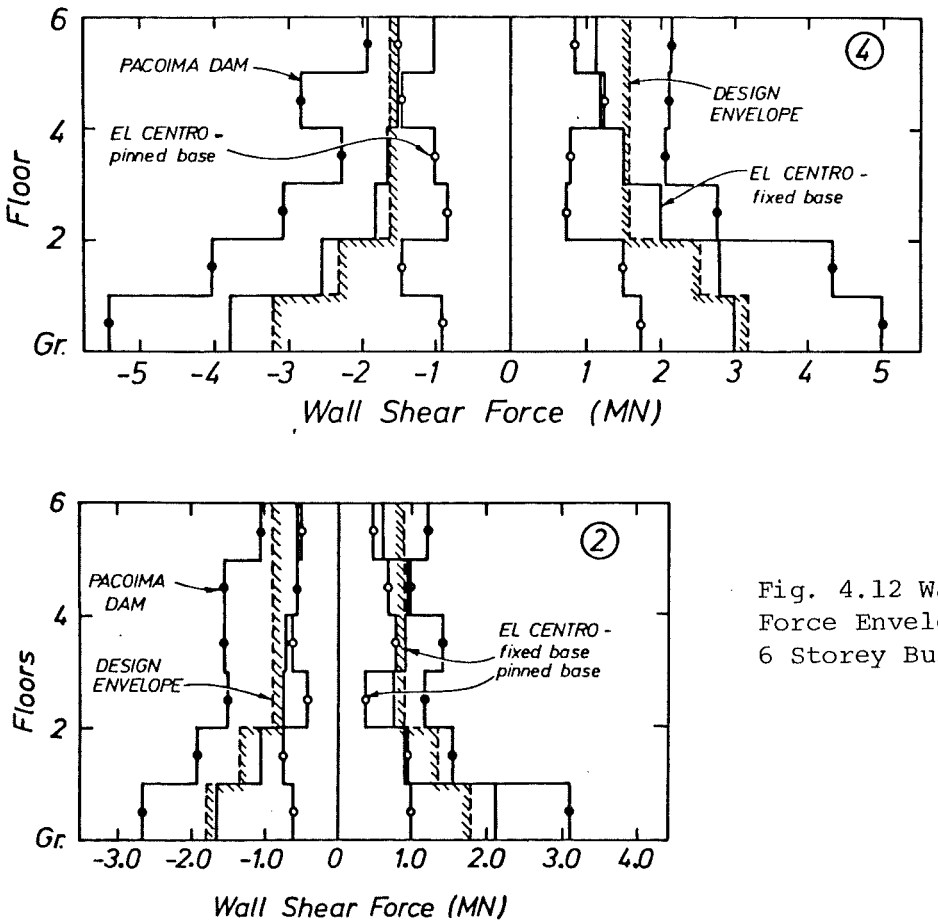

Fig. 4.12 Wall Shear Force Envelopes - 6 Storey Buildings.

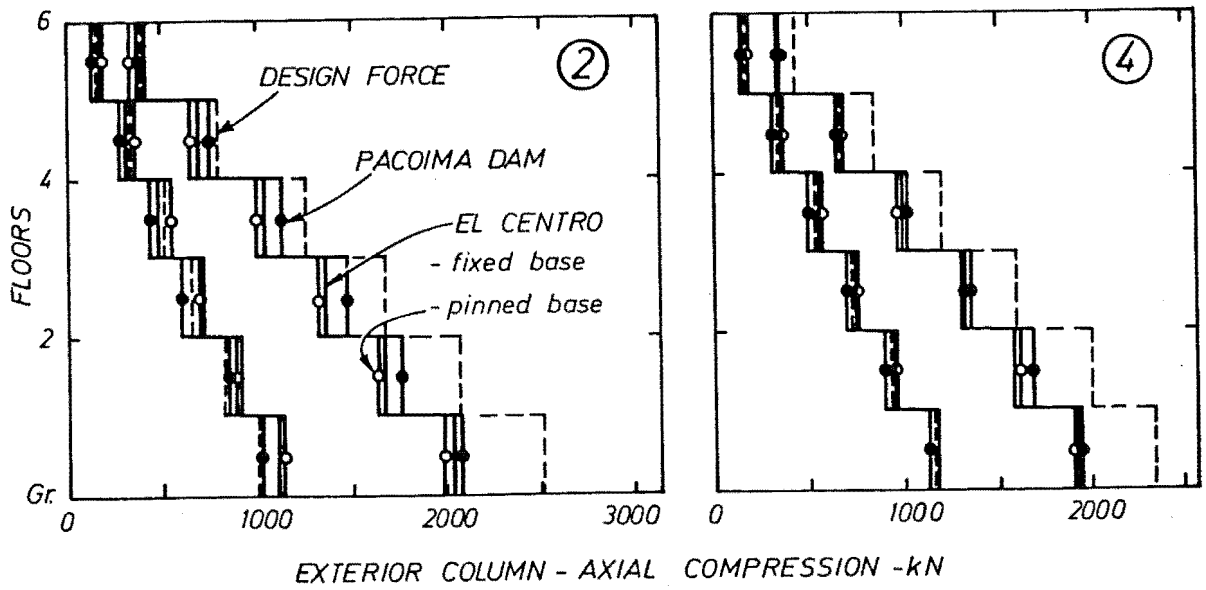

Fig. 4.13 Column Axial Force Envelopes - 6 Storey Buildings.

4.2.4.5 Column bending moment

Peak column moments recorded during both excitations are shown in Fig. 4.14. Also shown are probable member strengths, calculated as follows. The axial force in the column at the time of the maximum recorded moment was obtained and, together with the known member reinforcement content, used to calculate a column moment capacity. Column interaction charts [50] were used for this purpose. The moment capacity so determined was factored by 1.13 and 0.95 for the reasons discussed in Section 4.2.2.2, to give the probable strengths indicated in the figures.

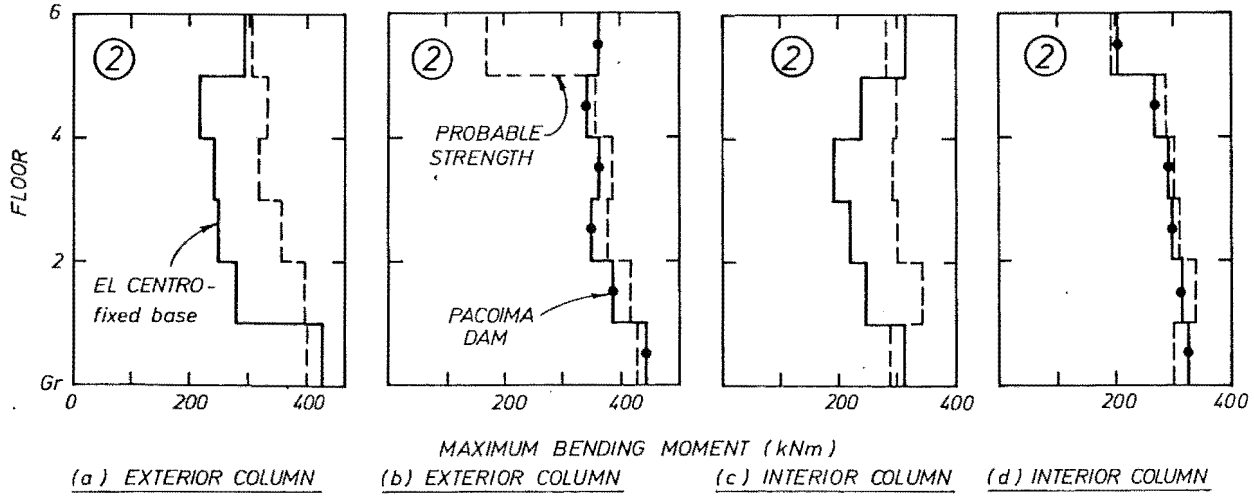

Fig. 4.14 Column Moment Envelopes - 6 Storey Buildings.

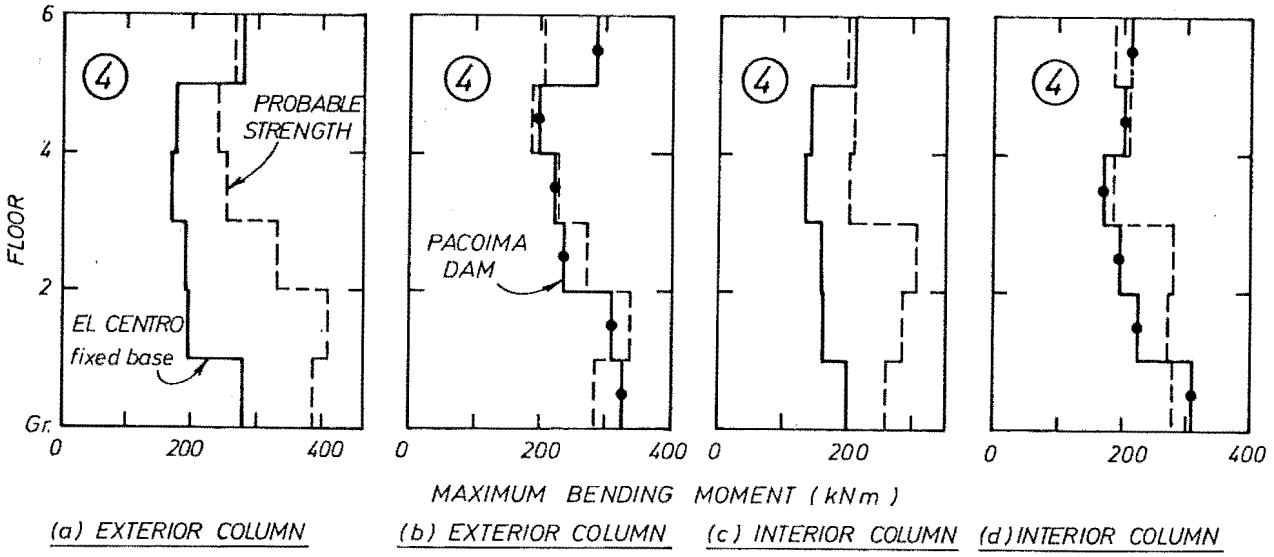

Fig. 4.14 (Continued)

As is seen for the El Centro excitation, column yield was restricted to top and bottom levels of the buildings, specifically to the top of the 6th storey columns and the bottom of the first storey columns. The protection afforded to columns, measured as the ratio of probable strength to peak observed imposed moment, (the "protection ratio"), was no less than approximately 1.20 for both interior and exterior columns, i.e. flexural strength capacities were at least 20% in excess of demands. It should be noted that this means of assessing "column protection factors" may not indicate the smallest (i.e. critical) factor. This is due to the influence of axial force on column strength, which may be such that at a moment smaller than the maximum, the probable section strength exceeds the flexural demand by a smaller degree than that indicated in Fig.4.14. However, the protection ratios suggested by this figure do indicate the general level of protection enjoyed by the columns. Under the Pacoima Dam event less protection was available, although no yielding was predicted in the 2nd, 3rd or 4th floors. The maximum protection ratio there was 1.11.

The basic column dynamic magnification factor used in design ($\omega = 1.20$) is considerably lower than that recommended for the columns of 6 storey frames [39] ($\omega = 1.75$ and 1.50 for the 2 and 4 m walled structures respectively, based on periods of vibration obtained from the modal analyses). However, this lower value appears to offer an adequate level of column protection except at ground and top floor levels, where yielding should be anticipated. At this level adequate transverse reinforcement is required [34] to ensure full hinge development.

The consequences of a "protection ratio" less than or equal to unity are not necessarily serious. Provided that adjacent beams hinge at the same time, columns will not form plastic hinges but undergo softening due to limited yielding. In addition, the duration times of column yielding are low (< 0.1 sec) and at no stage during the analysis was there sufficient yielding indicated to allow the formation of a collapse mechanism.

4.2.4.6 Column shear force

Figure 4.15 presents envelopes of maximum column shear force indicated by the analyses, and design column shears, calculated according to Step 6 of the summarised design procedure (Section 4.1.1). Observed shears are generally well estimated by the design method, although the design forces are over-conservatively large at the base

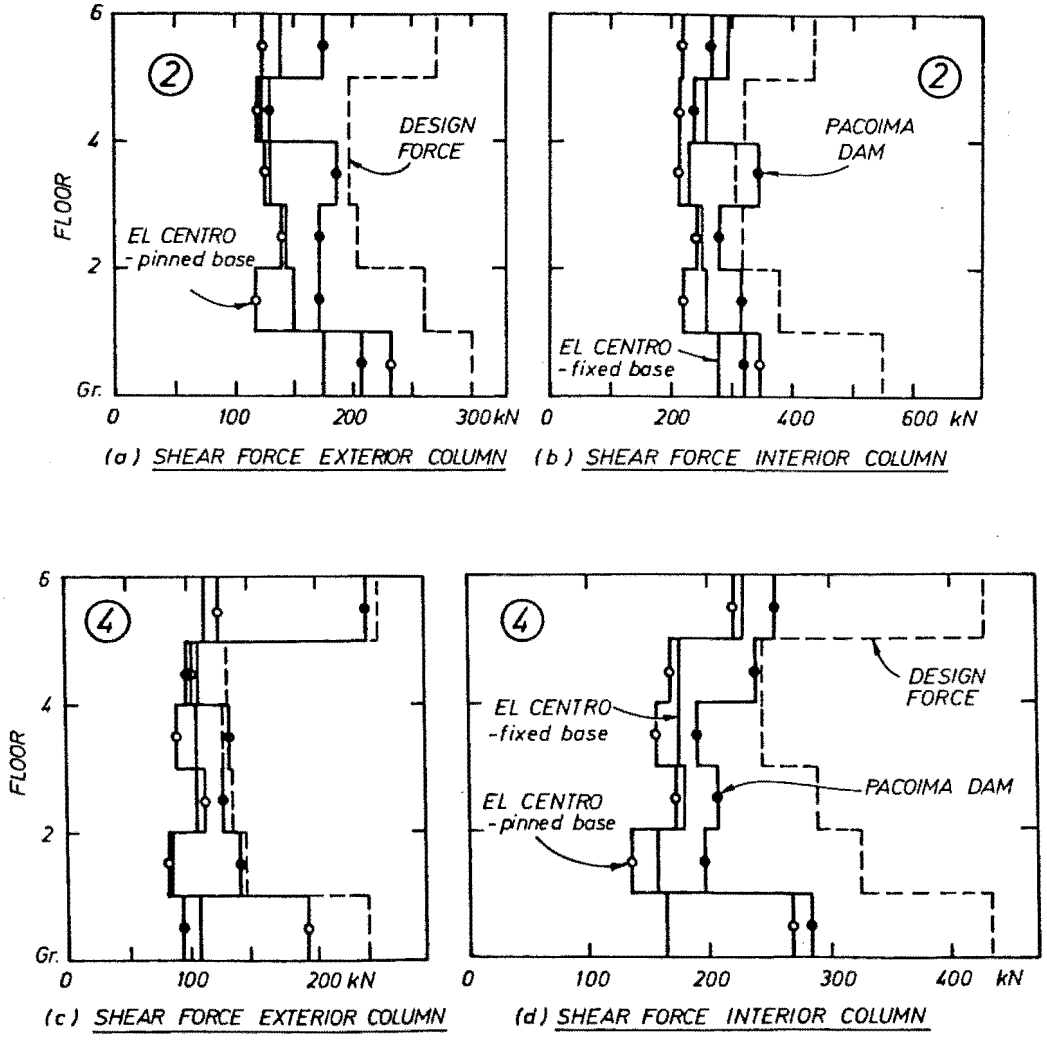

Fig. 4.15 Column Shear Force Envelopes - 6 Storey Buildings.

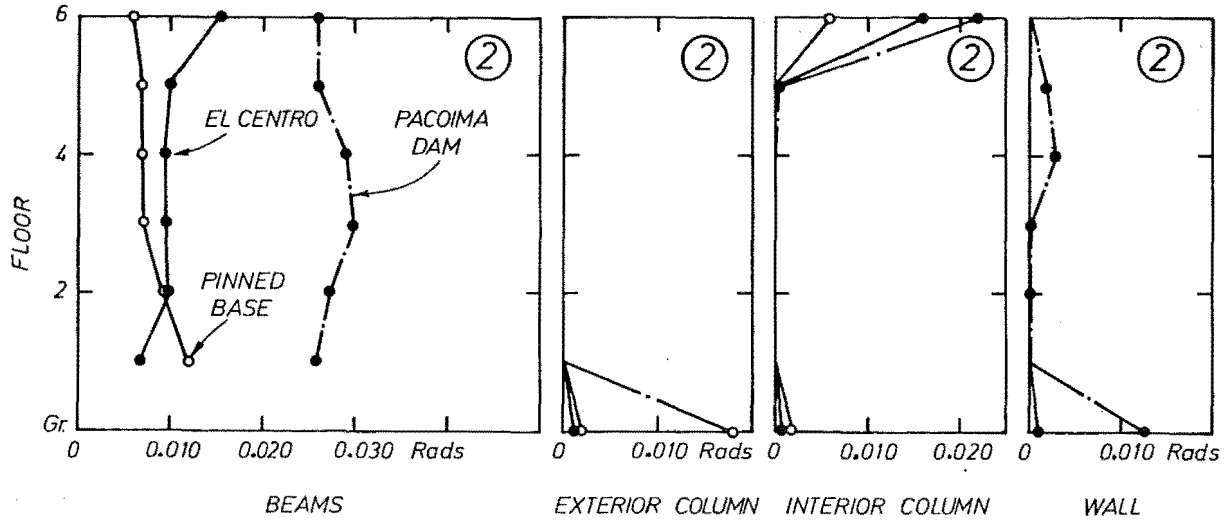

(a) Plastic Rotations - 2m walled structure

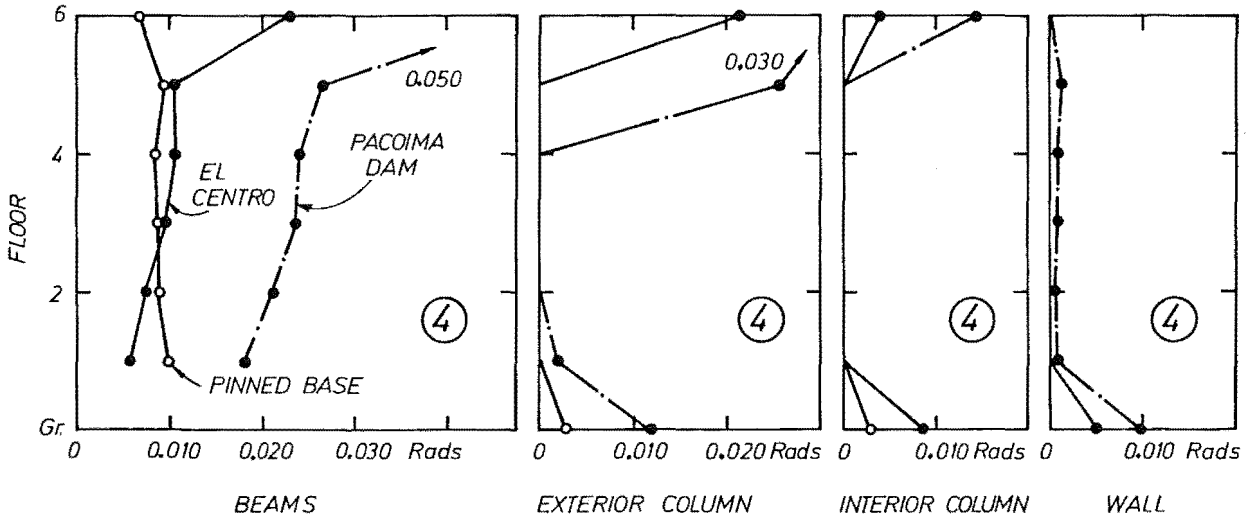

(b) Plastic Rotation - 4m walled structure

Fig. 4.16 Plastic Rotation Envelopes - 6 Storey Buildings.

and top floor levels. Levels of column shear force encountered were similar for the two accelerograms considered, with those values for the Pacoima Dam record generally slightly in excess of those for the El Centro record.

4.2.4.7 Plastic rotation demands

Envelopes of maximum (positive or negative) plastic rotations recorded for beams, columns and walls are shown in Fig. 4.16. Beam hinge rotations are approximately constant with height, at a typical value of 0.010 rads for the El Centro excitation. Rotations encountered during the more severe Pacoima Dam record were typically 0.030 rads, which is close to the value of 0.035 rads, an upper limit of rotation capacity considered [1] to be available to well detailed sections. The low levels of beam rotation observed during the El Centro excitation are taken as an indication that the moment redistribution procedure used in design is reasonable.

Plastic rotations undergone by those columns which yielded were small, generally less than 0.005 rads during the El Centro record. Such inelastic deformations are unlikely to cause significant distress to the columns. Although plastic rotation figures calculated for wall sections are of limited value, for the reasons outlined in Section 3.7.3, these are also given. Values of $\theta_p < 0.0015$ rads during the El Centro excitation, and 0.013 rads (Pacoima Dam) are indicated.

4.3 TWELVE STOREY BUILDINGS

The following section describes the computed response of three 12-storey frame-wall buildings to the NS El Centro 1940 and S16°E Pacoima Dam 1970 accelerograms. The design process used was identical to that previously described for the 6 storey buildings, with similar modelling assumptions. These are not restated in detail.

4.3.1 Structural Layout and Description of Buildings

The three twelve storey buildings studied were based on the structures originally used by Carter [49]. The buildings utilized the same floor plan as the six storey buildings discussed previously (Fig. 4.4), while a typical frame elevation is shown in Fig. 4.17. All beams (main, secondary and transverse) have dimensions 750 x 400 mm and a slab thickness of 160 mm was used throughout. Variation in the proportion of frame-wall stiffness was again achieved by holding

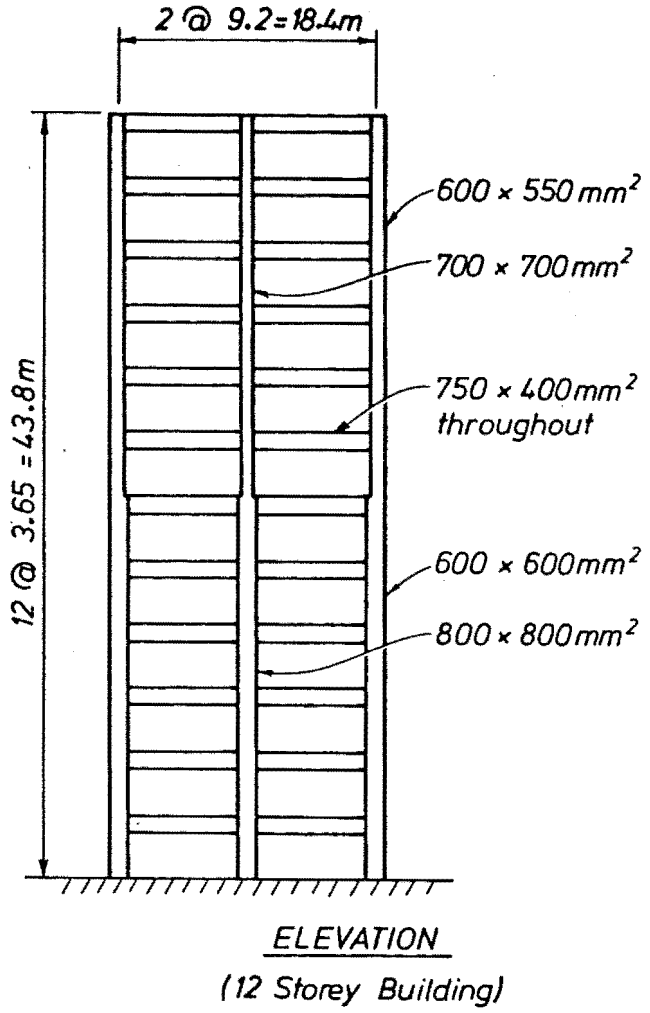

Fig. 4.17 Elevation of the Frame Component of 12 Storey Buildings.

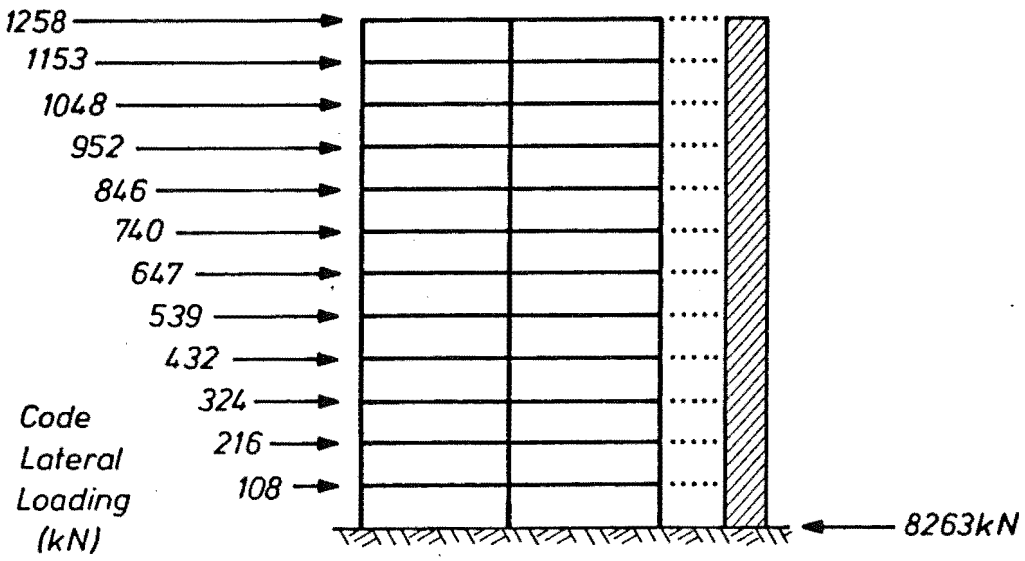

Fig. 4.18 Code Lateral Loading for 12 Storey Buildings.

constant the frame components, and varying the dimensions of the structural walls, as shown in Table 4.4. The 3 buildings are described by reference to the length (ℓ_w) of the structural walls present in them.

TABLE 4.4 : DIMENSIONAL VARIATION OF STRUCTURAL WALLS - 12 STOREY BUILDINGS

Wall		3.0 m	3.6 m	7.0 m
ℓ_w	(m)	3.00	3.60	7.00
b_w	(m)	0.50	0.60	0.50
Floors (1 - 4) b_w	(m)	0.50	0.60	0.50
(5 - 8) b_w	(m)	0.40	0.50	0.40
(9 - 12) b_w	(m)	0.30	0.40	0.30

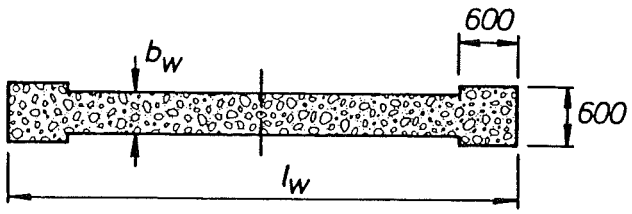

4.3.2 Design of Buildings

The 12 storey buildings were designed in an identical manner to the 6 storey buildings (Section 4.2.2). As the period of the first modes of vibration of all buildings were in excess of 1.20 sec. (see Table 4.5) the basic seismic coefficient used was C = 0.06 [9]. The static lateral loading used to establish "code" level actions for the structures is shown in Fig. 4.18. The 12 storey buildings had shear ratios (as defined in Eq. 4.8) of 0.44, 0.57 and 0.80 for the 3.0, 3.6 and 7.0 m walled structures respectively. The range in reinforcement contents required for the beams and columns was 0.56 - 1.68% and 0.80 - 1.60% respectively. As for the 12 storey buildings, f_y = 275 MPa was used for beams and f_y = 380 MPa for columns and walls.

TABLE 4.5 : FIRST MODE PERIODS OF VIBRATION FOR THE 12 STOREY BUILDING

Fixed Base Wall Unit = seconds	3.0 m Walled Structure	3.6 m Walled Structure	7.0 m Walled Structure
Modal Analysis	2.51	2.39	2.00
Apparent-El Centro	2.7	2.7	2.0
Pacoima Dam	1.6	1.6	1.7

Beam design is summarised in Fig. 4.19 which shows code earthquake moments, and combined earthquake and gravity moments ($D + L_R + E$) after horizontal and vertical redistribution, all actions occurring at column faces.

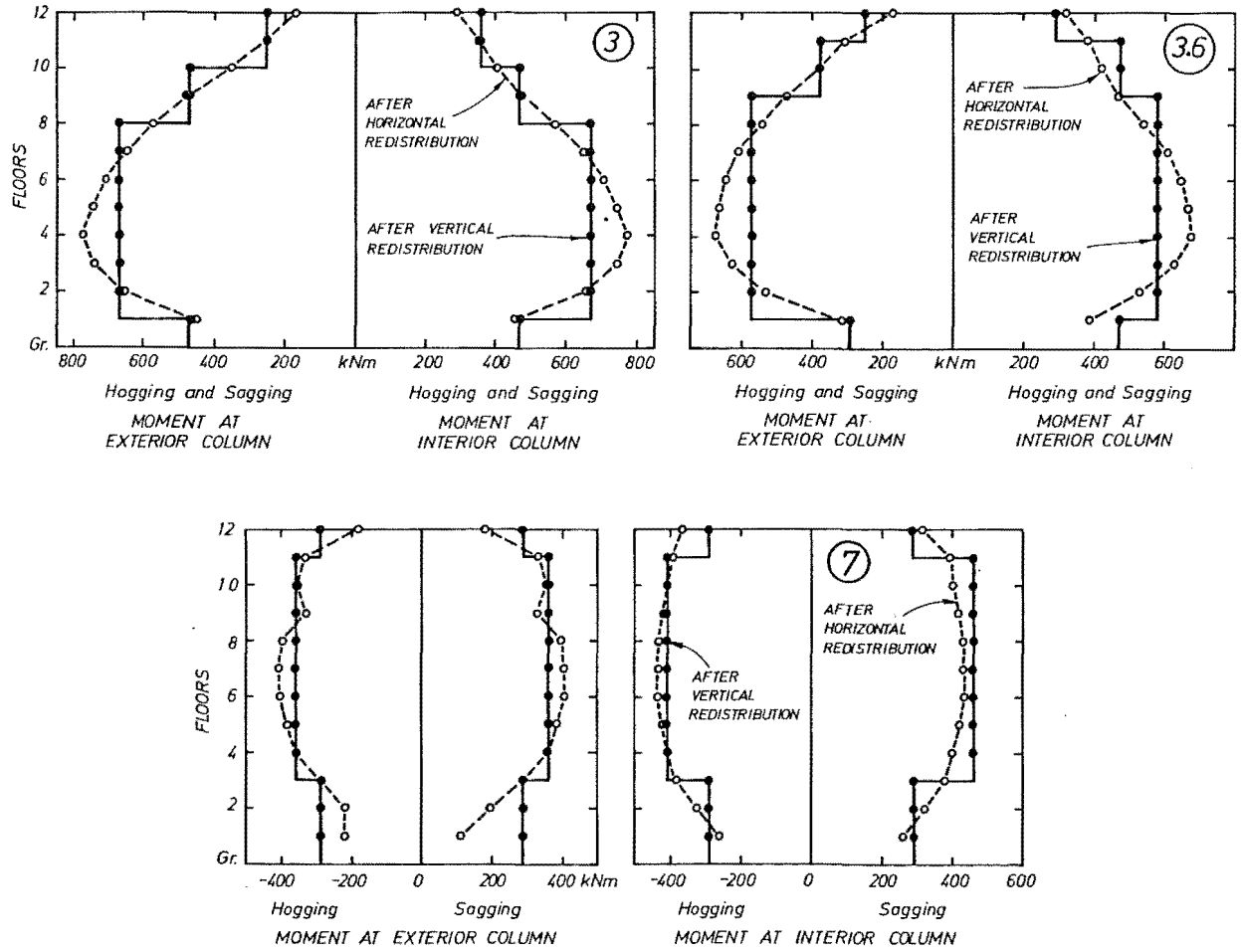

Fig. 4.19 Vertical Redistribution of Beam Moments - 12 Storey Buildings.

Appendix B contains tables illustrating the steps in the design process used for the columns. Assumptions similar to those employed for the design of the six storey structural walls were used for the 12 storey walls.

Input data for the dynamic analyses subsequently reported was similar in form to that used for the six storey buildings.

4.3.3 Response of the Twelve Storey Buildings

4.3.3.1 Displacement response

Time histories of horizontal displacement for the 3rd, 6th, 9th and 12th (top) floors of the 12 storey buildings subject to the El Centro and Pacoima Dam excitations are shown in Fig. 4.20. The displacements for the 3.0 and 3.6 m walled structures (El Centro) are somewhat different in trend to that of the 7 m walled structure, which compares more with the envelopes obtained for similar 12 storey buildings studied previously [2]. This difference is attributed to the relative sensitivity of the El Centro response spectrum in the period range of these structures. The form of the displacement curves is clearly dominated by the first mode of vibration, with approximately sinusoidal oscillation. In all 3 cases, the buildings acquire a locked-in plastic displacement or bias to the equilibrium position, although the final magnitude of this cannot be reliably estimated because of the possibility of some significant shaking after 10.0 seconds. Under the El Centro excitation the peak top floor displacements attained were 0.73, 0.78 and 0.69% of the total structural height for the 3.0, 3.6 and 7.0 m walled buildings respectively.

Lateral displacements experienced by the structures subjected to the Pacoima Dam excitation were considerably more severe, the response being dominated by the very large pulse occurring approximately 3 seconds after the record commenced. Again the structures appear to retain a locked-in plastic deformation at the end of 10 seconds of shaking. Peak recorded top floor deformations were 1.74, 1.66 and 1.51% of total height for the 3.0, 3.6 and 7.0 m walled buildings. The deflection histories for all 3 structures were similar in form and exhibit a larger degree of high mode participation than was evident in the El Centro response.

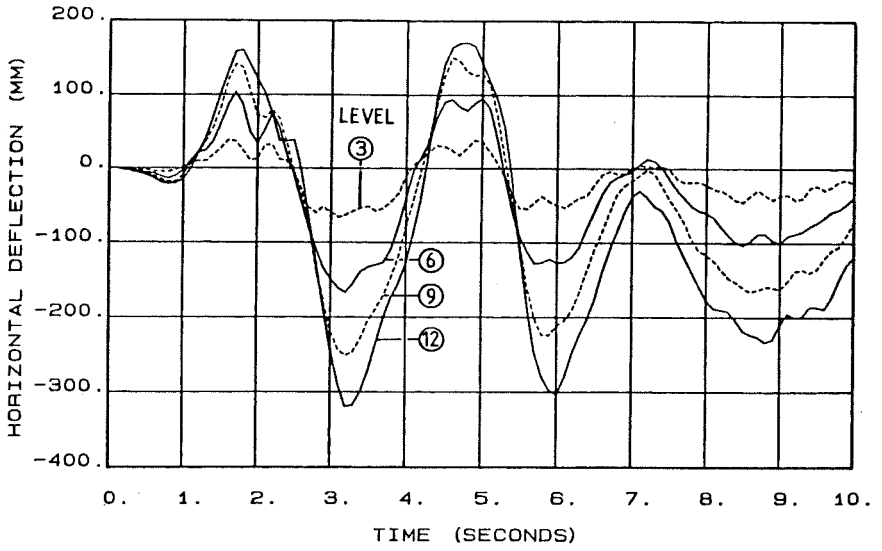

(a) 12 STOREY BUILDING 3.0M WALL FIXED BASE ELCENTRO

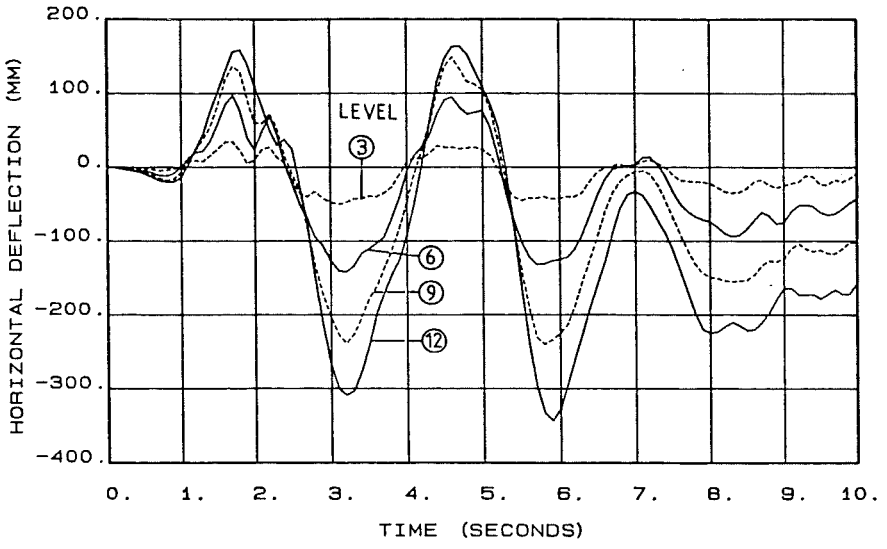

(b) 12 STOREY BUILDING 3.6M WALL FIXED BASE ELCENTRO

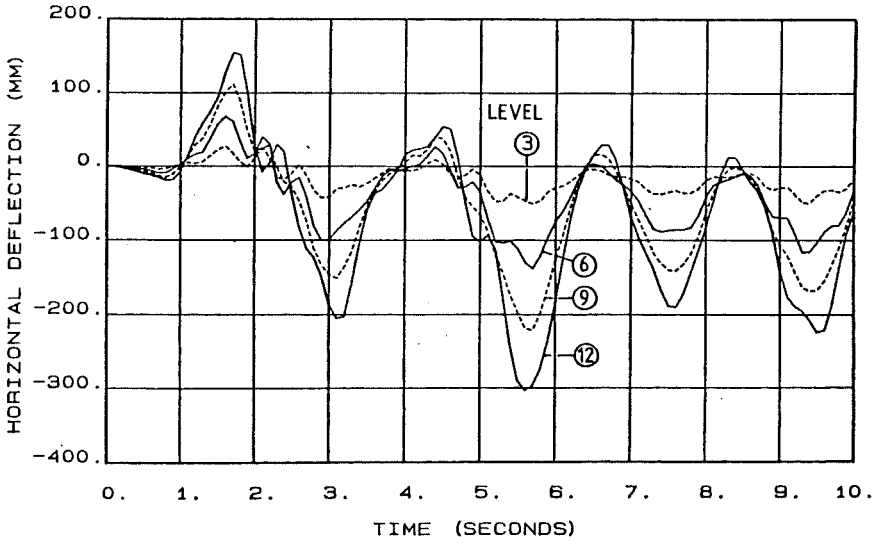

(c) 12 STOREY BUILDING 7.0M WALL FIXED BASE ELCENTRO

Fig. 4.20 Horizontal Displacement Histories - 12 Storey Buildings.

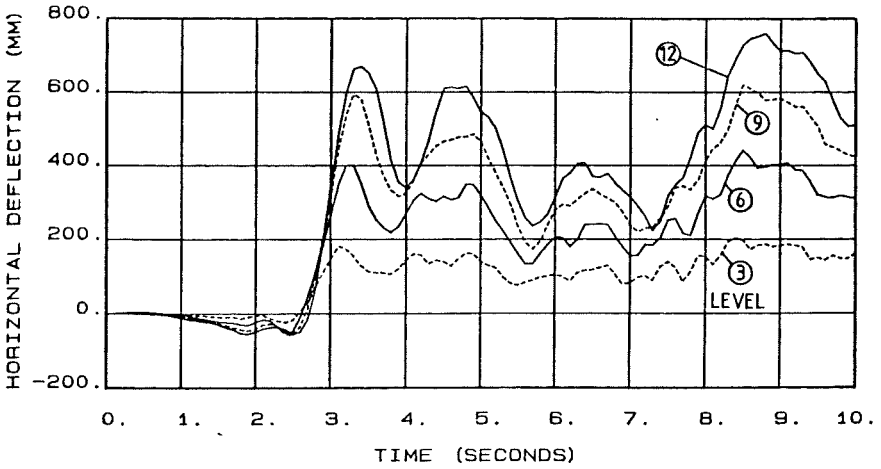

(d) 12 STOREY BUILDING 3.0M WALL FIXED BASE PACOIMA DAM

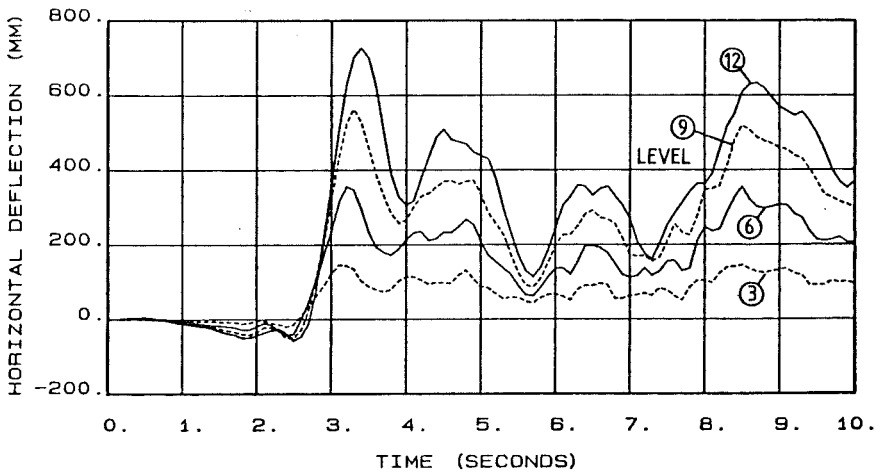

(e) 12 STOREY BUILDING 3.6M WALL FIXED BASE PACOIMA DAM

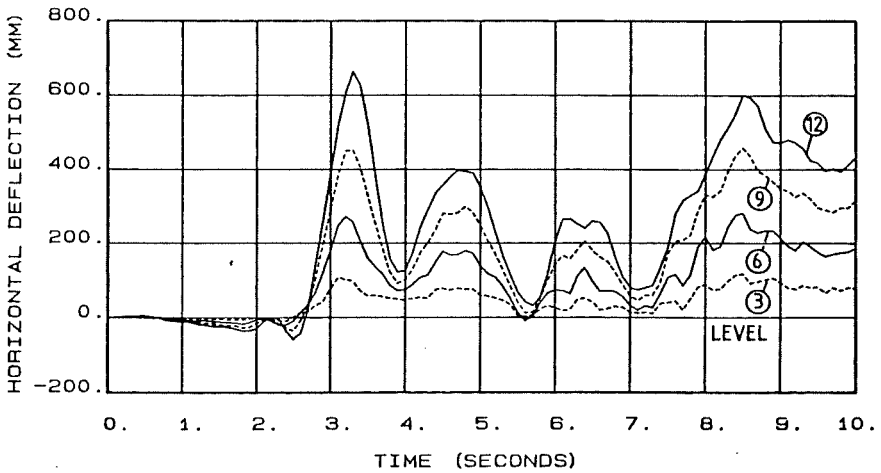

(f) 12 STOREY BUILDING 7.0M WALL FIXED BASE PACOIMA DAM

Fig. 4.20 (Continued)

Envelopes of peak interstorey drift indices, shown in Fig. 4.21, indicate that for the El Centro excitation deformations were generally less than the 1% code [9] limit for frame structures. Drifts were approximately constant over the top half of the structures, decreasing to close to half of that value at the first floor level. Drifts indicated by the Pacoima Dam analyses suggest that the buildings would

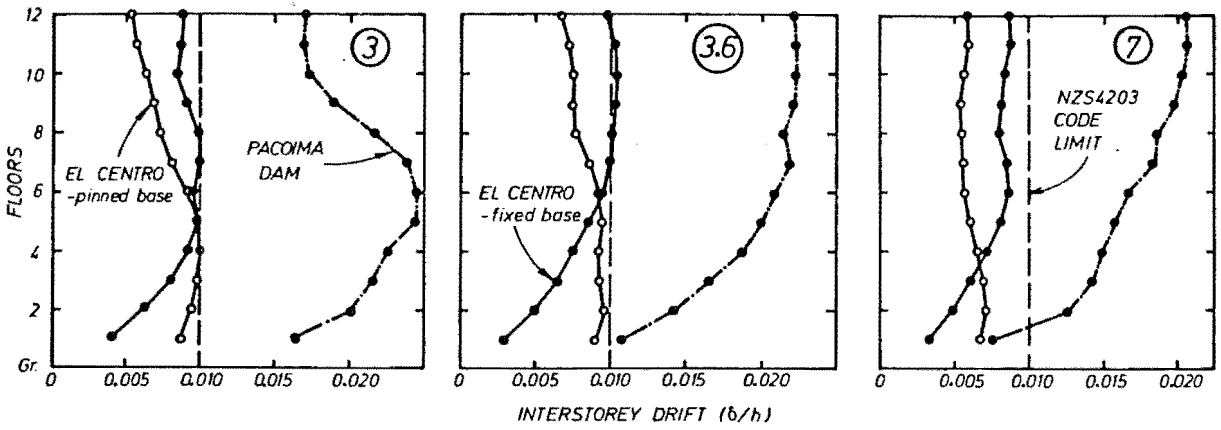

Fig. 4.21 Interstorey Drift Envelopes - 12 Storey Buildings.

be damaged to a significantly greater extent than under the El Centro excitation. A comparison of these drifts with the deformations observed in a 12 storey frame building [51] similar to the frame-wall structures discussed herein may be made, although this structure was modelled assuming a lesser reduction in gross stiffness properties than used in this study. Maximum drift indices of 0.0050 and 0.019 were obtained for the frame structure subject to the El Centro and Pacoima Dam excitations respectively.

4.3.3.2 Wall bending moment

Under the El Centro excitation, wall yield occurred only at the base section of the 3.0 and 3.6 m walls. Upper floor yielding experienced by the 7.0 m wall was minimal in extent (Fig. 4.22). The linear design envelope would appear to be well suited to matching wall flexural strength demand for the El Centro level of excitation. Response to the Pacoima Dam accelerogram indicated more widespread yielding, but as illustrated in Fig. 4.27, the levels of plastic deformation demand were small. Maximum base moments exceeded the design values by a considerable

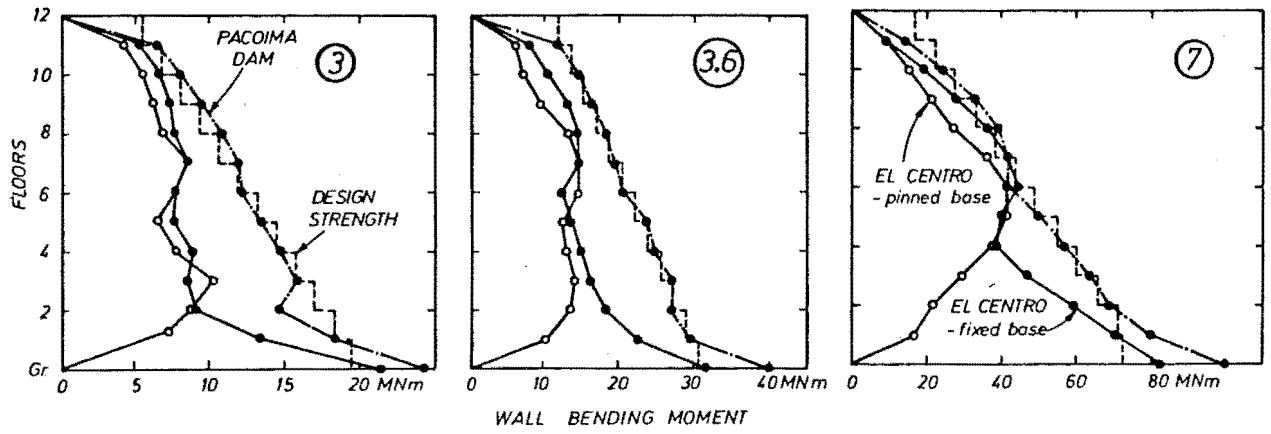

Fig. 4.22 Wall Moment Envelopes - 12 Storey Buildings.

amount for the Pacoima Dam analyses. This is attributed to the analytical model used to represent the wall base, wherein yield deformations are markedly underestimated and the relatively large inelastic rotation demand imposed on the base section causes a large apparent strength increase. This topic was discussed in Section 3.6.1.

4.3.3.3 Wall shear force

The extremes of wall shear force, together with the design envelope based on Fig. 4.3 (Section 4.1.1) are shown in Fig. 4.23. With regards the response to the El Centro record, design shear forces were exceeded at some lower levels for all three structures. Although these design forces were exceeded by as much as 40% (at the 2nd floor level of the 7.0 m wall), the design envelope generally estimated the observed El Centro shears well. Further comments regarding the levels of maximum wall shear are made in Section 4.4.

4.3.3.4 Column axial force

Extreme column axial load envelopes for the exterior column only are shown in Fig. 4.24. Good agreement between observed and design force levels may be observed, the forces associated with the Pacoima Dam excitation being slightly more extreme than those observed during exposure to the El Centro accelerogram. Variation in axial load for the interior

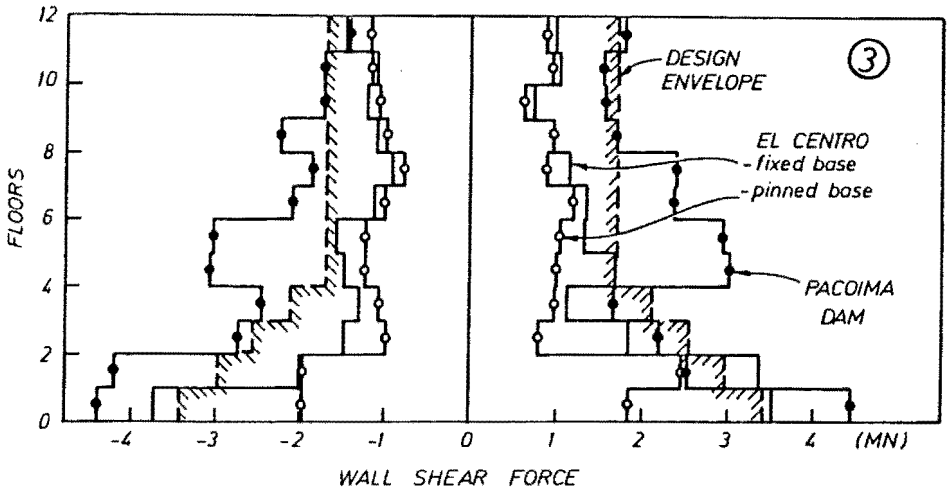

(a) 3.0 m walled structure

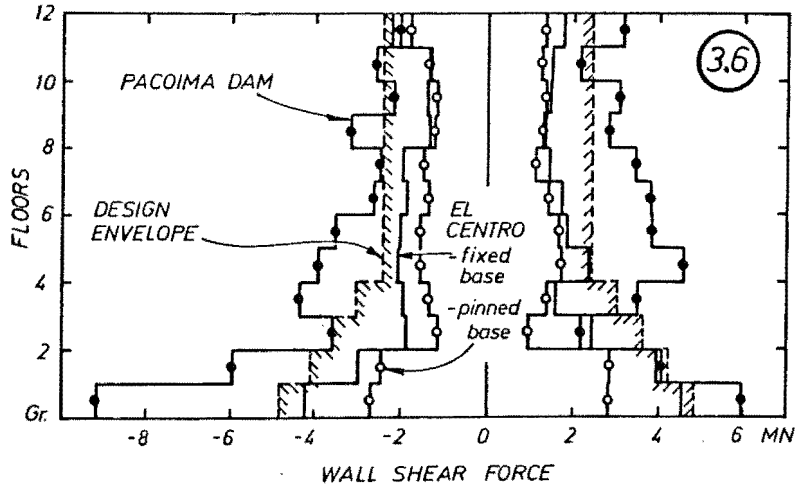

(b) 3.6 m walled structure

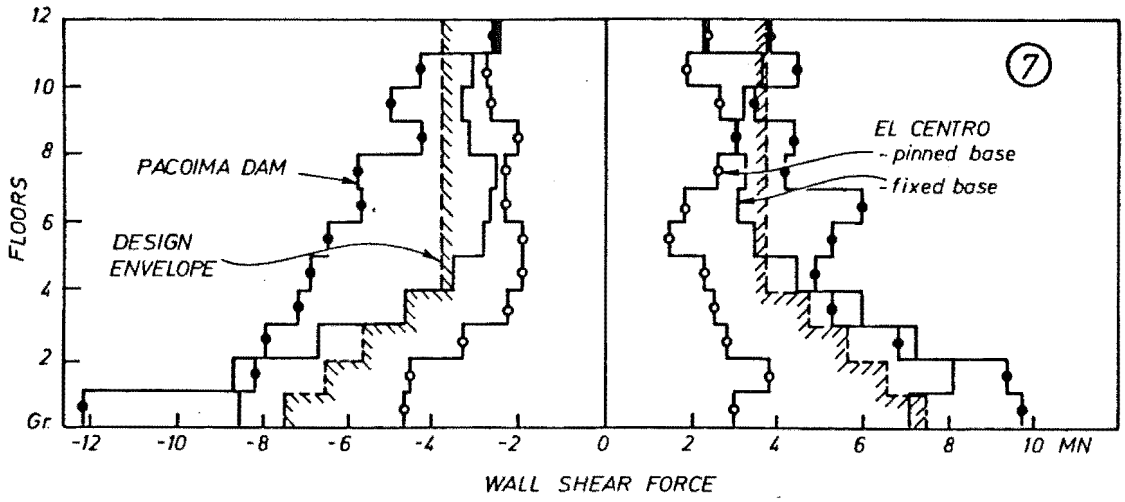

(c) 7.0 m walled structure

Fig. 4.23 Wall Shear Force Envelopes - 12 Storey Buildings.

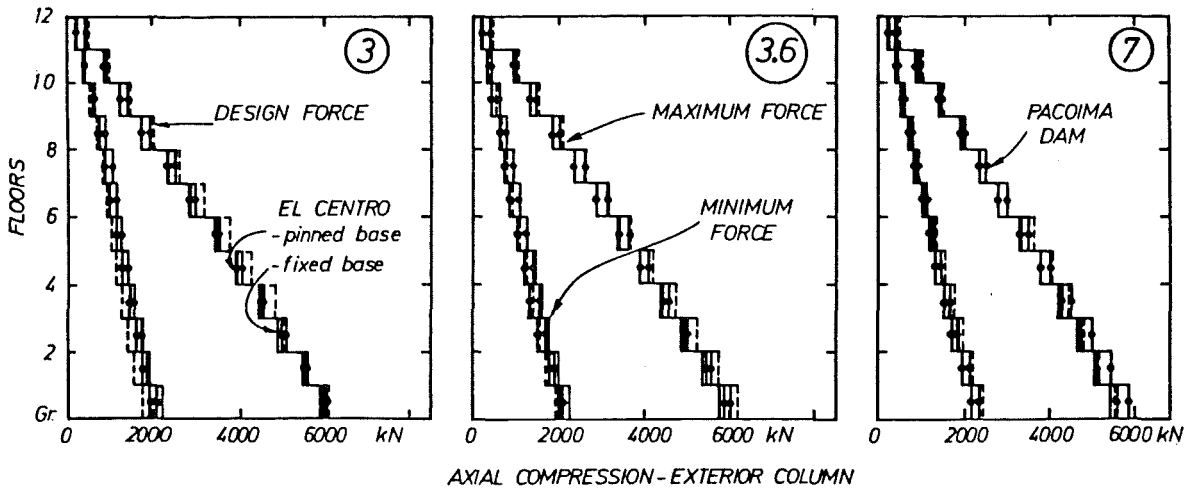

Fig. 4.24 Column Axial Force Envelopes - 12 Storey Buildings.

column was small, and hence is not shown. (Interior columns are subject to approximately equal and opposite seismically induced beam shear forces which give small variations from the gravity axial forces). Because of the dependence of column flexural strength on axial force, this latter is not of great significance when considered in isolation.

4.3.3.5 Column bending moments

The maximum observed column moments, and the probable flexural strengths (calculated at the time of the peak moment - see Section 4.2.4.5) are shown for interior and exterior columns in Fig. 4.25. Inelastic column response was restricted to ground and top floor levels. It should be noted that the ratio of probable strength to maximum moment demand cannot be obtained reliably by simply taking the ratio of probable strength to maximum moment demand. This is due to the influence of axial load on flexural strength at a point in the analysis other than when the maximum column moment was recorded. Column axial force may be such that the probable flexural strength exceeds the member demand by a smaller amount. Such a phenomenon is especially true for the exterior columns which are subject to large variations in axial load. However, checks did reveal that the degree of column protection suggested by Fig. 4.25 provided a good

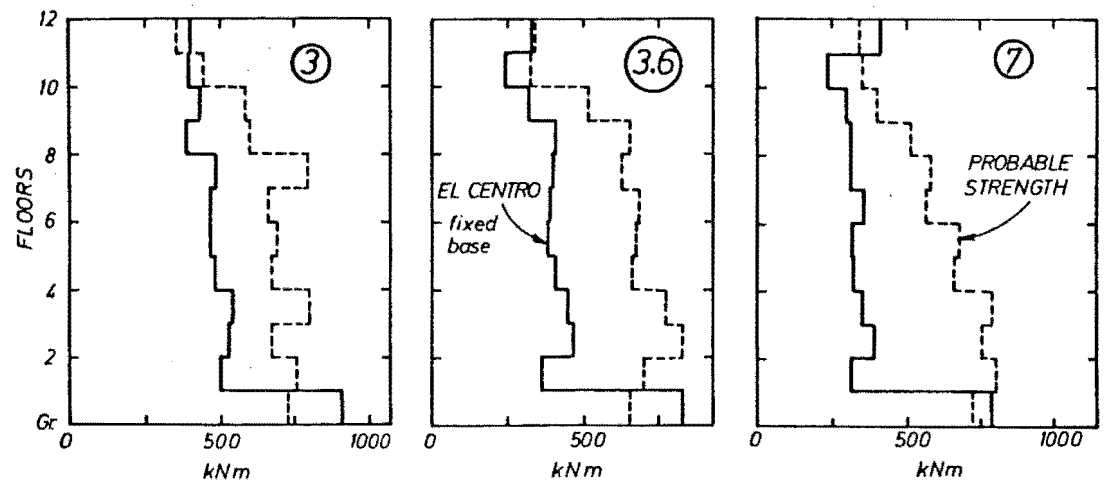

(a) EXTERIOR COLUMN - MAXIMUM MOMENT

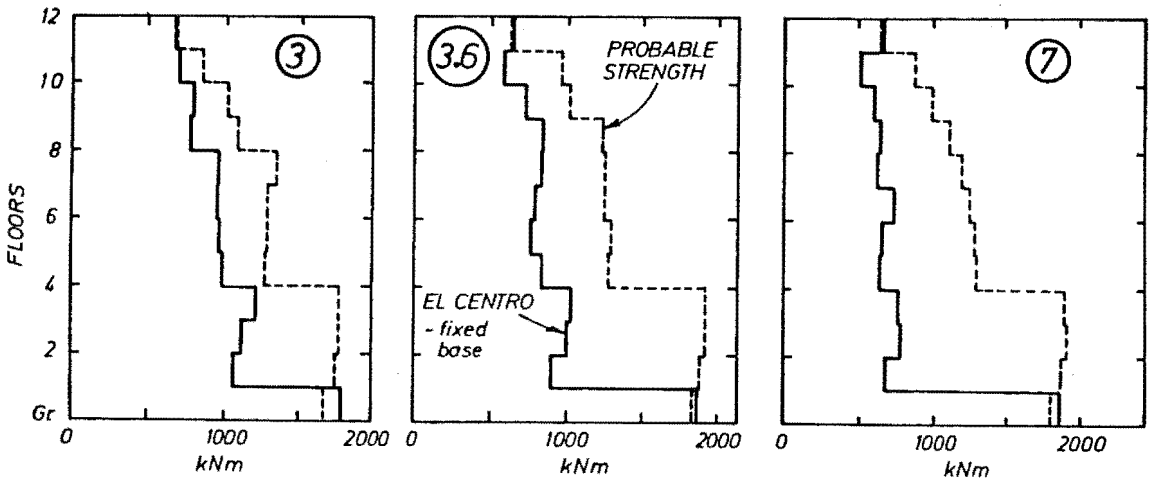

(b) INTERIOR COLUMN - MAXIMUM MOMENT

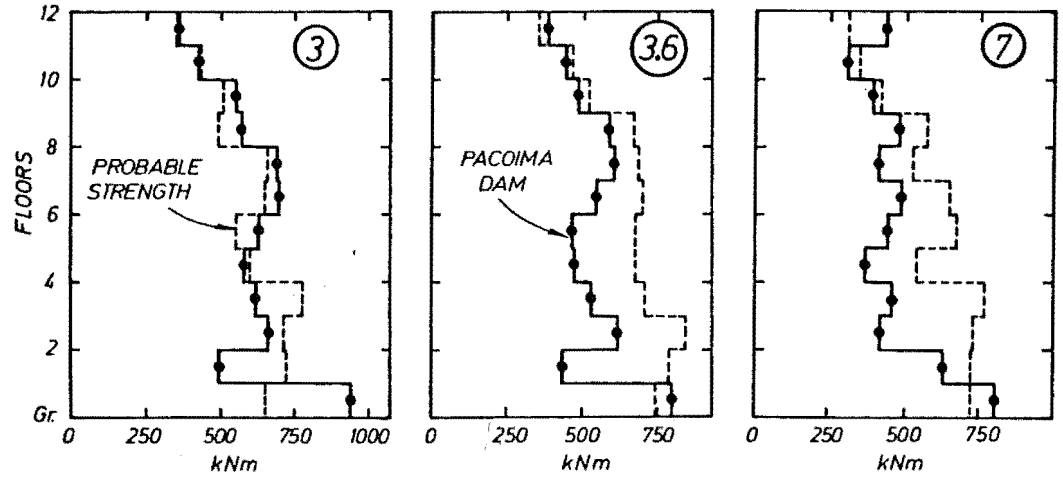

(c) EXTERIOR COLUMN - MAXIMUM MOMENT

Fig. 4.25 Column Moment Envelopes - 12 Storey Buildings.

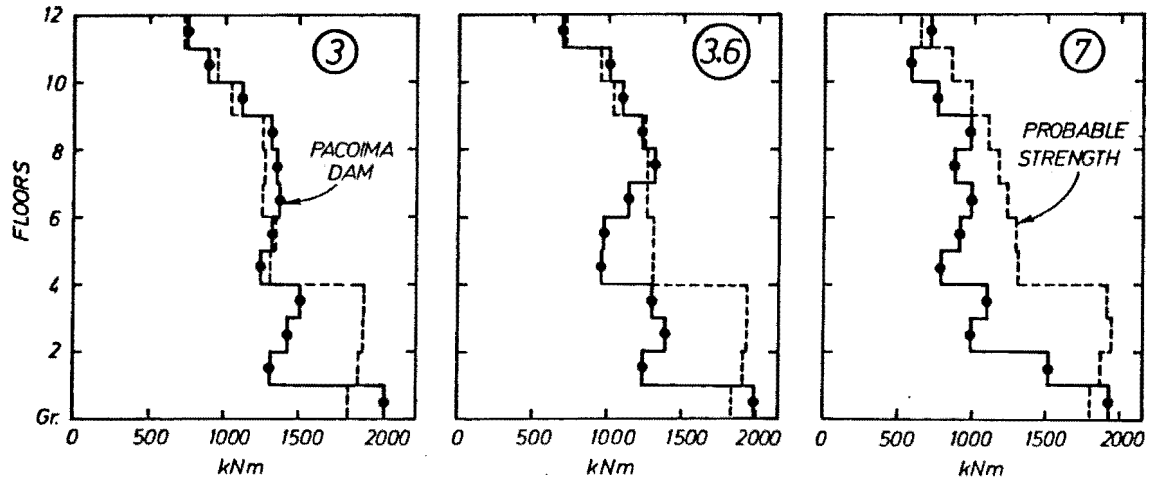

Fig. 4.25 (Continued)

indication of the margin of reserve strength with respect to plastic hinge formation. It is for this reason that moment envelopes for the two earthquake records have been presented separately. The large steps in probable strength (e.g. 3.0 m walled structure, exterior column, level 8 → level 9) generally indicate that peak moment occurred for a high axial load at one floor, and low axial load at the next. Interior columns are not generally affected in this way, and the flexural strength to demand ratios which may be deduced from Fig. 4.26 for these members do accurately reflect the protection they enjoy.

4.3.3.6 Column shear force

Levels of column shear force (Fig. 4.26) were conservatively estimated at all floors by the design forces, although the degree of conservatism at base and top floor levels was on occasions excessive. It is considered that the allocation of shear reinforcement to resist the design level forces (with allowance made for concrete shear strength where appropriate) would provide adequate protection against column shear failure. It has been shown [2] that critical tie area and spacing requirements for columns are generally governed by

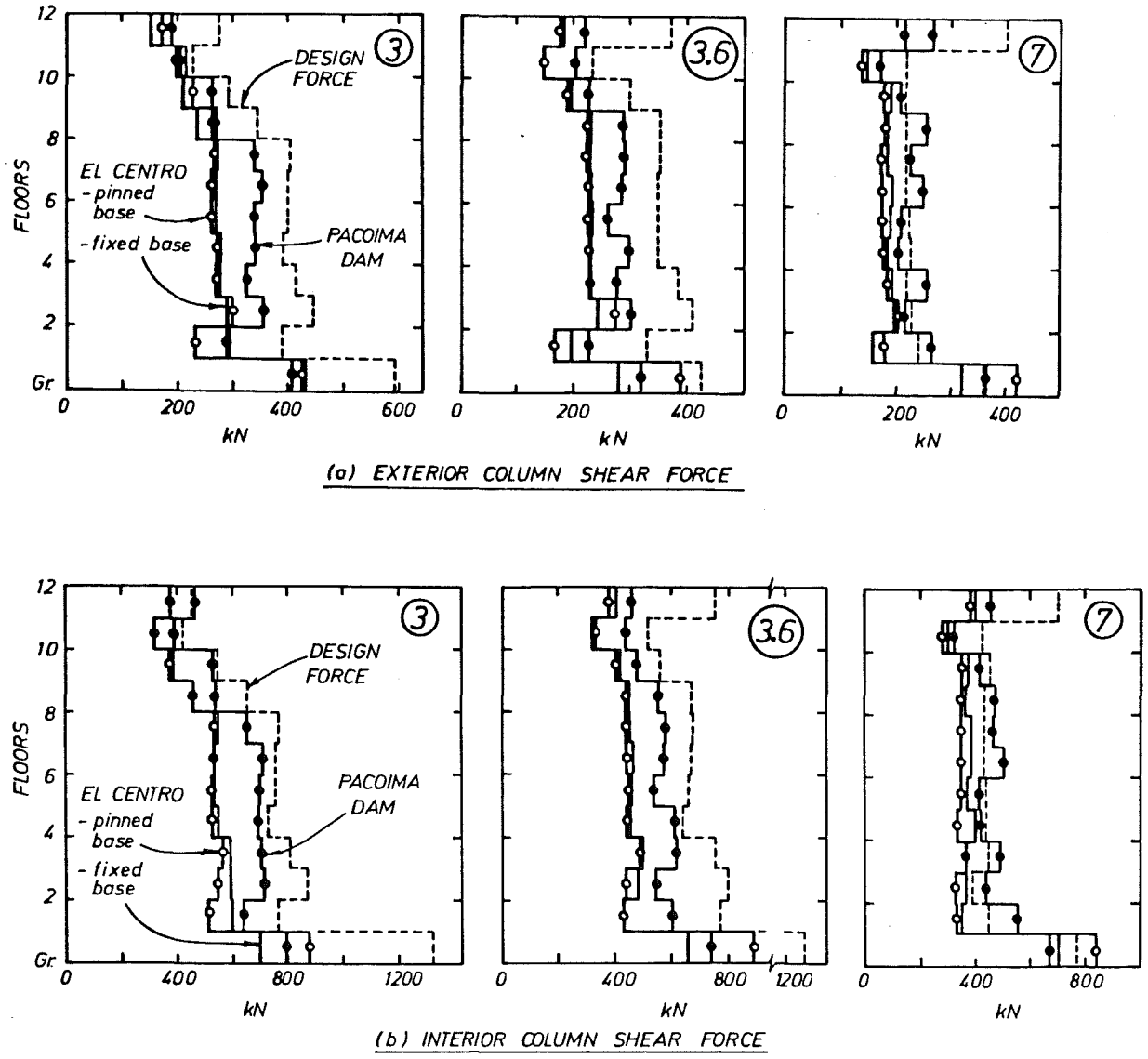

Fig. 4.26 Column Shear Force Envelopes - 12 Storey Buildings.

considerations of confinement, antibuckling and splicing of longitudinal bars rather than shear strength.

4.3.3.7 Plastic rotation demands

Plastic rotation demands calculated for the hinge zones of beam, column and wall elements are indicated in Fig. 4.27. For the El Centro excitation beam hinge rotations were generally less than 0.01 radians, well below the figure of 0.035 radians, which is taken to be the deformation level which well detailed beams can sustain [1]. These low levels of rotation are taken to indicate that the levels of moment redistribution used in design were not excessive. Higher, but still

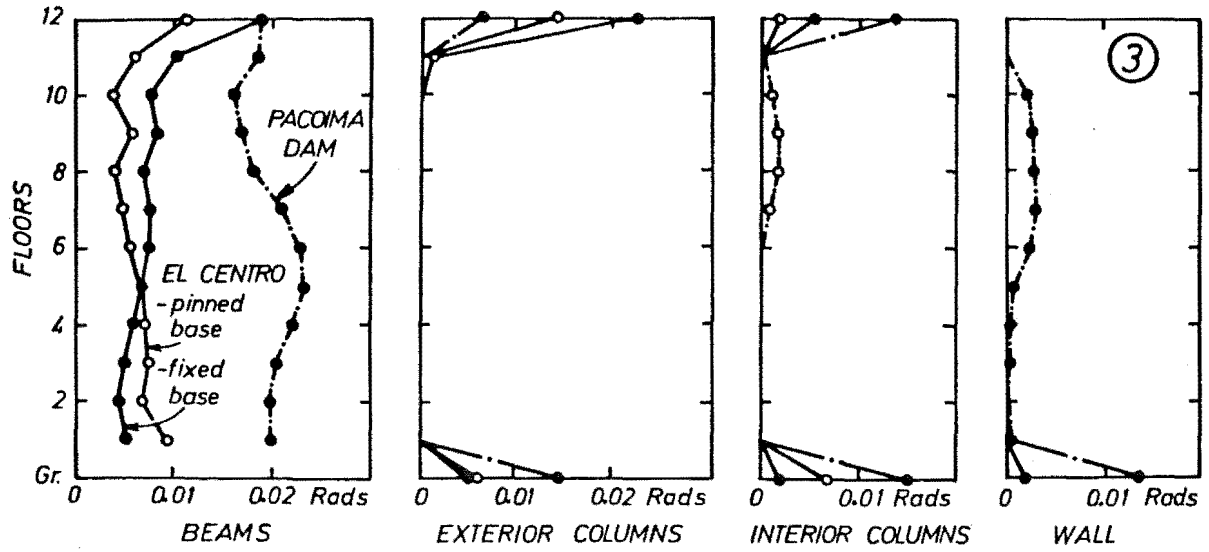

(a) PLASTIC ROTATIONS - 3.0m WALLED STRUCTURE

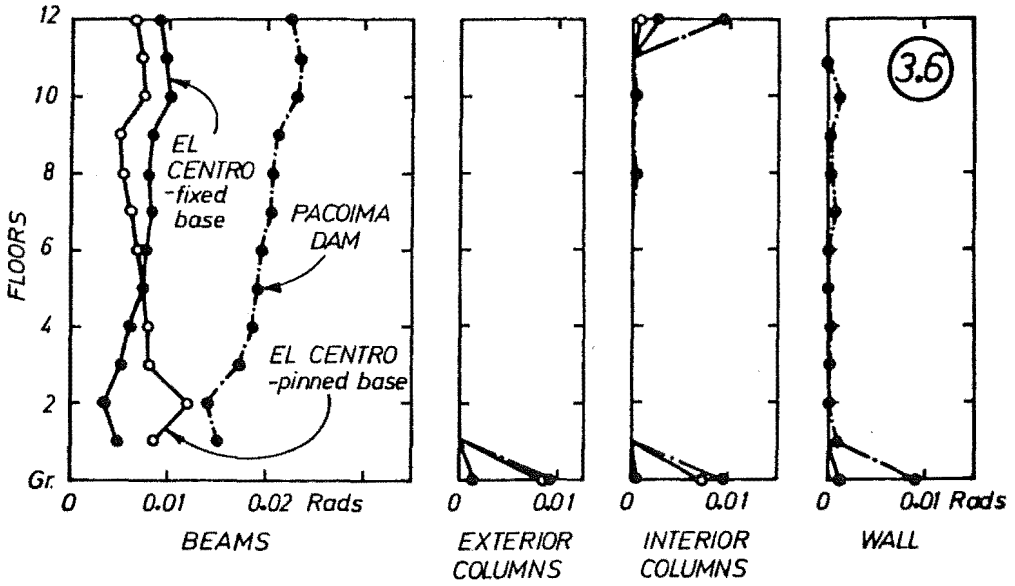

(b) PLASTIC ROTATION (RADIANS) - 3.6m WALLED STRUCTURE

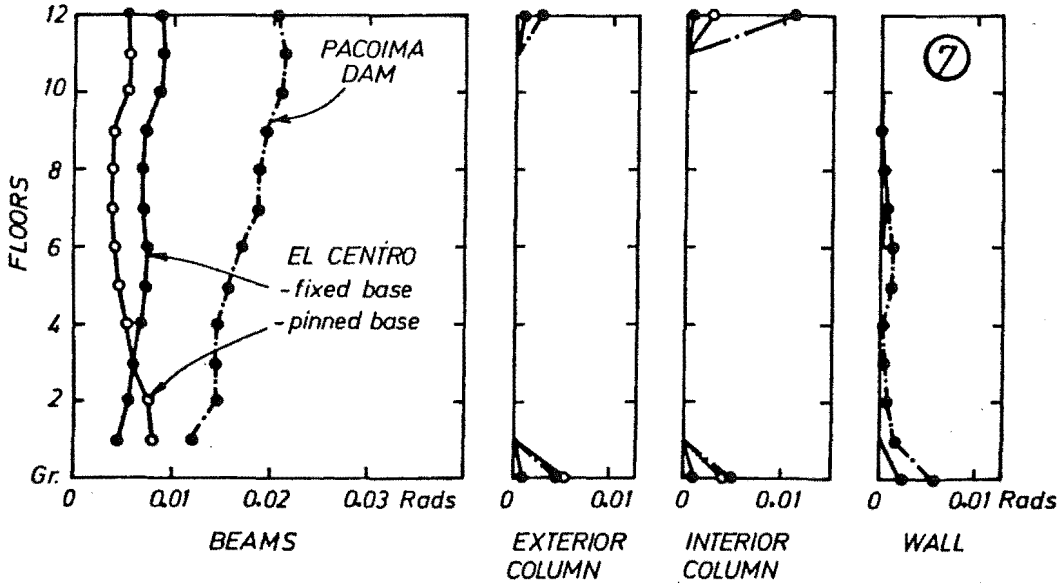

(c) PLASTIC ROTATIONS - 7m WALLED STRUCTURE

Fig. 4.27 Plastic Rotation Envelopes - 12 Storey Buildings.

sustainable levels of beam hinge deformation were indicated for the Pacoima Dam analyses. These envelopes show a uniformity of demand of inelastic rotations over the height of the structures in comparison to the envelopes predicted for "pure frame" structures [51]. This may be attributed to the influence of the structural wall elements which tend to distribute inelasticity evenly throughout the frame components of the structures.

Column inelasticity was restricted to top and bottom levels with generally infrequent and low levels of hinge rotation demands for the El Centro excitation. Base level column yielding is necessary for the formation of a full collapse mechanism, and appropriate section detailing would be provided to allow this. Although top floor column yielding is not necessary for the development of a mechanism, the analyses suggest that it should be expected, and hence the columns should be detailed for ductility. Because column axial loads are low in the upper floors, adequate ductility capacity should ensue even with the use of relatively small quantities of tie reinforcement. Top floor column yield may be due to the gain in top floor beam strength associated with the relatively large top level beam hinge rotations; that is, an effect of the modelling used rather than an indication of likely prototype response. Generally larger column hinge rotations were observed during exposure of the structure to the Pacoima Dam excitation.

Wall hinge rotations were small for the El Centro analyses, with significant inelasticity restricted to the base sections. As indicated in Section 3.6.7, care should be taken in the interpretation of wall hinge rotations determined using concentrated spring member ~~modes~~ models (as were used for these analyses). SEE ERRATA

4.4 DISCUSSION OF THE BEHAVIOUR OF THE SIX AND TWELVE STOREY BUILDINGS

4.4.1 General

The studies of the likely seismic response characteristics of 6 and 12 storey frame-wall buildings described in previous sections indicate that the previously postulated [2] design approach should ensure good aseismic performance. The primary energy dissipating mechanism, involving beam hinging, is effective while not placing

unreasonably high ductility demands on the beams. An adequate degree of protection against flexural yielding in column elements may be attained by the use of an established [34] procedure with a smaller dynamic moment magnification factor than is necessary for beam-column frame structures. Design column shear forces which require manageable quantities of transverse reinforcement and effectively proscribe shear failure, may be calculated readily. Inelastic column behaviour, which may be anticipated at ground and top floor levels, does not appear to be critical.

Structural wall elements present in the buildings may be designed in a manner similar to that advocated for cantilever walls [39]. Flexural design is based on a linear envelope of bending moment which, if matched by provided strength, will restrict significant inelastic deformations to the base of the wall.

The shear design of walls, however, should be viewed with some concern. The approach suggested involves the calculation of a base design force (Eq. 4.12) which is used to calibrate an empirically derived shear force envelope (Fig. 4.3). While the envelope closely estimates the shape of the analytically derived strength demand, it is the base shear force and in particular the appropriate magnitude of the dynamic magnification factor ω_v^*, which has not been conclusively resolved by the analyses undertaken. This factor is assumed to increase with both increasing number of storeys of the structure and an increasing structural wall content in the building. The latter is measured by the shear ratio (Eq. 4.8). Both trends are substantiated by the analyses presented. However, as shown in Fig. 4.28, the value of ω_v^* implied by the analyses, using the El Centro excitation (assumed to be more relevant to establishing "design" criteria than the extreme Pacoima Dam event), generally exceed the design ω_v^* values calculated from equation 4.11.

Despite this apparent shortcoming, and acknowledging the importance of avoiding a wall shear failure, it is believed that the level of shear strength suggested by the design scheme as previously described is realisitic. The basis for this view is presented subsequently.

4.4.2 Incidence of High Wall Base Shear Forces and Moments

The incidence of high wall base shear forces and moments was studied for the wall components of frame-wall structures in a similar manner to that used for the plain cantilever walls (Section 3.6.8). However, due to considerations of practicality and economy, it was found necessary to base this investigation on member status recorded

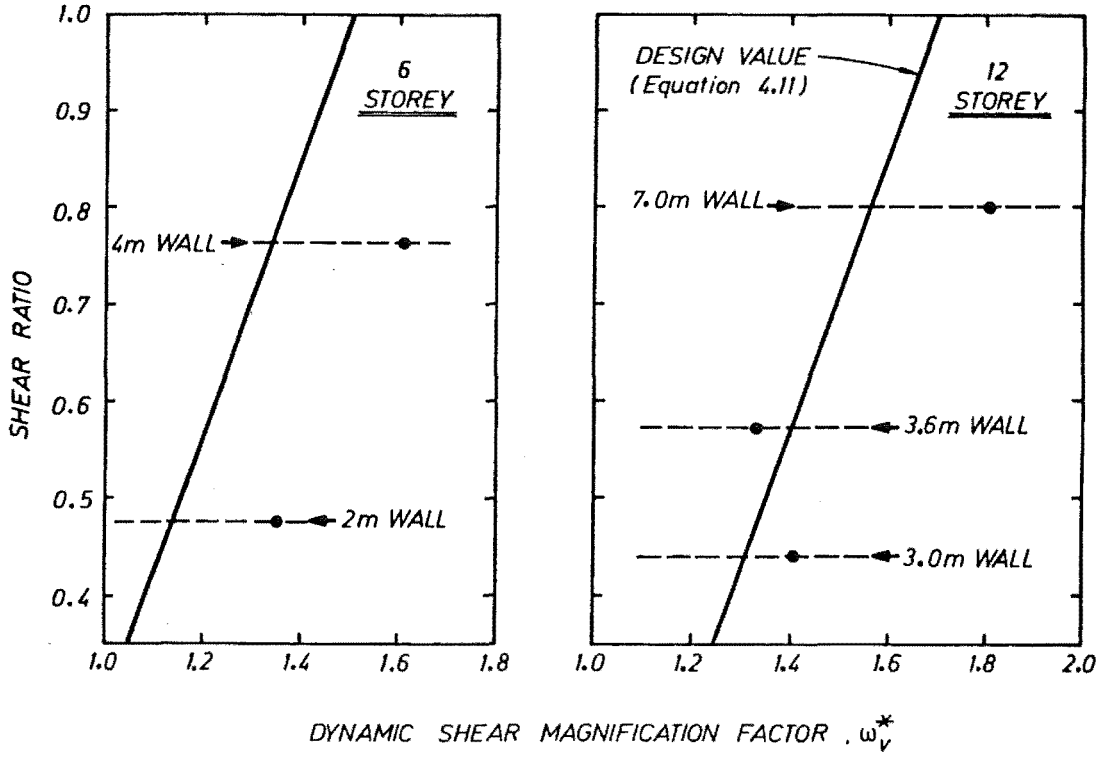

Fig. 4.28 Dynamic Wall Shear Magnification for 6 and 12 Storey Buildings.

at every 1/10 sec, although the dynamic analyses were made on the basis of calculations at a time step of 1/100 sec. Diagrams showing the frequency of occurrence of various proportions of peak base shear force, and yield moment, as well as the coincidence of these parameters are presented (Fig. 4.29). The analyses for which this information is presented are indicated on the figures. Full wall base fixity was assumed in this study. Estimated peak duration times of shear force and moment for each of the 4 intensity intervals considered are shown in Fig. 4.30. These values are also based on wall force and moment status at 1/10 sec. intervals, and interpolation as illustrated in Fig. 4.31 was used to calculate the duration times. Although this procedure is prone to inaccuracy as compared to that used for the cantilever walls, it was found that the errors involved were generally small and insufficient to affect the trends emerging from the diagrams. The horizontal axes show intervals where the recorded action (shear force or moment) exceeded 0.6, 0.7, 0.8 or 0.9 of the maximum observed values (V_{max} or M_{max}).

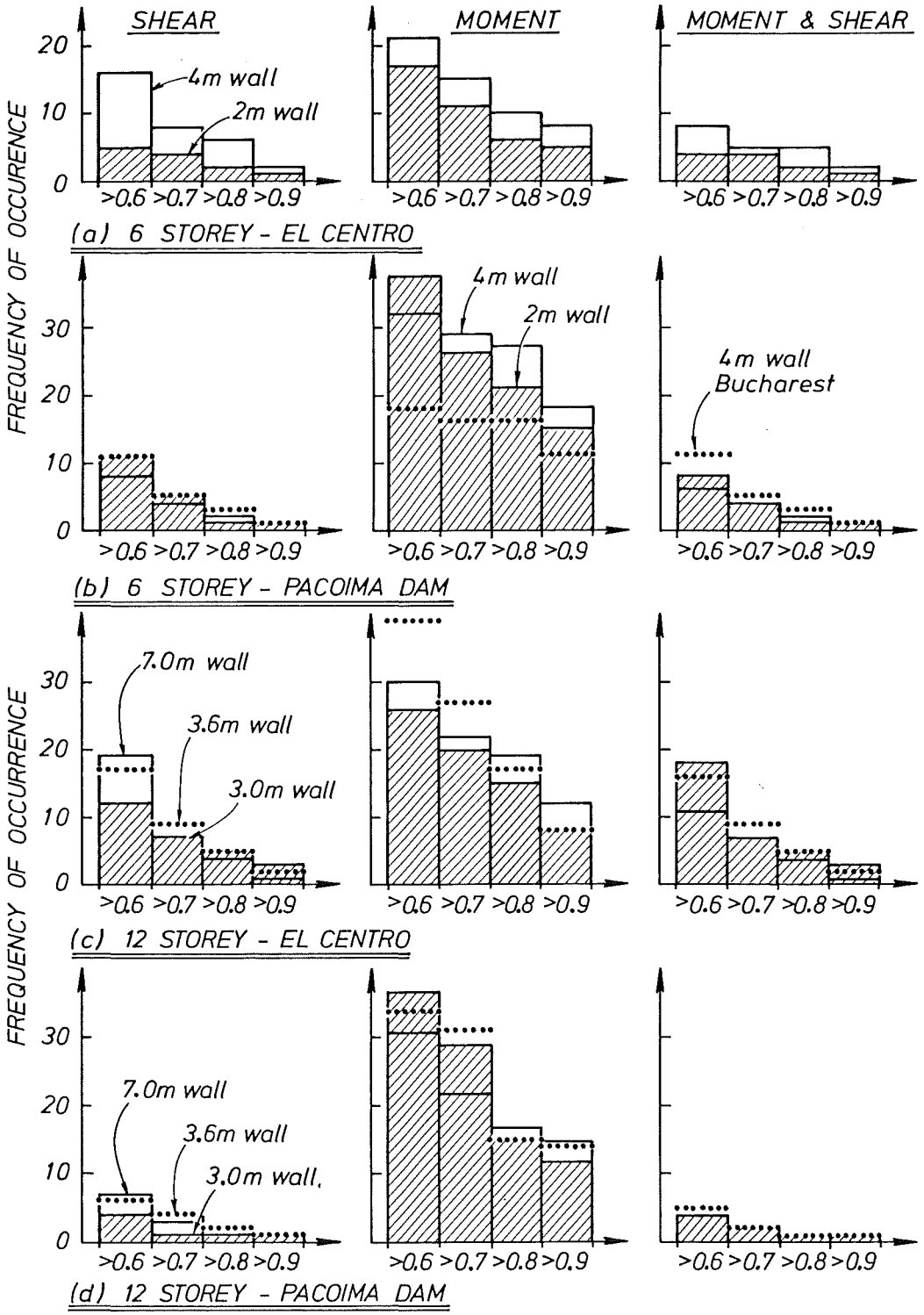

Fig. 4.29 Occurrence of High Wall Shear Force and Moment in Frame-Wall Buildings.

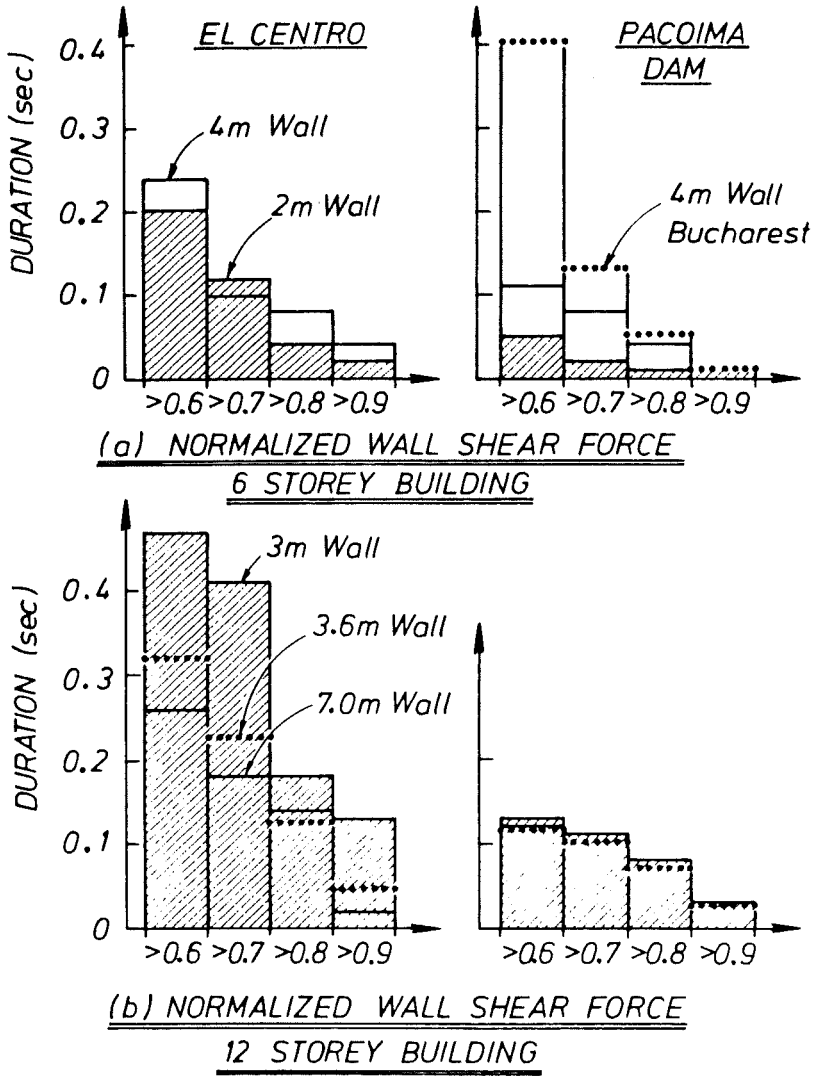

Fig. 4.30 Duration of High Wall Shear Force and Moment in Frame-Wall Buildings.

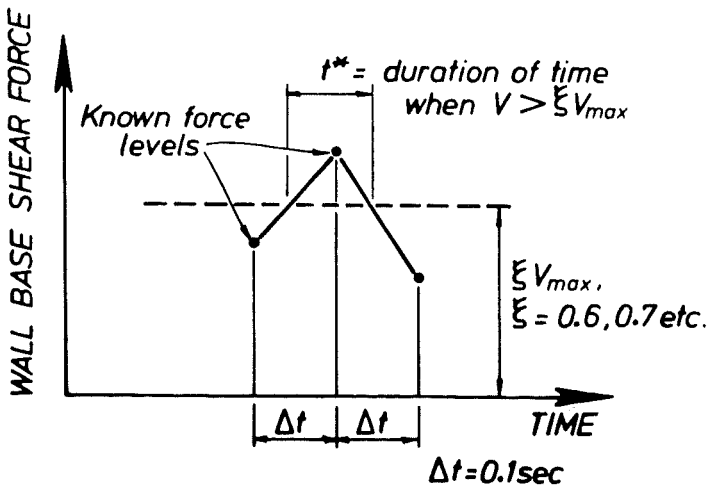

Fig. 4.31 Interpolation Scheme for Estimating Duration of High Wall Shear Force.

Figures 4.29 and 4.30 indicate the following points:

1. Wall base shear forces were high for a smaller proportion of the time than base moments for a given structure and excitation.
2. If the duration of strong shaking is taken to be 10 seconds for both the Pacoima Dam and El Centro accelerograms, shear forces of greater than 80% of the maximum occurred less than 10% of that time in all cases, and frequently less than 5% of the time. Moreover, wall shears greater than 90% of the maximum base shear occurred for less than 0.05 sec. in almost all cases.
3. High shear forces were generally coincident with high flexural strength demands. SEE ERRATA
4. The shear force duration diagrams indicate that in most cases force levels of 80% of maximum base shear force were applied for less than 0.1 sec.

It is reiterated that the design scheme proposed for wall shear strength is based on the peak observed wall shear forces recorded to have occurred during time history analyses. The facts that high wall shear forces occur at relatively few instances during most dynamic analyses, and than for only brief instants of time, are considered to be of relevance in the assessment of any wall shear design method. In addition, it seems doubtful that the rapid fluctuation in wall shear force (Fig. 3.32) indicated in analyses would be experienced by all walls simultaneously in a prototype structure subjected to a real seismic excitation. Equally, it does not seem probable that the exceedance of wall shear strength for a period of a few hundredths of a second would result in the failure of the whole structure.

Although it is stressed that the prohibition of shear failure is of paramount importance in structural response, the possibility of a small inelastic displacement due to shear may be acceptable, given the fact that the structure may be subjected to its most severe life-time seismic loading. Such shear yielding would of course be controlled by other structural elements in the building, which are all interconnected via floor diaphragms. In addition to the fact that peak column shear force demands were not generally coincident with peak wall demands (at the base level), it has been shown (Figs. 4.15 and 4.26) that columns generally enjoy some reserve shear strength which could absorb any temporary shortfall in overall structural shear resistance.

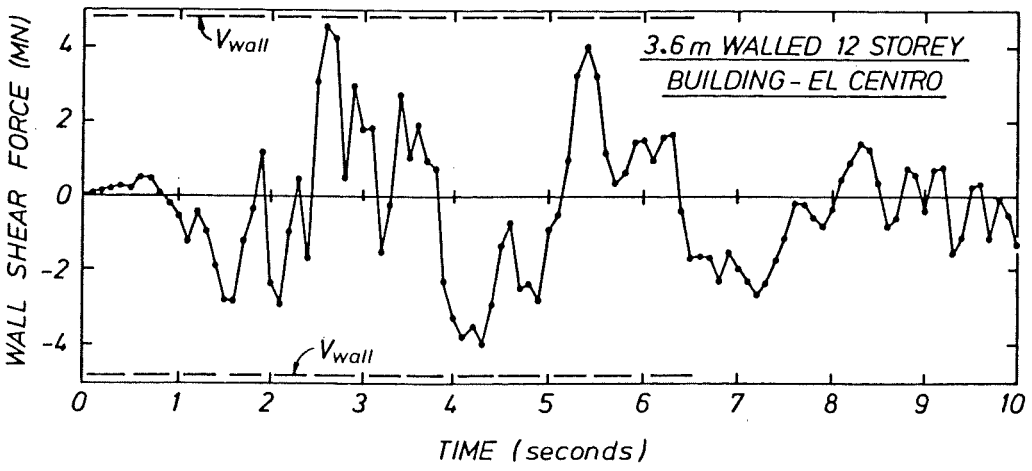

(a) El Centro

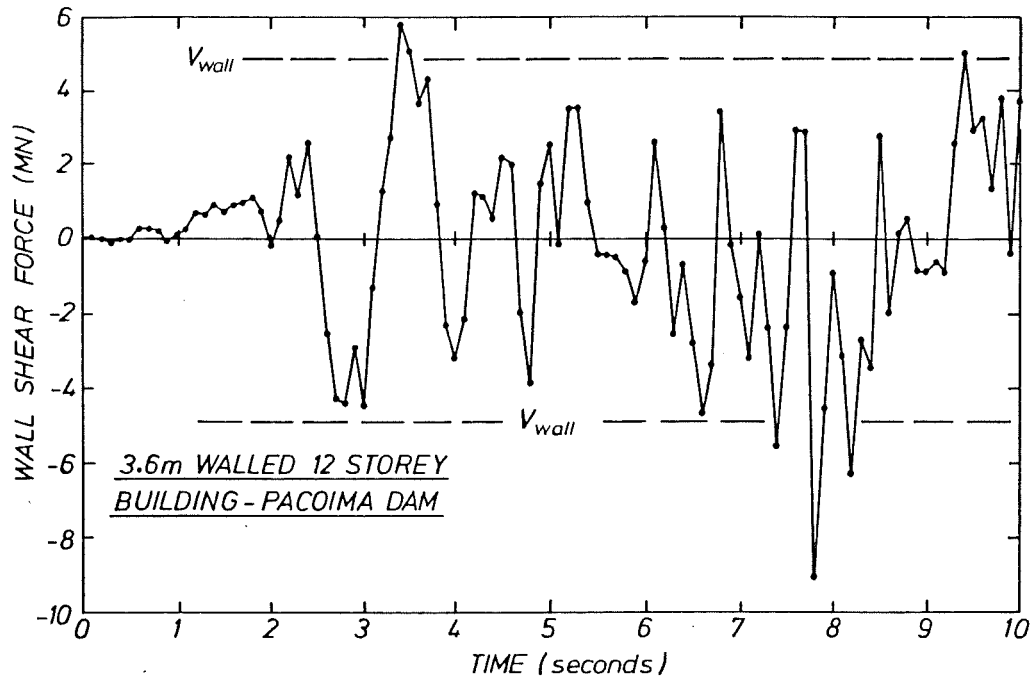

(b) Pacoima Dam

Fig. 4.32 Wall Base Shear Force Histories - 3.6 m Walled 12 Storey Buildings.

In view of the aforegoing discussion, and mindful of the fact that computer based dynamic analyses are based on many assumptions and simplifications, it is believed that the maximum observed levels of wall shear force should not be viewed with undue concern. It should be borne in mind that the proposed design approach requires the provision of these walls with potential shear strengths considerably larger than those derived from current seismic code provisions.

4.4.3 Eighteen Storey Buildings

A brief study was made of the behaviour of several simple 18 storey frame-wall buildings of similar form to the 12 storey structures. The results of this study are not presented in view of the fact that structural response illustrated no trends that were not exhibited by the smaller buildings described previously. The design methodology as proposed (Section 4.1) appears to be adequate for frame-wall structures of up to approximately 20 storeys. The approach is philosophically suitable for buildings of any height, although specific features may change, i.e. perimeter frames become more efficient than conventional beam-column frames with increasing height.

4.5 CONCLUSIONS REGARDING THE PERFORMANCE OF THE SIX AND TWELVE STOREY BUILDINGS

1. The computed response of the fixed base 6 and 12 storey frame-wall buildings to the El Centro accelerogram suggests that the design methodology (Section 3.1) will ensure good seismic performance of prototype structures.

2. Beam members designed with both horizontal and vertical moment redistribution were not subjected to high inelastic deformation demands, indicating that such redistribution is safe as well as convenient.

3. Columns designed using a basic dynamic magnification factor of 1.2 and a method previously developed for pure frame structures [34] enjoyed an adequate degree of protection against flexural yielding. Peak axial and shear force levels were predicted accurately with Eqs. 4.1-4.6.

4. Significant inelastic deformations in the walls were restricted to the base level plastic hinge zone as a consequence of using the linear moment design envelope of Fig. 4.2.

5. Wall base shear force levels for the El Centro excitation were somewhat underestimated by the design equation (4.12). However, this observation should be viewed in the context of the low frequency of occurrence and duration of high shear forces, and the general vagueries of dynamic analysis.

Chapter Five THE EFFECT OF FOUNDATION COMPLIANCE AND PARTIAL WALL HEIGHT ON THE RESPONSE OF FRAME-WALL BUILDINGS

5.1 INTRODUCTION

Foundation compliance is an aspect of the overall design problem that has traditionally received less detailed attention than the design of the "above ground" component or superstructure of a building. Although full base fixity of column and wall members is commonly assumed for the superstructure design, it is most unlikely that this can be achieved, especially for large cantilevered structural wall elements. The reluctance to address the problem of foundation flexibility is largely attributable to the fact that soil stiffness properties are difficult to estimate accurately. While it is known that soil stiffness is dependent on (among other factors) the frequency and amplitude of vibration of the foundation, the quantification of this phenomenon is extremely difficult. Although some theory exists, it is often based on models that are considerably removed from the physical realities of real foundation systems. Additional complexity may be introduced by non-linearity of soil response, and the interaction of several modes of footing response.

In the work reported subsequently, a simple approach to foundation compliance was adopted. The columns of the frame-wall structures were assumed to possess full base fixity, while the structural walls were assumed to be connected to flexible beams which permit rotational compliance which varies linearly with wall base moments, as illustrated in Fig. 3.10. The assumption of full fixity for column members may also be disputed but is considered reasonable in view of the comparative ease of fixing a column as compared to a structural wall of much greater flexural strength. Generally, the two extremes of full base fixity and a complete absence of flexural rigidity (i.e. effectively a pinned condition at the wall base) were used.

Both elastic response to static code lateral loading and inelastic response to historical accelerograms for the 6 and 12 storey buildings of Chapter 4, modelled to include foundation compliance, are discussed.

This chapter also examines the behaviour of buildings with structural walls of lesser height than that of the frame components (Section 5.5 onwards)

5.2 SIX STOREY BUILDINGS

5.2.1 Elastic Analysis

The six storey, 2 m walled building studied in Section 4.2 was used to investigate the effect of foundation compliance on the member actions associated with "code" (static lateral) loading. Elastic analyses were performed for four cases:

(1) Fully fixed base ($\theta = 0$),

(2) $\theta = 0.001$ radians,

(3) $\theta = 0.002$ radians,

(4) fully pinned base. (The base rotation associated with this condition was 0.0036 radians),

where θ is the wall base rotation as defined in Fig. 3.10. A trial and error process was used to determine suitable properties of the (imaginary) foundation beam so as to produce the desired base rotations. Selected envelopes of member actions and structural deformations are discussed subsequently. The most striking trend to emerge was the insensitivity of the building above the first floor to the degree of wall foundation compliance used. (Full ground level column fixity was assumed in these and subsequent analyses). Figure 4.4 shows the building superstructure.

5.2.1.1 Deflection and drift (Fig. 5.1): Structural deflected shapes for all four analyses were very similar in form. The effect of foundation flexibility is to allow a finite rotation of the wall base which accounts for most of the first floor deflection. As would be expected, increased foundation flexibility correlated with larger lateral displacement. While interstorey drifts were nearly independent of wall compliance over the top four levels, first floor drift almost doubled with the relaxation from fixed to pinned base walls.

5.2.1.2 Wall moments and shear force (Fig. 5.2): The pattern of wall bending moment is strongly influenced over the bottom storey by base fixity. At the first storey level, the reduction in moment demand associated with the transition from fixed to pinned base condition is only 25%. Increasing wall foundation compliance results in a slight lowering of the point of zero moment.

Wall base flexibility is associated with a reduction in wall shear force compared to the fixed base value. For flexibilities greater than those associated with a rotation $\theta = 0.023$ rad, the sense of base level

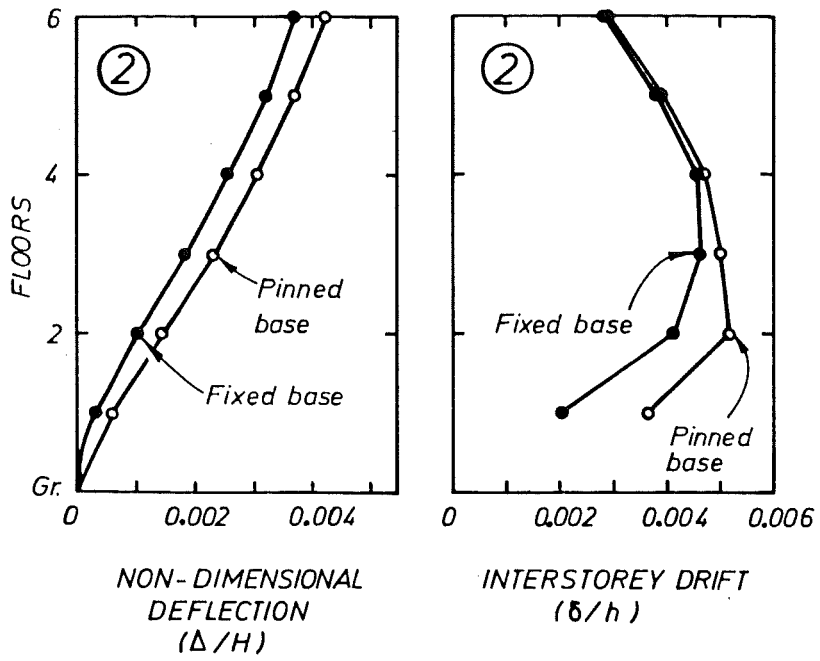

Fig. 5.1 Deflection and Drift Envelopes - 6 Storey 2 m Walled Building with Different Base.

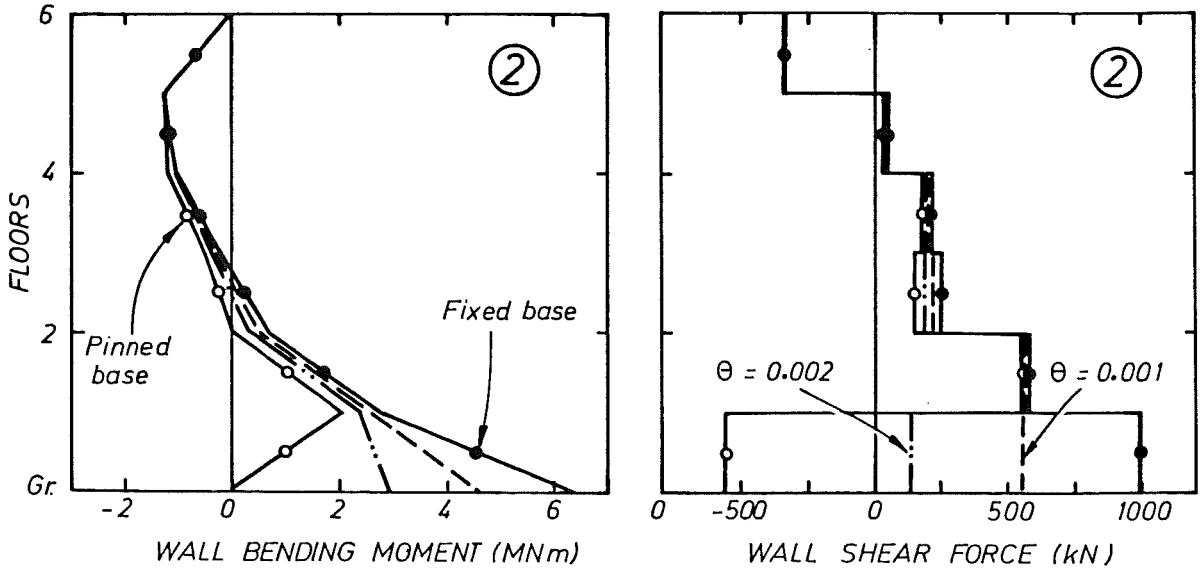

Fig. 5.2 Wall Moment and Shear Force Envelopes - 6 Storey 2 m Walled Building with Different Base.

wall shear force is the same as the applied load (and the same sense as top level shear force). This has the effect of requiring the columns of the frame component of the frame wall building to resist more than the total applied lateral load when foundation compliance is high. Above the bottom storey, however, patterns of wall shear force are barely affected by variations in wall base fixity.

5.2.1.3 Beam moment and column shear force (Fig. 5.3): The envelopes of beam bending moment associated with variable degrees of wall fixity are very similar. The strength of the frame component of the frame-wall structure can be measured in terms of the aggregated beam moment capacity (defined as the sum of the code lateral load analysis beam moments for all levels). This quantity increases by a modest 15% as wall fixity changes from full fixed to pinned. Figure 5.3 shows beam end moments.

Column shear force envelopes were also remarkably insensitive to wall foundation compliance except at the bottom level. The large increases in shear force with increasing wall base flexibility correlate with the reduced wall shear forces. Bottom storey column shear forces associated with the pinned wall were approximately 2.5 times the fixed base wall values. Column moment envelopes (not shown) necessarily illustrate similar trends.

The static response of the 4 m walled 6 storey building (not shown) indicated similar trends.

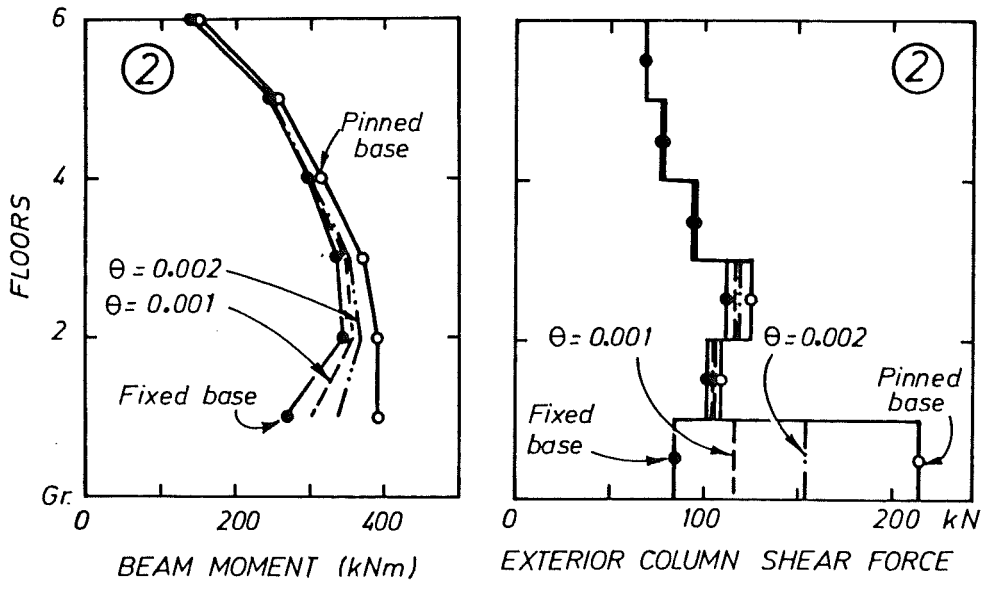

Fig. 5.3 Beam Moment and Column Shear Force Envelopes - 6 Storey 2 m Walled Building with Different Base.

On the basis of the elastic analyses presented, it might be postulated that a frame-wall structure designed for strength, assuming full column and wall fixity, might generally perform reasonably well in a time-history analysis (except perhaps at the first floor level) if some degree of wall base compliance was permitted. With this in mind the analyses reported subsequently were undertaken.

5.2.2 Response to the NS El Centro 1940 Component

This section describes the response of the 2 and 4 m walled 6 storey structures of Section 4.2, identical in all respects except for the assumption of pinned rather than fixed base walls, to the El Centro excitation. It is emphasized that member strengths used in the analyses described subsequently were derived for structures with fixed base walls, even though the dynamic analyses assumed pinned base walls. As was noted earlier (Section 4.2.4) some of the results of these analyses were presented earlier, with the results of the fixed base wall structures. This facilitates the comparison between these extremes in wall fixity.

5,2.2.1 Displacement response: Figure 5.4 indicates the time history of lateral displacement of the pinned base structures. Comparison with the fixed base deflection histories (Fig. 4.10) indicates greater structural flexibility and higher estimated first mode periods of vibration (Table 5.1). Maximum top floor deflection was increased by 9% for the 2 m walled structure and reduced by 25% for the 4 m walled structure. This compares with the peak deflection increases of approximately 15% in the elastic lateral load analysis.

Interstorey drifts (Fig. 4.9) were more nearly constant with height in the case of the pinned wall building. Drifts were lower for the 2 m walled structure, for which the stiffness reduction led to a lesser load attraction for the El Centro excitation. For the 4 m walled building, drifts were more nearly equal in the pinned and fixed wall buildings. It is believed that the lesser load attraction was offset by the greater severity of the loss of wall fixity for this building which has a more significant wall component than the 2 m walled structure.

5.2.2.2 Wall actions: As illustrated in Fig. 4.11, the linear envelope of wall flexural strength (derived assuming a fully fixed base wall) was adequate to prevent beam hinging at all levels. Interestingly, at the second to third floor levels, where the elastic analyses for pinned walls indicate low moment levels (Fig. 5.2), the maximum levels of wall moment are encountered during the dynamic response.

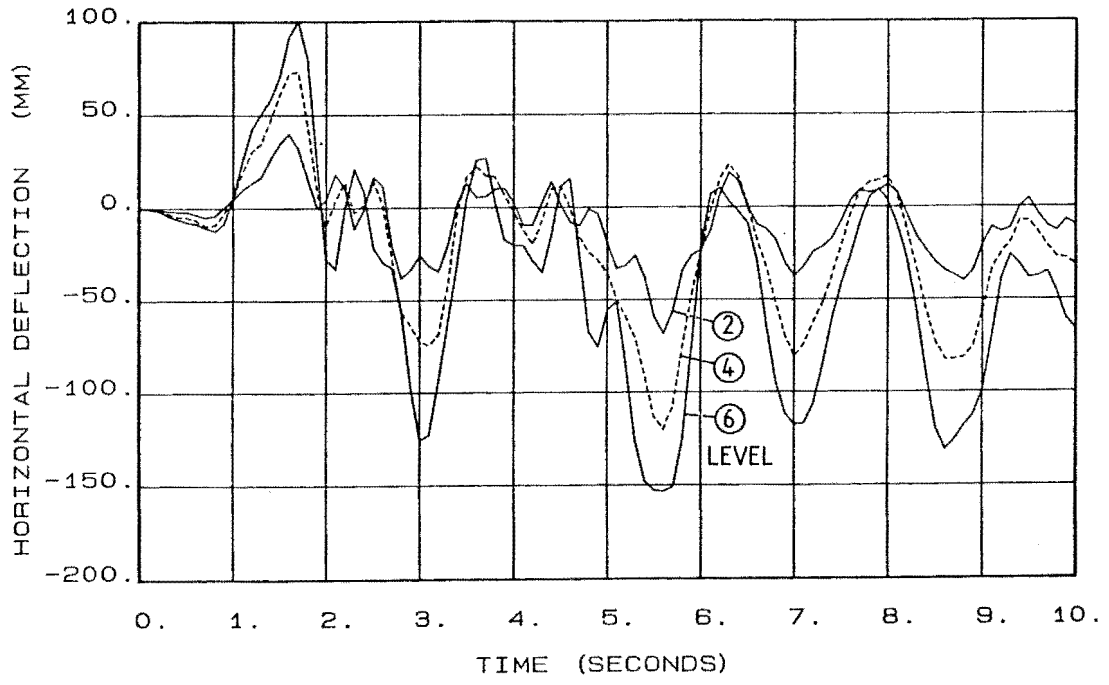

(a) 6 STOREY BUILDING 2M WALL PINNED BASE EL CENTRO

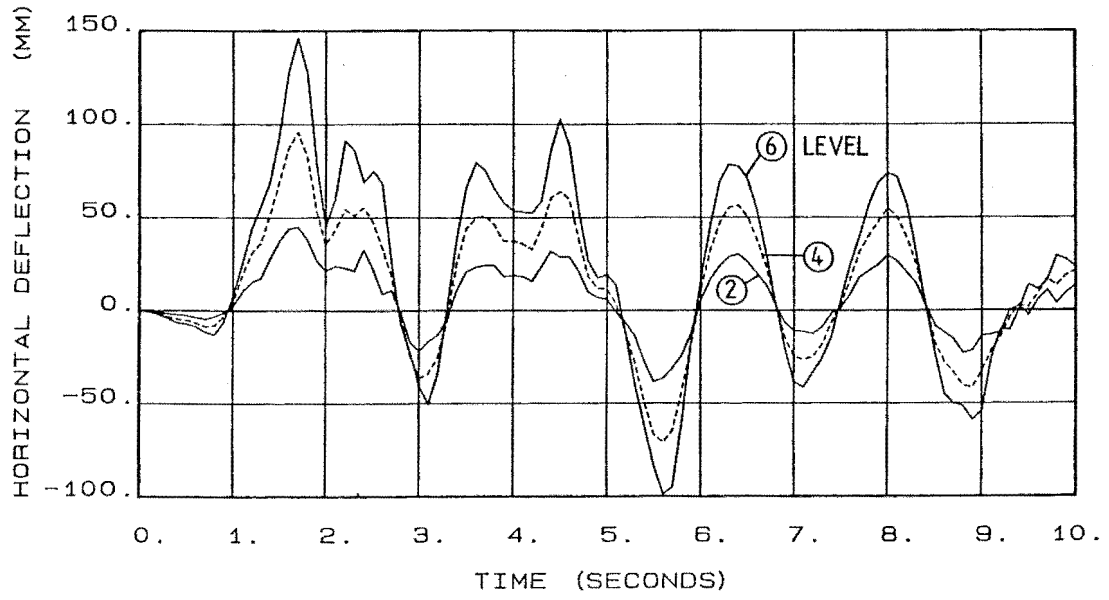

(b) 6 STOREY BUILDING 4M WALL PINNED BASE EL CENTRO

Fig. 5.4 Horizontal Displacement Histories - 6 Storey Pinned Wall Buildings.

The wall shear force envelope (Fig. 4.12) indicates an approximately constant level of shear force with height which is well estimated by the design force distribution. Base level shear force was generally of opposite sign to the force present in the second and upper floors, in conformity with the predictions of the elastic analysis.

5.2.2.3 Column actions: Fig. 4.13 indicates very similar extreme column axial forces for the pinned-wall and fixed wall structures. The design forces estimate the observed actions adequately.

Envelopes of maximum column bending moments and the associated probable strengths, calculated as indicated in Section 4.2.4.5, are provided in Fig. 5.5. The columns generally enjoy levels of protection against yielding in excess of those pertaining to the fixed base wall analysis (see Fig. 4.14). At the bottom level, where code column moment demands for the pinned wall structure greatly exceed those for the fixed base structure, excessive moment demands were not evident. This is also confirmed by the magnitude of inelastic hinge rotations in this region (Fig. 4.16).

Levels of column shear force (Fig. 4.15) are generally slightly lower for the pinned-wall structure than the fixed base structure, except at the bottom level. In this region, the pinned-wall shear forces observed were not in excess of the fixed base values by the ratios suggested by the elastic analyses, and were conservatively estimated by by the design shear forces.

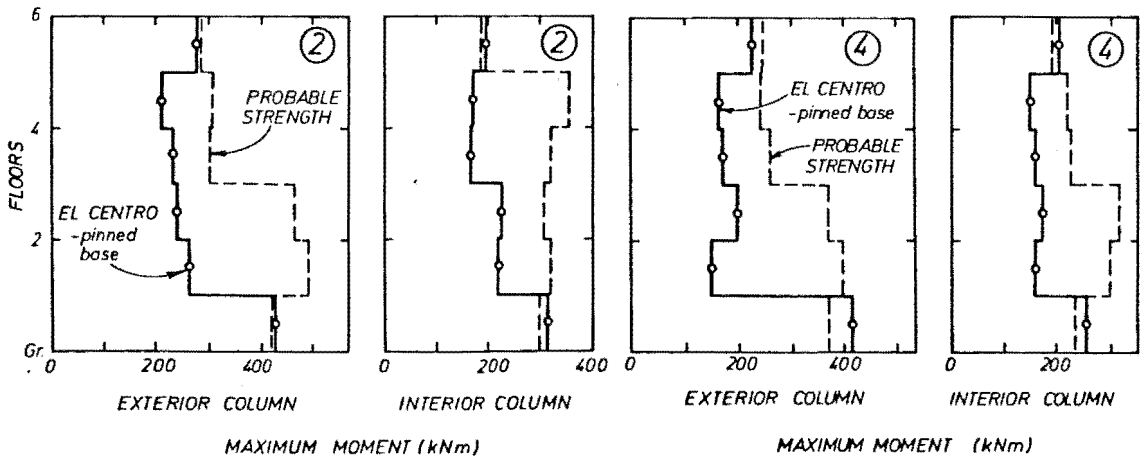

Fig. 5.5 Column Moment Envelopes - 6 Storey Pinned Wall Buildings.

5.2.2.4 Plastic rotation demands: Levels of plastic hinge rotations are indicated in Fig. 4.16. Beam hinge rotations are of comparable magnitudes with those levels recorded for the fixed base wall El Centro analyses, and do not indicate the increased top level deformations of those analyses. Low levels of column hinge rotations were also observed at the bottom of the ground floor and top of the 6th floor columns. No wall inelasticity was recorded.

5.2.2.5 Discussion of behaviour: In conclusion, it would appear that the 6 storey frame-wall structures,apportioned strength on the basis of having fully fixed structural wall elements, performed satisfactorily under the El Centro excitation when the walls were assumed to be pin-based. Deformations, while larger than for the fixed wall analyses, were within acceptable levels. Wall actions were significantly reduced for the pinned-wall structures, and despite the trends exhibited by elastic (code) static lateral load analyses, excessive ground floor column moments and shear forces did not eventuate. Lower demands on beam inelastic deformation capacity were also made for the pinned wall building. In summary, for these analyses the loss of wall base fixity was actually responsible for more favourable structural response in some respects.

A note of caution is sounded against the generalization of this admittedly most welcome result, which effectively suggests that loss of wall base fixity may not be of great importance in the response of a frame-wall building. The loss in overall structural stiffness which accompanies an increase in wall foundation compliance may, however, lead to unacceptable response, depending on the frequency characteristics of the accelerogram used. The loss of wall base fixity would be expected to become of increasing importance as the wall content of the frame-wall system increases. In addition, the loss of wall fixity may be increasingly critical with increasing structural height. Further studies, discussed subsequently, were carried out with a view to investigating these possibly significant factors.

5.2.3 Response of the 4 m Walled Building to the NS Bucharest 1977 Component

The response of the 6 storey, 4 m walled structure of Section 4.2 to the NS Bucharest 1977 excitation was investigated. Strength properties as derived in Section 3.2 were used for the two analyses made, the sole variable being the wall base condition assumed. Again the

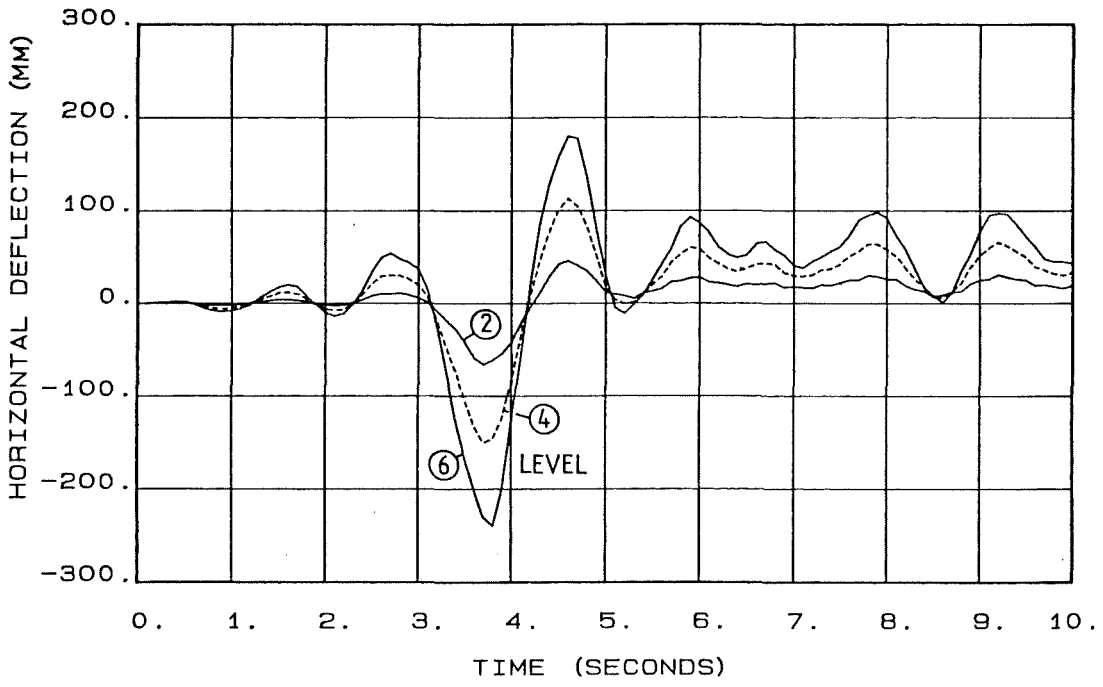

(a) 6 STOREY BUILDING 4M WALL FIXED BASE BUCHAREST

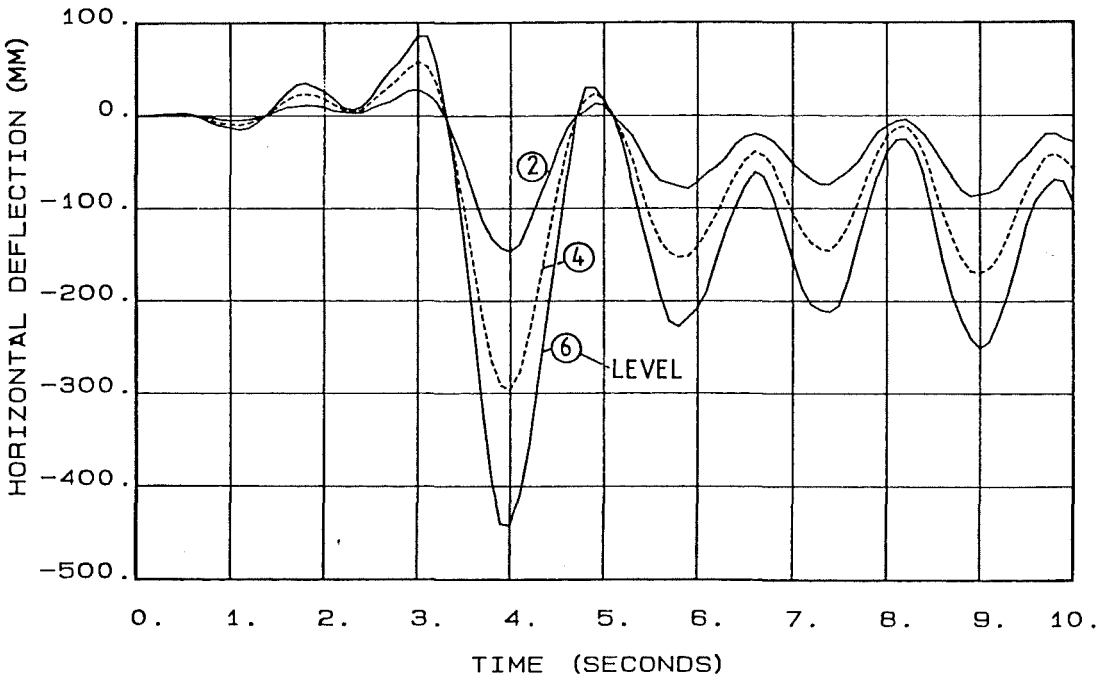

(b) 6 STOREY BUILDING 4M WALL PINNED BASE BUCHAREST

Fig. 5.6 Horizontal Displacement Histories - 6 Storey 4 m Walled Building With Different Base.

extremes of full fixity and pinned wall base were used. A modal analysis indicated that the relaxation from full fixity to a pinned condition increased the first mode period of vibration (T_1) from 1.08 to 1.46 sec. (Table 5.1). This latter figure is only marginally less than the 1.49 sec. period of the pinned 2 m walled structure. The nature of the Bucharest excitation is such that the increase in first mode period would likely be to give a considerably less favourable response for the pinned wall building (See Section 5.2.3.6).

5.2.3.1 Displacement response: The horizontal floor displacements(Fig. 5.6) indicate a considerable difference in gross structural response for the fixed and pinned wall walled buildings. Large, approximately equal, negative and positive excursions occurred for the fixed base wall building between 3 and 5 seconds of the record after which little oscillation occurred and residual permanent deformations were small. In contrast, the pinned wall structure never recovered from the negative displacement pulse (over the 3 to 4 second interval) and relatively large oscillations continued with a negative displacement bias. Maximum top floor displacements, normalised with respect to building height, were 2.03% and 1.10% for the pinned and fixed base wall structures respectively. From these diagrams it could reasonably be concluded that the pinned base structure was excited to a greater level of response than the fixed base building.

Maximum interstorey drift envelopes (Fig. 5.7) show that the pinned wall building underwent drifts typically 60% in excess of those for the fixed base building. The 1% code drift limit for frame structures [9] was consistently exceeded for the pinned wall building.

5.2.3.2 Wall actions: The linear design moment envelope proved adequate to restrict wall yielding to the base section only, a region detailed to accommodate this inelasticity. (Fig. 5.8). Levels of wall moment were uniformly low for the pinned base wall, and similarly, wall shear force demands were also low for this building (Fig. 5.9). The envelope of wall shear force for the fixed base building was not well predicted by the design force distribution, with a maximum shortfall of approximately 25%.

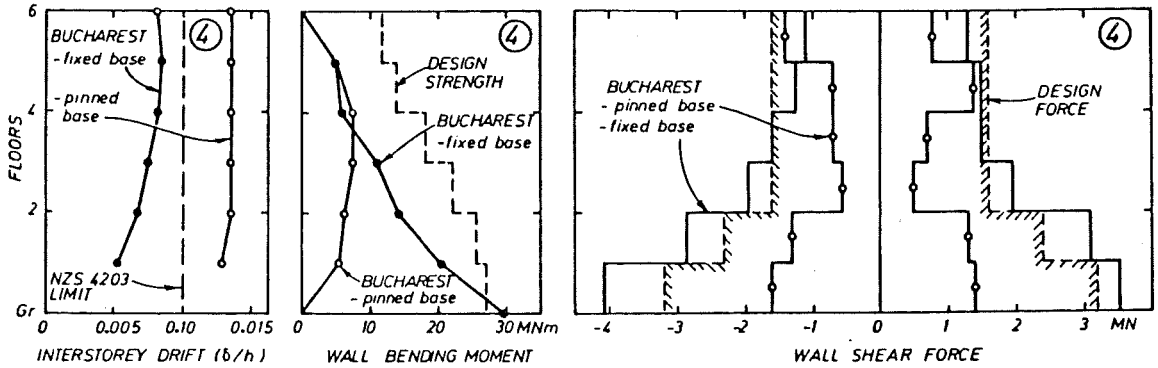

Fig. 5.7 Interstorey Drift Envelope -

Fig. 5.8 Wall Moment Envelope -

Fig. 5.9 Wall Shear Force Envelope -

6 Storey 4 m Pinned Wall Building With Different Base.

5.2.3.3 External overturning moment: A comparison of total base overturning moment was made for the fixed and pinned wall structures. The overturning moment was calculated as

$$M_o = \Sigma M_{wall_{base}} + \Sigma M_{col_{base}} + \Sigma P_{eq} \ell' \text{ where}$$

$M_{wall_{base}}$ = base wall moment (= 0 for pinned wall structure),

$M_{col_{base}}$ = ground level column moments, and

P_{eq} = earthquake induced axial forces at the base of exterior columns, these columns being $2\ell'$ apart.

Fig. 5.10 illustrates the time histories of M_o for both the El Centro and Bucharest excitations. Both diagrams show a considerable reduction in overturning moment attributable to the loss of wall base fixity. The fixed and pinned base curves are somewhat out of phase because of the period shift associated with this change. Although the general performance of the pinned wall structure was superior under the El Centro excitation and comparable for the Bucharest accelerogram (compared with fixed wall structure response) this could not readily be attributed to differences in base overturning moment, i.e. both

TABLE 5.1 : FIRST MODE PERIODS OF VIBRATION FOR THE 6 STOREY BUILDINGS WITH WALL FOUNDATION COMPLIANCE

Wall Base Condition	2 m Wall	4 m Wall
Modal Analysis:		
Fixed	1.37	1.08
θ = 0.001 rads[1]	1.41	-
θ = 0.002 rads	1.44	-
Pinned	1.50	1.46
Estimated from Dynamic Analysis:		
Pinned - El Centro	1.5	1.5
Fixed - Bucharest	-	1.5
Pinned - Bucharest	-	1.6

Note: (1) θ is defined in Section 5.2.1.

TABLE 5.2 : FIRST MODE PERIODS OF VIBRATION FOR THE 12 STOREY PINNED BASE WALL BUILDING

Pinned Base Walls	3.0 m Walled Structure	3.6 m Walled Structure	7.0 m Walled Structure
Modal Analysis	2.65 (2.51)[1]	2.62 (2.39)	2.54 (1.99)
Apparent - El Centro	2.7	2.7	2.5

Note: (1) Period of fixed base wall structures are shown in brackets.

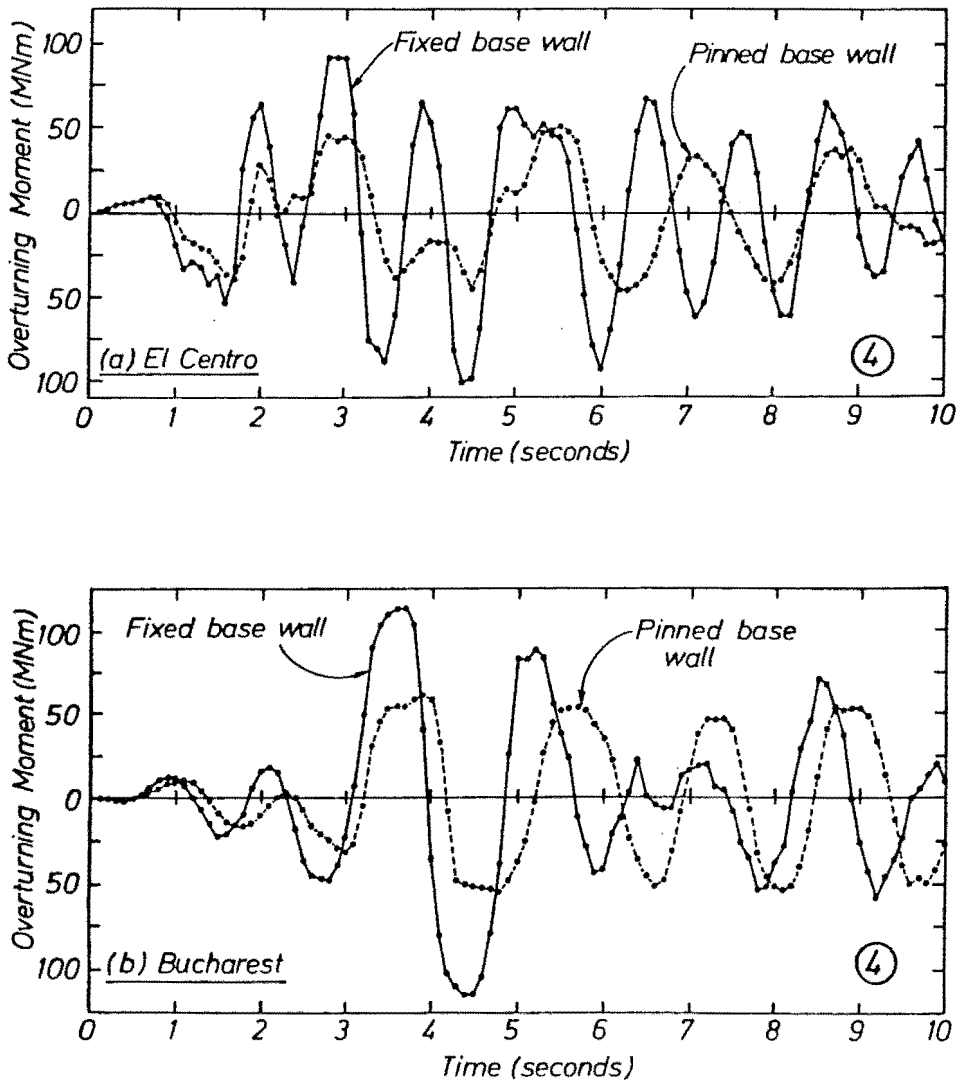

Fig. 5.10 Overturning Moment History - 6 Storey 4 m Wall Building With Different Base.

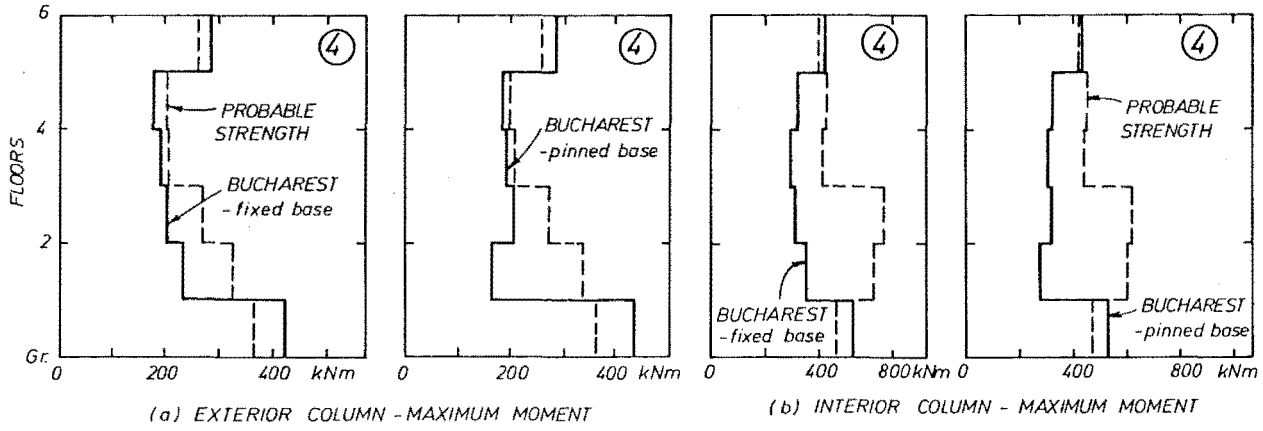

Fig. 5.11 Column Moment Envelopes - 6 Storey 4 m Wall Building With Different Base.

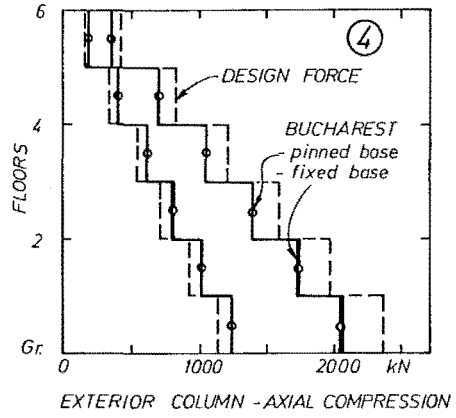

Fig. 5.12 Column Axial Force Envelope - 6 Storey 4 m Wall Building With Different Base.

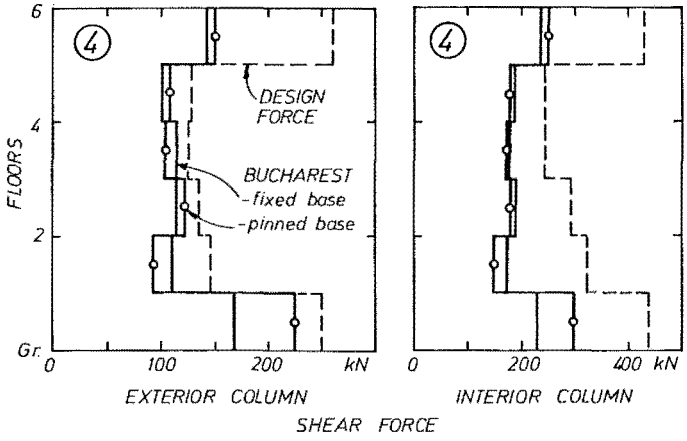

Fig. 5.13 Column Shear Force Envelope - 6 Storey 4 m Wall Building With Different Base.

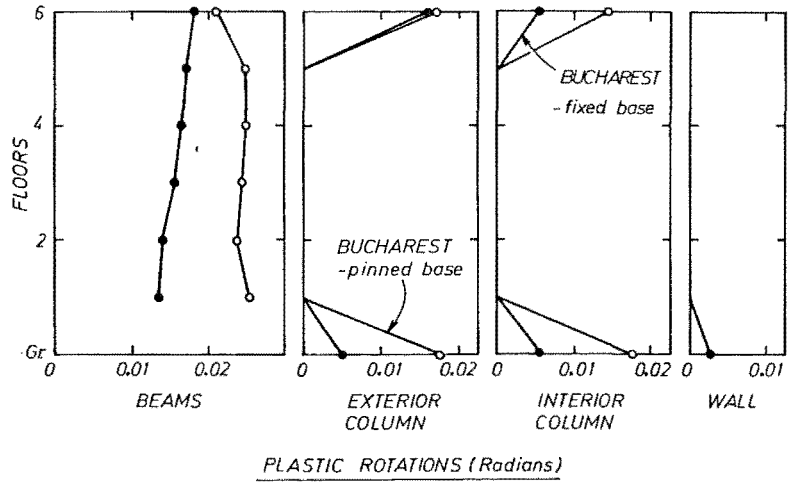

Fig. 5.14 Plastic Rotation Envelope - 6 Storey 4 m Wall Building With Different Base.

diagrams show similar reductions in peak overturning moments associated with wall fixity loss.

5.2.3.4 Column actions: Column moments (Fig. 5.11) were of similar magnitudes for the two analyses, the interior columns enjoying a higher degree of protection than the exterior. Yielding of top and bottom floor columns occurred in all cases, although (as indicated in Fig. 5.14) rotational demands were larger for the pinned wall structure. Column axial load (Fig. 5.12) was conservatively estimated by the maximum and minimum design forces. The pinned and fixed wall structures experienced very similar extreme column forces. Similar levels of maximum column shear force were recorded (Fig. 5.13) although the ground floor columns in the pinned wall structure experienced somewhat larger shear forces. Again, the design force levels, based on the fixed base structure elastic load force patterns, adequately predict the maximum forces at all levels.

5.2.3.5 Plastic rotation demands: As indicated in Fig. 5.14, levels of inelastic rotation undergone by the beams of the pinned wall building were approximately 60% larger than those of the fixed wall structure. Both envelopes of rotation demand are within sustainable limits. Column hinge rotations are considerably larger for the pinned wall structure, but again could be sustained given the provision of adequate transverse reinforcement in the hinge zones. The wall base hinge rotation demand (for the fixed wall structure) is small.

5.2.3.6 Discussion of behaviour: In conclusion it is considered that the overall structural response of the 4 m walled building to the Bucharest excitation was aggravated by the transition from a fixed to a pinned wall base. This is attributed to the fact that the period shift associated with the wall base relaxation made the building susceptible to a more severe degree of excitation for the particular accelerogram used. Displacements and drifts were made unacceptably larger and although wall actions were at low levels for the pinned wall case, beam and column inelastic demands were appreciably greater. very high column shear forces that might have been anticipated on the basis of a static elastic analysis did not eventuate, however.

The conclusion can reasonably be generalised to contend that a relaxation in wall base fixity (from the full fixity used in the design of the frame-wall building) to the most extreme case of an effectively pinned base wall will have an effect dependent on the frequency characteristics of both the structure and the accelerogram used. The

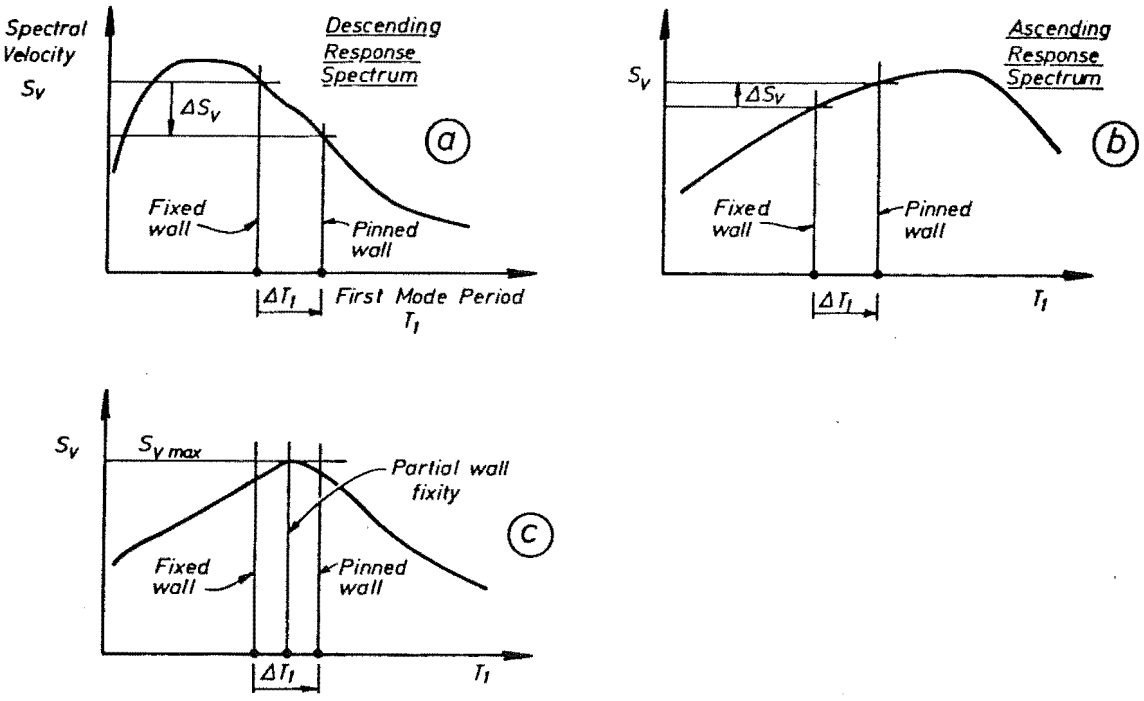

Fig. 5.15 Effect of Period Shift on Seismic Loading of Structures.

loss of overall structural stiffness (i.e. period increase) associated with foundation compliance may improve or worsen response (compared with the fixed base structure), depending on the characteristics of the accelerogram. (See Fig. 5.15(a) and (b)). It is also clear that a partial loss of wall base fixity could conceivably expose a structure to an excitation greater than that associated with either a fully fixed or pinned wall building. (Fig. 5.15(c)).

The magnitude of the very large horizontal forces introduced to the walls at the first floor level (via. the slab) is viewed with concern, In all analyses discussed, it has been assumed that the floor slabs act as infinitely rigid diaphragms, distributing inertia forces to walls and columns. It is unlikely that this would be a valid assumption in the case of the pinned wall structures studied, for which slab-wall interface shear stresses of as much as 5 MPa are associated with the peak shear forces calculated in the dynamic analyses. Local thickening of the floor slab above the assumed thickness of 160 mm and special reinforcement would be required to reduce and adequately transfer these stresses. Inelastic behaviour of the slab-wall (or slab-column)

connections greatly complicates the distribution of lateral load throughout the structure [52] and this consideration is not pursued further herein. This aspect of response is one of the least satisfactory regarding the behaviour of pinned base wall structures, and it is clear that the likelihood of high wall-slab shear stresses should be recognised in frame-wall structures where wall fixity cannot be ensured.

5.3 TWELVE STOREY BUILDINGS

The twelve storey buildings of Section 4.3 were used to further investigate the effects of wall foundation compliance on both "code" force distribution and the inelastic response of the structures. Again the extremes in wall base condition of full fixity and a fully pinned connection were used in this study. Column members were assumed to have full base fixity for both cases of wall fixity. The results of these investigations are presented and discussed subsequently.

5.3.1 Elastic Analysis

The general trend exhibited by the twelve storey buildings was the correlation between larger wall size and greater alteration due to base deformations,and member actions, as compared with those of the fixed base wall analyses. The period shifts associated with the loss of wall base fixity are indicated in Table 5.2. Interstorey drifts (Fig. 5.16) illustrate this trend, the differences in drifts being extreme in the case of the 7 m walled structure. Beam moment patterns (Fig. 5.17) demonstrate the manner in which fixed base actions are increasingly altered (by loss of wall base fixity) with increasing wall stiffness. The aggregated beam moment demand (Section 5.2.1.3) which may be taken as an indication of the load resisted by the frame component of the building, increased by 8, 13 and 60% for the 3, 3.6 and 7 m walled structures respectively, with the loss of wall base fixity. In addition, the 3.6 and 7 m walled structures had aggregated beam moment demands of 93 and 97% of the 3 m walled structure demand, suggesting that once wall base fixity is lost, wall size in this respect is of little importance. In general terms, the top half of the 3 m walled building is not sensitive to wall base fixity. The top several storeys of the 3.6 m walled structure are similarly not affected by wall fixity, while beam moments at all levels of the 7 m walled structure are significantly affected. These comments apply also to the other envelopes of member actions presented in this section.

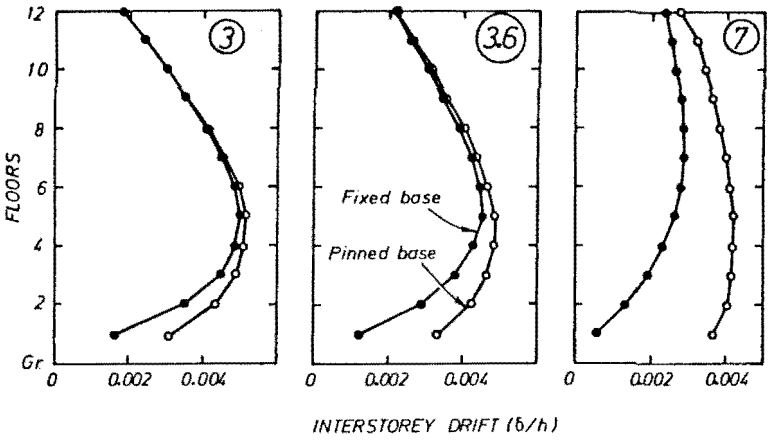

Fig. 5.16 Interstorey Drift Envelopes - 12 Storey Wall Buildings With Different Base.

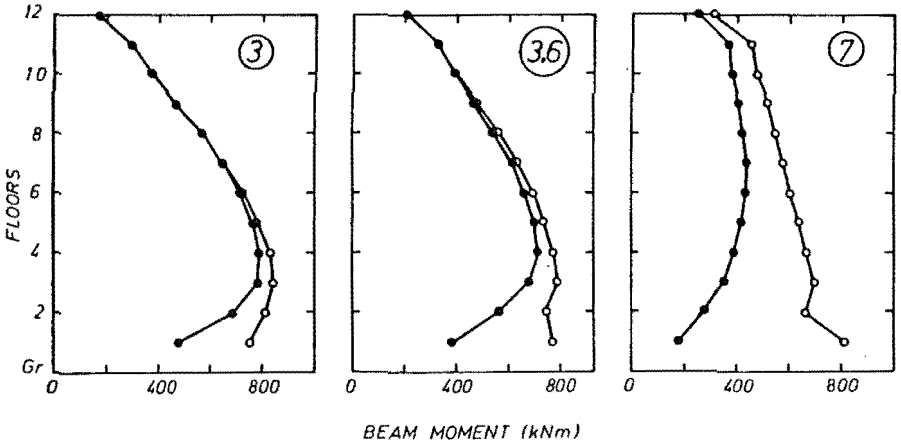

Fig. 5.17 Beam Moment Envelope - 12 Storey Wall Buildings With Different Base.

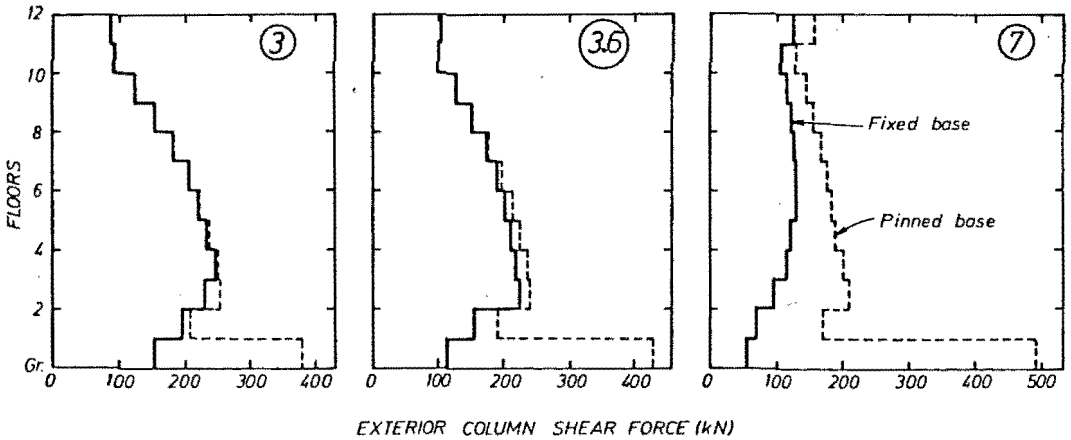

Fig. 5.18 Column Shear Force Envelopes - 12 Storey Wall Buildings With Different Base.

Exterior column shear force envelopes (Fig. 5.18) indicate the transfer of lateral load resistance from wall to frame components, and the large increase in bottom storey column shear force due to the transition from a fully fixed to a pinned wall base. Wall bending

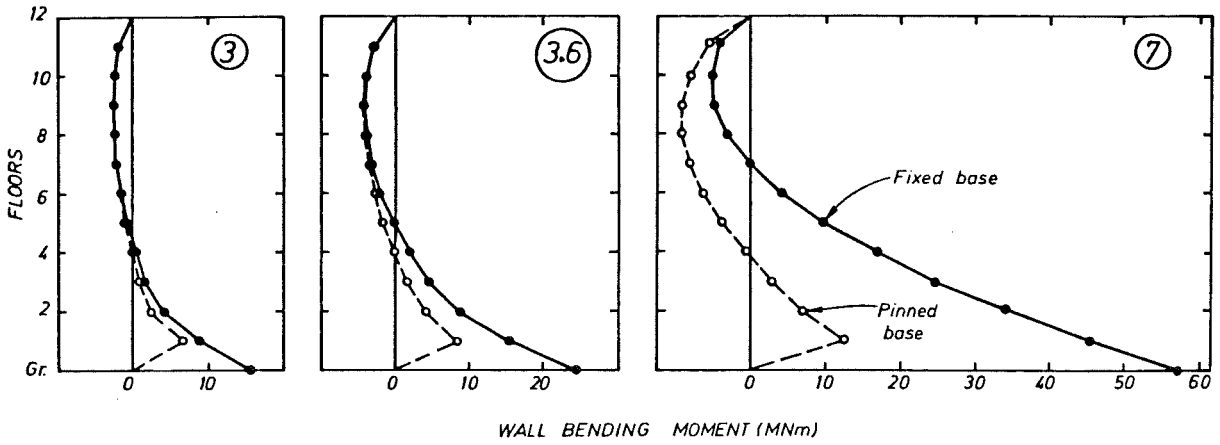

Fig. 5.19 Wall Moment Envelopes - 12 Storey Wall Buildings With Different Base.

moment patterns (Fig. 5.19) also illustrate the redistribution of load away from the walls associated with base fixity loss. Upper level wall moments increase at an increasing rate with wall size, with the transition from full to zero moment fixity. The point of zero moment also drops further. Finally, wall shear force patterns due to code lateral loading are shown in Fig. 5.20. The massive shear force reversal associated with base fixity loss is indicated, and for the case of the 7 m walled structure the magnitude of the base level shear force for the pinned wall analysis was greater than that for the fixed base analysis. The concept of "shear ratio" (Section 4.1.1) used to assess frame:wall stiffness is not useful in the case of buildings with non rigid foundations due to the reversal of the sense of wall shear force between first and second storeys.

Wall moment at the first floor of the 3 m walled structure shows particularly little influence due to fixity. This suggests an analogy between a fixed base wall and a pinned base wall one storey higher, i.e. in some cases, pinned base walls are nearly 'fixed' at first floor level. In the latter case, high first storey shear forces are commonly passed to peripheral walls.

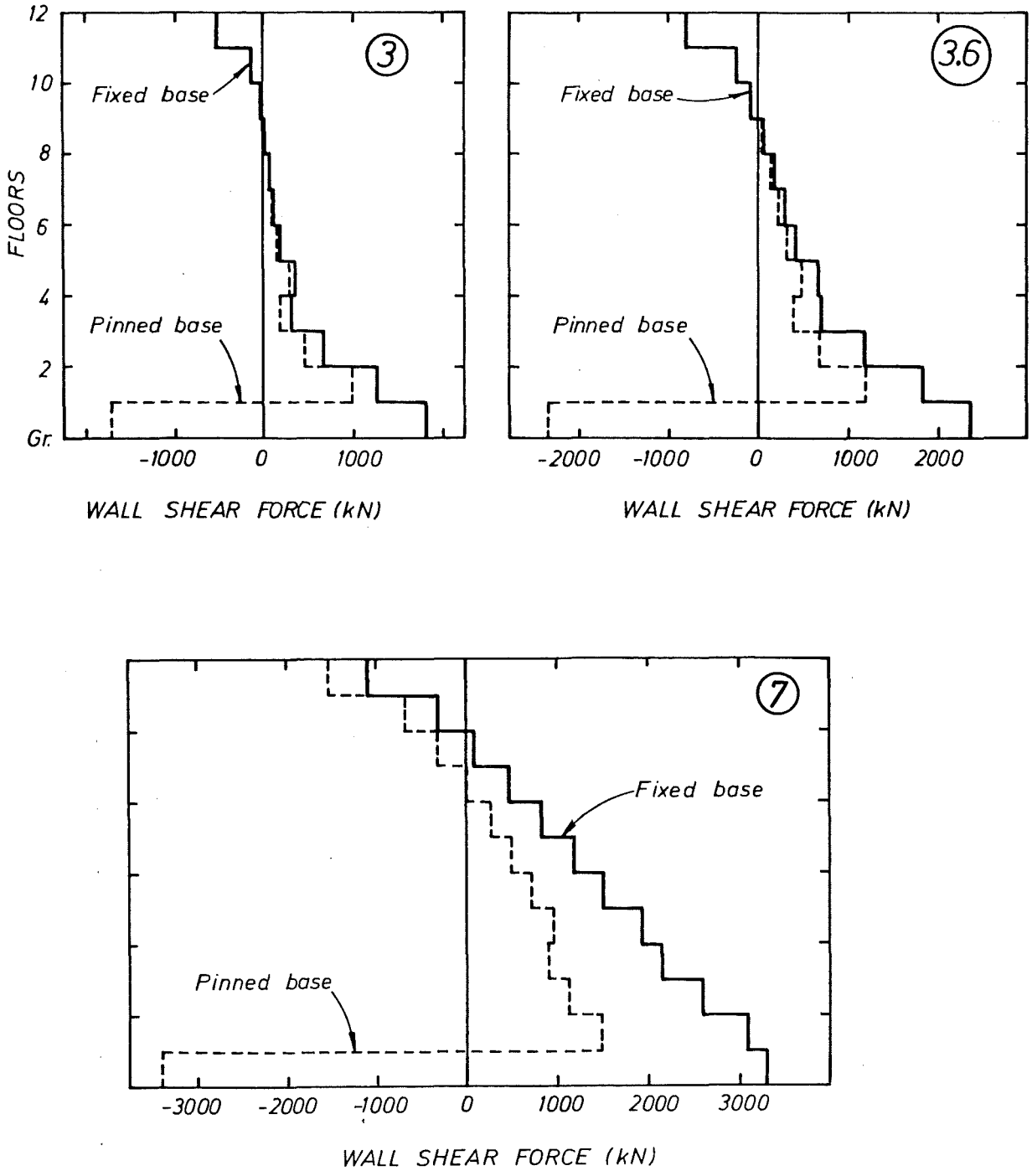

Fig. 5.20 Wall Shear Force Envelopes - 12 Storey Wall Buildings With Different Base.

5.3.2 Response to the NS El Centro 1940 Component

The response of the 12 storey pinned wall structures to the El Centro component is described in this section. The structures analysed were identical in all details (strength and stiffness) to those discussed in Section 4.3 except for the provision of a moment release at the base of the lumped walls. As was done for the 6 storey structures, some of the results of these analyses are indicated on the envelopes of the corresponding fixed base walled structures presented earlier (Section 4.3).

5.3.2.1 Displacement response: The time history records of horizontal displacement for the 12 storey pinned wall structures are shown in Fig. 5.21 Comparison with those obtained for the corresponding fixed base structures (Fig. 4.20) indicates similar levels of response were attained. The loss of wall base fixity resulted in nearly equal first mode periods for the 3 structures which is reflected in the similarity between the diagrams in Fig. 5.21. Estimated values of first mode period are shown in Table 5.2.

Interstorey drifts (Fig. 4.21) were of a similar level to those recorded for the fixed base analyses remaining within the code [9] limitations of 1%. The difference between drift patterns indicated by static lateral analysis (Fig. 5.16) and those in Fig. 4.21 is marked.

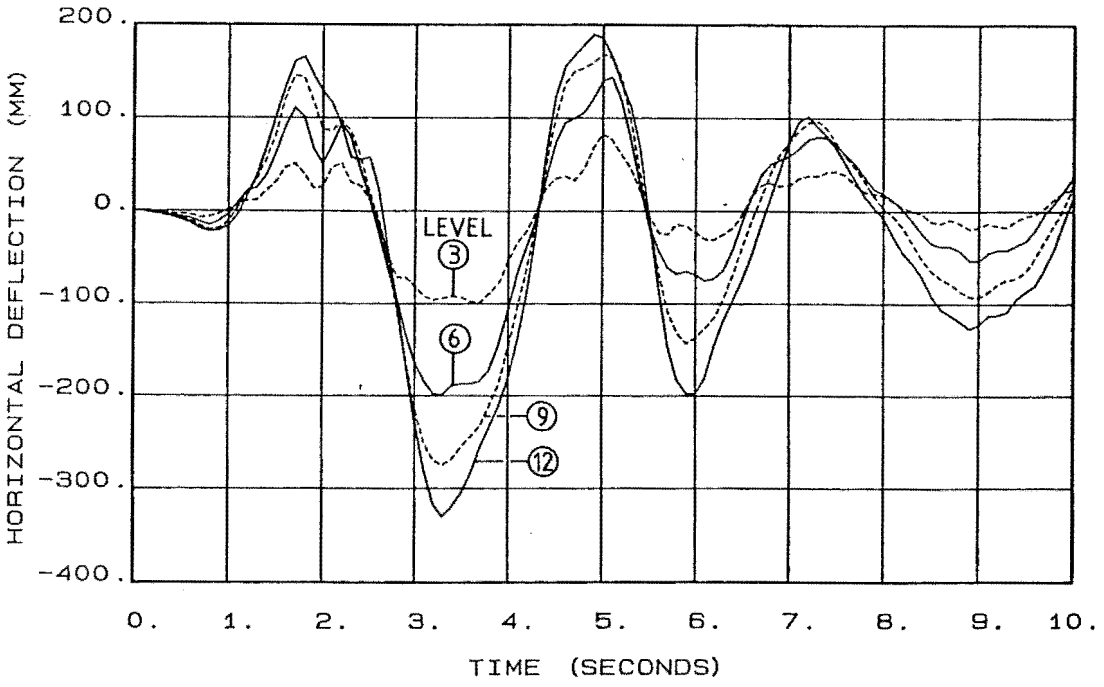

(a) 12 STOREY BUILDING 3.0M WALL PINNED BASE ELCENTRO

Fig. 5.21 Horizontal Deflection Histories - 12 Storey Pinned Wall Buildings.

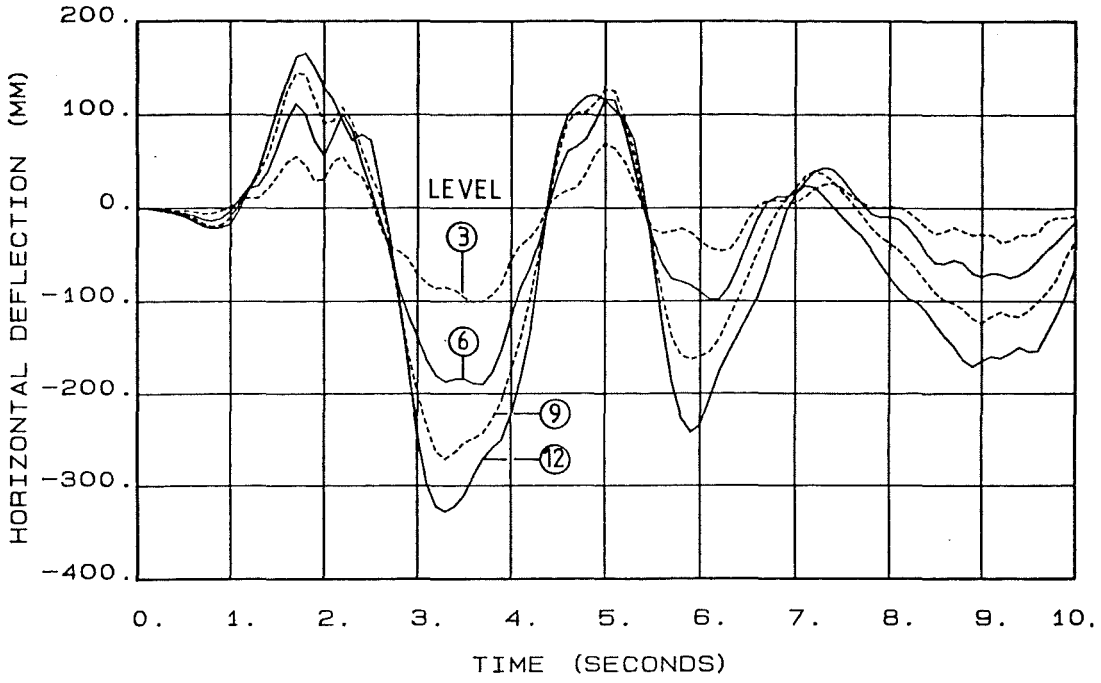

(b) 12 STOREY BUILDING 3.6M WALL PINNED BASE ELCENTRO

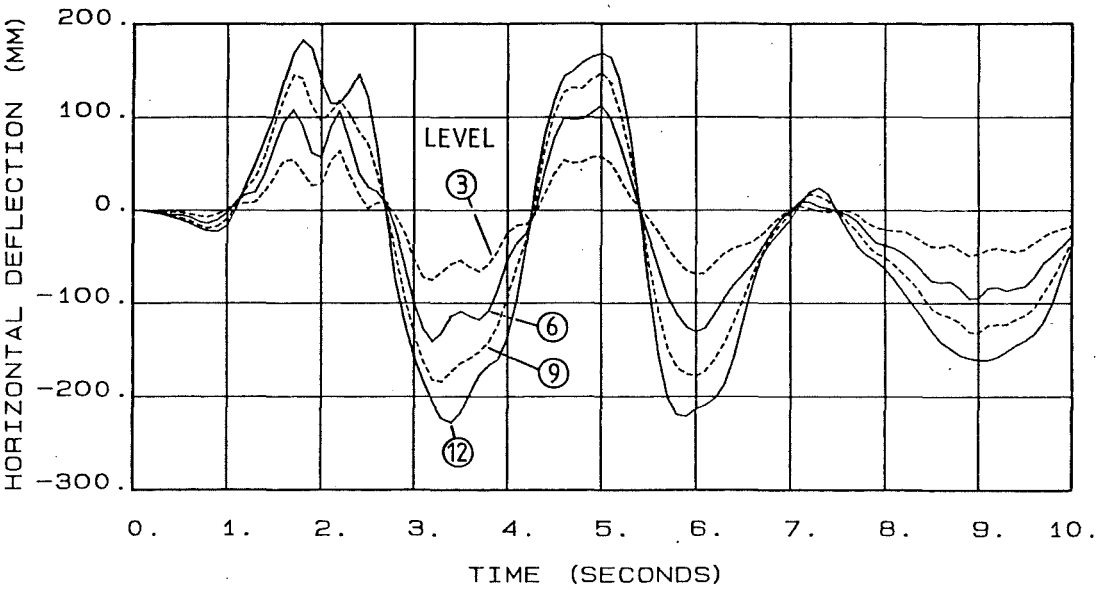

(c) 12 STOREY BUILDING 7.0M WALL PINNED BASE ELCENTRO

Fig. 5.21 Horizontal Deflection Histories - 12 Storey Pinned Wall Buildings.

Drifts for the pinned 7.0 m walled building, subjected to dynamic loading, compare more favourably with those for the fixed wall building for dynamic rather than static loading.

5.3.2.2 Wall actions: Levels of wall bending moment encountered for the pinned base walls were within the design strength envelope, this latter based on the assumption of full base fixity (Fig. 4.22). Upper floor moments for the 7.0 m pinned wall structure were closest to the design strength, which is not surprising given the comparatively high moments in this region for static loading (Fig. 5.19).

Pinned wall shear force levels (Fig. 4.23) were similarly contained by fixed base design strength envelopes, with wall shear force maximums approximately constant with height. The high levels of base shear force suggested by elastic analysis load patterns (Fig. 5.20) did not eventuate in these dynamic analyses, although the trend of a differing sense between ground floor wall and frame shear force was manifested. This latter phenomenon could subject the 1st floor diaphragm (floor slab) to higher levels of inplane actions than might exist for those of fixed base buildings.

5.3.2.3 Column actions: The flexural yielding of columns was restricted to ground and top floor locations, with levels of protection similar to those enjoyed by the columns of fixed base walled buildings existing elsewhere (Fig. 5.22). Column axial force levels were well predicted by the design force envelopes (Fig. 4.24) although they were marginally larger than those of the fixed base wall buildings. Fig. 4.26 indicates that levels of column shear forces generally very similar to those experienced by the fixed base wall buildings occurred for the pinned base wall buildings. Base level forces were higher and sometimes exceeded the design force levels but did not approach the magnitudes suggested by elastic analysis patterns (Fig. 5.18). This is because column shear forces are controlled by wall shear force levels. These were not magnified to the same extent as in the fixed base wall buildings.

5.3.2.4 Plastic rotation demands: Comparable levels of beam hinge plastic rotations within fixed- and pinned-wall base buildings are indicated in Fig. 4.27. The larger rotations at lower levels for the pinned wall structures could be anticipated from the elastic

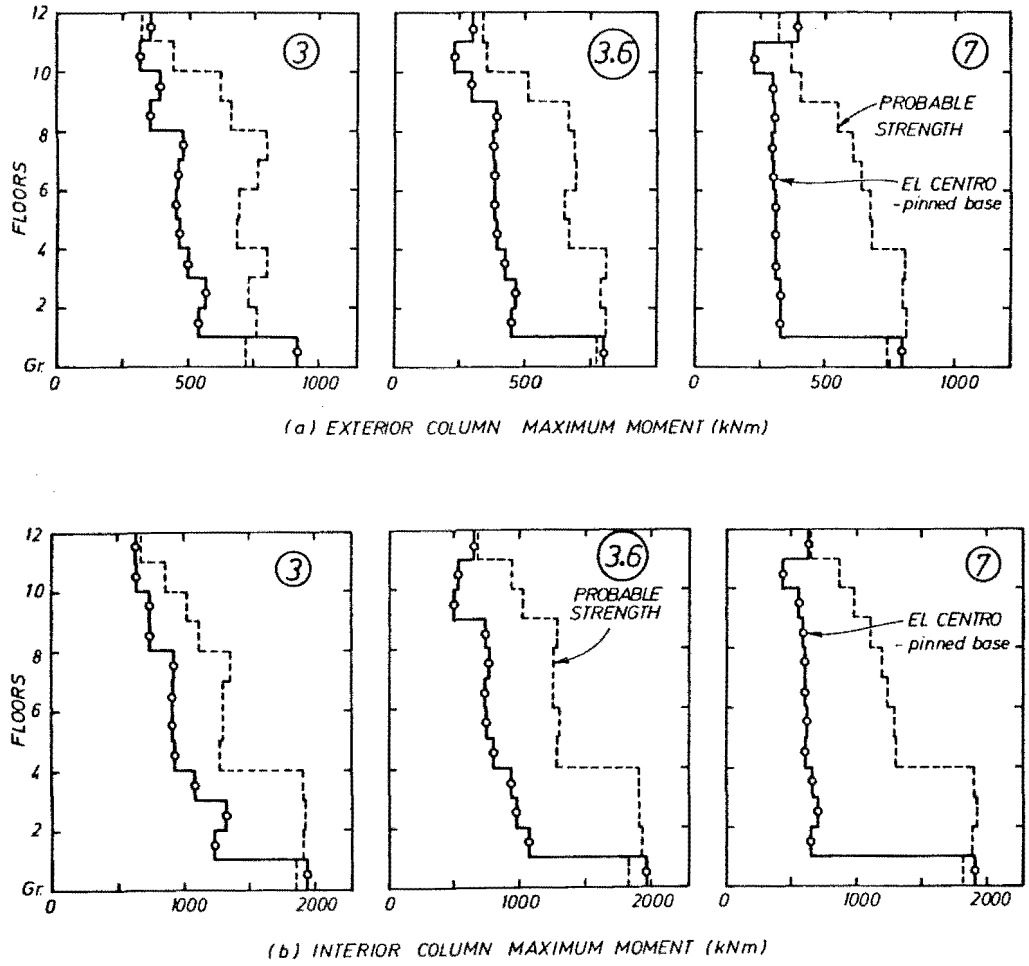

Fig. 5.22 Column Moment Envelopes - 12 Storey Pinned Wall Buildings.

analyses (Fig. 5.17) which indicate that beams designed for fixed base load patterns would have a shortfall in strength in this region. Column rotational demands were also similar and no yielding was observed in the pinned base walls.

5.3.2.5 Discussion of behaviour: The dynamic response of the 12 storey structures modelled with pinned wall base conditions was good in most respects. (It is reiterated that the structures had strength apportioned on the basis of code lateral load analyses assuming full base fixity). In comparison with the response to the results of the fixed wall base analyses, maximum deformations were similar, as were peak column forces and moments. The extreme levels of column shear force indicated in first storey members by the elastic pinned wall analyses did not eventuate. Wall flexural and shear strength demands were also within the fixed base design envelopes. Despite the apparently acceptable performance of these 12 storey structures with complete loss of wall base fixity, the dependence of response on the characteristics of the particular input accelerogram used (Section 5.2.3) is, however, strongly emphasised.

5.4 CONCLUSIONS REGARDING THE EFFECTS OF FOUNDATION COMPLIANCE

The following conclusions are drawn regarding the seismic response of frame-wall buildings with flexible wall base conditions:

1. The influence of a loss in wall base fixity on overall structural response is dependent on the frequency characteristics of the particular accelerogram used. Complete loss of wall base fixity was demonstrated to result in both improved and deteriorated performance, depending on the base excitation selected.
2. In general, without specific consideration of the likely ground motions at a given locality, it would appear that a frame-wall structure with strength apportioned using the design methods described herein, and assuming full base fixity, is likely to behave in an acceptable manner should full wall base fixity not be available in reality.
3. Levels of structural deformation (e.g. interstorey drift indices, plastic hinge rotations) are influenced by the loss of wall base fixity. Whether these deformations increase or decrease depends on both the change in seismic load (1. above) and the loss in structural stiffness associated with an increase in foundation compliance.

4. Member force patterns indicated by static lateral load analyses for these structures suggest extreme first storey column moment and shear strength demands. High column actions at base level were not indicated in the dynamic analyses performed, however, due to the occurrence of base level column hinging.
   The large shear force reversal that takes place at the first storey level of partially fixed walls implies high inplane slab shear stresses. The possible loss of rigidity of the wall-slab connection in this region may significantly affect load distribution patterns indicated by dynamic analyses.
5. The levels of wall shear force encountered during the dynamic analyses were conservatively predicted by envelopes derived assuming full base fixity. Wall flexural strength demands were also within the bounds of the fixed base design envelopes.
6. There was no apparently important influence of building height or structural wall content (expressed in terms such as "shear ratio" Section 4.1) on these observations which could not be attributed to the influence of period shift on structural stiffness.
7. Although full base fixity is generally assumed in design and known to be unavailable, these results suggest that a degree of compliance is not likely to seriously affect dynamic performance.

5.5 FRAME-WALL STRUCTURES WITH WALLS OF PARTIAL HEIGHT

5.5.1 Introduction

The frame-wall buildings considered in the foregoing sections have all incorporated structural wall elements extending over the full height of the buildings. While this is a common practice the use of structural walls extending only partially up the height of a building is by no means unusual, and the influence of this variation in structural form on seismic behaviour is described in succeeding sections. It is stressed that the buildings examined had wall elements extending from various heights continuously to ground level, i.e. walls were not terminated above ground level. This latter form of construction,with gross stiffness discontinuity near the base of the structure, is considered most unsatisfactory in aseismic design.

5.5.2 Description of Buildings and Elastic Analysis

The response to static lateral (code) loading was investigated for a series of buildings based on the 3.0 and 7.0 m walled structures of Section 4.3. The full range in wall height was considered, with buildings of 3, 6, 9 and 12 storey (i.e. full height) walls included in the study, as well as the response of the frame component only. The wall height transition is illustrated diagramatically in Fig. 5.23. These partial height walled structures had identical geometrical and stiffness properties to their parent structures.

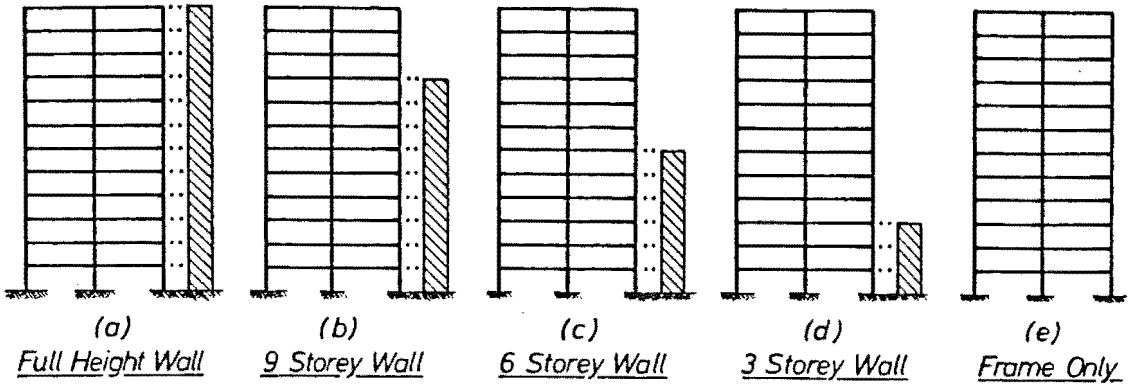

Fig. 5.23 Diagrammatic Representation of 12 Storey Partial Height Walled Buildings.

Both fully fixed and pinned base walls were used. The same lateral loading (as given in Fig. 4.18) was used for each building, despite the fact that a 20% lesser loading is allowable in NZS 4203 for the pure moment resisting frame. This was done so as to allow meaningful comparison to be made of the levels of member actions for this frame structure and the frame-wall buildings. Envelopes of structural deformation and member actions are subsequently presented and compared. It should be noted that the discussion is related to static elastic loading only, and that inelastic response patterns and trends may be different.

5.5.2.1 Interstorey drifts: Decreasing wall height had little effect on the drifts experienced by the 3 m fixed base wall structures (Fig. 5.24). This is because of the relatively high flexibility of this wall; the loss of this element makes comparatively little difference to the total structural stiffness. Similarly, the further loss in stiffness associated with the pinned wall structure does not dramatically increase lateral drifts. An interesting feature of the

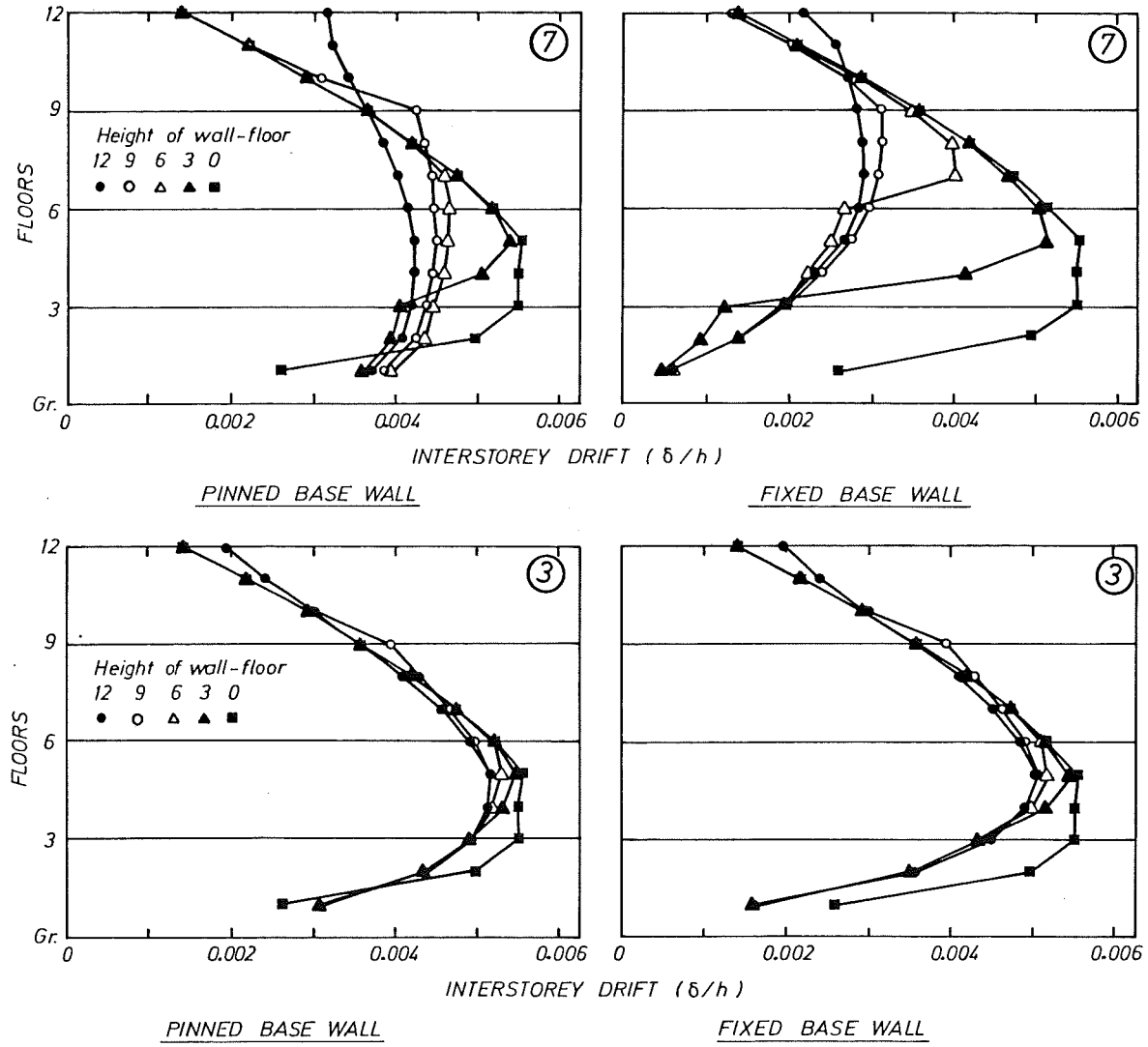

Fig. 5.24 Interstorey Drift Envelopes - 12 Storey Buildings - Code Loading.

drift envelopes is the fact that the loss of the structural wall element at the top of the building actually leads to reduced drifts over the top four storeys. This may be explained by consideration of the different modes of response to lateral loads of uncoupled wall and frame elements. Fig. 2.1 illustrates the manner in which a frame restrains a full height wall over the upper levels of a coupled frame-wall building, and it is clear that the absence of a wall component in that region will reduce the displacements of the frame elements.

In the case of the 7 m walled structure (fixed base), the loss of wall height alters drift patterns more dramatically due to the relatively larger stiffness of the 7 m wall. Drifts above the top of the shortened walls quickly converge to the drift envelope of the pure frame structure. As would be expected from stiffness considerations, the pinned base structures were less sensitive to a loss in wall height.

5.5.2.2 Frame Actions:

1. Beam Moment

Envelopes of beam moment (Fig. 5.25) for both the fixed and pinned base wall structures are similar in form to the interstorey drift envelopes. Due to this similarity in trends, they are not discussed further.

2. Column Shear Force

The loss of wall height exerts little influence on column shear force envelopes for the 3 m fixed base wall structure (Fig. 5.25 (a)(b)). The complete absence of a wall does somewhat increase column shears over the lower 3 storeys however. In the pinned 3 m wall structure partial height wall envelopes are similarly consistent, although the pure frame bottom storey shear force is markedly less than the large bottom storey forces associated with the pinned wall structures.

More complex trends are indicated by the 7 m walled structure. Firstly, for the fixed base wall structure the 9 storey wall envelope is similar to that of the full height wall. The 3 and 6 storey wall structures have envelopes of column shear force which follow the pure frame envelopes down the structure until the wall top, where a sudden decrease occurs as lateral load is taken by the wall. The negative shear indicated for the 3 storey walled structure occurred because of the restraint afforded the frame at the 3rd floor level by the very stiff short 7 m wall. Trends exhibited by the 7 m pinned wall structures are similar to those of the 3 m pinned wall structures.

5.5.2.3 Wall actions: Envelopes of wall bending moment for the 3 m fixed base wall structures (Fig. 5.26) show virtually no change over the bottom 3 storeys, despite the decrease in wall height. The negative upper floor moments recorded for the 6 and 9 storey walls indicate that the frames help restrain the tops of these shorter walls, as occurs for the case of the full height wall. The 3 storey wall is too stiff to exhibit this reversal in curvature. For the 3 m pinned

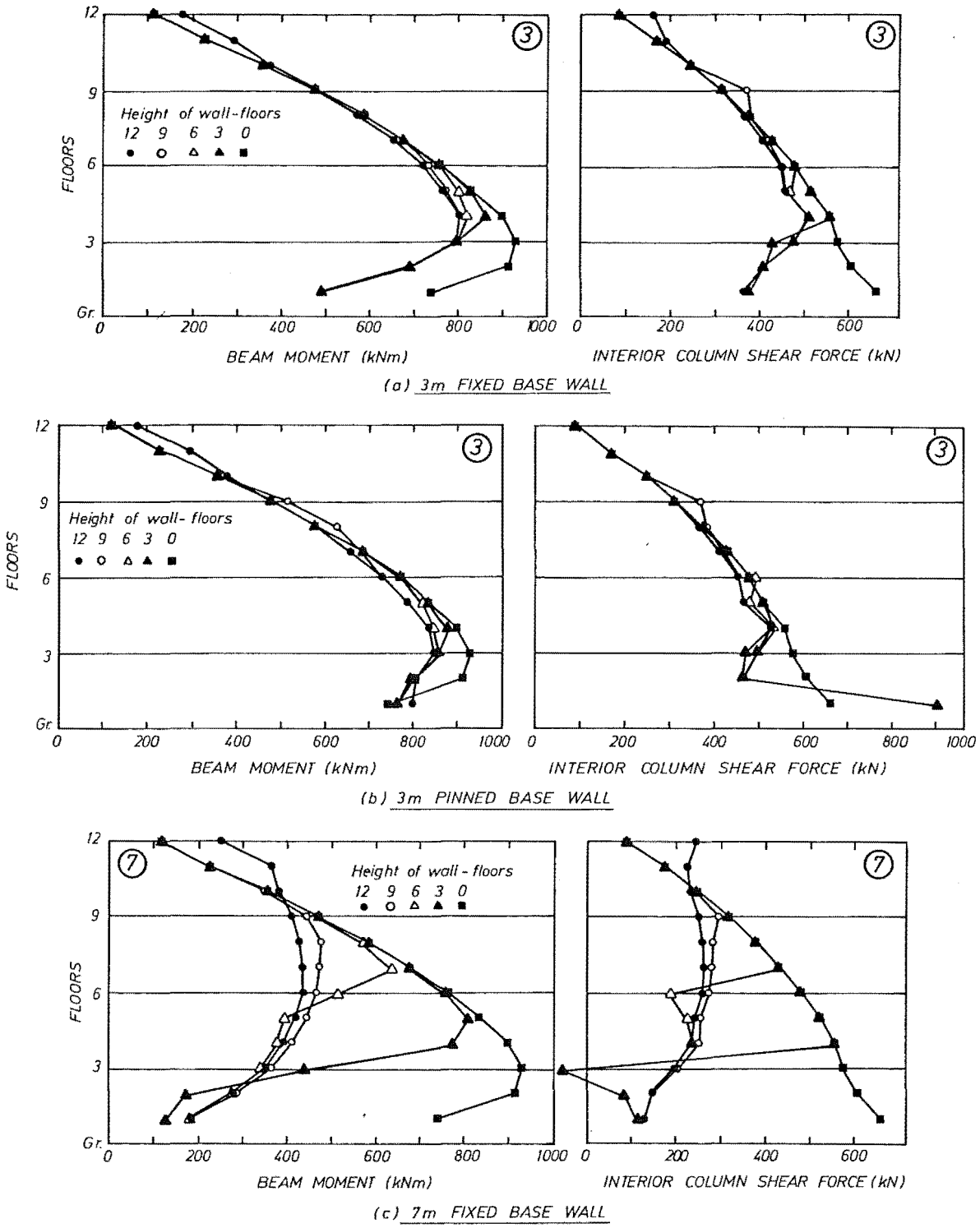

Fig. 5.25 Beam Moment and Column Shear Force Envelopes - 12 Storey Buildings - Code Loading.

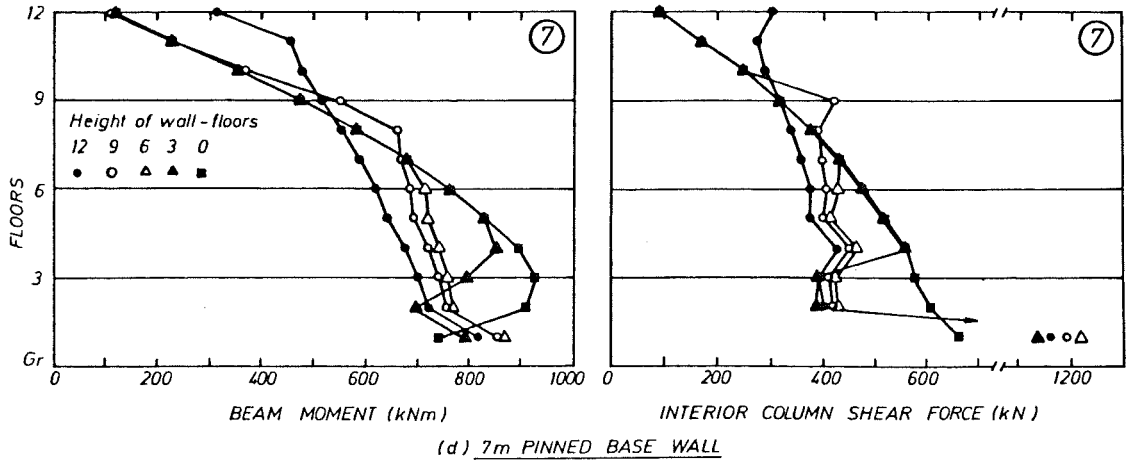

(d) 7m PINNED BASE WALL

Fig. 5.25 (Continued)

wall, moment envelopes quickly converge to that of the full height wall.

No such negative wall moments occur for the 7 m fixed walls, indicating the comparatively greater stiffness of these shorter walls. Moments for the 3 storey wall do not approach the full height wall envelope as do the 6 and 9 storey wall envelopes. Envelopes of pinned wall moment exhibit no unexpected trends.

As illustrated (also in Fig. 5.26) reduction in wall height resulted in little deviation from the full height wall shear force distribution for both fixed and pinned wall types. A general trend, however, was for a small increase in shear over the force for the full height wall structure at a height corresponding to the top of the shorter walls. The comparative invariance of ground level wall shear force means that the structures of varying wall height will have similar shear ratio parameters.

5.6 RESPONSE OF PARTIAL HEIGHT WALL BUILDINGS TO DYNAMIC LOADING

5.6.1 General

The seismic response of the two series of 3 and 7 m walled frame-wall structures to the NS El Centro 1940 accelerogram was investigated. The six buildings (two each with wall height 9,6 and 3 storeys) were designed in the manner described in Section 4.1, assuming full wall base fixity. To reiterate briefly, this procedure entailed firstly the

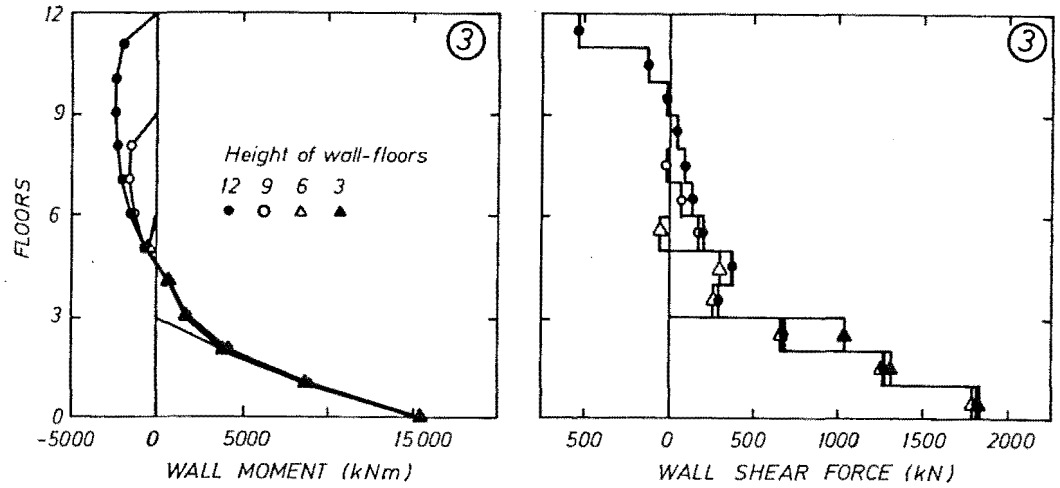

(a) 3m FIXED BASE WALL

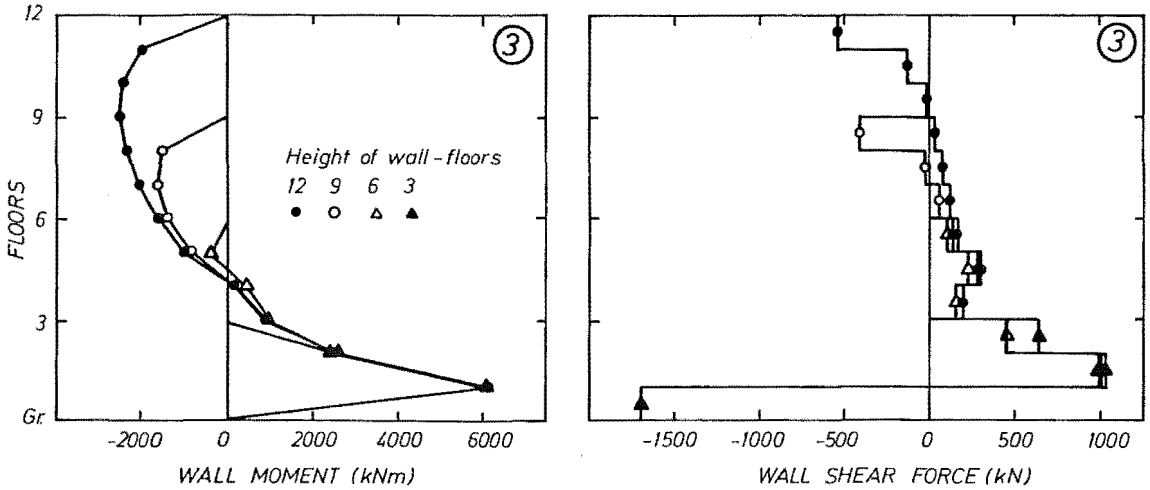

(b) 3m PINNED BASE WALL

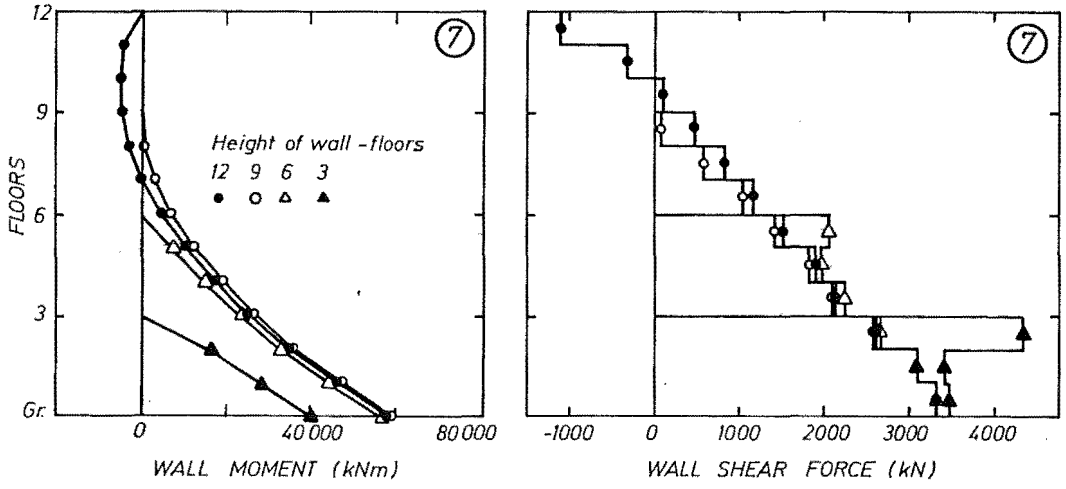

(c) 7m FIXED BASE WALL

Fig. 5.26 Wall Moment and Shear Force Envelopes - 12 Storey Buildings - Code Loading.

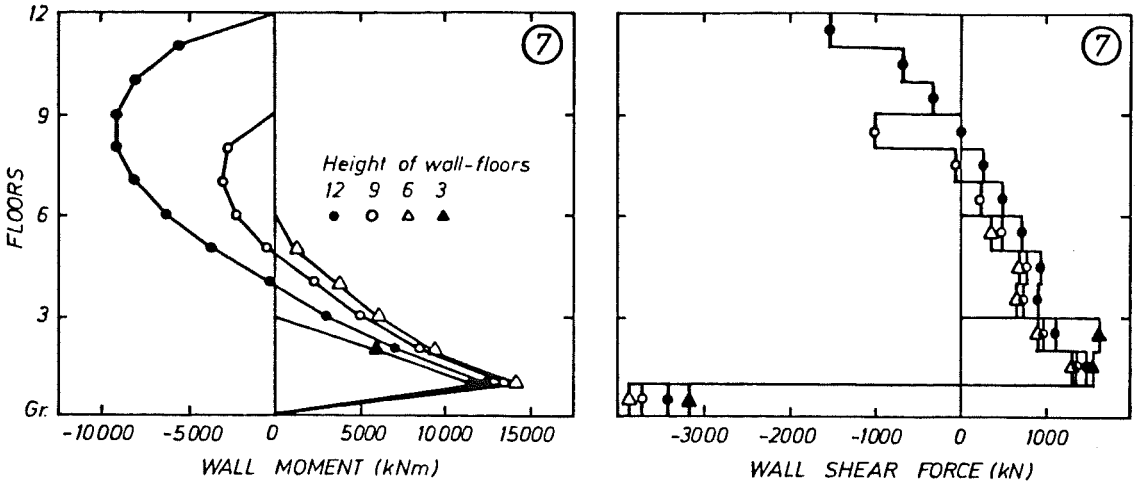

Fig. 5.26 (Continued)

design of beam members utilizing both horizontal and vertical moment redistribution. Columns were designed for actions factored up from the static lateral (code) analyses, recognizing the likelihood of both beam flexural overstrength moment input and dynamic magnification of code forces. A basic dynamic magnification factor of $\omega = 1.2$ was again used.+ Walls were designed for linear envelopes of flexural strength as shown in Fig. 4.2 when reverse curvature of the walls occurred in the code analyses, or for a similarly constructed linear envelope [39] where single wall curvature was apparent.

In addition, the response of the "no wall" or frame only structure was investigated. This structure was designed according to the codified procedure for ductile multistorey frames [34], assuming the building to be a one-way frame. In recognition of the pure frame configuration of this structure, code actions based on a structural type factor of $S = 0.8$ were used ($S = 1.0$ has been used throughout the hybrid frame-wall structures). The basic dynamic magnification factor used for column design was $\omega = 1.8$, the recommended value [34] for this building. Although some column reinforcement requirements were relatively high (up to $\rho_t = 2.7\%$) and would in practice probably necessitate an increase in member size, the same structural geometry as used for the frame component of the frame-wall buildings was retained for consistency.

+ both above and below the wall cut-off point.

The dynamic response to the El Centro accelerogram of the six frame-wall structures, and the pure frame building was investigated. In addition, the behaviour of the six frame-wall structures modified to a pin base wall condition (but in all other details identical to their respective fixed wall counterparts) was examined. Only those features of response which are considered most important are discussed, with other aspects only briefly commented upon.

5.6.2 Horizontal Deflection

Time history diagrams of horizontal deflection are not shown as they illustrate no significant differences from previously presented findings (Section 4.3.3.1). Envelopes of maximum interstorey drift indices are shown in Fig. 5.27. They show a lesser variation in drifts with varying wall height for the 3 m walled structures as compared to the

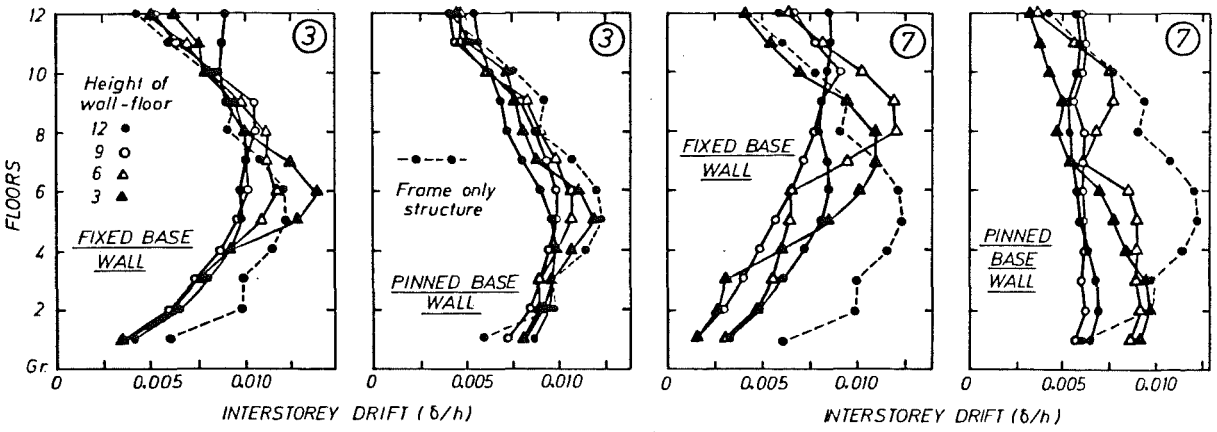

Fig. 5.27 Interstorey Drift Envelopes - 12 Storey Buildings.

7 m buildings, a trend also evident under static lateral loading (Section 5.5.2.1). The levels of deformation experienced by the frame-only structure are excessively large, reflecting the high flexibility of the frames when uncoupled to structural walls. Pinned wall buildings indicate drift indices which are more constant over the height of the structure, with lesser discontinuities in the envelope associated with wall termination.

5.6.3 Wall Actions

Wall flexural strength demands were well estimated by the linear envelope used in design with significant yielding restricted to the base sections of the fixed walls. No yielding was indicated over the height of the pinned base walls which were allocated the same strength distribution as the corresponding fixed walls.

Wall shear force envelopes are shown in Fig. 5.28 for for both wall fixity conditions. Also indicated are design envelopes, derived as follows: the design base forces were determined using the procedure of Section 4.1, with the basic cantilever wall dynamic magnification factor ω_v as prescribed in Ref. 34, based on actual wall height. These values were 1.5 for 6 and 9 floor walls and 1.2 for the 3 storey walls. Shear ratio values were calculated and a base overstrength value of 1.45 was used. Design forces at higher levels were taken as the larger of either (i) that force calculated using the envelope of Fig. 4.3 assuming H to be the total structural height rather than the actual wall height, or (ii) the force $\phi_o \omega_v^* V_{code,i}$, where $V_{code,i}$ is the code shear force at the ith level being considered.
The former method gave the critical force in most cases, with the latter approach necessary only for the 3 storey 7 m wall, where the 3rd floor code shear force exceeds the base level value. As may be seen from Fig. 5.28 the observed levels of wall shear force (both for fixed and pinned base walls) are well predicted by this method at most levels.

5.6.4 Column Moments

Envelopes of maximum column moment demands and the probable section capacities (calculated in the manner described in Section 4.2.4.5) are shown in Fig. 5.29. In general, those columns, at least one storey below the wall top are well protected against yielding, except at base level where yielding is expected. Columns above the wall top and in the uppermost storey where the wall is present enjoy a lesser level of reserve strength and indeed their capacity is often less than the strength demand calculated in the dynamic analyses. This tendency was reduced for the columns of the pinned wall structures. These columns attracted smaller flexural strength demands than the corresponding fixed wall base columns. There was no evidence of abnormally large column strength demands at the level of the wall top.

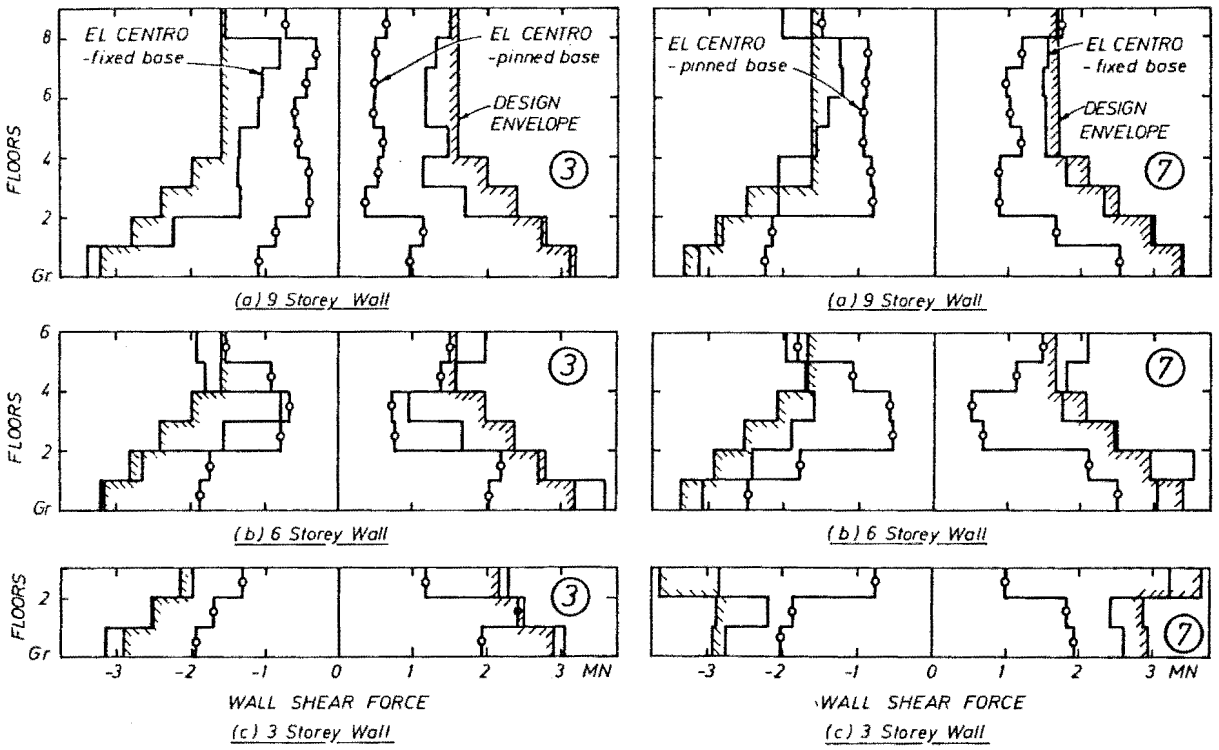

Fig. 5.28 Wall Shear Force Envelopes - 12 Storey Buildings.

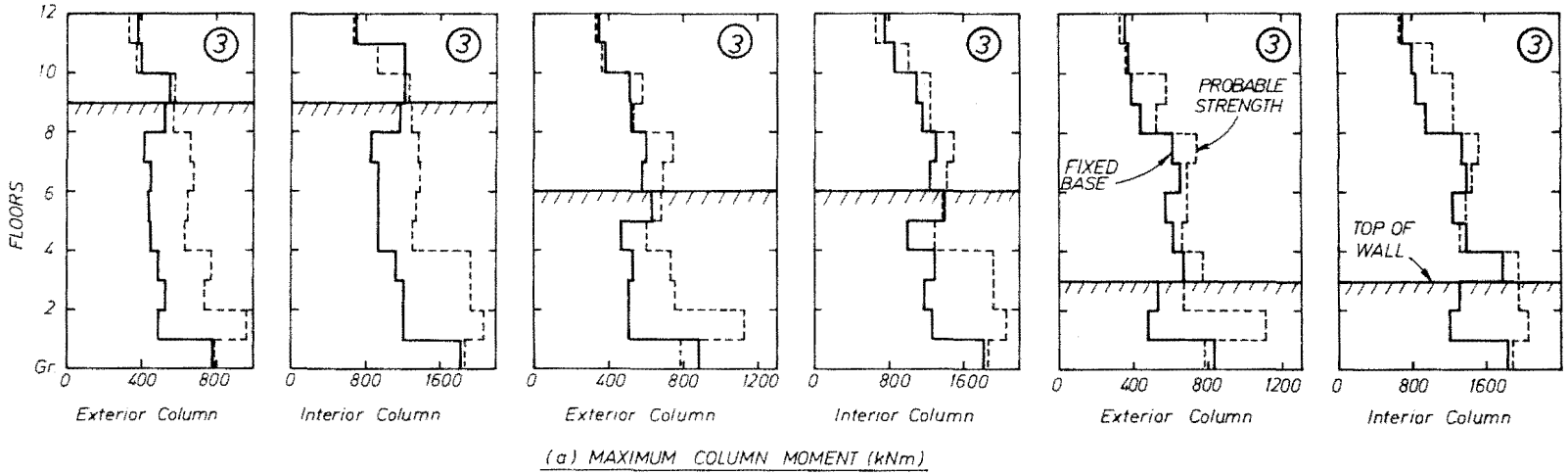

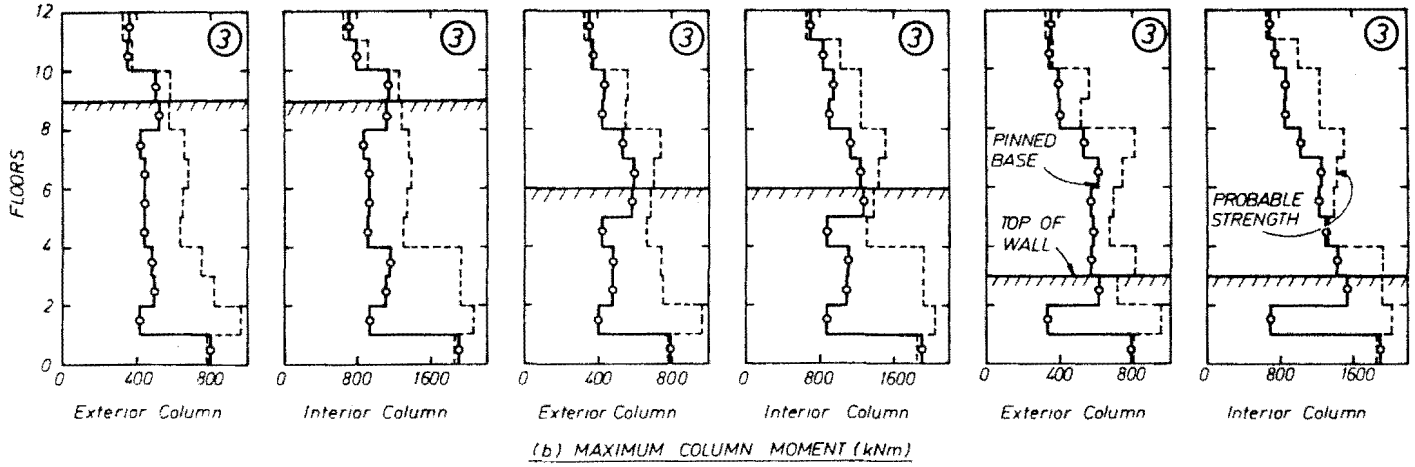

Fig. 5.29 Column Moment Envelopes - 12 Storey Buildings.

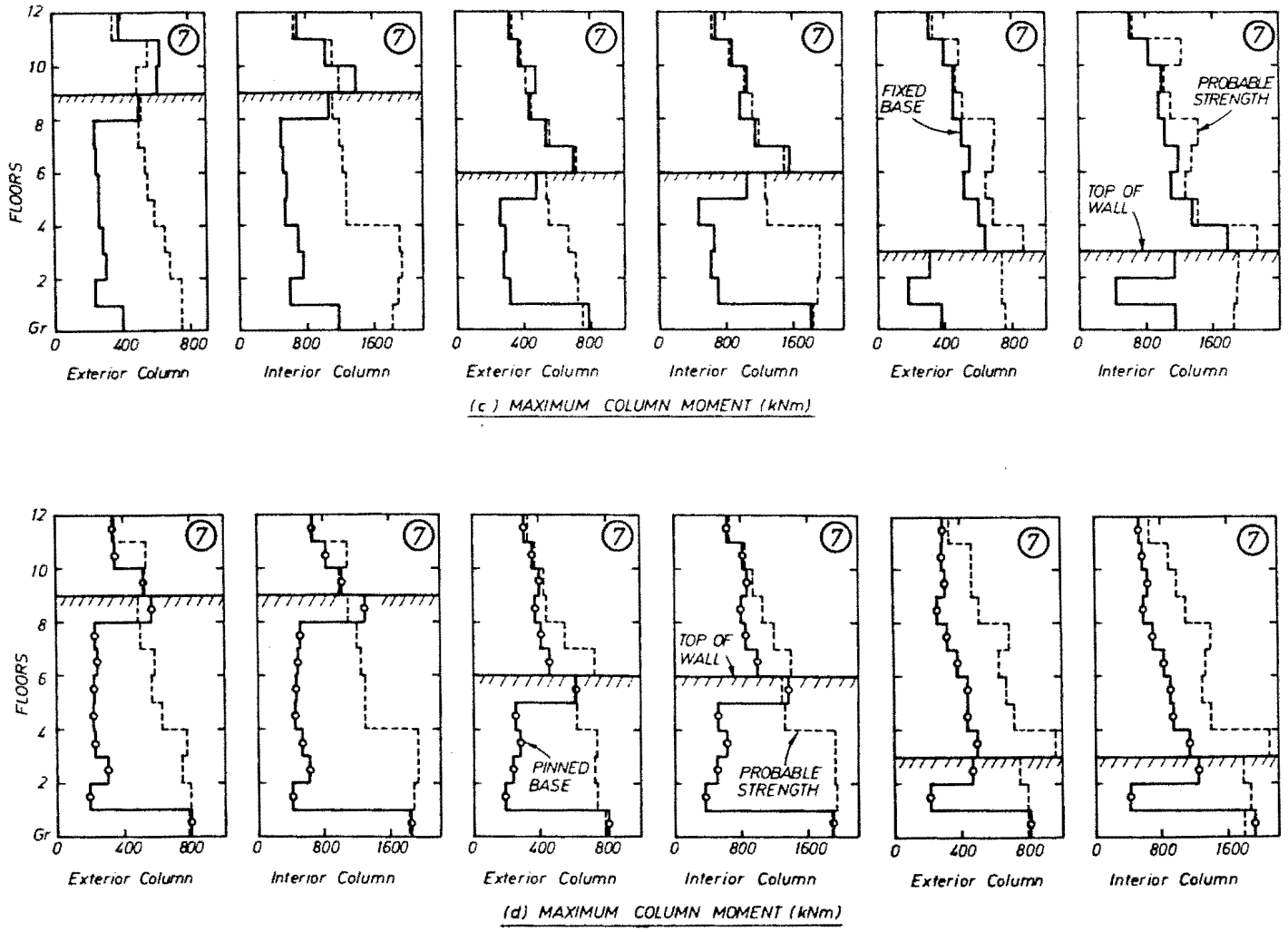

Fig. 5.29 (Continued)

Although the magnitudes of the plastic rotations associated with this upper level yielding are low (< 0.005 radians), it is apparent that higher column strengths are desirable if the intended hierarchy of plastic hinge formation is to be maintained. This would be done most appropriately by the use of larger dynamic magnification factor (ω) in the design of those columns at and above the level of the wall top. Such an approach is reasonable in view of the fact that above the wall top the building is a pure frame structure, and hence values of ω (in excess of 1.2, which has been found appropriate for coupled frame-wall configurations) should be used [34]. Because even a partial wall presence exerts some control on high mode participation during seismic response, it seems unreasonable to use the full "frame only" ω values for the above wall region (which could be as large as 1.9). Check calculations reveal that a value of $\omega = 1.5$ used in the design of the above wall frame would be sufficient to eliminate column yielding in that area. The proposed column ω value scheme for frame-wall structures with walls of partial height is shown in Fig. 5.30.

Column moment and shear force demands for the frame only building are shown in Fig. 5.31. Column yielding was restricted to top and ground floor levels. A value of $\omega = 1.8$ was used in the flexural design of the columns.

5.6.5 Column Shear Force

Maximum levels of column shear force encountered during the analyses are presented in Fig. 5.32, together with design forces based on the fixed base wall code actions, and calculated according to the method of Section 4.1. Again, the design envelope predicts the maximum forces well over the height of the structure except as follows:

(i) at the levels at which the 7 m wall was terminated, design shear forces consistently under-estimated the calculated peak forces. This was due to the low code (static) shear forces in these areas. This shortcoming may be readily overcome by using the same design force as for the floor above the wall top.

(ii) in the first storey, design shear force values, calculated as the maximum of $2.5\phi_o V_{code}$ or $(M^o_{col} + 1.3\phi_o M_{code,top})/(\ell_n + 0.5h_b)$ (Section 4.1.1) are often well in excess of the maximum demand for the fixed base wall structures indicated by the dynamic analyses. However, check calculations reveal that the quantities

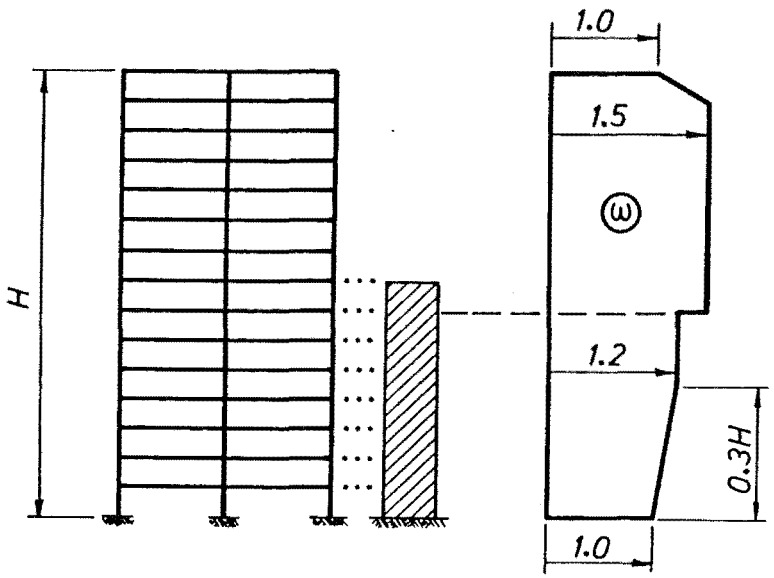

Fig. 5.30 Column ω Factor for Partial Height Wall Structures.

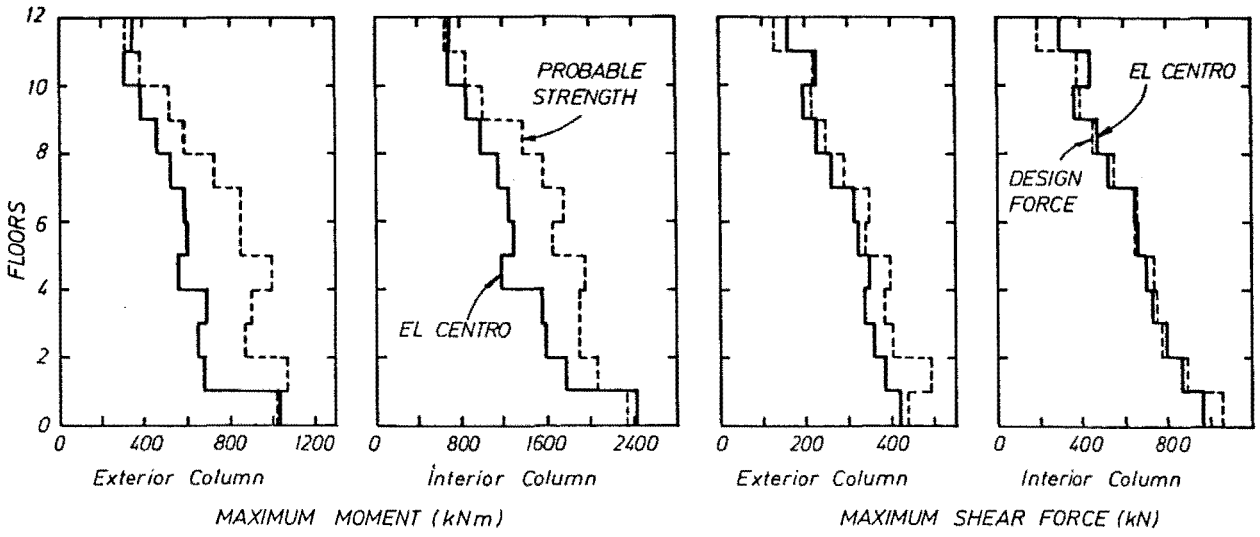

Fig. 5.31 Column Moment and Shear Force Envelopes - Frame Only Building.

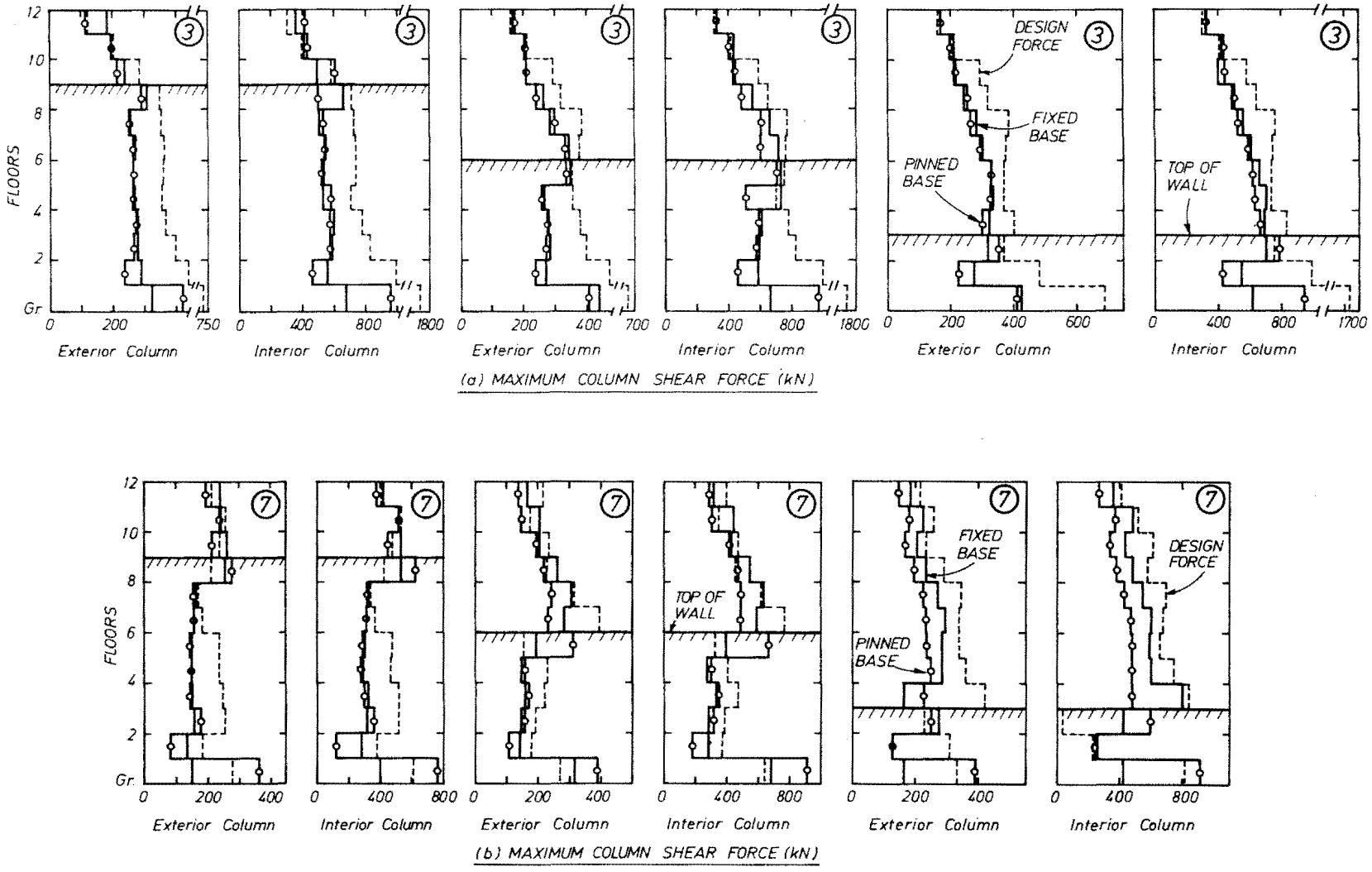

Fig. 5.32 Column Shear Force Envelopes - 12 Storey Buildings.

of transverse reinforcement required to sustain these design forces are not excessive, and hence these design force levels may be considered to be acceptable.

Forces associated with the pinned wall structure exhibit familiar trends (cf. Section 5.3.2.3). Fixed base structure design forces adequately envelope all but the ground floor shear forces for the 7 m wall, and the forces at levels corresponding to the last storey with a structural wall presence. The latter shortcoming may be remedied by the method suggested in (i) above. It is not surprising that design force levels based on an analysis assuming fixed base structural walls are unable to envelope base level column shear forces for a pinned wall structure. If doubts are held as to wall base fixity, it would appear prudent to design base level columns for a level of shear force that is considerably in excess of that derived for a fixed base structure. The force associated with the development of the flexural overstrength of both the top and bottom of ground floor columns is a conservative upper bound value which may be used. The quantities of transverse reinforcement required to resist such forces are not likely to be prohibitive provided that low column reinforcement ratios are used.

Levels of column shear force in the frame-only building, shown in Fig. 5.31, were well estimated by the relevant design level forces.

5.6.6 Plastic Rotations

Levels of plastic rotations in beam column and wall members were of similar levels to those encountered in the full height wall analyses and are for this reason not discussed further.

5.7 CONCLUSIONS REGARDING THE PERFORMANCE OF PARTIAL HEIGHT WALL BUILDINGS

1. It is considered that the analyses performed indicate that good seismic response may be expected from well detailed frame-wall structures in which the structural wall component extends from ground level to only partway up the building. Unduly high local ductility demands in frame members near the wall termination point were not observed.

2. The design methods proposed for frame-wall structures incorporating full height structural walls appear to be applicable to these

partial-height walled structures with relatively few modifications. The most important of these involves the use of a column moment dynamic magnification factor larger than 1.2 for those members at the level of and above the wall top. This procedure recognises the change in structural form, from coupled frames and walls to frame-only, which characterises these buildings.

3. Adequate levels of design wall shear force may be obtained using the previously proposed methods, with the envelope of forces constructed using the total building height rather than the actual wall height. Special care and possibly more sophisticated modelling may be required when short, squat wall elements are involved.

4. Loss of wall base rigidity, investigated by consideration of the behaviour of pinned base wall structures, may not lead to seriously impaired performance as was found for the full height walled buildings discussed previously.

Chapter Six INTRODUCTION TO EXPERIMENTAL INVESTIGATION OF STRUCTURAL WALLS

6.1 INTRODUCTION

Many buildings depend on relatively thin structural walls for all or part of their lateral load resistance. These elements may be plain cantilevers or coupled walls, and may be used in conjunction with moment resisting frames. The desirability of well detailed structural walls being incorporated in buildings at risk to seismic attack is due to:

1. The protection afforded the building and its contents at low intensity seismic attack due to the high stiffness of wall elements,
2. The strength of walls which limits structural damage at moderate design levels of earthquake loading, and
3. The deformation and energy dissipation capacities of walls which can ensure structural survival during extreme seismic events. SEE ERRATA

There are several groups of issues related to the design of structural walls. These are, the basic philosophy of design; the geometric details and arrangements of wall elements in the building; the apportioning of flexural and shear strength and the relationship between these; and the detailing of the walls which permits the development of large inelastic deformations in certain preselected locations. The approach taken to structural wall design in New Zealand [34] is discussed in the subsequent section.

Relatively few experimental investigations of structural wall behaviour have been undertaken, with the notable exceptions of the on-going studies made by the Portland Cement Association [53,54] and at the University of California, Berkeley [55,56]. A description and summary of some major findings of these programs is given in Section 6.3.

The experimental work described herein was undertaken with the primary objectives of assessing the adequacy of current code [34] provisions for (i) the prevention of premature inelastic instability, and (ii) the allocation of hoop reinforcement in regions subjected to high compression strains. The test set up, design, construction and instrumentation of the wall units and test procedures are described in the last section of this chapter.

6.2 THE APPROACH TO STRUCTURAL WALL DESIGN IN NEW ZEALAND

6.2.1 General

This section contains a description of some of the background to and details of the design procedure recommended for slender cantilever structural walls by NZS 3101, the New Zealand Code of Practice for the Design of Concrete Structures [34]. A more detailed treatment of this subject is given elsewhere [39]. It is emphasised that this discussion is relevant to slender, fixed base cantilevered walls designed for fully ductile response to seismic attack.

6.2.2 Preliminary Design

The earliest decisions made with regards the design for lateral load resistance are without doubt most crucial for ensuring favourable seismic response. Structural walls should be arranged in a symmetrical manner, with the avoidance of significant discontinuities in mass or stiffness. In order to minimise the effects of accidental torsion, walls should ideally be placed on the periphery of the structure. Consideration of the feasibility of the intended foundation system should also be made at an early stage.

6.2.3 Loading

Given the relevant details of dead and seismic live loads, structural geometry, site location and characteristics, the design loads for a structure are assessed using NZS 4203, the Code of Practice for the General Structural Design and Design Loadings for Buildings [9]. The total design horizontal seismic static force $V = C_d W_t$, where the seismic design coefficient C_d = CRSM, these four factors being defined in the Notation. Of particular importance are the Structural Type factor, S, and the Material factor, M. The former takes values of 1.2 and 1.0, depending on whether there is one or two or more approximately symmetrically arranged ductile cantilever walls in the structure. For reinforced concrete, the same as for structural steel, the Material factor is 0.8. This reflects the high degree of confidence held in reinforced concrete construction detailed in accordance with the requirements of NZS 3101.

An elastic analysis is generally used to determine the lateral load taken by each wall in the structure, and so the design actions (subsequently designated with the subscript "code") are obtained. These are in the form of shear force and bending moment envelopes, etc.

6.2.4 Capacity Design Philosophy [1]

The capacity design philosophy embodies the a priori selection of a desired response to seismic loading, whereby a favourable failure limit state is chosen. The critical locations in such a structure are detailed in a manner which allows the selected mechanism to develop. Sufficient reserve strength is provided elsewhere throughout the structure so as to preclude the formation of any alternative mechanism. For a cantilever structural wall, the most desirable inelastic response is realised via the flexural hinging of the base section of the wall, a process permitting the dissipation of considerable seismic energy. Thus the wall base section must be detailed to allow the development of large inelastic rotations, and it is generally more economical to make the upper regions sufficiently strong to ensure that significant inelastic deformation demands are not made there. This removes the need for confining reinforcement, stringent requirements for lap splices and conservatively low estimates of concrete shear capacity in the upper region of a structural wall. A wall designed according to this philosophy must also be prevented from failing in a shear mode. The subsequent sections outline the manner in which these aims may be achieved.

6.2.5 Flexural Design

Given the required flexural strength of the critical (ground level) wall section, M_{code}, the necessary flexural reinforcement content is obtained using conventional engineering principles. Irrespective of the intensity of axial compression a strength reduction factor (ϕ) of 0.9 is used. To restrict flexural yielding to this base section, the upper levels of the wall are designed for moments higher than the code moments, as given by the envelope shown in Fig. 6.1. Analytical studies [36, 38] have shown that during seismic attack, strength demands on a wall are unlikely to exceed the capacity of a wall designed to this linear envelope.

The maximum flexural strength of the base section is also assessed at this stage. This so-called flexural overstrength (M^o) typically exceeds M_{code} by a factor of approximately $\phi_o > 1.39$, when $f_y = 275$ MPA and $\phi_o > 1.56$ when $f_y = 380$ MPa. This increase is attributable to such factors as strain hardening of reinforcement, likely concrete strength in excess of the design value, and the possibility of a larger axial load than was used in the determination of the flexural reinforcement. The wall overstrength factor is calculated as $\phi_o = M^o/M_{code}$, where both moments refer to the critical base section.

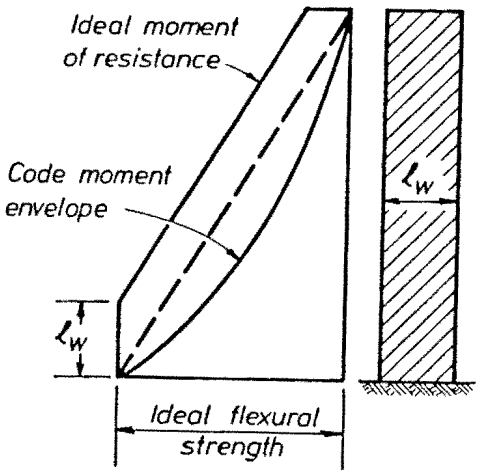

Fig. 6.1 Moment Design Envelope for Cantilever Structural Walls.

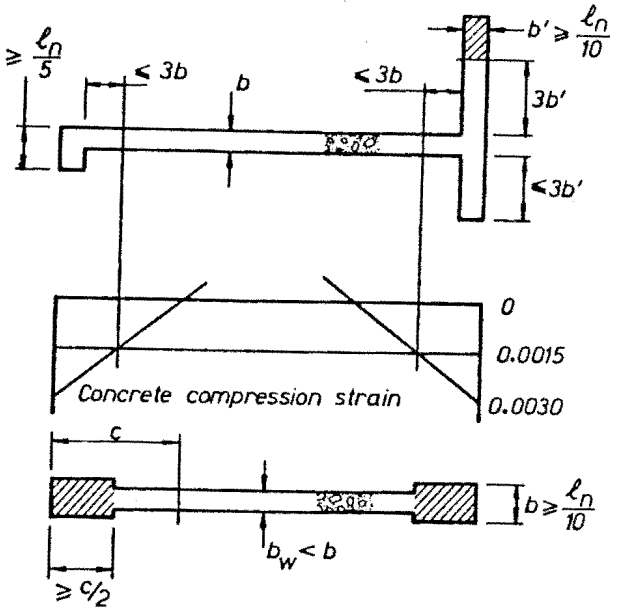

Fig. 6.2 Parts of a Wall Section to be Considered for Instability.

6.2.6 Detailing for Ductility

To enable the inelastic rotations associated with wall base hinging to develop, special detailing of the wall base section (plastic hinge zone) is necessary. These provisions consider three aspects: (a) Dimensional limitations are imposed to prevent premature out of plane instability of the base section. (b) Hoop reinforcement is provided to prevent the premature degradation of wall compression zones. This reinforcement is required to confine the outer regions of the compression zone and thus enable significant plastic curvatures to develop. The hoops also delay the onset of inelastic buckling of the principal vertical reinforcement. (c) Adequate shear reinforcement is required to ensure that diagonal tension failure of the section does not occur.

6.2.6.1 Dimensional limitations: It is recommended that in the outer half of the calculated compression zone, the wall thickness to clear storey height ratio should not be less than 1 to 10. This need not be complied with if the fibre of compression strain of 0.0015 is within a distance of the lesser of 2b or $0.15\ell_w$ from the extreme compression fibre. In such a case it is considered that the compressed area of the wall is sufficiently small to be adequately stabilized by adjacent parts of the wall. Figure 6.2 shows other cases in which dimensional limitations may also be of importance, and affected by the presence of flange elements. Part of a wall subject to compression strains in excess of 0.0015 but within a

SEE ERRATA

distance of 3b of a supporting flange are not subject to the $b \geq \ell_n/10$ limitation, although parts of flanges further than 3b' from the wall web should comply with this criterion. Where a flange is not present, a boundary element of length at least $\ell_n/5$ may be formed that satisfies the slenderness limit to provide lateral support to the web.

It is stressed that these dimensional limitations are empirical and were based on intuitive judgement due to the absence of experimental data on wall stability at the time NZS 3101 was being drafted.

6.2.6.2 Hoop reinforcement: The following empirical rules are suggested for the provision of hoop reinforcement:

(a) Confinement: when the critical computed neutral axis depth exceeds the critical value $c_c = 0.10\phi_o S\ell_w$ (6.1)

or the value

$$c_c = \frac{8.6\phi_o S\ell_w}{(4 - 0.7S)(17 + h_w/\ell_w)} \quad (6.2)$$

the outer half of the compression zone where strains exceed 0.0015, should be provided with transverse confining reinforcement as below, over a height equal to the wall length. Confinement in the form of polygonal hoops with or without supplementary cross ties should surround the longitudinal bars in the region to be confined, such that

$$A_{sh} = 0.3 s_h h'' \left(\frac{A_g^*}{A_c^*} - 1\right) \frac{f'_c}{f_{yh}} \left(0.5 + 0.9 \frac{c}{\ell_w}\right), \text{ and} \quad (6.3)$$

$$A_{sh} = 0.12 s_h h'' \frac{f'_c}{f_{yh}} \left(0.5 + 0.9 \frac{c}{\ell_w}\right) \quad (6.4)$$

where c/ℓ_w need not be taken more than 0.8. In addition, vertical spacing of hoop sets, s_h, should not exceed 6 times the diameter of the vertical bars confined, one third the thickness of the confined wall, or 150 mm, whichever is less. It should be observed that by complying with these recommendations for the provision of confinement reinforcement, the need for a detailed calculation to estimate curvature ductility capacity is avoided. Equations (6.3) and (6.4) are extensions of similar requirements developed for columns. There is little experimental evidence regarding hoop reinforcement requirements in walls.

(b) Antibuckling: where 2 or more layers of potentially yielding longitudinal reinforcement are present with an area ratio of $\rho_\ell = \Sigma A_b/(b s_v)$ in excess of $2/f_y$, transverse ties satisfying the

following requirements should be provided:each bar or bar bundle near a wall surface should be restrained against buckling by a 90° bend or at least a 135° standard hook of a tie. When two or more bars no more than 200 mm apart are so restrained, any bars between them are exempted from this requirement. The area of one leg of a tie, A_{te}, in the direction of potential buckling of the longitudinal bar should be such that

$$A_{te} = \left(\frac{\Sigma A_b f_y}{16 f_{yh}} \cdot \frac{s}{100}\right) \qquad (6.5)$$

where ΣA_b is the sum of the areas of the longitudinal bars (including those exempted from support as mentioned previously) being restrained by the tie. In addition, the tie spacing s should not exceed 6 times the diameter of the longitudinal bar being restrained.

6.2.6.3 Shear design: Although some aspects of the background to structural wall shear design were discussed in Chapter 3, this information is presented again for completeness. The main features of the shear design advocated by NZS 3101 are to magnify the "code" shear force distribution and to allocate horizontal reinforcement for that part of the design stress that cannot be sustained by concrete shear resisting mechanisms.

The magnification of the code shear force distribution is done in two parts. Firstly, it is assumed that a shear force larger than V_{code} could develop at any level in the structural wall. This is associated with the attainment of the flexural overstrength of the base section. This force is $(M^o/M_{code}) \times V_{code} = \phi_o V_{code}$ Secondly, it is assumed (on the basis of dynamic analyses [38] that during seismic attack the frequency characteristics of the excitation may be such as to induce significant participation of modes of vibration other than the first. (The codified distribution of shear force is intended to represent that associated with the first mode of vibration of the structural wall). The critical effect of higher mode participation is to lower the centroid of the inertia forces on the wall and thus with the development of the overstrength base moment a higher moment gradient will be associated with a base shear larger than $\phi_o V_{code,base}$. This dynamic shear magnification, the subject of the study discussed in Chapter 3, is assumed to be dependent on the number of storeys in the structure. The dynamic shear magnification factor, ω_v, takes values between 1.0 and 1.8. Thus the design base shear force is $V_{wall,base} = \phi_o \omega_v V_{code,base}$,

and in general, at any level of a structural wall, $V_{wall} = \phi_o \omega_v V_{code}$. The rationale behind the magnification of code shear force is illustrated in Fig. 6.3.

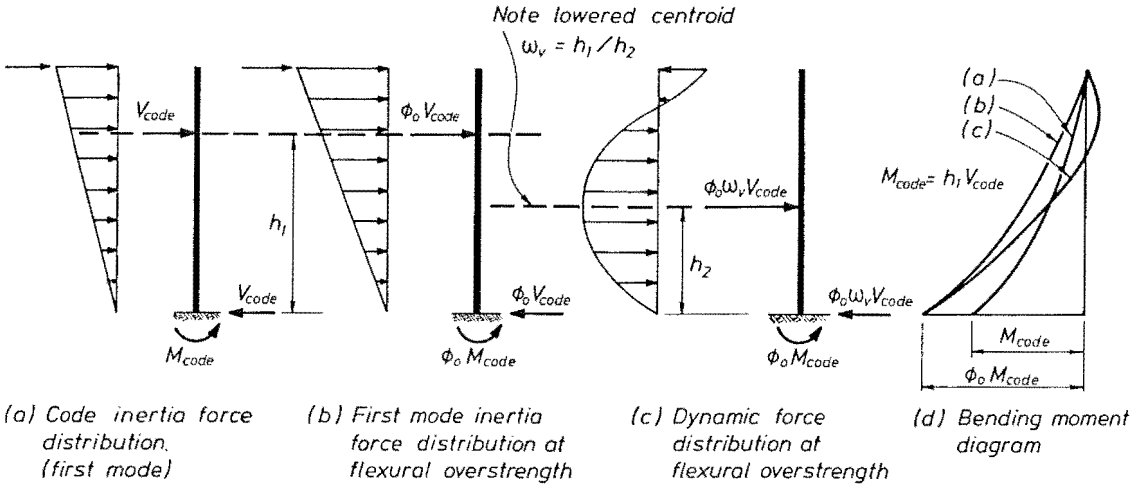

Fig. 6.3 A Comparison of Code and Dynamic Lateral Loading.

With the design shear forces thus established, the required quantity of shear reinforcement may be determined over the height of the wall. The base section only is dealt with herein, as it is of critical importance. The shear stress index

$$v_i = V_{wall}/(b_w d) \tag{6.6}$$

where d need not be taken less than $0.8\ell_w$, is subject to two limitations as follows:

$$v_{i\ max} < (0.3\phi_o S + 0.16)\sqrt{f'_c} \tag{6.7}$$

$$v_{i\ max} < 0.9\sqrt{f'_c} \tag{6.8}$$

where f'_c is in MPa units and S is the structural type factor. The development of these two criteria in New Zealand was stimulated by the findings in the tests by the Portland Cement Association [53,54] and the University of California, Berkeley [55,56], discussed in Section 6.3. The former expression contains a basic concrete shear capacity $(0.16\sqrt{f'_c})$ and trades off stress level against implicit ductility demand (ϕ_o vs S), the forementioned tests having indicated that shear failure depends on both stress level and inelastic deformation demands.

Where the structural type factor is large (typically S ≥ 1.6) and a limited displacement ductility demand is expected, a larger shear stress may be sustained than for a more ductile wall. Similarly, the value of ϕ_o being larger than the minimum (given in Section 6.2.4) indicates that strength in excess of that required by code loading has been provided and this is expected to result in a reduction of ductility demand. The limitation of $0.9\sqrt{f'_c}$ was considered to be a reasonable upper bound on allowable reversed shear stress in potential plastic hinge regions, to preclude premature diagonal compression failure. SEE ERRATA

When the design shear is derived from capacity design procedures, as given in Eq. 6.6, the value of the strength reduction factor, ϕ, is unity.

Having established v_i, the concrete contribution to shear strength is calculated as

$$v_c = 0.6\sqrt{(P_u/A_g)} \tag{6.9}$$

in the plastic hinge zone. In the upper regions of the wall, the value of v_c may be taken as that appropriate to members subject to gravity (non seismic) load only. These provisions are summarised below. Unless a more detailed calculation is made, in accordance with Eqs. 6.12 or 6.13 below,

$$v_c = 0.2\sqrt{f'_c} \tag{6.10}$$

for walls in compression, and

$$v_c = 0.2(\sqrt{f'_c} + P_u/A_g) \tag{6.11}$$

for walls subject to P_u in tension (taken to be negative). MPa units should be used for these non-homogeneous equations. Alternatively, v_c may be taken as the lesser of the following two expressions:

$$v_c = 0.27(\sqrt{f'_c} + (P_u/4A_g)) \tag{6.12}$$

$$v_c = 0.05\sqrt{f'_c} + \frac{\ell_w(0.1\sqrt{f'_c} + 0.2(P_u/A_g))}{(M_u/V_u) - (\ell_w/2)} \tag{6.13}$$

again where MPa units should be used for stresses. P_u is negative for tension, and when $(M_u/V_u) - (\ell_w/2)$ is negative, Eq. 6.13 should not be used. Expressions 6.10 - 6.13 are based on the results of studies made by the ACI [27].

Finally, the required quantity of horizontal reinforcement required to sustain the stress $(v_i - v_c)$ may be computed as

$$A_{sv} = (v_i - v_c)\, b_w s/f_y \qquad (6.14)$$

Design in this manner is considered adequate to preclude the diagonal tension and compression failures of a structural wall.

Although failure via a sliding shear mechanism is unlikely for a fully ductile (and thus probably slender) structural wall, it is recommended that horizontal construction joints, where shear friction is relied upon to transfer shear, be crossed by a minimum amount of vertical reinforcement. The required area of shear friction reinforcement is given by

$$A_{vf} = (V_{wall} - \phi\mu P_u)/\phi\mu f_y \qquad (6.15)$$

The coefficient of friction, μ, takes values of 1.4 for clean interfaces roughened to a full amplitude of more than 5 mm, and 1.0 for 2 - 5 mm amplitude roughness.

6.3 PREVIOUS EXPERIMENTAL STUDIES OF STRUCTURAL WALL BEHAVIOUR

6.3.1 General

Research into the seismic response of reinforced concrete structures has been concentrated principally in three countries - Japan, New Zealand and the United States of America. A considerably smaller effort has been devoted to the study of structural wall behaviour than has been accorded moment resisting beam-column frames, although this trend has been altering in recent years. However, despite the comparative paucity of information regarding structural wall behaviour, only those test programmes considered to be most significant and relevant to design in areas of significant seismicity are outlined here. An extensive bibliography of previous research in this topic is given elsewhere [7]. The conclusions made in the summaries following are as reported by the

authors of the original work. Comments are offered on some aspects of these experimental studies.

6.3.2 Portland Cement Association (PCA) Tests [54]

6.3.2.1 General description of test program: An important series of tests, investigating the behaviour of isolated (i.e. free standing cantilevered) earthquake resistant structural walls, has been carried out by the PCA [54]. 16 tests were reported, with controlled variables being axial load, wall cross-sectional shape (rectangular, barbell and flanged), the quantity of flexural, hoop and shear reinforcement, concrete compression strength, load history and repair techniques. The primary aim of the experimental program was to investigate the ductility, energy dissipation and strength of walls subject to reversing lateral loads.

The test walls were approximately one-third full size, of constant length ℓ_w = 1.90 m (75") and subjected to a lateral point load acting at a lever arm of 4.57 m (15') to the critical section. The non-dimensional moment to shear ratio was $M/V\ell_w$ = 2.40. Typical specimen cross sections, and the experimental set up are shown in Fig. 6.4. No lateral supports (out of wall plane) were provided. Generally, nominal reinforcement yield strength, f_y, and concrete compression strength, f'_c, were 414 MPa and 41.4 MPa respectively.

The observed behaviour of most wall units was distinguished by the nominal shear stress present on the section, $v = V/(0.8\ell_w b)$, with low stress defined as $v \leq 0.26\sqrt{f'_c}$ (MPa units) and high stress as $v \geq 0.58\sqrt{f'_c}$. Walls subjected to low nominal shear stress developed mainly horizontal cracks, along which shear was transferred by dowel action and interface shear. Although these walls yielded initially in flexure, secondary failure modes of inelastic bar buckling and fracture, or lateral instability of the walls developed.

Units with high ($v \geq 0.58\sqrt{f'_c}$) applied shear stress developed inclined shear flexure crack patterns with shear transfer via a truss mechanism. The most common form of failure was by web crushing at the base of the web-flange junction where diagonal compression struts converged (Fig. 6.5). This form of failure was associated with high rotational ductility demands at the critical section, in addition to the high applied shear stresses.

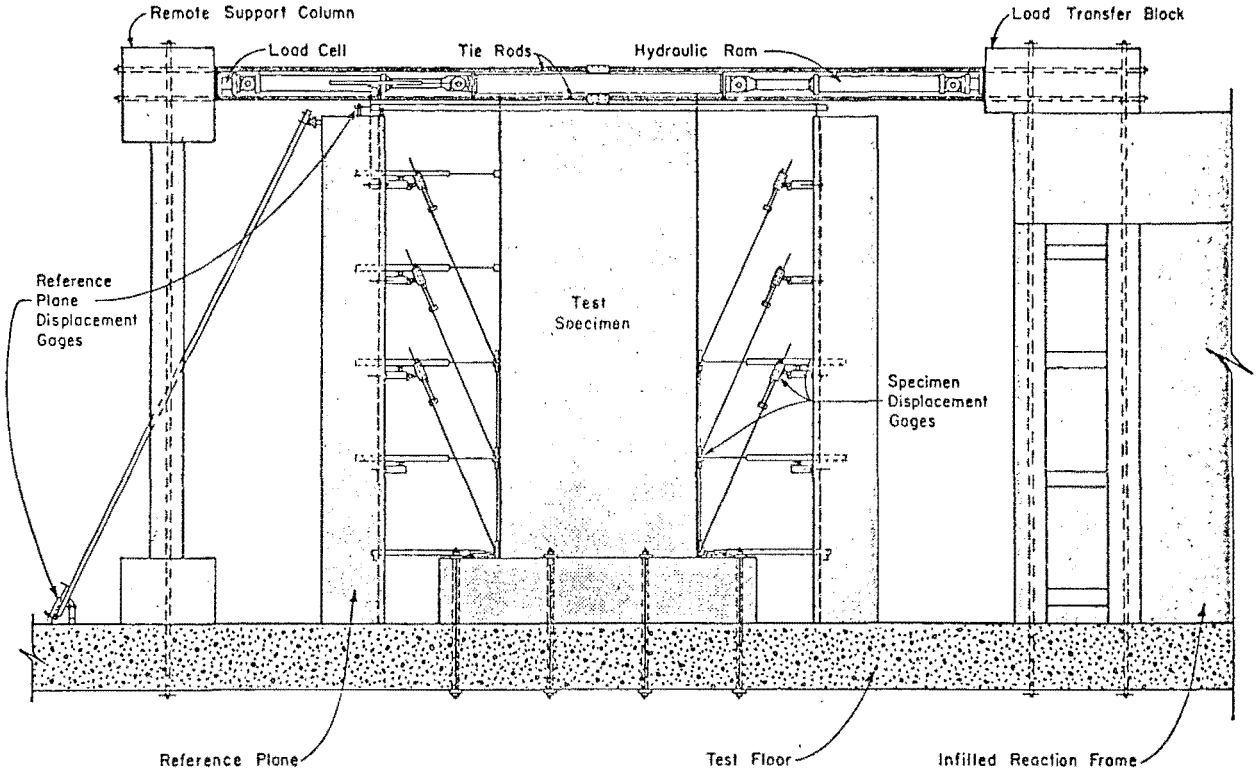

(a) ELEVATION OF TEST SET-UP

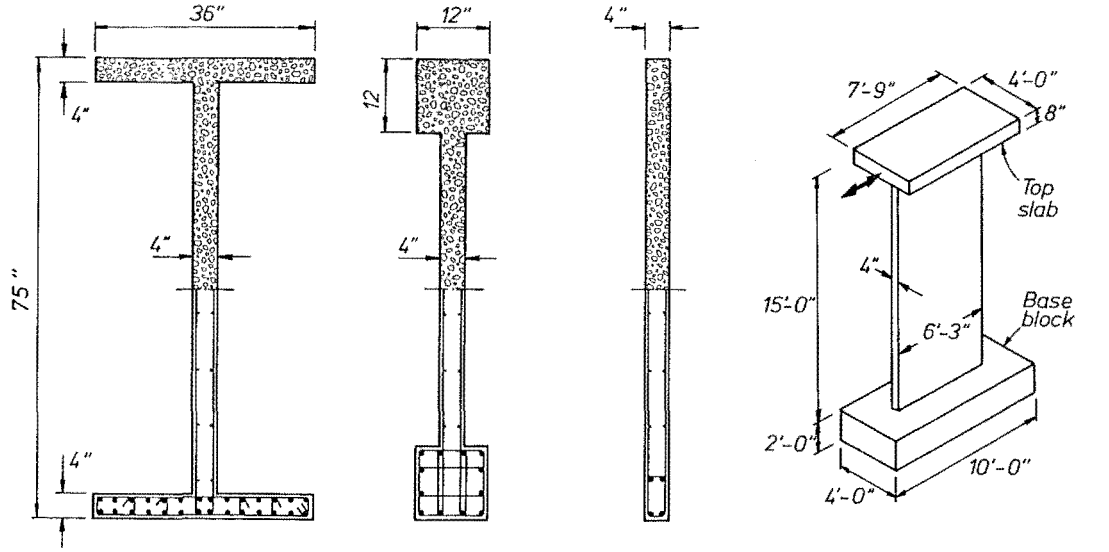

(b) FLANGED SECTION (c) BARBELL SECTION (d) RECTANGULAR SECTION (e) NOMINAL DIMENSIONS OF RECTANGULAR SECTION TEST SPECIMENS

Fig. 6.4 Details of PCA Tests [54].

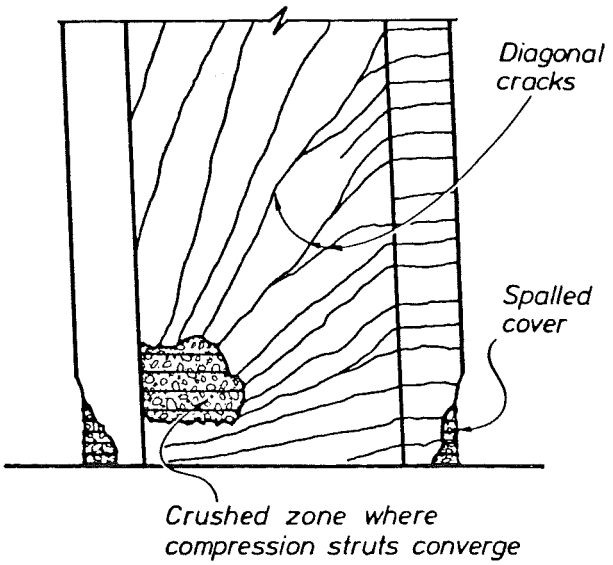

Fig. 6.5 Compression Strut Crushing Failure Mechanism.

6.3.2.2 Effects of program variables on wall behaviour: In this section observations made by the PCA investigators are summarised.

1. Wall Shape

Rectangular walls are most susceptible to out of plane instability, the lateral stiffness being controlled by wall width. Only one case of failure due to lateral instability of the entire wall compression zone was observed, however. For equivalent moment to shear ratios, rectangular sections are generally subject to lower shear stresses. Both barbell and flanged walls have larger out of plane stiffness, but are more susceptible to web crushing failures by virtue of their generally higher moment to shear capacities. The boundary elements of barbell walls may limit shear sliding by acting as large dowels. Flanged walls have a greater potential for flexural resistance and hence larger shear stresses can develop while the web remains relatively thin

2. Quantity of Reinforcement

The walls were tested under a constant moment to shear ratio so that flexural strength (and thus applied shear force) was controlled by the quantity of flexural reinforcement present. More heavily reinforced sections were more prone to a web crushing failure in the compression zone.

Shear reinforcement was allocated on the basis of that force associated with the development of the design moment, based on nominal material strengths. It was concluded that the reinforcement supplied ought to be based on the likely maximum flexural capacity, calculated assuming strain hardening of the flexural reinforcement. The quantity

of horizontal reinforcement supplied was observed to have little effect on shear stiffness after significant inelastic excursions, this parameter being influenced most strongly by the level of the previous maximum imposed deformation.

The presence of hoop reinforcement gave better inelastic performance due to the capacity to develop large core compression strains, the antibuckling support afforded the vertical flexural reinforcement and the increased shear capacity and stiffness of wall boundary elements. Hoop reinforcement was provided only in the boundary elements of barbell and flanged walls and over a distance of $\ell_w/10$ at the ends of the rectangular sections. A high degree of hoop reinforcement was not needed in lightly reinforced walls, nor outside the critical region which extended over a height approximately equal to ℓ_w above the critical (base) section.

3. Axial Load

Only 7 of the 16 units tested had axial load present, and this was generally in the range of $0.06 - 0.09 f'_c A_g$. Axial load of this intensity is too small to exert a noticeable effect on curvature ductility, especially when barbells or flanges are present. The primary effect of axial load was found to be in reducing shear deformations and allowing walls with axial load to sustain more cycles of reversed loading at higher base rotation levels prior to web crushing.

4. Concrete Strength

Concrete compression strength (f'_c) was observed to influence boundary element crushing strength, web crushing strength and abrasion resistance at crack interfaces.

5. Load History

Three types of load history were used: monotonic, "incrementally reversing" (gradually increasing amplitude reversing cycles with small amplitude cycles between the higher amplitude excursions) and "modified reversing" (single reversed cycles of alternate high and low amplitude excursions). It was found that stiffness degradation was primarily a function of the previous maximum imposed deformation, rather than the load history type.

6. Repair Techniques

Two barbell section walls were repaired by removing and recasting panel concrete in the damaged area. Retesting of these walls indicated reduced initial stiffness compared to the virgin specimens, but similar strength and stiffness in the inelastic regime.

Many of these conclusions also follow from first principles and are not in need of experimental confirmation.

6.3.2.3 Conclusions

1. Two types of wall response to reversing lateral load were identified, depending on the level of applied shear stress:
(a) low shear stress ($v \leq 0.26\sqrt{f'_c}$ MPa): good inelastic performance (which may be defined qualitatively as the capacity to demonstrate a stable, non degrading hysteretic response) may be limited by bar buckling, concrete core degradation or lateral instability.
(b) high shear stress ($v \geq 0.64\sqrt{f'_c}$ MPa): web crushing governs inelastic performance, with the onset of this phenomenon governed by both shear stress level and the imposed rotational ductility demand. The use of additional horizontal reinforcement does not significantly enhance strength or ductility in this situation. No quantitative estimate of permissible maximum rotational ductility was made in this report, however.

2. Wall behaviour is dependent more on the maximum previously attained deformation level, rather than the details of the load history. Shear deformations, which were found to be a significant fraction of overall displacement (up to 70%), were especially affected in this manner.

3. Confinement of boundary elements over the height of the plastic hinge zone significantly improves performance by delaying bar buckling and allowing high compression strains to develop.

4. Out of plane instability can control the behaviour of rectangular walls.

Appendix C compares the provided transverse reinforcement of the PCA walls (and the EERC/UCB units described subsequently) with the requirements of NZS 3101 [34].

6.3.3 EERC/UCB Tests [55,56]

A second important research program devoted to the study of structural walls is in progress at the Earthquake Engineering Research Center, University of California, Berkeley. Two series of tests carried out under this program are outlined [55,56].

6.3.3.1 Description of wall units: Six approximately one third scale models of prototype walls were tested, comprising 4 barbell and 2 rectangular sections (see Fig. 6.6). High strength steel (nominally 414 MPa) was used for vertical and transverse reinforcement with concrete compression strengths of approximately 35 MPa. The 3 storeyed walls had constant axial loading of order $0.07f'_cA_g$, and were loaded so as to give moment to shear ratios ($M/\ell_w V$) of 1.84 and 1.60 for the barbell and rectangular sections respectively. After testing, the units were comprehensively repaired and retested. Parameters studied included wall cross sectional type, the type of transverse reinforcement used in the boundary elements (rectangular hoops vs spirals), loading type (monotonic vs cyclic) and repair techniques.

6.3.3.2 Observed behaviour:

1. Force-displacement hysteresis loops for the wall units are shown in Fig. 6.7. Stiffness was observed to degrade with successive cycling at a given displacement. Various limit state strengths were reasonably well predicted using conventional theory.

2. Flexural,shear and fixed end rotational components of displacement remained in approximately constant proportions during the tests - 60-70% ; 25-30% ; 5-10%. Energy dissipation, measured as the area enclosed by the load-deflection curves, was primarily attributable to flexural actions and increased approximately linearly with lateral deflection.

3. Two main types of failure mechanism were identified:

Buckling Failures

(a) Buckling of longitudinal reinforcement - inelastic bar buckling between hoops after cover had spalled and hoops had ruptured.

(b) Buckling of boundary elements after cover spall - asymmetric spalling of cover and associated eccentricity of axial load caused buckling of the compression zone over a height approximately equal to wall boundary element thickness.

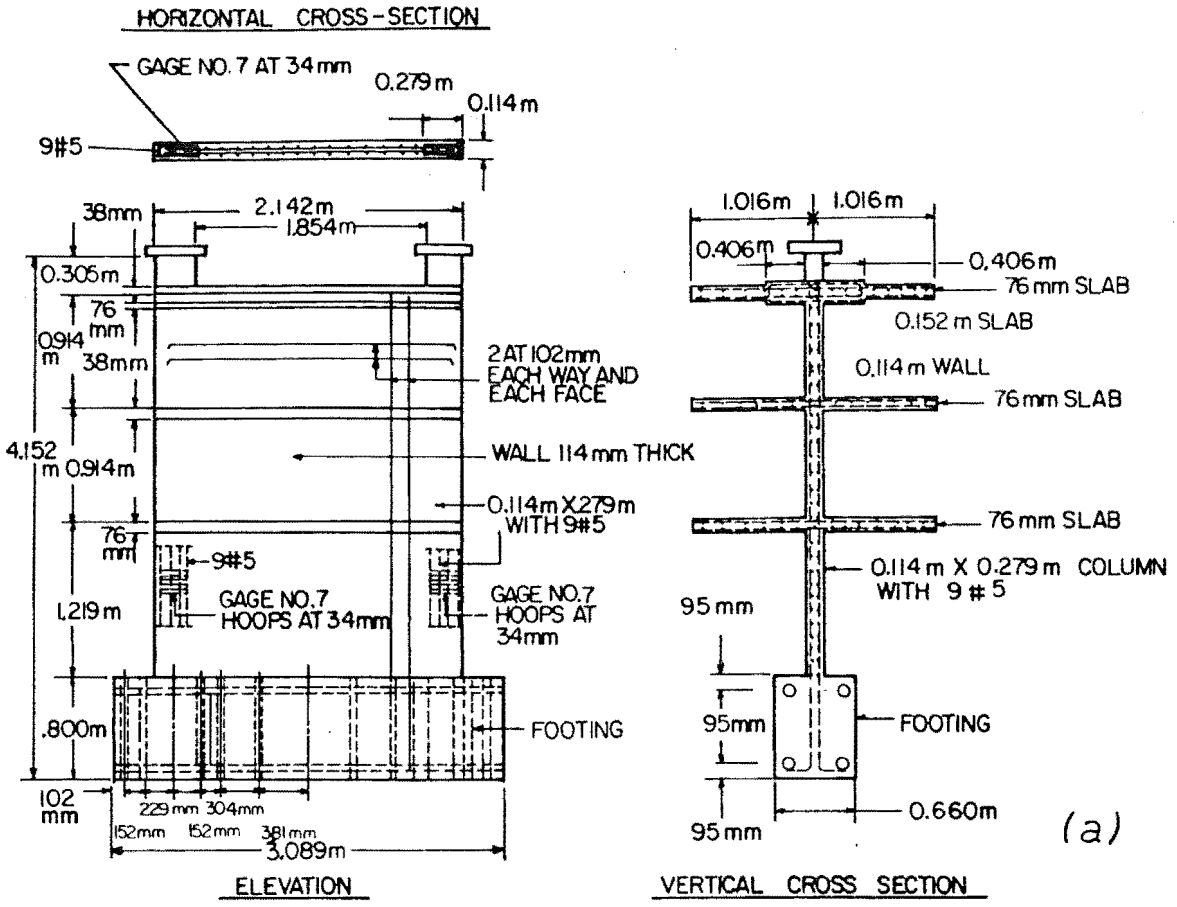

(a) General plan of test rig.

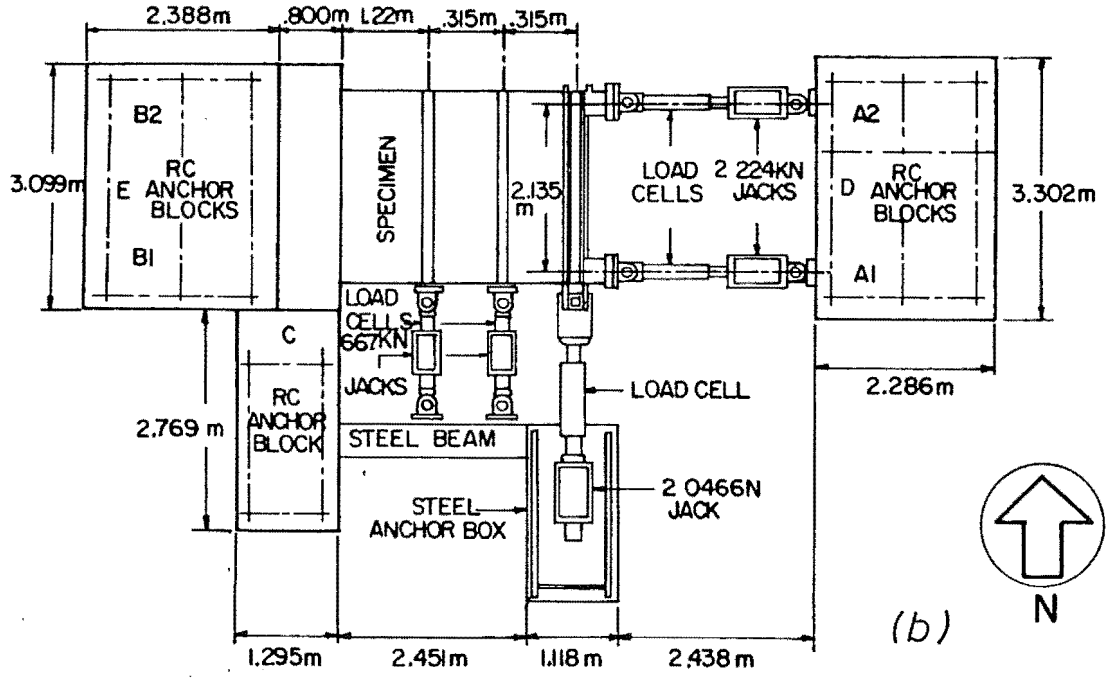

(b) Details of rectangular sections.

Fig. 6.6 Details of EERC/UCB Tests [55,56].

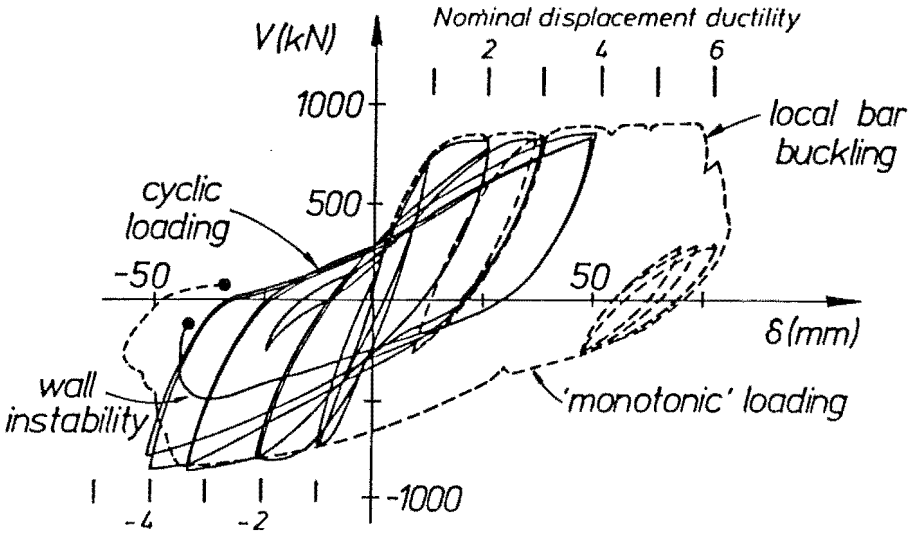

(a) RECTANGULAR SECTION UNITS

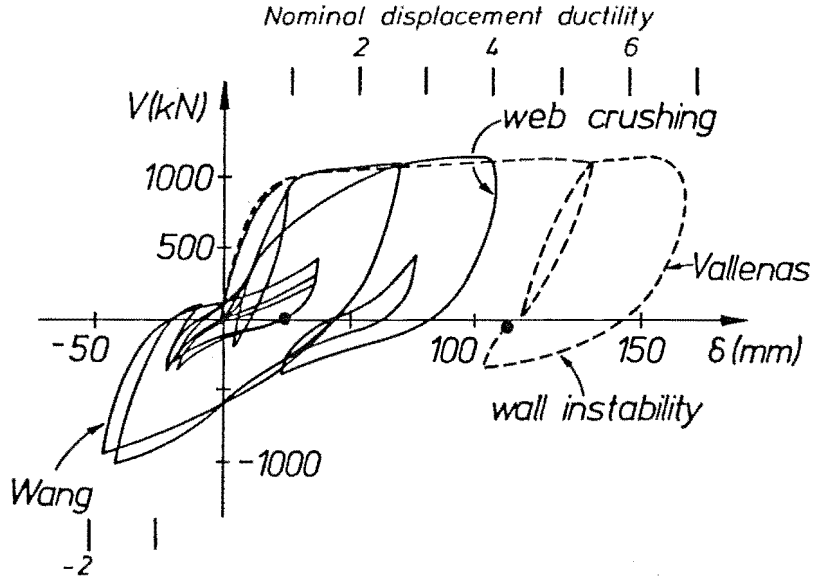

(b) "MONOTONICALLY" LOADED BARBELL UNITS

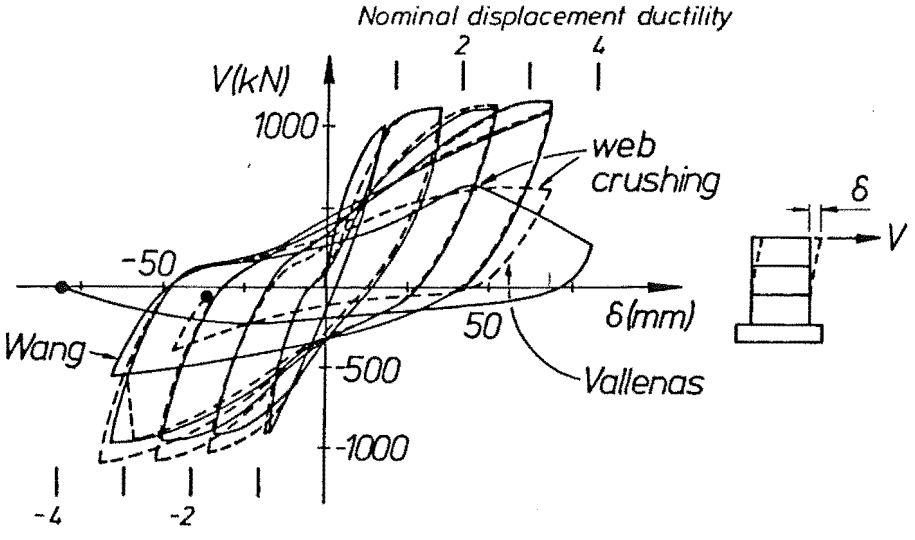

(c) CYCLICALLY LOADED BARBELL UNITS

Fig. 6.7 Hysteretic Response of EERC/UCB Wall Units.

(c) Buckling of boundary element with residual open cracks occurred in units where a compressive force had to be transferred via vertical reinforcement only across wide tensile cracks which had opened in the previous load cycle. In this case, buckling occurred over the full first floor height.

Shear Failures:

(a) Crushing of panel concrete - web crushing was observed to occur at large displacement ductilities for monotonically loaded units.

(b) Sliding shear at base - cyclically loaded specimens generally developed horizontal failure planes across which shear resistance degraded due to the grinding of adjacent surfaces and only the confined boundary elements provided effective shear resistance (via dowel action). Shear deformations increased from about 50% to more than 90% of total deformations.

4. All wall units were repaired by removal of the damaged (bottom storey) zone, the welding in of replacement reinforcement and recasting of a thickened panel concrete. On retesting, initial stiffness was lower but strength and post yield stiffnesses compared favourably with the virgin specimens. However, problems were encountered with the brittle rupture of welded connections, the crushing of the second floor panel (at shear stress $v = 1.12\sqrt{f'_c}$ MPa) and sliding at construction joints.

6.3.3.3 Conclusions:

1. Flexural strength at various limit states may be predicted adequately by using realistic material models and the plane-sections hypothesis. However, UBC [26] shear design equations are inadequate in that they neglect the true flexural strength which is enhanced by strain hardening of flexural reinforcement and actual material strengths in excess of those assumed in design.

2. Maximum nominal shear stresses of $1.12\sqrt{f'_c}$ and $0.78\sqrt{f'_c}$ MPa were recorded for barbell and rectangular section walls respectively. Under high moment and shear, structural walls develop wide diagonal cracks and a diagonal tension failure mechanism can develop. Well confined boundary elements were effective in providing shear resistance when a sliding shear failure occurred in the wall web.

3. Cyclic loading of walls constitutes a more severe regimen than does monotonic loading, as both deformation capacity and strength degrade with load reversals.

4. Inelastic bar buckling may be controlled by closely spaced spiral or hoop reinforcement in the boundary elements, with the former providing more efficient confinement. Hoop spacing to bar diameter ratios (s/d_b) of 1.78 and 2.14 were used for the barbell and rectangular walls respectively.

5. Lateral instability of rectangular sections may govern the structural response and appears to be affected by the clear height to web width in the lowest floor of the wall,width of tensile cracks and longitudinal reinforcement strains.

6.4 DESIGN OF CANTILEVER WALL UNITS

6.4.1 Introduction and Aims of the Test Programme

The experimental study reported herein was conducted with the primary objective of examining current code provisions [34] for (i) the prevention of premature inelastic instability, and (ii) the supply of hoop reinforcement for confinement of regions subjected to high compression strains. In view of the potentially high inelastic deformation demands on slender cantilever walls (Chapters 3 and 4), experimental verification of the empirically derived rules (see Sections 6.2·6.1, 6.2.6.2) was considered desirable. Four wall units, three rectangular sections and one tee section, were tested under a fully reversing cyclic lateral load program simulating seismic actions. The design, construction and instrumentation of the wall units, and the test procedure employed, are described subsequently.

6.4.2 Limitations Imposed by Laboratory Facilities

The design of the structural wall test units was subject to many practical constraints, the most important of which were:

(a) the availability of an MTS ±500 kN hydraulic jack (to be used for the application of lateral loads), and

(b) the clear height (4.425 m) available between the platens of the 10 MN Dartec Universal Testing Machine (hereinafter simply termed "the Dartec").

These two factors imply a limit on the maximum flexural strength of a test unit. It was decided to use the reaction frame used previously [57], which was constructed to satisfy the same constraints.

6.4.3 Variable Eccentric Axial Load Concept

As discussed earlier an important aspect of the experimental program was the examination of the lateral instability or buckling phenomenon. The compression zone of a structural wall is likely to buckle given firstly, a high axial load on the section, and secondly, a previous loading history which makes the wall susceptible to instability. Thus is was decided to employ the following type of variation in axial and lateral load during testing: (See Fig. 6.8).

(a) Moment at critical section is $M_1 = P_1.e - V_1.h_w$, where V is negative according to the assumed sign convention (Fig. 6.9). For a small value of P_1 (of order $0.05f'_c A_g$ for the section) wide tensile cracks were expected to develop at the east end of the wall,

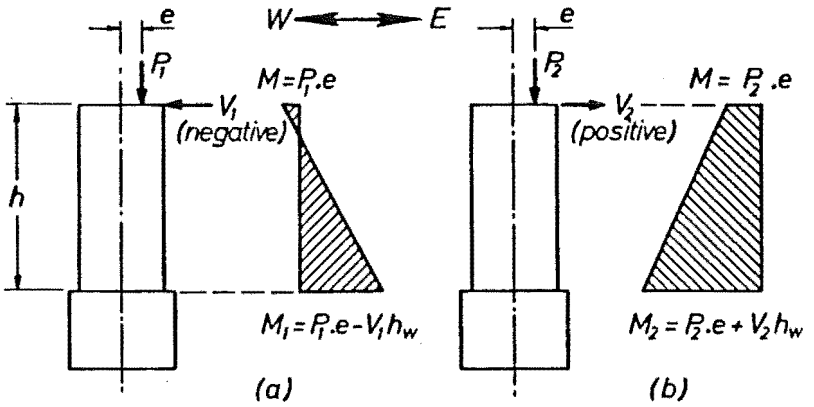

Fig. 6.8 Bending Moment Patterns Applied to Test Specimens.

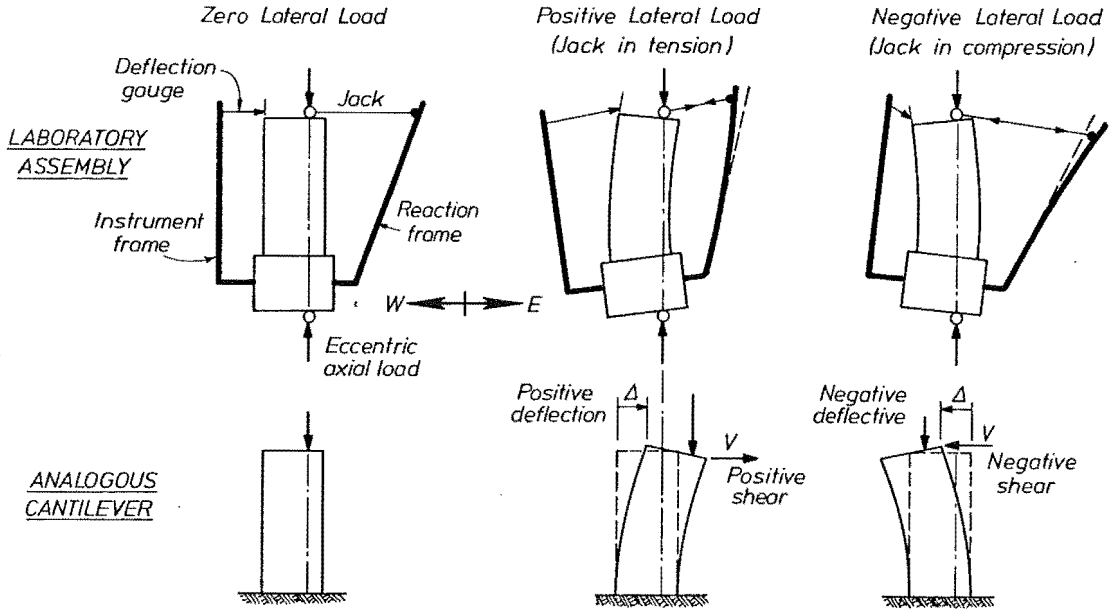

Fig. 6.9 Sign Convention for Wall Tests.

thus softening it. This load combination is not of great interest in itself because even at large displacement ductilities, little major distress should be evident.

(b) With reversed direction of lateral load, the wall bending moment diagram becomes as shown in Fig. 6.8 (b), with moment at wall base $M_2 = P_2.e + V_2.h_w$. For a large axial compression P_2 (of order $0.20f'_c A_g$), the neutral axis depth becomes large. In addition, the compression must first be carried across the open cracks present from the previous reverse load cycle via the vertical flexural reinforcement only. This large compression force, taken across an extensively cracked zone is likely to induce instability, a problem which should becomes more critical with increasing levels of inelastic deformation.

In addition to the softening action of this loading regime, the eccentricity of axial load has the effect, in case (b), of decreasing the moment gradient on the unit. This simulates an increase of the lever arm of the applied lateral load (the situation of greater interest), advantageously increasing the shear span of the unit (see Appendix D). The axial load limits chosen for P_1 and P_2 (Fig. 6.10) SEE ERRATA could be considered as being typical for the extreme load expected in the tension and compression legs of a coupled structural wall.

Figure 6.9 shows diagramatically the essential elements of the test set up and indicates the deformations imposed on these elements as lateral load is cycled. Initially, with zero lateral load, the wall is aligned vertically by the adjustment of concrete blocks on the counter-balance arm (Fig. 6.11). Because the pin connections between unit and test machine can not be displaced laterally, the base block rotates to maintain compatibility between wall deformation and (horizontal) jack stroke. As shown, this net rotation is anticlockwise for positive lateral load. In addition, it may be observed that the reaction frame is itself subjected to some deformation, which was of order 4 mm per 100 kN of jack force, measured horizontally at reaction frame top. The test set up was self-equilibriating in terms of lateral load, with no external horizontal reactions required.

Also shown in Fig. 6.9 is the analogous situation for a fixed base cantilever wall. As may be noted, the fact that the instrument frame undergoes the same rotation as the base block means that the

lateral displacements so measured are independent of this rigid body rotation and apply directly to the analogous cantilever situation.

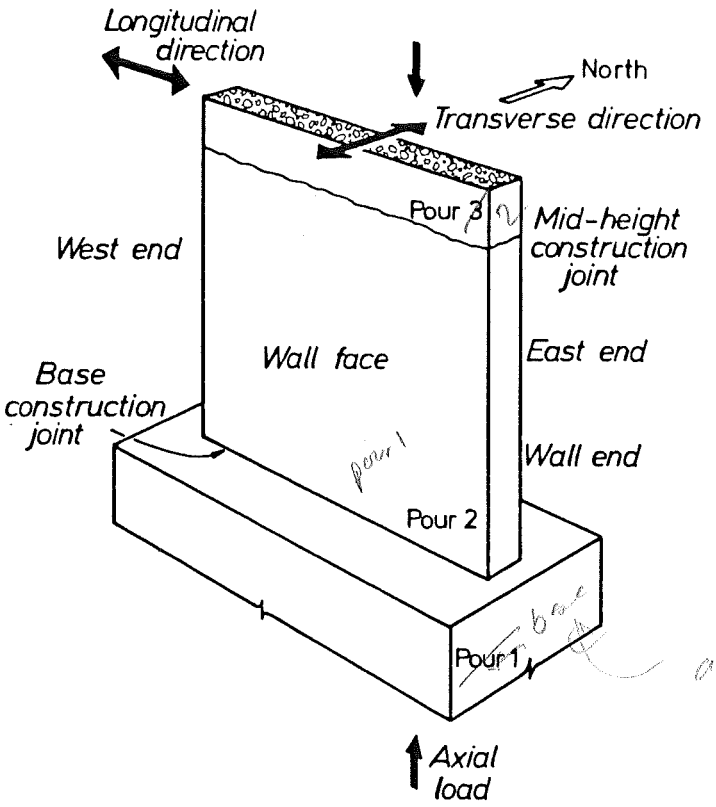

Fig. 6.10 Terminology Diagram for Wall Units.

6.4.4 General Notes on Design

Given the constraints of available lateral force and lever arm, a trial and error process was used to determine section dimensions and reasonable arrangements of flexural reinforcement. Although the units were not intended to be scale models of any particular prototypes, an attempt was made to keep relative section dimensions in proportion. The units constructed could be viewed as 1/4 - 1/3 full sized models of the bottom few storeys of medium rise walls. Realistic materials were used: commercially available deformed bars for flexural reinforcement, plain bars for stirrups and hoops and appropriately scaled (9 mm) aggregate size for the concrete. Realistic construction practices were also used wherever possible, although no splices were used in the units. 10 mm cover was provided to the hoops and stirrups, which is somewhat large. This means that an abnormally large proportion of section width is lost on spalling. However, it was not considered practical to construct with a smaller cover thickness. Assumed material properties

used for the preliminary design were: concrete strength f'_c = 25 MPa; flexural reinforcement strength Grade 380 steel was used but, acknowledging the probable higher strength, a design value of f_y = 440 MPa was used.

Appendix D contains detailed design calculations relevant to each unit tested. Figure 6.10 indicates some terminology used in the following sections regarding the sense of loading on the walls. Figure 6.11 shows the general testing arrangement and defines the various components thereof. Details of the model structural walls tested, and their instrumentation, are provided subsequently for each wall.
Table 6.1 summarises section geometry and reinforcement content.
Table 6.2 summarises the material properties of concrete and reinforcement used in the units, with reinforcement stress-strain curves shown in Fig. 6.12. Concrete test cylinders for the wall proper were cured both in a fog room (100% humidity) and in the laboratory, i.e. in the same environment as the wall units. Laboratory cured cylinder strengths were generally higher, and these values were used for theoretical strength calculations in preference to fog room cured cylinder strengths.

6.4.4.1 Slab stubs: It was considered important in the design of the units to model as accurately as possible the deformation constraints that would be present in the bottom regions of a prototype structural wall. Because of the moment gradient in the test set up, it was anticipated that only the bottom storey of the walls would need to have well modelled boundary conditions. Specifically it was decided to provide a floor slab stub, and ensure that by adequate detailing, lateral sway of the wall is prevented at that floor slab level. This was done by providing 100 mm thick slab stubs either side of the wall and bearings between these and the 310 UB 40 steel beams bolted to the base block. (See Fig.7.1). Slab stubs were attached by high strength bars, with a plaster packed joint between wall and slab. A series of holes was provided in the units so that slabs could be positioned vertically as required, thus varying the unsupported floor height to wall thickness ratio.

6.4.4.2 Base block beams (Fig.7.1(b)): The 310 UB 40 steel beams attached to the base block via. recoverable 24 mm dia. bolts had several uses, which for convenience are listed here:

(a) for use in bracing wall and top block formwork during construction.
(b) to provide stability to the units (during storage and transportation) which, when the top block was poured, were very flexible about their weak north-south axis.

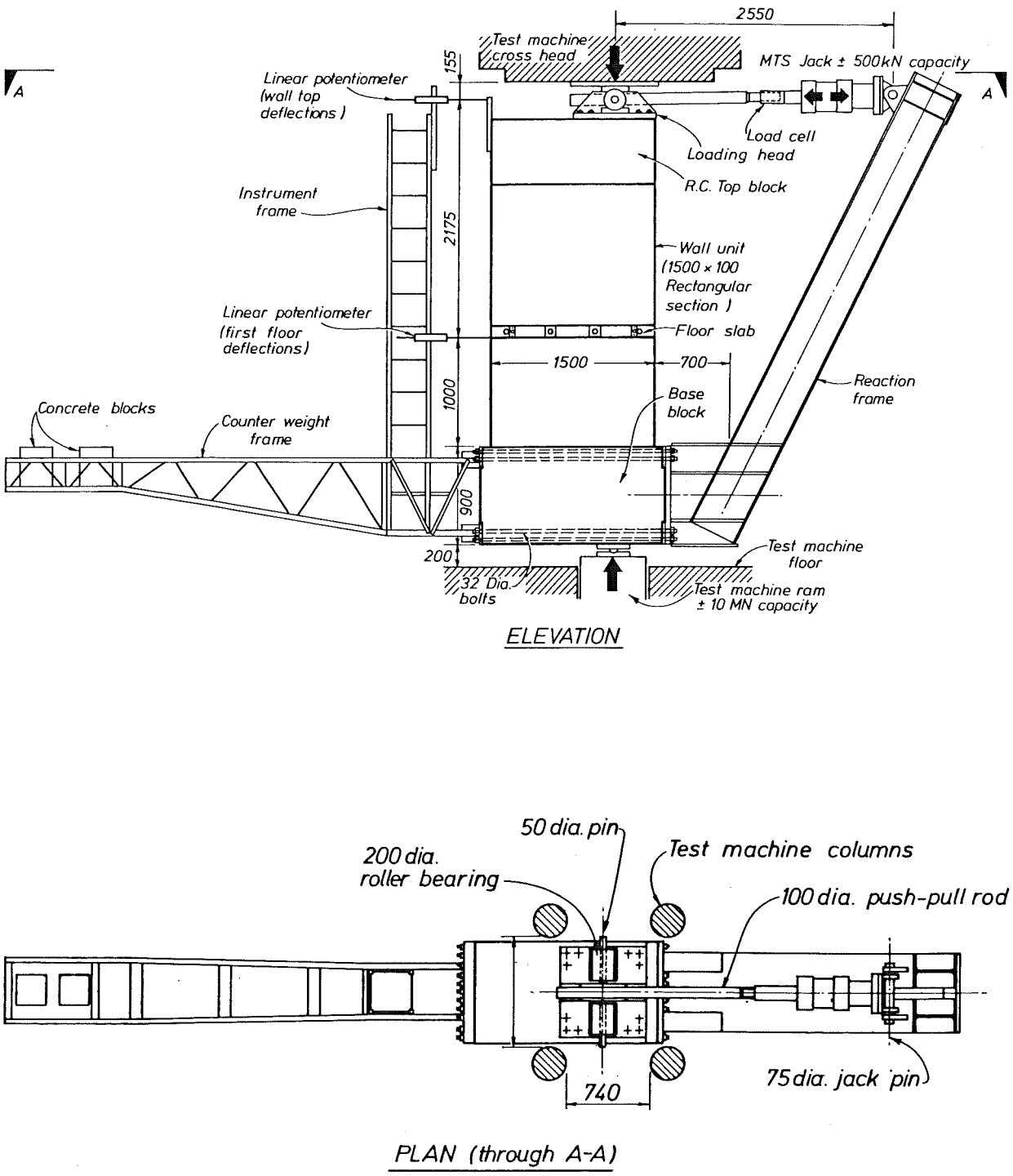

Fig. 6.11 Elevation and Plan of Test Assembly.

TABLE 6.1 : GEOMETRY AND REINFORCEMENT CONTENT OF WALL UNITS

	WALL 1	WALL 2	WALL 3	WALL 4
Wall Shape	Rectangular	Rectangular	Tee	Rectangular
ℓ_w mm	1500	1500	1300	1500
b_w mm	100	100	100	100
ℓ_f mm	-	-	700	-
b_f mm	-	-	100	-
ρ_f (2)	0.0471	0.0471	0.0393 (1)	0.0471
ρ_d (3)	0.0094	0.0094	0.0076 (1)	0.0094
ρ_h (4)	0.0032	0.0032	0.0028	0.0032
ρ_v (5)	0.0071	0.0071	0.0057	0.0071
ρ_s (6) east end	0.0221	0.0133	0.0193	0.0221
ρ_s (6) west end	0.0133	0.0133	0.0107	0.0133
ρ_t (7)	0.0173	0.0173	0.0107	0.0173

Notes:

1. For east (unflanged) end of wall.
2. ρ_f = ratio of main flexural reinforcement area to end zone area.
3. $\rho_d = A_s(\text{end zone})/0.8\ell_w b_w$.
4. ρ_h = ratio of distributed flexural reinforcement area to area of wall web, i.e. $\rho_h = \Sigma A_b/(b_w s_v)$ where the web bars (of total area ΣA_b) are spaced at s_v.
5. ρ_v = ratio of shear reinforcement area to area of a vertical section of wall, i.e. $\rho_v = A_{sv}/(s\, b_w)$ where shear reinforcement of area A_v is at a spacing s.
6. ρ_s = volumetric ratio of hoop reinforcement to confined core.
7. ρ_t = ratio of total vertical wall reinforcement area to total gross section area.

TABLE 6.2 : MATERIAL PROPERTIES OF THE WALL UNITS

Property	WALL 1	WALL 2	WALL 3	WALL 4
CONCRETE STRENGTH[1] (MPa)				
Base block, lab. cured	35.4	32.7	40.3	39.8
Wall, pour 1, lab. cured[2]	28.6	25.3	33.8	36.5
fog cured	30.2	23.2	29.0	28.9
pour 2, lab. cured	26.1	34.3	34.2	27.1
fog cured	27.5	30.4	31.0	26.4
Top block, lab. cured	39.0	33.9	40.0	38.2
REINFORCEMENT				
Main flexural bars - size	HD12	HD12	HD10	HD12
f_y (MPa)	450	450	400	345
ε_y	0.0023	0.0023	0.0019	0.0016
E_s (GPa)	195	195	210	216
f_{ult} (MPa)	692	692	590	610
Yield plateau length	$4\varepsilon_y$	$4\varepsilon_y$	$7\varepsilon_y$	$3\varepsilon_y$
Distributed flexural bars & shear reinforcement	R6		R6	R6
f_y (MPa)	360		380	335
ε_y	0.00175		0.0175	0.0015
E_s (GPa)	206		217	220
f_{ult} (MPa)	497		500	450
Yield plateau length	$3\varepsilon_y$		$6\varepsilon_y$	$10\varepsilon_y$
Hoop reinforcement - size	R5			
f_y (MPa)	290			
ε_y	0.0014			
E_s (GPa)	207			
f_{ult} (MPa)	395			
Yield plateau length	$12\varepsilon_y$			

Note: (1) As found from 100 mm dia. x 200 mm cylinders tested immediately prior to the testing of the wall units.

(2) Used for theoretical strength calculations.

(3) The strength of the 100 mm dia. x 200 mm cylinders is approximately 4% greater than would have been obtained for standard (6" dia. x 12") cylinders.

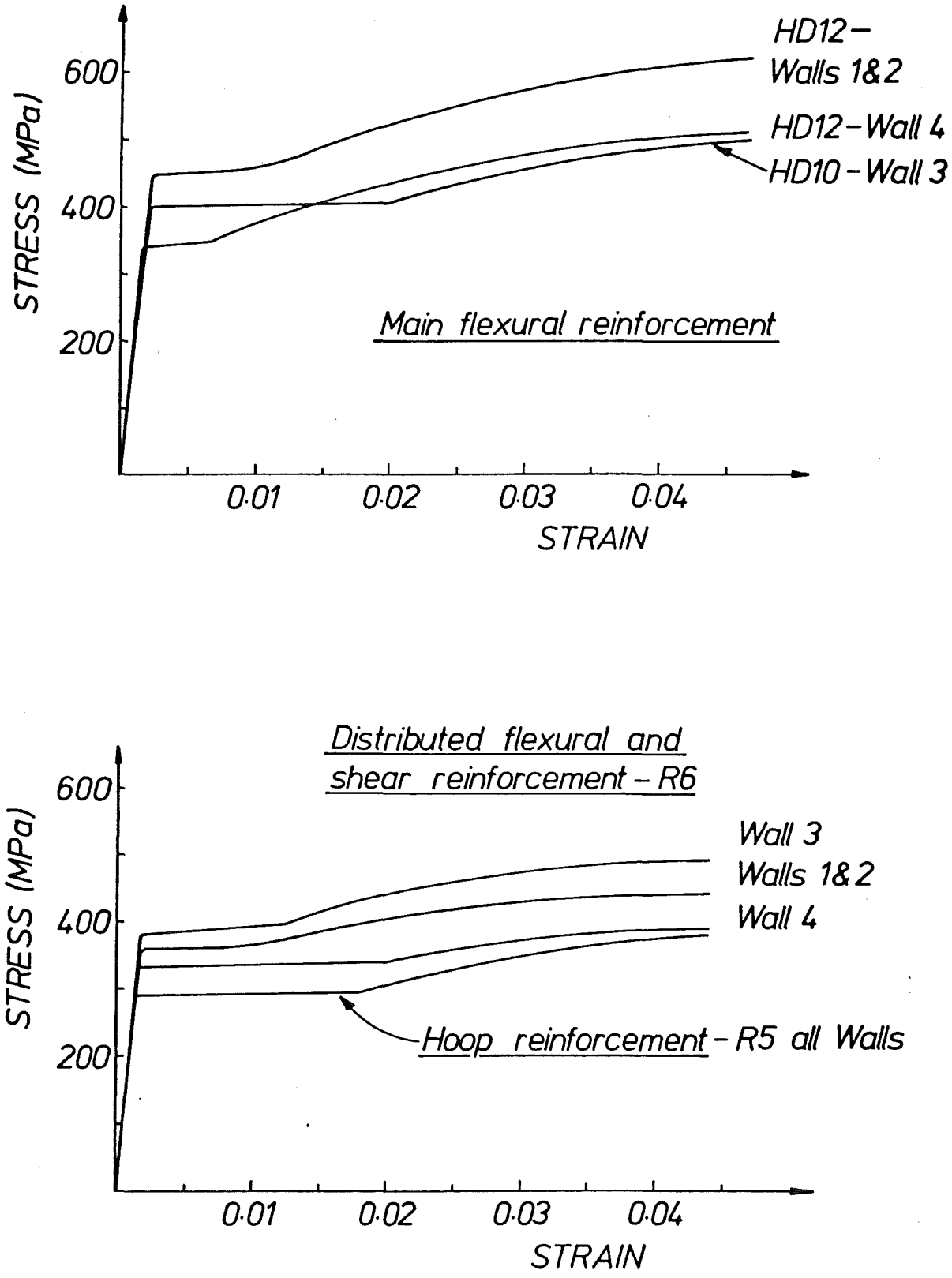

Fig. 6.12 Stress-Strain Curves for Reinforcement Used in Wall Units.

(c) to constrain the movement of the slab stubs at right angles to the plane of the wall during the test.

6.5 CONSTRUCTION OF WALL UNITS

The major steps in the construction of the wall units are summarised here, the procedure being similar for all walls constructed.

6.5.1 Base Block

(1) An 8 mm steel plate with a rectangular hole for seating the bottom roller bearing was bolted to a construction base made from steel channel sections.

(2) A 5 mm steel template for the vertical (flexural) reinforcement was welded to the 8 mm plate, and vertical bars, with strain gauges already in place, were welded into position.

(3) Ends of the base block formwork, constructed from 18 mm laminated plywood, were erected. 25 mm thick steel end plates (Fig. 7.1(a)) were attached to the formwork.

(4) PVC tubes of internal diameter 36 mm were placed between the base block ends to accommodate the 32 mm dia. reaction frame bolts. The use of plastic sleeves was to allow recovery and reuse of the 32 mm bolts.

(5) A light basketing cage of D12 bars was tied in around the sleeved bolts.

(6) Plywood formwork sides were erected and transverse PVC tubes (housing 24 mm bolts, used later for the attachment of 310 UB 40 members) were installed. The side and end panels were braced in preparation for pouring. (See Fig. 6.13(a).

(7) Base block concrete was poured using a mix of nominal strength 35 MPa and slump 75 mm. The construction joint area was treated with a chemical retarder and brushed down 24 hours after pouring to remove laitence and expose the aggregate.

(8) The block was left to moist cure 7 days, then stripped of formwork and removed from its construction base.

6.5.2 Wall Proper

(1) Hoop and shear reinforcement was tied up the full height of the wall. Instrumented sets of reinforcement were strain gauged before placement, as this allowed considerable convenience in the fixing of the strain gauges (see Fig. 6.13(b)).

(2) Potentiometer and dial gauge mounting rods, and PVC tubes for the slab stub attachment holes (Fig. 7.1 (a)) were positioned.

(3) One full height (2.4 m) formwork panel was erected on one face of the wall, and braced to 310 UB 40 steel beams, themselves bolted to the base block via 24 mm dia. bolts. Figure 6.13(c) shows the completed wall reinforcement cage for wall 4. Side formwork was constructed from 18 mm plywood sheeting, with horizontal 100 x 50 timber stringers at 250 mm vertical centres and further backed by vertical 64 x 38 RHS soldiers.

(4) A half-height (1.2 m) panel was erected on the other face of the wall and similarly braced. Wall ends were then put in place to complete the bottom half formwork.

(5) Strain gauge leads were led out of the wall via holes in the forms.

(6) A theodolite was used to control the verticality of the formwork panels and ensure that the wall to be constructed was perpendicular to its base plate. Tolerances of 3 mm and 6 mm (over the full height of the units) were achieved for North-South and East-West verticality respectively.

(7) The bottom half of the wall proper was poured with the construction joint for the next pour prepared as previously indicated. High slump/low aggregate size (175 mm/9 mm) was used to ensure adequate workability in the thin walled sections which were congested due to the closely spaced hoops and quantity of strain gauge leads. The use of a 3/4 inch dia. immersion vibrator and an external vibrator bolted to the wall side proved satisfactory. Despite the relatively wet mixes used, no significant shrinkage cracking occurred.

(8) The formwork for the top half of the wall proper was positioned, checked for alignment and concrete for the top half poured two to three days after the bottom section. 7 days moist curing was allowed.

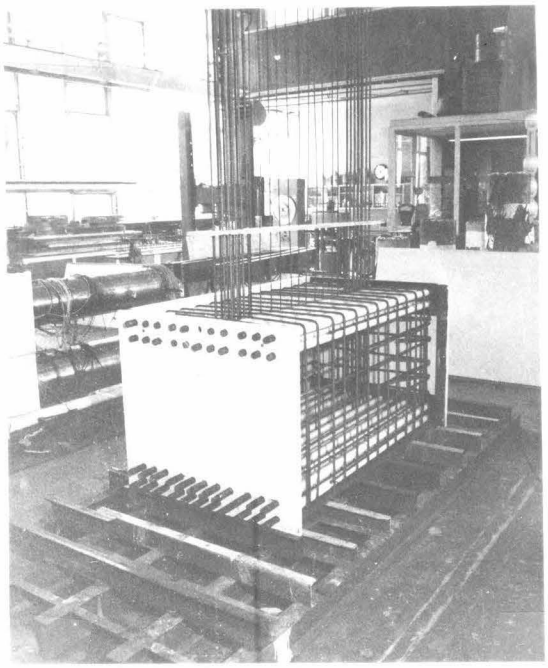

(a) Base block under construction.

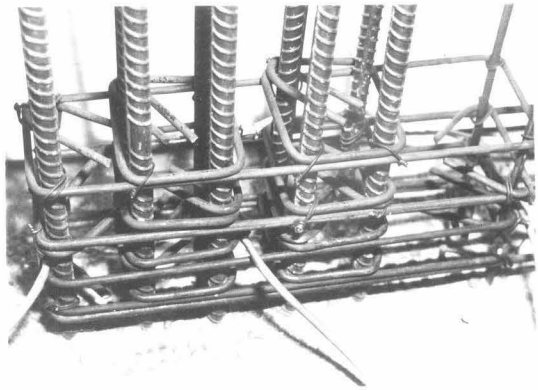

(b) Detail of hoop reinforcement.

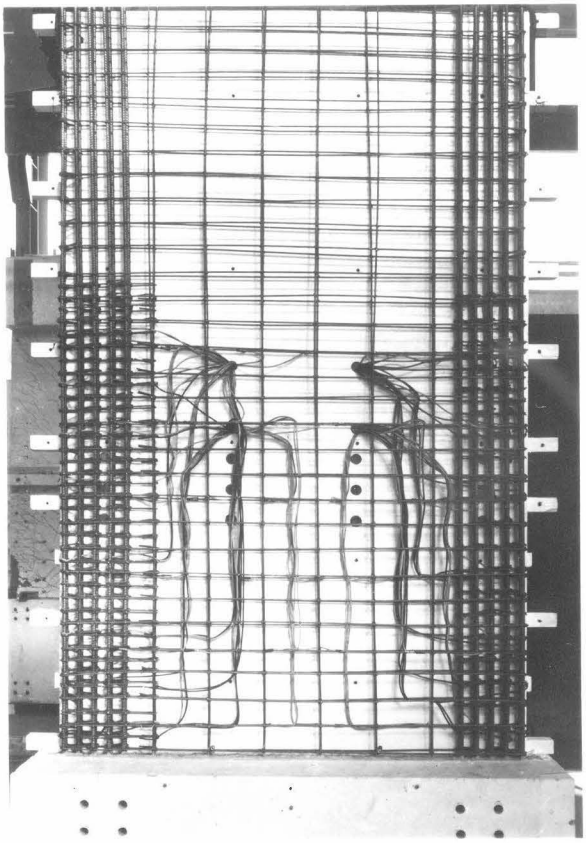

(c) Wall reinforcement cage.

Fig. 6.13 Construction of Wall Units.

6.5.3 Top Block

(1) Formwork for the top block was erected, comprised of ~~playwood~~ plywood SEE ERRATA panels and 100 x 50 timber soldiers. This formwork was braced off the 310 UB 40 steel beams and the already poured wall itself.

(2) A moderately heavy reinforcing cage, tied on the ground, was craned into position.

(3) Transverse 24 mm dia. bolts encased in PVC sleeves were installed, permitting further bracing of formwork to the 310 UB 40 beams.

(4) 24 mm dia. bolts necessary for the attachment of the steel loading head (Fig. 7.1(c)) were positioned via the use of templates.

(5) The top block was poured and cured in standard fashion.

6.6 INSTRUMENTATION

The provision of instrumentation for the units involved finding a balance between the following factors:

(a) the desire for comprehensive information regarding wall response to load,

(b) practicality of installation,

(c) expense, both direct and labour costs,

(d) the desire to avoid significant alteration of the walls' true characteristics by the provision of excessive instrumentation,

(e) constraints imposed by the available data acquisition systems.

Detailed layouts of internal and external instrumentation provided for each unit are supplied subsequently. Brief notes regarding the instrumentation used, and its intended purpose, are given here. Instrumentation was concentrated over the lower part of the wall, where greater damage was expected.

6.6.1 Strain Gauges

Electrical resistance strain gauges are useful indicators of relatively low levels of strain. However, because of their small gauge length, the high values of strain they indicate may not accurately reflect the true average strain rate of a reinforcing bar. Details of the type of gauge used and methods of attachment are given elsewhere [58].

Flexural Reinforcement: Vertical bars were gauged to enable assessment of the extent of yield penetration into the base block (bar anchorage zone) and up the height of the wall.

Hoop Reinforcement: Hoop legs transverse to the axis of loading were provided with gauges to monitor strains induced by the combined requirements of confinement and antibuckling.

Shear Stirrups: Strain gauges were spaced relatively closely on stirrups so as to assess the strain distribution along the bars, as well as up the height of the wall.

The presence of large numbers of 5 mm thick strain gauge leads in the thin (100 mm) wall sections was initially viewed with some concern. However, test behaviour gave no cause to suspect that this aspect of instrumentation significantly affected the units. On average 2% of strain gauges were destroyed during wall pouring and vibrating.

6.6.2 Linear Potentiometers

These gauges enable measurements to be made of the relative displacements of 2 gauge points. Such gauges are available in a range of sensitivities: gauges of travel length 7.5 mm to 300 mm were used. Steel brackets were used for the mounting of the potentiometers in the cases where the distance between gauge points was much larger than the available travel. This type of gauge was typically used for the purpose as shown below for Wall 1. (See also Fig. 7.3).

Channel	Purpose
1	Monitor for voltage supply to data acquisition system.
2,3	Rotation of base block (Fig. 7.3(c)).
4,5	Attached to instrument frame to measure lateral displacement of wall independent of base block rotation (Fig. 6.11).
6,7	Transverse (out of plane) deformations of potential buckling compression zone. Those potentiometers were located 150 mm from the east end of the wall. SEE ERRATA
8-27	Measurement of vertical displacement for curvature calculations.
28-31	Determination of shear deformations.
32-33	Monitor sliding shear at wall base construction joint.
34	Measurement of gross elongation of wall at level of floor slab.

6.6.3 Data Acquisition

Strain gauges and linear potentiometers were connected to a Solatron Data Acquisition system. This equipment can monitor up to 200 channels and records information (voltages) on paper tape. Details of the system may be found in Ref. 58.

6.7 TESTING PROCEDURE

6.7.1 Loading

Loading is discussed with reference to the sign convention shown in Fig. 6. 9. Lateral loading essentially followed the procedure commonly used at the University of Canterbury of 2 fully reversing cycles to about 3/4 theoretical yield strength, then successive (displacement controlled) fully reversing cycles to approximate displacement ductilities of 2, 4, 6, etc. until failure. These lateral loads were incremented and decremented in a nominal, stepwise manner. This scheme was complicated somewhat by the desire to vary axial load on the unit with direction of loading. Details of how this was achieved are given for each unit in turn. As discussed earlier, negative lateral load, with associated low axial load, is of no great interest in itself. The main purpose of this loading was to soften up the east end of the wall and enhance the likelihood of instability of this zone during positive lateral load. Diagrams of load condition v load increment number are supplied for each unit in turn.

6.7.2 Test Procedure

The following general notes on installation and testing are applicable to all units.

(1) The unit was transported to approximate position, with loading head beneath the top platen of the Dartec. The steel reaction frame, with MTS jack already attached, was bolted to the base block using 1850 mm long by 32 mm dia. bolts.

(2) Counter balance arm and instrument frame were bolted to the base block. Weights were added to the arm so as to balance the wall/reaction frame system, which at this stage hung from a 50 mm pin from the crosshead of the Dartec.

(4) The total test assembly was attached loosely with 4-3 tonne chain hoists to the Dartec crosshead via brackets mounted on the four 310 UB 40 columns. This was done as a safety measure to enable

support of the assembly in the event of failure of the Dartec hydraulics.

(5) Bearings between slab stub and 310 UB 40 beams were fitted.

(6) Potentiometers and dial gauges were mounted on their respective brackets and centred at mid travel.

(7) Strain gauge and potentiometer leads were connected to the Solatron data acquisition system and initial readings taken.

(8) After each subsequent load increment, axial and lateral load was noted and all strain gauges and potentiometers scanned by the Solatron system. Continuous graphical output of the lateral load - top level displacement was arranged to aid assessment of performance during the test procedure.

(9) Cracks were marked on the white painted units after each load change and photographs taken as it was deemed appropriate. Clear photographs showing the whole wall, or major portions of it, could not be taken because of the numerous obstructions surrounding the unit such as the Dartec machine legs and slab restraint columns.

(10) Fig. 6.14(a)-(c) shows the test set-up from various angles. The aerial view (Fig. 6.16(a)) shows the reaction frame and 500 kN MTS jack at left attached to Wall 4 in position in the Dartec 10 MN Universal Test Machine. The counter weight frame and Solatron Data Acquisition system are visible at right. Fig. 6.14(b) is an elevated view from the south-east.

The south-west elevation (Fig. 6.14(c)) shows the Solatron , counter balance arm and the vertical instrument frame used to monitor lateral (east-west) displacements.

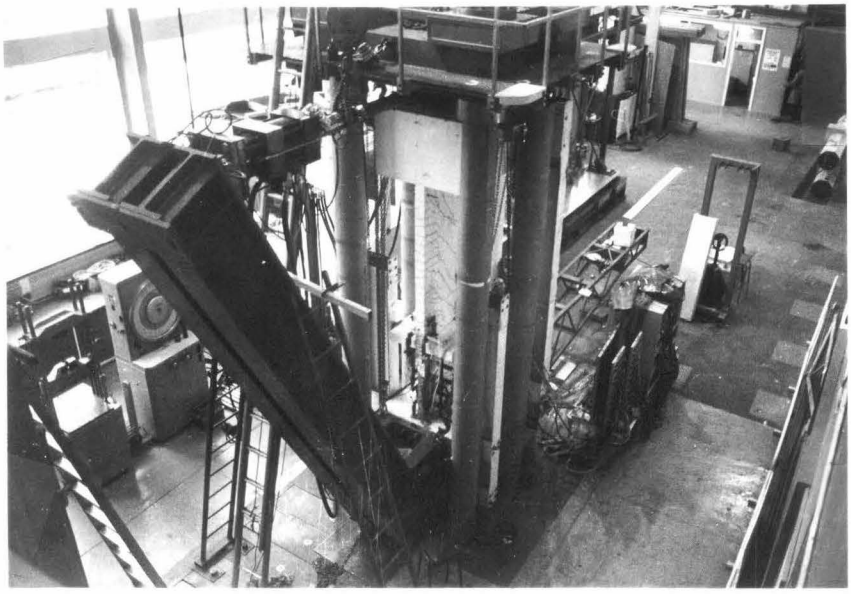

(a) Aerial view from northeast.

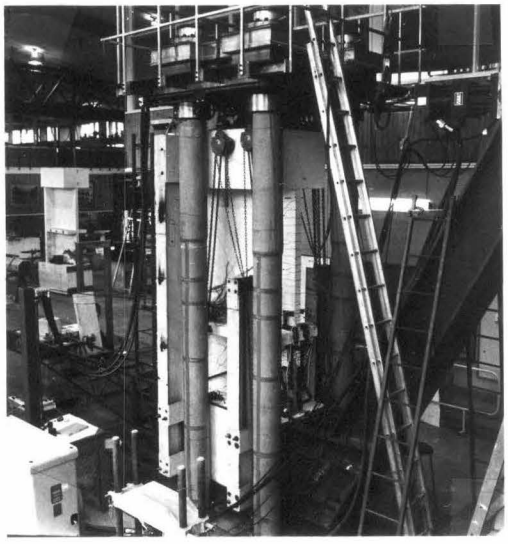

(b) Elevation from southeast.

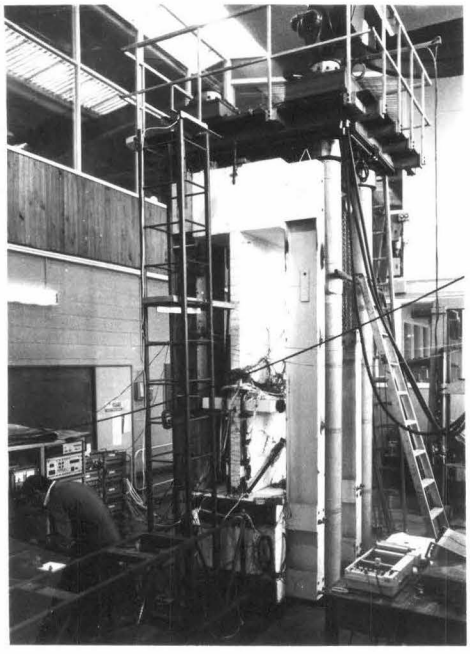

(c) Elevation from southwest.

Fig. 6.14 Views of Test Assembly.

Chapter Seven EXPERIMENTALLY OBSERVED BEHAVIOUR OF MODEL STRUCTURAL WALL UNITS

7.1 INTRODUCTION

This chapter contains the results of tests conducted on four approximately 1/3 scale model structural wall units. The characteristics and behaviour of each unit are discussed separately. The description of experimentally observed response includes specimen strengths and deformations as well as strain measurements for longitudinal and hoop reinforcement. The chapter concludes with a general discussion of the more important aspects of response and a summary of observed experimental behaviour. Particular stages in a test are referred to by the relevant load point numbers or the nominal displacement ductility (μ_Δ) attained.

7.2 WALL 1 - DESCRIPTION OF TESTING AND RESULTS

7.2.1 General Notes

This rectangular section wall was designed for nominal axial load variation of $0.05f'_cA_g$ (negative lateral load) to $0.30f'_cA_g$ (positive lateral load). Code [34] required hoop steel was provided as follows:

east end ($P = 0.30f'_cA_g$ nominal) 6 legs of R5 bar @ 40 mm (h"/2) vertical centres over outermost half of theoretical compression block at ideal strength, i.e. full code required confinement.

west end ($P = 0.05f'_cA_g$ nominal) 5 legs of R5 bar @ 72 mm ($6d_b$) vertical centres, corresponding with code antibuckling requirements.

Details of wall geometry, reinforcement and instrumentation are given in Figs. 7.1, 7.2 and 7.3 respectively.

The actual test variation of axial load for Wall 1 was $0.05\ f'_cA_g$ - $0.26\ f'_cA_g$, using the measured value of f'_c. Axial load application was carried out prior to the incremental cycling of lateral load, remaining constant for the duration of each positive or negative excursion. At zero lateral load, axial load was then changed and the next half cycle of lateral load begun. Fig. 7.4 shows the incremental loading sequence used for the test.

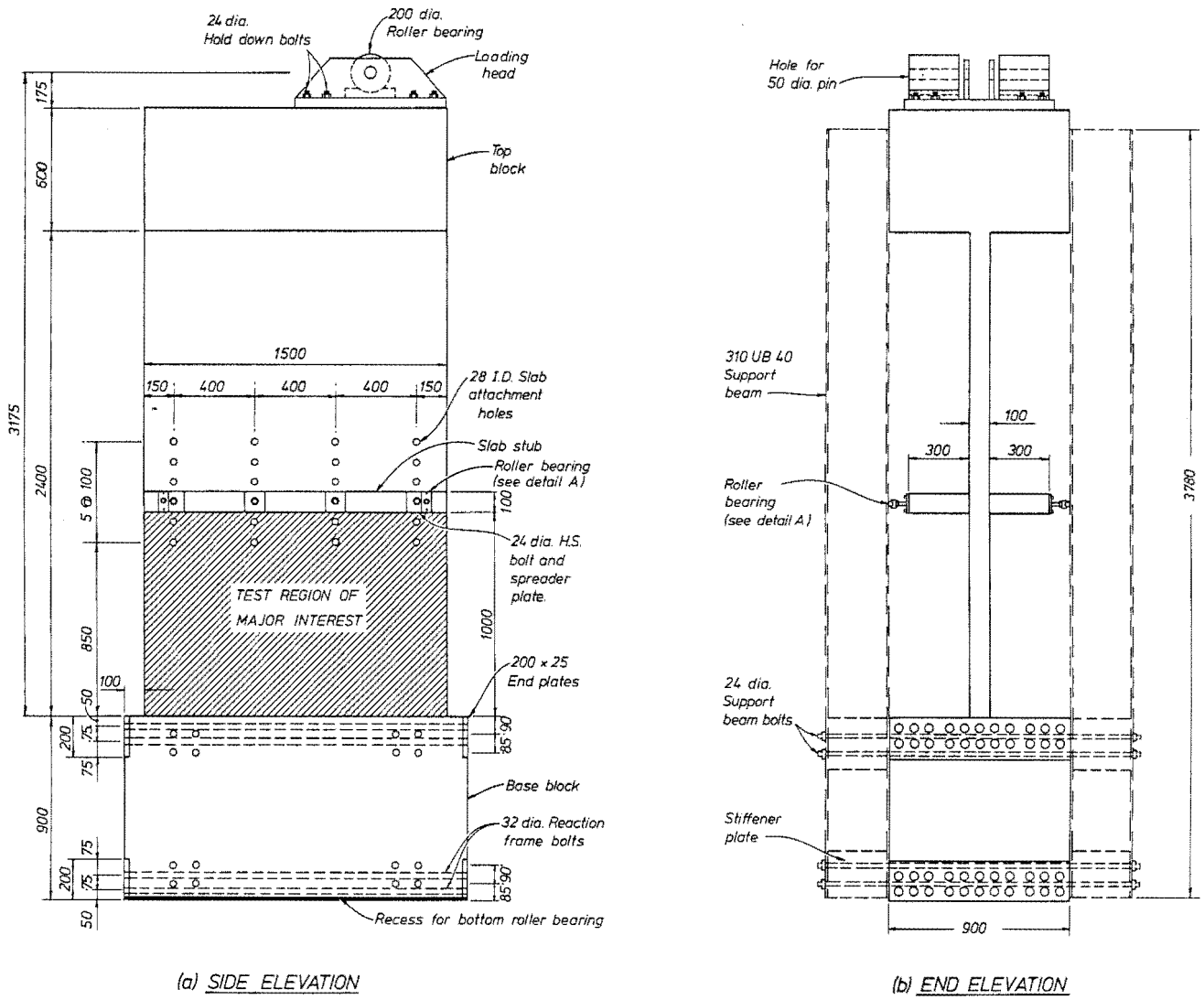

Fig. 7.1 Details of Wall Geometry - Walls 1 and 2.

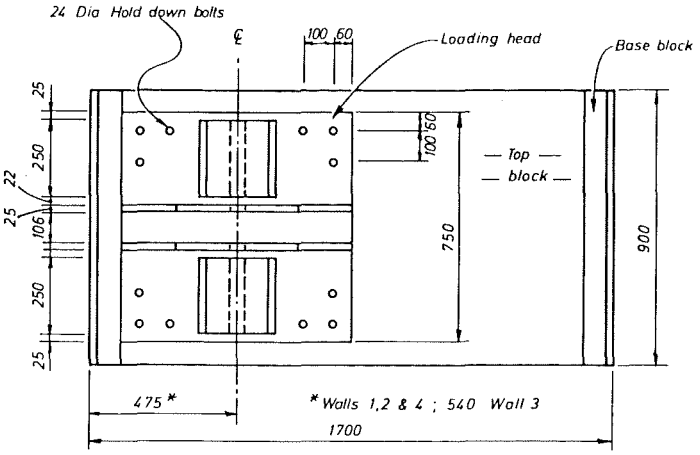

(c) PLAN VIEW OF TOP BLOCK

Fig. 7.1 (Continued)

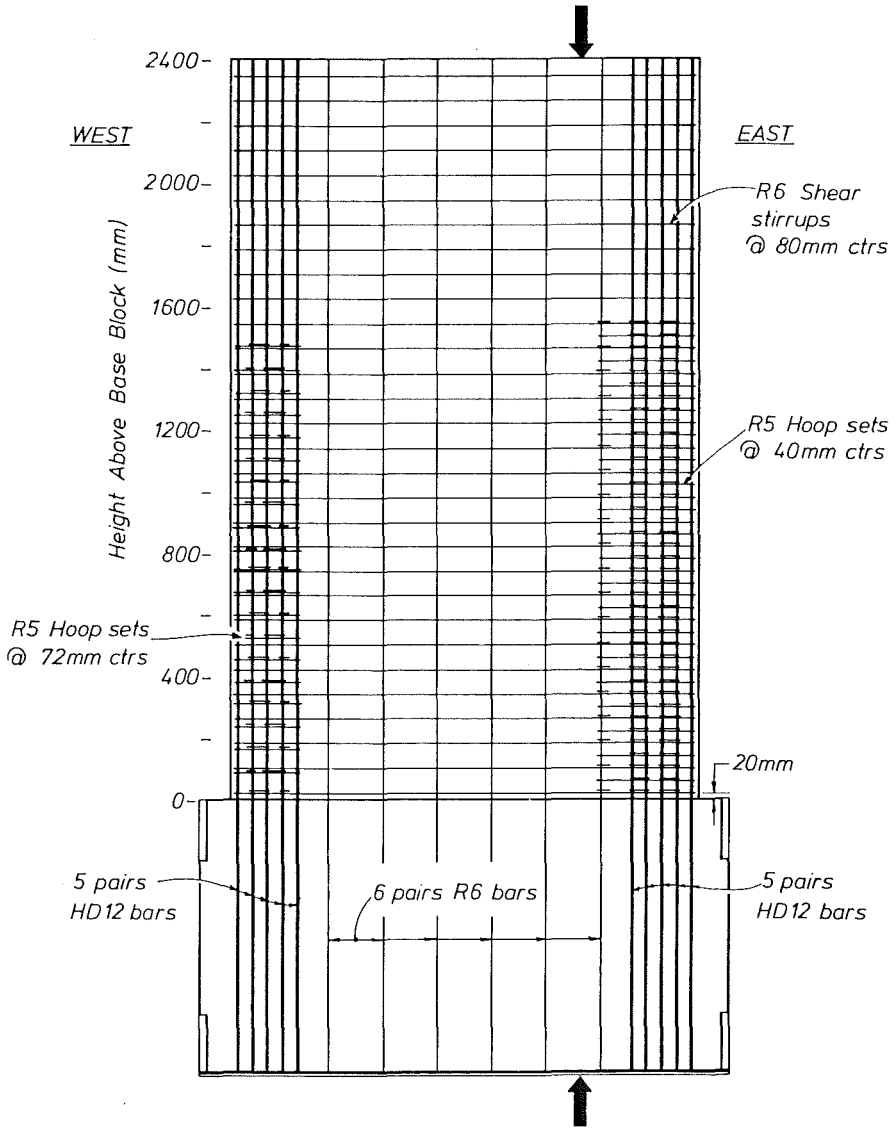

(a) SIDE ELEVATION

Fig. 7.2 Reinforcement Details - Wall 1.

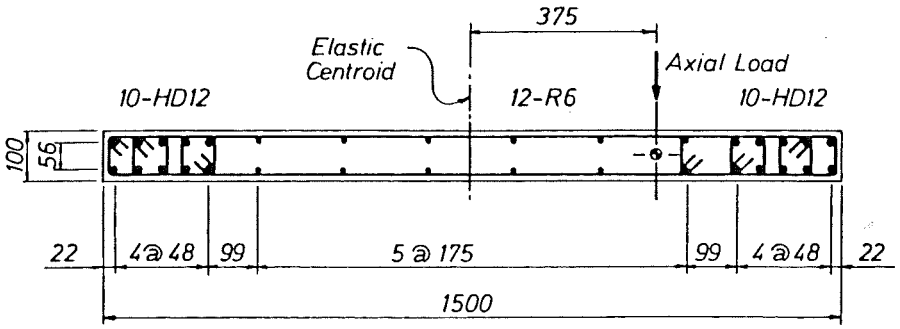

(b) CROSS SECTION

Fig. 7.2 (Continued)

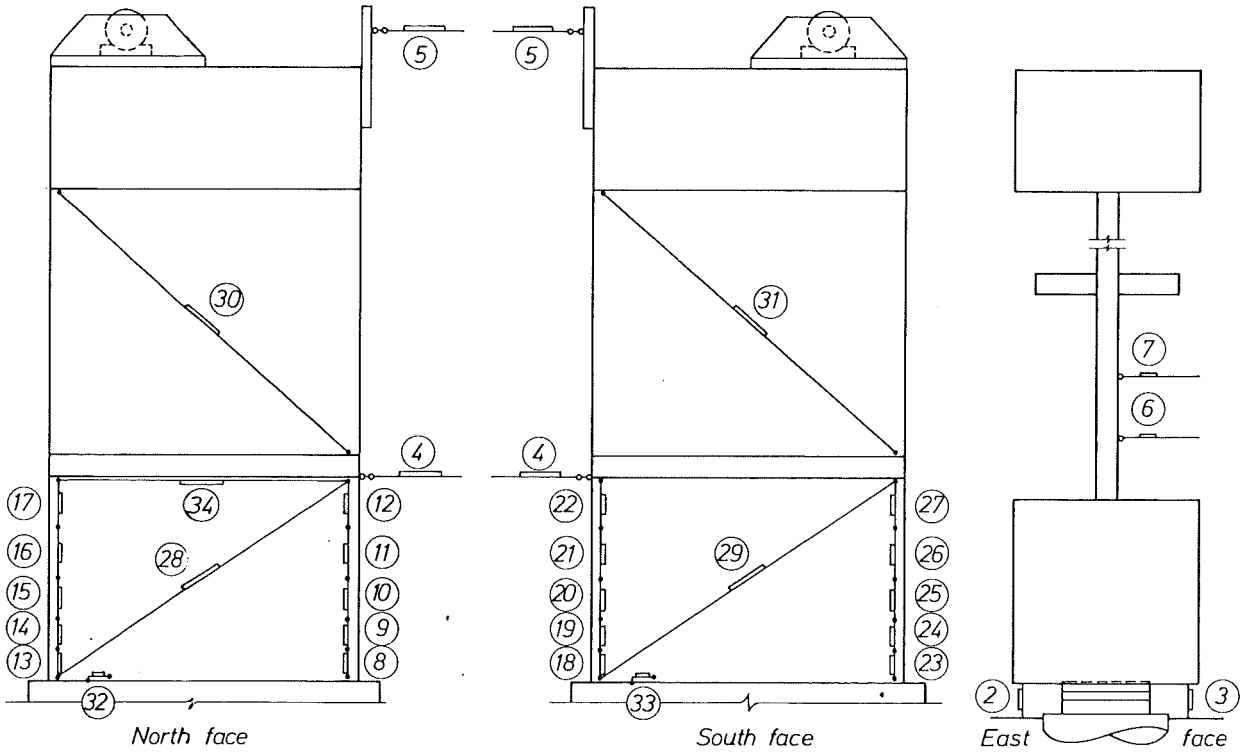

(a) EXTERNAL INSTRUMENTATION

Fig. 7.3 Details of Instrumentation - Wall 1.

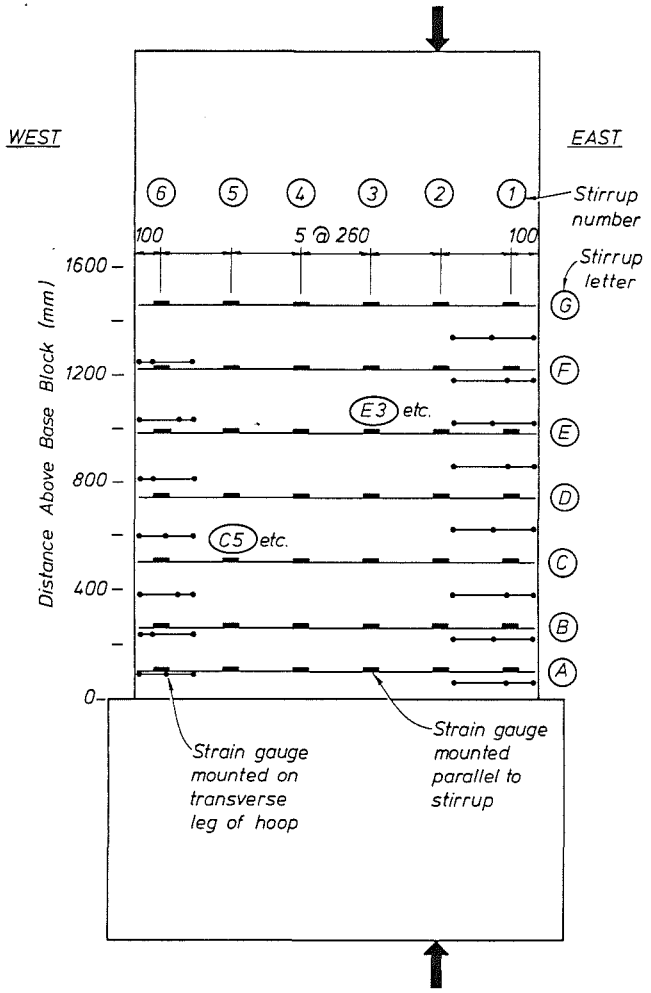

(b) HOOP AND STIRRUP GAUGES

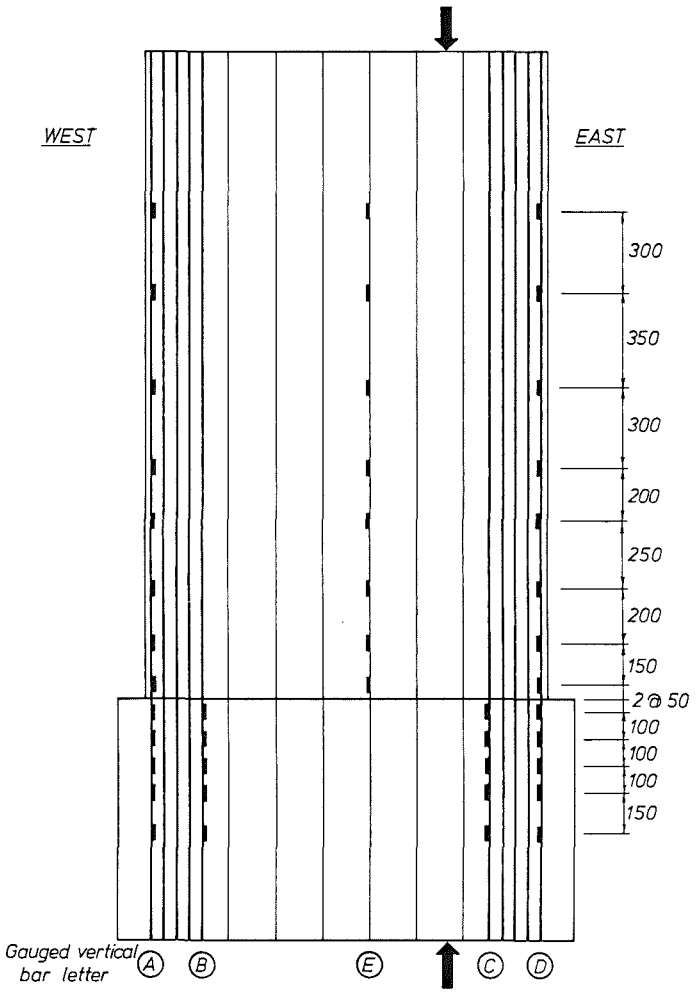

(c) LONGITUDINAL BAR GAUGES

Fig. 7.3 (Continued)

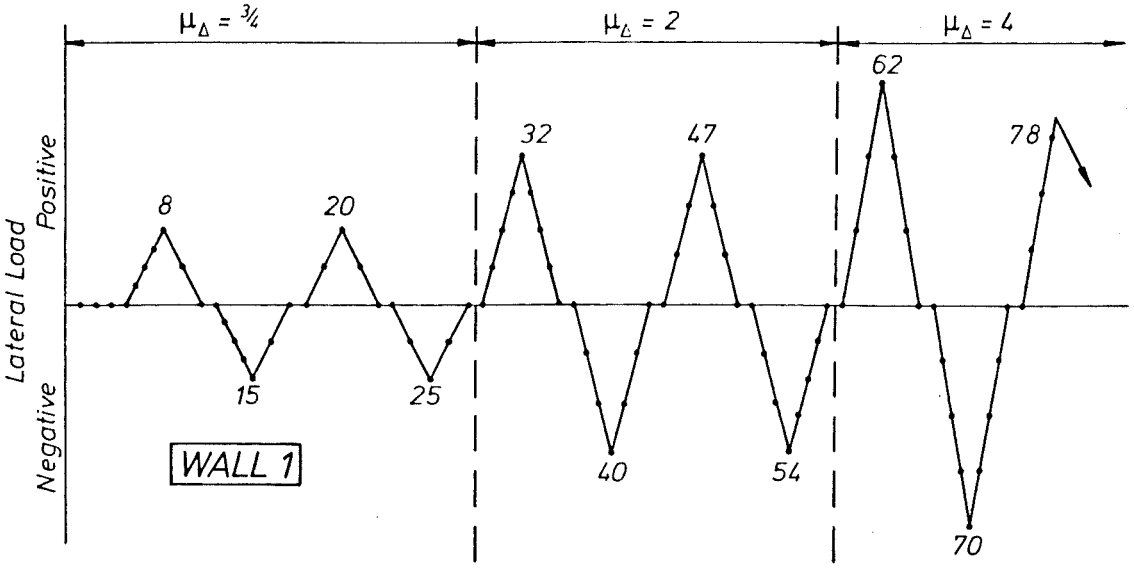

Fig. 7.4 Incremental Loading Diagram Showing Load Point Numbers - Wall 1.

7.2.2 Description of Observed Behaviour

Load Point (shown above in Fig. 7.4)

6. Fine cracking became visible on west end of wall to a height of 1.5 m above the critical section.
8. Cracks penetrated 500 mm in from the west end, and further up the wall height.
13. Horizontal cracks opened on the east end of the wall.
14. Four main diagonal cracks propagated about 900 mm in from extreme tensile fibres.
15. A horizontal crack spread across the wall at height 950 mm above the wall base (through a line of slab stub attachment holes, which act as crack initiators being local points of weakness). Diagonal cracks extended to within 500 mm of the compression face. Cracks at each end of the wall were present up the full height of wall to the underside of the top block.
20. No significant increase in cracking, as compared with load point was observed.
25. Cracks at the east end of the wall were present over the full wall height, i.e. up to the underside of the top block. The construction joint between the wall and base block opened slightly with

no visible horizontal (shear) displacements. The mid-height wall joint remained uncracked.

32. Vertical splitting of east end cover occurred to a height of 400 mm above the block base (see Fig. 7.5(a)).

40. Deformations were concentrated at existing major diagonal cracks. At the wall ends these inclined cracks branched into numerous smaller, essentially horizontal, cracks aligned with hoop reinforcement sets. Although the base construction joint in the web opened vertically approximately 2 mm, this width was much reduced at the east end. This is due to the more favourable clamping action of the end group of deformed bars as compared with the widely spaced plain bars in the central part of the unit. Slight vertical splitting developed over the lowermost 150 mm of the west face (see Fig. 7.5(b)).

47. Vertical splitting and spalling at the east end of the wall at this load point, the second cycle to $\mu_\Delta = 2$, is shown in Fig. 7.5(c).

54. Diagonal cracks extended to within 150 mm of the west face, where vertical splitting increased slightly in extent. Cover concrete at the east end was loosened.

62. The severely spalled east end of the wall is shown in Fig. 7.5(d). Diagonal cracks of width 3-4 mm were observed, with a well defined horizontal crack (260 mm above the base block, coincident with a stirrup) also developing. No significant shear slip was noted at the base construction joint.

70. Cover spalled over the bottom 100 mm of the west end of the wall. A 100 mm square slab of cover spalled off the north face of the wall some 300 mm from the extreme tension fibre. Diagonal panel cracks opened to 4 - 5 mm in width.

79. Failure of the wall occurred as loading proceeded towards $\mu_\Delta = +4$ for a second time. Some warning of the likelihood of failure could be obtained from the load-deformation curve produced during testing, which indicated a major reduction of stiffness. Failure was essentially in a compression mode, occurring suddenly and being non-ductile. Preset deflection control trips limited the travel of the Dartec ram so that no damage was done to the testing facilities.

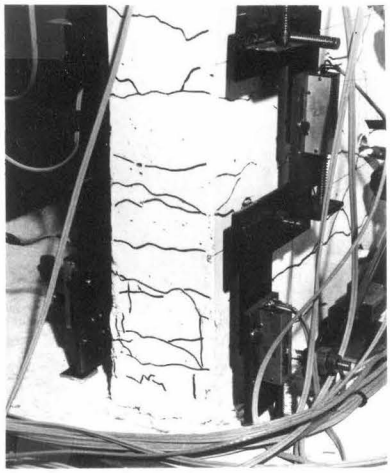

(a) Vertical splitting of east end cover μ_Δ = 2 x 1

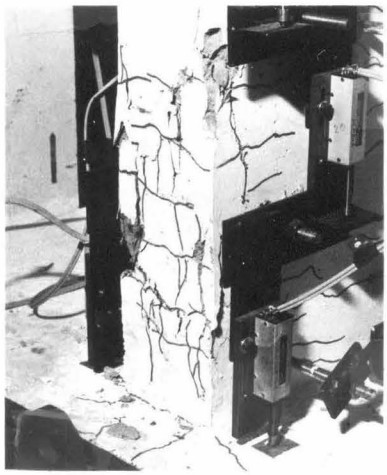

(b) Vertical splitting of west end cover μ_Δ = 2 x 1

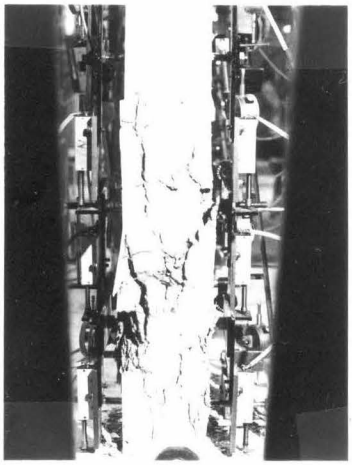

(c) Spalling of east end cover μ_Δ = 2 x 2

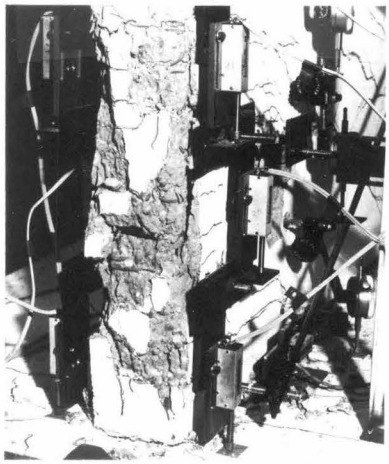

(d) East end μ_Δ = 4 x 1

Fig. 7.5 Wall 1 During Testing.

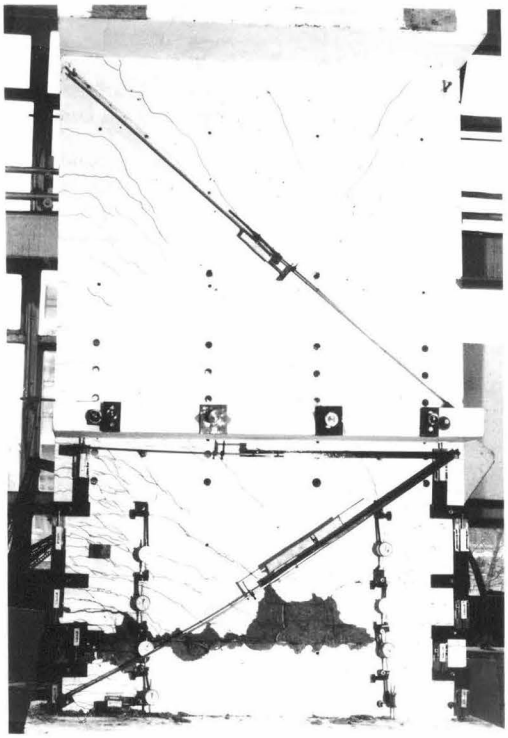

(e) North face, end of test.

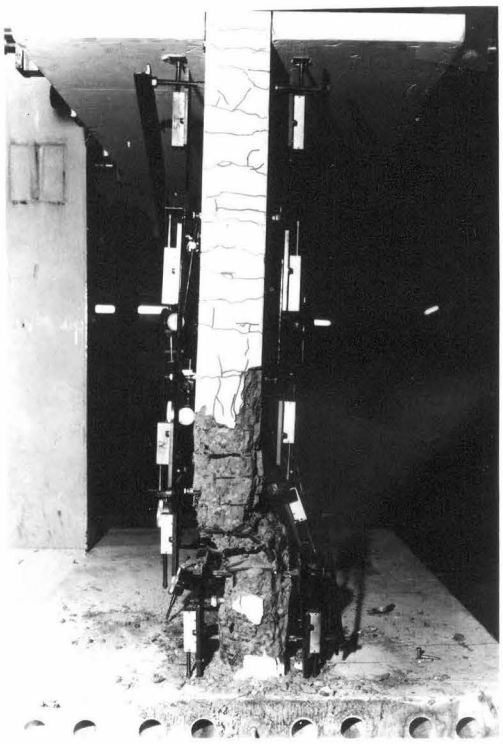

(f) East face, end of test.

(g) South face, end of test.

Fig. 7.5 (Continued)

7.2.2.1 Description of failure mechanism and the failed unit:

The east end of the wall underwent both a compression failure and a lateral movement of order 35 mm to the south, the failure zone being 250 mm above the base block. (See Fig. 7.6). This lateral shift occurred over a small vertical height (≃ 50 mm) and associated buckling was of a local nature only. This offset reduced to zero 1200 mm into the section. Concrete in the confined core was crushed to a fine powder in the failure zone, while remaining intact elsewhere. No fracture of flexural or hoop reinforcement was observed, although at the failure zone, plastic strains of about 30% were noted in transverse hoop legs. Outside the well confined zone concrete, failure was via the formation of a diagonal sliding plane transverse to the wall.

After testing the wall was taken out of the test rig and photographs made to illustrate the post failure condition of the unit (Fig. 7.5(e)-(g)). These photographs show crack patterns, potentiometer and dial gauge instrumentation and the extent of damage incurred during the test program.

It is considered likely that failure was initiated by the crushing of the unconfined concrete immediately adjacent to the well confined zone. The peak compression strain (on the south face of this section) was approximately 0.011 at the previous cycle to $\mu_\Delta = +4$. Thus it was doubtful whether attempts to attain similar strains with full resistance capacity a second time would be successful. As lateral load (and compression block depth) increased, this unconfined concrete would lose significant load carrying capacity. To maintain (and further increase) compression capacity as lateral load increased, both strains in the confined core and neutral axis depth would increase. Such a progressive westward shift in neutral axis position is likely to have caused further crushing in the unconfined concrete and increased the load required to be sustained by the intact confined core, until this latter failed itself in the crushing mode observed. After failure, it was noted that a vertical 6 mm bar located 670 mm from the compression face was buckled. This suggests a considerable westward migration of the neutral axis from its position ($c \simeq 690$ mm) at the first cycle to $\mu_\Delta = +4$.

The critical section where failure was observed was approximately 250 mm above the wall-baseblock construction joint, the theoretical critical section. The confining effect of the comparatively massive base block

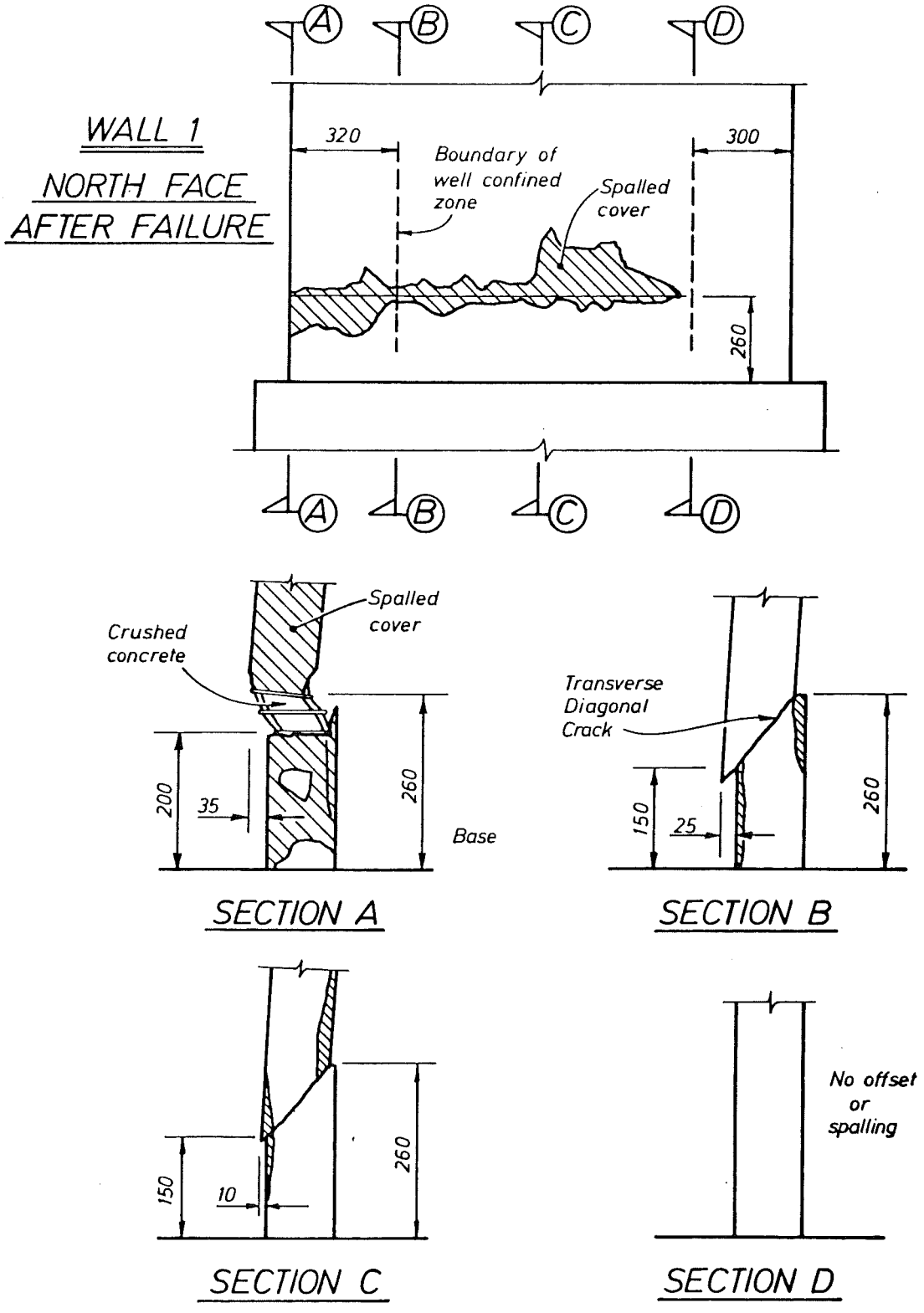

Fig. 7.6 Diagram of Wall 1 After Failure.

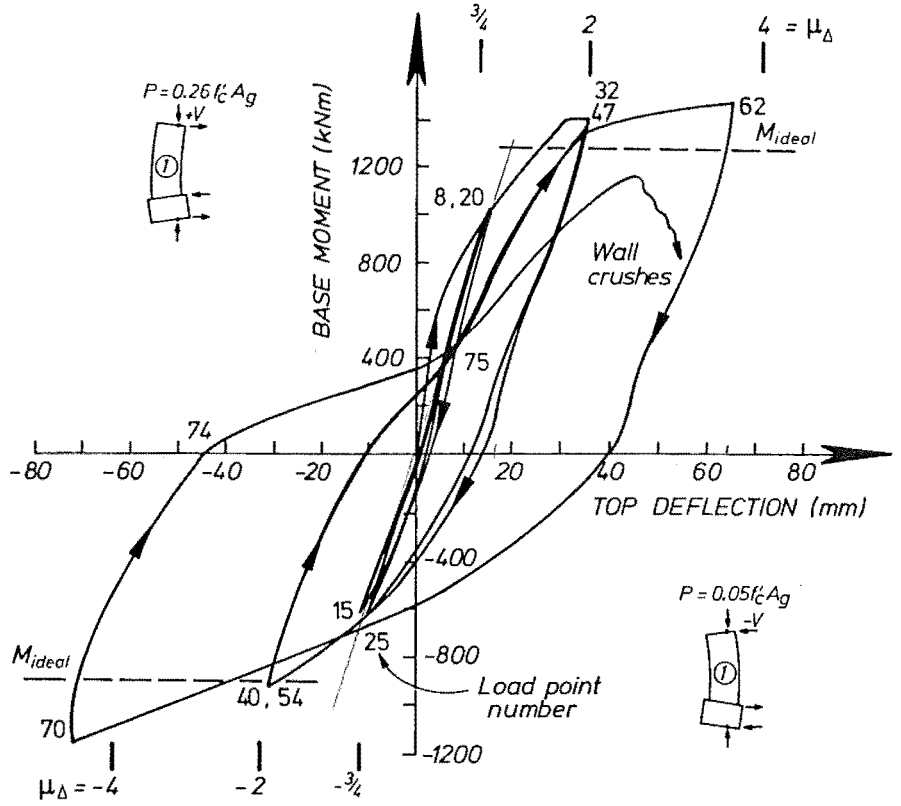

Fig. 7.7 Moment - Wall Top Displacement Relationship - Wall 1.

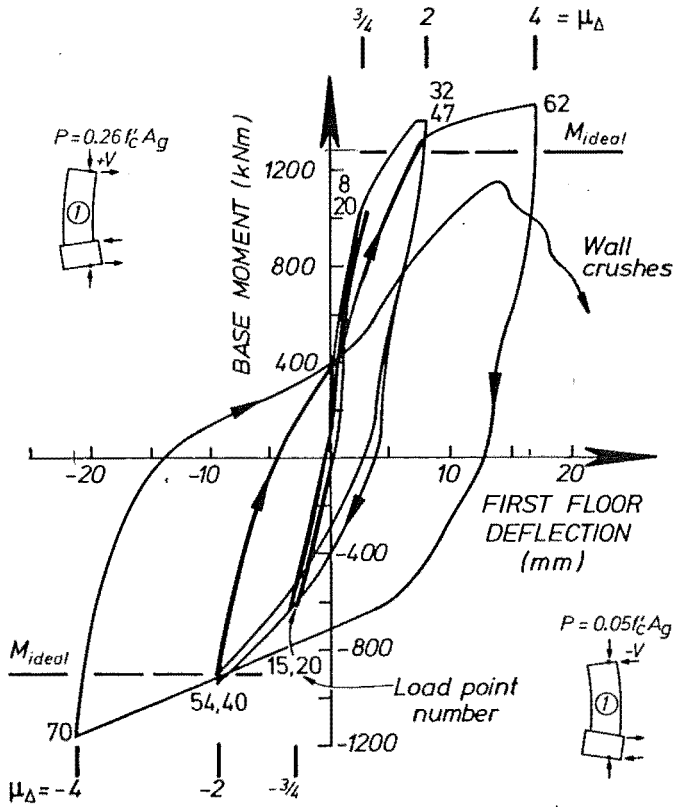

Fig. 7.8 Moment - First Floor Displacement Relationship - Wall 1.

is responsible for forcing the critical zone upwards. An estimate of the extent of this shift is taken as one half the theoretical compression block depth (i.e. 0.5 x 600 = 300 mm), a reasonable distance in this case.

7.2.3 Test Results

The following sections discuss envelopes and distributions of maximum displacements, strains, etc. deduced from strain gauge and potentiometer readings. A feature common to almost all observations is the high level of consistency between first and second cycle readings (at a given ductility), unless specifically noted to the contrary.

7.2.3.1 Moment-deflection hysteresis relationship: Moment vs. horizontal displacement hysteresis loops are presented in preference to lateral load (shear) - displacement loops because of the effect of the varying eccentric axial load which contributed to the total applied moment. The moments referred to are those at the theoretical critical section (the wall-base block interface), whilst "top deflection" is as measured at the level of the applied lateral load (see Fig. 6.10).

With respect to the moment-deflection relationship of Fig. 7.7, the initial cycles to $\mu_\Delta = \pm 3/4$ show good repeatability, although the initial positive loading branch indicates greater stiffness. The (expected) difference between stiffness associated with positive and negative loading is due to the difference in concurrent axial loading. The step changes in axial load occurred between positive moments of 70 and 420 kN.m and caused significant changes in stiffness. This effect is more noticeable when increasing the axial load (i.e. at the transition from negative to positive lateral loading); this loading subjects the entire height of the wall to a constant moment and, for a given base moment, induces larger deformations than those which result from the linearly decreasing moment patterns associated with negative loading. The unloading branches from positive loading indicate a corresponding increase in unloading stiffness as axial load is reduced (causing the applied moment to drop from 420 to 70 kN.m). The final loading branch, from $\mu_\Delta = -4$ until the wall crushing failure shows a severe softening of the moment-displacement relationship, especially between load points 74 and 75 over which interval (see Section 7.2.3.13) an out of plane displacement of the east end of the section occurred immediately prior to failure. However, stiffness had increased and the attainment of $\mu_\Delta = 4$ for a second time seemed likely.

Ideal flexural strengths were exceeded by 12 and 28% for positive and negative loading respectively, these strengths calculated using the maximum and minimum applied axial loads respectively. Good repeatability of response is demonstrated by the two cycles at $\mu_\Delta = 2$, where the strength loss between first and second cycles is less than 5%. Yield points are not well defined by the loops, especially for negative loading. The usual decrease in apparent flexural strength with increasing lateral displacement (the so called P-Δ effect) does not significantly modify ideal section strengths for the walls tested. This is because the rotation of the walls during testing causes only a small displacement of the critical section and thus a small change to axial load eccentricity. The magnitude of this P-Δ moment is of the order of 1% of the section strength at $\mu_\Delta = 4$.

The base moment-first floor level deflection relationship is shown in Fig. 7.8. Similar features to those exhibited in Fig. 7.7 are evident, although there is a higher proportion of negative to positive deflection, attributed to higher shear deformations in the lower storey for negative loading.

7.2.3.2 Moment-Curvature Relationship: A comparison was made between a theoretical moment-curvature relationship and experimentally determined points. The theoretical calculation was made in a standard manner, using such assumptions as the plane sections hypothesis and ignoring the influence of shear. The section was split into about 40 discrete blocks, each subdivided into areas of steel and confined or plain concrete. A modified Kent-Park [59] stress strain relationship was used to model concrete behaviour, and a realistic stress-strain model for the steel was used (linear first and second branches with a quadratic strain hardening branch). The monotonic moment-curvature relationship so obtained forms an envelope to the relationship that would be obtained under cyclic loading.

The experimentally determined curvatures were evaluated over the bottom 150 mm of the wall. Because the lowest level potentiometers (numbers 8, 13, 18 and 23, Fig. 7.3) were targeted on the base block, the deformations recorded by them included anchorage deformations. True first level wall curvatures were obtained by subtracting this component, as calculated from the integration of longitudinal bar strains (see also Section 7.2.3.9). As can be seen from Fig. 7.9 generally good agreement exists between the theoretical relationship and experimental points. Experimental pre-yield stiffness was somewhat high for positive loading,

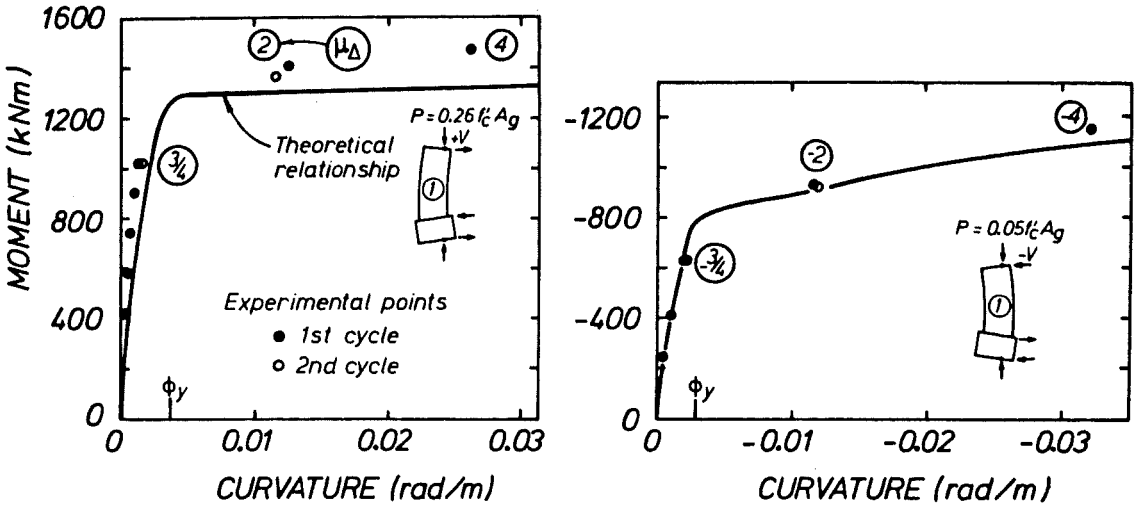

Fig. 7.9 Moment-Curvature Relationship - Wall 1.

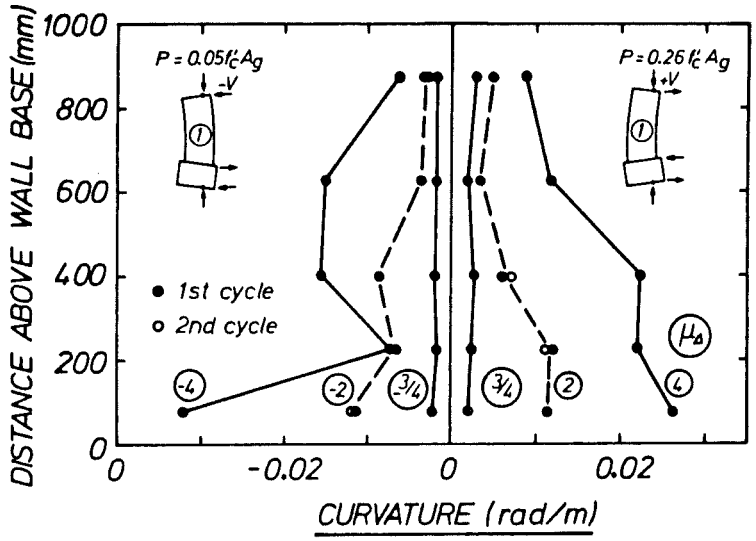

Fig. 7.10 Wall Curvature Distribution - Wall 1

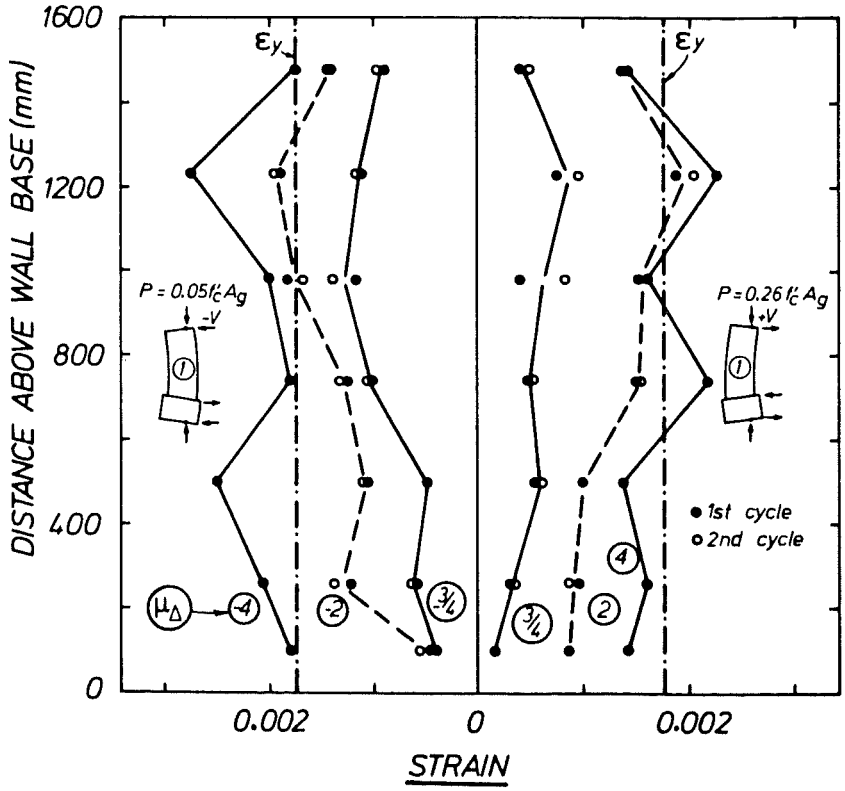

Fig. 7.11 Stirrup Strain Distribution - Wall 1

and the peak recorded strength is 10% in excess of the theoretical value. Agreement is excellent for negative loading. The theoretical yield curvatures indicated in the figure were determined from the intersection points of best fit lines modelling the pre and post yield sections of the curves.

7.2.3.3 Wall curvature distribution: Curvatures were calculated at each level by finding the average strains of north and south face potentiometers at both ends of the wall and calculating the strain gradient. These values are also used to determine the flexural component of first floor deflection. As may be seen from Fig. 7.10, curvatures are approximately constant with height at $\mu_\Delta = \pm 3/4$, while for higher ductilities the expected trend of larger curvatures near wall base is observed. For negative loading, observed level 2 curvatures are lower than might be expected from level 1 and 3 values. This is due to the random nature of crack distribution, which is such that level 2 happens to contain fewer significant diagonal cracks, where deformations are concentrated. The curvature distributions would suggest that wall plastic hinge length was of the order of $0.7\ell_w$.

By simple numerical integration of these wall curvatures it is possible to estimate the rotation undergone by the bottom storey of the wall. (Such a calculation gives maximum rotations of 0.0177 and 0.0245 radians for $\mu_\Delta = +4$ and -4 respectively). These values cannot be taken as full plastic hinge rotations (given the definition of plastic hinge length ℓ_p equalling ℓ_w). Based on these rotations, rotational ductilities of 4.9 and -7.2 were achieved during testing (Table 7.1).

7.2.3.4 Shear reinforcement strains: Figure 7.11 shows envelopes of maximum strain recorded along each of the gauged stirrups in the wall. Strains are relatively uniform with height (the section is subject to constant shear), with a maximum strain of $1.6\varepsilon_y$. There is no marked difference in strain magnitudes for positive and negative loading, although reinforcement should be considerably more highly stressed for negative loading (Appendix D). Strains at the section 980 mm above the base block are somewhat smaller than strains above and below, which is possibly due to the influence of the floor slabs which were close to this height. Maximum observed to design shear force ratios are 1.16 and 1.14 for positive and negative load respectively.

The average slope of diagonal tension cracks was approximately 45°, with no obvious difference attributable to loading direction. Although explicit measurement of crack widths was not made during this test, it was clear that crack width increased with increasing μ_Δ achieved.

Calculations based on code [34] equations for concrete and steel shear capacities, using actual rather than design material properties, suggest that the stirrups should have reached about 80% of yield strain at the extreme (positive or negative lateral loads attained). Although gauges indicated strains well in excess of ε_y, strains observed along the stirrups (Section 7.2.3.6) indicate an average less than yield strain.

7.2.3.5 Strain history of gauge F4: The strain in gauge F4 is plotted against applied shear in Fig. 7.12. Also shown is a theoretical envelope based on code [34] equations for concrete shear capacity and the usual 45° truss analogy for steel shear strength. This theoretical envelope estimates the experimental load demand well. Loading in the negative sense gives a greater strain increase for a given applied shear increment because of the lesser concrete capacity associated with this sense of loading (less efficient aggregate interlock associated with lower axial compression). Reasonable consistency between cycles at a given ductility is shown. A given positive or negative excursion of lateral load is associated with a loop in the strain history diagram. For a given shear force (attained twice during such a cycle of loading) it may generally be observed that the stirrup strains associated with the unloading part of the loop are larger. This increased dependence on the steel resisting mechanism implies some degradation of the concrete shear transfer mechanism. As ductility increases, the gauges indicate an increasing residual strain present at zero lateral load.

7.2.3.6 Strain distributions along stirrups: Strain distributions along stirrups C, E and G (Fig. 7.3) are shown in Fig. 7.13. These indicate the general trends of increasing strain levels with μ_Δ and second cycle strains slightly larger than first cycle, attributed to a slight breakdown in concrete shear resisting mechanism. Strains are generally lower at stirrup ends, with one or two identifiable regions where larger strains are concentrated. These regions, marked with Roman numerals, can be identified with areas where major diagonal cracks intersect the stirrups - see Fig. 7.14.

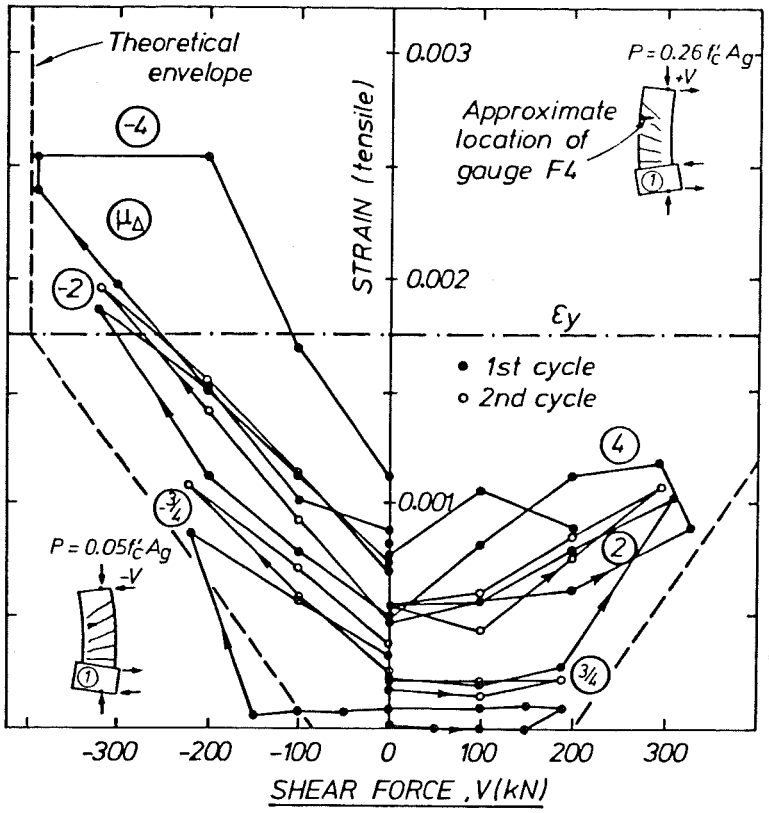

Fig. 7.12 Strain History of Stirrup Gauge F4 - Wall 1.

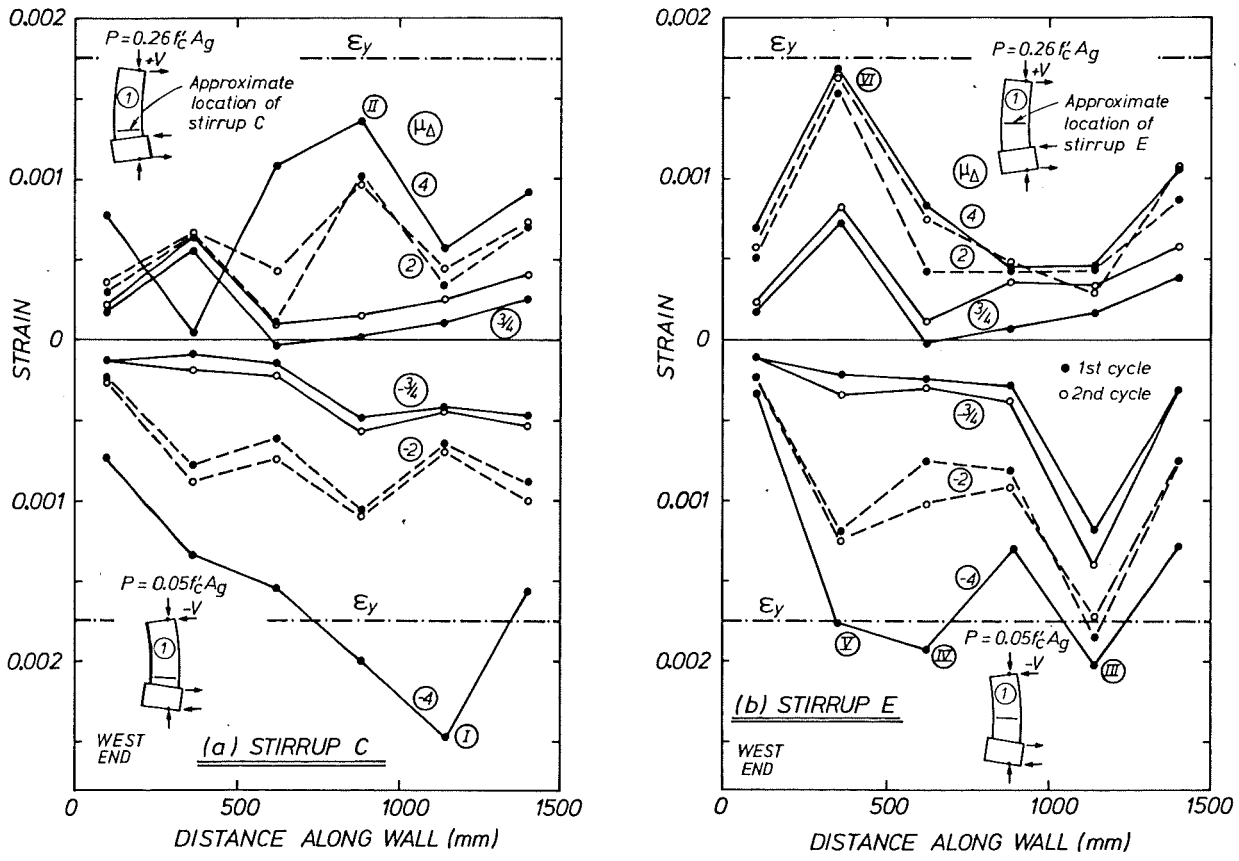

Fig. 7.13 Strain Distribution in Stirrups C, E and G - Wall 1.

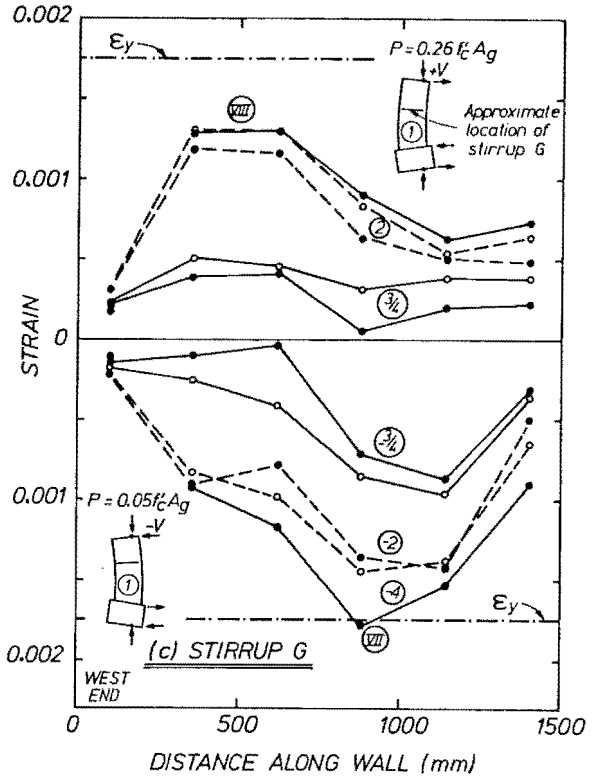

Fig. 7.13 (Continued)

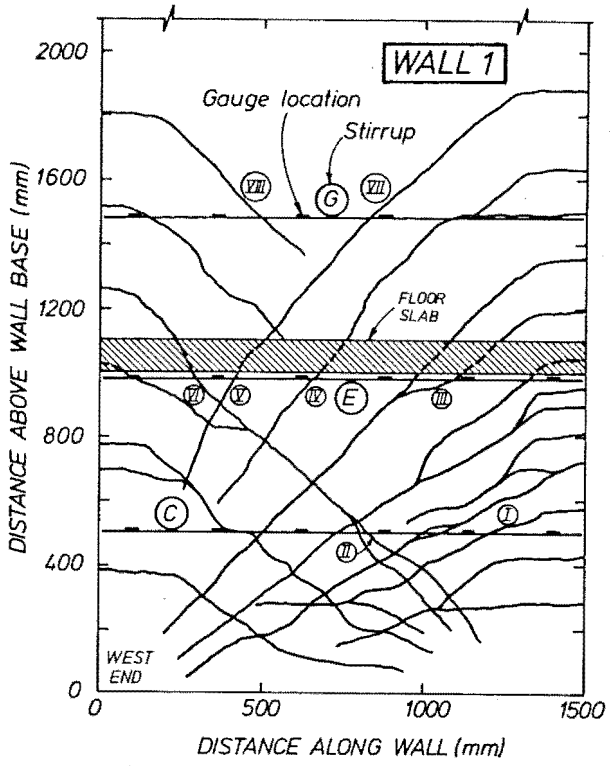

Fig. 7.14 Major Diagonal Cracks - Wall 1

7.2.3.7 Hoop reinforcement strains: Fig. 7.15 shows maximum tensile strains observed in hoop reinforcement sets when the east end zone was both in compression (positive load) and tension. The most striking observations is that strain levels during tension loading of the east end (i.e. during negative ductilities) are comparatively high. During positive lateral loading, blocks of previously cracked core concrete are compressed, with the tendency for expansion of the core restricted by the hoop ties which are put into tension. During negative lateral loading, these displaced blocks of aggregate are unlikely to fit back together neatly and consequently significant strains may remain in the the hoops. Levels of observed strain were generally low, never in fact attaining yield strain. In view of the large vertical strain sustained by the core concrete (of order 2%) the supplied quantity and vertical extent of this reinforcement were more than sufficient.

Similar comments apply to the west end hoop strains, which were generally even lower than the east end values (see Fig. 7.16). It should be remembered that these hoops were supplied in an antibuckling rather than confining role. Also compression strains were expected to be much less.

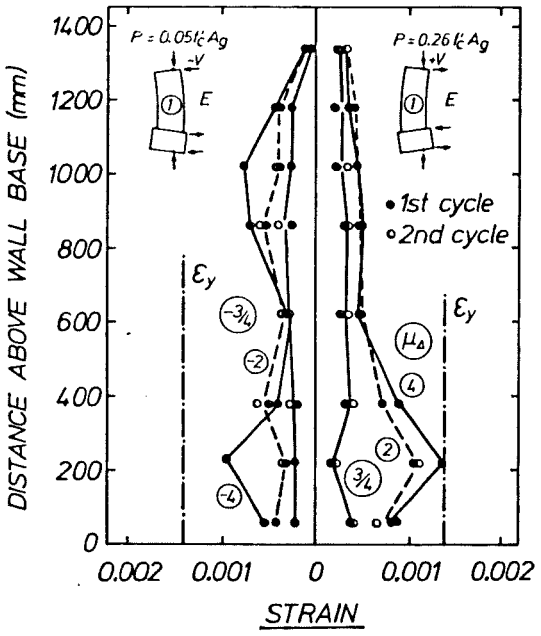

Fig. 7.15 East End Hoop Reinforcement - Wall 1

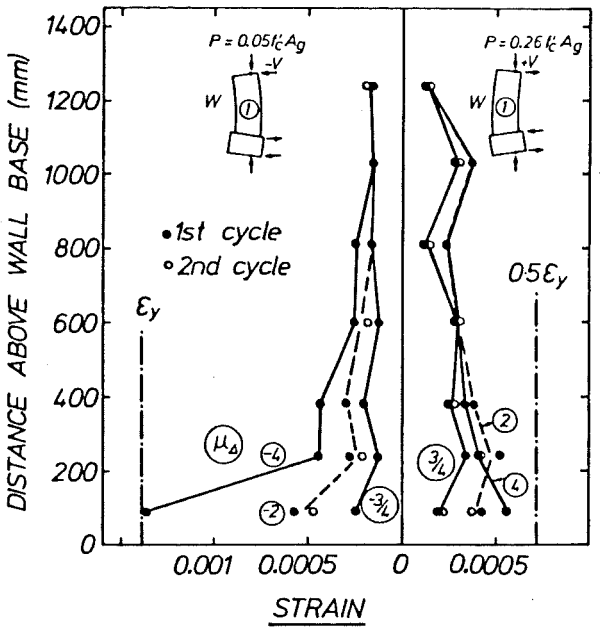

Fig. 7.16 West End Hoop Reinforcement - Wall 1

7.2.3.8 Steel strains above base level: Distributions of strains in vertical bars are given, with 2 scales of diagrams being provided. (The locations of the bar gauges are given in Fig. 7.3(c)). The fine scale figures (7.17(a), 7.18(a)) allow details of strains at low ductility levels to be observed, while the coarse scale figures (7.17(b), 7.18(b)) indicate the magnitudes of large tensile strains encountered. Compression strains were generally less than or close to ε_y. It may be noted that, when an end zone was in net compression, the bars sometimes retained tensile strains due to the severe inelastic tensile elongations induced in the previous load cycle. The maximum observed strain of 2.6% ($\cong 11\varepsilon_y$) indicates that bars were often well into the strain hardening range. Fig. 6.11 indicates a stress of approximately 560 MPa at this strain, an increase of about 25% above yield stress. Strains significantly in excess of ε_y occurred up to a height of approximately 1 m above wall base, where the moment on the section is about 70% of the base value. Tensile strains were largest 200-400 mm above the wall base, suggesting that even for flexure the true critical section is not at the wall base.

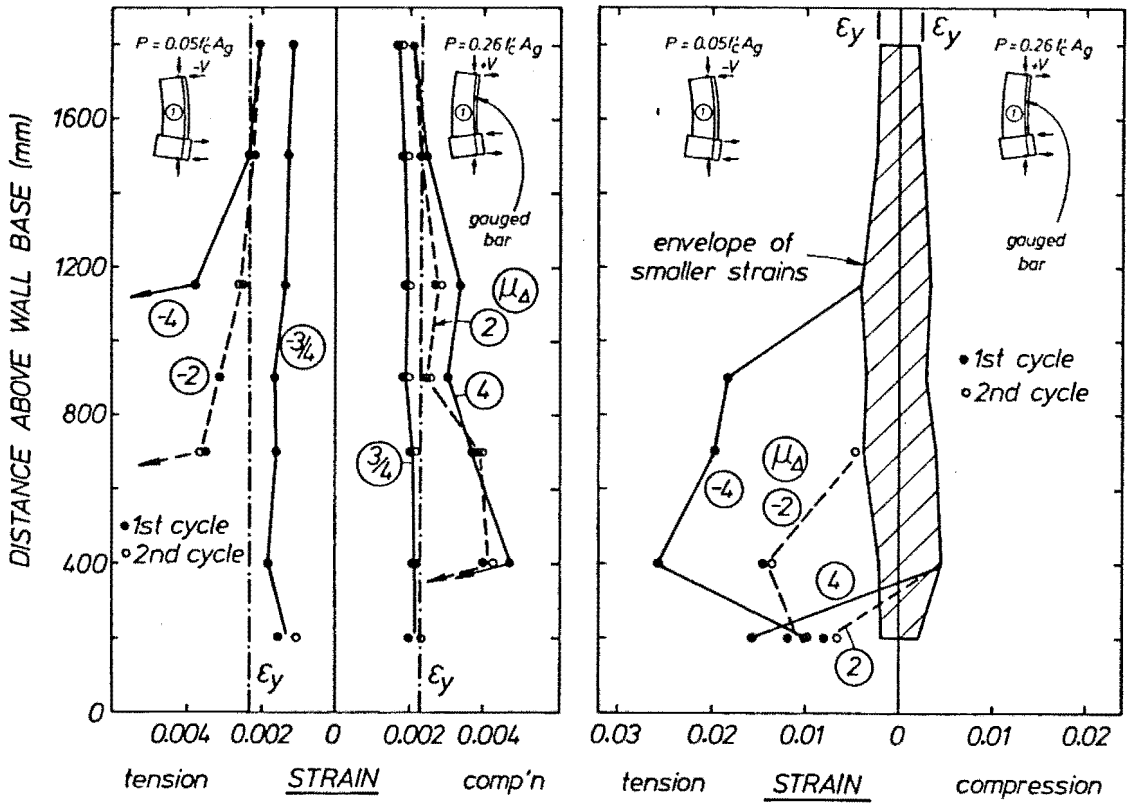

Fig. 7.17 East End Flexural Reinforcement Strains - Wall 1.

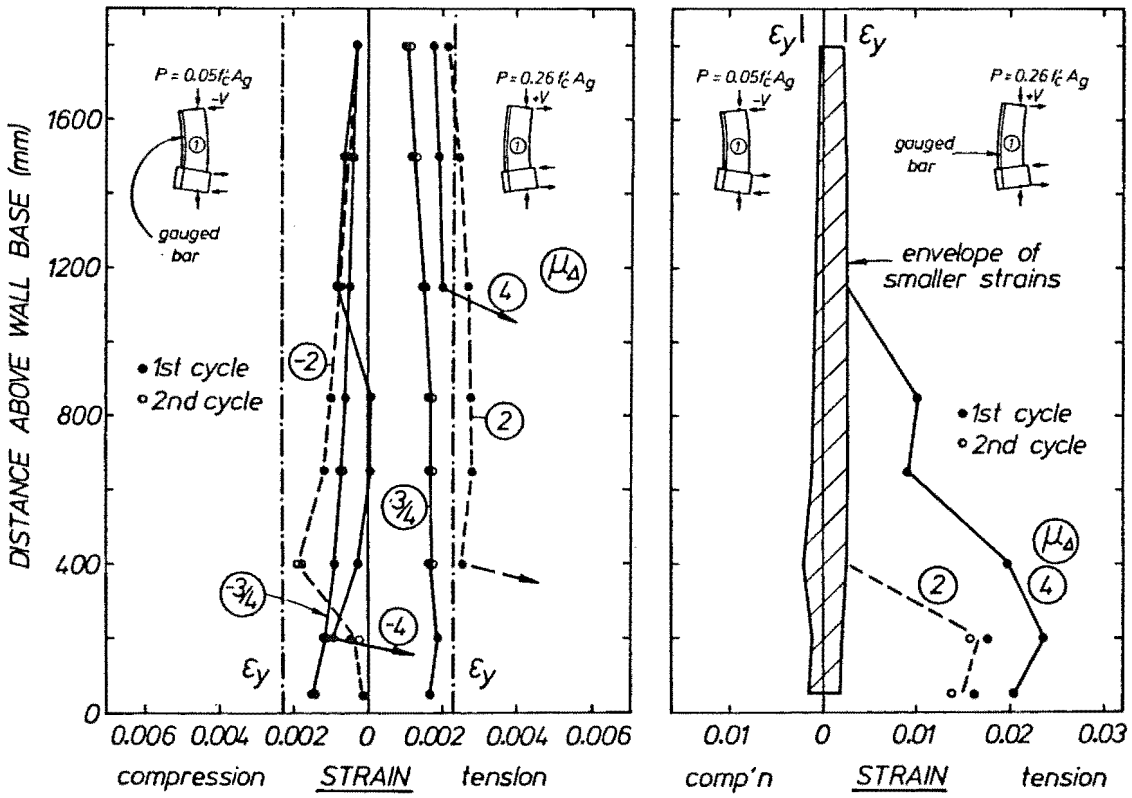

Fig. 7.18 West End Flexural Reinforcement Strains - Wall 1.

7.2.3.9 Strains below wall base level: As before, fine and coarse scale diagrams are presented (Figs. 7.19, 7.20). Compression strains were generally less than ε_y, although residual tensile strains in the compression zones were sometimes recorded as noted previously. Maximum tensile strains of approximately $5\varepsilon_y$ indicate that strain hardening was just commencing at $\mu_\Delta = 4$. Tensile yield strains were recorded as deep as 250 mm, i.e. 20 bar diameters into the base block. Both tensile and compressive strains were negligible at an embeddment length of 500 mm. At high strains, the strains in bars B and C were significantly less than those for A and D, although the distance of the bars from the neutral axis was not proportionally smaller. Strains at

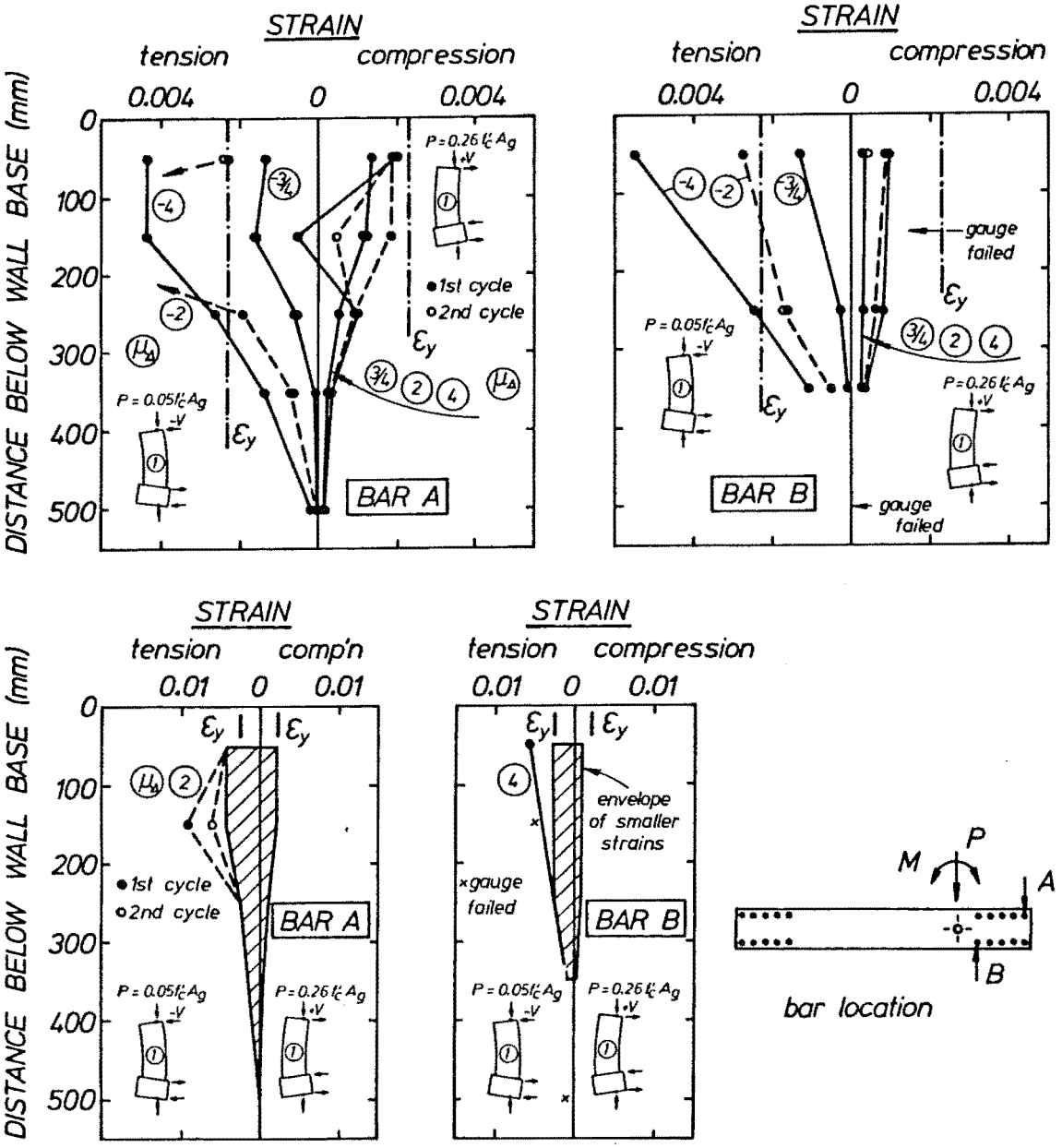

Fig. 7.19 East End Anchored Flexural Reinforcement Strains - Wall 1.

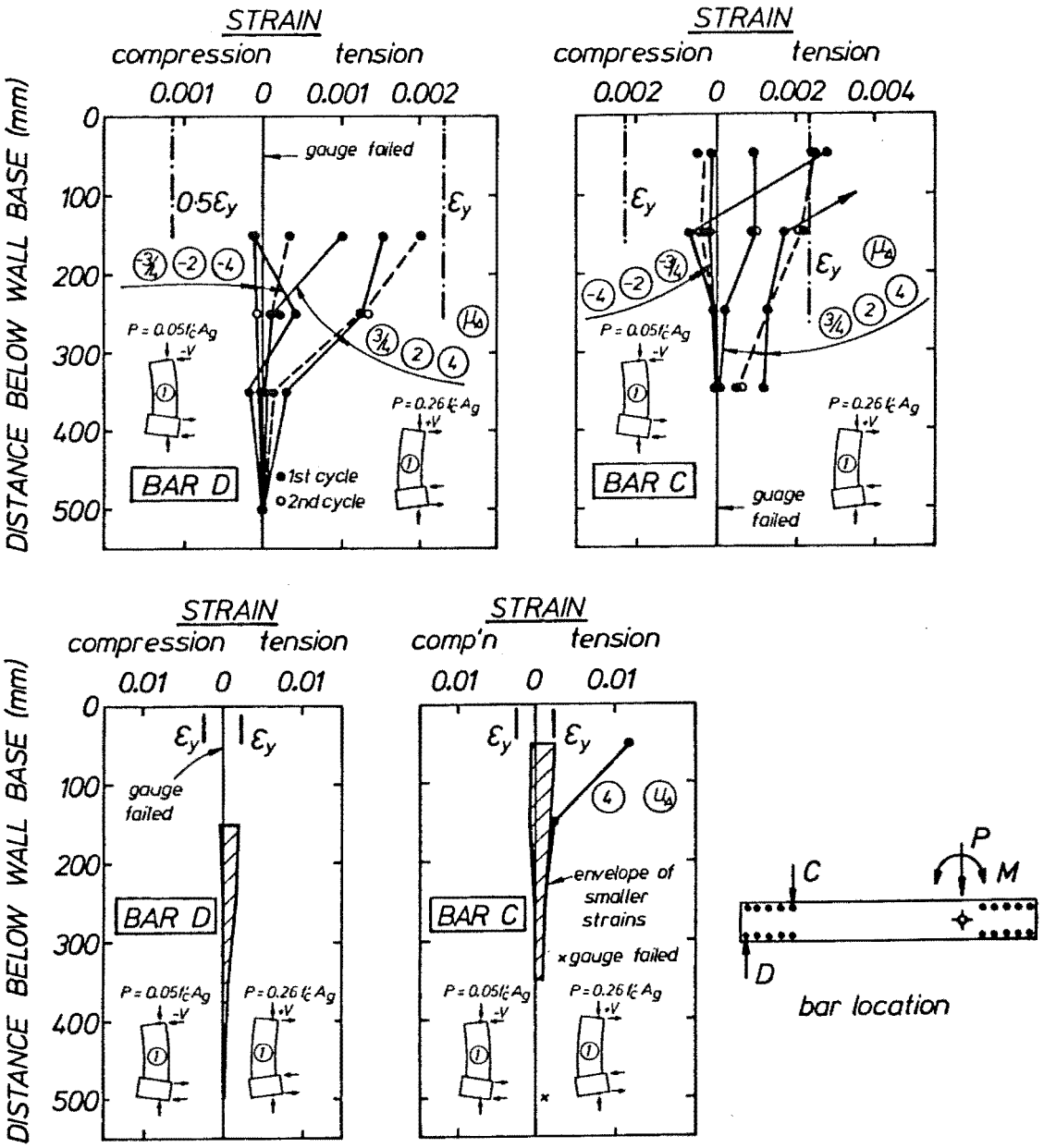

Fig. 7.20 West End Anchored Flexural Reinforcement Strains - Wall 1.

low deformation levels are in better proportion, in line with a "plane sections" hypothesis for embedded bars.

7.2.3.10 First floor level deflection: The decomposition of measured total first floor displacement into flexural, shear and fixed end components is illustrated in Fig. 7.21(a). Flexural deformation was estimated from a numerical integration of the first moment of area of measured wall curvatures taken about the level of the first floor. Curvatures shown in Fig. 7.10 were used. Shear deformations were calculated using a truss analogy (see Fig. 7.22) and deformations indicated by the diagonally mounted potentiometers (Fig. 7.3). Average base shear level shear slip was added to give the total shear displacement. Fixed end deformation (due to anchorage pull-out) was obtained from the tensile and compressive strain profiles recorded in the

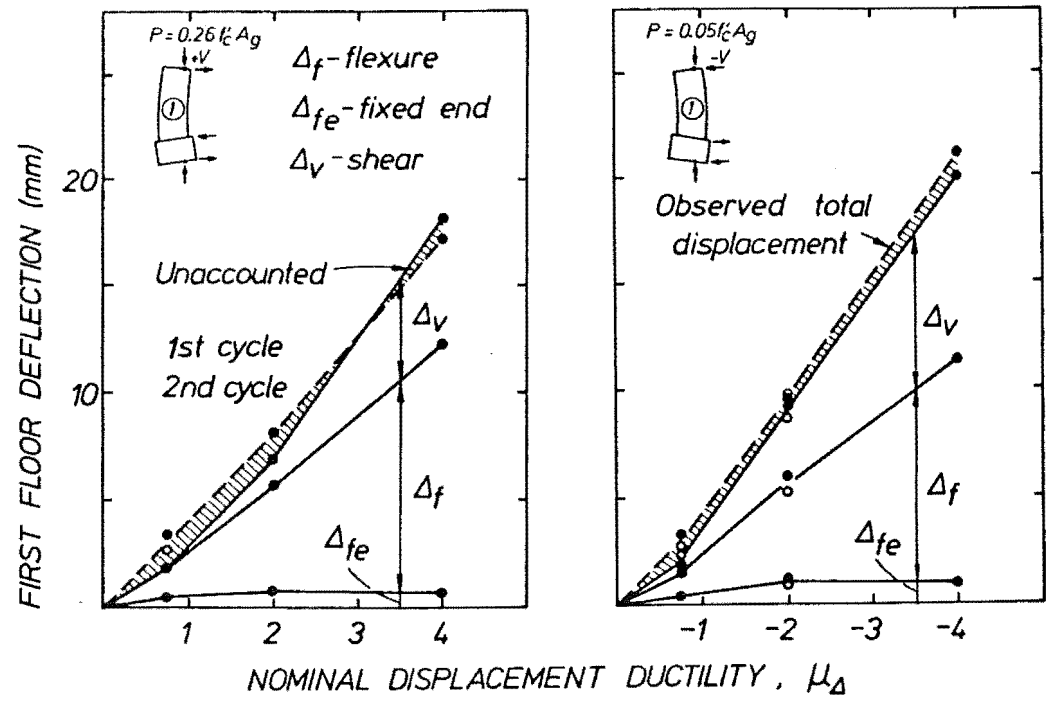

(a) components of deflection

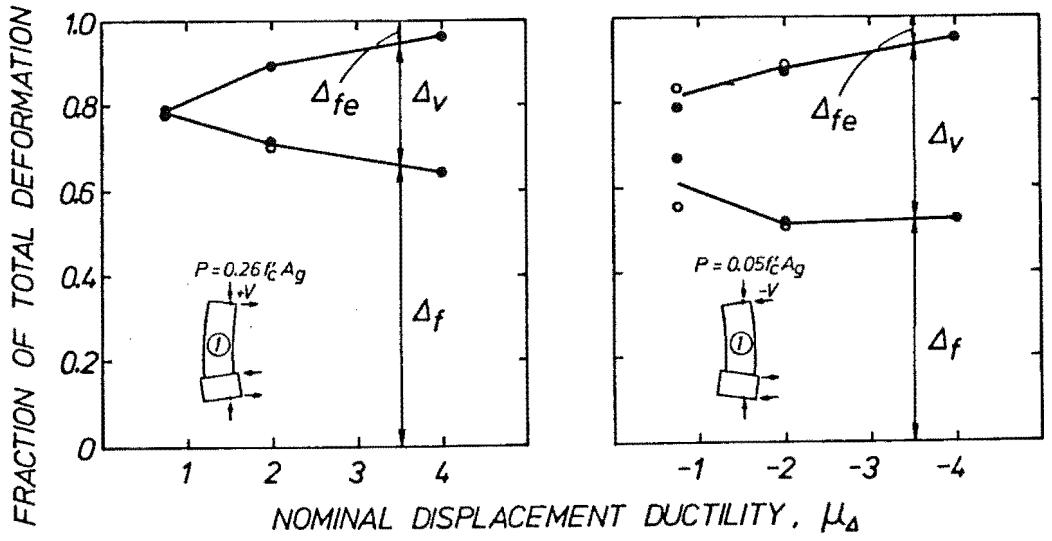

(b) relative proportions

Fig. 7.21 First Floor Displacements - Wall 1.

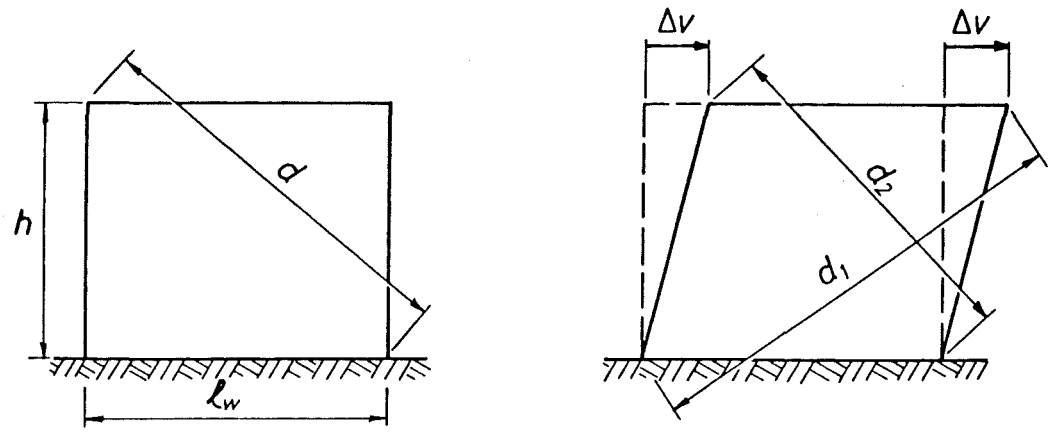

$$d_2^2 = h^2 + (\ell_w - \Delta v)^2 \quad , \quad d_1^2 = h^2 + (\ell_w + \Delta v)^2 \quad \therefore \quad \Delta v = \frac{1}{4\ell_w}(d_1^2 - d_2^2)$$

Fig. 7.22 Method Used to Calculate Shear Deformations.

embedded bars. (Figs.7.19 and 7.20). From the numerical integration of these strain diagrams, a value of pullout deformation can be found and the associated east-west displacement deduced. Finally, an estimate of the error involved in the calculations may be found by subtracting the previous 3 quantities from the recorded displacement at the slab level. This error is large at $\mu_\Delta = -4$ and may be attributed to inadequate assessment of shear displacement.

Also shown (Fig. 7.21(b)) are the relative proportions of each type of deformation. This figure (and Figs. 7.46(b), 7.62(b), 7.74(b)) assumes the total deformation to be equal to the summation of the derived flexural shear and fixed end components. The fixed end component is the smallest, dropping as total deformation increases from 15% to less than 5% of the total for both positive and negative lateral load. Shear deformations are proportionally larger for negative rather than positive load than the difference in positive and negative shear forces would predict. This more flexible negative shear transfer mechanism is due to the associated lower axial load. Shear deformations are largest at $\mu_\Delta = \pm 4$, representing 30-45% of total deformation. Flexural deformations are approximately half the size of shear deformations at this stage. Sliding shear at base construction joint level constituted at most about 13% of shear deformation and less than 3% of total first floor displacement. SEE ERRATA

7.2.3.11 Wall elongation: The wall exhibited a general trend for elongation during testing, due to an accumulation of residual tensile strains at first one wall end and then the other (Fig. 7.23). SEE ERRATA (Slight compression did occur at $\mu_\Delta = +3/4$, where high axial load compressions at this low lateral load level exceeded tensile elongations). As would be expected, greater elongations were observed for negative loading, where axial load is smaller. At $\mu_\Delta = -4$, wall elongation corresponds to a vertical strain of about 0.6%.

7.2.3.12 Shear slip at base construction joint: The average values of of shear slip monitored at the wall-base block interface are shown in Fig. 7.24. This deformation was only 0.2 mm at $\mu_\Delta = +4$ and less than 1 mm at $\mu_\Delta = -4$, despite the low level of axial load associated with this loading. Such good performance is evidence of the adequacy of the method of construction joint preparation. Slip at this base level joint was observed to be non-uniform along the length of the wall, and greatest in the central regions, remote from the well confined end bundles of longitudinal bars. Maximum shear slip at higher levels (say 200-400 mm above base) across intersecting flexural-shear cracks from reversed lateral loading was estimated at 3 mm, well in excess of base slip.

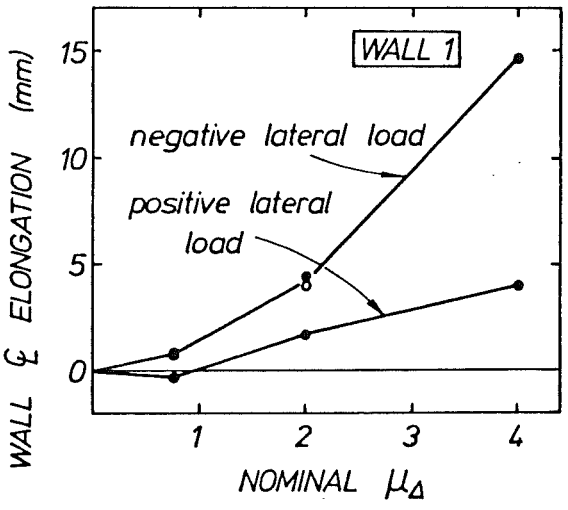

Fig. 7.23 Axial Elongation of Wall 1.

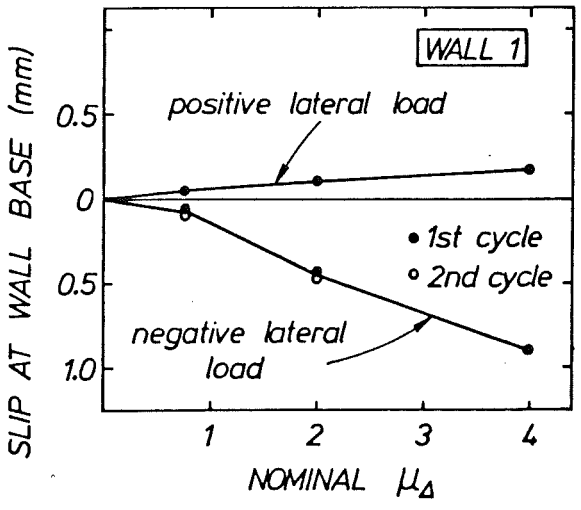

Fig. 7.24 Slip at Base Construction Joint - Wall 1.

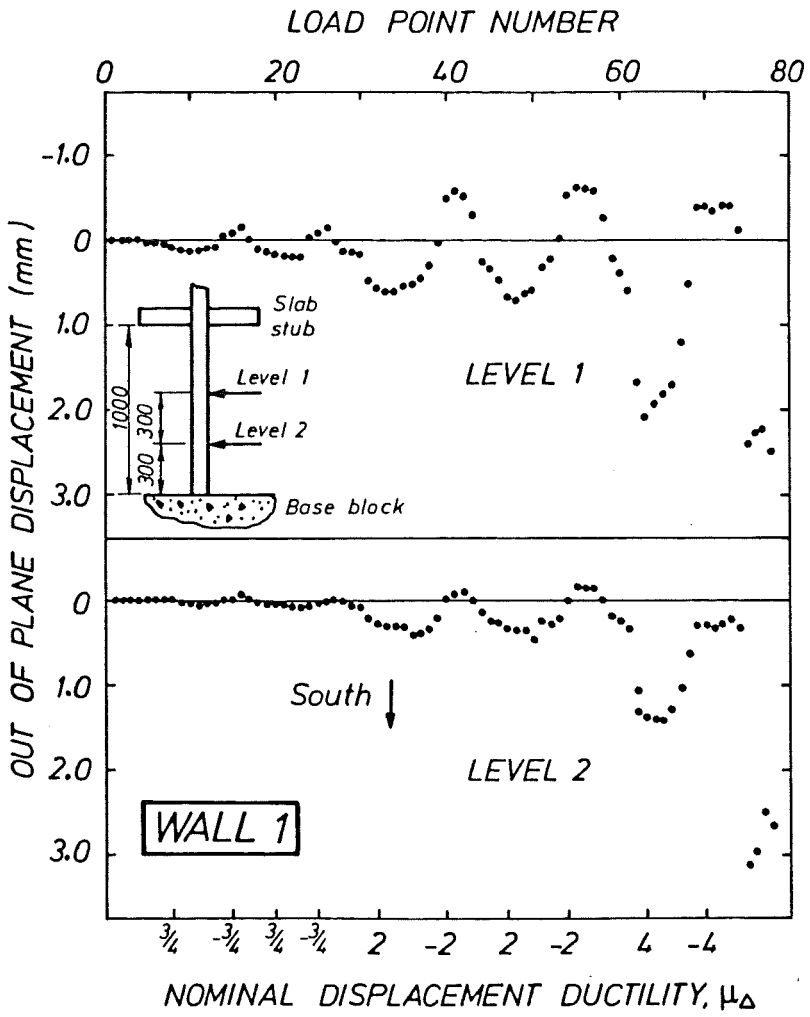

Fig. 7.25 Out of Plane Displacement History - Wall 1.

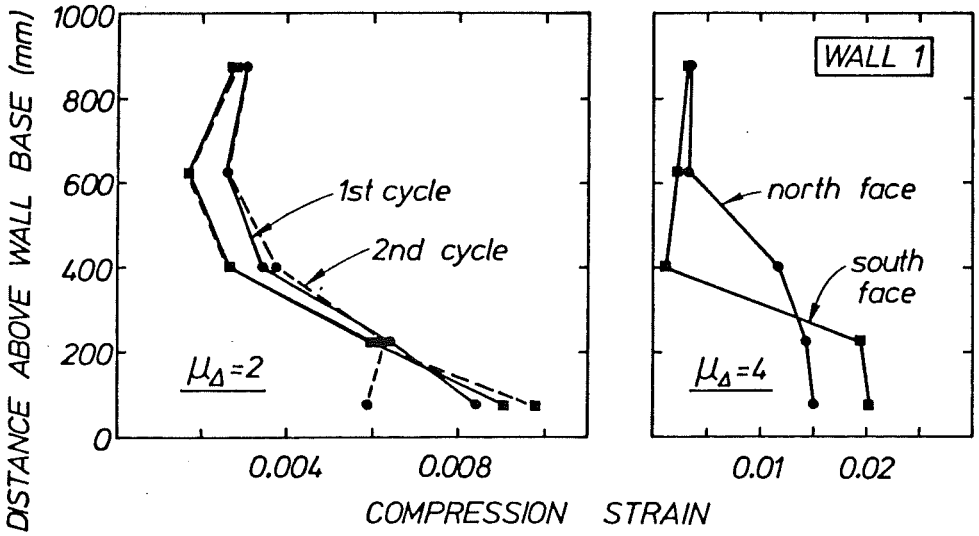

Fig. 7.26 Compression Strains at East End of Wall 1.

7.2.3.13 Out of plane displacement history: Figure 7.25 shows the displacements, recorded by the 2 potentiometers mounted transversely to the east end of the wall, as a function of load increment number. Deformation is clearly periodic, albeit slightly different in form for the 2 potentiometers, varying with applied lateral load. Displacement from vertical is discernible from the first negative excursion onwards, with southwards movements associated with ~~negative~~ positive lateral load. SEE ERRATA Displacement amplitude increases with ductility level but remains fairly constant between successive cycles at the same ductility. The pre-failure transverse deformations are a small proportion of first storey height (0.3% at load point 75). The "equilibrium position" (mid point of oscillation extremes) drifted southwards as the testing progressed. Two types of major southward shift may be observed from the figure (see also Fig. 7.4):

type 1 - increments 30-31, 46-47, 61-62, 78-79

type 2 - increments 43-44, 58-59, 74-75

The former type of displacement is associated with an increase in positive lateral load at an already considerable axial load and is probably due to out-of-plane curvatures caused by unequal north and south face compression strains (see later). The type 2 displacement occurs as axial load, at zero lateral load, is incremented from 0.05 $f'_c A_g$ to 0.26 $f'_c A_g$. This increase is sufficient to yield in compression the 10-HD12 end zone flexural bars, thus closing the cracks opened at the east end during the previous negative lateral load cycle. The observed lateral sway for this case may be explained by the model outlined in Section 7.6.6.

7.2.3.14 Vertical compression strains at the wall east end: Fig. 7.26 gives distributions of vertical compression strain measured between potentiometers at the east end of the wall on both north and south faces. It may be observed that over the bulk of the first storey height, north face strains are higher, which, with the aid of the figure may be interpreted as indicative of southwards displacement. Although these observations, and the more direct measurements discussed above both illustrate the tendency the wall had for lateral movement, it should be remembered that the cause of failure was a plain material compression failure. Had this mode been suppressed in some manner (say by the provision of more extensive hoop reinforcement) it is considered likely that an instability failure (see later) would eventually have resulted.

7.3 WALL 2 - DESCRIPTION OF TESTING AND RESULTS

7.3.1 General Notes

It was originally intended to test this unit in the same manner as Wall 1, i.e. between nominal axial load extremes of 0.05 and $0.30f'_cA_g$. Wall 2 was constructed with identical flexural and shear reinforcement but with only the code requisite antibuckling hoop reinforcement (5 legs R5 @ $6d_b$ = 72 mm) in both end zones. In view of the performance of Wall 1, however, it was decided to vary axial load between nominal limits of 0.03 and $0.15f'_cA_g$. In addition, axial load was changed in a step wise manner with lateral load. This was done in order to avoid the large step in lateral displacement which occurred for Wall 1 at zero lateral load when axial load was increased from 0.05 to $0.26f'_cA_g$. In addition, such gradual variation in axial load is similar to what might be expected for one wall in a coupled structural wall system. The changes in axial loads naturally alter the flexural strength of the section, but as illustrated in Appendix D, these changes are not great. Shear design is still controlled by east-west loading and the shear reinforcement supplied is very close to that required, the small drop in demand being compensated by a decrease in concrete shear strength. In addition, the volume of hoop reinforcement provided (the antibuckling requirement only for Wall 1 loading) proved to be close to that required for full code confinement at the lower axial load. The code spacing provisions were not met however, the hoops being spaced at 72 mm, which is considerably greater than the required spacing (h"/2 = 40 mm).

Details of external wall geometry are not provided, this unit being externally identical to Wall 1 (Fig. 7.1). However, details of reinforcement and instrumentation are given in Figs. 7.27 and 7.28.

The achieved limits of axial load variation were $0.04 - 0.16f'_cA_g$, using actual concrete strength. For this wall, axial load started from the average value of $0.10\ f'_cA_g$ and was stepped along with lateral load so that extreme (maximum or minimum) compression was applied at theoretical (positive or negative) flexural strength. In proceeding from one load point to the next, the axial load adjustment was made prior to that for lateral load. Fig. 7.29 shows the incremental loading used for the test.

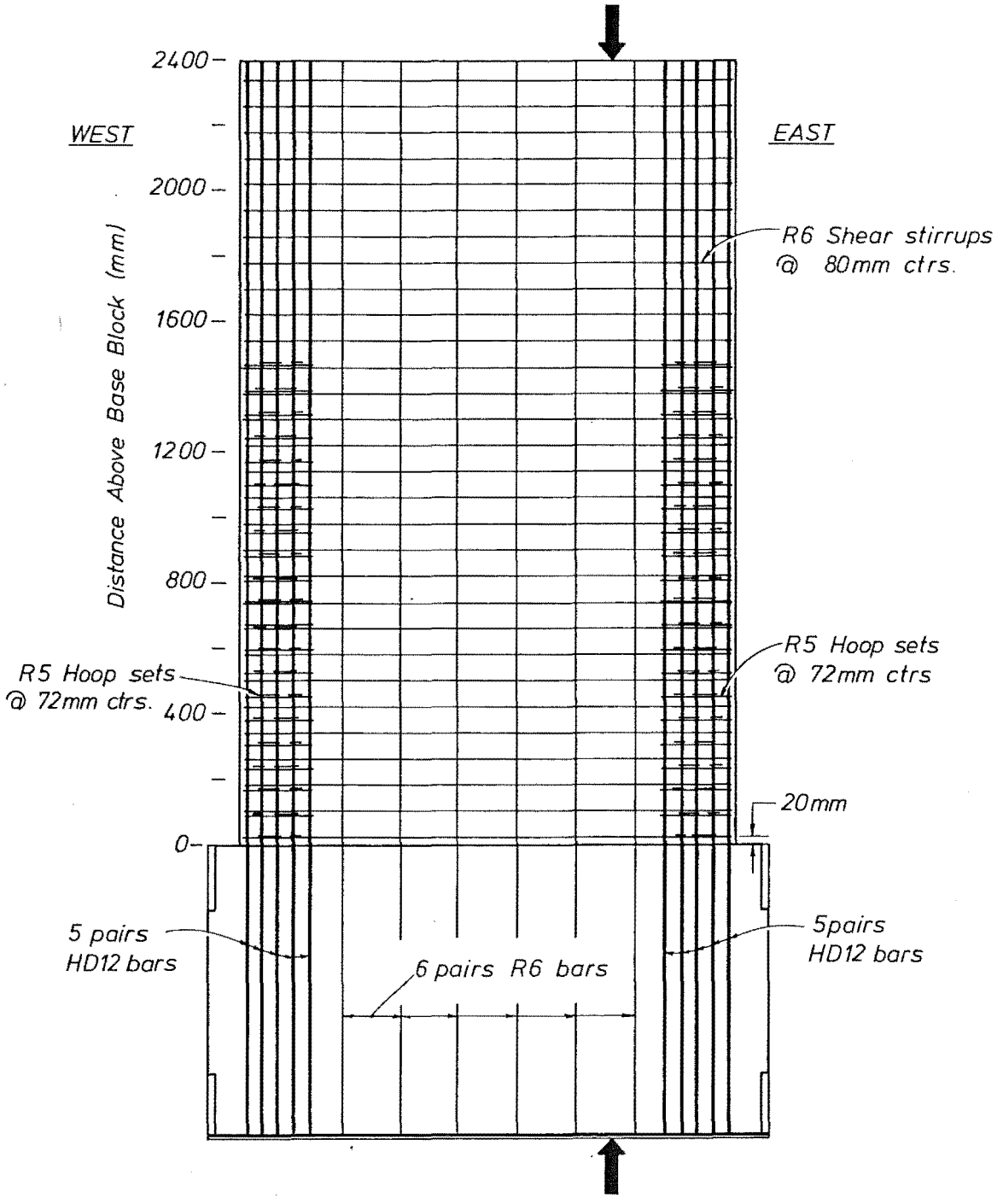

Fig. 7.27 Reinforcement Details - Wall 2.

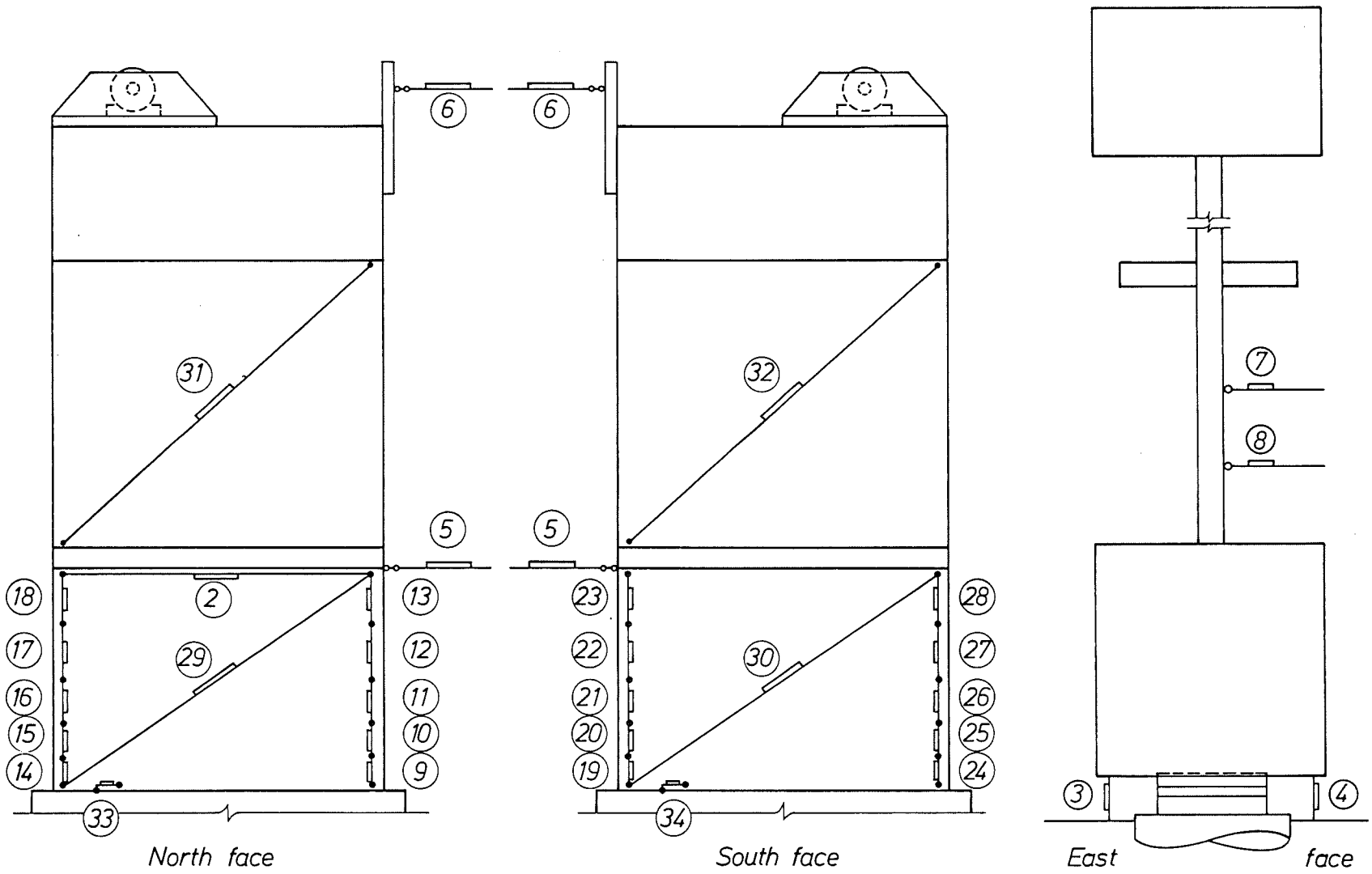

(a) EXTERNAL INSTRUMENTATION

Fig. 7.28 Details of Instrumentation - Wall 2.

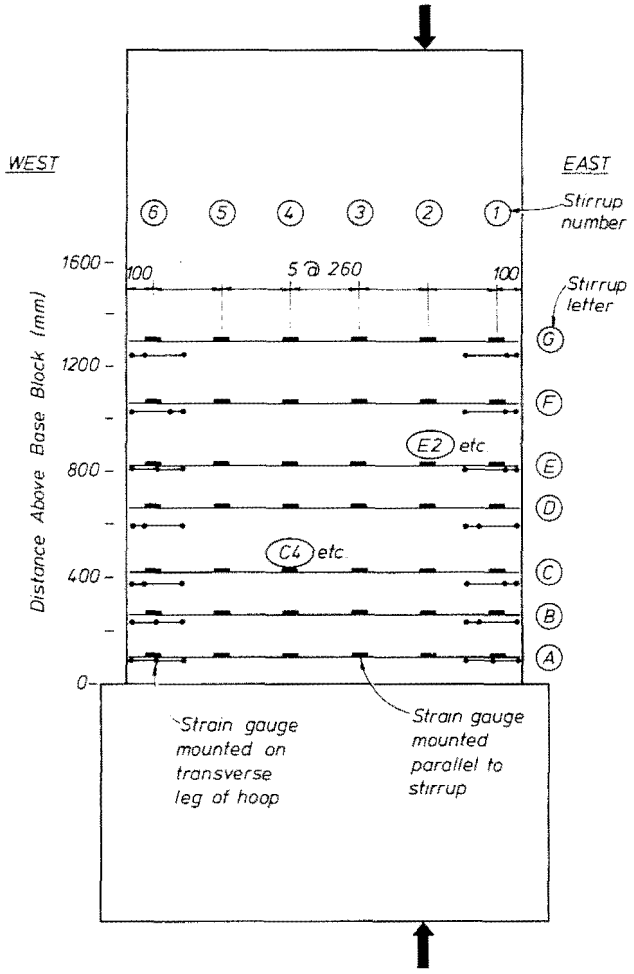

(b) HOOP AND STIRRUP GAUGES

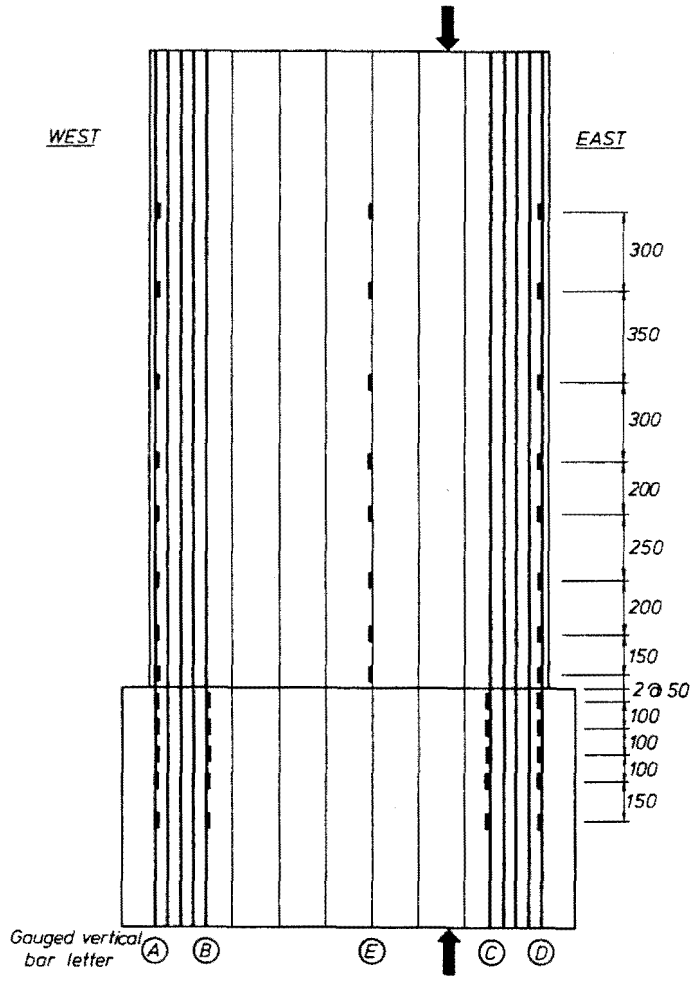

(c) LONGITUDINAL BAR GAUGES

Fig. 7.28 (Continued)

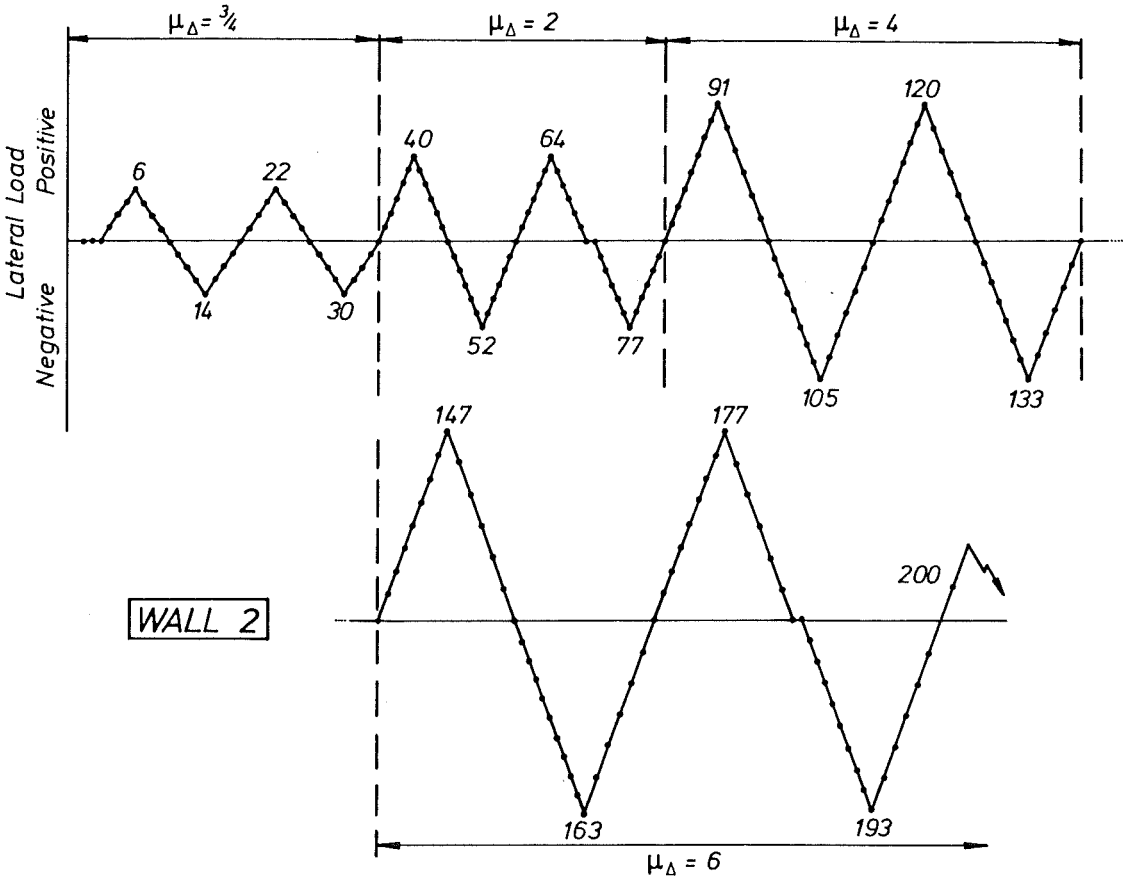

Fig. 7.29 Incremental Loading Diagram Showing Load Point Numbers - Wall 2.

7.3.2 Description of Observed Behaviour

Load Point

4. Fine cracks appeared at the west end of the wall, extending up 1.5 m.
5. Fine diagonal cracks were visible on the face of the wall, extending to within 600 mm of the compression edge. The base construction joint was faintly cracked.
6. Cracks in the west end of the wall extended vertically to the underside of top block.
11. East end of wall developed slight horizontal cracks.
13. Diagonal cracks had spread 800 mm into the section. The mid-height construction joint was cracked along its whole length but no slip was visible. Wall face cracks were initiated at the level of hoops and stirrups (where cover is least). The cracks were

generally horizontal 200-300 mm into the section and inclined thereafter due to the influence of shear.

22. Few more significant cracks had formed, although existing cracks grew in length slightly. Maximum diagonal crack width was approximately 0.3 mm.

30. Maximum diagonal crack width observed was approximately 0.4 mm, again with no significant growth in number or extent of cracks.

40. Diagonal cracking became slightly more extensive, opening to 0.4 - 0.5 mm in width. Base construction joint crack opened approximately 1 mm at wall centre but was much smaller at both ends. This was similar to the behaviour observed for Wall 1. Slight vertical splitting over the lowermost 300 mm of the east end of the wall was observed.

52. Diagonal cracking (maximum recorded width 0.6 mm) had extended to within 250 mm of the compression edge, with some shear deformation visible across these cracks. No shear slip was visible at the wall base, despite crack opening at the centre of the wall of approximately 2 mm. Fine vertical splitting was observed up to 150 mm above the base block at the west (compression) edge.

64. A slight increase was observed in the amount of vertical splitting at the compression edge. No significant increase in the extent of diagonal cracking was observed over load point 40.

91. Vertical splitting of cover concrete extended 400 mm up the wall and 100 mm onto the panel face, at the east edge of the wall. Diagonal crack widths were up to 2.0 mm, and despite close to 3 mm opening of the base construction joint (at wall centre) no significant shear slip was noted there.

105. Face crack widths of 2.8 mm were recorded, with vertical splitting (but no spalling) of west end cover to a height of 200 mm above wall base.

120. North side of the compression zone (east end of wall) had noticeably more vertical splitting, suggesting that spalling would commence there and thus make more probable a tendency for southwards lateral movement (see Fig. 7.30(c)).

133. Despite large crack widths, the wall displayed no marked loss of structural integrity.

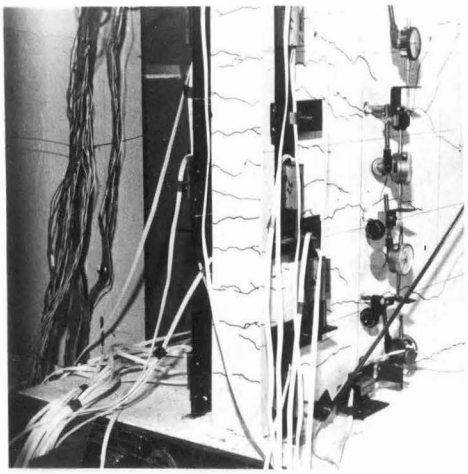

(a) View from south west,
μ_Δ = 2 x 1.

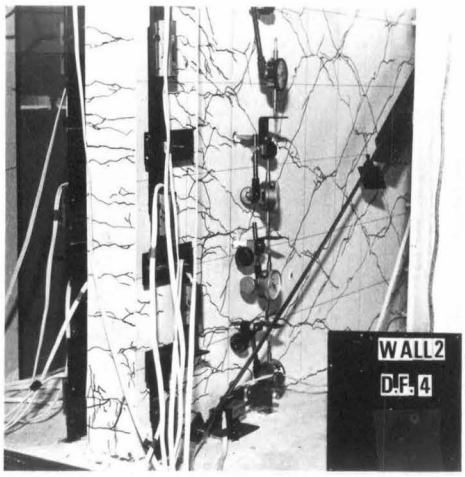

(b) View from north east.
μ_Δ = 4 x 1.

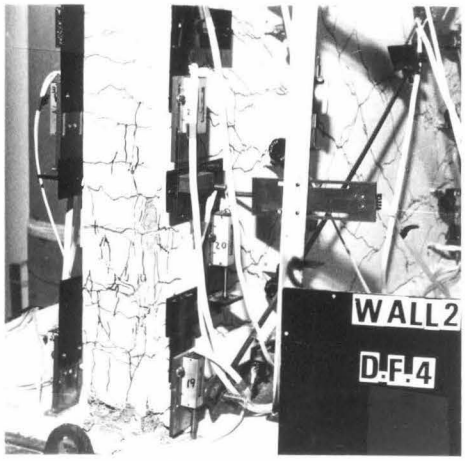

(c) View from north east,
μ_Δ = 4 x 2.

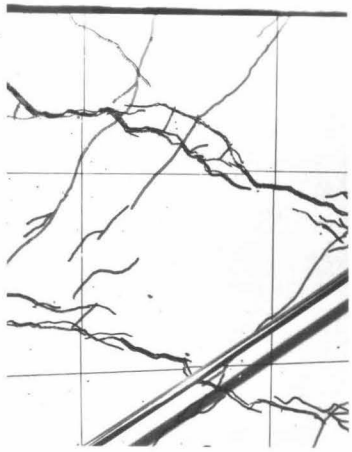

(d) Horizontal deformations
at diagonal cracks.

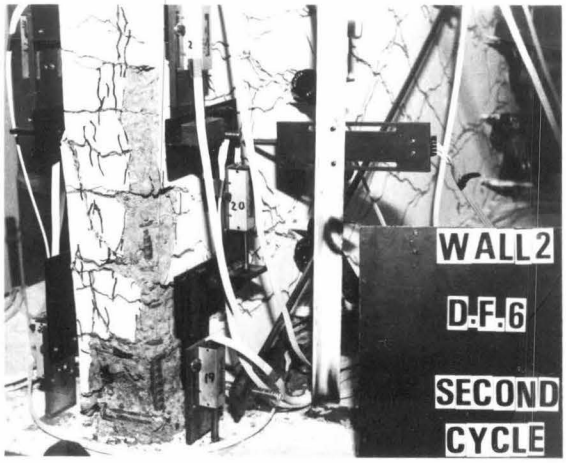

(e) View from south east,
μ_Δ = 6 x 2.

Fig. 7.30 Wall 2 During Testing.

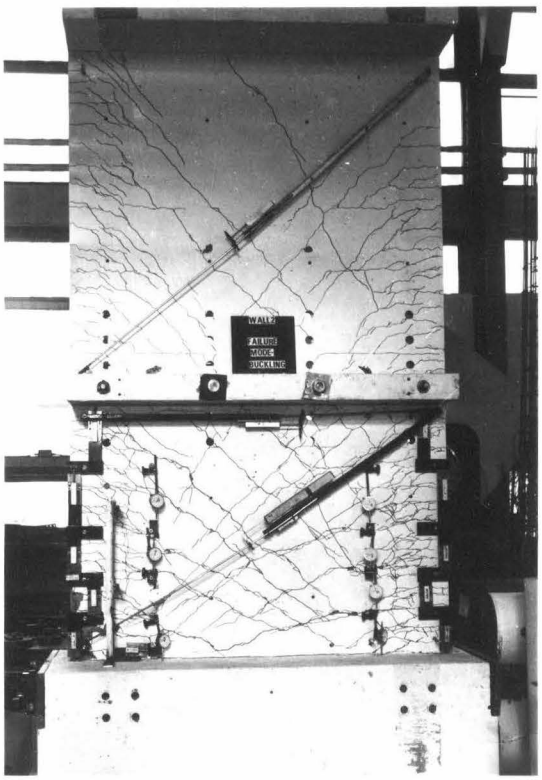

(f) North face, end of test.

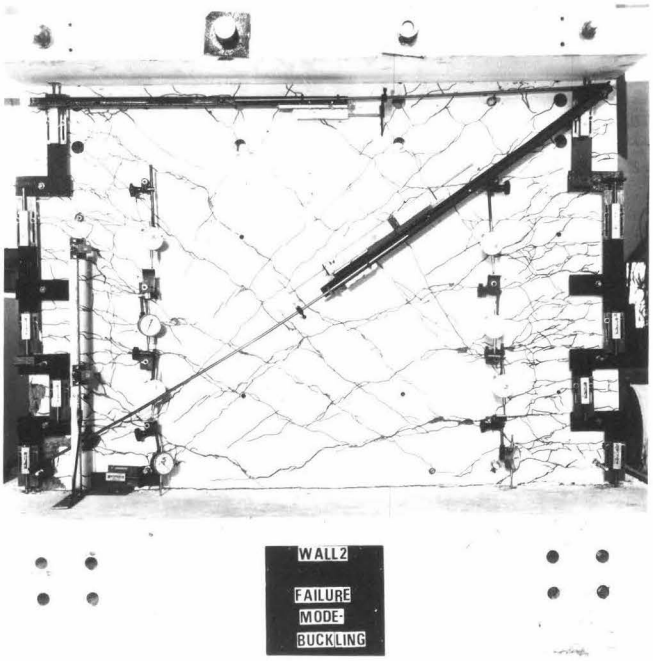

(g) North face, bottom panel, end of test.

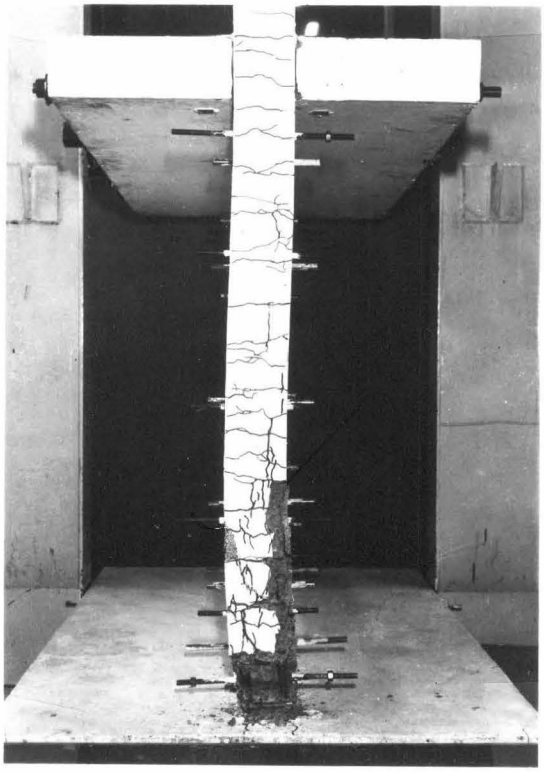

(h) East end, showing buckling to south.

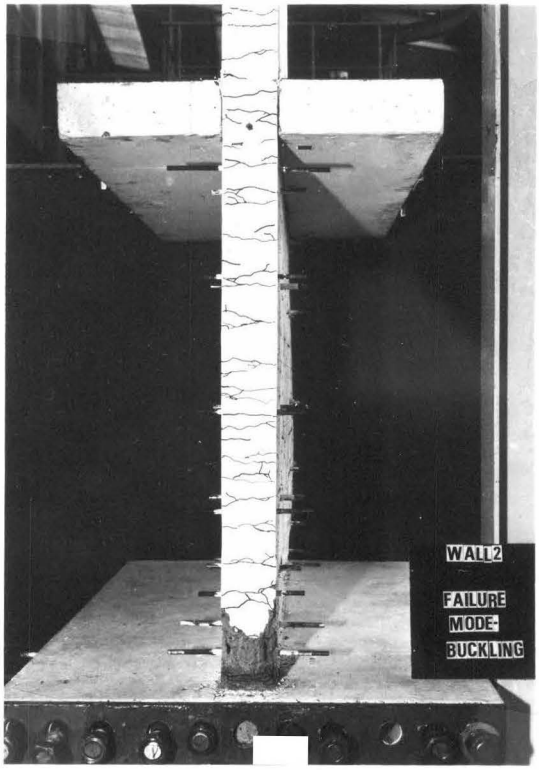

(i) West end, end of test.

Fig. 7.30 (Continued).

147. Vertical splitting of compression edge cover developed to a height of 500 mm above the base block, although spalling occurred only over the bottom 30 mm of the wall edge. Vertical splitting was also observed about 200 mm from the extreme compression fibres, suggesting possible distress of the unconfined concrete.

163. Deformations were concentrated at the major diagonal cracks, which opened as much as 4 mm (see Fig. 7.30(d)). Slight spalling was observed at the compression zone and also where large diagonal cracks intersected 6 mm plain vertical bars.

177. Horizontal shear deformations of order several millimetres were observed across diagonal cracks, with slight and zero shear slip recorded at base and mid height construction joints. Fig. 7.30(e) shows the extent of spalling at the east end of the wall at this increment.

193. Considerable loosening of the tension zone cover was recorded, with spalling 150 mm around the sides of the wall.

200. Failure at a relatively low load occurred during positive lateral loading while attempting the attainment of $\mu_\Delta = +6$ for a third time, the mode of failure being lateral instability (see below). Testing halted when preset limits on the Dartec actuator stroke were reached. At this stage, lateral and axial loads were +86 kN and approximately 500 kN respectively.

7.3.2.1 Description of failure mechanism and the failed unit:

Figures 7.30(f) to (i) illustrate the condition of the wall after testing was completed. They show the distribution of diagonal cracks and the generally low levels of visible degradation during inelastic cycling, along with the out of plane deformations that occurred at the east end.

As stated above, the unit failed via buckling of the compression zone (Fig. 7.31). The deformation occurred over the full height of the wall between base block and floor slab. The maximum (southwards) displacement was approximately 40 mm (occurring 400 mm above the base block), the zone of transverse deformation extending some 600 mm from the eastern edge. The presence of the floor slabs was clearly observed to have influenced this behaviour, the wall remaining essentially vertical at floor level. In contrast, the wall underwent a large concentrated rotation (transverse to the axis of lateral load) at base level. An appropriate model of this behaviour is shown in Fig. 7.31. Apart from this deformation, the wall appeared to be in good condition given the severity of its load history.

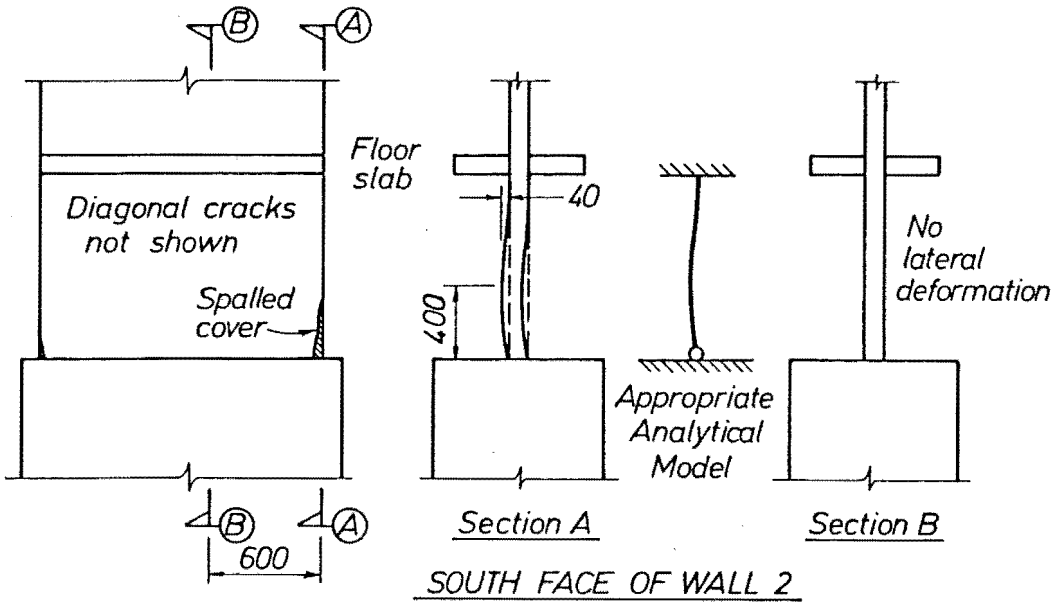

Fig. 7.31 Failure Configuration of Wall 2.

The failure of Wall 2 was sudden and although not catastrophic, could well have been had lateral load continued to be applied. The most disturbing aspects of the failure mode were the lack of warning prior to buckling and the low level of lateral load capacity at which the failure occurred. Admittedly the unit was severly cracked and significant spalling had occurred, but there was no marked difference in appearance between the wall prior to the second cycle to $\mu_\Delta = 6$ and immediately preceding failure. It is likely that the lower level of axial load in this test (c.f. Wall 1) was responsible for the occurrence of full floor height instability rather than a localised material failure. Maximum strains in the plain concrete adjacent to the confined core at the second cycle to $\mu_\Delta = 6$ were approximately 0.5%, compared with 0.9% in Wall 1 prior to its failure. This figure is appropriate to the height of the true critical section, taken to be $c_i/2$ above the wall base, where c_i is the ideal neutral axis depth. The maximum compression strain measured over the lowermost section of the wall at the plain concrete-confined core boundary was in excess of 2%, an observation confirming the confining influence of the base block.

There are considered to be two other contributing causes to the instability failure. Firstly, it was observed that more cover was lost on the north face of the compression zone than the south. This would lead to a transverse eccentricity of axial load, tending to bow the wall to the south. Secondly (and unfortunately not verifiable by observation) it is thought likely that a previously postulated mechanism, involving disturbance to aggregate particles was generally responsible for the failure of the wall (see Section 7.6.6.2).

7.3.3 Test Results

The following sections discuss envelopes and distributions of displacements, strains, etc. deduced from strain gauge and potentiometer readings. A feature common to almost all observations is again the high level of consistency between first and second cycle readings (at a given ductility) unless specifically noted to the contrary.

7.3.3.1 Moment-deflection hysteresis relationship: The moment - top level deflection relationship shown in Fig. 7.32 indicates the excellent response of this unit. A high degree of repeatability in both stiffness and strength is evident for the second cycle at a given displacement ductility, with a maximum 1st to 2nd cycle strength loss of 8%. Ideal positive and negative moment strengths are exceeded by 19% and 28% respectively at $\mu_\Delta = \pm 6$, but are within 5% of the recorded strength at $\mu_\Delta = \pm 2$.

Because of the relatively smooth variation of axial load adopted for this test, the large changes in stiffness exhibited by Wall 1 at low positive moment are not indicated for this second unit. Loading (and unloading) stiffnesses are continually affected by the changes in axial load and the anticipated general trend of stiffness to decrease with lower axial load is evident. Superimposed on this trend is a small but discernible degree of loop pinching during positive loading. This phenomenon, common to all the walls tested and discussed more fully in Section 7.6.1, is attributable to large shear deformations occurring during large changes in neutral axis position. This feature exerts no great effect on the overall hysteretic response,however, which is considered to be indicative of excellent seismic performance.

Failure of the wall occurred at a low positive lateral load (and moderate axial load) after an excursion to $\mu_\Delta = -6$, and unloading along a similar path to that of the first excursion. The large horizontal

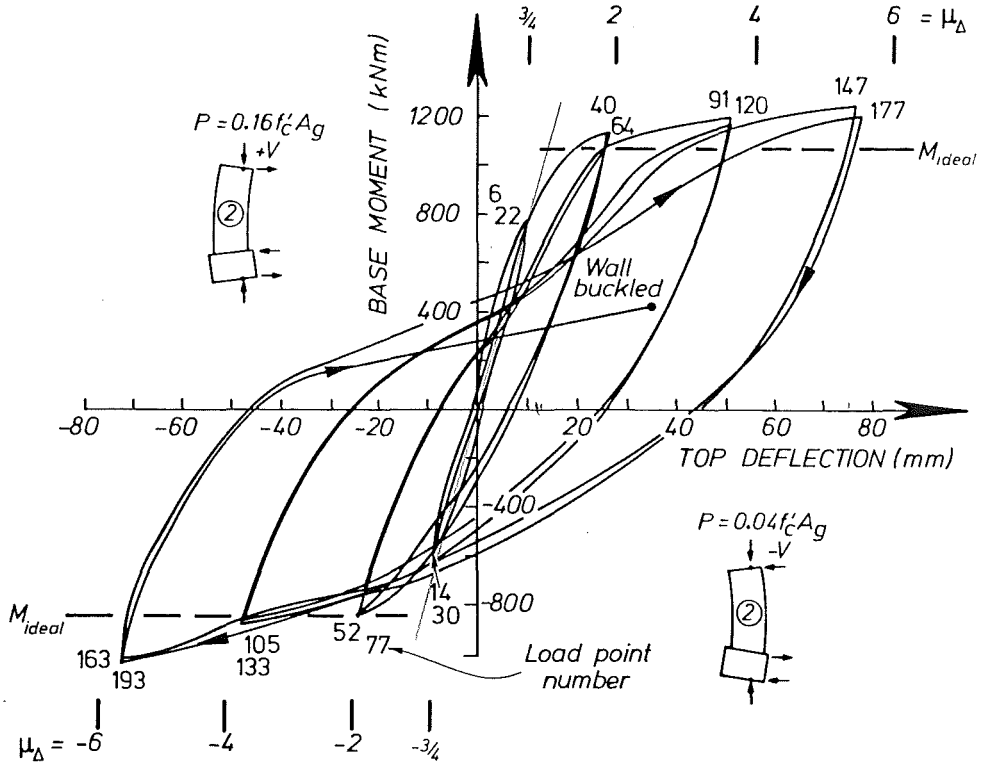

Fig. 7.32 Moment - Wall Top Displacement Relationship - Wall 2.

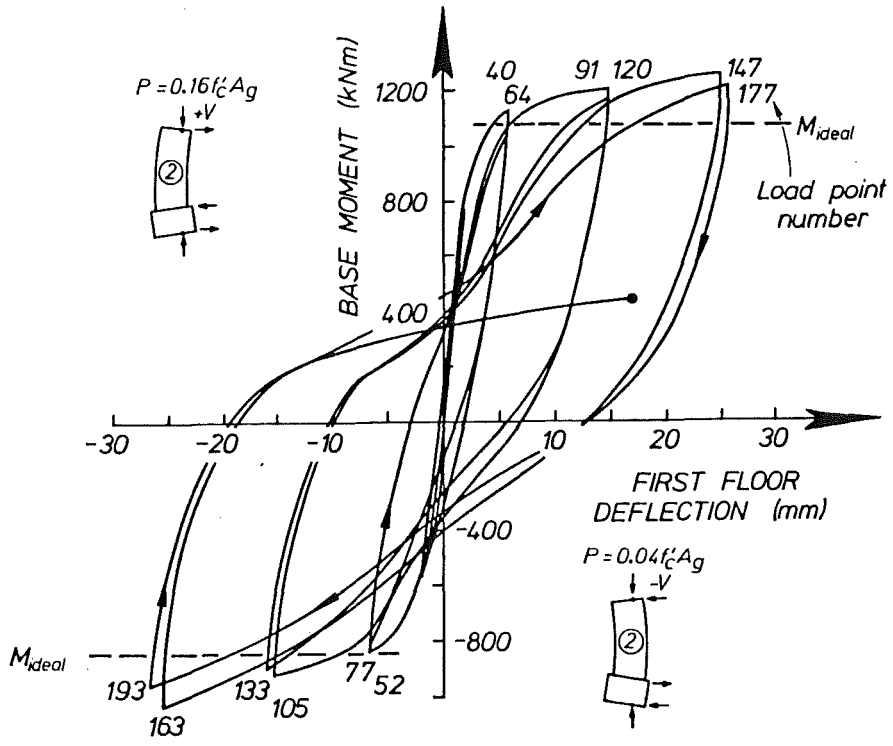

Fig. 7.33 Moment - First Floor Displacement Relationship - Wall 2.

displacement associated with a small increase in lateral load is consistent with the buckling failure mode observed.

The moment - first floor deformation response is shown in Fig. 7.33 and illustrates similar trends to those in Fig. 7.32. Deflection at this level increase from 17% to 36% of top level deflection as μ_Δ was increased from 3/4 to 6 (23% to 36% for μ_Δ = -3/4 to -6) indicating the progressively greater concentration of damage in the lower region of the wall. There is also a higher degree of loop pinching evident during both positive and negative loading, attributable to the higher proportion of shear deformations in the bottom storey of the wall.

7.3.3.2 Moment curvature relationship: Very similar comments to those made for Wall 1 are applicable to this unit (Fig. 7.34). Good agreement between experiment and theory is generally obtained with experimental pre-yield stiffness again higher than predicted for positive loading. Recorded post yield strengths are slightly in excess of theoretical values, with a discrepancy of less than 10% in most cases.

7.3.3.3 Wall curvature distribution: As was observed in the case of Wall 1, the uneven distribution of major cracks distorts the expected curvature envelopes (Fig. 7.35). The trends are still clear, however, with effective plastic hinge length (for the particular moment gradients used) of order 1 m = $2/3\ell_w$. Lowest level negative curvatures are lower

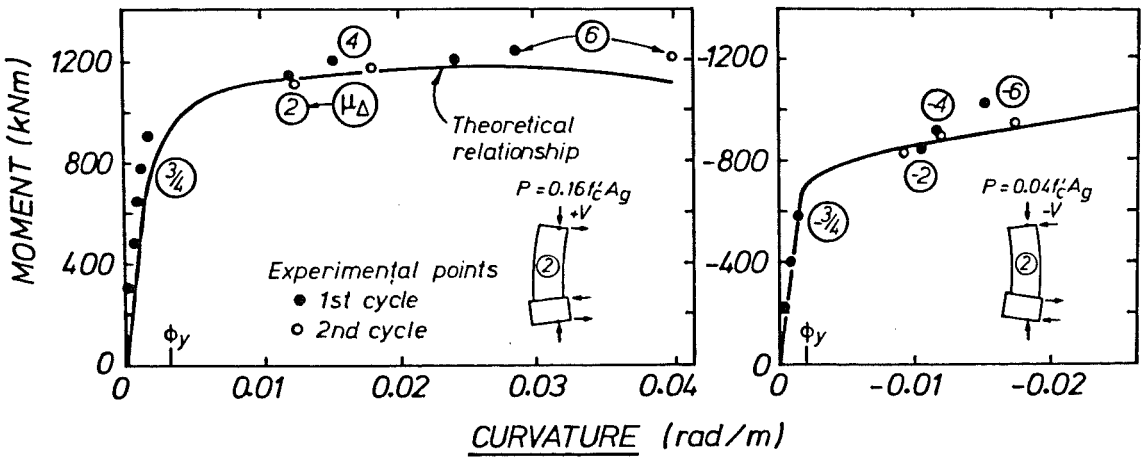

Fig. 7.34 Moment-Curvature Relationship - Wall 2.

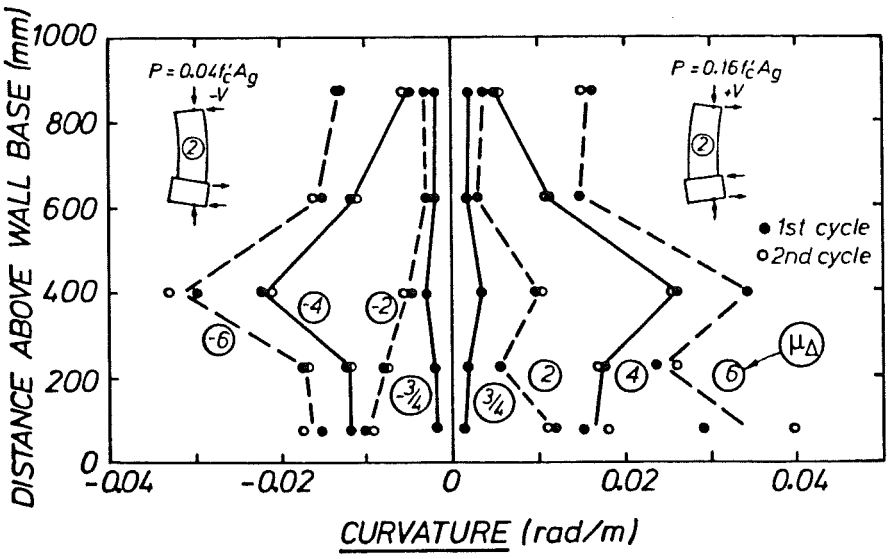

Fig. 7.35 Wall Curvature Distribution - Wall 2.

than might be expected, although this may be attributed to unreasonably high estimates of fixed end deformations which are subtracted from the curvatures calculated from potentiometers 9, 14, 19 and 24 (Fig. 7.28). By simple numerical integration of wall curvatures, an estimate of rotations may be made over the bottom storey of the wall. Such a calculation gives maximum rotations of 0.0256 and 0.0214 radians for positive and negative lateral loading respectively. It should be noted that these rotations are those occurring over the lowermost $2/3\ell_w$ height of the wall. If one accepts a plastic hinge length $\ell_p = \ell_w$ then these rotations are less than the true plastic hinge rotations. Based on these rotations, achieved rotational ductilities are approximately +6.4 and -7.6 for positive and negative lateral loading respectively.

7.3.3.4 Shear reinforcement strains: The envelopes of maximum recorded stirrup strains (Fig. 7.36) indicate essentially uniform strains with height as would be expected with the constant applied shear. Strain levels between successive displacement ductilities show strain increases which are much larger than would be needed to match the (slightly) larger section strength. This phenomenon is taken as evidence of the decreasing efficiency of concrete shear resistance with large deformations. Strains recorded for negative loading are generally larger for negative than for positive loading (with resisted shear forces similar) indicating, as expected, less concrete shear resistance with decreasing axial load.

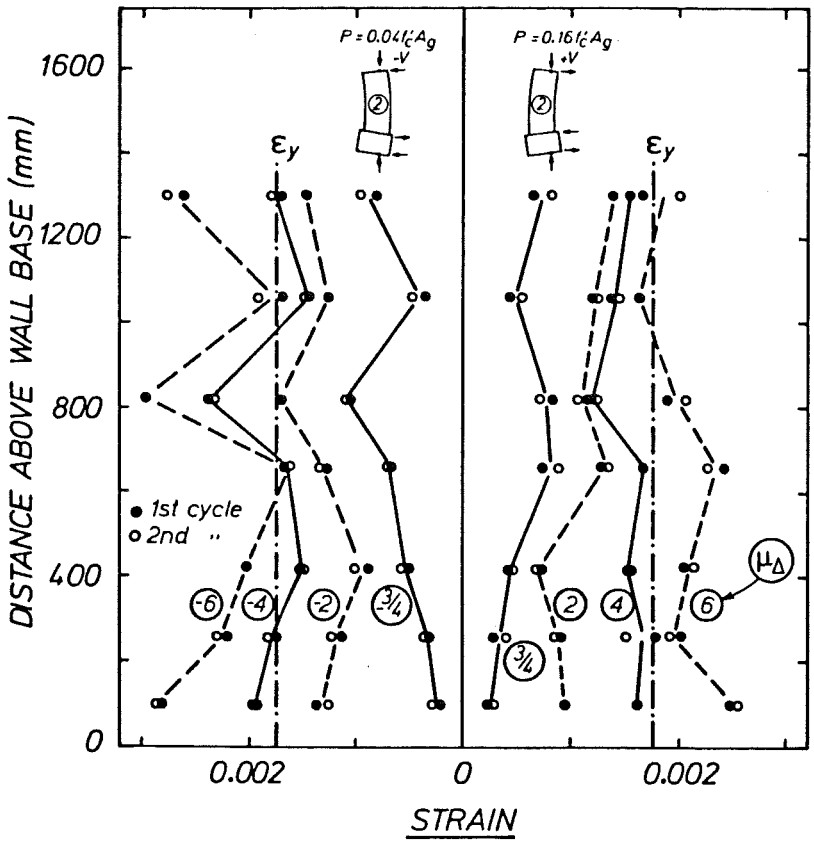

Fig. 7.36 Stirrup Strain Distribution - Wall 2.

7.3.3.5 Strain history of Gauge E3: The strain history of gauge E3 (Fig. 7.28) is plotted against applied lateral load in Fig. 7.37. The theoretical envelope contains the experimental response quite well. Remarkable consistency is shown between first and second cycles of negative load, while the positive load trace indicates greater reliance on the steel shear resistance during the second cycle at a given ductility. The relative contributions of concrete shear resisting mechanisms can be assessed from the figure. For a given applied shear and ductility level, stirrup strain is greater for negative loading. Also, for a given shear force increment, the associated strain increase is larger for negative loading.

7.3.3.6 Strain distribution along shear stirrups: Figure 7.38, indicating strain distributions in stirrups C, E and F (see Fig. 7.28) illustrates trends to the similar series of figures presented for Wall 1. High strains are concentrated at one or two locations along each stirrup, generally at differing locations for positive and negative loading. These locations may be correlated (via the Roman numerals, Fig. 7.39) with major diagonal cracks.

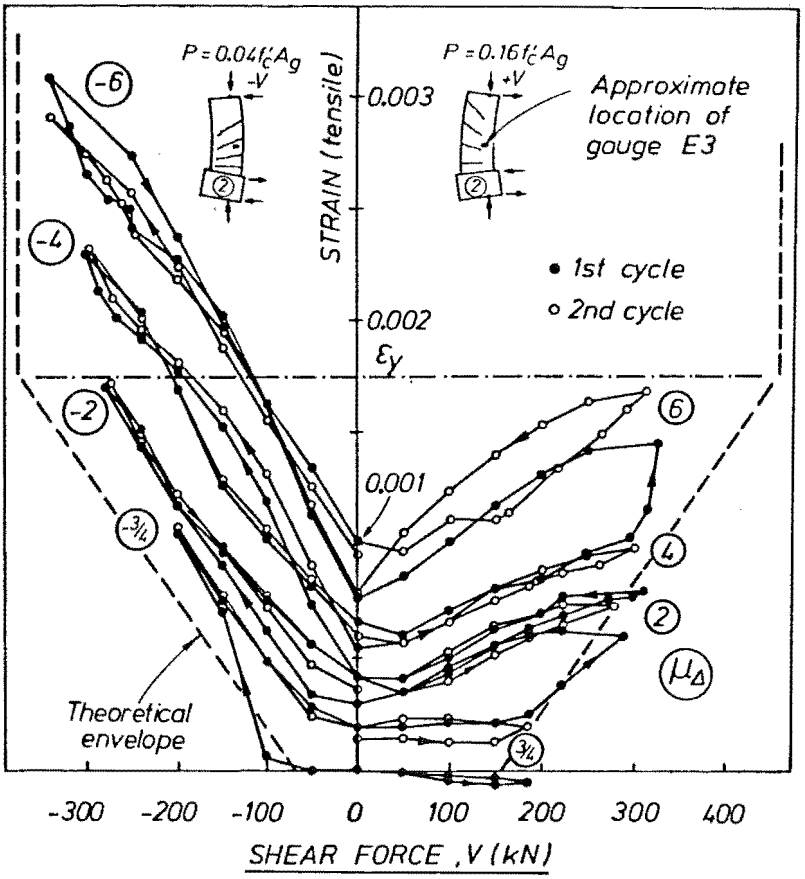

Fig. 7.37 Strain History of Stirrup Gauge E3 - Wall 2.

7.3.3.7 Hoop reinforcement strains: As illustrated in Fig. 7.40 there is an unexpectedly large similarity between strain levels in the east end loops for both negative and positive loading. It would be expected that under negative lateral loading tensile strains in east (tension zone) hoops would be very small. However, as discussed in Section 7.2.3.7, these strains may be attributed to the only partial recovery of lateral deformations undergone by blocks of aggregate during previous compression loading.

The maximum strain encountered ($\cong 2\varepsilon_y$ at $\mu_\Delta = +6$) is relatively small, and corresponds to a simultaneous vertical compression strain of about 2%. This, together with the evidently low levels of hoop strain recorded more than 600 mm above the base block suggests that the hoop steel supplied was quite adequate. It may be recalled (Section 7.3.1) that the hoop reinforcement provided was at approximately twice the code recommended pitch [34].

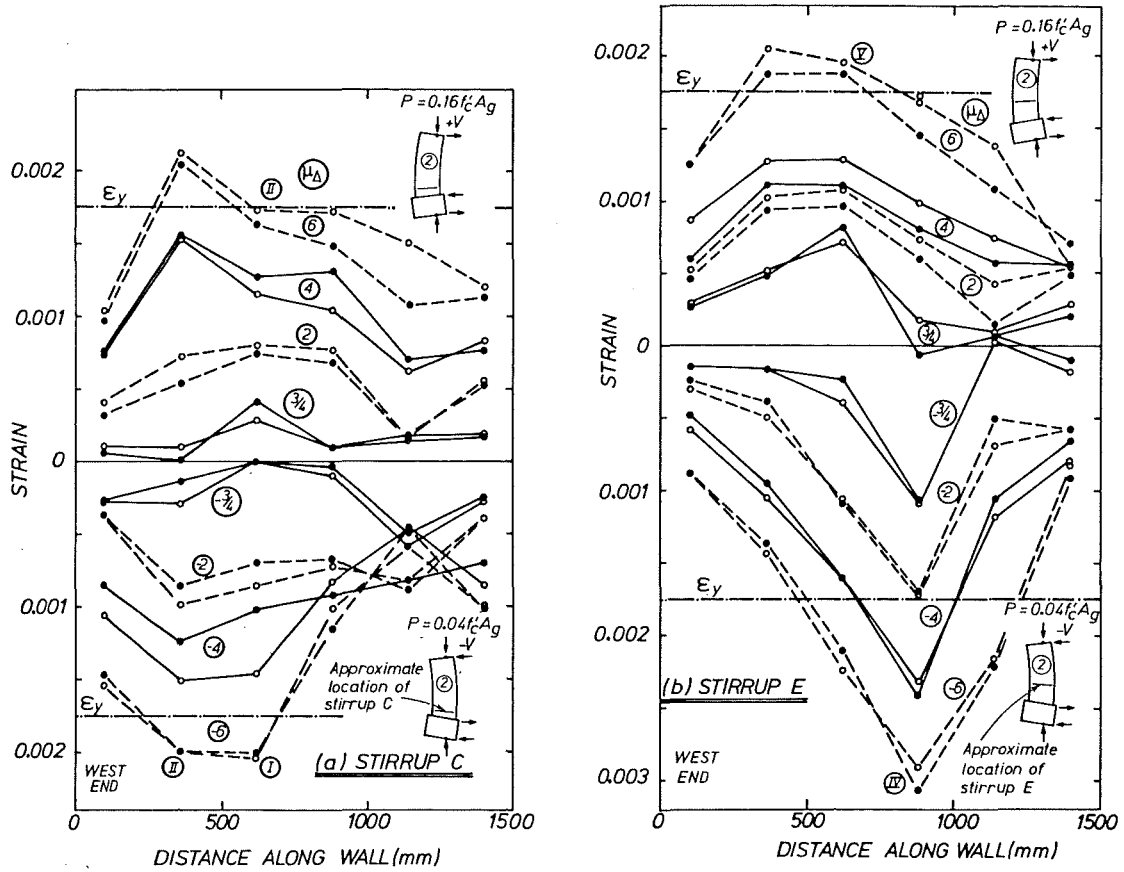

Fig. 7.38 Strain Distribution in Stirrups C, E and G - Wall 2.

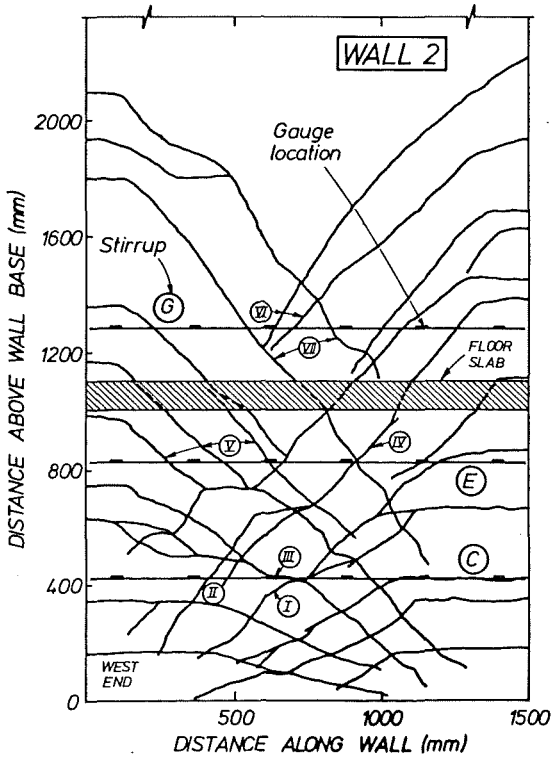

Fig. 7.39 Major Diagonal Cracks - Wall 2.

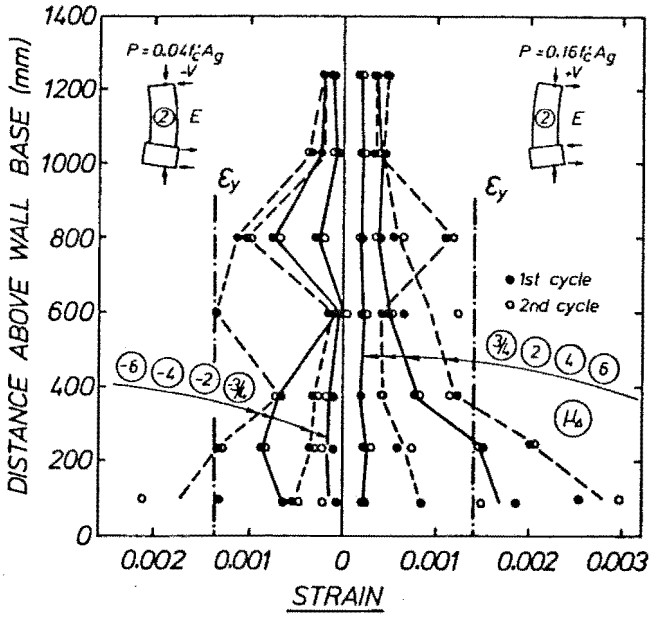

Fig. 7.40 East End Hoop Reinforcement Strains - Wall 2.

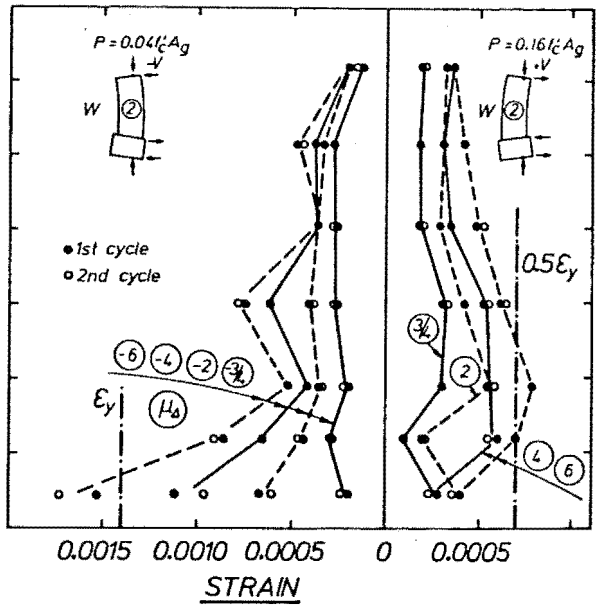

Fig. 7.41 West End Hoop Reinforcement Strains - Wall 2.

General strain levels in west end hoops are low (Fig. 7.41), with yield being attained only near wall base at $\mu_\Delta = -6$. These lower levels of strain are consistent with the lower axial load associated with compression of the west end. Appreciable ($0.6\varepsilon_y$) strains are recorded when this end is in tension.

7.3.3.8 Strains in longitudinal reinforcement above wall base:

Figures 7.42 and 7.43 show both small scale details and larger strains attained at higher ductilities for flexural bars in both the east and west ends of the wall. At $\mu_\Delta = \pm 3/4$, observed strains are nearly constant with height and less then ε_y. At higher ductilities, large plastic tensile elongations develop progressively at higher sections in the wall, with eventual maximum strains of $14\varepsilon_y$ ($\mu_\Delta = 6$) near wall base. However, 1500 mm ($= \ell_w$) above wall base, maximum strain attained was less than $2\varepsilon_y$. Compressive strains, especially at high ductilities, are influenced by previous large, unreversed tensile deformations, and bars supporting a compressive load often retain a net tensile strain. There is thus often a considerable discrepancy between first and second cycle compressive strains. Maximum obtained compression strains, recorded usually at low μ_Δ levels, only slightly exceed ε_y.

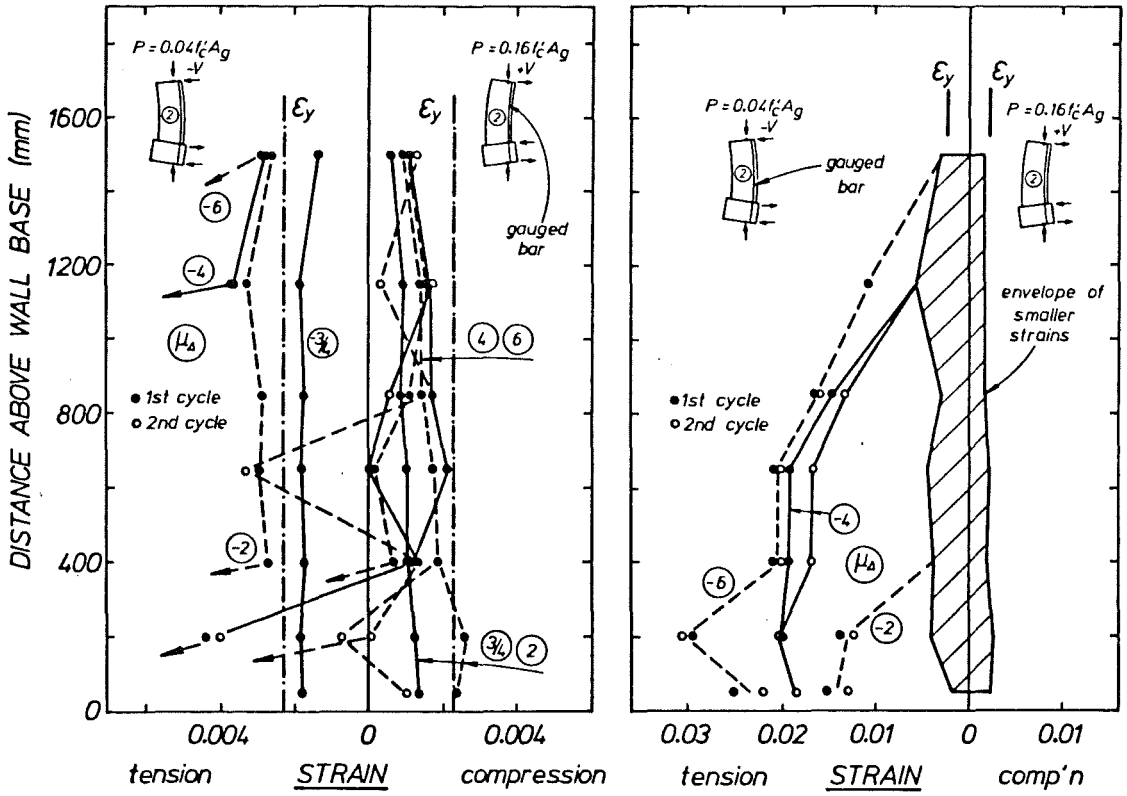

Fig. 7.42 East End Flexural Reinforcement Strains - Wall 2.

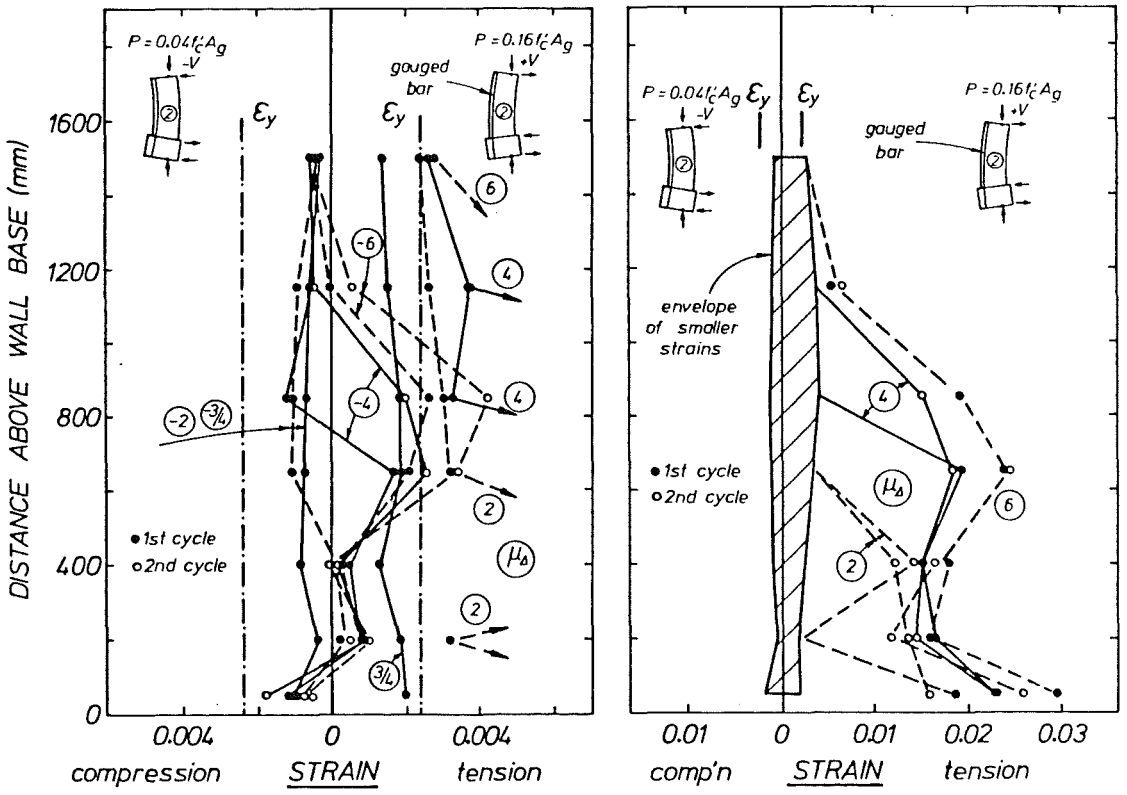

Fig. 7.43 West End Flexural Reinforcement Strains - Wall 2.

7.3.3.9 Strains in longitudinal reinforcement below wall base:

Figures 7.44 and 7.45 indicate the fine and coarse scale variation in strains and are influenced by large tensile elongations as was outlined previously. Maximum tensile strains were of order $11\varepsilon_y$, with compressive strains just exceeding ε_y. Gauges at a depth of 500 mm below wall base indicated maximum strains of less than $0.2\varepsilon_y$, with yield strains recorded to a depth of about 250 mm (= $20d_b$).

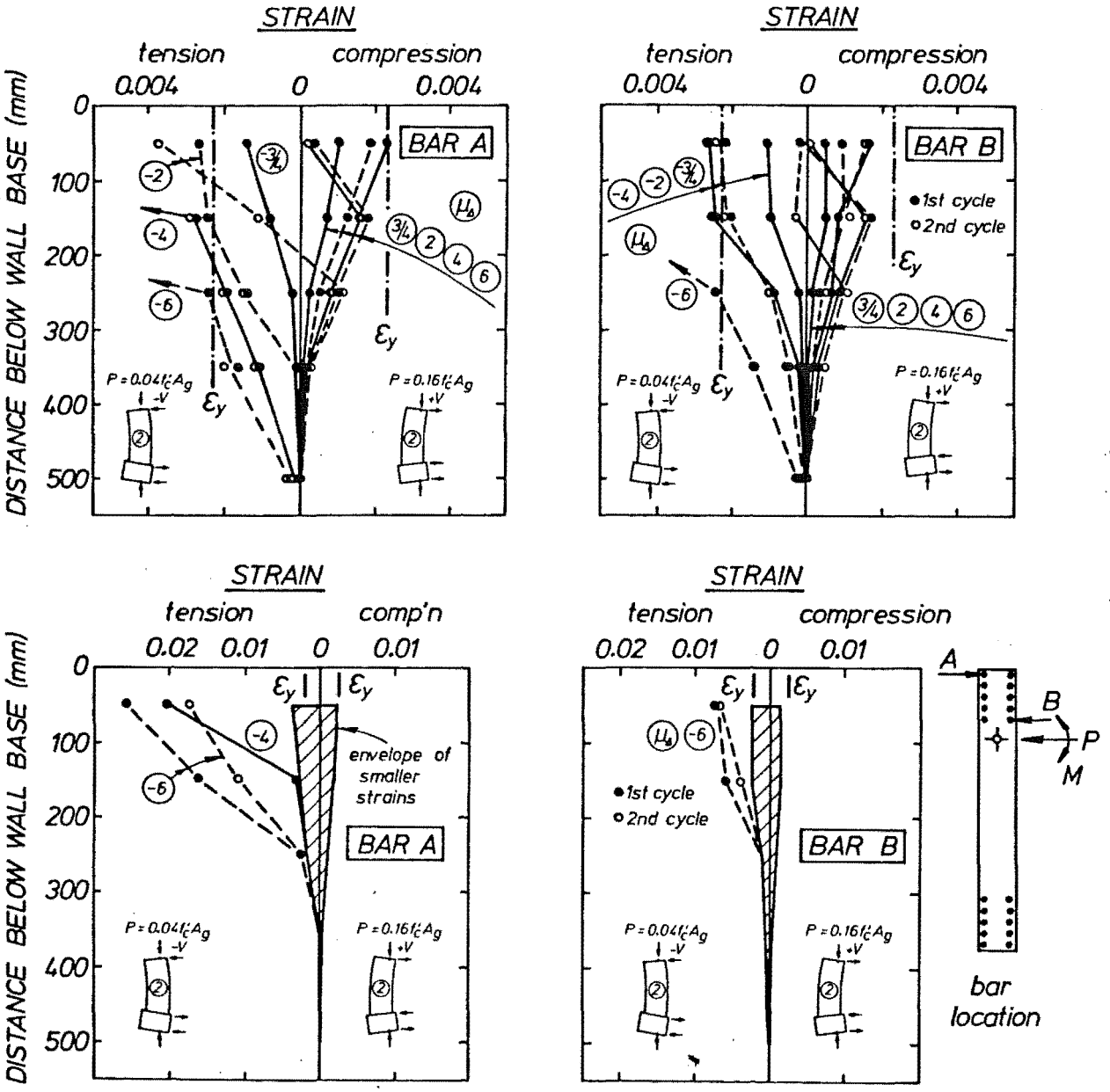

Fig. 7.44 East End Anchored Flexural Reinforcement Strains - Wall 2.

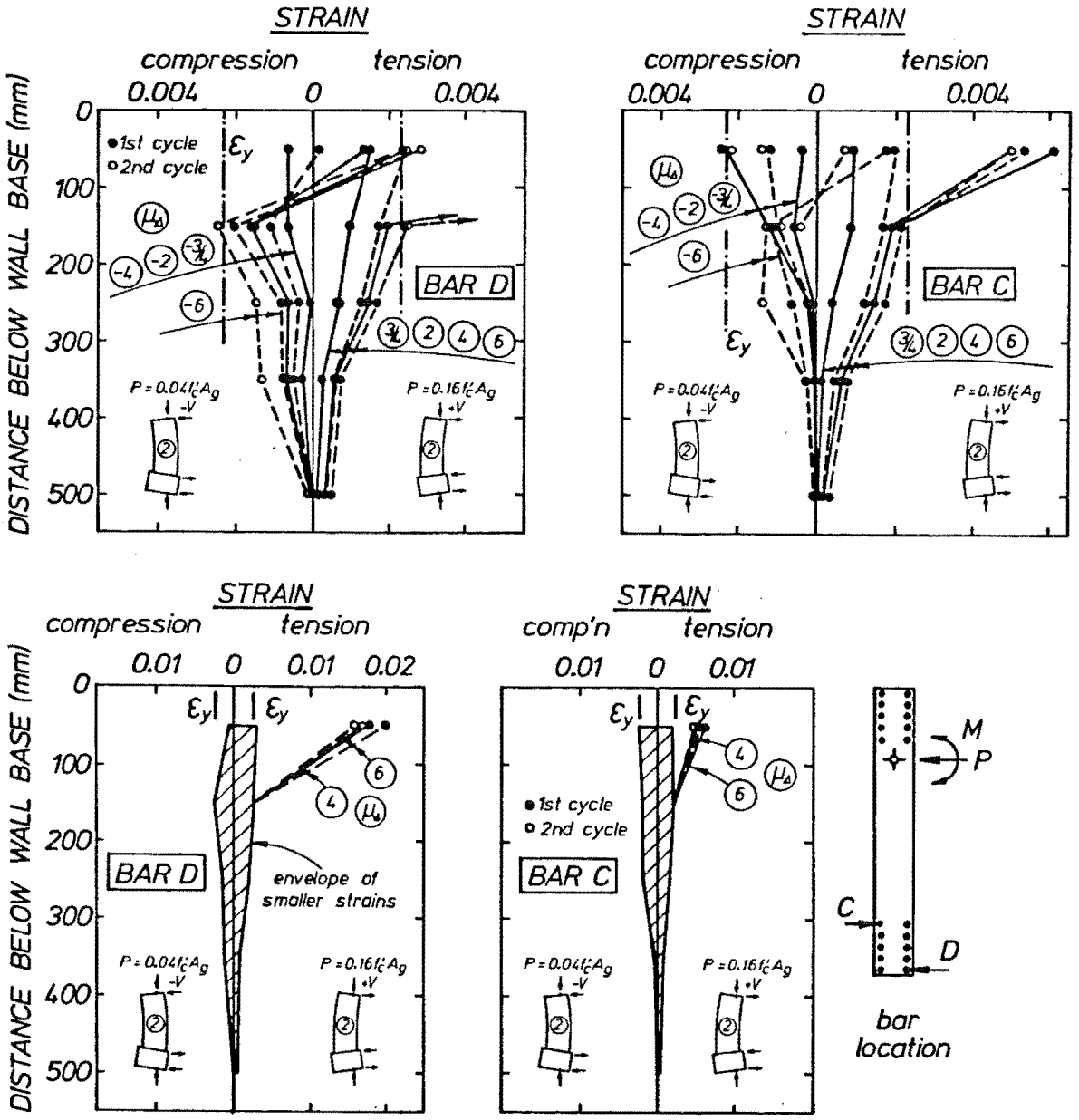

Fig. 7.45 West End Anchored Flexural Reinforcement Strains - Wall 2.

7.3.3.10 First floor level deflection: Flexural, shear and fixed end components of first floor, evaluated as previously (Section 7.2.3.10) are shown in Fig. 7.46(a), with relative proportions shown in Fig. 7.46(b). This latter shows the decreasing contribution of flexural deformation and an increasing shear component with increasing ductility. Fixed end deformations constitute about 10% of total deformations at the first floor level and a maximum of 4% of total wall top deflection. Shear deformations were virtually zero at $\mu_\Delta = +3/4$ but close to 25% of total displacement at $\mu_\Delta = -3/4$, and increased to about 30% and 40% of the total at

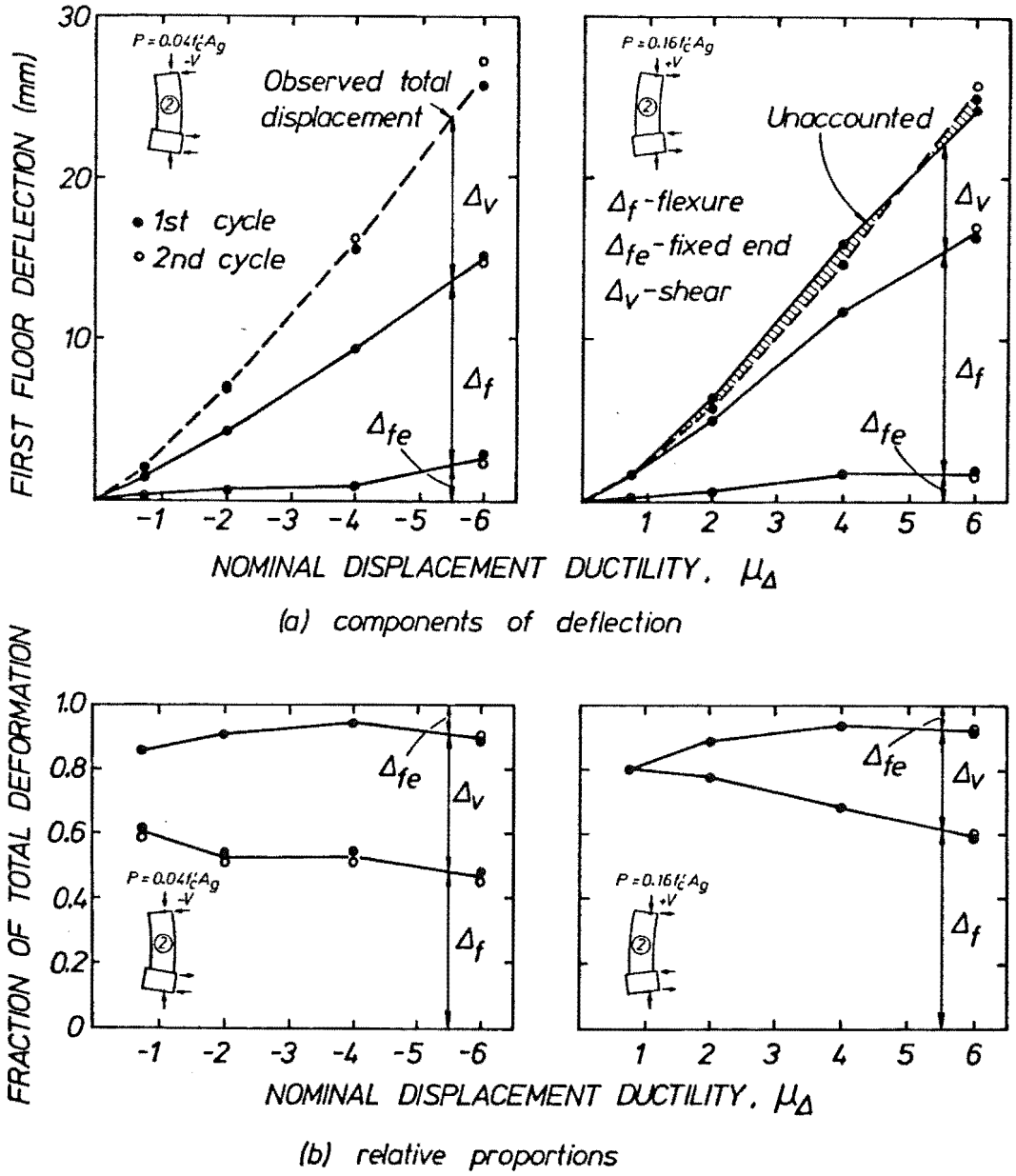

Fig. 7.46 First Floor Displacements - Wall 2.

μ_Δ = +6 and -6 respectively. The relative proportions of shear deflection are due in large part to the axial load difference between positive and negative lateral load: the lower axial load associated with negative lateral load is associated with wider shear-flexural cracks and hence greater shear deformations are needed to close these on reversal of lateral loading.

7.3.3.11 Wall elongation: Figure 7.47 shows the almost linear increase of wall centreline length observed with increasing displacement ductility. The trend of greater elongation associated with lower axial load (negative lateral load) is not unexpected. Good consistency between first and second loading cycles is evident.

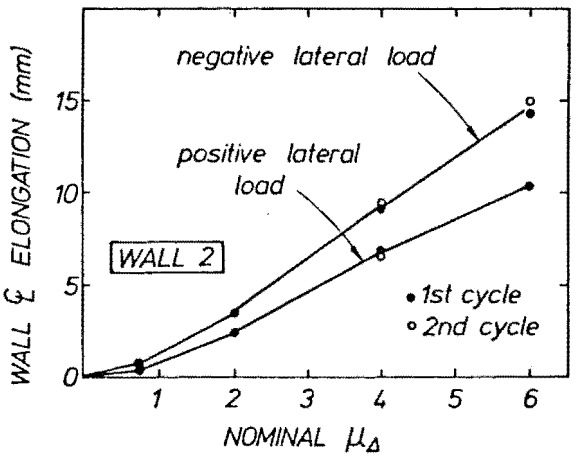

Fig. 7.47 Axial Elongation of Wall 2.

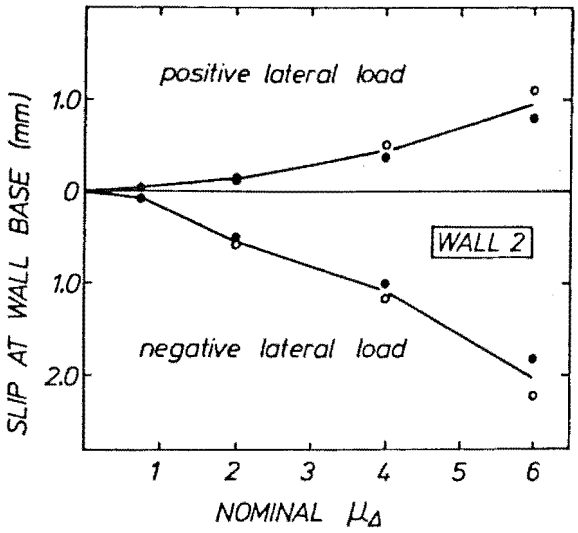

Fig. 7.48 Slip at Base Construction Joint - Wall 2.

7.3.3.12 Shear slip at base level construction joint:

Levels of slip at the base level construction joint are indicated in Fig. 7.48. Good correlation exists between these observations, and those for Wall 1 at comparable displacement ductility levels, taking account of axial load differences. Measured slip was larger for the second cycle at a given μ_Δ, indicating some degradation of the resisting mechanism. Visual observation suggested that sliding shear deformations were concentrated at this base construction joint level, although shear slip was not monitored elsewhere. The construction joint at the mid height of the wall was not even cracked along the whole of its length at the end of the test. Similarly, no other complete horizontal crack formed across the wall during testing.

7.3.3.13 Out of plane displacement history: Figure 7.49 shows a lateral displacement history response that is clearly cyclic, although different in form to that obtained for Wall 1. Again, the oscillation begins centred about the initial (vertical) position and a net southward migration of the east end of the wall occurs with increasing displacement ductility. Two distinct, repeating types of large (southward) displacement jumps are discernible:

Type 1 : load points 112 → 113, 139 → 140, 169 → 170, 199 → 200 - failure

Type 2 : load points 104 → 105, 132 → 133, 162 → 163, 193 → 194 (see Fig. 7.29).

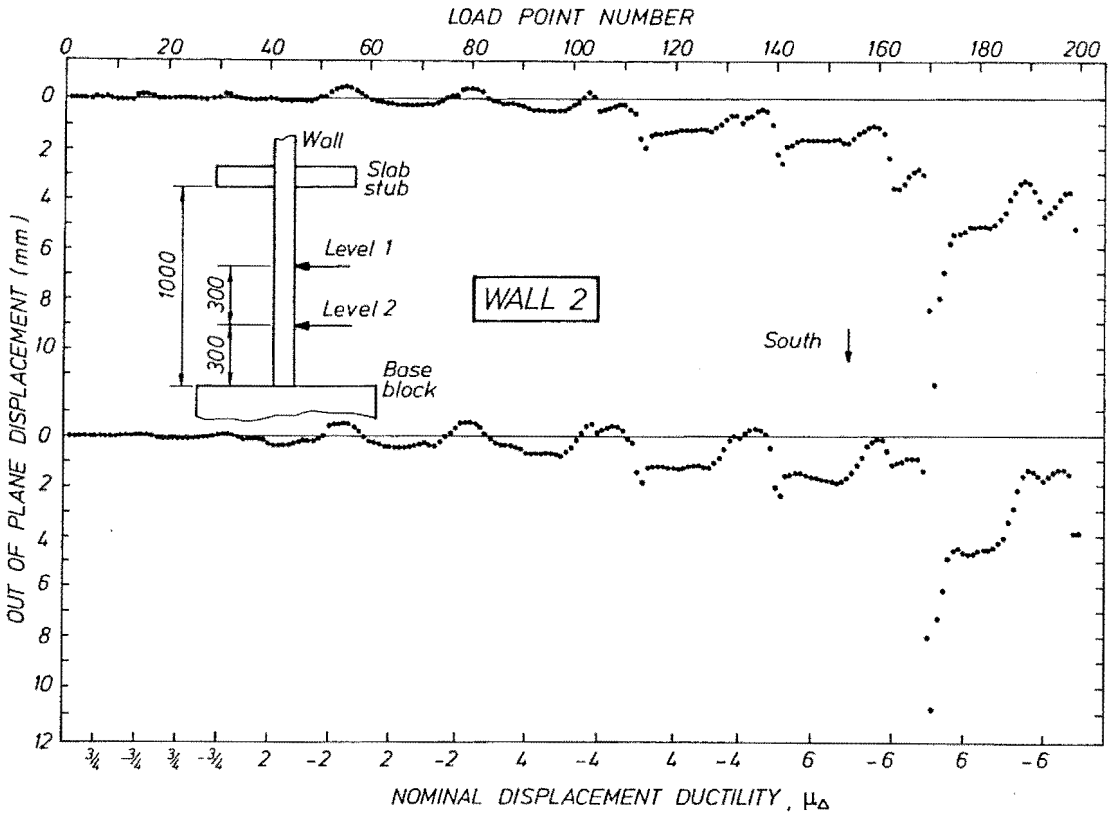

Fig. 7.49 Out of Plane Displacement History - Wall 2.

The Type 1 initial load points have axial loads insufficient to cause yield of the main end zone reinforcement (10 - HD12 bars). However, at the next load step, axial and lateral loads were increased to a level sufficient to yield these bars in compression and close the cracks opened during the previous negative load cycle. Lateral movement associated with this process can be explained by the mechanism discussed in Section 7.6.6. Type 2 displacements occur prior to the attainment of large negative ductilities, at which time the east end of the wall is in tension. The lateral movements occurring at such times were considerably less than Type 1 displacements but occurred regularly. A possible explanation for these displacements is that if the west end of the wall moved transversely northwards at these times of high negative lateral load, the east end of the wall could conceivably move south in sympathy. Unfortunately, transverse movement of the west end was not monitored and verification of this was not possible.

Unequal longitudinal strain measurements on north and south faces of the eastern end of the wall also indicate the existence of considerable transverse displacements. For the second cycle to $\mu_\Delta = 6$ (load point 177), tensile strains were recorded at the south face of the

core at levels 2 and 3 despite a considerable net compression force on this end of the wall (see Fig. 7.50). The transverse curvature

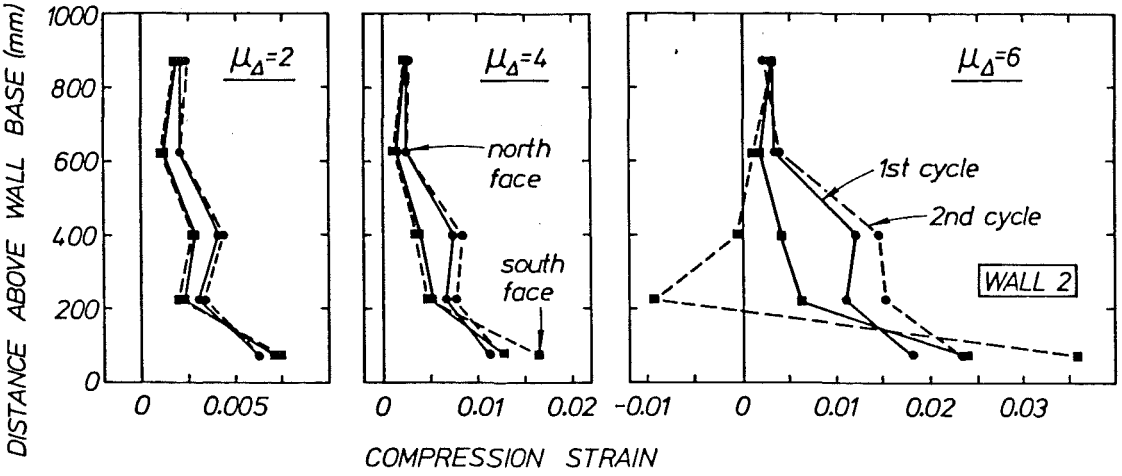

Fig. 7.50 Compression Strains at East End of Wall 2.

associated with this strain pattern was close to 0.10 rad/m over the region 300-500 mm above the wall base level.

7.4 WALL 3 - DESCRIPTION OF TESTING AND RESULTS

7.4.1 General Notes

The third unit tested was a tee-section wall, loaded so that a relatively high axial force and positive lateral load produced compression at the stem (eastern) end of the section. Negative lateral loading, together with a low axial load level ensured a very shallow compression block in the flange and high tensile strains at the east end of the web, predisposing this region to instability in subsequent lateral load reversals. Details of wall geometry, reinforcement and instrumentation are shown in Figs. 7.51, 7.52 and 7.53, respectively. Although the section was designed for axial load extremes of $0.03f'_cA_g$ - $0.16f'_cA_g$, those achieved were $0.02f'_cA_g$ - $0.12f'_cA_g$, based on actual concrete properties. The eastern end of the wall was supplied with hoop reinforcement over 89% of the theoretical compression block depth, the quantity of reinforcement being slightly in excess of the code

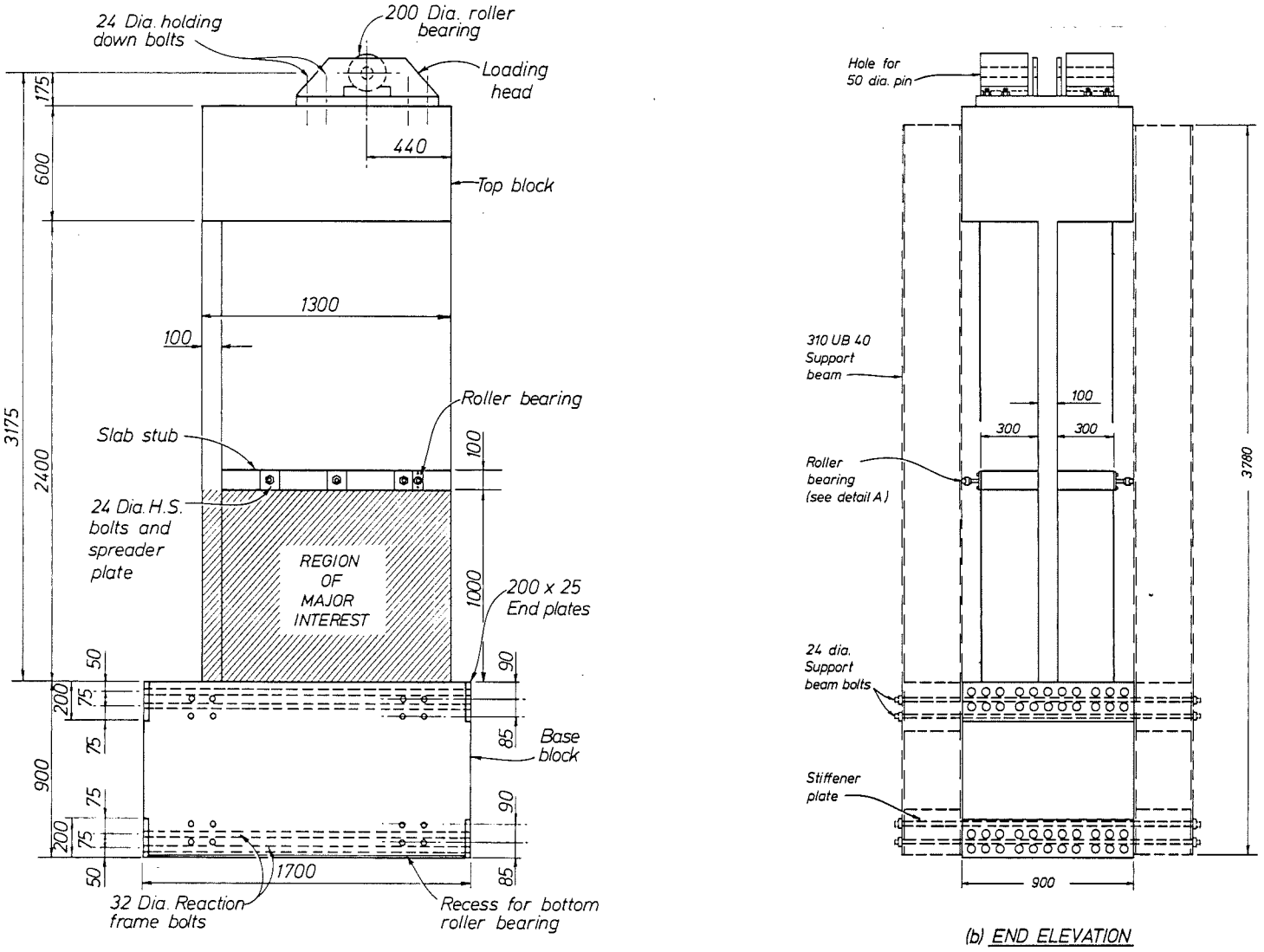

Fig. 7.51 Details of Wall Geometry - Wall 3.

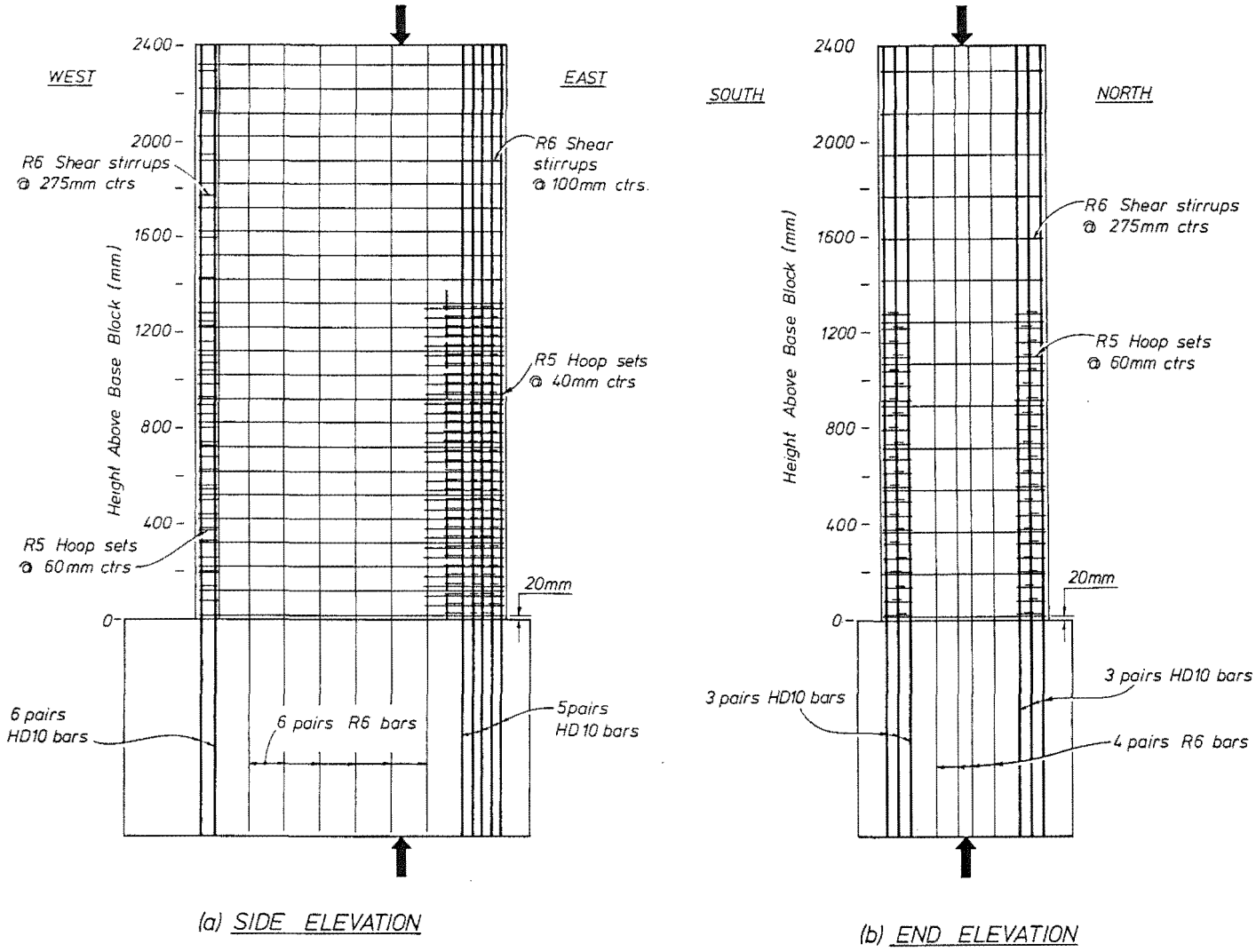

(a) SIDE ELEVATION

(b) END ELEVATION

Fig. 7.52 Reinforcement Details - Wall 3.

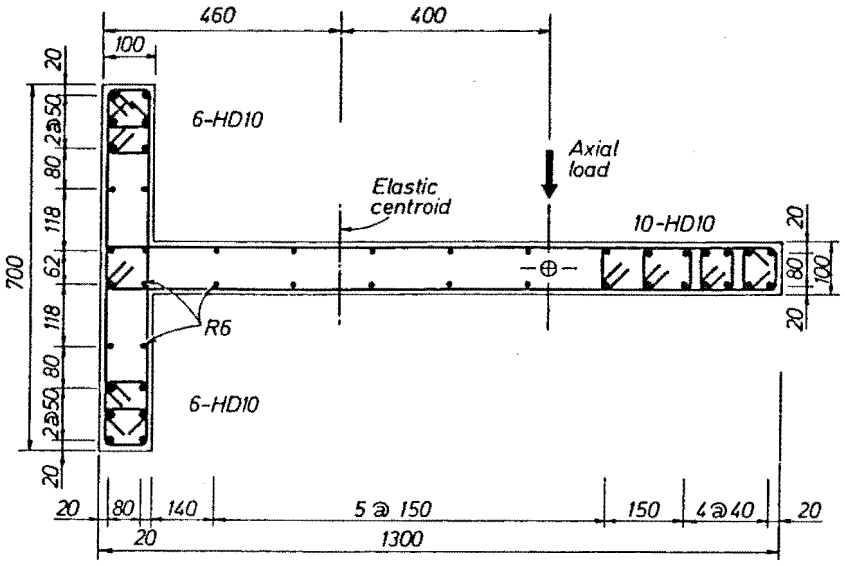

(c) CROSS SECTION

Fig. 7.52 (Continued)

requirements. The western end of the section had hoop reinforcement complying with code antibuckling requirements, i.e. R6 legs restraining only the 10 mm primary longitudinal reinforcement at 60 mm centres.

Because of the stability to out of plane movement afforded by the flange element, the floor slab (1.00 m above the base block) was braced in the manner of Walls 1 and 2 at the eastern end only. A stepwise variation of axial and lateral load was used during the testing of this wall to give maximum/minimum axial forces at the attainment of the theoretical ultimate positive/negative flexural strengths respectively. The incremental loading diagram for Wall 3 is shown in Fig. 7.54.

7.4.2 Description of Observed Behaviour

Load Point

3. Axial load of $0.070 f'_c A_g$ applied, with zero lateral load.
4. First cracking of the western (flanged) end of the wall was observed, the cracks spreading into the wall web.
6. Crack widths of approximately 0.15, 0.50 and 0.25 mm were recorded in the bottom storey web, top region web and in the west face (flange) regions respectively.
10. Faint cracking of the eastern edge of the web became visible.

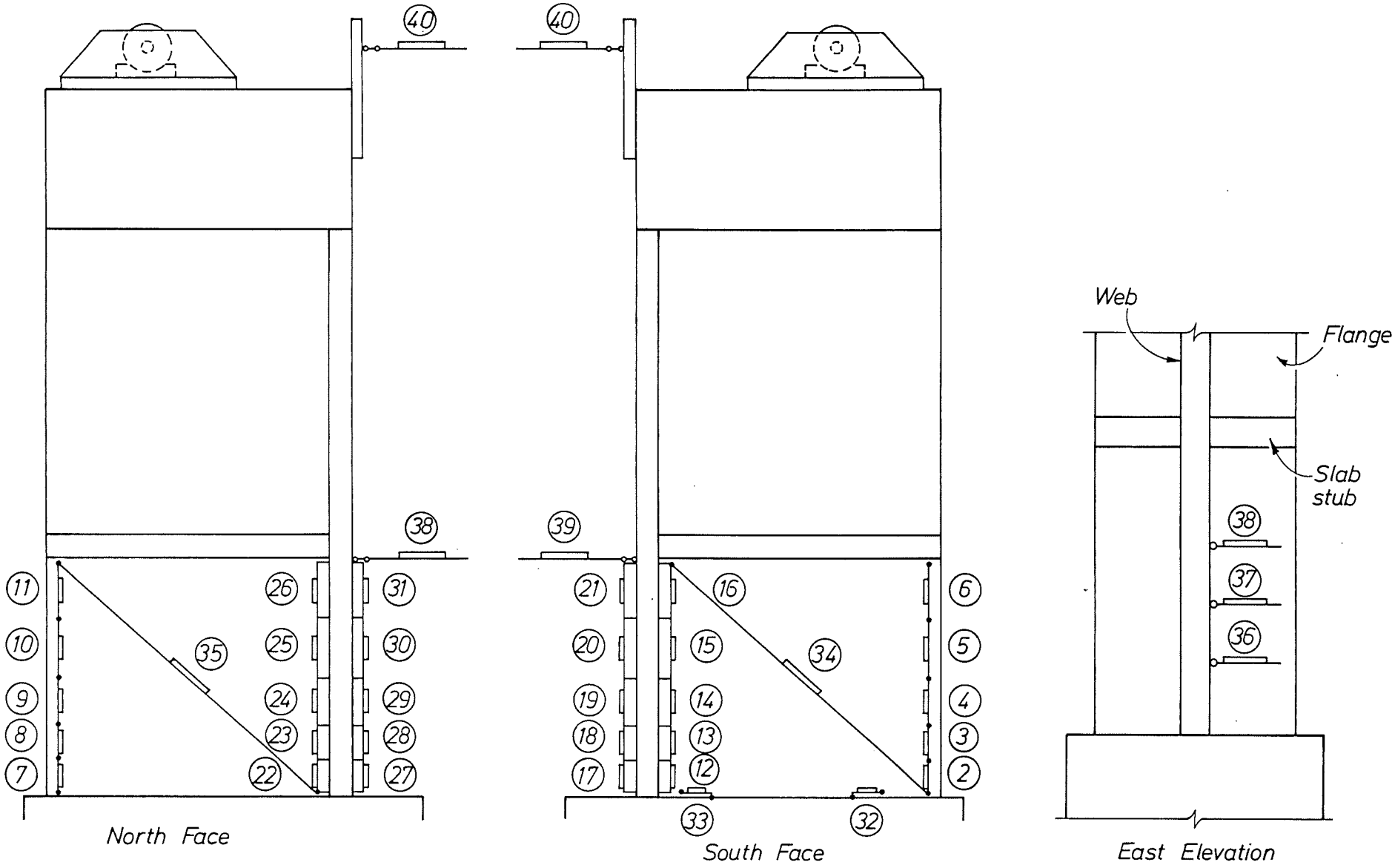

(a) EXTERNAL INSTRUMENTATION

Fig. 7.53 Details of Instrumentation - Wall 3.

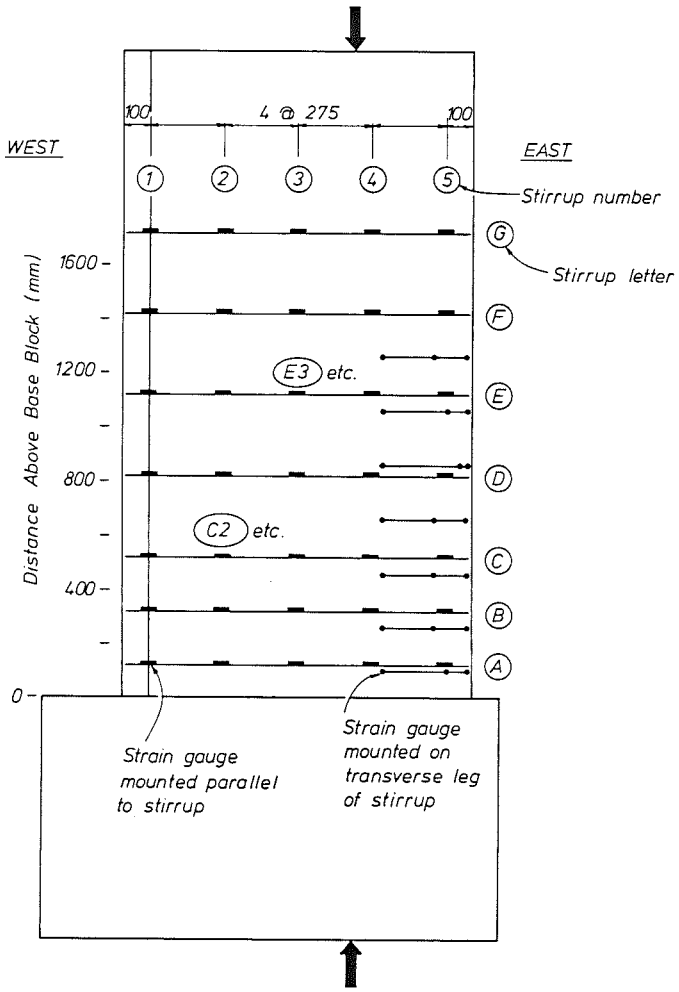

(b) HOOP AND STIRRUP GAUGES IN WEB

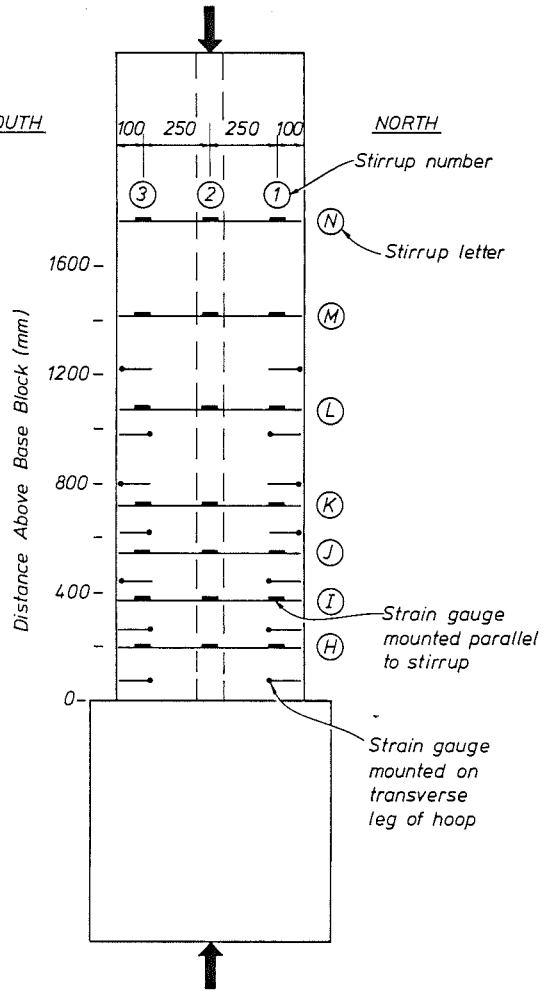

(c) HOOP AND STIRRUP GAUGES IN FLANGE

Fig. 7.53 (Continued)

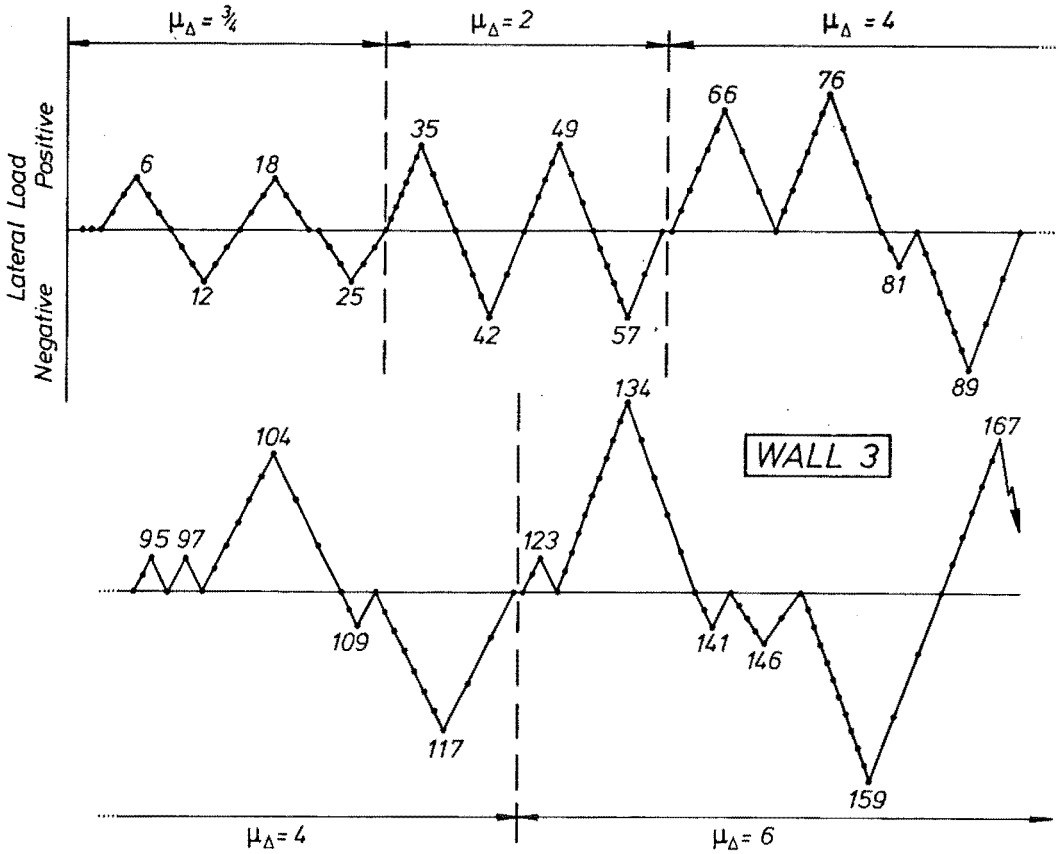

Fig. 7.54 Incremental Loading Diagram Showing Load Point Numbers - Wall 3.

12. Crack widths comparable to those at load point 6 were recorded. Two diagonal cracks extended to the wall flange. Diagonal cracks were relatively few in number as compared with the many closely spaced horizontal cracks extending 200-300 mm in from the east end of the wall.

18. Little spreading or increase in numbers of cracks, as compared with load point 6, was noted. Diagonal web cracks extended to within 500 mm of the east end of the wall. The flange crack pattern was composed mainly of horizontal cracks which were fine and closely spaced at the flange edges but fewer and of greater width in the central region. The construction joint between the wall proper and base block had opened slightly under both positive and negative lateral loading.

32. Fine vertical splitting cracks opened on the eastern edge of the web, up to 300 mm above the base block.

35. Vertical splitting spread to 600 mm above the wall base, and 50 mm onto the north and south faces (Fig. 7.55(a)), with little increase in the formation of other cracks. Diagonal crack widths of 1.0-1.2 mm were observed, with west face (flange) crack widths of 1.60 and 0.7 mm in central and edge regions respectively.

42. The western face of the flange developed fine vertical cracks at this load point, in line with the flange-web junction (Fig. 7.55(b)). Horizontal cracks of width 0.3-0.6 mm were noted in the end region of the flange, with 0.6-0.9 mm wide diagonal cracks in the bottom storey of the web. The differences in crack widths in the edge and central regions of web and flange are attributable to the presence of deformed or plain bars crossing the cracks.

66. Cover on the eastern edge of the web was severely degraded at this load point, with splitting and loosening of cover extending 300 mm onto both faces of the web.

75. Spalling of cover on the eastern edge of the web up to a height of 700 mm above the base block occurred, together with some south face cover loss (Fig. 7.55(c)). West face (flange) crack widths of 4.0 and 1.2 mm were noted in flange centre and edges respectively.

89. Very little evidence of concrete distress on the western face of the flange was observed, although cracking at the web flange junction increased. Diagonal cracking spread from the wall web into the flange, indicating a very small neutral axis depth.

104. Further loss of cover on the south face of the web occurred, the spalled zone extending 300 mm from the east end of the wall.

134. Crack widths of 5-6 mm and 1-2 mm were recorded in the central and edge regions of the wall flange at this load point. Web diagonal crack widths were up to 4 mm. There were no significant sliding shear displacements visible at the wall-base block construction joint.

159. The relatively few diagonal cracks opened to widths of up to 7 mm, while the wall-base block interface crack was up to 5 mm wide in the wall web region where deformed vertical reinforcement was not provided. Distress associated with the compression strains on the western face of the flange remained virtually non-existent.

161. A northwards lateral displacement of the eastern end of the wall became apparent. This displacement indicated a gross instability of the bottom 800 mm of the section (Fig. 7.55(d)).

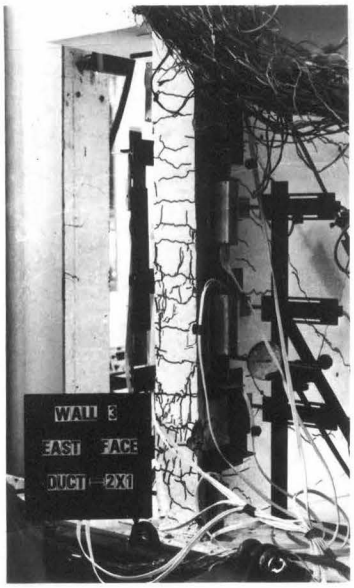

(a) Vertical splitting at east end, μ_Δ = 2 x 1.

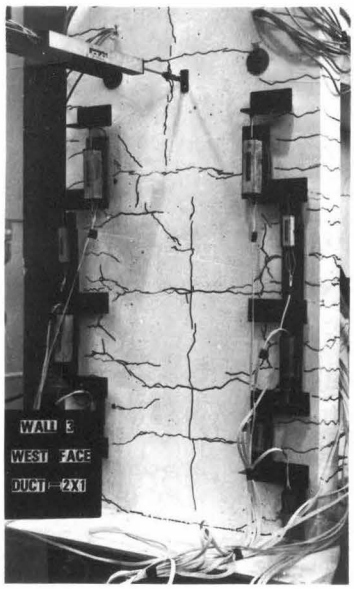

(b) Cracking at west end, μ_Δ = 2 x 1

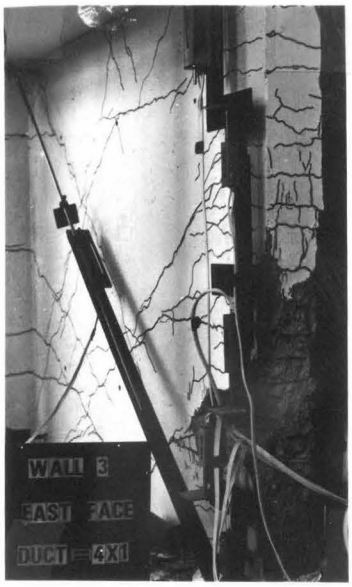

(c) East end, μ_Δ = 4 x 1

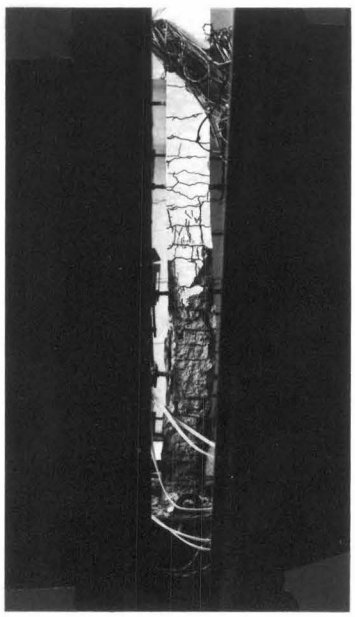

(d) East end, load point 161.

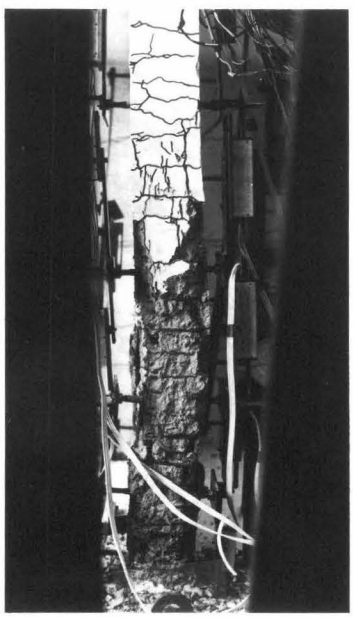

(e) East end, load point 162.

(f) East end after failure.

Fig. 7.55 Wall 3 During Testing.

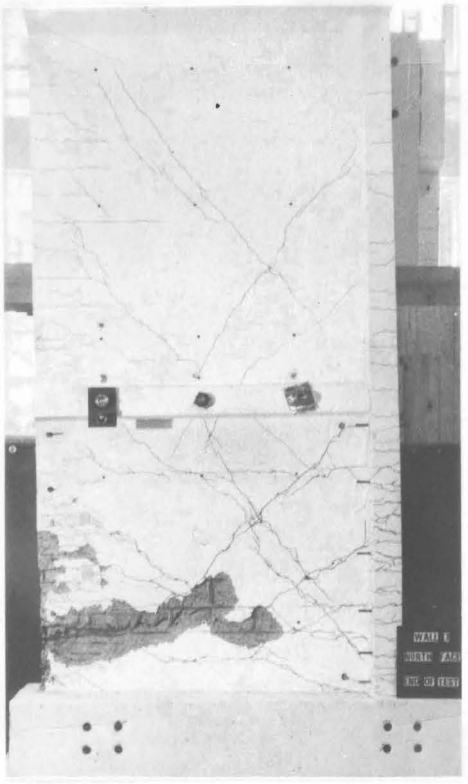

(g) North face, end of test.

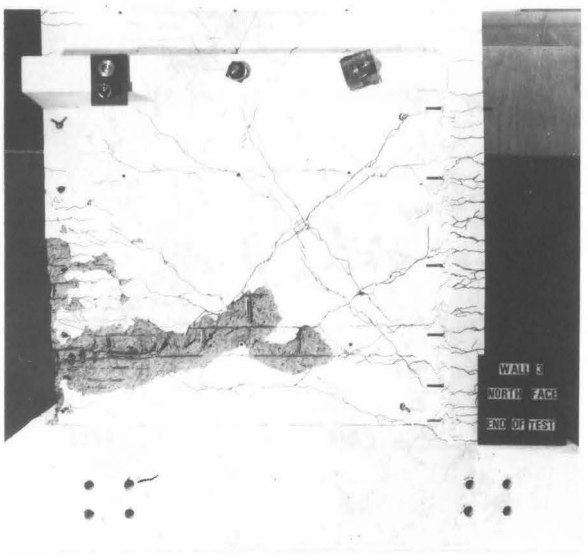

(h) North face, lower panel, end of test.

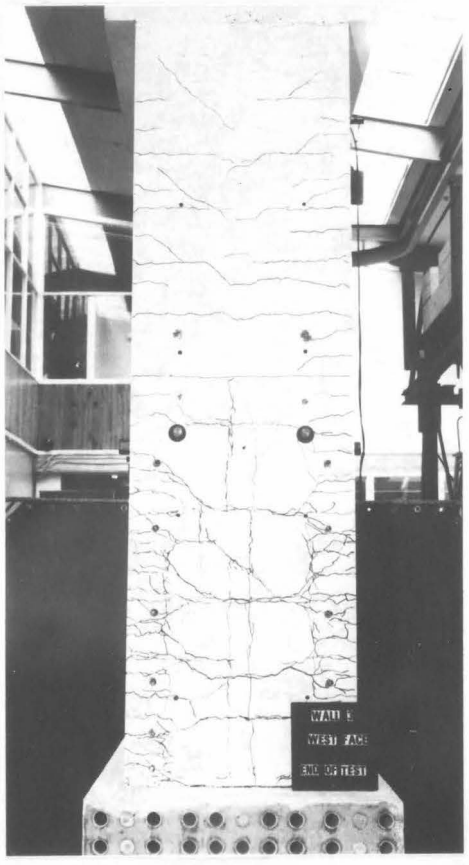

(i) West face, lower panel, end of test.

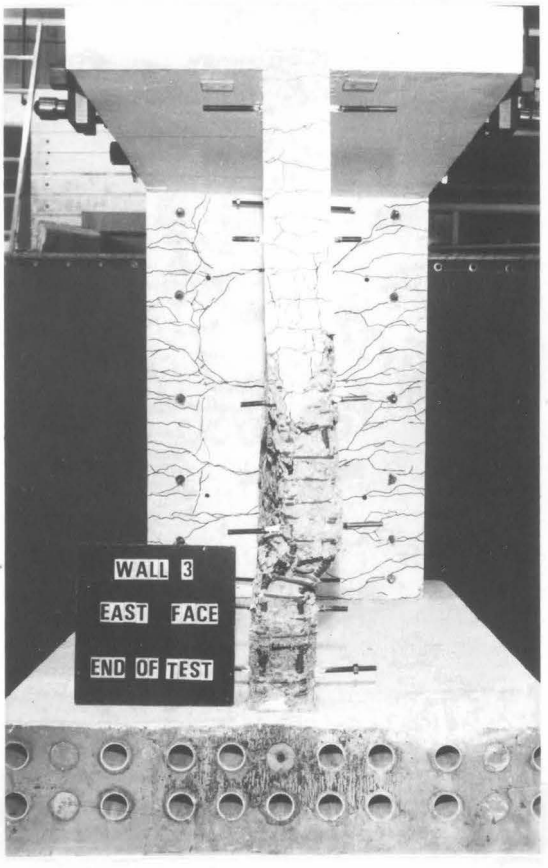

(j) East end, end of test.

Fig. 7.55 (Continued)

162. Further lateral deformations occurred (Fig. 7.55(e)) with the compression zone slowly creeping northwards, while maintaining the required axial load.

165. The stability of the wall apparently increased at this stage, with southward out of plane deformations indicated by a laterally mounted dial gauge. The load carrying capacity of the section increased normally.

167. During the taking of readings at this load point the unit suddenly failed in a material compression failure mode. Compression load carrying capacity was abruptly lost, and in an endeavour to recover this, the Dartec machine increased the compression strain on the unit. This process was automatically arrested and the test stopped when preset limits in compression deformations were attained. Axial and lateral loads at the time of failure were 700 and 216 kN respectively. Fig. 7.55(f) illustrates the east end of the wall after failure.

7.4.2.1 Description of failure mechanism and the failed unit:

The failure of Wall 3 combined aspects of behaviour exhibited by both Walls 1 and 2. Prior to the explosive material compression failure which terminated the testing, the east end of the wall had adopted a northwards out of plane buckled profile. This was similar to the failure mode of Wall 2 except that, for Wall 3, lateral wall displacements terminated some 200 mm below the floor slab, rather than extending over the full first floor height as was the case for Wall 2. A comparison of Figs. 7.30(h) and 7.55(e) indicates this similarity.

The continued application of increasing axial and lateral loading to the wall after the development of this lateral deformation resulted, initially, in an increase in stiffness of the section. Out of plane deformations actually reduced somewhat (Section 7.4.3.9) and the attainment of a second excursion to a nominal displacement ductility of +6 seemed likely. However, a sudden material compression failure occurred at load point 167 and the unit was left in a very similar condition to that of Wall 1 after its failure. Figures 7.55(g)-(j) illustrate the wall after the completion of testing. The final failure of Wall 3 is believed to have been initiated in the unconfined concrete on the south face of the web immediately adjacent to the confined core and approximately 350 mm from the extreme compression fibre. This concrete was subjected to high compression strains due to axial and lateral loading which was further

increased on the south face of the wall by the northwards out of plane displacement present. At the height above the base block, where ultimate failure occurred, a peak compression strain in the critical unconfined region of approximately 0.024 was indicated immediately prior to failure. The failure of concrete adjacent to the core would cause the neutral axis depth to increase in order to maintain the compression force capacity needed to resist the applied loads. This results in progressive over-straining and failure of the unconfined concrete from the core back towards the flange, and in addition, the eventual overloading of the confined core. After failure, there was an inclined failure plane in the unconfined region of the web, with a localised abrupt kink in the confined core associated with a compression failure there. Core concrete in this kinked zone was severely degraded to little more than powder. This process, as for Wall 1, occurred very rapidly and was halted only when preset compression deformation limits on the Dartec actuator travel were attained. The strong similarity between final failure patterns may be seen from a comparison of Figs. 7.30(g),(j), and 7.55(e) and (g). The section where local kinking of the longitudinal reinforcement occurred was approximately 250 mm above the theoretically critical base section. It is believed that the confining effect of the relatively massive base block is responsible for this commonly observed effect. In addition, the maximum observed transverse displacements (Section 7.4.3.9) were recorded at this height.

7.4.2.2 Crack patterns: Several aspects of cracking which developed in the web and flange regions of the wall are worthy of note. Firstly, in comparison with Walls 1 and 2, relatively fewer major diagonal cracks formed in the web region, which resulted in larger crack widths being recorded for Wall 3 (compare Figs. 7.30(g) and 7.55(h)),i.e. 3-4 c.f. 6-8 cracks. As all walls tested had similar (but not identical) quantities of horizontal and vertical plain 6 mm bars in the web regions,which would be thought to influence crack formation, the difference is attributed to greater tensile strength of the concrete in Wall 3 compared to that in Walls 1 and 2. Although this tensile strength was not directly measured there is no doubt that tensile strength increases with compressive strength, albeit not proportionally [1] . Table 6.2 shows Wall 3 concrete compressive strength to be significantly greater than that of Walls 1 and 2. Larger tensile strength implies greater crack spacing and for similar overall deformation levels, larger crack widths.

Crack patterns for the web element are shown in Fig. 7.55(i). Although approximately 20 horizontal cracks are present at the edges of the bottom storey area, only 5 major horizontal cracks (including that at the wall-base block interface) formed in the central region of the flange. This is attributed to the influence of the deformed longitudinal bars present at the edges of the flange in the region well defined by the crack pattern. Due to the more efficient development of bond forces along deformed bars compared with plain bars, cracks in regions reinforced with deformed bars are more numerous and less wide. This mechanism is also responsible for the close spacing of horizontal cracks at the east end of the flange, and the wider spacing of flexure-shear cracks which become inclined away from this end region (Fig. 7.55(h)).

Flange cracking above the floor slab level was significantly less severe than below it,and cracks are generally horizontal, with some slight diagonal cracking and vertical cracking along the web-flange junction. No indication of punching of the web through the flange was present at the base. A prototype wall unit would almost certainly be provided with deformed vertical panel reinforcement and thus it would exhibit a more uniform distribution of web and flange cracking than indicated in this wall.

7.4.3 Test Results

7.4.3.1 Moment-Deflection Hysteretic Relationship: Figure 7.56 shows the relationship between base section moment and equivalent horizontal wall deflection at the level of lateral load application. The asymmetric nature of the curves is due to the geometry of the section and the changing axial load used during testing. The small load reversals indicated (e.g. on the descending branches from $\mu_\Delta = 4$) are associated with adjustments made to the position of the push-pull rod (Fig. 6.13(a)). Two full cycles to nominal displacement ductilities of 3/4, 2 and 4, and one full cycle to $\mu_\Delta = 6$ were obtained prior to failure of the wall. The positive flexural strength remained approximately constant after $\mu_\Delta = 2$ at a level 20% greater than the theoretical ideal strength. Negative moment strength increased markedly between $\mu_\Delta = -2$ and -4, the ideal negative strength being approximately equal to the observed capacity at $\mu_\Delta = -2$. This increase (of close to 50%) is predicted by analysis (Section 7.4.3.2) and is attributable to the strength enhancement due to high tensile strains (up to 6%) in longitudinal reinforcement at the

SEE ERRATA

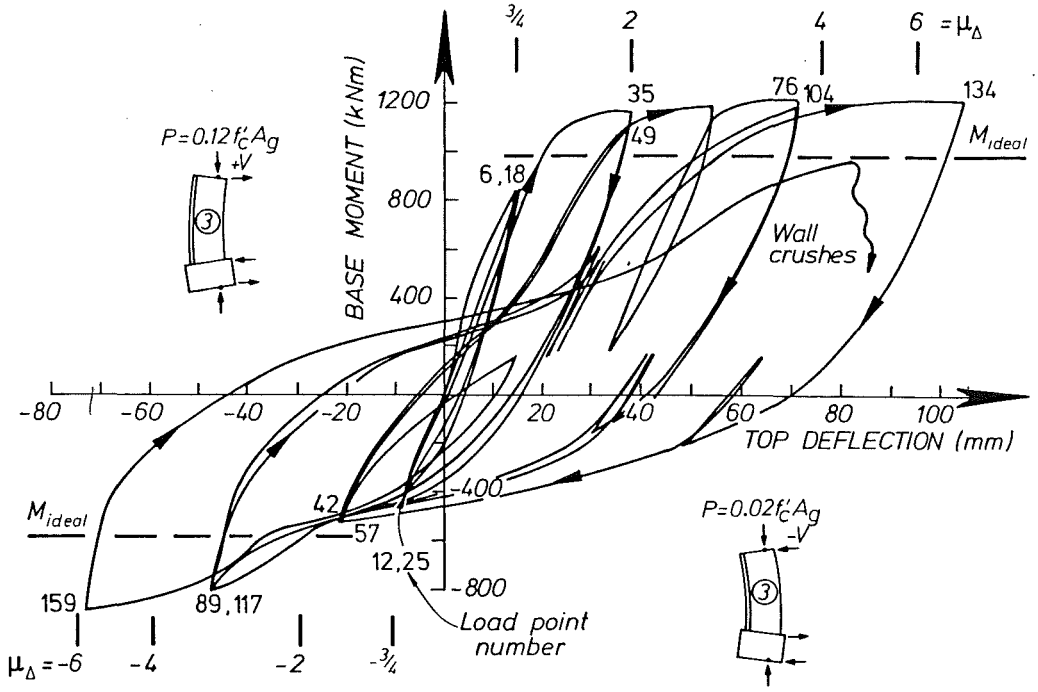

Fig. 7.56 Moment-Wall Top Displacement Relationship - Wall 3.

east end of the wall. During negative loading a very small neutral axis depth was maintained, with longitudinal reinforcement in the eastern face of the flange, and all web reinforcement in tension.

Good repeatability of load carrying capacity at a given displacement is exhibited, with decreases in strength in successive cycles less than 5% of the first cycle strength. The reloading of the section in the positive sense at displacement ductilities of 2 and larger is accompanied by significant pinching of loops. This temporary loss in stiffness is due in part to the influence of the increasing external axial load applied with increasing moment. The primary source of this phenomenon is, however, the horizontal (shear) displacements needed to close the wide diagonal cracks opened in the previous negative loading excursion, as discussed more fully in Section 7.6.1.

The base moment-first floor level deflection hysteresis relationship exhibits similar trends to Fig. 7.56 and is not shown.

7.4.3.2 Moment-curvature relationship: Figure 7.57 illustrates the theoretical monotonic moment-curvature relationship and experimental points

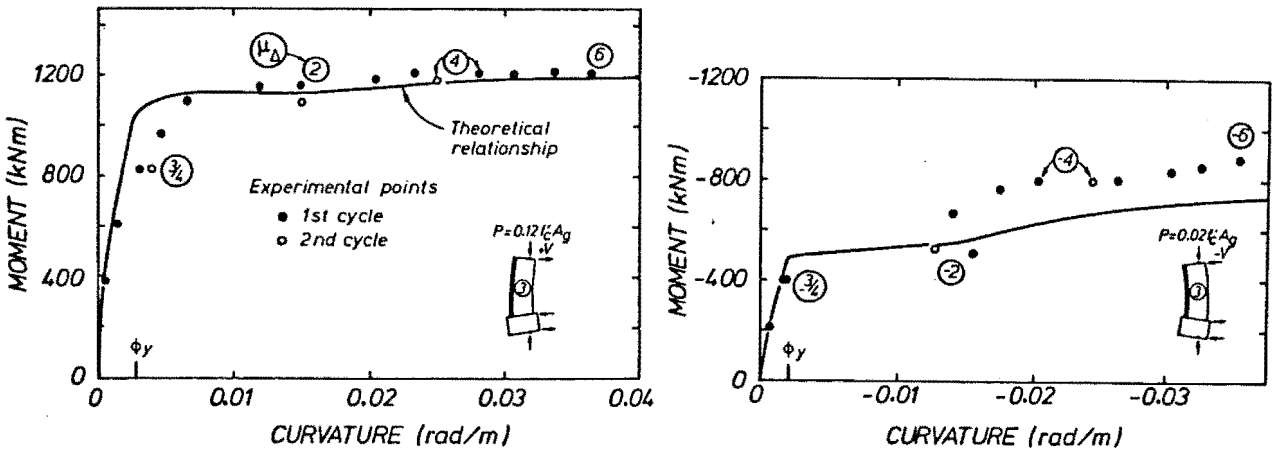

Fig. 7.57 Moment-Curvature Relationship - Wall 3.

observed over the bottom-most 150 mm of the wall. Experimental curvatures were calculated using averaged strains from the 4 west end and 2 east end potentiometers respectively. Good agreement is shown for positive loading at high curvatures where a discrepancy of less than 4% exists between theoretical and analytical points. Agreement at low post yield curvatures is poor, with experimentally observed points indicating approximately twice the theoretical curvatures for a given moment, i.e. the theoretical stiffness is twice the observed stiffness. This is attributed to an inadequate estimation of the influence of anchorage deformations on curvatures at this lowermost level.

Paradoxically, pre-yield agreement between experimental points and the theoretical curve is excellent, while at negative displacement ductilities greater than 2, recorded strengths are up to 25% in excess of those predicted. This is caused by a significant increase in strength of the east end flexural reinforcement due to repeated loading to high strains (of order 5% at the critical section). The monotonic moment-curvature envelope does not recognise this effect.

7.4.3.3 Wall curvature distribution: The distribution of curvature over the bottom region of the wall is shown in Fig. 7.58. The values were calculated as indicated in the previous section. For positive loading, curvatures are distributed in an approximately linear manner and suggest a plastic hinge length of close to the section dimension ($\ell_p \simeq \ell_w$). The low second level negative load curvatures are attributed to the

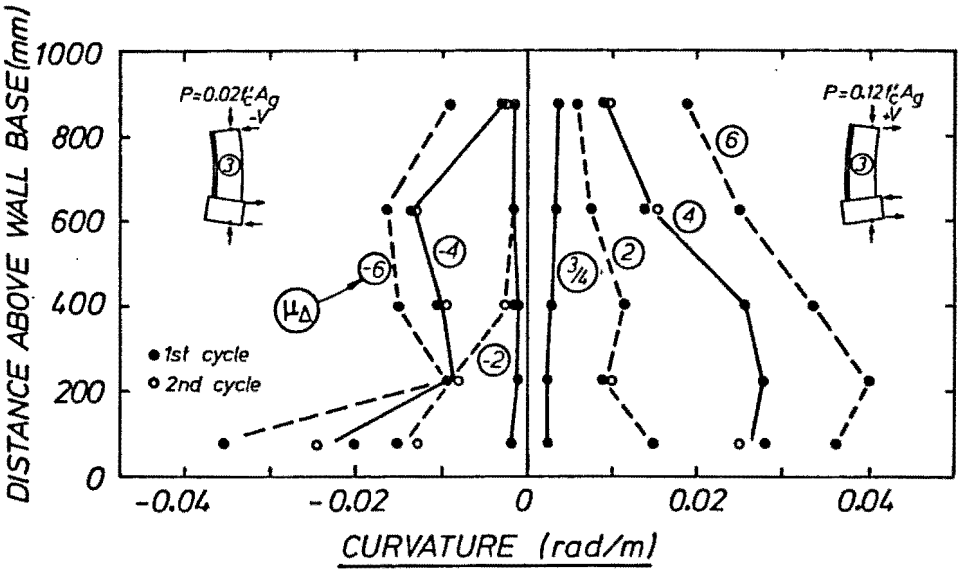

Fig. 7.58 Wall Curvature Distribution - Wall 3.

(random) concentration of deformations outside this region. The gauge regions are crossed by relatively few cracks (generally 3-5) and invariably cracks form at the potentiometer attachment rods. Deformations at these latter cracks contribute consistently to the curvatures measured over one or other of the adjoining gauge regions. Thus deformations at the cracks between regions 1 and 2 and 2 and 3 could contribute to curvatures in regions 1 and 3 respectively, giving low curvatures in region 2. The negative load curvatures indicate a restriction of inelastic deformations to a lower region of the wall than for positive loading, which is consistent with the steeper gradient of the negative bending moment diagram. Negative curvatures accrue almost totally from the high east end tensile strains due to the small negative load neutral axis depth. Yield strains were indicated 1 m above the wall base at $\mu_\Delta = -2$, with a strain of 1.3% at that height at $\mu_\Delta = -6$. Concrete compression strains remained less than 0.002 on the western face of the flange even at $\mu_\Delta = -6$. Inelastic tensile strains occurred on the eastern side of the flange at large negative displacements, however.

7.4.3.4 Shear reinforcement strains: The maximum recorded web stirrup strains are shown in Fig. 7.59(a). Strains were approximately constant with height, and generally less than 1.5 times yield strain. The high strains recorded on the third gauged stirrup set (gauge C4) for negative loading are due to the exact coincidence of this gauge with

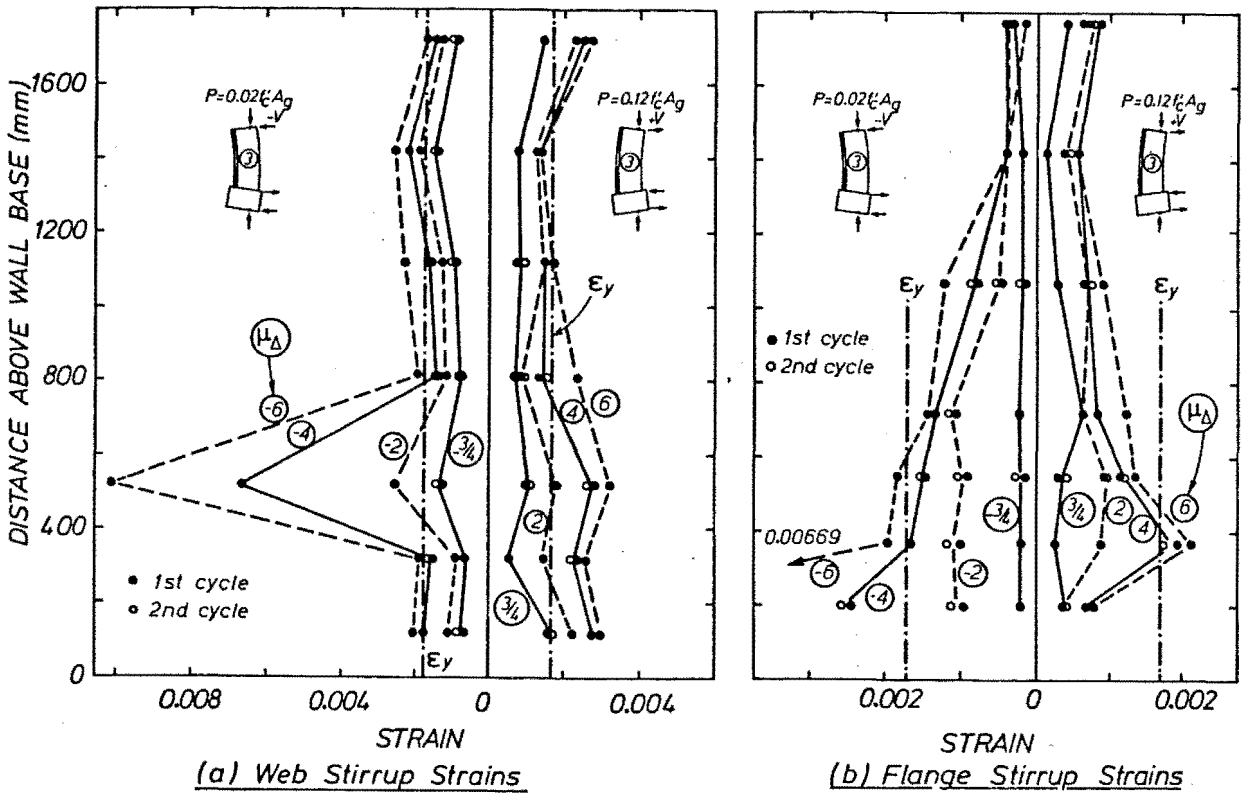

Fig. 7.59 Stirrup Strains - Wall 3.

a major diagonal crack which opened under this loading. Peak shear forces of +287 and -296 kN were sustained (at $\mu_\Delta = \pm 6$) corresponding to nominal shear stresses ($v = V_{max}/0.8b_w\ell_w$) of $0.473\sqrt{f'_c}$ and $0.488\sqrt{f'_c}$ MPa respectively. Given the similarity of applied shear forces and stirrup resistance for positive and negative loading, the concrete shear capacity does not appear to have been strongly influenced by the difference in axial force for positive and negative loading. An apparent anomaly is that the plastic elongation consistent with the high 3rd level stirrup strains at $\mu_\Delta = -4$ was not recorded at $\mu_\Delta = +4$, indicating an inelastic shortening to have occurred at the gauge.

The flange stirrup strains (Fig. 7.59(b)) are also generally less than or equal to yield strain, indicating an adequate level of shear reinforcement in the flange.

7.4.3.5 Hoop reinforcement strains: East and west end hoop strains, shown in Figs. 7.60 and 7.61, are generally less than yield strain of 0.0014. (See also Fig. 7.53 for details of hoop strain gauge layout). East end strains are, as would be expected, low for negative loading and increase with increasing μ_Δ for positive loading (which puts the

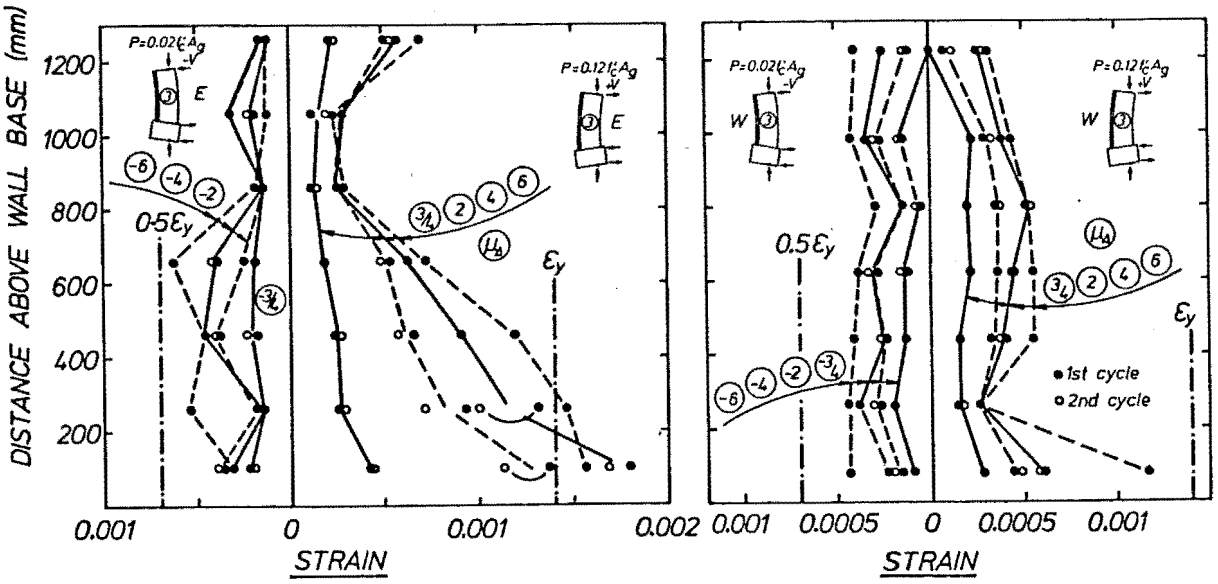

Fig. 7.60 East End Hoop Reinforcement Strains - Wall 3.

Fig. 7.61 West End Hoop Reinforcement Strains - Wall 3.

east end of the wall in compression). A peak average core compression strain of approximately 2.5% was indicated at $\mu_\Delta = 6$, while immediately prior to failure (load point 167) a strain of 3.3% was indicated at the southern face of the confined core. West end hoop strains are low for both senses of lateral loading which is not surprising given the low levels of compression strain imposed on the flange. The low strain levels recorded suggest that the quantity of hoop reinforcement supplied in the east end of the wall was sufficient to give good confinement to that region. It is believed, however, that the failure of the wall would have been delayed by the provision of hoop reinforcement over a deeper portion of the east end of the web. This subject, together with general design recommendations for hoop reinforcement, is pursued further in Section 7.6.4.

7.4.3.6 Strains in longitudinal reinforcement: Although some longitudinal bars were provided with strain gauges in both the base block and wall proper, detailed results for these gauges are not presented. The trends exhibited are similar to those shown for Walls 1 and 2.

7.4.3.7 First floor level deflection: The decomposition of first floor deflection is shown at μ_Δ values of 3/4, 2, 4 and 6 in Fig. 7.62(a), the flexural, shear and fixed end components calculated as described in Section 7.2.3.10. The relative proportions of these deformation modes are shown in Fig. 7.62(b), and conform to trends exhibited by Walls 1 and 2. Fixed end deformations are an approximately constant fraction of the whole,

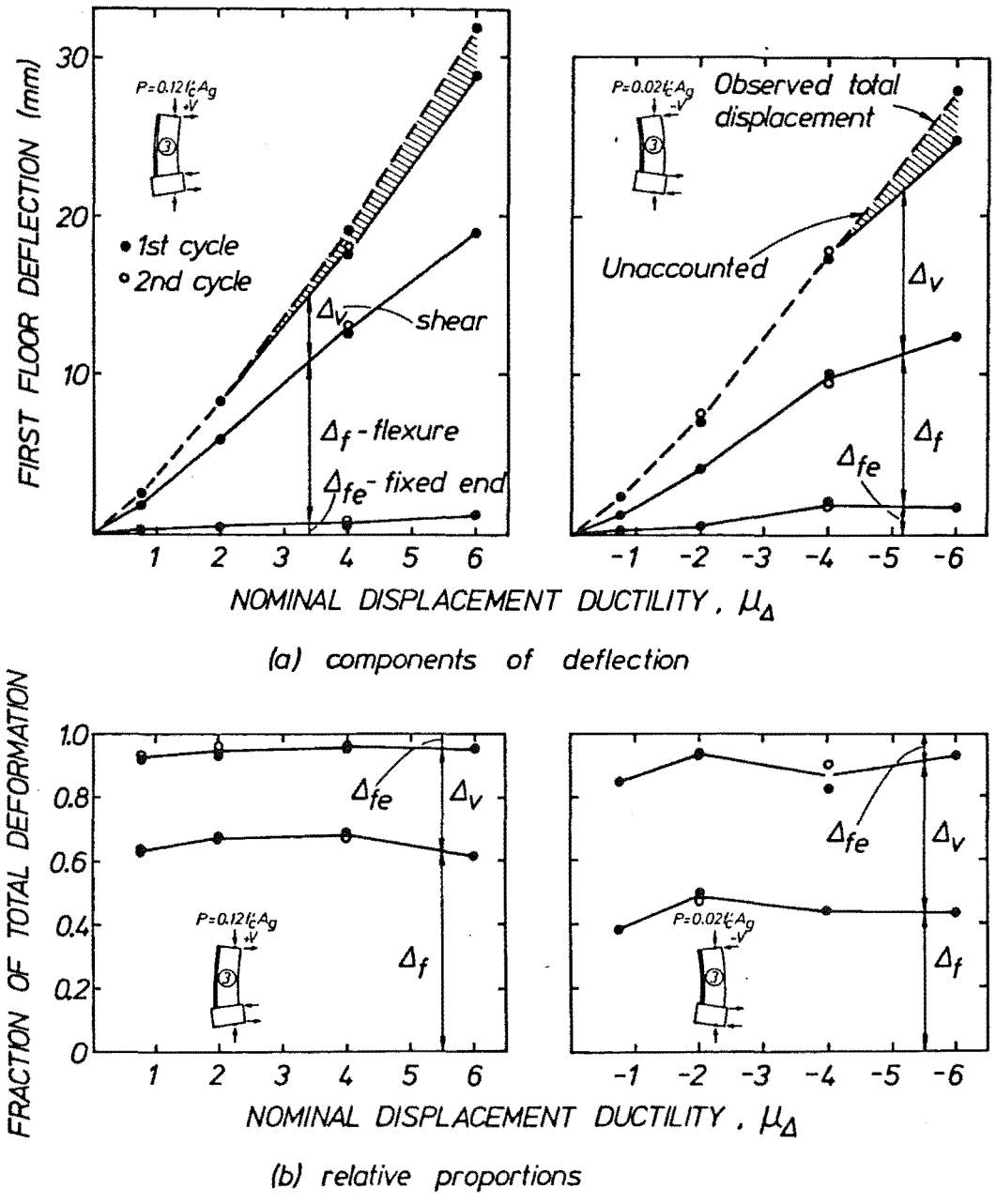

Fig. 7.62 First Floor Displacements - Wall 3.

while shear deformations form a larger fraction for negative loading (≃ 45%) compared with 30% for positive loading. This is attributed to the lower stiffness of the concrete shear resistance mechanism due to the wide diagonal cracks and very small neutral axis depth accompanying negative loading. The discrepancy between observed and deduced deflections at $\mu_\Delta = \pm 6$ was 10% and 14% of the total for positive and negative loading respectively, though less than half these amounts at lower deformation levels.

7.4.3.8 Shear slip at base construction joint: As shown in Fig. 7.63, an extremely low level of base level shear slip was recorded for positive lateral loading. The slip associated with negative loading (and lower axial loading) was, as would be expected, greater, but always less than 5% of the total first floor displacement. There was no indication of any tendency for the web to punch through the flange, a mode of behaviour more common for squat walls [39].

7.4.3.9 Out of plane displacement history: Figure 7.64 shows the out of plane displacement history of a vertical section some 150 mm from the east end of the web. Early on in the test, displacements at all 3 levels monitored were southwards, with the tendency for reversed (northwards) deformations initiating at level 1 and spreading up the wall. The oscillatory nature of the out of plane displacements is again evident, northwards movements occurring during periods of positive loading (compression on the east end of the wall). The largest jumps in northwards

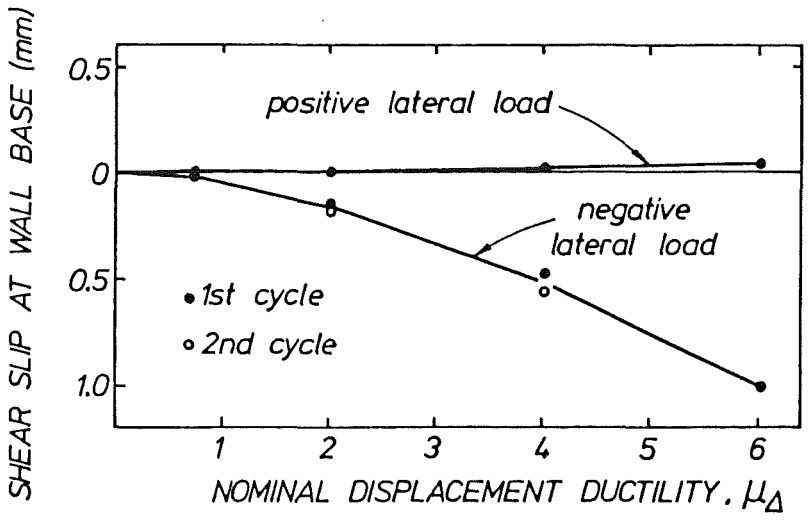

Fig. 7.63 Slip at Base Construction Joint - Wall 3.

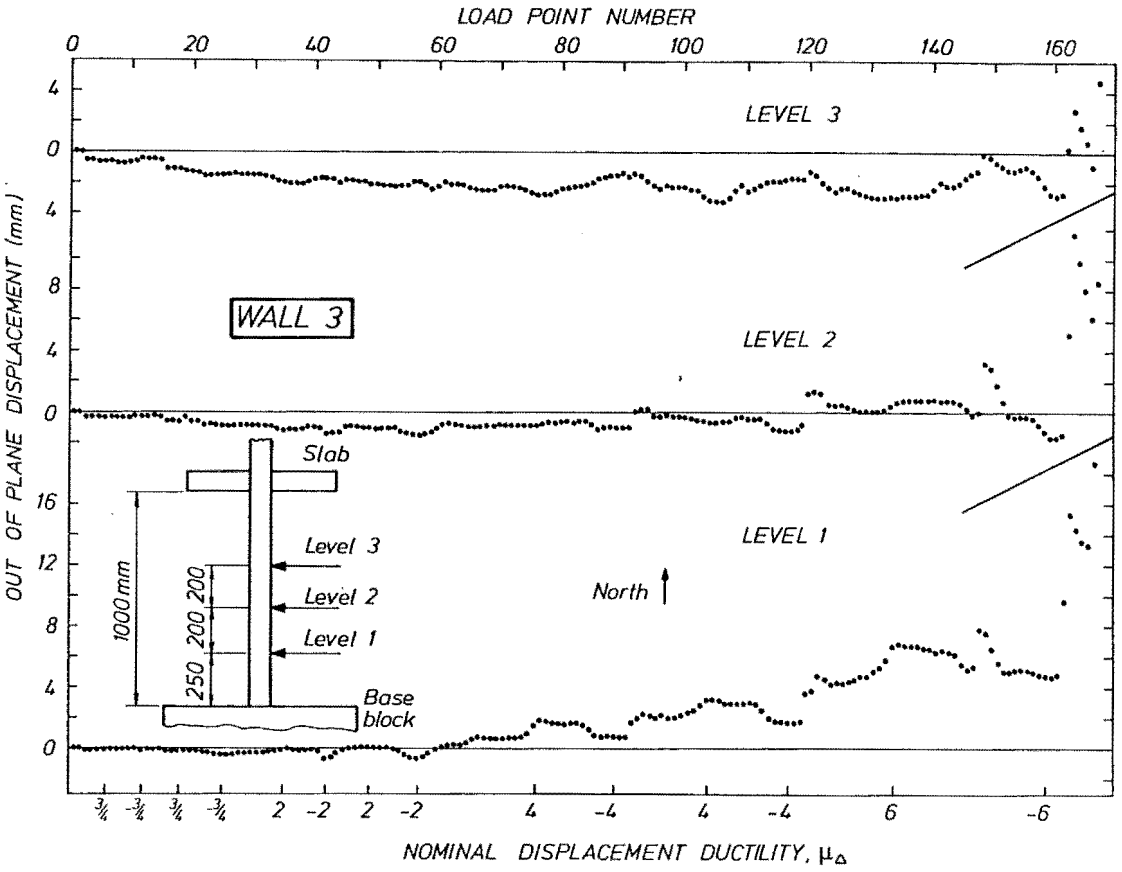

Fig. 7.64 Out of Plane Displacement History - Wall 3.

displacement occur during the change from axial/lateral forces of 330/-50 kN to 400/0 kN, e.g. load points 91 → 92, 119 → 120, 147 → 148, 161 → 162. This force transition is that necessary to cause closure of residual tensile cracks at the east end of the wall and is the period at which the compression zone is least stable. After these cracks close and concrete compression strains develop, out of plane displacements continue to occur but at a reduced rate. With reversal of lateral load direction, and consequent tension at the east end of the wall, the straightening of longitudinal reinforcement causes some recovery towards verticality of the section.

At load point 162, a northwards deflection at all 3 levels monitored was indicated, but despite increasing average compression strains, a southwards web displacement occurred between points 162 and 166, Immediately prior to failure, this southward tendency reversed. Figure 7.65 illustrates transverse displacement profiles at various stages of the test, and suggests how the top region of the wall (deflecting

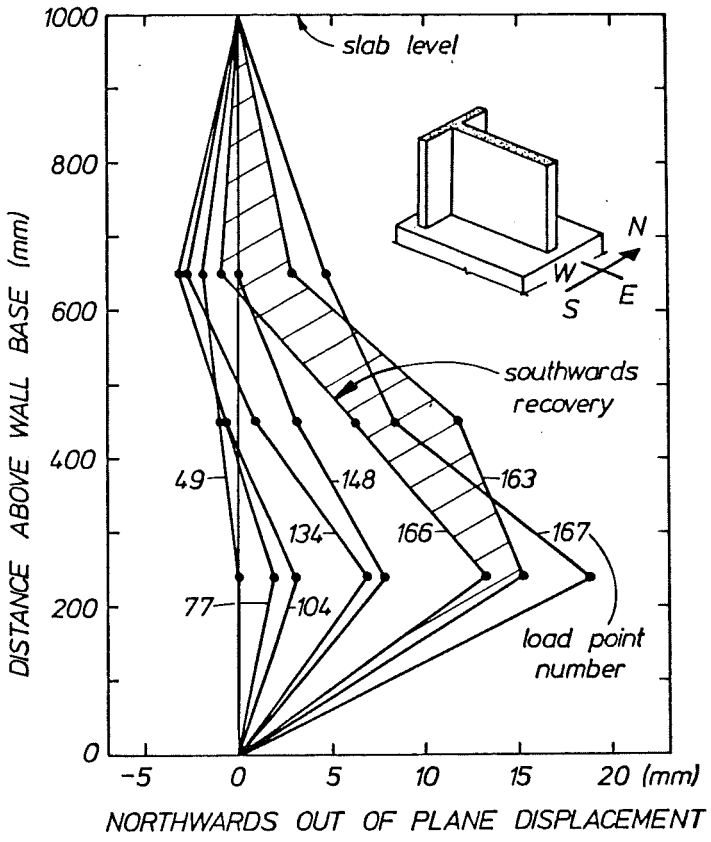

Fig. 7.65 Out of Plane Displacement Profiles - Wall 3.

southwards) helped to restrain the base. It is believed that had the centre first floor section commenced moving northwards during compression loading, an earlier failure would have occurred.

The observed phenomenon of the northwards movement halting at load point 163 and reversing thereafter is explained in terms of a stress redistribution in the east end of the web. In order to sustain the increasing external lateral and axial loading, the tensile strains on the north face of the web gave way to the compressive strains needed to develop compressive stresses and provide the necessary internal compression forces. This redistribution was accompanied by the southwards lateral movement observed.

7.5 WALL 4 - DESCRIPTION OF TESTING AND RESULTS

7.5.1 General Notes

The fourth and final wall unit tested was of rectangular section and almost identical in geometry, instrumentation and reinforcement layout to Wall 1 (see Figs. 7.1, 7.2 and 7.3). The sole difference was the positioning of the slab stub to give a first storey slenderness ratio of 8 to 1. The extremes of axial load attained based on actual material properties, were $0.15f'_cA_g$ and $0.03f'_cA_g$ for positive and negative lateral loading respectively. Again, axial load was varied in a stepwise fashion with lateral load so as to give maximum/minimum axial force at the theoretical ideal positive/negative flexural strengths. The high axial load was such that at the ideal positive flexural strength, three quarters of the compression block was supplied with the code [34] required quantity of confinement reinforcing. Code antibuckling reinforcement only was supplied at the western end of the section. Figure 7.66 shows the incremental loading scheme used for this unit.

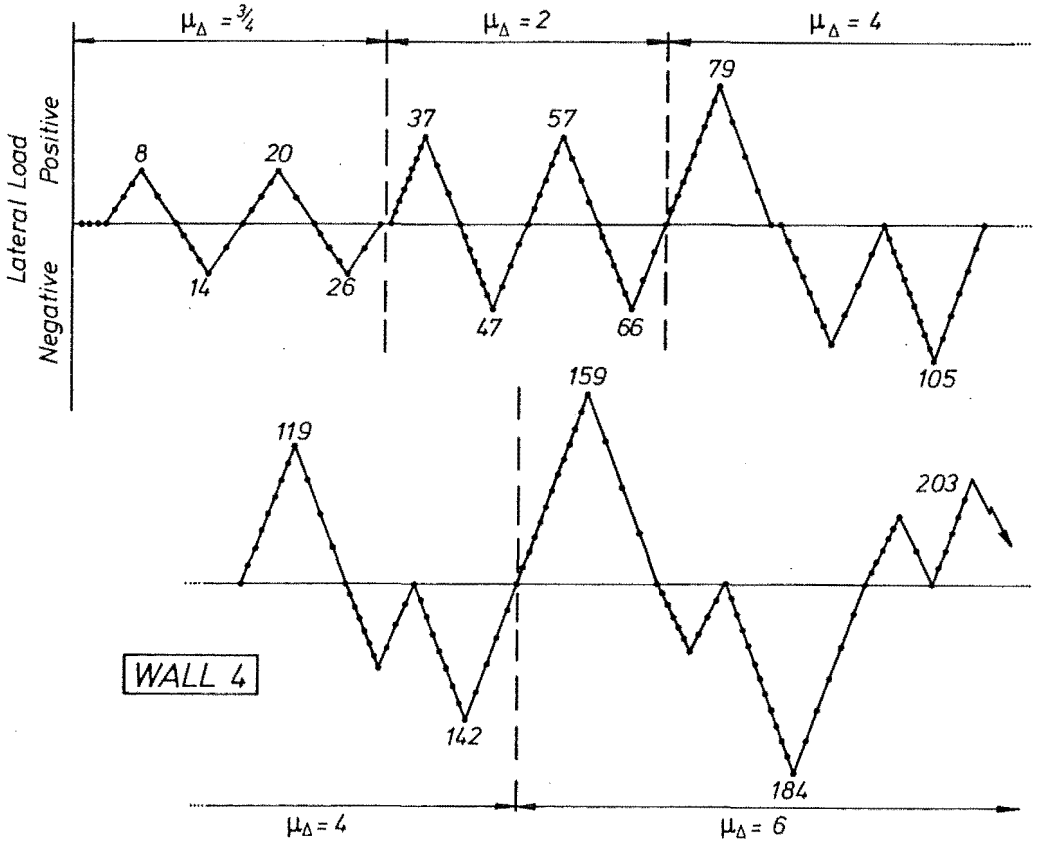

Fig. 7.66 Incremental Loading Diagram Showing Load Point Numbers - Wall 4.

7.5.2 Description of Observed Behaviour

Load Point

8. Diagonal cracks both above and below the floor slab extended to within 700 mm of the east face of the wall. Typical crack widths in these upper and lower regions were 0.03 and 0.13 mm respectively.

14. Diagonal cracks in the other direction of widths similar to those at scan 8 extended to within 500 mm of the west end of the wall.

20. Only slight extension of cracks (as compared with scan 8) was observed.

37. Vertical splitting cracks opened over the entire bottom storey height (800 mm) of the east face. Diagonal cracks of width up to 0.8 mm lengthened to within 550 mm of the east edge of the wall.

47. Slight vertical splitting occurred over the lowermost 100 mm of the west face. A vertical opening of the wall-base block interface crack of approximately 1.0 mm was observed, although this was not accompanied by any appreciable horizontal (shear) displacement.

57. Splitting of east face cover concrete became more extensive, with some spalling of loosened material (Fig. 7.67(a)).

79. Splitting of cover concrete spread 300 mm into the section on both north and south faces to approximately equal degrees. East face cover had substantially spalled (Fig. 7.67(b)). Bottom storey diagonal cracks of up to 2 mm in width extended to within 500 mm of the east face.

105. Spalling of the lowermost 100 mm of west face cover concrete occurred, although vertical splitting above this level was slight (Fig. 7.67(c)). Diagonal and base level cracks were of width up to 3.5 mm. East end cover was also loosened and dislodged.

159. An apparent slight southwards lateral displacement of the east end (compression face) was evident at this excursion to $\mu_\Delta = 6$. (Fig. 7.67(d)). However this impression is attributed to the unevenness of cover spalling on the north and south faces of the section, as no significant out of plane displacements were recorded at this load point (Fig. 7.76). In addition, cover thickness was several millimetres greater on the northern face which probably added to the visual illusion.

184. The wall-base block interface crack opened to a width of approximately 5 mm in the central region of the wall, although less

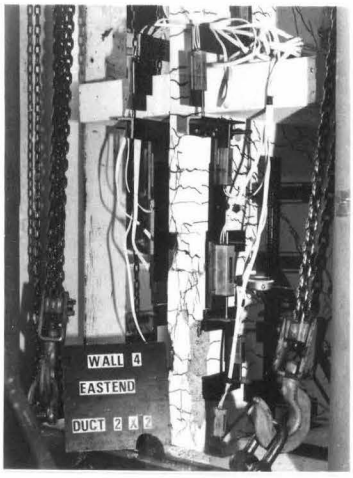

(a) East end, μ_Δ = 2 x 2

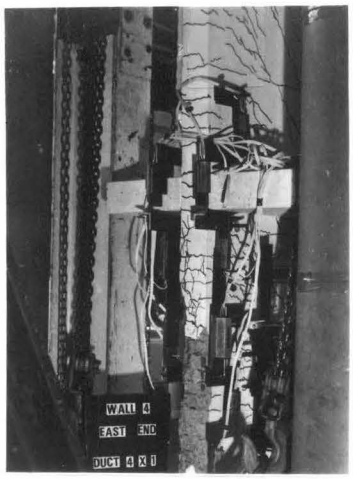

(b) East end, μ_Δ = 4 x 1

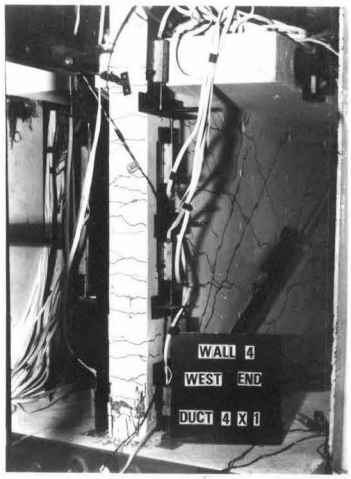

(c) West end, μ_Δ = 4 x 1

(d) East end,
μ_Δ = 6 x 1

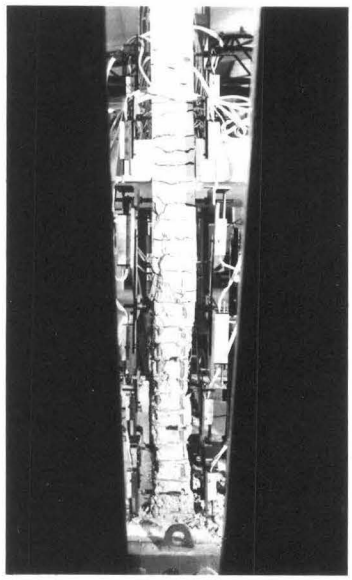

(e) East end,
load point 189

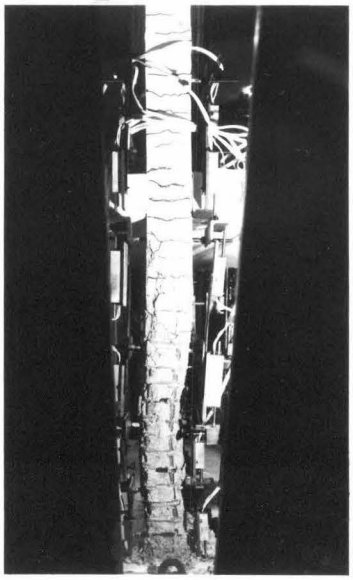

(f) East end,
load point 196

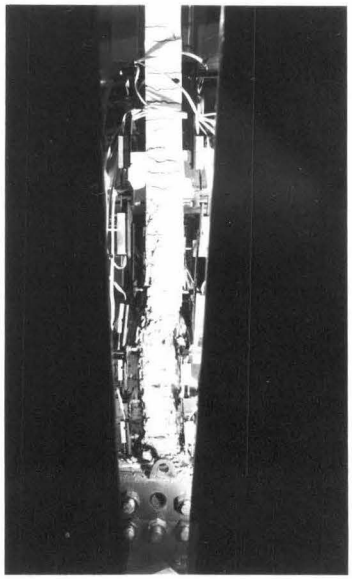

(g) East end,
load point 200

Fig. 7.67 Wall 4 During Testing.

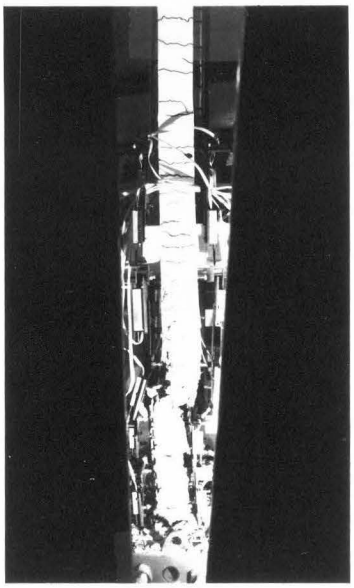

(h) East end, at failure.

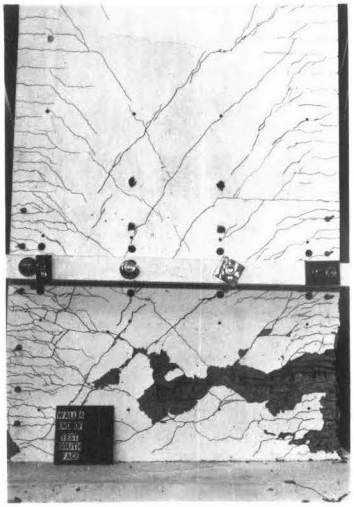

(i) South face, end of test.

(j) North face, lower panel, end of test.

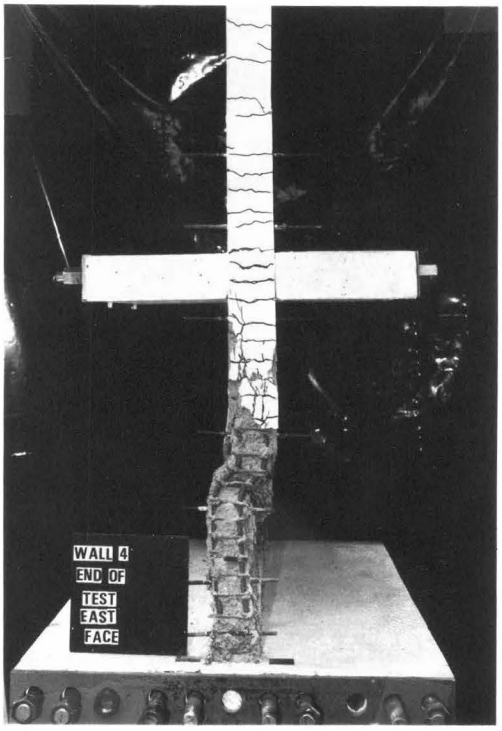

(k) East end, end of test.

Fig. 7.67 (Continued).

than half this at the east end due to the influence of the bundle of deformed bars there. Westwards shear slip at this level was of the order of 1 mm. The four major diagonal cracks, of width 3-4 mm, extended to within 150 mm of the west end of the wall, where spalling and vertical splitting extended some 200 mm above the base block.

189. A distinct southwards displacement of the lower 500 mm of the compression zone became apparent at this point, although above this the wall remained essentially vertical. With increasing positive lateral load, this movement steadily increased.

199. At this load point the overall southwards movement of the lower region of the wall halted and reversed somewhat, and lateral movement concentrated in a smaller region, between 300 and 500 mm above the wall base.

204. A sudden failure of the section occurred after load point 203, at axial and lateral loads of 850 and 230 kN respectively. The test was terminated when the preset axial displacement trips of the Dartec test machine were activated. The out of plane displacements of the east end of the wall during the latter stages of testing are indicated in Fig. 7.67 (e) - (i).

7.5.2.1 Description of the failure mechanism and the failed unit:

The failure mechanism and post-testing appearance of the fourth wall were very similar to those of Wall 3. Figures 7.67(i)-(k) illustrate the wall after failure.

The failed section, some 350 mm above the base block, exhibited features similar to those of Walls 1 and 3 after failure, a kinked and crushed zone of depth approximately 100 mm in the well confined core, and failure plane inclined across the 100 mm width of section in the unconfined area extending back towards the west (tension) end of the section. The mechanism of this failure, involving rapid progressive failure of the unconfined area of the section and overloading of the confined region is as described for Wall 3 (Section 7.4.2.1). Peak compression strains of 0.026 and 0.036 were indicated in these two areas respectively immediately prior to failure (load point 203).

7.5.2.2 Crack patterns: Wall 4 exhibited fewer major diagonal cracks compared with Walls 1 and 2, similar to the trend in Wall 3. This is attributed to greater concrete tensile strength for units 3 and 4 compared with 1 and 2, as reflected by the higher compression strengths of the concrete used for the former walls (Table 6.2)

7.5.3 Test Results

7.5.3.1 Moment-deflection hysteretic relationship: The moment-wall top deflection relationship for Wall 4 is shown in Fig. 7.68, the small internal loops being associated with relocation of the push-pull rod - see Section 6.4.4. Wall 4 had a slightly lower initial stiffness, hence

SEE ERRATA

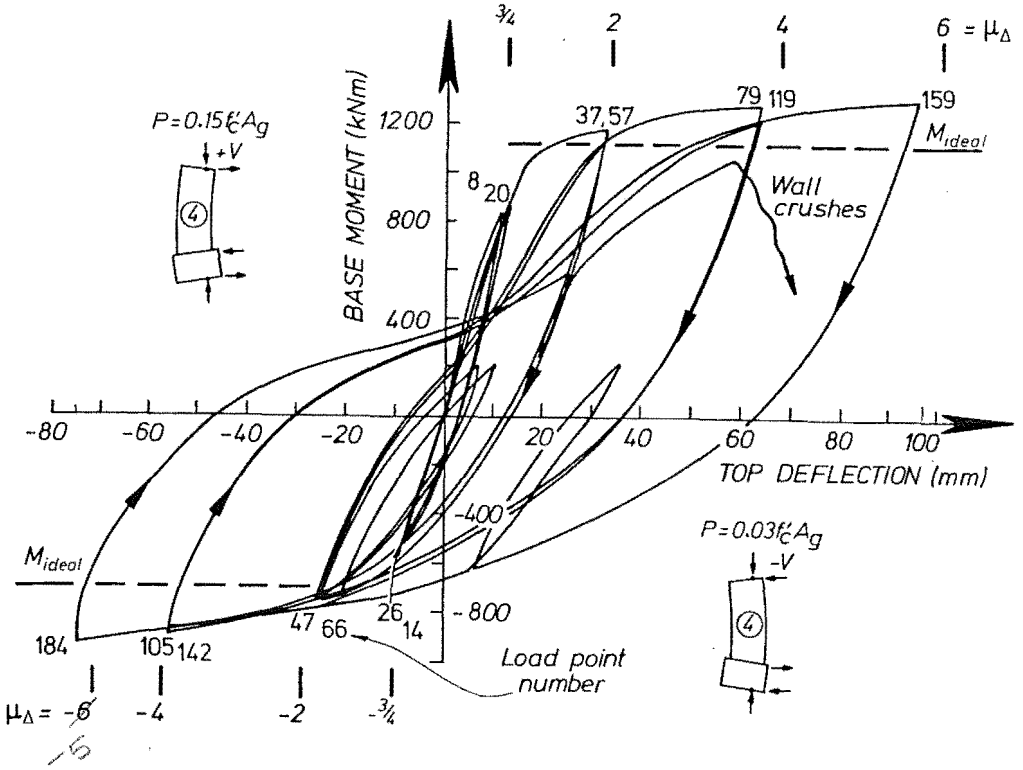

SEE ERRATA

Fig. 7.68 Moment - Wall Top Displacement Relationship - Wall 4.

a larger yield displacement compared with Wall 2 (see Table 7.1) which is unexpected in view of the higher concrete strength of Wall 4. Thus larger displacements were necessary to achieve similar displacement ductility (μ_Δ) factors. The loops show a good degree of repeatability with low strength loss at repeat attainment of a given μ_Δ value. Ideal flexural strengths underestimate peak recorded strengths by 15 and 30% for positive and negative loading respectively. A slight pinching of the loops during the transition from negative to positive loading is again evident. The final positive loading branch shows good stiffness and strength (approximately 95% of the ideal strength at $\mu_\Delta \simeq 4$),

immediately prior to failure. Wall 2 showed no similar increase in strength or stiffness during its final positive excursion (see Fig. 7.32) indicative of the different failure mechanisms exhibited by these walls.

7.5.3.2 Moment-curvature relationship: Figure 7.69 illustrates theoretical monotonic moment-curvature relationships and experimental points for the lowermost gauged region of the wall. The theoretical pre-yield stiffness is reasonably well estimated by the experimental points. At higher deformations, good agreement exists between the analytical and experimental trends, with discrepancies of less than 8% occurring for both directions of loading.

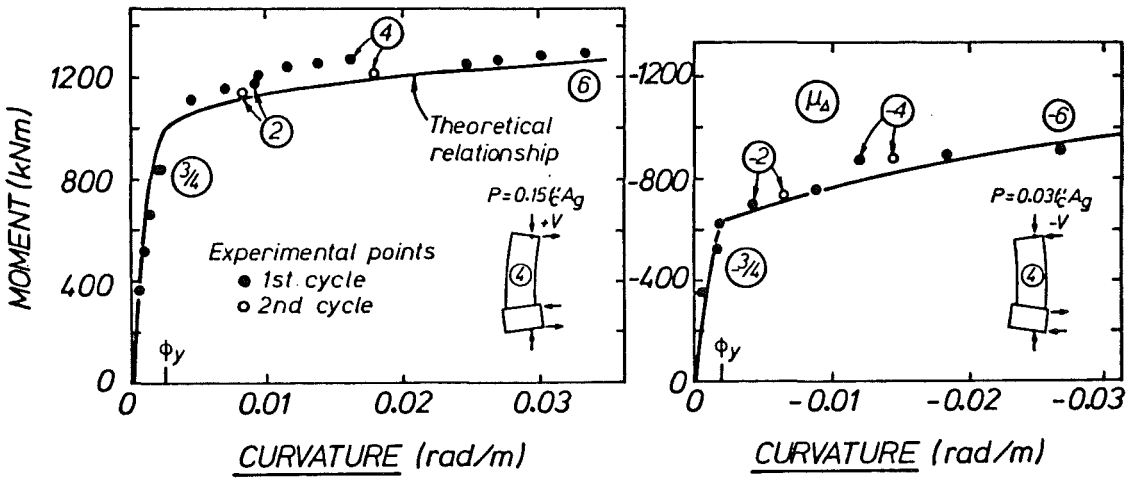

Fig. 7.69 Moment-Curvature Relationship - Wall 4.

7.5.3.3 Wall curvature distribution: The distribution of wall curvatures (Fig. 7.70) is similar to those derived for the previous sections. Curvatures are approximately constant with height at $\mu_\Delta = 3/4$ and increase linearly at successively higher ductilities. Low curvatures for both positive and negative loading indicated over the second lowest gauge region are attributed to the fortuitous process of deformation concentration discussed earlier (Section 7.4.3.3).

7.5.3.4 Shear reinforcement strains: Patterns of peak shear stirrup strains (Fig. 7.71) are also similar to the envelopes shown previously for the other walls. Strains are approximately constant with height and larger with increasing ductilities achieved. The magnitudes of the strains recorded are generally less than or slightly in excess of yield strain (ε_y),

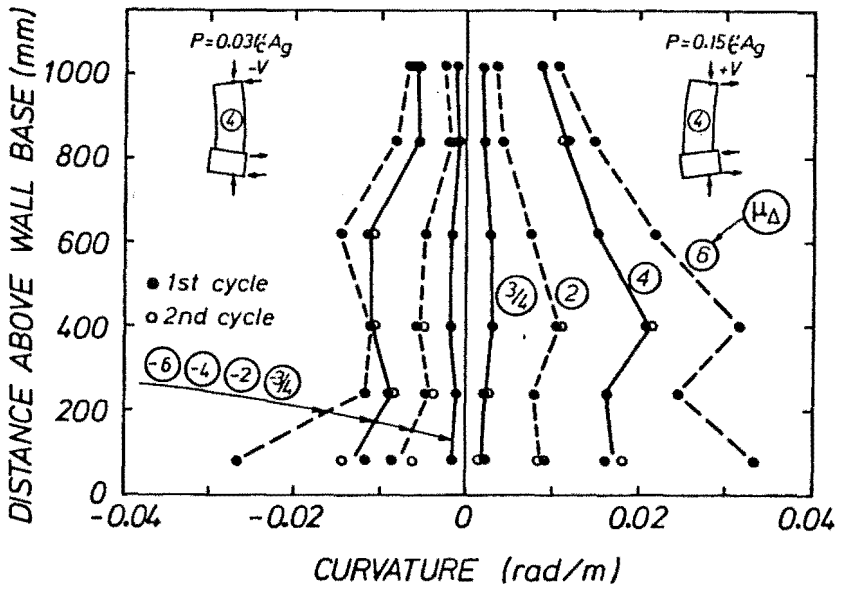

Fig. 7.70 Wall Curvature Distribution - Wall 4.

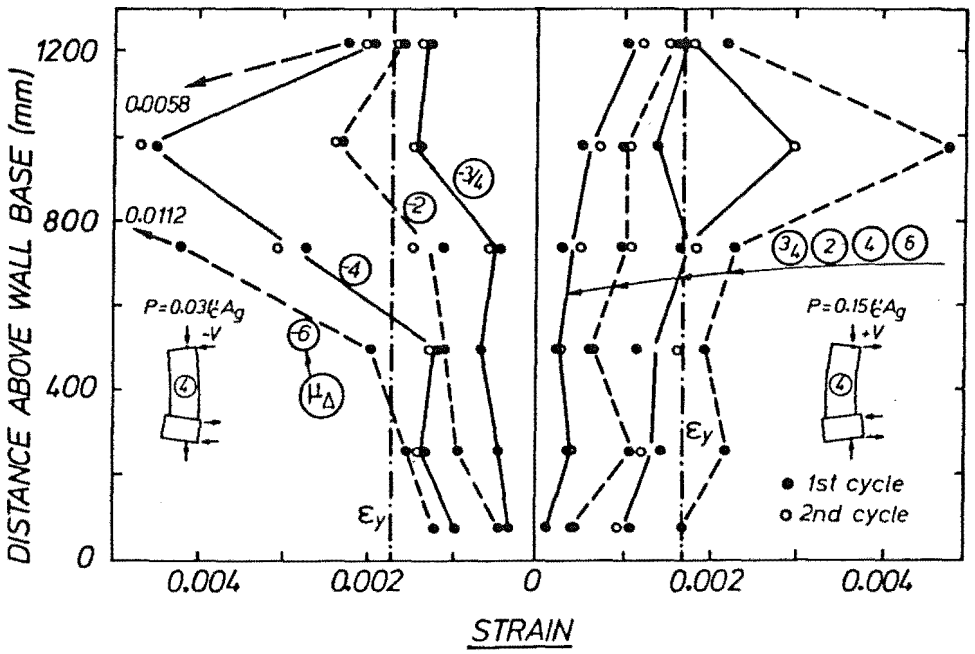

Fig. 7.71 Stirrup Strain Distribution - Wall 4.

although several gauges close to major diagonal cracks indicated strains of nearly $6\varepsilon_y$. A peak nominal shear stress of 2.56 MPa or $0.42\sqrt{f'_c}$ MPa was sustained in both positive and negative loading.

7.5.3.5 Hoop reinforcement strains: Maximum strains in the east end hoop reinforcement are shown in Fig. 7.72 and are distributed somewhat unusually in comparison with the strains for previous walls. Up to and including the first excursion to $\mu_\Delta = -4$, strains follow the pattern common to all the walls tested: strains are generally less than yield strain and larger for positive loading (which puts the east end of the wall in compression). On the attainment of $\mu_\Delta = 4$ for the second time, strains of close to $3\varepsilon_y$ were recorded in the upper regions of the wall where the need for significant confining stresses had not been demonstrated by Walls 1 to 3. More unusual still is the fact that at $\mu_\Delta = -4$ (second cycle) these strains had reduced to less than $0.5\varepsilon_y$, which could only occur with the compression yielding of these hoop legs. At higher ductilities, similar trends are evident, with some high strains ($\simeq 4\varepsilon_y$) at lower levels where residual tensile strains were recorded at $\mu_\Delta = -6$. The lack of obvious distress in these high regions of the wall (such as spalled cover concrete) together with previously established trends (Walls 1, 2 and 3) suggest that these results are spurious.

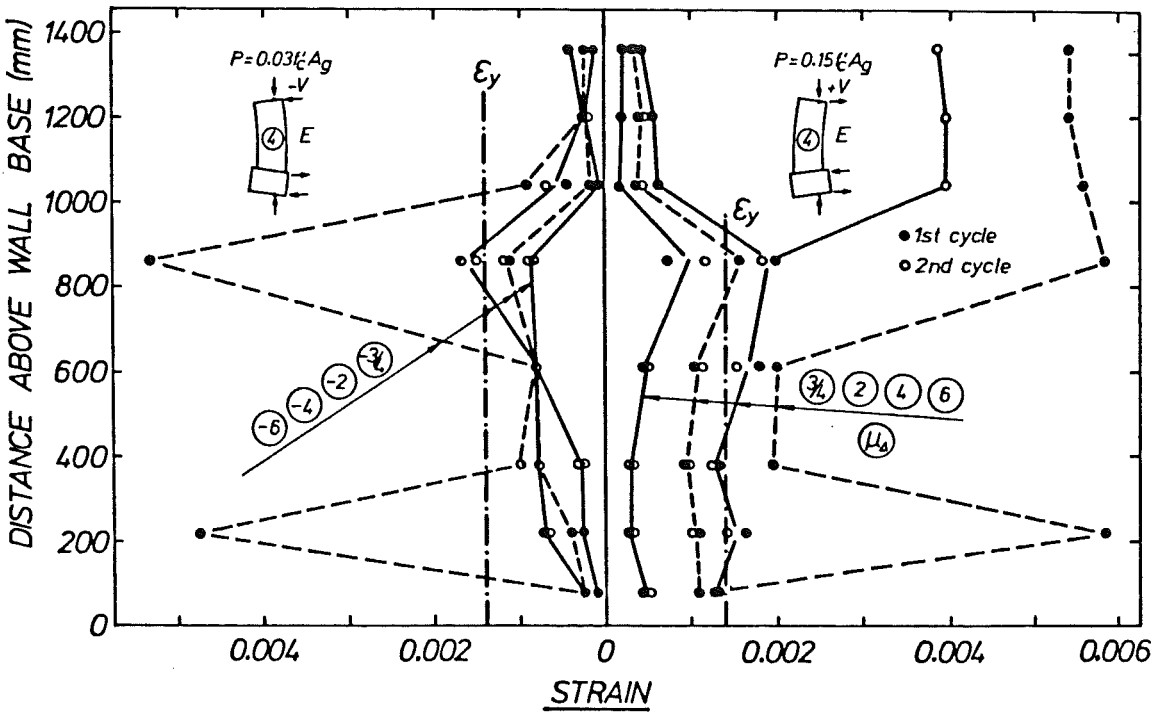

Fig. 7.72 East End Hoop Reinforcement Strains - Wall 4.

West end hoop strains (Fig. 7.73) do follow established patterns. Strains are generally less than ε_y for both senses of lateral loading, exceeding yield strain at the bottommost gauged hoop set only (where cover spall did occur).

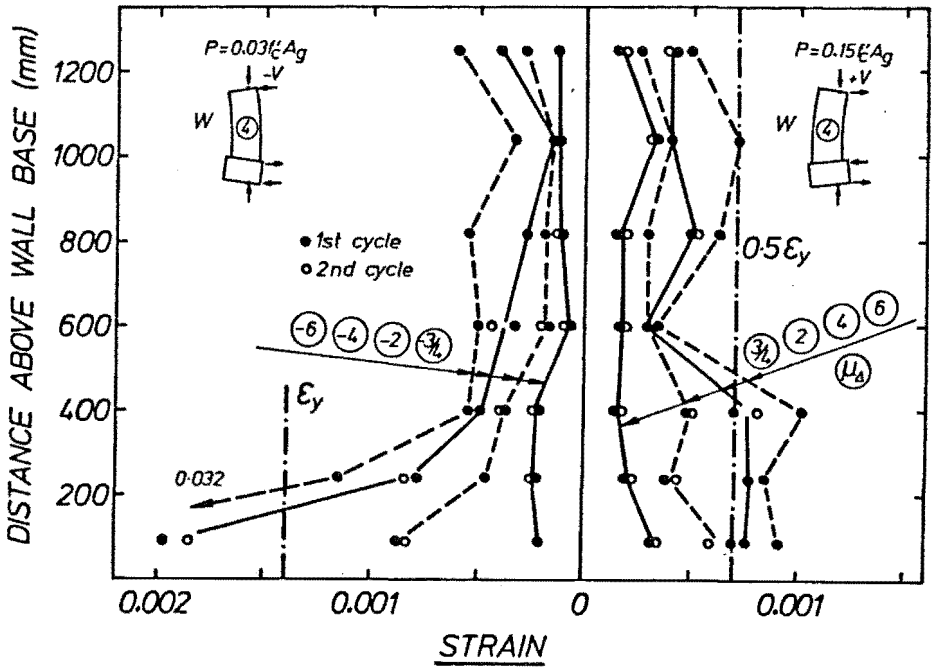

Fig. 7.73 West End Hoop Reinforcement Strains - Wall 4.

7.5.3.6 Strains in longitudinal reinforcement: Strain histories for those longitudinal bars which were gauged are not presented. The trends exhibited again were similar to those shown for Walls 1 and 2.

7.5.3.7 First floor level deflection: Figure 7.74 shows the decomposition of first floor deflection into flexural, shear and fixed end components. The unaccounted for displacement is, as for the previous walls, larger for negative loading and represents 20% of the total observed deformation at $\mu_\Delta = -6$. Flexural deformation represents approximately 65% of the whole for positive loading, 45% for negative loading, while the fixed end rotation contribution is of the order of 10 to 15%. Thus shear deformations are, as would be expected, larger for negative loading, and become a slightly larger component of total deformation with increasing ductility.

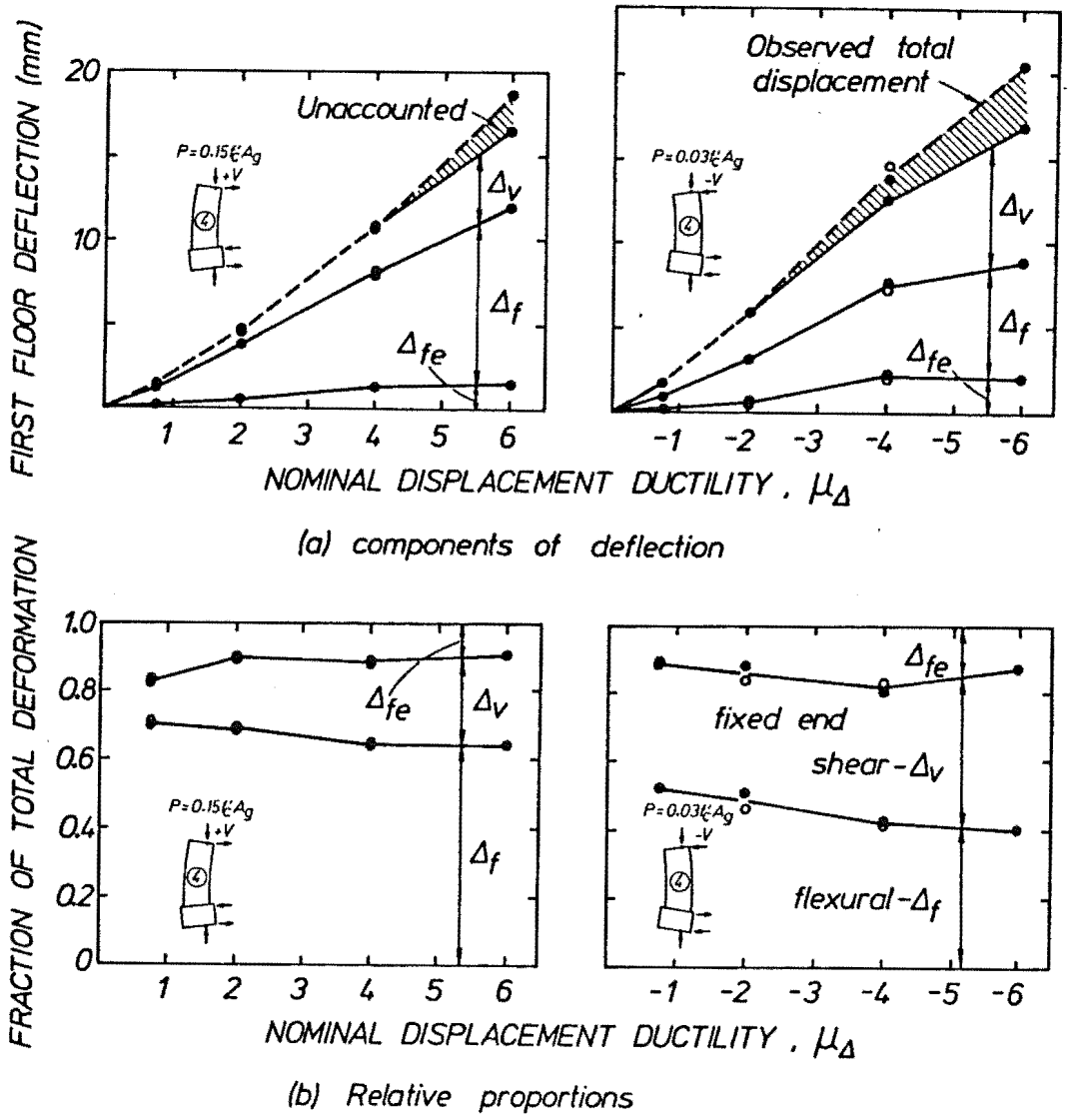

Fig. 7.74 First Floor Displacements - Wall 4.

7.5.3.8 Shear slip at wall base: Base slip, averaged from the two potentiometers mounted across the wall base block construction joint, is shown in Fig. 7.75 to be very small. The largest slip, at $\mu_\Delta = -6$, is less than 0.1% of the first floor height.

7.5.3.9 Out of plane displacement history: The out of plane displacement history of the east end of Wall 4 was monitored at four levels as indicated in Fig. 7.76. Prior to load point 60, these measurements were small (less than 1 mm) and are not shown. The overall impression given by this diagram is a less consistent pattern of lateral displacements as compared with the previous walls. The correlation

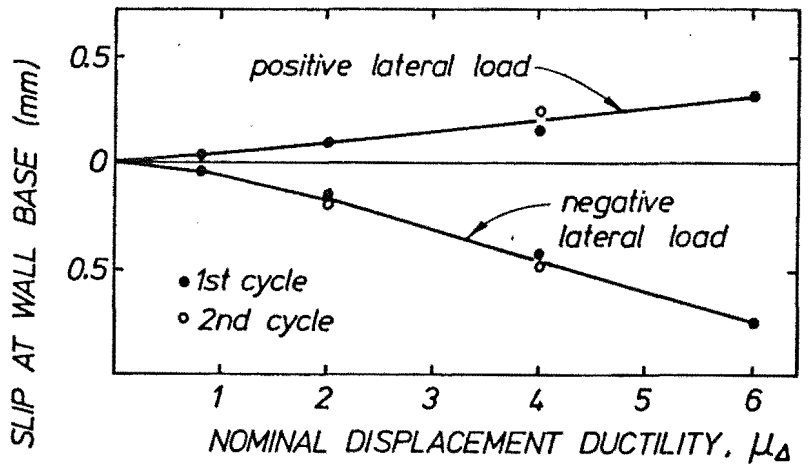

Fig. 7.75 Slip at Base Construction Joint, Wall 4.

between movements in one particular direction (north or south) and the sense of lateral loading is erratic. In addition, the potentiometers at the four levels do not indicate consistent trends over the whole first storey height. For example, while at load point 66 (μ_Δ = -2 for the second time) a local peak in northwards displacement is recorded at all four levels, a local southwards displacement peak occurs for most levels at load point 105 (μ_Δ = -4 first cycle). From load points 120 to 140 little variation in out of plane displacement occurred except at level 1. At load point 190, where lateral movement was clearly apparent at the time of testing, levels 3 and 4 of the wall (although displaced southwards) were actually moving northwards.

During the final positive loading sequence (load points 198 to 204) the wall moved slightly northwards with increasing lateral (and axial) load, as occurred for Wall 3. Again this is attributed to the development of an internal stress redistribution, whereby tensile south face strains reduced in order to provide the extra compression capacity needed to sustain the external loading. After failure, levels 1 and 2 were displaced southwards; levels 3 and 4 northwards. This less coherent lateral deformation history indicates a greater inherent resistance to instability than was shown by Wall 2, even though the latter sustained two full cycles at μ_Δ = 6 before buckling.

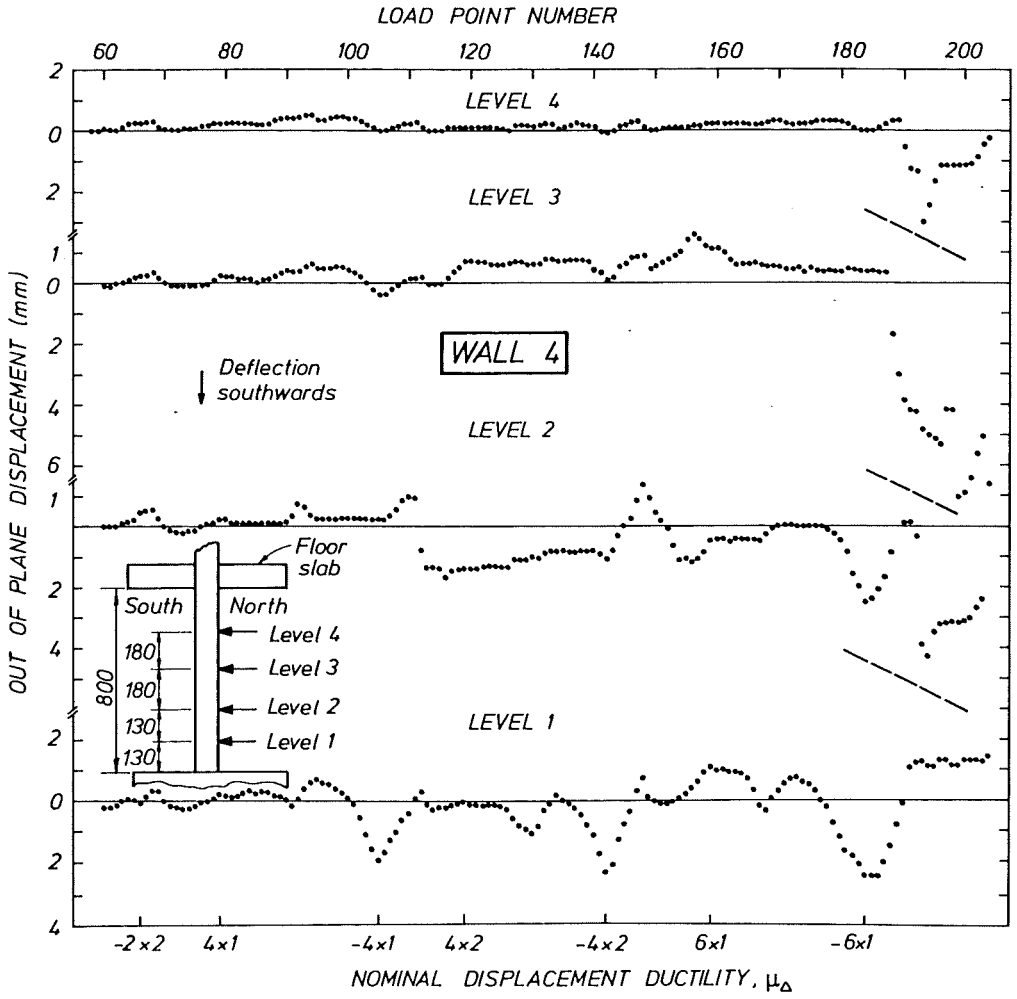

Fig. 7.76 Out of Plane Displacement History - Wall 4.

7.6 DISCUSSION OF IMPORTANT ASPECTS OF RESPONSE

This section contains a discussion of especially interesting or important aspects of response. A summary of the experimental behaviour of the four wall units tested is given in Section 7.7. Table 7.1 summarises the strength and deformation data of the units.

7.6.1 Pinching of Moment-Displacement Hysteresis Loops

The moment-displacement relationships presented for the four walls tested all exhibit pinching, or temporary loss in stiffness, during periods of low, increasing positive moment. This loop pinching causes a reduction in energy dissipation and is concurrent with out of plane movements of the wall compression zone.

TABLE 7.1 : SUMMARY OF STRENGTH AND DEFORMATION RESPONSE

Lateral Loading	WALL 1		WALL 2		WALL 3		WALL 4	
	+	-	+	-	+	-	+	-
1. P (kN)	1159	222	594	145	750	143	837	152
2. $\frac{P}{f'_c A_g}$	0.263	0.051	0.163	0.040	0.118	0.022	0.153	0.028
3. M_i (kN.m)	1280	-897	1057	-839	980	-584	1114	-703
SEE ERRATA 4. C_i (mm)	580	252	427	254	383	44	443	192
5. V_i (kN)	266	-309	263	-281	214	-202	236	-241
6. V_{design} (kN)	286	-343	307	-321	285	-243	326	-344
7. M_{max} (kN.m)	1466	-1158	1286	-997	1218	-883	1294	-916
8. M_{max}/M_i	1.15	1.29	1.22	1.19	1.24	1.51	1.16	1.30
9. V_{max} (kN)	329	-387	326	-340	287	-296	307	-308
10. V_{max}/V_{design}	1.15	1.13	1.24	1.21	1.01	1.22	0.94	0.90
11. v_{max} MPa	2.74	3.22	2.72	2.83	2.76	2.85	2.56	2.57
12. $v_{max}/\sqrt{f'_c}$	0.500	0.587	0.551	0.575	0.473	0.488	0.423	0.425
13. Δ_y (mm)	18.0	-16.0	14.0	-13.0	19.0	-15.0	17.0	-14.5
14. μ_Δ	3.7	-4.4	5.6	-5.6	5.5	-4.9	5.6	-5.2
15. θ_y (rad)	0.0036	-0.0034	0.0039	-0.0034	0.0046	-0.0026	0.0032	-0.0034
16. μ_θ	4.9	-7.2	6.5	-6.3	6.6	-6.6	8.4	-4.9
17 ϕ_y (rad/m)	0.0020	-0.0030	0.0022	-0.0018	0.0032	-0.0020	0.0030	-0.0020
18. μ_ϕ	12.6	-10.7	18.2	-9.6	11.3	-17.7	11.1	-13.3

Notes

1. Axial load (at wall base section) associated with peak moment.
2. Non-dimensional axial load.
3. Ideal flexural strength (based on measured material properties - see Table 6.2 and axial force P-Note 1.
4. Neutral axis position associated with M_i measured from east and west ends of wall for positive and negative lateral loading respectively.
5. Shear force (or lateral force) associated with M_i.
6. Design shear force.
7. Maximum observed flexural strength.
8. Ratio of M_{max} to M_i.
9. Maximum recorded shear force.
10. Ratio of V_{max} to V_{design}

(Notes continued on next page)

11. Maximum nominal shear stress = $V_{max}/(0.8\ell_w b_w)$.
12. Non-dimensionalized shear stress.
13. Top level yield displacement, estimated from the moment-displacement relationship. Δ_y values were calculated from the intersection points of best fit lines modelling pre and post-yield response. These lines were constructed by eye.
14. Maximum displacement ductility achieved, i.e. maximum imposed displacement normalised with respect to Δ_y.
15. Yield base rotation as determined from the moment rotation relationship (for rotations measured over the bottom storey regions). These may be regarded as plastic hinge rotations only in so far as the plastic hinge length may be taken as equal to first storey height.
16. Maximum rotational ductility.
17. Yield curvature, also as determined from the moment-curvature relationship.
18. Maximum curvature ductility.

Figure 7.77 illustrates the phenomenon. The distinct pinching of the loop over G A B is not accompanied by a similar effect over D E (see Figs. 7.7, 7.32, 7.56 and 7.68). At a particular displacement ductility level tangent stiffnesses at points G and B are similar to those at E and D respectively, while between G and A stiffness is at a minimum, and approximately half that at the aforementioned points.

The severity of the loop pinching may be assessed in terms of the reduction in the energy dissipation capacity of the section compared with a non pinching hysteretic response. Calculations (see Section 7.6.2) show that the loop area lost to pinching (area ABG, Fig. 7.77) is typically 10% of the actual loop area (area ABCDEFGA), where loop area is proportional to energy dissipation. Given this fact, and the observations that after the pinching phase stiffness increased and loops were very repeatable with minimal strength loss, the adverse influence of loop pinching on wall behaviour is minimal. Notwithstanding this, the mechanisms involved in this aspect of behaviour remain of interest.

The behaviour of Wall 4 is used to illustrate the following discussion. The load point sequences over which pinching was worst are (from Fig. 7.68) 49 → 52, 68 → 70 (μ_Δ = 2), 108 → 113, 145 → 149 (μ_Δ = 4) and 187 → 194 (μ_Δ = 6), where the last numbers are the points at which stiffness increases. These points are indicated on Fig. 7.78(a), the first floor deflection-moment hysteresis relationship for Wall 4. Also shown (Fig. 7.78(b) and (c)) are the shear and flexural deformation-moment relationships for the wall, where the deformations were calculated

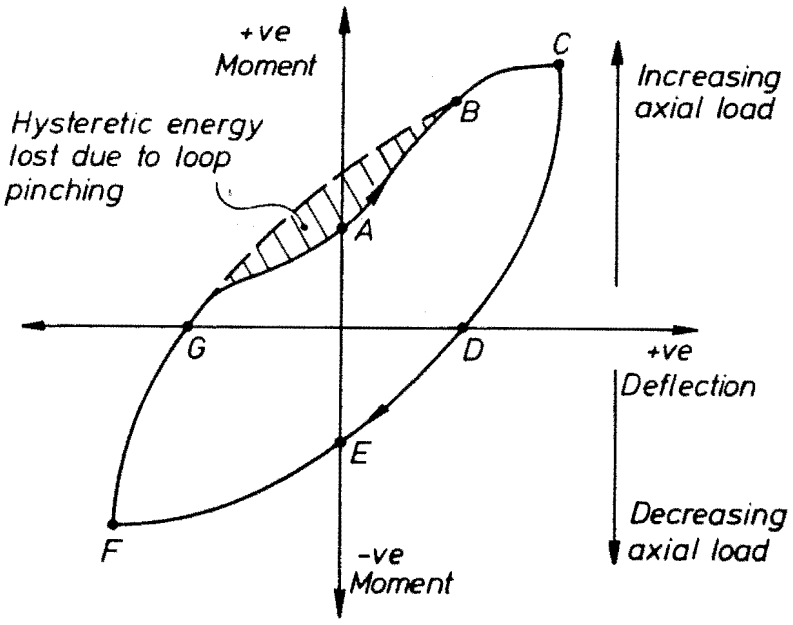

Fig. 7.77 Typical Form of Wall Moment-Deflection Hysteresis Loop.

from experimental measurements. The former illustrates the larger shear displacements associated with negative loading and a marked softening of response at low positive moments after excursions to μ_Δ = -4 and -6. After the considerably smaller positive shear displacements at μ_Δ = 4 and 6, there is only slight pinching of loops at low negative moments. The low axial load associated with negative loading lessens the efficiency of the aggregate interlock mechanism of concrete shear resistance [1]. Shear stirrup resistance must increase and diagonal shear-flexure cracks become wide to allow the development of adequate stirrup strains at high negative displacement ductilities. When loading is reversed (to positive) the neutral axis migrates eastwards and large shear displacements occurr across the open diagonal cracks before they close and the aggregate interlock mechanism stiffens response.

The flexural deformation-moment loop (Fig. 7.78(c)) encompasses relatively more area than the previous figure, especially in the positive displacement direction. This illustrates the better energy dissipation available via flexural yielding although the proportion dissipated by shear is certainly of value. (The ratio of moment to shear loop area at μ_Δ = 6 is 1.79 to 1). There is a slight degree of loop pinching at low positive load with no corresponding feature at low negative load.

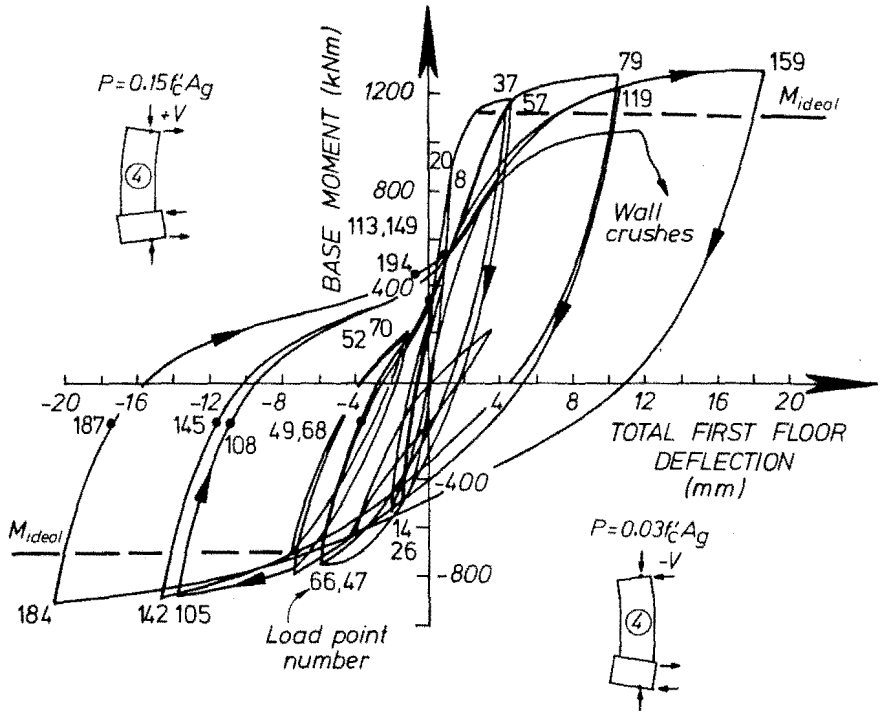

Fig. 7.78 (a) Moment-First Floor Total Deflection Hysteretic Response - Wall 4.

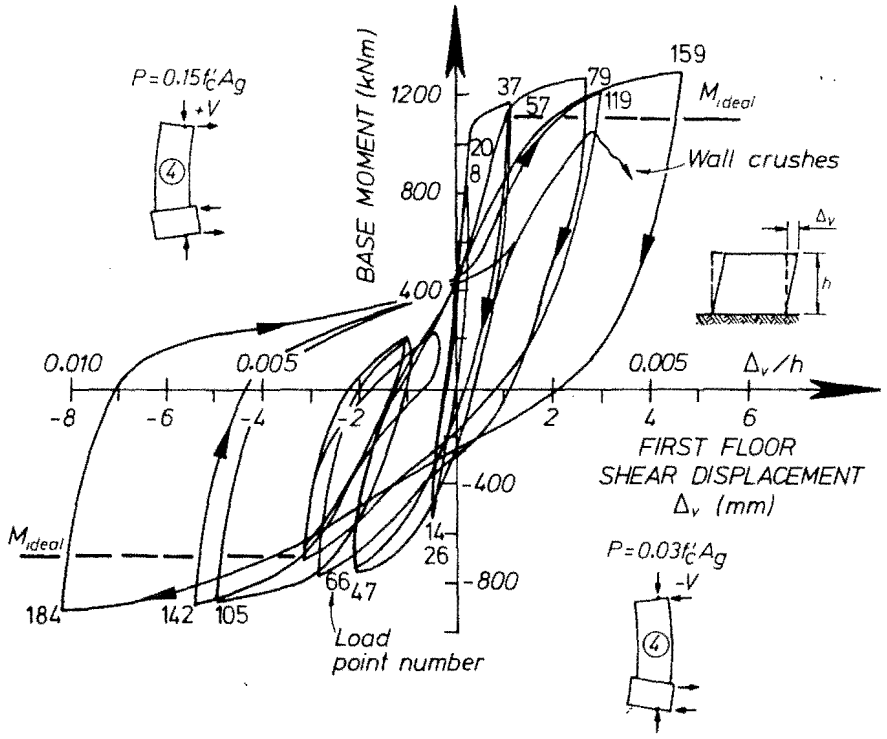

Fig. 7.78 (b) Moment-First Floor Shear Displacement Hysteretic Response - Wall 4.

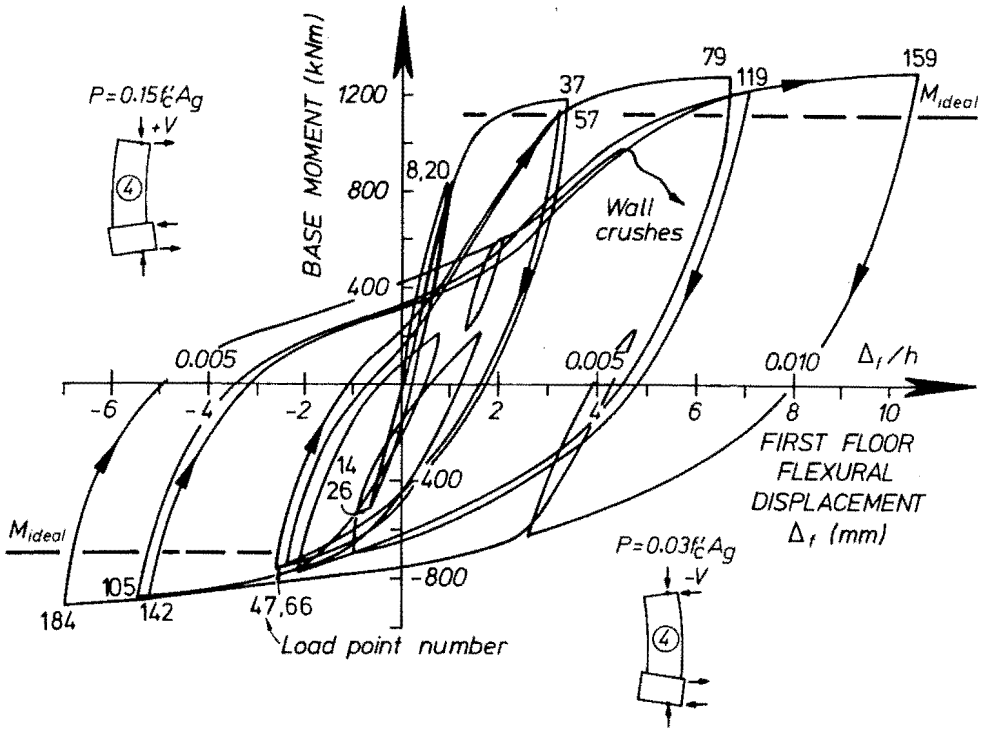

Fig. 7.78 (c) Moment-First Floor Flexural Displacement Hysteretic Response - Wall 4.

This pinching is attributable to the influence of changing axial load on tangent stiffness. Positive lateral loading (giving positive moment greater than 216 kN.m for Wall 4) and stepwise increasing axial load causes an increase in tangent stiffness which is visually more apparent after appreciable inelastic load cycling than at low deformation levels. This trend of increasing stiffness halts when the positive section strength is approached. Negative lateral loading (and decreasing axial loading) results in curves of continuously decreasing stiffness, devoid of apparent pinching. In this case, the softening is due to both a reducing axial force and the approaching of negative flexural strength.

In summary, the larger reduction in shear stiffness after, and as a consequence of, large shear displacement excursions and the effect of axial load on flexural stiffness combine to give a temporary reduction in total observed tangent stiffness.

7.6.2 Energy Dissipation

The areas described by the moment-top level deflection hysteretic loops, which are proportional to the energy dissipated via inelastic deformation, were determined at nominal displacement ductilities of 2, 4 and 6. In addition, the areas enclosed by bilinear response models

which best represented pre- and post-yield stiffnesses were obtained. The loop area lost due to the pinching phenomenon (Section 7.6.1) was also estimated by approximating curve G B by eye and determining area A B G (refer to Fig. 7.77). Table 7.2 shows that the bilinear model always overestimates actual response loop area, although less severely at higher deformation levels. Second cycle areas are as much as 30% less than first cycle areas. In normal design ~~practice~~ practice, however, SEE ERRATA specified material properties are used to calculate ideal member strenths. Probable or likely strength is thus underestimated, which compensates for the shortfall in actual loop area due to the bilinear idealisation. Loss in energy dissipation capacity due to loop pinching is of the order of only 10%.

These observations, together with a simple inspection of the hysteresis loops themselves, indicate that a bilinear modelling of wall hysteresis may considerably overestimate loading stiffness and energy dissipation. A hysteresis model such as that proposed by Takeda [28], which allows for a softened loading stiffness, appears to be more suitable. The generally good repeatability of loops suggests that an allowance for the degradation of stiffness due to repeated cycling at a particular displacement is of secondary importance.

Figure 7.79 shows a Takeda hysteretic model superimposed on the experimental moment-deflection relationship of Wall 4. Parameters α and β (see Fig. 3.11) were chosen as 0.3 and 0.0 respectively, and experimental initial and bilinear stiffnesses used. A good overall correlation between the experimental curve and the model exists, although a smaller value of the unloading parameter α would give a better fit for negative moment. The Takeda formulation, which is based on the behaviour of traditionally designed Japanese sections for which shear deformations are significant, appears to be suitable for the modelling of the experimental wall sections.

TABLE 7.2 : AREAS ENCLOSED BY MOMENT-WALL TOP DEFLECTION HYSTERESIS LOOPS

SEE ERRATA

Units = $kN.m^2$	WALL 1	WALL 2	WALL 3	WALL 4
$\mu_\Delta = 2$				
a. Bilinear	63.1	59.2	74.0	66.0
b. Actual 1st Cycle	30.6	22.8	29.1	32.0
c. 2nd Cycle	24.4	16.0	19.6	24.8
b:a	0.48	0.39	0.39	0.48
c:a	0.39	0.27	0.26	0.38
μ_Δ				
d. Bilinear	202.2	147.2	178.4	180.8
e. Actual 1st Cycle	102.5	72.9	83.2	102.4
f. 2nd Cycle	-	66.2	69.2	92.0
g. Loss due to Pinching	12.5	6.4	9.6	9.6
e:d	0.51	0.50	0.47	0.37
f:d	-	0.45	0.39	0.51
g:average of e and f	0.12	0.09	0.13	0.10
$\mu_\Delta = 6$				
h. Bilinear		233.6	291.2	276.0
i. Actual 1st Cycle		124.0	144.8	164.8
j. Loss due to pinching		9.2	18.8	16.8
i:h		0.53	0.50	0.60
j:i		0.07	0.13	0.10

TABLE 7.3 : WALL STIFFNESSES IN TERMS OF MOMENT - TOP DEFLECTION (UNITS = MN.m/m)

	WALL 1	WALL 2	WALL 3	WALL 4
Experimental values				
Positive Loading: K_o (1)	78	76	54	65
K_1	2.4	2.3	0.6	1.5
Negative Loading: K_o	44	61	38	55
K_1	5.3	4.6	3.5 (2)	3.3
Positive bilinear factor	0.03	0.03	0.01	0.02
Negative bilinear factor	0.12	0.08	0.09	0.06
Calculated values				
Positive loading: K_o	74	69	59	83
Negative loading: K_o	69	69	54	81

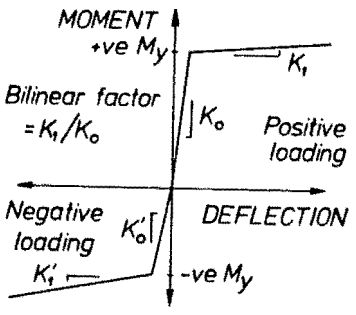

Notes: (1) See adjacent diagram

(2) Measured between $\mu_\Delta = -4$ and -6

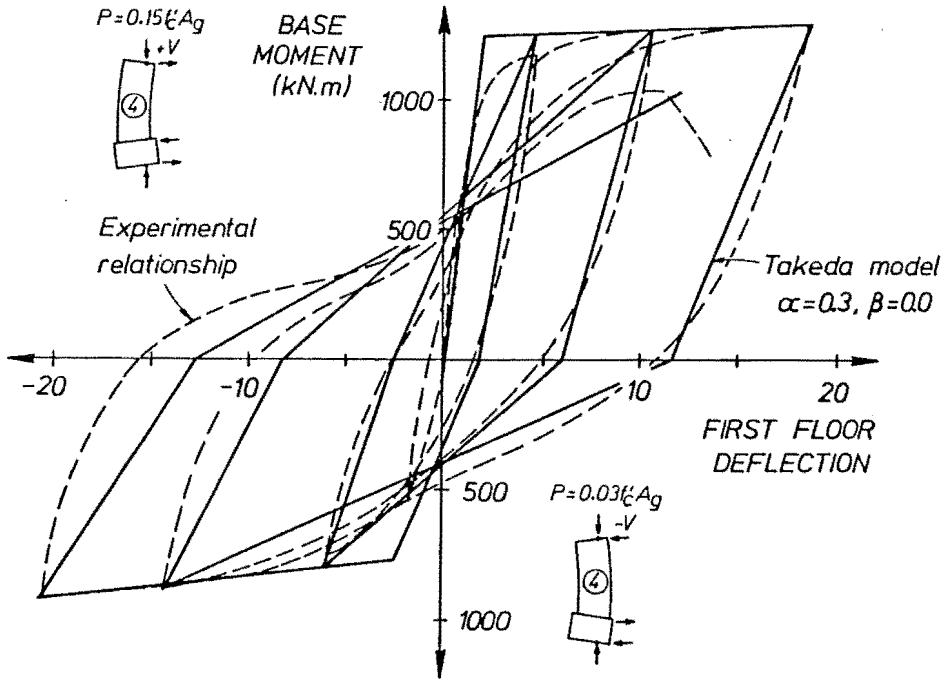

Fig. 7.79 Takeda [28] Modelling of Wall 4 Response.

7.6.3 Moment-Displacement Stiffness

Initial loading stiffness (K_o) and post yield stiffness (K_1) for positive and negative load were estimated from the moment - top level deflection hysteresis loops (Table 7.3). Bilinear factors are also shown, although it should be noted that different factors would be obtained from moment-rotation or moment-curvature relationships. The trends of greater positive initial stiffness and negative bilinear stiffness are clearly shown, however.

In addition, K_o values calculated using a method proposed by Paulay [39] are shown. This method requires the calculation of an effective second moment of area using a cracked section-transformed area approach. Concrete moduli of elasticity of 25 GPa (Walls 1 and 2) and 30 GPa (Walls 3 and 4) were used, these values reflecting the relative concrete compression strengths of the walls. Effective second moments of area were approximately $0.5I_g$ and $0.4I_g$ for positive and negative loading respectively. Flexural, shear and anchorage deformations were then estimated. The respective proportions of these components of deformation were consistently close to 0.75 : 0.10 : 0.15.

Experimental positive loading stiffnesses are reasonably well estimated by the calculated values, while the calculated negative loading stiffnesses are consistently high. The relative proportions of the three deformation components may be compared with the experimentally obtained proportions at μ_Δ = 3/4 (Figs. 7.21(b), 7.46(b), 7.62(b) and 7.74(b)). For positive loading there is generally good agreement. For negative loading however observed shear deformations constitute approximately 40% of the total and flexural deformations are thus less than the calculations indicate. Underestimation of shear deformations is responsible for the high calculated values of negative loading stiffness.

SEE ERRATA

7.6.4 Confining Reinforcement

7.6.4.1 Strain levels encountered: The provision of confining reinforcement in the compression region of the potential plastic hinge zone of a structural wall must address the two inter-related issues of quantity and placement. In this section the results of the four wall unit tests are used to examine these questions, and formulate recommendations for design practice. (The current New Zealand code provisions relevant to confinement are summarised in Section 6.2.6.2).

Table 7.4 shows observed neutral axis depths (i.e. the extent of the compression regions) and several derived ratios for the walls at peak positive displacement ductilities. The experimental values were determined at the actual critical sections of the walls, generally gauge level 3, some 300-500 mm above the theoretically critical section at the wall-base block interface. Strain readings at north and south faces of the wall were averaged and a linear strain profile between east and west end strains assumed. In some cases, due to the influence of out of plane or transverse bending, large differences between "north face" and "south face" compression block depths exist. Neutral axis positions at first and second cycles to a given deformation level were averaged. Also shown are the compression block depths associated with the ideal positive flexural strength (c_i in Table 7.1) and the extent of hoop reinforcement, the so-called confined depth. The values of neutral axis position for Wall 2 at μ_Δ = 4 and 6 are almost certainly in error, although a cause for this could not be found.

TABLE 7.4 : NEUTRAL AXIS POSITIONS FOR POSITIVE LATERAL LOADING

Units = mm	WALL 1	WALL 2	WALL 3	WALL 4
1. c_i (I)	580	427	383	433
2. c (μ_Δ = 2)	560	405	564	712
3. c (μ_Δ = 4)	690	279	502	637
4. c (μ_Δ = 6)	-	273	499	648
5. Confined depth (II)	326	228	340	326
6. Confined depth/c_i	0.56	0.53	0.88	0.75
7. Confined depth/c(μ_Δ = 6)	0.47 (III)	0.84	0.68	0.50

Notes:

I. Neutral axis depth, measured from east end of wall, associated with ideal moment strength.

II. Depth of section supplied with closely spaced sets of hoop reinforcement.

III. Actually for μ_Δ = 4.

TABLE 7.5 : MAXIMUM CONCRETE COMPRESSIVE STRAINS IN THE WALL UNITS

Displacement Ductility	WALL 1		WALL 2		WALL 3		WALL 4	
	unconfined zone	confined zone	unconfined zone	confined zone	unconfined zone	confined zone	unconfined zone	confined zone
μ_Δ 4 x 1	0.0111	0.0196	0.0022	0.0079	0.0086	0.0172	0.0105	0.0175
μ_Δ 4 x 2	-	-	0.0029	0.0087	0.0086	0.0184	0.0111	0.0183
μ_Δ 6 x 1	-	-	0.0040	0.0123	0.0150	0.0266	0.0139	0.0249
μ_Δ 6 x 2	-	-	0.0071	0.0137	-	-	-	-
Prior to Failure	0.0088	0.0136	tension	tension	0.0243	0.0350	0.0257	0.0363

Walls 1, 3 and 4 all exhibited material failure mechanisms resulting from the high compression strains implied by the large neutral axis depths. The ratios of confined depth to ideal and actual compression block depths show the actual confined region of the compression block to be considerably smaller than expected. At $\mu_\Delta = 6 \times 1$, the code provision for half the compression zone to be confined is well satisfied by Walls 3 and 4, although this degree of confinement was demonstrably insufficient to allow a second excursion to $\mu_\Delta = 6$.

Table 7.5 indicates peak core concrete and unconfined concrete compression strains, again calculated at the actual failure zone (above the base) using the plane sections hypothesis and linear interpolation between measured strains. In this way, the most probable peak compression strains due to both lateral loading and (unintentional) out of plane displacements were obtained. Core strains were determined at the north east or south east corner of the confined region, the cover concrete having spalled. Strains in the unconfined concrete were calculated at the north or south face of the (unspalled) wall, at the plain concrete - core interface, i.e. the westernmost end of the core. The measurements indicate high levels of plain concrete strains in Walls 1, 3 and 4 at $\mu_\Delta = 4$ and 6 and it is surprising that a material compression failure did not occur sooner for these units. Immediately before failure, the derived plain concrete strains are very high for Walls 3 and 4; the relatively low value for Wall 3 is due to the last pre-failure readings being made at a low deformation level ($\mu_\Delta \cong 2$). Wall 2 strains, admittedly of dubious accuracy, are considerably lower. It is emphasized that the strain calculations are heavily dependent on the assumption of linear strain profiles.

Core strains are also high, but apparently non critical, given the generally low levels of hoop strain encountered. Hoop strains were generally below yield level for Walls 1, 2 and 3, with higher (and probably spurious) strains recorded in Wall 4 hoops only.

The information presented suggests that in regions where hoop reinforcement was supplied, it was adequate. The material failures observed in Walls 1, 3 and 4 could probably have been averted by the provision of hoop reinforcement further back in the sections. Thus detailed,it is believed that these walls could also have sustained larger out of plane displacements and that their failure mechanism would have been either that shown by Wall 2 - out of plane buckling, or compression failure of the confined core region.

The considerable transverse displacements exhibited by Wall 3 (Fig. 7.65) suggest that a buckling failure would have occurred, probably after a second excursion to $\mu_\Delta = -6$, had more extensive hoop reinforcement been provided. The high axial load and small out of plane displacements of Wall 1 (Fig. 7.25) suggest a compression failure in the core. However, as shown by Wall 3, (Fig. 7.64) out of plane displacements and thus the potential for buckling can increase very rapidly. The conjectured mode of failure of Wall 4, should more extensive hoop reinforcement have been supplied, is, for similar reasons, uncertain.

7.6.4.2 Design Recommendations

The present code [34] requires hoop confinement in the outer half of wall compression zones when the design neutral axis depth exceeds a critical value (Eqs. 6.1 and 6.2). This critical depth is primarily a function of the structural type factor S [9] and the flexural overstrength factor ϕ_o, both of which are related to the ductility demand expected on the section. S varies from 5 for an elastically responding structure to 0.8 for walls in a ductile, slender coupled wall system. These latter elements are detailed the same way as cantilever structural walls. The maximum implied displacement ductility demand (μ_Δ) is $5/0.8 \simeq 6$. Although it is suggested [9] that for reasonably regular frames, four fully reversed cycles to a ductility of 4 constitutes a reasonable performance criterion, no such criterion exists explicitly for structural wall elements. While it is acknowledged that for ductile walls $\mu_\Delta = 6$ may be required, this extreme demand will probably occur only once and other, lesser, demands will occur with greater frequency, e.g. 2 cycles at $\mu_\Delta = 5$, 5 cycles at $\mu_\Delta = 3$, etc. It may reasonably be presumed that compliance by a wall with the four cycles at $\mu_\Delta = \pm 4$ criterion would enable such occasionally larger demands to be sustained. The overstrength factor also influences

the ductility demand on a section: a value of ϕ_o in excess of the normal value ($\cong$ 1.4) means that the wall is stronger than the design S factor requires and thus a lesser ductility capacity than is implied by that value of S may be needed.

It is considered that the extent of the well confined region of a structural wall ought to depend on the ductility demand implied by the S and ϕ_o factors. This may conveniently be achieved by incorporating the critical compression block depth c_c (a function of both S and ϕ_o) in the estimation of that region which ought to be well confined, as indicated subsequently. Figure 7.80 illustrates the critical section strain profiles for a wall in the cases when (1) the neutral axis depth is equal to c_c, (2) $c > c_c$, i.e. high axial load may be present. Typical S and ϕ_o values of 1.0 and 1.4 have been used in Fig. 7.80. The ultimate curvature demand ϕ_u is assumed to be the same for both cases. It is further assumed that it is necessary to confine all concrete which is subjected to strains in excess of 0.004 at the attainment of ϕ_u. The present codified approach requires the provision of hoop reinforcement over the outer half of the compression block when $c \geq c_c$. For case (1) (Fig. 7.80) when $c = c_c$ no confinement is required although the hoop reinforcement supplied to prevent inelastic bar buckling will in fact provide some confining action. For case (2) where $c > c_c$, the region where $\varepsilon_c > 0.004$ is αc, and it is this region of the section, rather than the outermost 0.5c, where hoop confinement ought to be supplied. From the geometry of the figure, $c = \alpha c + c_c$, whence $\alpha = 1 - \frac{c_c}{c}$. Somewhat more conservatively, if a maximum strain of only 0.003 is permitted in the unconfined region, from Fig. 7.80, $c = \alpha c + \frac{3}{4} c_c$, whence $\alpha = 1 - 0.75 \frac{c_c}{c}$, or say

$$\alpha = 1 - 0.7 \frac{c_c}{c} \qquad (7.1)$$

whenever $c_c/c < 1$. When c is just a little larger than c_c, Eq. (7.1) would give a very small and rather impractical value for α. In line with current code recommendations [34] it is suggested that when $c_c/c < 1$, at least one half of the theoretical compression zone be confined, i.e. $\alpha \geq 0.5$.

Equation 7.1 was used to calculate the relative depth of confinement, i.e. α factors, for the wall units tested (with positive lateral load). The results are summarised in Table 7.6. An S factor of 0.8 is justified when the walls are considered as parts of a coupled wall structure.

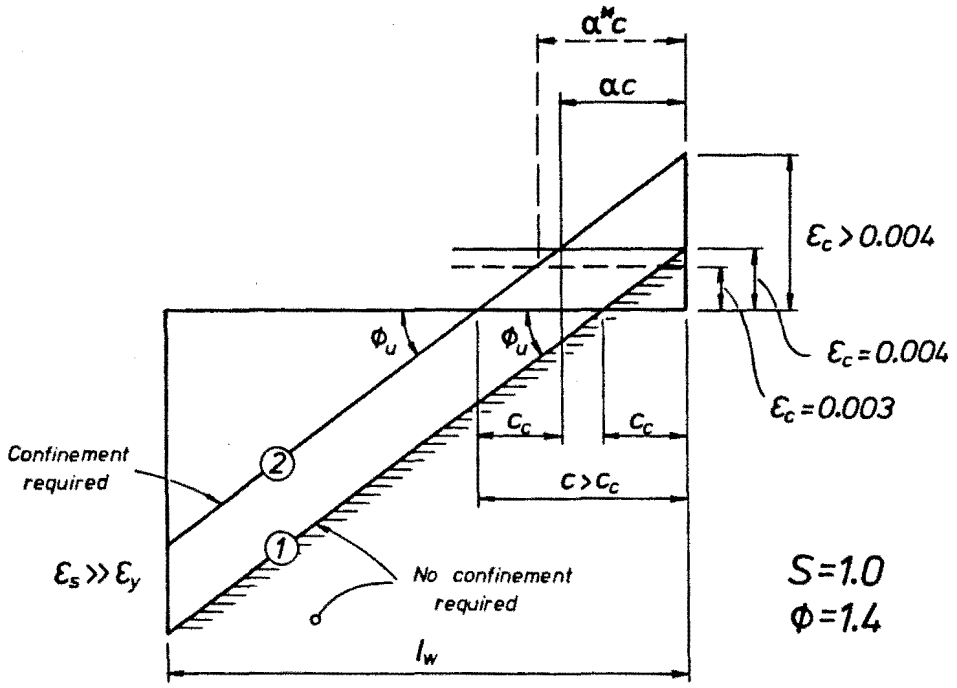

Fig. 7.80 Strain Patterns for a Rectangular Section Wall.

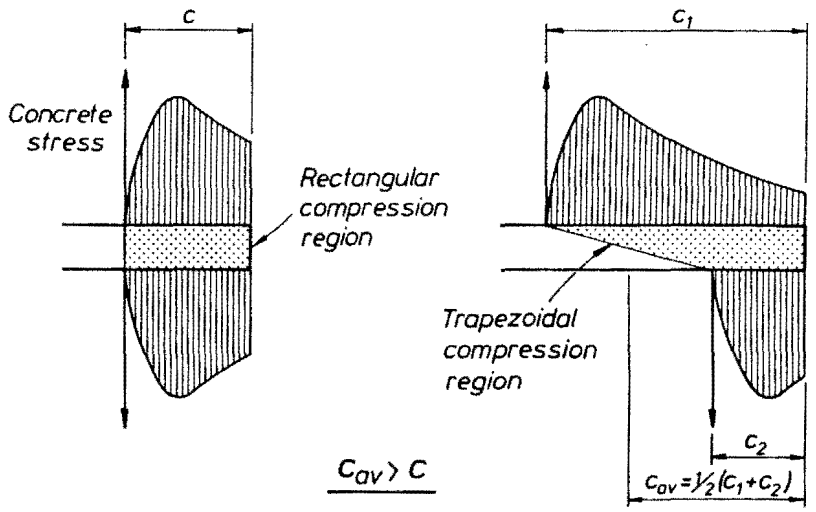

(a) No out of plane bending (b) Significant out of plane bending

Fig. 7.81 Skewing of Wall Stress Distributions due to Out of Plane Bending.

TABLE 7.6 : EXTENT OF HOOP REINFORCEMENT FOR WALLS USING PROPOSED DESIGN METHOD

Wall	ϕ_o (1)	c_c mm (2)	c_i mm (3)	c_i/ℓ_w	α (4)	α (5)
1	1.32	159	580	0.39	0.81	0.77
2	1.31	158	427	0.28	0.74	0.69
3	1.30	136	383	0.29	0.75	0.70
4	1.30	156	433	0.29	0.75	0.70

Notes: (1) Calculated from the interaction diagrams of Appendix D using actual axial force (Table 7.1) and assuming the ideal strength to be related to a hypothetical "code" strength demand by a factor ϕ = 0.9. The values of ϕ_o are somewhat less than the typical values of approximation because the ideal strength calculations were based on reinforcement yield strength of 440 MPa rather than the nominal 380 MPa which would normally be used.

(2) Calculated as $0.1\phi_o S\ell_w$, where S = 0.8.

(3) From Table 7.1

(4) From Eq. (7.1).

(5) Based on ϕ_o = 1.56 which would normally be used for f_y = 380 MPa.

The table indicates that in accordance with the proposed requirement for the extent of hoop confinement embodied in Eq. (7.1), the wall units tested would have required hoop reinforcement over approximately the outer 75% of the theoretical compression block. Row 6 of Table 7.4 indicates the actual confined proportions of the compression zones for the wall sections. Units 3 and 4 comply with the requirements of Eq. (7.1), so that no improvement in the performance of these two walls would be expected from the proposed requirement. It is likely, however, that the material compression failure of Wall 1 could have been delayed significantly had α = 0.81 been used. Wall 2 did not exhibit distress attributable to high compression strains.

It should be noted that this scheme for determining the required extent of hoop confinement is based on the ideal neutral axis depth determined from an ACI type calculation [27]. As has been demonstrated (Table 7.4), this value may be considerably less than the actual average neutral axis position of a wall unit at significant displacement ductilities. This increase in neutral axis depth is due to three main factors:

1. As strains increase, cover concrete capacity decreases as splitting and spalling occurs, necessitating an increase in compression block depth if axial force is to be maintained. This effect is particularly severe for the model walls tested,wherein the cover constituted an abnormally large proportion of the gross section. ACI [27] strength calculations were made ignoring the cover concrete subjected to strains in excess of 0.003 at $\mu_\Delta = 6$ (4 for Wall 1) as determined from the experimental observations. Compression block depths up to 20% in excess of those values in column 3 of Table 7.6 were indicated.

2. Significant strain gradients in the out of plane sense were recorded in all walls (e.g. Wall 2, Fig. 7.50). This induces a skewed rather than rectangular stress block (Fig. 7.81). Because of the nature of the concrete stress-strain relationship, whereby stress decreases with high inelastic strain, this skewness must increase nonlinearly if axial and flexural capacity is to be maintained. Thus the average neutral axis depth, $0.5(c_1 + c_2)$, as calculated from experimental data and presented in Table 7.4 for example, is larger than the theoretical value c (Fig. 7.81). In this way out of plane displacements have the effect of increasing average neutral axis depth.

3. Because of the strength degradation accompanying the cyclic loading of even well confined concrete to a particular displacement ductility [57], neutral axis depth must progressively increase to maintain the compression load on the wall. This is indicated by the wall curvature distributions shown previously (Figs. 7.10, 7.35, 7.58 and 7.70), wherein at high ductilities second cycle curvature generally equals or exceeds the first cycle value.

The notion of requiring confined depth to be a function of expected neutral axis depth, calculated for a specific ductility demand, is, although theoretically attractive, impractical in the context of routine design procedures. The proposed scheme embodied in Eq. (7.1), and based on a standard strength design calculation, is believed to offer a simple and rational improvement to wall confinement allocation. The existing code equations governing the quantity of hoop reinforcement required (Eqs. 6.3, 6.4) are believed to be adequate, and no alteration to these is proposed. The testing of otherwise identical walls with a range of hoop reinforcement content, using a constant extent of confinement, would need to be conducted to allow an assessment of these equations to be made.

7.6.5 Shear Strength

A capacity design approach was used for the apportioning of shear reinforcement in the walls (see Appendix D). The design shear force (based on an assumed flexural reinforcement overstrength) was generally exceeded during the tests, as shown in Table 7.1. Stirrup strain readings presented earlier generally show peak strains of less than ε_y at $\mu_\Delta = \pm 2$, increasing to approximately $2\varepsilon_y$ at $\mu_\Delta = \pm 4$ or 6. The highest recorded strain was 0.011 (Wall 4). Distributions of stirrup strain (Figs. 7.13 and 7.38) indicate that these high strain zones correspond with major diagonal cracks and strains in other parts of the stirrups are significantly less than ε_y. The increase in strains with displacement ductility is due to (a) an increase in section strength and, primarily, (b) the increased width and spreading of diagonal cracks which accompanies flexural yielding. Despite the high stirrup strains recorded in some areas, overall shear response was good with no significant deterioration of shear resistance observed. The maximum nominal shear stresses sustained (Table 7.1) were considerable in terms of stresses envisaged by Reference 34.

Table 7.7 indicates the concrete shear resistance, v_c, required at the development of the peak nominal shear stresses, v_{max}, assuming full stirrup yield force develops. The codified allowable concrete resistance is $0.6\sqrt{P/A_g}$ (Eq. (6.9)), while the peak demand of $0.\overset{81}{\cancel{66}}\sqrt{P/A_g}$ was met without distress. Although the tests reported were not specifically designed to examine the adequacy of the code approach to shear design [34], shear resistance was good and the design method was proved adequate. SEE ERRATA

TABLE 7.7 : MAXIMUM DERIVED CONCRETE CONTRIBUTION TO SHEAR STRENGTH OF THE STRUCTURAL WALL UNITS

	WALL 1		WALL 2		WALL 3		WALL 4	
1. Loading Sense	+	-	+	-	+	-	+	-
2. v_{max} MPa	2.74	3.22	2.72	2.83	2.76	2.85	2.56	2.57
3. v_s MPa	2.54	2.54	2.54	2.54	2.15	2.15	2.37	2.37
4. v_c MPa	0.20	0.68	0.18	0.29	0.61	0.70	0.19	0.20
5. $\sqrt{P/A_g}$ MPa	2.78	1.21	1.99	0.98	1.99	0.87	2.36	1.00
6. $v_c/(\sqrt{P/A_g})$	0.07	0.56	0.09	0.29	0.31	0.81	0.08	0.20

Notes:

1. Sense of lateral load, positive or negative.
2. Maximum nominal shear stress, from Table 7.1
3. Shear stress resisted by stirrups = $(A_v f_y)/(b_w s)$, where
   A_v - area of 2 stirrup legs, mm^2
   f_y = stirrup yield strength (Table 6.2), MPa
   b_w = wall web width (= 100 mm), and
   s = stirrup spacing (= 100 mm, walls 1, 2 and 4, 80 mm wall 3)
4. Concrete shear stress = $v_{max} - v_s$
5. P = axial force at maximum shear stress (Table 7.1) and
   A_g = gross section area, m^2
6. Ratio of rows 4 and 5.

7.6.6 Out of Plane Instability

The mechanism of the development of out of plane instability or buckling in a susceptible region of a structural wall, as exhibited most clearly by Walls 2 and 3, is described with reference to the test arrangement and established sign conventions.

7.6.6.1 Description of mechanism

1. At high negative ductilities, large tensile strains are imposed on east end longitudinal reinforcement (Point A, Fig. 7.82). Wide, approximately horizontal cracks are present across the extent of the confined region at the east end of the wall (Fig. 7.83(a)).

2. Unloading from high negative displacements (i.e. reducing lateral load) is accompanied by an increase in axial load. The point of zero

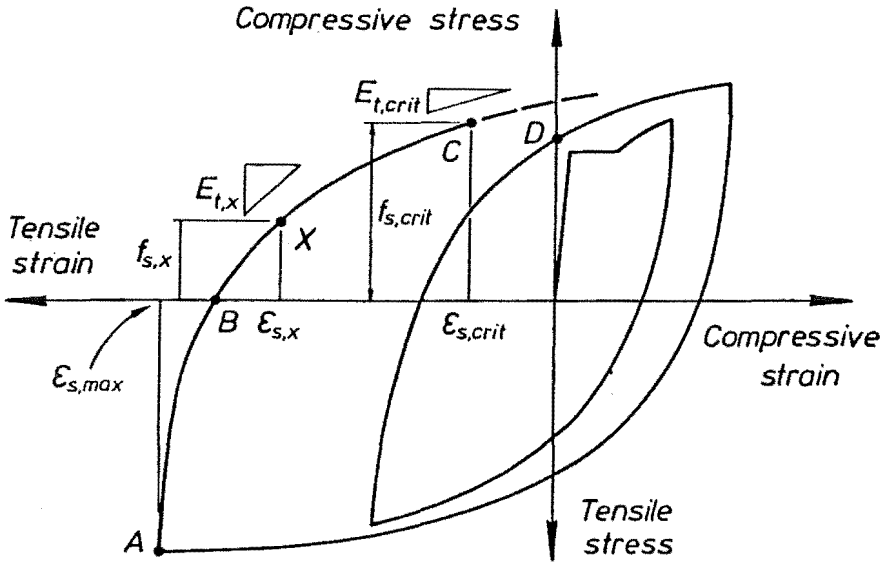

Fig. 7.82 Reinforcement Stress-Strain Relationship Prior to Buckling.

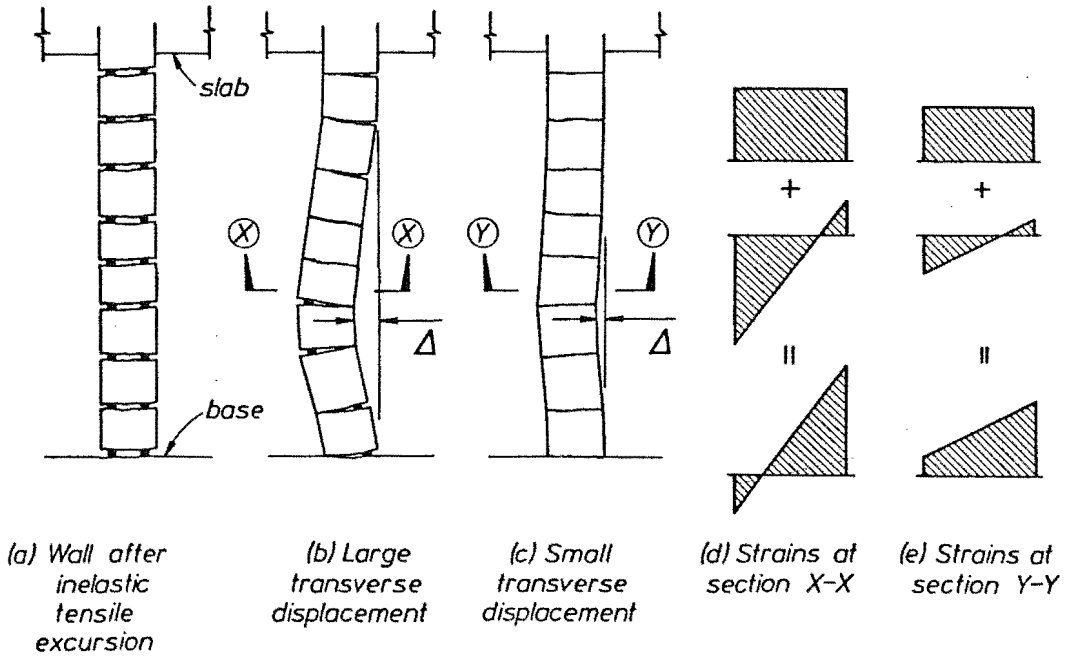

Fig. 7.83 Deformations and Strain Patterns in a Buckling Zone.

stress in the longitudinal reinforcement (Point B, Fig. 7.82) is reached when tensile strains associated with negative lateral loading,still present are balanced by compression strains due to both axial load and the positive moment caused by axial load eccentricity. From this point further reversal from negative loading induces compression stresses in the reinforcement.

3. With continued loading, reinforcement compressive stresses increase in the potential buckling zone, the longitudinal bars sustaining all the compression force,assuming cracks to be still open. This will be the case if sufficiently large negative deformations were imposed and the bars retain some residual tensile strain.

4. Out of plane buckling (Fig. 7.83(b) and (c) will occur at a stage when the tangent modulus of the reinforcement reaches a critically small level while residual tensile cracks are still open (Point C, Fig. 7.82). The modulus of each layer of bars will be different, as will the compression load they sustain. The boundary conditions on the first storey wall panel are complex, with partial transverse rotational restraint at the base block and floor slab levels, and restraint of the west end of the wall due to a tensile stress field there (Fig. 7.84). In addition vertical stresses over the height of the first storey panel are not constant (due to the applied lateral loading), so that the tangent Young's modulus of each layer of bars also varies with height. Nonetheless, a critical condition may develop at which transverse instability of the eastern part of the wall does occur. If the horizontal cracks close before a critical condition is attained (Point D, Fig. 7.83), concrete compression stresses will develop and greatly stiffen the section, effectively prohibiting transverse instability of the reinforcement.

5. Assuming buckling to have occurred, transverse displacements will cease if and when the section can develop a redistributed stress state which permits the resistance of both longitudinal loading (lateral and axial forces) and the effective transverse loading caused by the out of plane eccentricity of these "longitudinal vertical forces". The deformations needed to achieve this stress state may be considerable.

6. Continued increases in lateral and axial load effectively increase the out of plane loading on the section. In order that both types of loading be equilibrated, the net compressive stresses, and the transverse gradient of these stresses, must continue to rise, and the high transverse curvatures that result serve to further increase out of plane displacements. The behaviour of Walls 2 and 3 illustrate the range of response to this

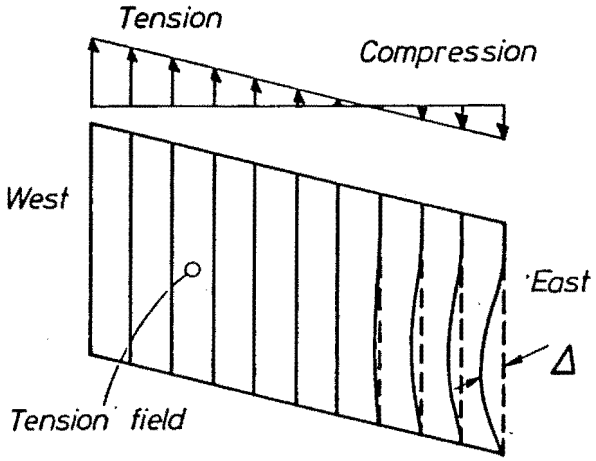

Fig. 7.84 Buckling Pattern for a Wall Panel.

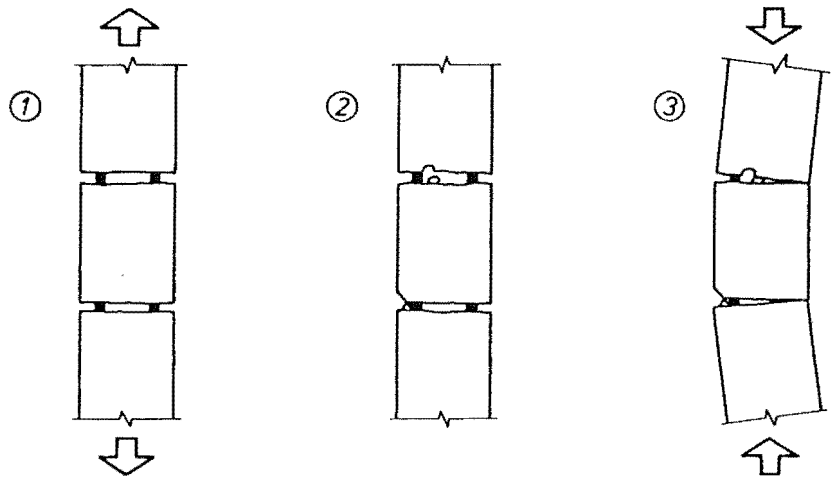

Fig. 7.85 Effect of Aggregate Disturbance on Wall Instability.

very severe loading situation, discussed as points 7 and 8.

7. Out of plane displacements may continue to increase rapidly, even if increases in lateral and axial loading are slight. This is especially likely if crack widths are still wide immediately prior to initial instability, and consequently large out of plane displacements occur from the outset of buckling. The flexural resistance associated with such deformations is not sufficient and instability is not arrested. Wall 2 behaved in this manner.

8. After the initial instability, out of plane displacements may not increase markedly. This will happen when initial out of plane displacements are small, a situation which may arise when residual crack widths prior to buckling are small, or where only a small part of the wall panel buckles due to the stability afforded by those parts of the wall that are in tension. Subsequent increases in lateral and axial loading may take place without significant changes in transverse displacement. However, at high positive displacement ductilities high compression strains will develop. In view of the stress-strain behaviour of concrete, confined or otherwise, whereby stress decreases with increasing high strain, a larger compression area will be required to provide the compression force. This deepening of the compression block may raise strains in the concrete outside the confined core to an untenable level and a material compression failure, as occurred for Wall 3, results.

9. The desired positive displacement ductility may be achieved despite the out of plane deformations on the section. On unloading from this point, the out of plane deformations may be reduced by the straightening of the east end longitudinal bars when they are put in tension. Nevertheless, on the next load reversal from a high negative ductility, the east end of the wall is likely to have been left with some residual out of plane displacements which increase the tendency for further displacements.

7.6.6.2 Additional factors affecting stability: The foregoing discussion has ignored,or mentioned only briefly,several important considerations. These are discussed as follows.

1. The effect of disturbance of aggregate particles. A mechanism long believed to influence the transverse stability of slender sections is illustrated in Fig. 7.85. It is postulated (and unfortunately not verified experimentally despite the sensible nature of the mechanism) that aggregate disturbed during tensile loading may partially block full closure of the attendant horizontal cracks. On load reversal, the uneven closure of these cracks may result in an eccentricity of axial load which induces

a transverse (destabilising) moment on the section. This is clearly a random, unpredictable process which may act with or against other destablising influences.

2. Effect of shear forces. Although shear force levels were low at times when critical conditions existed for out of plane buckling, shear deformations are believed to have two possible effects on stability:

(a) shear displacements will contribute to random aggregate misfit which may or may not enhance out of plane deformations,

(b) shear displacements cause earlier contact of crack faces (upon load reversal) and hence the development of internal concrete forces which stiffen the potential buckling zone.

3. The effect of cyclic loading. The strain history of longitudinal reinforcement is a critical paremeter related to out of plane instability. The most important aspect of strain history is the magnitude of the tensile strain which occurs prior to compression of the potentially unstable zone. This may be sufficient to allow large steel compression stresses and a very low tangent modulus to develop while tensile cracks are not yet fully closed. Specimen 3, a barbell section wall tested by Vallenas [56] exhibited an out of plane buckling failure when lateral load was reversed after essentially monotonic loading to a displacement ductility of approximately 8. In this case, the behaviour was influenced by the local buckling of some longitudinal bars which occurred prior to complete load reversal. Cyclic loading of small amplitude is not sufficient in itself to induce out of plane instability.

4. The effect of axial load level. Axial load level is a further important parameter, and although high loads cause more adverse conditions, sections with low axial forces are undoubtedly prone to out of plane buckling. The stress-strain condition of the reinforcement in the region of potential instability is of primary importance, with the relative contribution to compression stresses of direct (axial load) or indirect (lateral load) actions a secondary concern. High axial load will be more likely to cause the material compression failures which are accelerated by transverse instability. The compression block depth measured in terms of the parameter c/ℓ_w is more significant than the axial load alone, as it takes account of section geometry as well.

5. The effect of cover spall: uneven spalling of cover concrete has previously been postulated as a cause of out of plane instability failure [56]. Uneven spalling may dictate the direction of out of plane displacements but is not considered to be an unduly significant contributory

factor to the buckling phenomenon, provided that confining reinforcement is present. The load carrying capacity of cover concrete becomes low at comparatively small compression strains, although actual spalling may not occur until significantly larger strains are attained.

6. Spacing of hoop reinforcement. In addition to confining the core concrete, hoop reinforcement also provides the longitudinal bars with restraint against local buckling. It has been assumed that sufficient restraint is available to the flexural reinforcement to prevent local bar buckling when tension cracks are about to close. Given this, the effect of hoop spacing on initial wall instability is minimal. However, hoop spacing, as it affects confinement, is obviously of importance.

7. Scale of the wall section. Because of the small scale of the wall units (approximately 1/3 - 1/4 full size) and the use of 10 mm thick cover concrete, the section geometry was somewhat atypical of prototype design. In particular, the transverse distance between the primary reinforcement layers along the north and south faces of the units (56 mm = $0.56b_w$) was significantly less than what would be typical for a prototype wall ($\simeq 0.65b_w$) This parameter (raised to the second power) strongly influences the out of plane rigidity of the wall at the critical time when compression is being transferred across residual tensile cracks via the bars only. Because of this factor, the experimentally tested units may indicate the onset of buckling earlier than would be expected for prototype walls.

8, Analytical model: the development of an analytical model describing the out of plane buckling of wall sections was considered beyond the scope of this experimental study. Such a model ought to recognise the following factors:

(a) the geometry of the wall,
(b) the axial and flexural load history,
(c) realistic cyclic stress strain behaviour for reinforcement and concrete,
(d) modelling of the boundary conditions of the wall panel, including the stiffening effect of the tension zone,
(e) the resistance of out of plane (P-Δ) moment on the section after initial Euler-type instability,
(f) partial recovery of the critical zone with load reversal,
(g) allowance for imperfect crack closure and aggregate disturbance.

A finite element approach, whereby the wall panel is modelled as an assemblage of small regions, may be suitable. Section 8.4.7 outlines a very simple analytical model based on the behaviour of the prism units discussed in the next chapter.

7.6.6.3 Design recommendations: On the basis of this experimental study, it is considered that the present codified [34] dimensional requirement for wall thickness to equal or exceed one tenth the clear wall height in potential hinge regions need not be changed. The adequacy of performance of the units is difficult to assess because of the absence of an explicit codified performance criterion. It was observed that Wall 4, with a web width to floor height ratio of 1:8 sustained only one full cycle at $\mu_\Delta = 6$, whereas Wall 2 (with a slenderness ratio of 1:10 and presumably more prone to instability) sustained two cycles at $\mu_\Delta = 6$. However, this observation alone is not considered sufficient justification to require a slenderness limitation more severe than 1:8 for example. The 1:10 constraint is often difficult enough to satisfy. The proposed increase in the extent of hoop confinement (Section 7.6.4) will not prevent the onset of out of plane instability, but it should delay the material failure observed to be associated with such instability.

It is suggested that wherever possible, boundary elements should be supplied at the ends of structural walls because of their stabilizing influence. (Such elements are often required from considerations other than that of stability, e.g. to form a column element into which transverse beams are framed).

The stablizing potential of flange elements or cross walls was not investigated, as it was clear that plain rectangular sections are most susceptible to instability. Thus, no modifications to the codified provisions regarding these elements are suggested.

7.7 SUMMARY OF EXPERIMENTAL RESPONSE

1 General Behaviour During Testing

Widespread shear-flexure cracks developed early in the tests and subsequent deformations concentrated at these locations. Crack spacing was lower in regions reinforced with deformed bars, i.e. at the extremities of web and flange elements. Concrete cover suffered vertical splitting and loosening at a displacement ductility of 2 and spalling at the east face of the units was widespread at $\mu_\Delta = 4$. All walls initially demonstrated flexural yielding, which was not significantly affected by shear deformations. Testing was terminated with material compression or out of plane buckling failures as detailed subsequently.

2. Failure Mechanisms

Wall 1 sustained a material compression failure initiated in the unconfined concrete adjacent to the confined core, spreading westwards into the section and causing a compression failure in the overloaded core. The failure, which occurred while loading towards $\mu_\Delta = 4 \times 2$, was not influenced by out of plane deformations and is attributable to the high axial load ($0.26f'_c A_g$) present on the unit.

Wall 2 suffered significant loss of lateral load resistance after the second fully reversed cycle at $\mu_\Delta = 6$. The east (compression) end of the unit developed a large out of plane displacement over the full first storey height. Wall geometry was such as to give a storey height to wall thickness (i.e. slenderness) ratio of 10:1, equal to the maximum code permitted slenderness [34].

Wall 3 developed a material compression failure of east end plain and core concrete while approaching $\mu_\Delta = 6 \times 2$. Large out of plane displacements occurred on reloading from $\mu_\Delta = 6 \times 1$ and large lateral displacement ($\mu_\Delta \simeq 4$) at the time of failure combined to produce unsustainable compression strains on the south face of the wall.

Wall 4, with a slenderness ratio of 8:1 rather than 10:1 cf. the preceding units, also demonstrated a compression failure in the confined concrete zones of its east end. Out of plane displacements were present prior to failure but these were not indicative of full storey instability (as in Walls 2 and 3) and were considered to be less instrumental in causing the failure.

3. Moment-Displacement Hysteresis Response

The moment-displacement relationship for the units confirmed the generally excellent nature of response. Loops are full and show only a small loss in energy dissipation capacity, i.e. pinching. Repeated cyclic loading produced a stable repeatable response with little stiffness or strength degradation. Both positive and negative strength increased with increasing displacement ductilities up to 6. The variation in axial load concurrent with lateral force is responsible for the generally greater stiffness with positive lateral loading and the unsymmetrical nature of the response curves.

4. Moment-Curvature Relationships

A good correlation exists between theoretical monotonic moment-curvature relationships and experimental points forming an envelope of actual response. Observed pre-yield stiffness is estimated reasonably

well by the analytical value, while post yield comparisons of strengths show discrepancies of 10% at most.

5. Wall Curvature Distributions

Wall curvatures were measured over the bottom storey and indicate approximately linear distributions at μ_Δ = 2, 4 and 6. Curvatures at the second lowest gauged level are often unexpectedly low, believed to be because of the fortuitious contribution of deformations at the boundaries of that area to curvature at levels 1 and 3. Inelastic strains in flexural reinforcement were recorded above the floor slab level. The curvature distributions suggest effective plastic hinge lengths of $l_p \simeq 2/3\ell_w$ although this is influenced by the relatively steep moment gradients used. (Design shear spans (ℓ_v) of approximately 2 and 3 were used for negative and positive loading respectively - see Appendix D). Slender prototype walls are likely to have larger shear spans, i.e. less steep moment gradients and thus a wider spread of plasticity and larger plastic hinge lengths, but a reduced effect of diagonal tension, i.e. tension shift.

6. Strains in Shear Reinforcement

Levels of shear force sustained by the sections were, as a result of the varying eccentric axial loading used, generally similar for positive and negative lateral loading. Maximum nominal shear stresses ($v = V/(0.8\ell_w b_w$ of 0.42 to $0.57\sqrt{f'_c}$ MPa were applied to the units. Maximum stirrup strains in the plastic hinge region were approximately constant with height and generally less than yield strain at $\mu_\Delta = \pm 2$, and less than $2\varepsilon_y$ at $\mu_\Delta = \pm 4$. Some local strains of up to 1% were recorded where gauges coincided exactly with major diagonal cracks. Strains showed little increase from the first to second excursions to a particular deformation level, indicating minimal degradation of the concrete shear resistance mechanism during the relevant two cycles. Although some high stirrup strains were recorded, the design method for shear resistance is considered adequate, as discussed in Section 7.6.4.

7. Hoop Strains

Strains measured in the east end hoops of all walls were generally less than ε_y even at $\mu_\Delta = 6$, when the applied axial load was large necessitating the highest degree of confinement. It is considered that the satisfactory performance obtained prior to the eventual failure of the units indicates that both the amount and the configuration of the hoop reinforcement provided was adequate. This is in spite of the fact that at high deformation levels, the reinforcement supplied was considerably less than would be required by the code. There is evidence which suggests that

the provision of hoop reinforcement deeper into the sections of Walls 1, 3 and 4 would have prevented or delayed the material failures exhibited by these units. West end hoop reinforcement, supplied in quantities required for antibuckling purposes only, was almost always below yield strain level and frequently strained to less than $0.5\varepsilon_y$. Cover concrete, which was generally not badly degraded at the west end of the walls, is believed to have been effective in assisting the prevention of bar buckling.

8. Longitudinal Bar Strains

Above the base block, yield progressed up the bars with increasing displacement ductility, reaching the level of $0.5\ell_w$ at $\mu_\Delta = 2$ and ℓ_w at $\mu_\Delta =$ Maximum tensile strains of approximately 3% were recorded. Because tensile strains exceeded compression strains, gauges often indicated residual tensile strains when the bars were sustaining a compressive load. This phenomenon was also noted in bars embedded in the base block where yield penetration was up to a length of $24d_b$ at $\mu_\Delta = 6$.

9. First Floor Deflection

The fixed end, flexural and shear components of lateral deflection at the first floor level were derived separately from experimental measurements and compared with the observed deformations. Actual displacement was generally underestimated, the discrepancy increasing with μ_Δ to as much as 15% of the observed total value, although the agreement is often considerably better than this. Fixed end(anchorage) deformations constituted approximately 10% of the total for both directions of loading, the function decreasing somewhat with increasing μ_Δ. The proportion of flexural deformations also decreased with increasing displacement, and was of the order 60 to 70% for positive loading and 40 to 50% for negative loading. Shear deformations consequently increased in importance during the tests and were a greater proportion of the whole for negative loading than for positive loading because of the lower axial load present for the former situation. Shear stiffness was low at times of change from negative to positive lateral loading, when wide diagonal cracks existed and shear resistance from the aggregate interlock mechanism was low.

10. Wall Elongation

An almost linear growth in wall centreline height, attributable to the accumulation of residual tensile strains, was observed with increasing μ_Δ. Elongation was larger at negative displacement ductilities, but still appreciable for positive ductilities despite the higher axial compression loads present.

11. Shear Slip at Wall Base

Slip across the base level construction joint was minimal and made up less than 5% of total first floor deformations in most cases. This shear deformation was greater for negative lateral loading due to the adverse influence of the accompanying low axial load. Slip was not constant along the base, being greatest in the lightly reinforced central region of the walls.

12. Out of Plane Deflection History

The diagrams of out of plane displacement at the east end of the walls versus load point number show initially oscillatory deflections which gradually acquire a northwards or southwards bias. With compression loading on the east end of the wall, out of plane displacements increase (northwards or southwards), and on reversal of the lateral load to give tension at the east end, these out of plane deformations recover somewhat. The largest changes in out of plane displacement occurred when the axial/lateral load combination was sufficient to yield the main east end longitudinal reinforcement in compression and close the cracks which had opened under previous negative lateral load. Walls 2 and 3 displayed good out of plane stability prior to the first cycle of loading to $\mu_\Delta = -6$ after which instability increased markedly. The out of plane deflection history of Wall 4 showed inconsistent trends at the monitored levels, suggesting that the tendency for out of plane instability over the storey height reduces with decreasing wall slenderness.

Chapter Eight BEHAVIOUR OF AXIALLY LOADED PRISMATIC UNITS

8.1 INTRODUCTION

After the tests on the cantilever wall units, the potential for out of plane instability was further investigated by observing the behaviour of prismatic bodies subject to cyclic tensile and compressive strains. Alternate tension and compression intended to model the strain regime imposed on the end zone of a structural wall subject to reversing lateral load. Figure 8.1 illustrates the wall elements under consideration. The use of these subassemblage elements rather than models of complete wall units meant considerable savings in experimental effort.

The prisms were constructed to various heights to thickness (i.e. slenderness) ratios and subjected to uniform strains of magnitudes typical of those imposed on structural wall end zones during seismic attack. During periods of compression loading, the units were constrained to behave as short pin-ended columns. The out of plane movement of these units was monitored, together with gross vertical deformations and strains in hoop reinforcement.

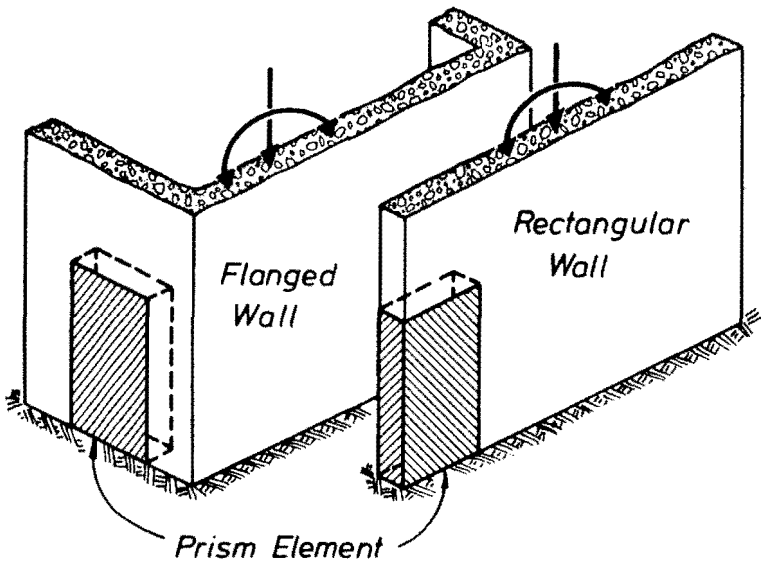

Fig. 8.1 Location of Prism Elements in Prototype Walls.

This experimental programme was intended to provide insight into the mechanism of out of plane inelastic buckling,and stimulus for the formulation of a suitable mathematical model that could be used for theoretical predictions. The tests did not fulfill expectations, however, due to an oversight in the modelling of the end conditions of the prisms. For this reason the results of the tests are not discussed in the detail with which the model wall tests were described. Although disappointing, the prism tests do offer some additional insight into the phenomenon of inelastic instability. The testing methods used, the units themselves and typical performance during testing are described subsequently.

8.2 DESCRIPTION OF THE PRISM UNITS

The design of the prism units was somewhat arbitrary with respect to size but was influenced by the desire to use close to full size and realistic materials. The dimensions, reinforcement contents and material strengths of the prisms are summarised in Table 8.1, while Fig. 8.2 illustrates a typical unit. All units were of cross-sectional dimensions 160 x 480 mm with 6 pairs of evenly spaced HD16 longitudinal bars providing a gross reinforcement ratio of 0.0314. Initially 4 prisms were constructed giving a height between end rollers (Fig. 8.3) of 1120 mm. This corresponds to an effective slenderness ratio (height between end rollers : prism width) of 7 : 1, while subsequent units were constructed at ratios of 5.5 : 1 and 4 : 1. In view of the behaviour of Wall 2 (Fig. 7.31) where buckling occurred at an effective pin-ended slenderness ratio of approximately 7 : 1, these slenderness ratios were expected to span the transition range over which instability in prototype structures would be prevented.

Hoop reinforcement was provided with R5 or R6 bars, both nominally mild steel, with measured properties as shown in Table 8.1. Assuming the prisms to be parts of structural walls designed to satisfy code [34] provisions for confinement (see Section 6.2) and that $0.10 \leq c/\ell_w \leq 0.15$, Equation 6.4 was used to estimate appropriate hoop reinforcement contents. Assuming f'_c = 25 MPa and using measured hoop yield strengths, this equation required single hoop leg areas of approximately $0.48s_h$ and $0.38s_h$ mm^2 for R5 and R6 bar respectively, where s_h is the vertical hoop spacing in mm.

TABLE 8.1 : DIMENSIONS, REINFORCEMENT CONTENT AND MATERIAL PROPERTIES OF PRISM UNITS

Prism Number	1	2	3	4	5	6	7	8	9
1. Slenderness ratio	7:1	7:1	7:1	7:1	7:1	5.5:1	5.5:1	4:1	4:1
2. Height between pins, mm	1120	1120	1120	1120	1120	880	880	640	640
3. Size of hoop bars	R5	R6	R6	R5	R5	R5	R5	R5	R5
4. Hoop pitch, mm	64	64	96	64	64	64	64	64	64
5. Volumetric hoop ratio, ρ_s	0.0067	0.0096	0.0064	0.0067	0.0067	0.0067	0.0067	0.0067	0.0067
6. Concrete strength[1], MPa	24.1	24.1	24.1	24.1	29.0	29.0	29.0	29.0	29.0
7. Reinforcement properties		HD16			R5			R6	
8. f_y, MPa		442			290			350	
9. ε_y		0.0022			0.0014			0.0018	
10. f_u, MPa		660			410			510	
11. Yield plateau length		$4\varepsilon_y$			$12\varepsilon_y$			$3\varepsilon_y$	

Note: (1) Compression strength at time of prism testing.

The tie spacing most commonly used (64 mm = 4 x diameter of HD16 bars) corresponds to bar areas of $0.3ls_h$ and $0.44s_h$ for R5 and R6 hoops respectively. The code antibuckling requirements (Section 6.2) were satisfied for all units.

Prism reinforcing cages were tied using steel end templates (Fig. 8.2) to keep the longitudinal bars evenly spaced. In the case of prisms 5 - 9, all longitudinal bars were strengthened over the end regions as indicated in Fig. 8.2(a). Resistance strain gauges were attached to hoop legs in the transverse direction and provision was made for the attachment of longitudinal and transversely mounted potentiometers. The units were poured using concrete with 20 mm aggregate size and a target 28 day compression strength of 25 MPa. External instrumentation consisted of the 4 control potentiometers (Section 8.3), 3 sets of 4 potentiometers mounted at the corners of the prism to monitor axial strains in the top, central and bottom thirds of the units, and pairs of transversely mounted potentiometers used to monitor out of plane displacements (see Fig. 8.2(b)).

8.3 EXPERIMENTAL SET-UP AND TEST PROCEDURE

Figure 8.3 shows the assembly used to test the prism units. It indicates the various components involved. Prior to installation in the Dartec Universal Test Machine, the prism was attached via the protruding longitudinal bars (A)+ to the steel end plates (B) using welded connections (C). The bars were preheated to 400°C prior to welding and the connections performed well before testing. The 60 mm thick end plates were provided with slotted holes to pass 10 high strength bolts (D) which attached the prism to circular reaction plates (E). These standard reaction plates were in turn attached to the Dartec cross head (top) or ram (bottom) via 6 - 2" bolts (F). The end plates (B) were provided with seats to accommodate 50 mm diameter rollers (G) top and bottom, and roller seats (H) were placed between these rollers and the reaction plates. Provision was made for a plaster packing joint at the bottom roller seat (I).

During compression loading, force was transmitted from the Dartec ram to the prism ends (templates) directly via the reaction plate, roller and end plate. The longitudinal bars were not directly loaded in

---

+ This and subsequent letters refer to parts labelled in Fig. 8.3.

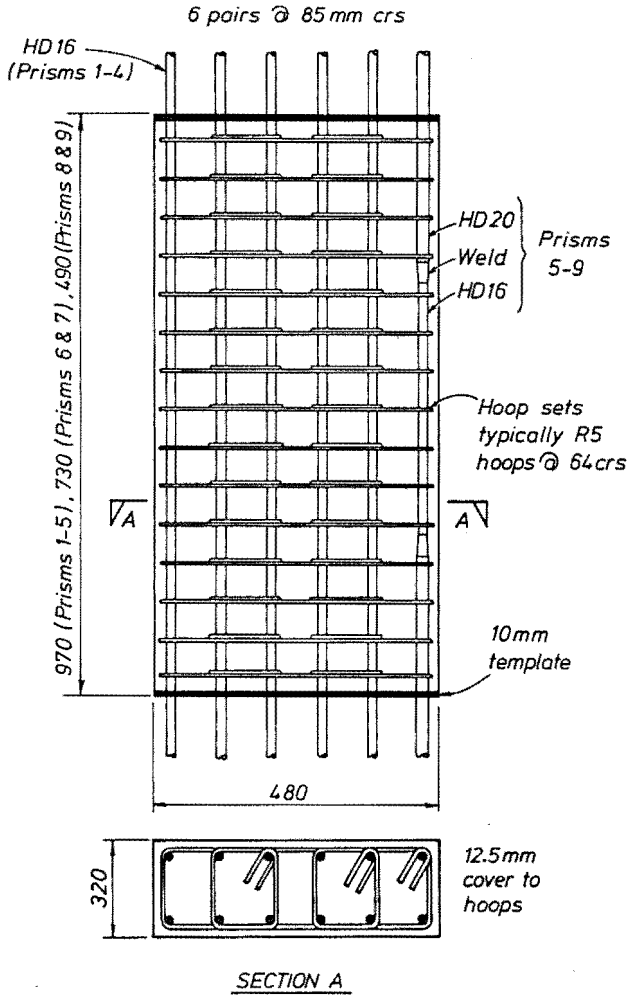

(a) Hoop and longitudinal reinforcement.

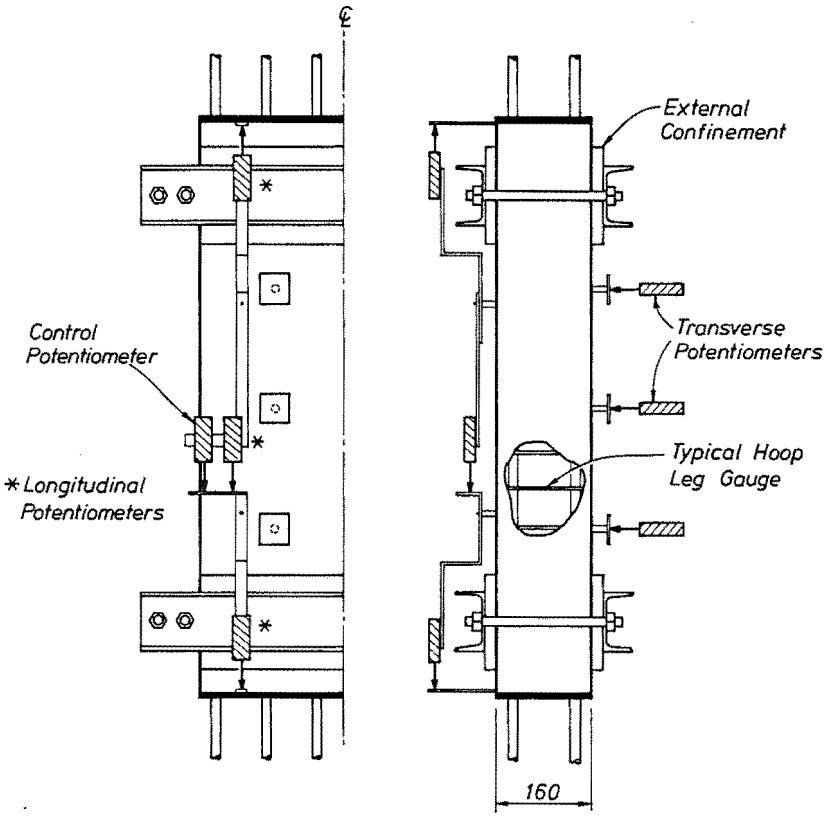

(b) External instrumentation and confinement.

Fig. 8.2 Typical Prism Details.

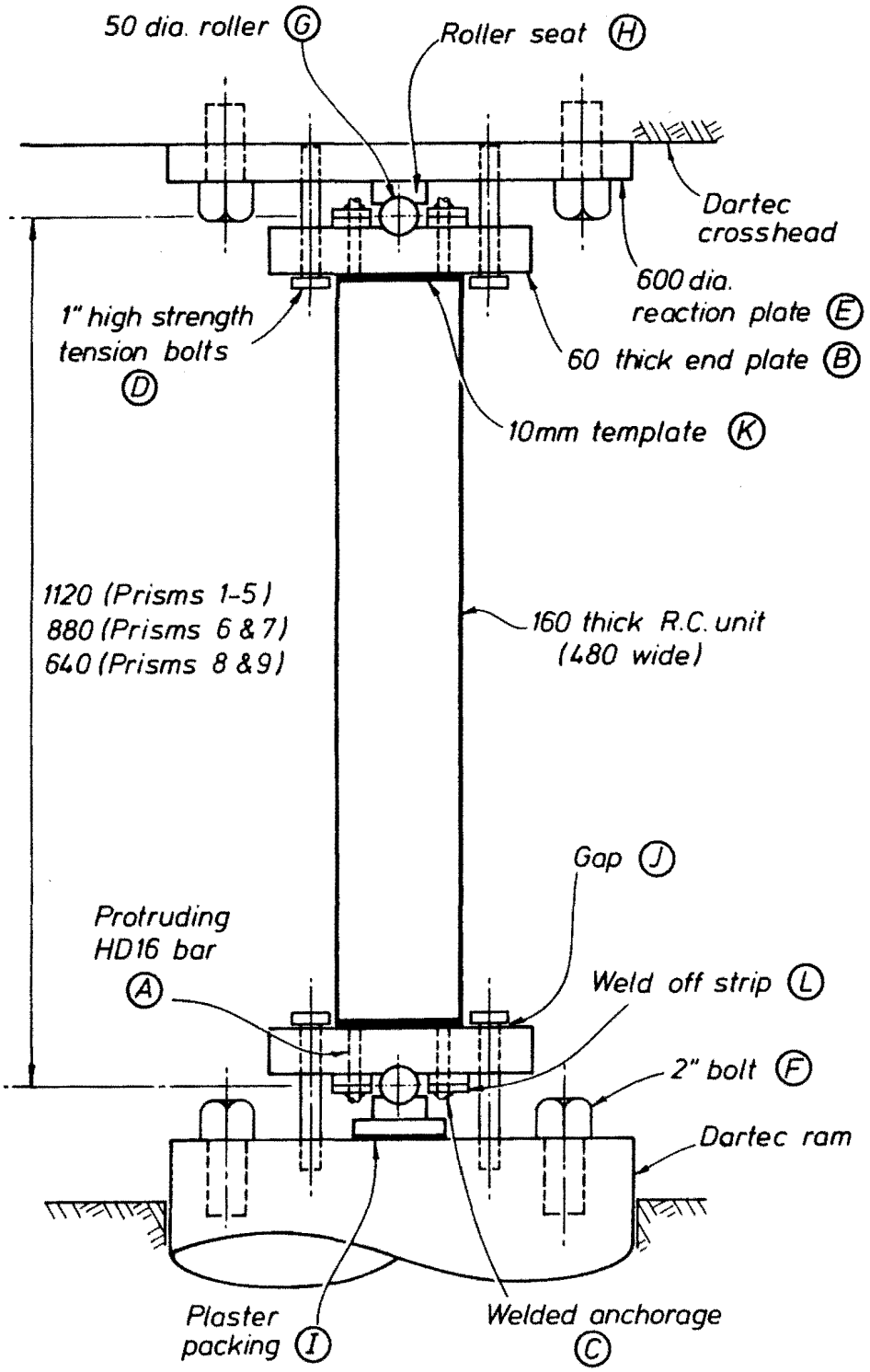

Fig. 8.3 Elevation Showing the Prism Testing Assembly.

compression at the prism ends. Tensile loading on the longitudinal bars was transmitted from the Dartec ram via the load path 2" bolts, reaction plate, 1" high strength bolts, end plate, and welded anchorages. During compression loading, the 1" bolts (D) were not tightened hard against the end plates, but left with a gap (J) to allow the rotation of the prisms ends which would accompany transverse instability.

The tests were controlled by the average strain measured over the central 4 control potentiometers (Fig. 8.2). With the test machine in stroke control, axial deformations were applied to give the desired tensile or compressive strain. The prisms were tested at increasing levels of strain with two fully reversed cycles imposed before deformation levels were incremented.

8.4 BEHAVIOUR OF THE PRISM UNITS

8.4.1 General Description

Prism 1 was tested without the external confining plates shown in Fig. 8.2(b). Damage was concentrated in the upper third of the prism, although the test was controlled by central region strains, which, during compression loading, were much smaller than upper level strains. Out of plane deformations did increase during testing. The concentration of damage at the ends of the prism was due to the deterioration of the compression force transfer mechanism between the concrete at the ends of the prism and the longitudinal bars. This mechanism is discussed in Section 8.4.5. In order to lessen end zone damage, external confining plates (Fig. 8.2(b)) were fitted to the succeeding prisms. The testing of prism 1 was halted when the plastic elongation of the bars protruding from the prism ends became sufficient to cause the weld-off strips (item L, Fig. 8.3) to foul the roller seats (item H, Fig. 8.3). In an attempt to reduce this elongation (and also reduce bond deterioration in the end regions), prisms 5 → 9 were provided with strengthened longitudinal bars as indicated for one bar in Fig. 8.2. This practice, in conjunction with the external confining plates, was effective in forcing damage to occur primarily in the central region of the units.

Prisms 2 and 4 behaved in a similar manner to prism 1, with damage concentrated outside the central region, and instability evident only at the end of the testing. Prism 3 was tested under monotonic loading and behaved well (see the load-strain curve of Fig. 8.5(a). Prism 5, the last of the most slender units, had damage concentrated in the central

region and behaved otherwise as units 2 and 4. Cover loss on the west face of the unit was accompanied by eastwards out of plane displacements.

Units 6 and 7, of height to thickness ratio 5.5 to 1, had damage concentrated relatively evenly on all faces and sustained greater inelastic deformations before finally exhibiting out of plane instability. Prisms 8 and 9 sustained even larger strains and although some out of plane displacements developed during testing, the failure of these was associated with crushing of the concrete rather than out of plane instability.

Some units (of each size) developed longitudinal bar bond failure, whereby some bars, especially corner bars, slipped at the ends right through the body of the prism during compression loading. These bars thus contributed very little to the compression strength of the affected units.

8.4.2 Load-Axial Strain Relationship

Figure 8.4 shows several axial force - strain relationships, the strains being calculated from the averaged readings of the four potentiometers at a particular level of load. The concentration of compression strains in the end regions of the units may be deduced from a comparison of Figs. 8.4(a) and (b), which are typical of the response of prisms 1 and 2 as well. Degradation of compression strength with strains in excess of 0.004, and with repeated loading to a given strain is evident, while tensile strength, as would be expected, increases with increasing strain. Compression loading stiffness is progressively lowered with increasing prior tensile strains. However, it increases above a load of approximately 1000 kN, at which stage cracks close and concrete compression capacity is developed. Figure 8.4(c) shows the much larger compression strains which were attained in the central region of prism 8 and also the more severe loss of stiffness in compression. The load-strain response of units 6 and 7 was intermediate between that of prisms 4 and 8.

Two concrete stress-strain relationships, (i) Modified Kent and Park [59] and (ii) Mander [57] , were used to predict the "monotonic" compression load-strain response of the prisms. The experimental points shown in Fig. 8.5 envelope the load-strain hysteresis loops obtained by testing, and may reasonably be used as an estimate of the monotonic load-strain response.

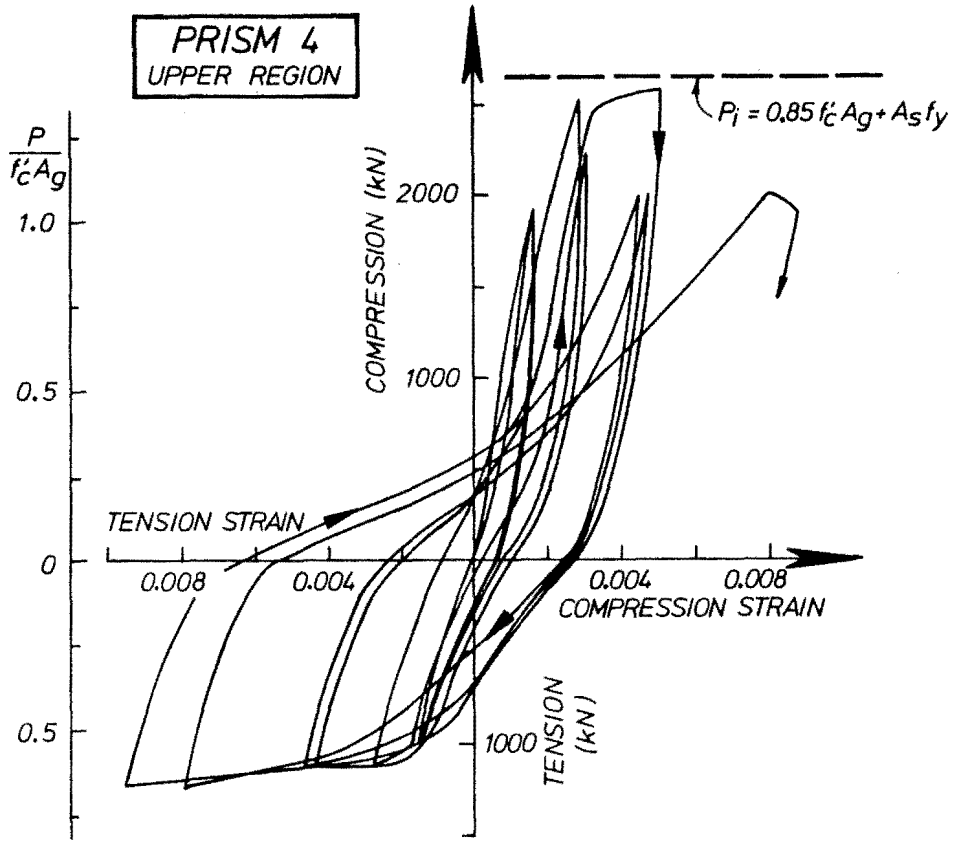

(a) Prism 4 - top level

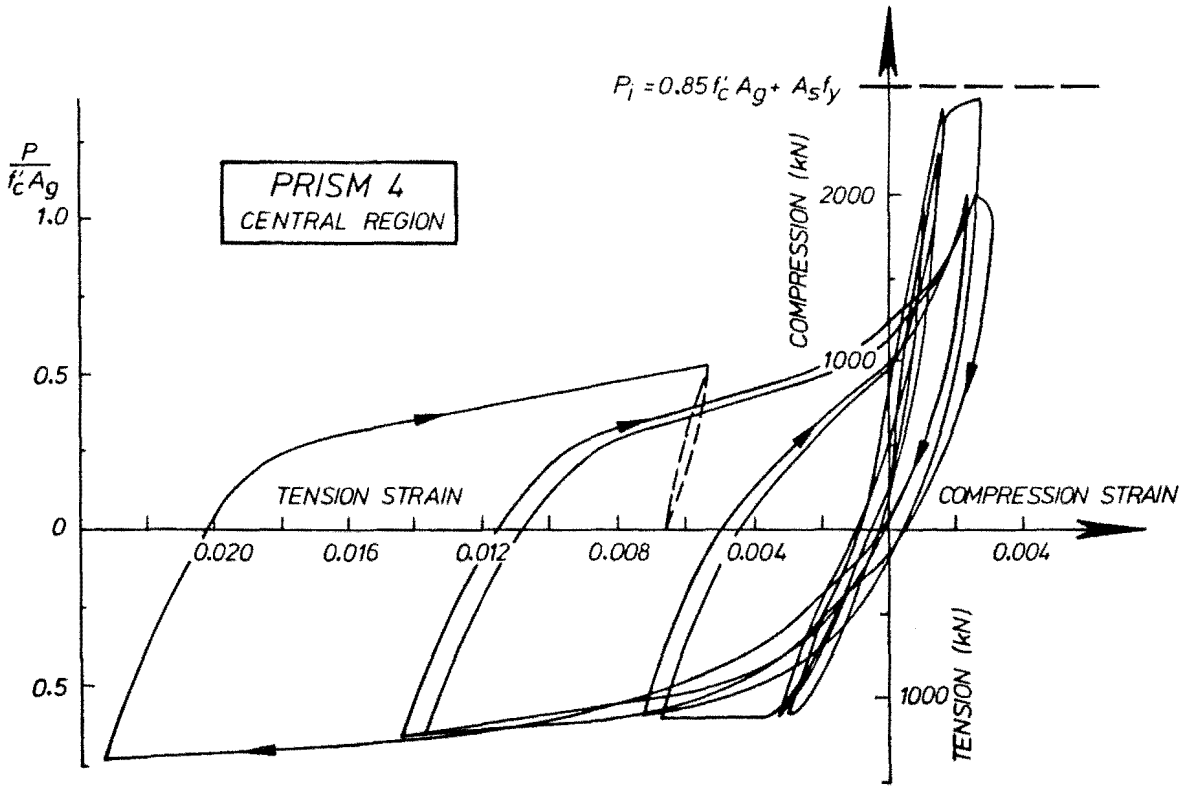

(b) Prism 4 - central level

Fig. 8.4 Load - Axial Strain Relationships.

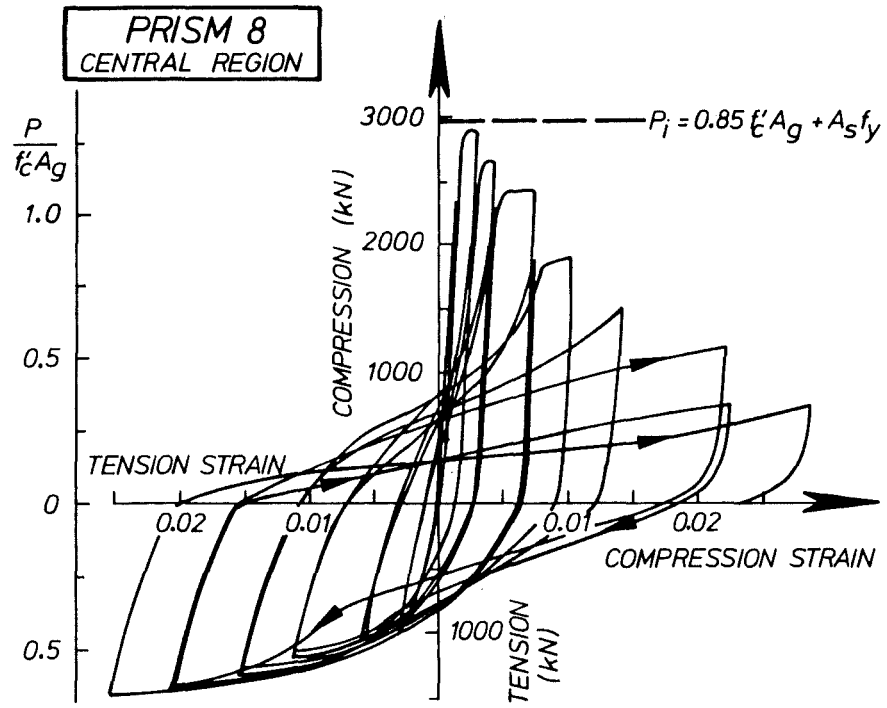

(c) Prism 8 - central level

Fig. 8.4 (Continued)

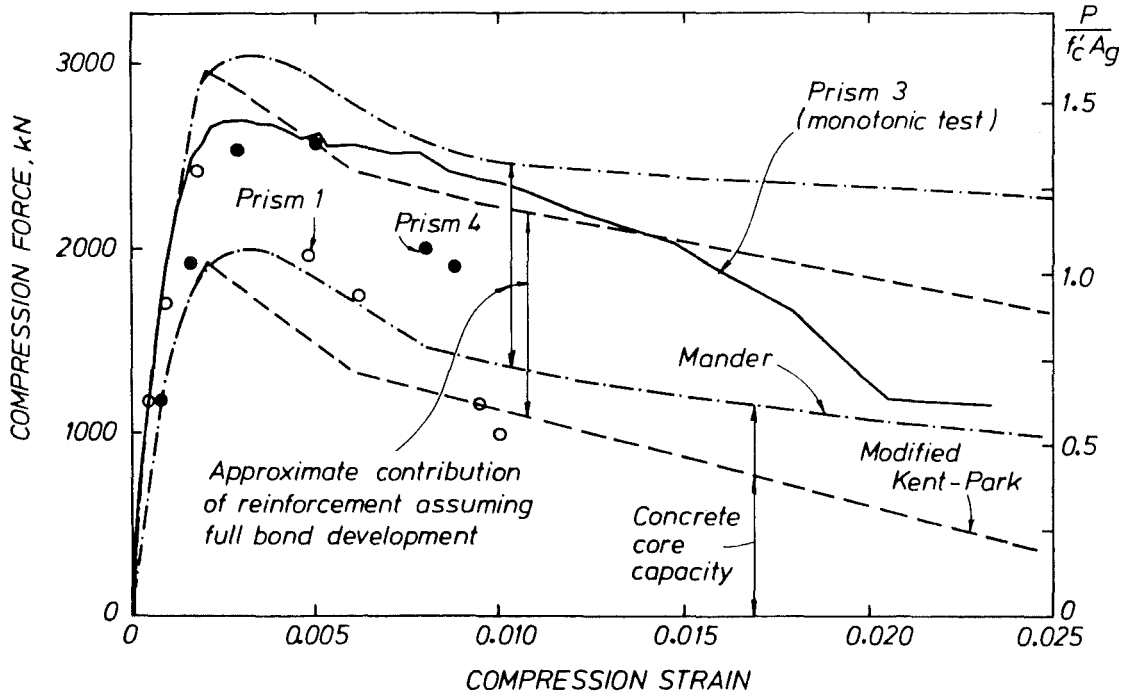

(a) Prisms 1 - 4

Fig. 8.5 Load - Axial Strain Comparison with Theoretical Models.

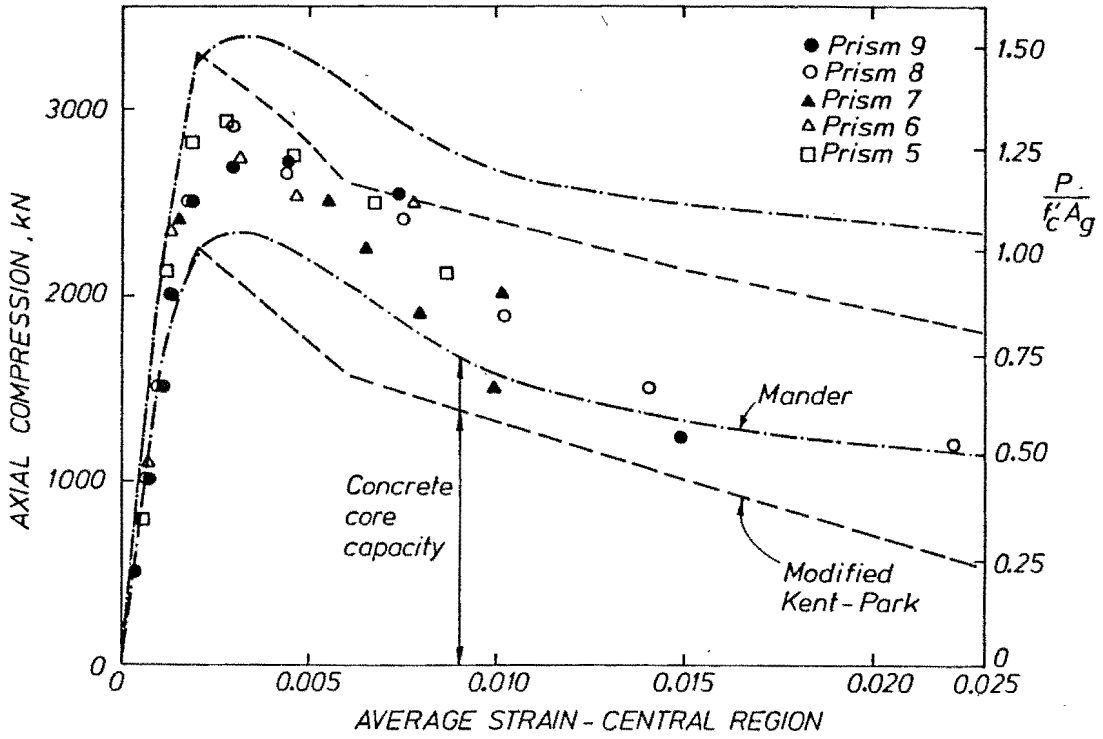

(b) Prisms 5 - 9

Fig. 8.5 (Continued)

Longitudinal reinforcement strength was calculated from the steel monotonic stress-strain relationship. Peak observed forces were over-estimated, typically by 15 and 20% for theoretical models (i) and (ii) above respectively, although prior to this stage good agreement between experimental results and the prediction exists. At higher strains strength degradation is more rapid than predicted. This is due to the deterioration of bond between the longitudinal reinforcement and the concrete, aggravated by cyclic loading, whereby the bars slipped through the concrete and took less force than the concrete strain suggests. Degradation is least for the truly monotonically tested prism 3.

8.4.3 Hoop Strains

Hoop strain patterns were quite predictable, with high strains (up to 4%) recorded in regions subject to high axial compression strains, and strain levels less than yield strain common elsewhere in the prisms.

8.4.4 Out of Plane Displacements

Out of plane displacement histories of prisms 2, 4, 6 and 9 are shown in Fig. 8.6, in conjunction with the variation in axial load to which the units were subjected. The cyclic variations in out of plane

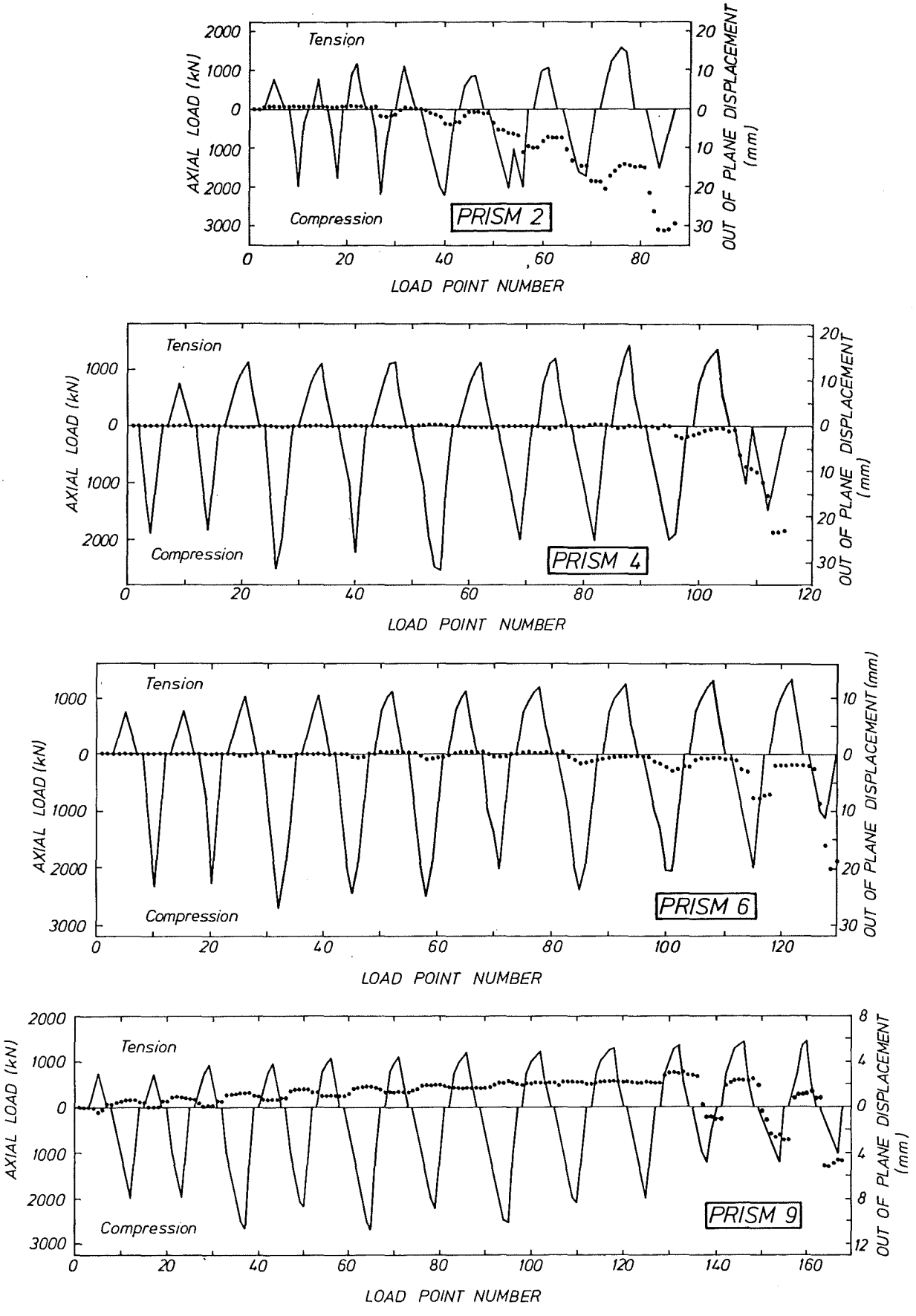

Fig. 8.6 Out of Plane Displacement Histories for Prisms 2, 4, 6 and 9.

displacements are very similar to those exhibited by the eastern end of the model wall units tested (see Figs. 7.25, 7.49, 7.60 and 7.75). Prism 2 displays a very similar deformation history to Wall 2, steadily trending to one particular transverse direction as the recovery towards verticality during tensile loading is less than the destabilising displacement of the previous compression excursion. The behaviour of prism 4 was similar to that of Wall 3, with generally small out of plane displacements prior to the large movements at the end of the test. It is interesting that the different modes of transverse response of Walls 2 and 3 (both units having the same first storey height to thickness ratios) was mirrored by prisms 2 and 4, also of the same geometrical slenderness. Prisms 6 and 9 also display a correlation between out of plane displacement and the sense of loading, although the displacements involved are considerably smaller than those associated with the more slender prisms. The sense of displacements during compression loading changes during the testing of prism 9, a phenomenon also exhibited by the response of Wall 4. (Note the displacement scale used for prism 9).

Displacement profiles at selected load points for prisms 2, 4, 6 and 9 are shown in Fig. 8.7. The concentration of deformations in the upper regions of units 2 and 4 is readily apparent. Unit 6 adopted a more symmetrical profile. The profiles for prism 9, the least slender unit, are similar to those of the least slender wall unit (Wall 4) and indicative of crushing rather than buckling failure.

Figure 8.8 shows these four units after testing was completed.

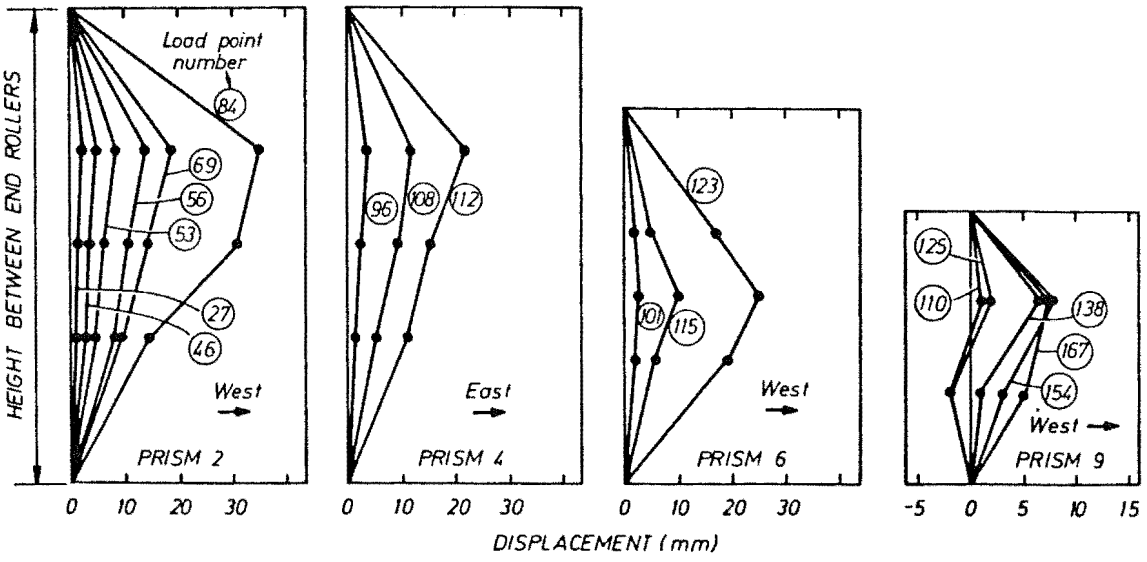

Fig. 8.7 Out of Plane Displacement Profiles for Prisms 2, 4, 6 and 9.

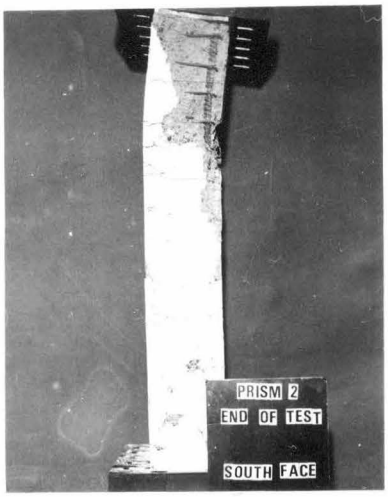

Prism 2

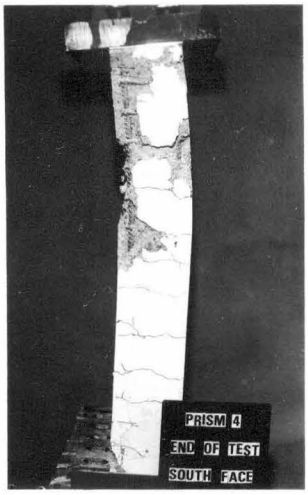

Prism 4

Prism 6

Prism 9

Fig. 8.8 Prisms After Testing.

8.4.5 Bond Conditions in the Prisms

Tensile loads were applied directly to the longitudinal bars (Section 8.3). Between the horizontal cracks which form when the concrete tensile strength is exceeded, some reduction of bar force occurs due to the transfer of forces to the concrete primarily via small compression struts bearing against bar deformations or ribs. This is illustrated in Fig. 8.9(a).

Compressive loads were applied at the prism ends to the concrete only, with compression force being transferred to the longitudinal bars, again via a bond mechanism involving internal inclined compression struts (see Fig. 8.9(b)). The horizontal crack in Fig. 8.9(b) will close either when the bar yield stress of the crack is exceeded or when

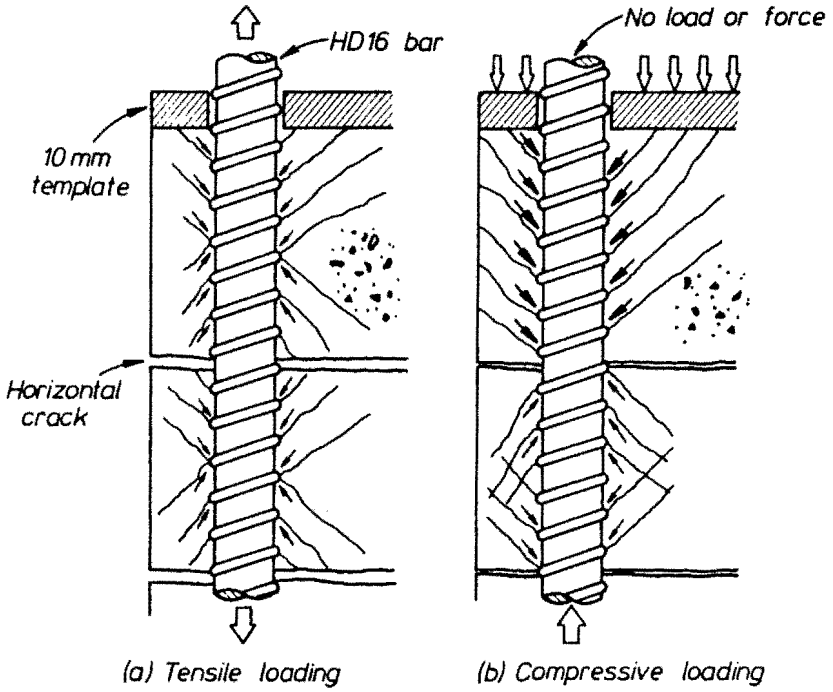

Fig. 8.9 Bond Conditions at the Prism Ends.

a bond failure occurs and the top block of concrete slides down along the relatively lowly stressed bar. Closure of the crack is possible only if the entire yield force of the bar is introduced to it over the length of the first block of concrete, extending between the end template and the first large horizontal crack. This involves extremely large bond stresses, of order 30 MPa assuming a concrete block depth equal to the hoop spacing. The range of possible total compression strengths of the prism at its ends thus extends from full combined core plus reinforcement capacity (complete compatibility between steel and concrete, with no bond degradation) to concrete strength only if all bars slip through.

Bond transfer efficiency deteriorated during the tests. A build up of crushed material at the tips of the diagonal concrete struts caused the shear strength of the cylindrical surface surrounding the bar to be exceeded, resulting in bar slippage. This deterioration was accelerated by the reversing direction of strut formation and the loss of cover concrete which reduced the effective perimeter of bar where force transfer may occur. This was most critical for corner bars and with progressively higher axial strains (both tensile and compressive) imposed. The use of external confining plates to reduce cover loss at end zones,and thus give a greater perimeter of bar for force transfer, merely delayed the inevitable.

Bond deterioration exerted a considerable adverse effect on the performance of the prism units, and it is likely that this would not have occurred had compression load been applied directly to the longitudinal reinforcement as well as to the concrete.

8.4.6 Prediction of Out of Plane Displacements

An attempt was made to compare the observed out of plane displacements of the prisms with those predicted by a very simple mechanism. Although relatively unsuccessful, the procedure is described briefly.

A cyclic loading stress-strain curve for the longitudinal reinforcement was obtained using an analytical model [57]. Given the maximum tensile strain recorded for each prism, and assuming tensile cracks to be perfectly open and uninfluenced by possible aggregate misfit, the stress-strain curve was used to determine whether or not Euler-type buckling would have occurred prior to crack closure. This was done as follows:

For a point X (Fig. 7.82), the tangent modulus $E_{t,x}$, compressive stress $f_{s,x}$ and tensile strain $\varepsilon_{s,x}$ were obtained. A buckling load of $\pi^2 E_{t,x} I/\ell^2$ was calculated, where I is the second moment of area of the 12 longitudinal bars alone for bending in the out of plane sense, and ℓ is the distance between the pin ends of the prism. This force was compared with the axial force capacity estimated as $f_{s,x}$ times the total bar area. Euler-type instability was considered to occur when the calculated buckling load was exceeded by the latter force capacity.

Only prism 4, which sustained a peak tensile strain of 2.4%, was found by this analysis to be unstable, all other units should have attained crack closure before the tangent modulus became critically low. This prediction is obviously at variance with the observed behaviour wherein all prisms eventually developed out of plane displacements. The reasons for this are discussed later.

An estimate of the out of plane displacement due to the predicted buckling of prism 4 was made assuming a circular arc deflected shape. This displacement is $\Delta \cong \varepsilon_{s,x} \ell^2/(8Z)$, where Z is the distance in the out of plane direction between the two layers of reinforcement in the prism. For prism 4 instability was indicated at an axial load of 850 kN, with $\Delta \cong 9$ mm. This compares well with the 10 mm/1000 kN recorded at load point 108 (Fig. 8.6).

Beyond this point the task becomes that of predicting the extent to which the prism continues to deflect in order to resist the out of plane moment 850 x 0.009 ≅ 8 kN.m in conjunction with the axial load. Moment curvature calculations indicated that at the curvature implied by the calculated deflection, sufficient strength should have been available to sustain the 1500 kN force imposed on the prism (load point 12, Fig. 8.6). However, this calculation was made assuming full bond between reinforcement and concrete. The degree to which bond had deteriorated at this stage of the testing of prism 4 could not be assessed quantitatively. Further calculations assuming all steel in compression to be debonded (i.e. slipping through the prism body) suggested that with an axial load of 1500 kN, a resisting moment of less than 1500 x 0.009 ≅ 13 kN.m would be available. This would lead to continued instability of the prism. In fact a peak out of plane displacement of 24 mm was recorded for prism 4 at load point 112.

It is most unfortunate that the deterioration of bond influenced the behaviour of prisms so markedly. This makes the comparison of observed behaviour and calculated response difficult, if not impossible. Prisms, other than unit 4, underwent out of plane deformations although these were not indicated by the simple calculation procedure described. It is likely that slippage of blocks of concrete past de-bonded bars was an uneven process which induced the movements observed. This effect would not contribute to instability in normal circumstances. The observed out of plane deformations for some prisms began at low tensile strain levels and these are almost certainly neither associated with Euler-type instability (e.g. prisms 2 and 9, Fig. 8.6), nor due to bond deterioration. These deformations are believed to have been caused by imperfect crack closure.

In conclusion, it is felt that the assessment of a model for the relatively simple situation of prism buckling (compared with wall instability) requires experimental data unaffected by extraneous influences such as bond problems.

8.4.7 Buckling of a Structural Wall End Region

A similar type of highly approximate calculation may be used to determine critical buckling conditions for the end region of a structural wall. Discounting the influence of aggregate misfit and stiffening due to the tension zone of the wall, instability should occur when the

force taken by the end zone flexural reinforcement equals the buckling load. i.e.

$$A_s f_{s,crit} = \frac{\pi^2 E_{t,crit} I}{\ell_e^2} \qquad (8.1)$$

where A_s is the area of the end region flexural reinforcement positioned in two layers a distance Z apart, f_{crit} and E_{crit} are as shown in Fig. 7.82, ℓ_e is the effective height of end zone and I is the second moment of area of the end zone reinforcement, i.e.

$$I = A_s Z^2/4 \qquad (8.2)$$

The behaviour of Wall 2 suggests $\ell_e \doteq 0.7h$ and hence Eq. (8.1) indicates the critical condition for Euler instability to be when

$$h \doteq Z\sqrt{\frac{5E_{t,crit}}{f_{s,crit}}} \qquad (8.3)$$

This expression may be used to establish a relationship between unsupported wall height (h) and wall thickness (derived from Z) as a function of the flexural steel properties and the expected peak tensile strain ($\varepsilon_{s,max}$, Fig. 7.82). The dependence of critical storey height on bar spacing Z rather than gross web width b_w is reasonable. An $h:b_w$ ratio (as expressed in the code [34]) has connotations of elastic instability with full web thickness remaining intact. However, the realities of inelastic instability are more likely to be affected by the "cover spalled" width, more closely related to Z.

A reasonable point at which to obtain $f_{s,crit}$ and $E_{t,crit}$ is when $\varepsilon_{s,crit}$ (Fig. 7.82) is zero. At this stage instability is imminent but displacements resulting from this cannot occur because residual tensile cracks are on the point of closure and out of plane stiffness is about to increase as concrete compression develops. By using f_{crit} and E_{crit} at this point, Eq. (8.3) will provide (within the limits of the model) a critical slenderness ratio (h/z).

For the walls tested, peak tensile strains of 2.5% were recorded, although a value of 2% is more realistic for strains spread over the whole first floor region. Using $\varepsilon_{s,max}$ = 2% and the steel stress-strain model of Mander [57], $f_{s,crit}$ and $E_{s,crit}$ values of 450 MPa and 9 GPa at $\varepsilon_{s,crit}$ = 0 were obtained for Wall 2. Eq. (8.3) suggests a critical

ratio of $h/Z \doteq 10$, which is equivalent to $h/b_w \doteq 5.6$ for Z and b_w values of 56 and 100 mm respectively.

For a prototype wall of width b_w = 400 to 500 mm, Z may be in the range $0.65 - 0.75b_w$. Examination of experimental stress-strain relationships [60] for high strength New Zealand steel indicates that the $E_{t,crit}$ and $f_{s,crit}$ values used above are also typical values for larger size bars. Thus Eq. (8.3) indicates safe clear wall heights of $6.5 - 7.5b_w$, compared to the codified value of $10b_w$.

8.5 CONCLUSIONS

Although the behaviour of the prisms was markedly affected by bond deterioration, the tendency for transverse instability was clearly observed to increase with increasing slenderness and increasing level of previous tensile strain. The pin ended slenderness of 5.5 : 1 appears to be close to the transition point above which instability, and below which crushing, controls behaviour. This corresponds to a wall first floor height to thickness ratio of approximately 8 : 1. The prism concept is a relatively economical means of examining transverse instability and it is believed that given refinement of the experimental arrangement, more valuable experimental data regarding the phenomenon could be obtained.

Chapter Nine SUMMARY AND RECOMMENDATIONS FOR FUTURE RESEARCH

9.1 ANALYTICAL STUDIES

A series of 6-18 storey cantilever structural walls were designed and subjected to inelastic time history analyses. Numerous factors influencing the dynamic magnification of wall base shear force were identified. These parameters include wall height and geometry, damping model, stiffness,model of member hysteresis, foundation compliance, base excitation (accelerogram) and member model type. Levels of shear magnification larger than those observed in previous theoretical research [36] were obtained. High shear forces, although occurring infrequently and for short periods of time, were generally contemporaneous with high moment demands. The magnitudes of the computed shear forces were found to be sensitive to small changes in many of the aforementioned parameters. The simple member models traditionally used for frame elements may not be suitable for walls in which inelasticity could spread over a height of several storeys.

A design methodology for interconnected frame-wall buildings was presented. The method used the capacity design philosophy [1] and incorporates procedures used for structural walls [39] and ductile moment resisting frames [34]. Firstly a routine static elastic lateral load analysis was made to determine "code" level earthquake actions. Beams were designed for this earthquake and factored gravity loading, with both horizontal and vertical moment redistribution permitted. Columns were then designed for moments in excess of the code values by factors recognising both the maximum input from beam flexural overstrength and moment magnification due to the participation of high modes of response. Walls were designed according to a linear flexural strength envelope. All elements were designed to sustain comparatively high levels of shear. Shear failure was not anticipated.

Simplified 6 and 12 storey buildings were designed using this approach and subjected to the El Centro and Pacoima Dam accelerograms. The generally good performance of the buildings for the El Centro excitation indicates that prototype structures so designed should exhibit good seismic response. Energy dissipation occurs primarily via sustainable flexural yielding at beam and wall base hinge zones.

Columns enjoy protection against flexural yielding except at the base and top floor levels. A basic dynamic magnification factor of 1.2 proved to be satisfactory. Column shear forces may be reliably predicted. Significant inelastic deformations are restricted to the wall base region by the provision of flexural strength for upper levels in accordance with the linear design envelope. Peak wall base shear forces were somewhat underestimated by the design procedure. However, this must be viewed in the context of the uncertainties involved in the analyses, the short duration times of these forces and the already large levels of design force advocated. The proposed wall shear force design envelope (Fig. 3.3) adequately estimates upper level forces. Deflections, interstorey drifts and inelastic deformation demands were of an acceptable level under the El Centro excitation.

Strength and deformation demands due to the extreme Pacoima Dam excitation were often at an unsustainable level.

The influence of wall foundation compliance on the performance of frame-wall buildings was studied with reference to the extreme case of zero wall moment fixity (with full column fixity). As expected elastic analyses indicated very high first floor column actions. Member forces in the upper regions of the building were not significantly affected by the loss of wall base fixity. Dynamic analyses were also performed for these pinned wall structures which were modelled with member strength properties identical to those used for the fixed wall buildings. The most important consequence of the loss of base fixity is the increase in first mode structural period. Depending on the frequency characteristics of the excitation accelerogram used, this period shift leads to a pinned base structural response that may be more or less favourable than the fixed base response. Although larger interstorey drifts were observed over the lower levels of pinned wall structures, extreme levels of column shear or moment did not occur. Shear and flexural strength levels provided in fixed base walls exceeded pinned wall strength demands. The first storey floor slab-wall junction may require special detailing, however, due to the large point shear force occurring at this level when wall compliance is high. This force is required to reduce the first floor level wall moment from a value, which may be as high as that for a fixed base wall to the low value at the base associated with the high degree of compliance.

The performance of frame-wall buildings with walls of less than full structural height was also studied. The design method established for full height wall buildings was found to be applicable with few modifications. A column dynamic magnification factor of 1.5 was found to be necessary to prevent column yielding above the wall cut off level. Special studies, with attention to wall modelling especially, may be required if squat wall elements are used (i.e. $h_w/\ell_w < 2$).

It is believed that the methodology developed is logical and straightforward and should provide buildings so designed, and carefully detailed, with excellent seismic resistance. The approach is capable of being extended to other structural configurations by the consistent application of capacity design principles.

9.2 EXPERIMENTAL STUDIES

Four model cantilever structural wall units were tested with the primary aims of investigating the New Zealand codified provisions [34] concerning hoop reinforcement and section instability. Three rectangular and one tee section, approximately 1/3 full size, units were designed and detailed in accordance with current New Zealand practice. Realistic reinforcement contents, materials and construction procedures were used. The model walls were tested with eccentrically acting axial load varying between 0.03 and $0.26f'_cA_g$, and subjected to increasing levels of fully reversing displacement controlled lateral load. Primary interest was in behaviour during the sense of lateral load for which axial load was increased with lateral load to produce large compression block depths at the development of flexural strength. The units were comprehensively instrumented with bar strain gauges and linear potentiometers. Out of plane displacements of the highly stressed compression zone were monitored.

Wall 1, tested at a peak axial load of $0.26f'_cA_g$ exhibited a material compression failure when a displacement ductility of $\mu_\Delta = 4$ was approached for the second time. This failure initiated in the highly strained plain concrete immediately adjacent to the well confined core. This failure was not significantly affected by the small out of plane displacements observed. Wall 2 ($0.11f'_cA_g$ peak axial force) sustained two fully reversed cycles at $\mu_\Delta = 6$ before developing a large out of plane displacement. This instability occurred without warning and severely limited lateral load resistance. Walls 3 and 4 (with axial compression

of 0.12 and $0.15f'_c A_g$ respectively) both exhibited material compression failures on approaching $\mu_\Delta = 6$ for the second time. Again failure initiated outside the confined core and was due to the combined effects of high ductility demands and axial force eccentricity arising from out of plane displacements.

Prior to failure, the general response of the units, assessed in terms of moment-deflection relationship, was very good. Strength was reasonably well predicted by routine monotonic moment-curvature calculations. Post yield strength increased with increasing ductility and degradation of strength due to repeated loading seldom exceeded 5%. Moment-displacement loops also indicated good stiffness response and energy dissipation characteristics. Shear deformations were generally less than 40% of the total first floor displacement, with anchorage deformations of order 10%. Slip at construction joints was negligible.

Hoop reinforcement, provided for both confinement and antibuckling roles, sustained generally low levels of strain. In view of the observed failure modes it is suggested that for sections with large design compression block depths, hoop reinforcement be extended further into the section than the outer half of the compression block, as is currently recommended. The increase should be a function of the expected ductility demand on the wall (Section 7.6.4).

It is recommended that the codified dimensional requirements for the potential hinge zones of rectangular section walls remain unchanged, i.e. a maximum slenderness of 1 to 10 be used for wall units where the design compression block is critically deep. Although the adequacy of the 1:10 ratio was not conclusively demonstrated by the study, this figure is considered to offer a reasonable degree of protection against section instability.

9.3 RECOMMENDATIONS FOR FUTURE RESEARCH

9.3.1 Analytical Work

It is felt that a comprehensive program of time history analyses of cantilever wall elements should be undertaken using a finite element type,well suited to modelling wall behaviour. A 'layered' element allowing for the spread of plasticity over a realistic hinge length may prove suitable. Provision for inelastic shear deformations would also be desirable, as would the use of a flexural hysteresis model more realistic than a simple bilinear scheme. Such a series of analyses

should provide a more reliable measure of the dynamic magnification of wall shear forces. The identification of damping schemes which reflect the true source of the phenomenon and accelerograms critical to the frequency characteristics of a particular wall are further important issues.

Aspects of the response of frame-wall structures which require additional research include the following: a study of different frame-wall configurations, involving coupled wall elements and tube or peripheral frames typical of taller buildings. It is felt that the basic approach taken for the cantilever wall - simple frame structures described herein will be well suited to those other hybrid frames. The use of more realistic wall modelling in these structures is also desirable. The influence of floor slab flexibility on response is worthy of closer study (especially where wall-foundation compliance is present and high shear stress levels occur at the first floor wall-slab interface). Three dimensional effects, i.e. skew or torsional loading of members may cause critical strength or ductility demands not indicated by the two dimensional analyses, and thus should be studied.

9.3.2 Experimental Work

The scope for the continued experimental study of structural wall or subassemblage units is wide. Effort should be concentrated on rectangular sections as these are clearly critical with regards instability and hoop reinforcement requirements for high axial loads. The testing of larger scale units allowing more realistic dimensional ratios (e.g. cover : web thickness) is also desirable. A series of tests, where the sole variable is the extent to which hoop reinforcement extends into the section, is seen as being of value. Tests are also required where the sole variable is the quantity rather than the extent of hoop reinforcement: this would indicate how conservative the present code equations (Eqs. 6.3, 6.4) are. The out of plane deformation history of such units should also be closely monitored.

The concept of concentric tension/compression load tests on prismatic units is felt to hold considerable promise for the study of out of plane instability, despite the poor performance of the prism tests described herein. The provision of loading blocks at prism ends, to give fixed rather than pinned end conditions, may prove suitable. It is a logical progression to derive and calibrate an analytical model which reflects prism buckling before tackling the more difficult task of rectangular

wall instability. An investigation of the influence of flanges and boundary elements on wall stability is the natural progression after the resolution of rectangular wall stability issues.

Aside from questions of confinement and stability, tests aimed specifically at checking the codified shear design procedures for plastic hinge zones are desirable, with special consideration to assessing the contribution of concrete shear strength, when subjected to reversed cyclic loading.

Appendices

APPENDIX A

COMPARISON OF DESIGN SHEAR FORCES AND MOMENTS FOR A STRUCTURAL WALL [38] USING NEW ZEALAND [34], UBC [26] AND PCA [38] RECOMMENDED PRACTICES.

The design example is a 20 storey cantilever structural wall of height 178.25 ft. with specified height and gravity loading. These calculations use the same units that were used originally.

1. PCA METHOD

Design moment = $2.0 \times 10^6/0.9 = 2\ 222\ 222$ K.in. from Fig. 32 [38], where 0.9 is the strength reduction factor used for flexural design common to all 3 methods.

Design shear force = 1470/0.85 = 1729 K, where 1470 kip is the value of ultimate shear force obtained from the PCA method and 0.85 is the strength reduction factor used in shear design.

2. UBC METHOD

Design moment = $298 \times 0.72 \times 178.25 \times 12/0.9$

= 509 938 kip in, where 298 kip is the UBC specified base shear (p54, [38]) and where for UBC (and NZ) code distributions of lateral load, $M_{code} \cong 0.72H\ V_{code}$ (Fig. 3.1), with H the total structural height.

Design shear force = 298 x 2.0/0.85 = 701 kip, where the specified base shear of 298 kip is multiplied by the UBC shear load factor of 2.0, and a shear strength reduction factor is used.

3. NZ METHOD

This calculation is based on the assumption of using the same basic value of "code" shear force as used by the UBC.

Design moment = 298 x 0.72 x 178.25 x 12/0.9 = 509 938 kip in, as per the UBC calculation.

Design shear force = 298 x 1.45 x 1.8/1.0 = 778 kip, where a typical base flexural overstrength factor of 1.45 is assumed, a dynamic magnification factor of 1.8, appropriate for a 20 storey wall

is used [34] and a strength reduction factor of unity is used in this capacity design approach.

TABLE A.1 : COMPARISON OF PCA, UBC AND NZ DESIGN ACTIONS

	Design Moment kip.in	Design Shear Force kip
PCA	2 222 222	1729
UBC	509 938	701
NZ	509 938	778

Note: 1000 K.in = 113 kNm
1 Kip = 4.45 kN.

The effective heights of application of the design shear force (M_{wall}/V_{wall}) are 0.31H, 0.34H and 0.60H for the NZ, UBC and PCA approaches respectively. Thus it is evident that despite the intention of the PCA formulation to recognise the effect of dynamic force magnification, the high design moment and a relatively low design shear force combination suggest that is the least conservative of the three methods considered. Although it may be argued that a PCA designed wall could resist elastically the highest level of lateral loading, a wall shear failure would be likely in the event of high levels of lateral loading, whereas the ductile flexural yielding unaccompanied by shear failure would be the likely response of the NZ and UBC walls in this example.

APPENDIX B : Column Design Calculations

Typical column design calculations for 6 and 12 storey buildings are given in tabular form in this appendix. The method is as described in Section 3.1 and all variables used are defined in the Notation.

TABLE B.1 : DERIVATION OF DESIGN AXIAL LOADS AND DESIGN MOMENTS - INTERIOR COLUMN, 6 STOREY STRUCTURE, 4 M WALL

Floor	$\Sigma V_{oe}^{+} = \Sigma V_{oe}^{+}$	0.9D	$D + L_R$	$P_{e\,max}^{+}$	$P_{e\,min}^{+}$	M_{code}	β	$\phi_o^{+} = \phi_o^{+} = \phi_o$	$\beta\phi_o M_{code}$	V_{col}	M_{m}^{+}	β_m^{+}	$M_{col,req}^{+}$	P_t	$P_{supplied}$	Column Size
	1	2	3	4	5	6	7	8	9	10	11	12	13	14	15	16	17
Units	kN	kN	kN	kN	kN	kN.m			kN.m	kN			kN.m	kN.m	%	%	
6	0	392	568	568	392	311+ 245	1.00	1.10+ 1.39	342+ 341	336+ 424	* n.c.	1.00	n.c.	282 + 265	1.51	1.8 + 1.5	500 x 500
5	0	785	1097	1097	785	247 246	1.20	1.39 1.37	412 404	244 241	n.c.	1.00	n.c.	368 361	1.26	1.5 1.3	500 x 500
4	0	1177	1618	1618	1177	252 249	1.20	1.37 1.35	414 403	244 242	n.c.	1.00	n.c.	370 359	0.95	I.3 1.2	500 x 500
3	0	1573	2040	2040	1573	296 333	1.20	1.35 1.50	480 599	260 289	n.c.	1.00	n.c.	433 547	1.17	1.2 1.2	550 x 550
2	0	1970	2661	2661	1970	169 243	1.20	1.50 2.20	304 641	220 324	n.c.	1.00	n.c.	264 529	0.89	1.2 0.9	550 x 550
1	0	2366	3179	3179	2366	65 225	1.00	2.20 1.40	143 315	435 277	n.c.	1.00	n.c.	65 338	0.80	0.9 0.9	550 x 550

* n.c. = non critical + Quantities for top and bottom of column respectively.

TABLE B.2 : DERIVATION OF DESIGN AXIAL LOADS AND DESIGN MOMENTS - EXTERIOR COLUMN, 6 STOREY STRUCTURE, 4 M WALL

Floor	$\overrightarrow{\Sigma V}_{oe}$	$\overleftarrow{\Sigma V}_{oe}$	0.9D	D + L_R	$\overrightarrow{P}_{e_{max}}$	$\overleftarrow{P}_{e_{min}}$	M_{code}	ω	$\overrightarrow{\phi}_o$	$\omega\overrightarrow{\phi}_o M_{code}$	$\overrightarrow{V}_{col}$	$\overrightarrow{R}_m$	$\overrightarrow{M}_{col,red}$	$\overrightarrow{\rho}_t$	$\overleftarrow{\phi}_o$	$\omega\overleftarrow{\phi}_o M_{code}$	$\overleftarrow{V}_{col}$	$\overleftarrow{R}_m$	$\overleftarrow{M}_{col,red}$	$\overleftarrow{\rho}_t$	$\rho_{t,supplied}$	Column Size
	1	2	3	4	5	6	7	8	9	10	11	12	13	14	15	16	17	18	19	20	21	22
Units	kN	kN	kN	kN	kN	kN	kN.m			kN.m	kN		kN.m	%		kN.m	kN		kN.m		%	mm x mm
6	76	66	253	362	428	177	170 133	1.00	1.10 0.79	187 105	158 142	1.00	159 107	1.13	1.10 1.82	187 242	156 258	1.00	159 196	0.80	1.1 1.1	450 x 400
5	145	130	506	694	824	361	130 127	1.20	0.79 0.78	123 119	79 79	1.00	142 138	0.80	1.82 1.75	284 267	129 124	0.97	261 245	1.00	1.1 1.0	450 x 400
4	214	192	759	1021	1213	545	130 133	1.20	0.78 0.78	122 124	81 81	1.00	141 145	0.80	1.75 1.75	273 279	126 126	1.00	250 256	0.80	1.0 0.8	450 x 400
3	279	252	1013	1351	1603	734	128 149	1.20	0.78 0.88	120 157	85 85	1.00	139 164	0.80	1.75 1.79	269 320	133 136	1.00	245 296	0.80	0.8 1.3	450 x 450
2	341	310	1268	1677	1987	927	79 130	1.20	0.88 1.39	83 217	64 83	1.00	83 184	0.80	1.79 2.56	170 399	102 146	1.00	138 340	1.28	1.3 1.3	450 x 450
1	401	366	1523	2002	2368	1122	30 135	1.00	1.39 1.40	42 189	136 137	1.00	18 164	0.80	2.56 1.40	77 189	250 137	1.00	32 164	0.80	1.3 1.3	450 x 450

Note: the unusually low values of $\overrightarrow{\phi}_o$ (column 9) are due to significant moment redistribution (which has the effect of making $\overleftarrow{\phi}_o$ values correspondingly high).

TABLE B.3 : DERIVATION OF DESIGN AXIAL LOADS AND DESIGN MOMENTS, INTERIOR COLUMN
12 STOREY STRUCTURE, 3.0 M WALL

Floor	$\Sigma V^{+}_{oe} = \Sigma V^{+}_{oe}$	0.9D	D + L_R	$^{+}P_{e,min}$	$^{+}P_{e,max}$	M_{code}	ω	$^{+}\phi_o = {}^{+}\phi_o$	$\omega\phi_o M_{code}$	V_{code}	$^{+}R_m$	$^{+}R_m$	$^{+}M_{col,red}$	$^{+}M_{col,red}$	ρ_t	$\rho_{supplied}$	Column Size
	1	2	3	4	5	6	7	8	9	10	11	12	13	14	15	16	17
Units	kN	kN	kN	kN	kN	kN.m			kN.m	kN			kN.m	kN.m	%	%	mm x mm
12	0	520	710	520	710	378 214	1.00	1.10 1.37	416 293	357 444	1.00	1.00	336 193	n.c.*	0.80	0.8 0.8	700 x 700
11	0	1041	1382	1041	1382	414 291	1.20	1.37 1.68	681 587	344 422	0.99	1.00	598 487	n.c.	0.80	0.8 0.9	700 x 700
10	0	1562	2045	1562	2045	522 389	1.20	1.68 1.36	1052 635	544 440	1.00	1.00	930 536	n.c.	0.84	0.9 0.9	700 x 700
9	0	2082	2705	2082	2705	631 501	1.20	1.36 1.62	1030 974	548 653	1.00	1.00	907 827	n.c.	0.80	0.9 1.3	700 x 700
8	0	2603	3364	2603	3364	721 608	1.20	1.62 1.42	1402 1036	767 672	1.00	1.00	1229 885	n.c.	1.23	1.3 1.3	700 x 700
7	0	3123	4020	3123	4020	794 704	1.20	1.42 1.29	1353 1090	757 688	1.00	1.00	1183 935	n.c.	0.95	1.3 1.0	700 x 700
6	0	3643	4675	3643	4675	846 791	1.20	1.29 1.22	1310 1158	753 712	1.00	1.00	1141 998	n.c.	0.80	1.0 0.8	800 x 800
5	0	4163	5329	4163	5329	859 815	1.20	1.22 1.19	1258 1164	728 710	1.00	1.00	1094 1004	n.c.	0.80	0.8 0.8	800 x 800
4	0	4695	5995	4695	5995	911 958	1.20	1.19 1.22	1301 1403	792 812	1.00	1.00	1123 1220	n.c.	0.80	0.8 0.8	800 x 800
3	0	5227	6661	5227	6661	740 1003	1.14	1.22 1.41	1029 1612	757 874	1.00	1.00	859 1415	n.c.	0.80	0.8 0.8	800 x 800
2	0	5759	7326	5759	7326	489 1009	1.07	1.41 1.43	738 1544	752 763	1.00	1.00	569 1372	n.c.	0.80	0.8 0.8	800 x 800
1	0	6291	7991	6291	7991	49 1289	1.00	1.43 1.40	70 1805	1312 1285	1.00	1.00	-225 1516	n.c.	0.80	0.8 0.8	800 x 800

* n.c. = non critical

TABLE B.4 : DERIVATION OF DESIGN AXIAL LOADS AND DESIGN MOMENTS, EXTERIOR COLUMN
12 STOREY STRUCTURE, 3.0 M WALL

Floor	$\dagger\Sigma V_{oe}$	$\dagger\Sigma V_{oe}$	0.9D	D + L_R	$\dagger P_{e,min}$	$\dagger P_{e,max}$	M_{code}	ω	$\dagger\phi_o$	$\omega\dagger M_{o\,code}$	$\dagger V_{col}$	$\dagger R_m$	$\dagger M_{col,red}$	$\dagger\rho_t$	$\dagger\phi_o$	$\omega\dagger M_{o\,code}$	$\dagger V_{col}$	$\dagger R_m$,	$\dagger M_{col,red}$	$\dagger\rho_t$	$\rho_{t,supplied}$	Column Size.
	1	2	3	4	5	6	7	8	9	10	11	12	13	14	15	16	17	18	19	20	21	22
Units	kN	kN	kN	kN	kN	kN	kN.m			kN.m	kN		kN.m	%		kN.m	kN		kN.m	%	%	mm x mm
12	100	100	299	413	199	513	194 130	1.00	1.10 1.29	213 168	197 230	1.00	169 116	0.80	1.10 1.55	213 202	197 276	1.00	169 140	0.80	0.8 0.8	550 x 600
11	197	197	598	797	401	994	202 152	1.20	1.29 1.59	313 290	163 200	0.94	276 245	0.80	1.55 1.80	376 328	195 227	1.00	332 277	0.80	0.8 1.1	500 x 600
10	342	342	896	1176	554	1491	258 200	1.20	1.59 1.29	492 310	258 210	0.96	434 263	1.12	1.80 1.46	557 350	293 237	1.00	491 297	0.80	1.1 1.1	500 x 600
9	483	483	1195	1553	712	2036	307 255	1.20	1.29 1.57	475 480	258 314	0.99	417 409	1.00	1.46 1.72	538 526	292 344	1.00	472 449	0.80	1.1 1.6	500 x 600
8	681	681	1494	1928	813	2609	353 307	1.20	1.57 1.37	665 505	369 322	1.00	584 433	1.55	1.72 1.51	729 556	405 353	1.00	638 476	0.80	1.6 1.6	500 x 600
7	872	872	1793	2302	921	3174	390 354	1.20	1.37 1.25	641 531	363 332	1.00	559 456	1.39	1.51 1.37	707 582	400 363	1.00	617 500	0.80	1.6 1.4	500 x 600
6	1056	1056	2092	2675	1036	3731	418 396	1.20	1.25 1.18	627 561	362 342	1.00	546 484	0.88	1.37 1.29	687 613	397 374	1.00	598 529	0.80	1.4 0.9	600 x 600
5	1234	1234	2390	3048	1156	4282	431 424	1.20	1.18 1.15	610 585	359 350	1.00	529 506	0.84	1.29 1.25	667 636	392 380	1.00	579 551	0.80	0.9 0.9	600 x 600
4	1405	1405	2691	3422	1286	4827	442 460	1.20	1.15 1.18	610 651	369 379	1.00	527 566	0.80	1.25 1.29	663 712	401 414	1.00	573 619	0.80	0.9 0.9	600 x 600
3	1578	1578	2993	3798	1415	5063	382 461	1.14	1.18 1.36	514 715	353 407	1.00	435 623	0.84	1.29 1.49	562 783	386 446	1.00	475 683	0.80	0.9 0.9	600 x 600
2	1748	1748	3292	4169	1544	5607	276 440	1.07	1.36 1.36	402 640	343 343	1.00	325 563	0.80	1.49 1.54	440 725	376 388	1.00	355 638	0.80	0.9 0.8	600 x 600
1	1847	1847	3593	4542	1746	6084	93 468	1.00	1.36 1.40	126 655	524 539	1.00	8 534	0.80	1.54 1.40	143 655	593 539	1.00	10 534	0.80	0.8 0.8	600 x 600

APPENDIX C

COMPARISON OF PCA [37,38] AND EERC [55,56] TEST SPECIMEN DETAILING WITH NZS 3101 [34] REQUIREMENTS

This appendix contains a comparison between the detailing used in the test units discussed in Section 6.3 and the corresponding details that would be required by a design according to NZS 3101 [34]. Specifically, the comparison examines hoops and shear reinforcement requirements, and is presented largely in tabular form. Comments are made as to the assumptions used for and the trends emerging from the comparison.

C.1 ASSUMPTIONS USED

The comparison is based on several levels of flexural strength of the tested units. These strengths were calculated by application of strain compatibility principles to wall sections having flexural reinforcement arrangements, axial loads and nominal (design) material properties as specified by the testing organisation (PCA or EERC). The calculations assumed a peak compression fibre strain of 0.003, a linear strain profile and took into account the distributed flexural reinforcement present in the section.

Capacity design principles were used to derive design shear forces in accordance with the spirit of New Zealand practice, as follows: flexural strengths, based on 1.25 and 1.40 times the nominal reinforcement yield strength and 1.0 times the nominal concrete compression strength, were calculated. One of these two values was selected for the member overstrength capacity; the $1.25f_y$ value if peak tensile strain was less than about 10 times yield strain, and the $1.40f_y$ value otherwise. A strength reduction factor (ϕ, typically 0.9 for flexure)was not used in the calculation. (The chosen overstrength value is indicated in columns 5 or 7 of Table C.1, and may be compared with the observed peak member strengths given in column 9 of that table). The design shear force was then obtained by dividing the overstrength moment by the (constant) lever arm at which the lateral load was applied.

The development of the comparison may be followed with reference to the notes for Tables C.1 and C.2 given subsequently.

TABLE C.1 : FLEXURAL STRENGTHS OF PCA AND EERC WALLS

UNIT	P	M_i	c_i	$M^o(1.25f_y)$	$c(1.25f_y)$	$M^o(1.40f_y)$	$c(1.40f_y)$	M_{max}	Failure Mode	ϕ_o
(1)	(2)	(3)	(4)	(5)	(6)	(7)	(8)	(9)	(10)	(11)
-	kN	kN.m	mm	kN.m	mm	kN.m	mm	kN.m	-	-
PCA										
R1	0	346	96	427	111	475	121	541	b.b.	1.52
R2	0	686	130	852	150	948	165	990	w.i.	1.53
B1	0	905	83	1120	100	1247	110	1241	b.b.	1.53
B3	0	905	83	1120	100	1247	110	1261	d.t./b.f.	1.53
B4	0	905	83	1120	100	1247	110	1531	d.t./b.f.	1.53
B2	0	2622	175	3224	191	3572	205	3107	b.b.	1.51
B5	0	2622	175	3224	191	3572	205	3484	w.c.	1.51
B6	930	2525	225	3117	252	3460	274	3772	w.c.	1.37
B7	1193	3522	256	4117	277	4463	294	4482	w.c.	1.30
B8	1193	3522	256	4117	277	4463	294	4470	w.c.	1.30
B9	1193	3522	256	4117	277	4463	294	4466	w.c.	1.30
B10	1193	3522	256	4117	277	4463	294	3233	b.b.	1.30
F1	0	2883	57	3589	65	4010	71	3821	w.c.	1.54
F2	1187	3945	83	4647	94	5064	101	4057	w.c.	1.42
EERC										
Rect	598	2830	470	3336	529	3621	568	3350	w.i.	1.31
Bar-bell	868	3613	340	4267	398	4644	437	4420	w.c.	1.31

Notes on Table C.1

1 Identification code for wall unit used by the testing organisation.

2 Axial load at critical section, ignoring self weight of units (typically less than $0.01f'_cA_g$).

3,4 Ideal flexural strength and neutral axis depth, based on nominal material properties (f'_c,f_y). The nominal (and actual) concrete and steel strengths were: PCA units; f'_c = 41.4 MPa (38.6 - 53.1 MPa), f_y = 414 MPa (410 - 543 MPa); EERC units; f'_c = 27.58 MPa (32.4 - 38.0 MPa), f_y = 414 MPa (444 - 507 MPa).

5,6 Flexural strength and neutral axis depth based on f'_c and $1.25f_y$.

7,8 Flexural strength and neutral axis depth based on f'_c and $1.40f_y$. Boxed values indicate the assumed design overstrengths.

9 Maximum recorded flexural strength.

10 Failure mode (specified by the testing organisation)

b.b. = inelastic bar buckling

w.i. = gross wall instability

d.t. = diagonal tension shear failure

b.f. = vertical bar fracture

w.c. = web crushing

11 Design flexural overstrength factor, taken as ratio of column 5 or 7 (as indicated) to column 3, and assuming a strength reduction factor of 0.9 relating ideal strength to a "code" strength demand..

TABLE C.2 : COMPARISON OF PCA AND EERC WALL DETAILING WITH NZS 3101 REQUIREMENTS

UNIT	d_b	s_h	d_h	n	$6d_b$	A_{te} required	A_{te} supplied	c_i	c_c	V	d	$0.8\ell_w$	v_i	v_c	v_s	ρ required	ρ supplied		v_{max}	$\frac{v_i}{v_{max}}$	Failure Mode
(1)	(2)	(3)	(4)	(5)	(6)	(7)	(8)	(9)	(10)	(11)	(12)	(13)	(14)	(15)	(16)	(17)	(18)	(19)	(20)	(21)	(22)
PCA	mm	mm	mm	-	mm	mm^2	mm^2	mm	mm	kN	mm	mm	MPa	MPa	MPa	%	%	%	MPa		
R1	9.5	102	4.95	1	57	4.5	19.2	96	350	104	1338	1524	0.67	0	0.67	0.16	0.31	52	3.67	0.18	b.b.
R2	9.5	34	6.00	1	57	1.5	28.2	130	352	207	1538	1524	1.32	0	1.32	0.32	0.31	97	3.69	0.36	w.i
B1	12.7	203	4.95	1	75	16.1	19.2	83	352	273	1272	1524	1.76	0	1.76	0.43	0.31	72	3.69	0.48	b.b.
B3	12.7	34	6.00	1	75	2.7	28.2	83	352	273	1272	1524	1.76	0	1.76	0.43	0.31	72	3.69	0.48	d.t./b.f.
B4	12.7	34	6.00	1	114	2.7	28.2	83	352	273	1272	1524	1.76	0	1.76	0.43	0.31	72	3.69	0.48	d.t./b.f.
B2	19.0	203	4.95	1	114	36.0	19.2	175	347	781	1680	1524	4.56	0	4.56	1.10	0.63	57	3.65	1.25	b.b.
B5	19.0	34	6.00	1	114	6.0	28.2	175	347	781	1680	1524	4.56	0	4.56	1.10	0.63	57	3.65	1.25	w.c.
B6	19.0	34	4.95	1	114	6.0	19.2	225	314	682	1680	1524	3.98	1.03	2.95	0.71	0.63	89	3.40	1.17	w.c.
B7	19.0	34	6.00	1	114	6.0	28.2	256	299	900	1680	1524	5.25	1.16	4.09	0.99	0.63	139	3.29	1.60	w.c.
B8	19.0	34	6.00	1	114	6.0	28.2	256	299	900	1680	1524	5.25	1.16	4.09	0.99	1.38	64	3.29	1.60	w.c.
B9	19.0	34	6.00	1	114	6.0	28.2	256	299	900	1680	1524	5.25	1.16	4.09	0.99	0.63	64	3.29	1.60	b.b.
F1	12.7	89	4.95	2	75	14.0	19.2	57	354	877	1753	1524	4.90	0	4.90	0.99	0.71	72	3.71	1.32	w.c.
F2	12.7	74	6.00	2	75	5.4	28.2	53	327	1108	1753	1524	6.20	1.09	5.11	1.23	0.63	51	3.50	1.77	w.c.
ERRC																					
Rect	15.9	34	4.47	1.5	95	6.3	15.7	470	398*	867	2070	1930	3.67	0.94	2.73	0.66	0.61	92	2.70	1.36	w.i.
Bar-bell	19.1	34	4.47	1	115	6.1	15.7	340	389	973	2190	1910	4.35	0.99	3.36	0.81	0.82	101	2.70	1.61	w.c.

* See page C6

Notes on Table C.2

1 Unit identification.

2 Diameter of smallest primary flexural reinforcing bar.

3 Vertical spacing of hoop reinforcement.

4 Diameter of hoop reinforcement.

5 Number of flexural bars restrained by one hoop leg.

6 Maximum hoop spacing allowed by NZS 3101 (= $6d_b$). Values enclosed by a box indicate NZS 3101 requirements not being met.

7 Hoop leg area required by NZS 3101 (equation 6.5).

8 Hoop leg area supplied.

9 Ideal neutral axis depth (column 4, Table C.1).

10 Critical neutral axis depth, calculated as the larger of equations 6.1 and 6.2, where ϕ_o is taken from column 11 of Table C.1 and S is taken to be 1.0. Values of h_w/ℓ_w were taken as 1.60, 1.59 and 1.84 for the PCA walls, EERC rectangular and barbell walls respectively.

11 Design shear force, calculated as M^o/h_w where M^o is given in column 5 or 7 of Table C.1 and the (constant) shear force lever arm h_w is 3.05, 3.85 and 4.385 m, for the PCA, EERC rectangular and EERC barbell walls respectively.

12 Distance from the extreme compression fibre to the centroid of the tensile reinforcement at flexural overstrength.

13 Minimum value of d which may be used (NZS 3101). The maximum value of columns 12 and 13 is used to derive column 14.

14 Design shear stress index $v_i = V/(b_w d)$.

15 Concrete shear stress capacity permitted by NZS 3101 $v_c = 0.6\sqrt{P/A_g}$, where P is the axial force on the section (column 2, Table C.1) and A_g is the gross sectional area of the wall. The self weight of the wall units was ignored in the calculation of v_c.

16 Shear stress required to be resisted by reinforcement, $v_s = v_i - v_c$.

17 Required shear reinforcement ratio, $\rho_h = \frac{v_s}{f_y}$ where f_y is the design yield strength used by the PCA or EERC as appropriate (usually 414 MPa = 60 ksi).

18 Supplied shear reinforcement ratio.

19 Ratio of supplied to required shear reinforcement contents.

20 Maximum shear stress index permitted by NZS 3101, calculated as the lower of $(0.3\phi_o S + 0.16)\sqrt{f'_c}$, $S = 1.0$, and $0.9\sqrt{f'_c}$ with f'_c in MPa units.

21 Ratio of design shear stress (column 14) to code allowable maximum stress.

C.2 COMPARISON OF SUPPLIED REINFORCEMENT AND NZ CODE REQUIREMENTS [34]

Columns 6 and 19 of Table C.2 give an indication as to whether or not the PCA and EERC test walls comply with NZS 3101 requirements for hoop and shear reinforcement. Antibuckling reinforcement was generally present in sufficient quantity and at a suitably small pitch to be effective. Of the 4 units which fail the New Zealand requirements, 3 did indeed exhibit inelastic bar buckling as the initiating failure mechanism. This experimental evidence lends good support to the codified provisions.

Because of the low levels of axial load used, compression block depths were generally small. Only the EERC rectangular section would require confining reinforcement in the end zones according to the provisions of NZS 3101. The section should be provided with hoop reinforcement in accordance with Eqs. (6.3) and (6.4). Because the expression $0.3(A_g^*/A_c^* - 1) = 0.3\ (470 \times 114/(470 - 15) \times (114 - 30)) - 1)$ $= 0.125 > 0.12$, the latter equation is critical.
In the direction perpendicular to the plane of the wall, this requirement is

$$A_{sh} = 0.125 \times 34 \times \left(\frac{470}{2} - 115\right) \times \frac{41.4}{414} \times \left(0.5 + 0.9 \times \frac{470}{2412}\right)$$

$$= 63.1 \text{ mm}^2$$

The provided reinforcement is 4 legs of 4.47 mm diameter, an area of 62.8 mm^2. This reinforcement is placed in the outer 270 mm of the section which complies reasonably with the NZS 3101 requirement for confinement to be located in the outermost half of the compression zone (235 mm in this case). The confined zones extended a height of 1.80 m above the critical (base) section, adequate in terms of New Zealand requirements.

The results of the shear design comparison are viewed with the most concern. Although about 3 units could be considered to have adequate shear reinforcement, the majority are seriously under reinforced. Despite the well defined relationship between shear force and moment for these test specimens, and the existence of comparatively reliable methods of assessing flexural strength, no consistent method of assessing a realistic level of design shear force has been used. While the provision of more shear reinforcement would have only delayed the onset of web crushing, the low levels of shear strength are believed to have considerably influenced the behaviour of many of the

PCA walls. For example, with regards the hysteretic response of these units, it is felt that the observed degree of hoop pinching can be attributed to inadequate shear strength rather than being an inherent feature of general structural wall behaviour. In the light of this, some of the conclusions drawn from the PCA tests may not necessarily be valid for walls of proportionally greater strength.

Although it was stated that only two walls displayed diagonal tension failures, it is felt that other units underwent this form of failure initially and the reported failure modes developed only after the continued application of large displacements. For all units associated with web crushing failure, the NZ code [34] limitation on permissible shear stress was exceeded (column 21, Table C2), while where $v_i/v_{max} < 1.0$, web crushing was not noted. It is acknowledged, however, that these failures did in some cases occur at a displacement ductility in excess of 5 (which is implied by an S factor of unity).

APPENDIX D

DESIGN OF EXPERIMENTAL STRUCTURAL WALL UNITS

This Appendix contains design calculations relevant to the determination of reinforcement required for the wall units tested. The design process is based largely on the relevant requirements of NZS 3101 which are summarised in Section 6.2.

D.1 WALL 1

As outlined in Section 6.4.3, it was decided to test the walls under eccentric axial loading, the magnitude of the load varying with the sense of the lateral load. The chosen axial loads were 0.05 and $0.30f'_cA_g$ for negative and positive lateral load respectively, and an eccentricity of $0.25\ell_w$ was selected for Wall 1. This maximum axial load was viewed as an extreme upper bound to the possible axial load on a structural wall under overload conditions. The minimum value of $0.05f'_cA_g$ was chosen to allow significant tensile yielding of flexural reinforcement prior to the application of higher axial compression. The eccentricity chosen was the largest possible within constraints imposed by existing testing facilities.

The assumed section size (1500 x 100 mm) with the layout of flexural reinforcement is shown in Fig. D.1. Material strengths of 25 MPa and 440 MPa were assumed for concrete and steel respectively, this latter figure being an estimate of probable yield strength for high strength (Grade 380) steel.

The moment-axial load interaction diagram for the section, covering the axial load range of interest is given in Fig. D.2. The figure shows the moment-axial load relationship for 3 combinations of material strengths (f'_c, f_y), the first (25,440) being the basic design curve as mentioned above. The (25,550) curve was used for shear design, while the (32.5, 550) curve provides an estimate of likely extreme overstrength of the section. Points on the curves were calculated on the assumption of an extreme compression fibre strain of 0.003 and a linear strain gradient, with all reinforcement present contributing to the section strength.

Reinforcement content ratios are given in Table 6.1.

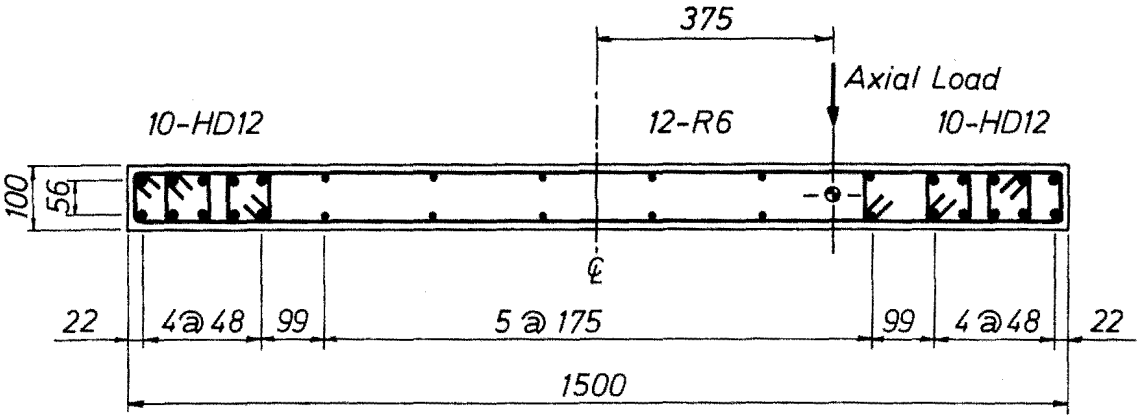

Fig. D.1 Rectangular Wall Cross Section.

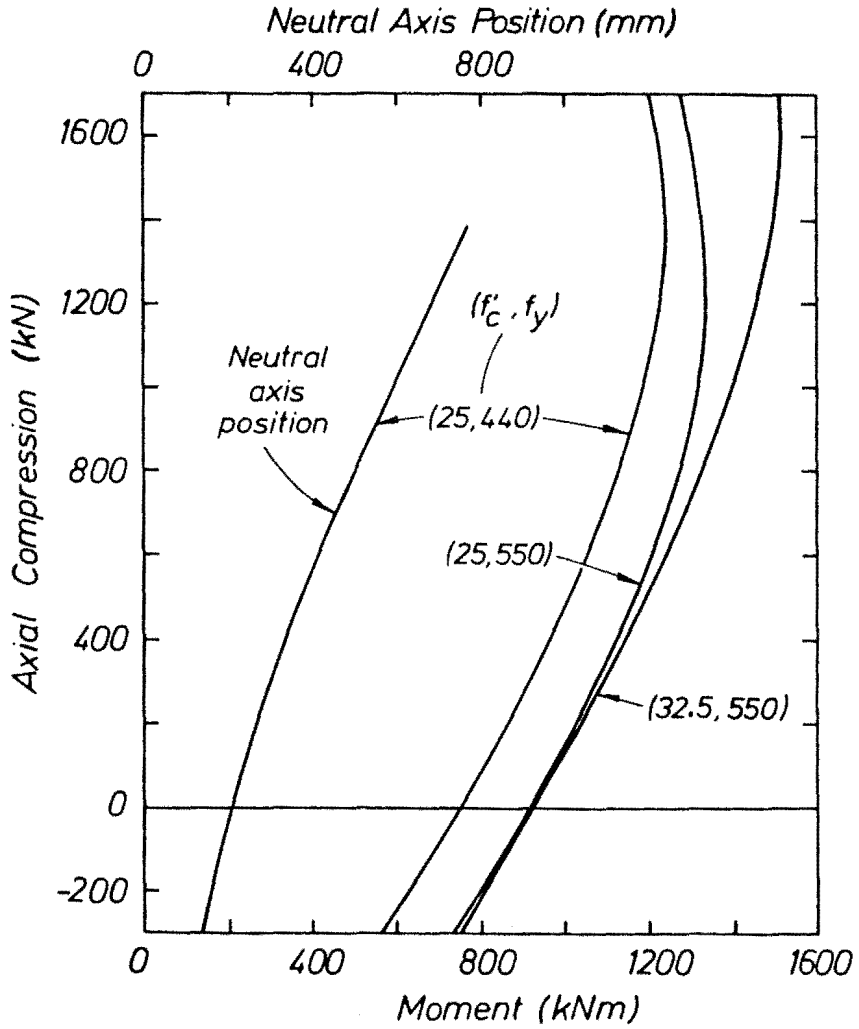

Fig. D.2 Rectangular Section Moment - Axial Force Interaction Diagram.

D.1.1 POSITIVE LATERAL LOAD

$$P = 0.3f'_c A_g = 0.3 \times 25 \times 1.5 \times 0.1 = 1125 \text{ kN}$$

From Fig. A.2 $M_i(25,440) = 1210$ kN.m, $c_i = 0.645$ m

$M_i(25,550) = 1330$ kN.m, $c_i = 0.670$ m

For the eccentricity $e = 0.25\ell_w = 0.25 \times 1.5 = 0.375$ m,

$P.e = 1125 \times 0.375 = 422$ kN.m.

Shear: The assumed design condition for shear is that corresponding to the development of the overstrength moment $M_i(25,550)$. The code approach involving a dynamic magnification factor is not appropriate because the lever arm of the applied shear is constant during the test. Thus, design shear force $V = (1330 - 422)/3.175 = 286$ kN where the jack lever arm at the critical section is 3.175 m. d, the distance from the extreme compression fibre to the centroid of the tension reinforcement (based on c = 0.67 m) = 1.356 m = $0.904\ell_w > 0.8\ell_w$.

$$\therefore \quad v_i = V/(b_w d) = 0.286/(0.10 \times 1.356) = 2.09 \text{ MPa}$$

$$v_c = 0.6\sqrt{P/A_g} = 0.6\sqrt{1.125/(0.10 \times 1.5)} = 1.64 \text{ MPa} - \text{Eq.6.9}$$

$$v_s = v_i - v_c = 2.09 - 1.64 = 0.45 \text{ MPa} \ldots \text{ non critical.}$$

Hoop Reinforcement:

I. Confinement. Half the compression block is confined, although the code equations (Eqns. 6.1, 6.2) for assessment of the critical compression block depth are not directly applicable.

Confine 0.5 x 645 = 322 mm, i.e. extend hoops to the first pair of R6 bars.

Assume R5 hoops (area = 19.64 mm^2) with 10 mm cover.

$$0.3\left[(A_g^*/A_c^*) - 1\right] = 0.3\left[\frac{321 \times 100}{311 \times 80} - 1\right] = 0.087 < 0.12$$

$\therefore$ Eq. 6.4 is critical rather than Eq. 6.3, and the required

hoop area $A_{sh} = 0.12 s_h h'' \frac{f'_c}{f_{yh}} (0.5 - 0.9 \frac{c}{\ell_w})$

Assume s_h = 40 mm, f_{yh} = 275 MPa, f'_c = 25 MPa

(i) h" = 311 mm. $A_{sh} = 0.12 \times 40 \times 311 \times \frac{25}{275} \times \left(0.5 + 0.9 \times \frac{645}{1500}\right) = 120.4$ mm

6 legs R5 = 6 x 19.64 = 117.8 mm^2 .... Ok

(ii) h" = 80 mm. $A_{sh} = 120.4 \times 80/311 = 31.0$ mm^2

2 legs R5 = 2 x 19.64 = 39.3 mm^2 .... Ok

Check spacing: $s_h < 6d_b = 6 \times 12 = 72$ mm

(Clause 10.5.4.5(6)
Ref. 34) $s_h < 0.5h" = 0.5 \times 80 = 40$ mm

$s_h < 150$ mm .... Ok

II. Antibuckling: The required hoop leg area

$$A_{te} > \frac{\Sigma A_b f_y}{16 f_{yt}} \cdot \frac{s_v}{100} \qquad \text{(Eq. 6.5)}$$

i.e. $A_{te} > \frac{113 \times 440}{16 \times 275} \cdot \frac{40}{100} = 4.52$ $mm^2 <$ 19.64 mm^2 .... Ok

Maximum Probable Strength

From Fig, D.2, $M_i(32.5,550)$ = 1430 kN.m. Maximum required lateral load = (1430 - 422)/3175 = 317 kN < 500 kN, which is the MTS jack capacity ..... Ok

D.1.2 NEGATIVE LATERAL LOAD

Design axial force $P = 0.05 f'_c A_g = 0.05 \times 25 \times 0.1 \times 1.5 = 188$ kN

From Fig. D.2, $M_i(25,440)$ = 855 kN.m, c = 0.31 m

$M_i(25,550)$ = 1020 kN.m, c = 0.32 m

Eccentricity e = 0.375 m, $\therefore$ P.e = 188 x 0.375 = 71 kN.m

Shear: Design shear force V = (1020 + 71)/3.175 = 343 kN

d, based on c = 0.32 m, = 1.264 m = $0.842\ell_w > 0.8\ell_w$

$\therefore v_i = V/(b_w d) = 0.343/(0.10 \times 1.264) = 2.71$ MPa

$$v_c = 0.6\sqrt{P/A_g} = 0.6\sqrt{0.188/0.1 \times 1.5} = 0.67 \text{ MPa}$$

$$v_s = v_i - v_c = 2.71 - 0.67 = 2.04 \text{ MPa} \ldots \text{ critical}$$

Assume 2 legged R6 stirrups, $f_y = 275$ MPa

$$\text{Required spacing } s = \frac{A_v f_y}{v_s b_w} = \frac{2 \times 28.3 \times 275}{2.04 \times 100} = 76.2 \text{ mm}$$

Use s = 80 mm, which is compatible with hoop spacing of 40 mm.

Hoop Reinforcement: Antibuckling reinforcement only is provided because of the small compression block depth. Spacing limitations (from Clause 6.5.3.3(d) Ref. 34)

$s < d/4 = 1264/4 = 316$ mm

$s < 6d_b = 6 \times 12 = 72$ mm

$s < 150$ mm

Thus choose s = 72 mm and check R5 hoops, $f_y = 275$ MPa.

$$\text{Required } A_{te} > \frac{\Sigma A_b f_y}{16 f_{yt}} \cdot \frac{s}{100} = \frac{113 \times 440}{16 \times 275} \cdot \frac{72}{100} = 8.1 \text{ mm}^2 < 19.64 \text{ mm} \ldots \text{ O}$$

Maximum Probable Strength

From Fig. D.2, $M_i(32.5,550) = 1035$ kN.m. Maximum lateral load = (1035 + 71)/3.175 = 348 kN < 500 kN .... Ok

Shear Span : The effective moment to shear ratios, non dimensionalised with respect to wall length, are 3.25 and 1.90 for positive and negative loading respectively. (See Fig. D.3).

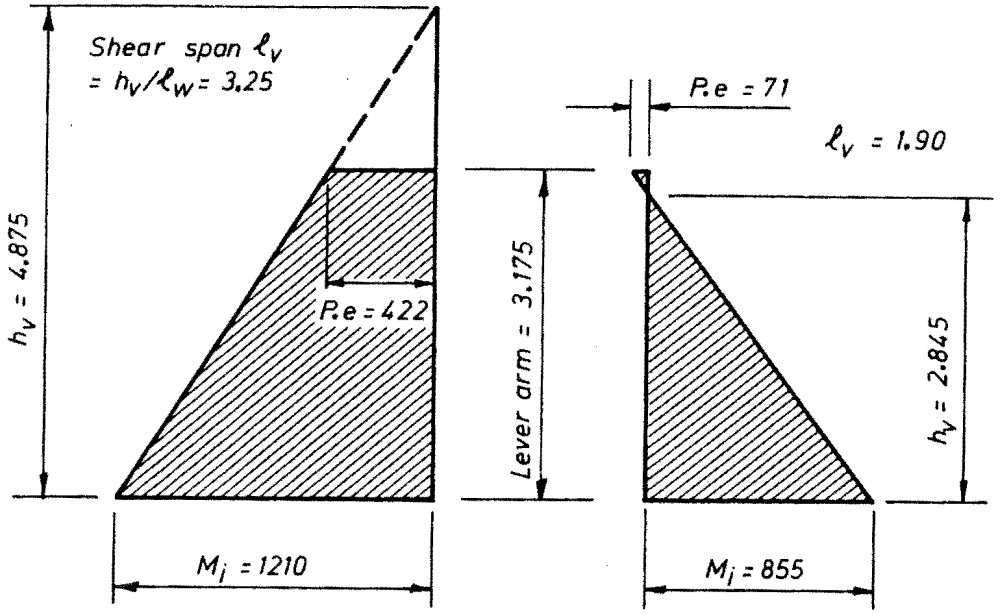

Fig. D.3 Design Bending Moment Diagram for Wall 1.

D.2 WALL 2

Initially it was proposed to construct a second wall almost identical to Wall 1 and test it under the same loading conditions. The sole difference was in the supplied hoop reinforcement: Wall 2 was provided with antibuckling reinforcement only, i.e. R5 sets at 72 mm vertical centres. However, given the behaviour of Wall 1, it was considered necessary to test Wall 2 under less severe conditions and it was decided that an axial load variation of $0.03 - 0.15 f'_c A_g$ (nominal) would be appropriate. Accordingly, calculations are presented for this loading, and any discrepancy between required and provided capacities is indicated.

D.2.1 POSITIVE LATERAL LOAD

$P = 0.15 f'_c A_g = 0.15 \times 25 \times 1.5 \times 0.1 = 562$ kN

From Fig. D.2 $M_i (f'_c = 25, f_y = 440) = 1030$ kN.m, $c = 0.40$ m

For eccentricity e = 0.375 m, P.e = 562 x 0.375 = 211 kN.m.

Shear: non critical.

Hoop Reinforcement:

I. Confinement. Half of the compression block, i.e. the outer 200 mm must be confined. Provided hoops to confine 207 mm into the section ..... Ok

$$0.3\left(\frac{A^*_g}{A^*_c} - 1\right) = 0.3 \times \left(\frac{207 \times 100}{197 \times 80} - 1\right) = 0.094 < 0.12$$

$$\therefore A_{sh} > 0.12 s_h h'' \frac{f'_c}{f_{yh}} \left(0.5 + 0.9 \frac{c}{\ell_w}\right) \quad , \quad h'' = 197{,}80 \text{ mm}$$

The provided hoop reinforcement is 5 legged R5 sets at 72 mm vertical centres. Thus, according to the above equation, the required hoop areas are with h" = 197 mm:

(i) $A_{sh} = 0.12 \times 72 \times 197 \times \frac{25}{275} \times \left(0.5 + 0.9 \times \frac{400}{1500}\right) = 108.6 \text{ mm}^2$

Supplied A_{sh} = 5 legs R5 = 5 x 19.64 = 98.2 mm^2 < 108.6 mm^2

i.e. supplied hoop reinforcement = $\frac{98.2}{108.6} \times 100 = 90.4\%$ of code requirement.

(ii) $A_{sh} = 108.6 \times \frac{80}{197} = 44.1 \text{ mm}^2$

Supplied A_{sh} = 2 legs R5 = 2 x 19.64 = 39.28 mm^2

i.e. 89.1% of code requirement.

In addition, the code maximum spacing (h"/2 = 40 mm, > 72 mm) is exceeded.

II. Antibuckling. Clearly Ok.

D.2.2 NEGATIVE LATERAL LOAD

$P = 0.03 f'_c A_g = 0.03 \times 25 \times 1.5 \times 0.1 = 112$ kN

From Fig. D.2, $M_i(25,440) = 810$ kN.m, c = 0.24 m

$M_i(25,550) = 980$ kN.m, c = 0.28 m

For eccentricity e = 0.375 m, P.e = 0.375 x 112 = 42 kN.m.

Shear: Design shear force V = (980 + 42)/3.175 = 321 kN

d, based on c = 0.28 m, = 1.264 m = $0.842\ell_w$

$$v_i = V/(b_w d) = 0.321/(0.1 \times 1.264) = 2.54 \text{ MPa}$$

$$v_c = 0.6\sqrt{P/A_g} = 0.6\sqrt{0.03 \times 25} = 0.52 \text{ MPa}$$

$$\therefore \quad v_s = 2.54 - 0.52 = 2.02 \text{ MPa}$$

This compared with a design value of 2.01 MPa for Wall 1 shear, so that it is clear that the altered axial load conditions do not change the shear reinforcement required.

Hoop Reinforcement: Antibuckling reinforcement provisions as for Wall 1 are clearly adequate.

Shear Span: Non-dimensional shear span values for positive and negative loading are 2.66 and 2.01 respectively.

D.3 WALL 3

A flanged (tee shaped) section was chosen for study after the two rectangular section walls. The relative dimensions of the section (Fig. D.4) show it to be stockier than is usual in prototype structural walls, but this was necessitated by practical condiderations. Because of the greater inherent stability of the flanged end of the section, higher axial load was supplied to the unflanged end of the wall where lateral instability is more likely. This unit was also initially designed for heavy axial load (of order $0.3f'_c A_g$) but in view of the performance of Wall 1, a less severe loading was deemed appropriate. Fig. D.5 shows an interaction diagram for the section and calculations pertinent to the reduced axial loads are subsequently provided. Axial load was applied at an eccentricity of 400 mm to the elastic centroid of this section, which is 460 mm from the west face of the wall.

D.3.1 POSITIVE LATERAL LOAD

As indicated above, the east end of this unit was originally designed for an axial load which required confining hoops over the outermost half of the theoretical compression block at ultimate strength. It was decided to test this third unit at an axial load such that the supplied hoop reinforcement extended over approximately 75% of the theoretical compression block depth

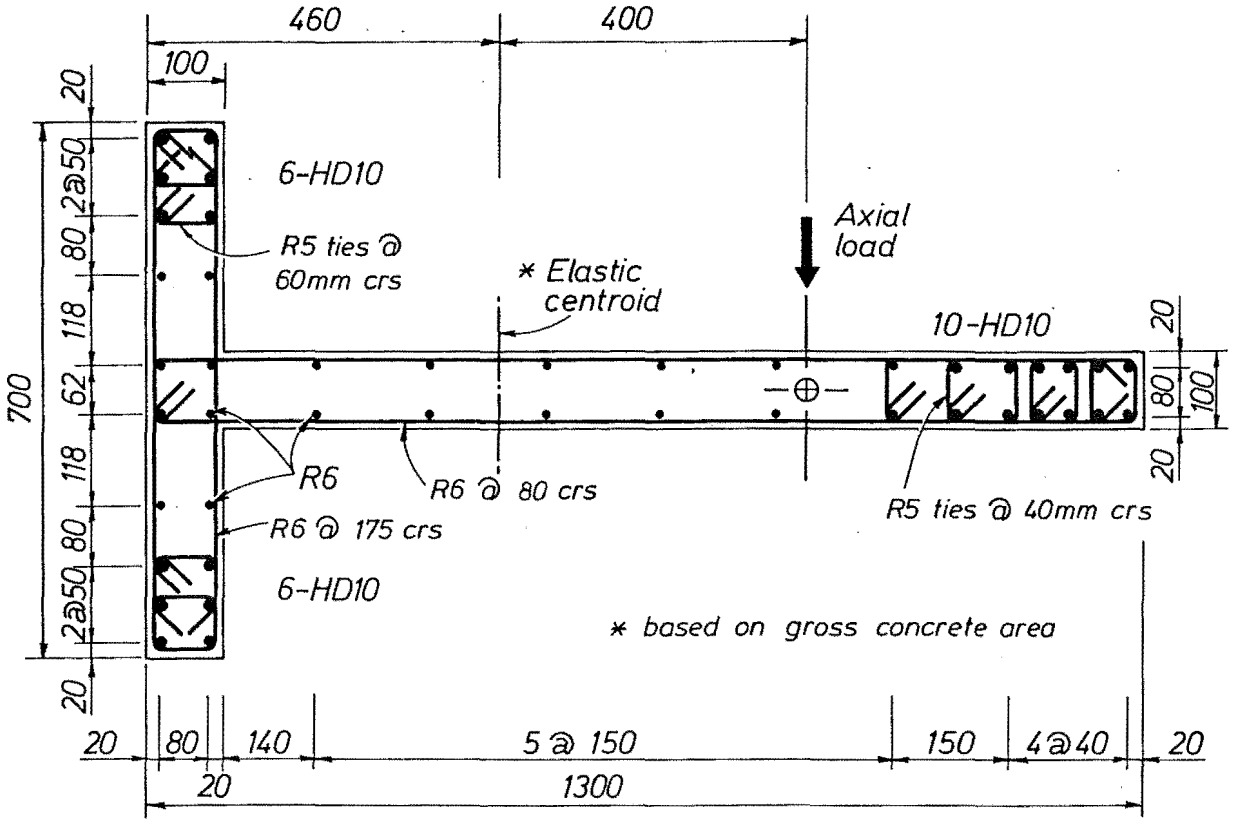

Fig. D.4 Tee Section Wall Reinforcement.

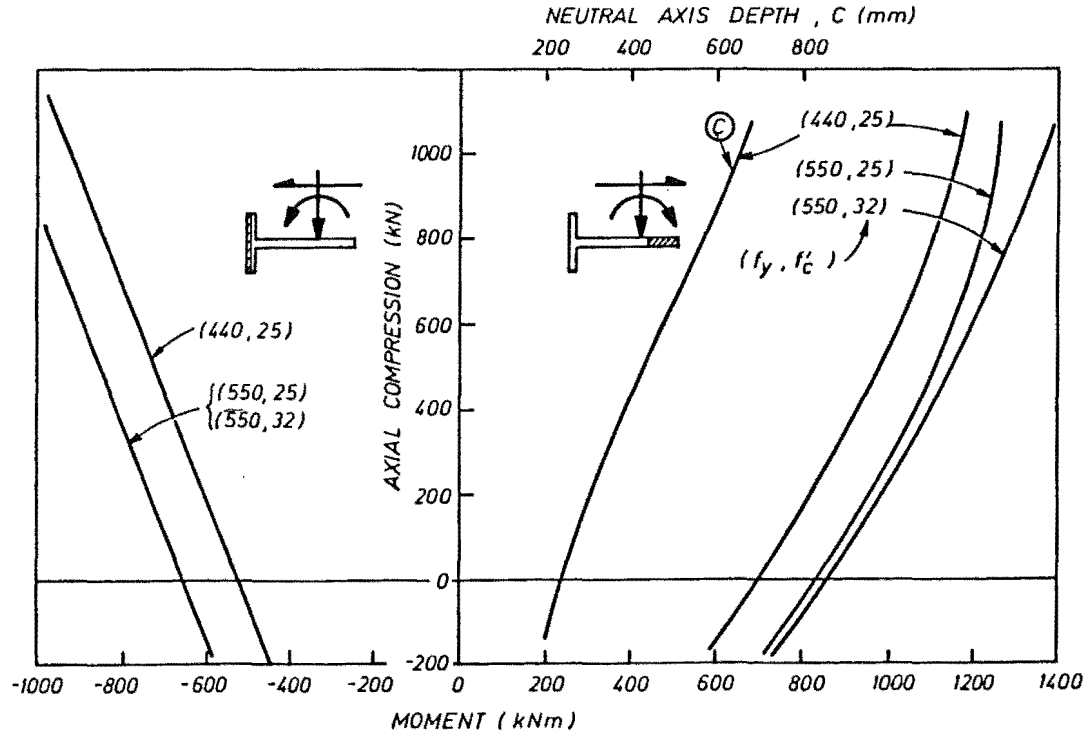

Fig. D.5 Tee Section Moment - Axial Force Interaction Diagram.

$3/4\ c = 408$ mm $\quad \therefore \quad c = 544$ mm

This corresponds to P = 750 kN ($= 0.16 f'_c A_g$),

M_i ($f'_c = 25$, $f_y = 440$) = 1085 kN.m from the interaction diagram.

Reinforcement ratios are given in Table 6.1.

Shear: Non critical

Hoop Reinforcement

I. Confinement. The code required confinement, based on a neutral axis depth of 544 mm and the hoop arrangement of Fig. D.6 is as follows:

$$0.3\left(\frac{A^*_g}{A^*_c} - 1\right) = 0.3\left(\frac{340 \times 100}{330 \times 80} - 1\right) = 0.086 < 0.12$$

Hence, for $s_h = 40$ mm, $f_y = 275$ MPa

(i) $h'' = 340$

$$A_{sh} = 0.12 s_h h'' \frac{f'_c}{f_y}\left(0.5 + 0.9\frac{c}{\ell_w}\right) = 0.12 \times 40 \times 340 \times \frac{25}{275}$$

$$\times \left(0.5 \times 0.9 \times \frac{544}{1000}\right) = 122.6 \text{ mm}^2$$

Provided area = 7 legs R5 = $7 \times 19.64 = 137.5$ mm^2, 12% in excess of the requirement. In addition, the hoop reinforcement is distributed over 3/4 of the compression block depth rather than the code required 1/2 depth. Because the original design of this section called for 7 legs of hoop reinforcement, a somewhat artificial device was used in the wall construction. This was to incorporate two extra R10 longitudinal bars (Fig. D.6) which were cut at 200 mm intervals to ensure no contribution to flexural strength. These bars permitted the inclusion of a seventh hoop leg.

(ii) $h'' = 80$ $\quad A_{sh} = 0.12 \times 40 \times 80 \times \frac{25}{275} \times \left(0.5 + 0.9 \times \frac{544}{1500}\right) = 28.8$ mm

Provided area = 2 legs R5 = $2 \times 19.64 = 39.3$ mm^2 .... Ok

II. Antibuckling - clearly satisfactory.

Maximum Probable Strength - non critical

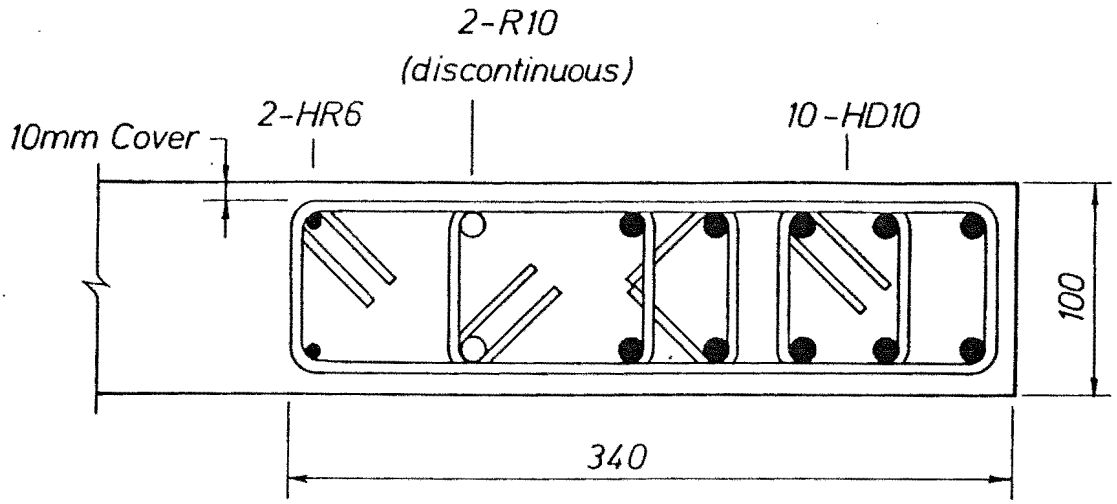

Fig. D.6 Tee Section East End Hoop Reinforcement Details.

D.3.2 NEGATIVE LATERAL LOAD

$P = 0.03f'_c A_g = 0.03 \times 25 \times 0.19 = 143$ kN

$M_i(25,440) = 580$ kN.m

$M_i(25,550) = 715$ kN.m, $c = 0.035$ m

$P.e = 143 \times 0.40 = 57$ kN.m

Shear: Design force $V = (715 + 57)/3.175 = 243$ kN

Taking $d = 0.8\ell_w = 0.8 \times 1.3 = 1.04$ m

$v_i = 0.243/(0.10 \times 1.04) = 2.34$ MPa

$v_c = 0.6\sqrt{P/A_g} = 0.6\sqrt{2143/0.19} = 0.52$ MPa

$v_s = v_i - v_c = 2.34 - 0.52 = 1.82$ MPa

The required spacing for 2 legged R6 stirrups, $f_y = 275$ MPa

is $s = \dfrac{A_v f_y}{b_w v_s} = \dfrac{2 \times 28.3 \times 275}{100 \times 1.82} = 85.4$ mm

Stirrups were provided at s = ~~80~~ 100 mm ..... Ok SEE ERRATA

Hoop Reinforcement: No confining reinforcement was provided in view of the small compression block depth. The D10 primary longitudinal reinforcement was provided with antibuckling hoops comprising R5 sets at $6d_b = 6 \times 10 = 60$ mm spacing in the flange.

Maximum Probable Strength - non critical

Shear Span: The non dimensional shear spans at ideal flexural strength are 2.70 and 1.91 for positive and negative loading respectively.

D.3.3 FLANGE ZONE

Shear reinforcement sufficient to withstand half of the design web shear stress was supplied in the flange region. 2 legged R6 stirrups at 175 mm spacing were used.

D.4 WALL 4

Wall 4 had an identical reinforcement arrangement to Wall 1 and differed only in the positioning of the floor slab to give a first storey span : wall thickness ratio of 8 : 1 (compared to 10 : 1 for Walls 1, 2 and 3). It was decided to test this unit at an axial load level which would result in the confined depth being approximately 75% of the ideal neutral axis depth. This was done on the basis of measured material strengths (Table 6.2) which were markedly different from the assumed properties (concrete strength of 36.5 MPa > 25 MPa, flexural reinforcement yield strength of 345 MPa < 440 MPa). The provided hoop and shear reinforcement contents are reviewed with respect to the axial load chosen and these measured material properties.

D.4.1 Postive Lateral Load

For c = (4/3) x 323 = 431 mm (where the confined depth = 323 mm), the ideal flexural strength based on measured material properties $M_i(36.5,345)$ = 1114 kNm, P = 973 kN.

Shear: Non critical.

Hoop Reinforcement: Eq. (6.4) is critical. The required hoop area, using the measured hoop strength (Table 6.2) is

$$A_{sh} = 0.12 s_h h'' \frac{f'_c}{f_y}\left(0.5 + 0.9\frac{c}{\ell_w}\right) = 0.12 \times 40 \times 313 \times \frac{36.5}{290} \times (0.9 \times 431/15$$

$$= 143.4 \text{ mm}^2$$

Provided area = 6 legs R5 = 6 x 19.64 = 117.8 mm^2, some 18% less than the code requires. In the event, an axial force of 923 kN = $0.169 f'_c A_g$ was used which compensated slightly for the shortfall in hoop reinforcement.

Maximum Probable Strength: Assuming measured concrete strength and reinforcement overstrength of 450 MPa, the maximum probable strength at an axial load of 923 kN is 1380 kNm, corresponding to a lateral load of (1380 - 923 x 0.375)/3.175 = 326 kN < 500 kN.

D.4.2 Negative Lateral Load

An axial load of $P = 0.03f'_c A_g = 0.03 \times 36.5 \times 0.1 \times 1.5 = 164$ kN was used for negative lateral loading. For the eccentricity e = 0.375 m, P.e = 164 x 0.375 = 62 kNm.

Shear: Assuming that the maximum negative shear develops with $M_i(36.5,450) = 1030$ kN.m (P = 164 kN), the design shear force V = (1030 + 62)/3.175 = 344 kN, d = 1.306 m = $0.87/\ell_w$.

$$v_i = V/(b_w d) = 0.344/(0.10 \times 1.306) = 2.63 \text{ MPa}$$

$$v_c = 0.6\sqrt{P/A_g} = 0.6\sqrt{0.164/0.15} = 0.63 \text{ MPa}$$

$$\therefore \quad v_s = v_i - v_c = 2.63 - 0.63 = 2.00 \text{ MPa}$$

For 2 legged R6 stirrups, f_y = 275 MPa, the required spacing $s = \frac{A_v f_y}{b_w v_s} = \frac{2 \times 28.3 \times 275}{100 \times 2.00} = 77.8$ mm, slightly less than the actual spacing of 80 mm. However, shear reinforcement is adequate because the actual stirrup strength of 335 MPa (Table 6.2) is well in excess of the 275 MPa assumed.

Hoop Reinforcement: Satisfactory with respect to antibuckling requirements.

Shear Span: The non dimensional shear spans for positive and negative ideal strengths are 3.07 and 1.95 respectively.